Effect of concrete composition and self-healing method on bond behaviour of cracked normal concrete and self-consolidating concrete

by

Seyed Sina MOUSAVI OJARESTAGHI

MANUSCRIPT-BASED THESIS PRESENTED TO ÉCOLE DE TECHNOLOGIE SUPÉRIEURE IN PARTIAL FULFILLMENT FOR THE DEGREE OF DOCTOR OF PHILOSOPHY
Ph.D.

MONTREAL, DECEMBER 19, 2020

ÉCOLE DE TECHNOLOGIE SUPÉRIEURE
UNIVERSITÉ DU QUÉBEC

BOARD OF EXAMINERS

THIS THESIS HAS BEEN EVALUATED

BY THE FOLLOWING BOARD OF EXAMINERS

Mr. Lotfi Guizani, Thesis Supervisor
Department of Construction Engineering, École de technologie supérieure

Mrs. Claudiane Ouellet-Plamondon, Thesis Co-supervisor
Department of Construction Engineering, École de technologie supérieure

Mr. Hakim Bouzid, President of the Board of Examiners
Department of Mechanical Engineering, École de technologie supérieure

Mr. Amar Khaled, Member of the jury
Department of Construction Engineering, École de technologie supérieure

Mr. Jean-Philippe Charron, External Evaluator
Department of Civil, Geological and Mining Engineering, Polytechnique Montréal

THIS THESIS WAS PRENSENTED AND DEFENDED

IN THE PRESENCE OF A BOARD OF EXAMINERS AND PUBLIC

ON NOVEMBER 26, 2020

AT ÉCOLE DE TECHNOLOGIE SUPÉRIEURE

ACKNOWLEDGMENTS

I have great pleasure in expressing my sincere gratitude to professor Lotfi Guizani and professor Claudiane Ouellet-Plamondon, Department of Construction Engineering, ETS Montreal, under whose guidance the present work has been carried out. Their in-depth knowledge and intellectual insights, especially in the area of structures and materials, helped me a lot in bringing out this thesis in the present form. I am thankful for their constant encouragement and constructive criticisms throughout this study.

I wish to express my thanks to ETS technicians staff of Concrete and Structure laboratories, Juan Mauricio Rios, Jonathan Auger, and other technicians who helped me a lot in carrying out the experiments.

I would like to thank Mr. Chandrasekhar B for his valuable help, suggestions, and discussion at different stages of work on concrete mixtures. His valuable comments on the microstructure and chemical properties of concrete helped me a lot.

I owe a lot to my parents for their patience, abundant love and affection.

Effet de la composition du béton et de la méthode d'auto-cicatrisation sur le comportement d'adhérence du béton normal fissuré et du béton autoplaçant

Seyed Sina MOUSAVI OJARESTAGHI

RÉSUMÉ

L'interaction entre la barre d'armature en acier et le béton environnant est un aspect crucial contrôlant l'efficacité du comportement composite des structures en béton armé. De plus, un bon comportement interfacial entre le béton et l'armature est nécessaire pour obtenir des performances durables pour une structure en béton armé. Cependant, la plupart des études précédentes se sont concentrées sur le comportement interfacial des barres d'armature avec le béton environnant intact et exempt de dommages. Il n'y a que peu de recherches sur le béton pré-fissuré avec différentes conditions de pré-fissuration. De plus, il existe un besoin de développer des solutions pratiques pour atténuer les dommages interfaciaux dus au phénomène de pré-fissuration. Par conséquent, cette thèse se propose d'étudier expérimentalement et analytiquement l'adhérence béton-acier d'armature en présence du phénomène de pré-fissuration. En outre, une approche pratique est étudiée pour déterminer la possibilité d'auto-guérison des fissures au niveau de l'interaction barres d'armature-béton. Deux types de polymères superabsorbants (SAP) sont utilisés dans les mélanges de béton, à des dosages de 0,25%, 0,50% et 1,0%, pour accélérer le processus d'auto-guérison. La méthodologie expérimentale consiste en un processus de pré-fissuration avec des périodes de cure pour cicatriser les fissures de fendage et la résistance. Le test de fendage (test brésilien) est utilisé pour simuler le préchargement et obtenir les fissures initiales. Des largeurs de fissures allant de 0.10 mm à 0,50 mm sont étudiées dans la présente thèse. Un nombre total de 230 essais d'arrachement sont réalisés pour obtenir la réponse interfaciale armature-béton en termes de courbes enveloppes adhérence-glissement, permettant l'examen de la contrainte initiale, de la résistance d'adhérence, de la résiduelle d'adhérence, de la contrainte d'adhérence moyenne et de l'énergie absorbée par le mécanisme d'adhérence. Sept types de béton sont testés dans la présente thèse, y compris le béton normal (NC) avec un affaissement normal, NC avec affaissement élevé (fluide), NC avec adjuvant entraîneur d'air (AE), béton autoplaçant (SCC), NC modifié avec SAP, NC modifié avec SAP incorporant de l'air -entrainé, SCC modifié avec SAP. Enfin, des analyses statistiques sont effectuées pour mieux analyser et mettre en évidence les principaux résultats. Les résultats expérimentaux montrent que la pré-fissuration engendre une réduction importante au niveau de la résistance de l'adhérence, la contrainte d'ahérence moyenne et la résistance résiduelle d'adhérence. La dégradation de la résistance d'adhérence est corrélée à la largeur de la fissure initiale. Les résultats montrent que des largeurs de fissures supérieures à 0,15 mm ont un impact considérable sur les propriétés de l'adhérence. De plus,

les résultats montrent que le béton autoplaçant (SCC) est moins sensible au phénomène de pré-fissuration que le béton normal (NC). L'affaissement plus élevé du mélange SCC peut être la raison principale de cette observation. Concernant la méthode d'auto-cicatrisation, les résultats indiquent que les particules de SAP favorisent de manière significative la reprise de résistance dans le béton pré-fissuré, exposé à des cycles humide-sec, surtout pour un dosage plus élevé de SAP et une largeur de fissure inférieure à 0,30 mm. L'adjuvant entraîneur d'air a un impact considérable sur les performances du processus d'auto-cicatrisation, de sorte que le béton contenant de l'AE a un facteur d'amélioration de cicatrisation plus élevé par rapport au mélange dépourvu d'AE. L'analyse par microscopie électronique à balayage (MEB) montre une grande quantité de calcium, d'oxygène et de carbone dans les produits de guérison déposés sur les surfaces internes et externes des fissures. Cette étude serait une première étude de la cicatrisation des fissures dans la région critique de l'interaction armature-béton, qui devrait être poursuivie par des recherches plus poussées, notamment l'effet de l'AE sur la cicatrisation des fissures du béton SAP et l'influence d'ajouts cimentaires (SCM) sur les résultats de la présente thèse. De plus, les résultats de la présente étude démontrent que les particules SAP sont plus efficaces dans les mélanges SCC, par rapport aux mélanges NC, pour cicatriser les fissures initiales à l'interface barres d'armature-béton. De plus, les résultats de la Microtomographie (Micro-CT) montrent que le facteur d'amélioration de la cicatrisation pour l'auto-scellement des fissures est plus élevé que celui de l'auto-guérison (récupération de la résistance), car plus d'efforts sont nécessaires pour la récupération de la résistance que la fermeture de la fissure.

Mots clés: adhérence-glissement, béton fissuré, composition du béton, polymère superabsorbant (SAP), béton autoplaçant, barres d'armature en acier

Effect of concrete composition and self-healing method on bond behaviour of cracked normal concrete and self-consolidating concrete

Seyed Sina MOUSAVI OJARESTAGHI

ABSTRACT

The interaction between the steel reinforcing bar and surrounding concrete is one of the most important issues that control the efficiency of the composite behaviour of reinforced concrete structures. Moreover, a good interfacial behaviour between concrete and reinforcement is necessary to achieve durable performance for a reinforced concrete structure. However, most previous studies have focused on the interfacial behaviour of reinforcing bars with the undamaged and intact surrounding concrete. There are only few researches on pre-cracked concrete with different pre-cracking conditions. Moreover, there is a need for developing practical solutions to mitigate interfacial damages due to the pre-cracking phenomenon. Hence, this thesis intends to experimentally and analytically study the reinforcing steel-concrete bond behaviour in presence of the pre-cracking phenomenon. Additionally, a practical approach is studied to determine the self-healing possibility of cracks at the rebar-concrete interaction. Two types of superabsorbent polymers (SAP) are used in concrete mixtures, in dosages of 0.25%, 0.50%, and 1.0%, to accelerate the self-healing process. The used methodology consists of a pre-cracking process along with re-curing periods (healing periods) for healing splitting cracks. Splitting test (Brazilian test) is used to simulate pre-loading and to obtain initial pre-cracking. Crack widths of 0.10-0.50 mm are studied in the present thesis. A total number of 230 pull-out tests are carried out to obtain the rebar-concrete interfacial response in terms of bond-slip envelope curves, allowing examination of the initial bond stress, bond strength, residual bond stress, average bond stress, and energy observed by the bond mechanism. Seven concrete types are tested in the present thesis including normal concrete (NC) with a normal slump, NC with flowing slump, NC with air-entraining admixture (AE), self-consolidating concrete (SCC), SAP modified NC, SAP modified air-entraining NC, and SAP modified SCC. Finally, statistical analyses are performed to better investigate and point out the main findings. Experimental results show that the pre-cracking phenomenon leads to a significant reduction in the bond strength, average bond stress, and residual bond stress. Bond strength degradation is presented as a function of crack width. Results show that crack widths larger than 0.15 mm have a considerable impact on bond properties. Moreover, Results regarding bond strength reduction due to pre-cracking show that compared to NC, SCC is less sensitive to this phenomenon. The higher value of slump flow can be the main reason for this observation. Regarding the self-healing method, results indicate that SAP particles significantly promote strength regaining in the pre-cracked concrete, exposed to wet-dry cycles, especially for a

higher dosage of SAP and crack width smaller than 0.30 mm. Air-entraining admixture has a considerable impact on the performance of the self-healing process so that concrete containing AE has a higher healing improvement factor as compared to the non-air-entraining mixture. Scanning electron microscopy (SEM) analysis shows a large amount of calcium, oxygen, and carbon in healing products at both internal and external surfaces of cracks. This study would be an initial investigation of the crack-healing in the critical region of the rebar-concrete interaction, which should be continued by further research, notably the effect of AE on the crack-healing of SAP concrete and influence of supplementary cementitious materials (SCMs) on the results of the present thesis. Moreover, results of the present study demonstrate that SAP particles are more efficient in SCC mixtures, as compared to NC mixtures, to heal the initial cracks at the rebar-concrete interface. Moreover, micro-CT scanning results show that the improvement healing factor for self-sealing of cracks is higher than self-healing (strength recovery) one, as more efforts are needed to regain strength recovery than the crack closure.

Keywords: bond-slip, cracked concrete, concrete composition, superabsorbent polymer (SAP), self-consolidating concrete, steel rebar

TABLE OF CONTENTS

Page

LIST OF TABLES

Page

LIST OF FIGURES

Page

LIST OF ABBREVIATIONS

AE	air-entraining admixture
ANOVA	analysis of variance
COV	coefficient of variation
EDS	energy dispersive x-ray spectroscopy
HPC	high performance concrete
IAE	integral absolute error
IF	improvement factor for self-healing performance
ITZ	interfacial transition zone
MC	Mohr-Coulomb
NC	normal concrete
Rebar	reinforcing bar
RF	reduction factor
RH	relative humidity
RMvt	resultant movement of concrete relative to the rebar
S	splitting failure mode
SAP	superabsorbent polymer
SCC	self-consolidating concrete
SEM	scanning electron microscope
SP	superplasticizer
UPV	ultrasonic pulse velocity

LIST OF SYMBOLS

A_b	area of reinforcing bar
B	length of the top horizontal and diagonal section of ribs
$\acute{B}$	length of the top horizontal section of ribs
c	concrete cover around the bar
c_C	concrete cover
C	cohesion strength of concrete
CP	response characteristic parameters
d_b	rebar diameter
E_0	area under the bond-slip curve of intact concrete
E_b	bond energy, area under bond-slip curve till slip of 10 mm
E_c	area under the bond-slip curve of pre-cracked concrete
$E_{1.0}$	bond energy, area under bond-slip curve till slip of 1.0 mm
E_c/E_0	normalized dissipated energy
E(X)	Mean of X
F	tensile force of pull-out test
f_R	relative rib area (bond index)
f_c	concrete compressive strength
f'_c	compressive strength of concrete
f_y	yield strength of steel reinforcing bar
f_u	ultimate strength of steel reinforcing bar
H	healing period (14 or 28 days)
h_r	rib height of rebar
IF_{τ_m}	improvement factor for average bond stress
IF_{τ_u}	improvement factor for bond strength
IF_{τ_r}	improvement factor for residual bond stress
K	reduction factor for horizontal steel-concrete interfacial pressure due to the pure shear failure in concrete shear-off

K_I	increase factor for development length
K_{tr}	effect of confinement by the stirrup (ACI 318M-14)
L	embedded length of steel bar in concrete specimens
L	a reduction factor for contact pressure due to the pre-cracking phenomenon (Chapter 3)
L_{heal}	threshold length of cracks healed by SAP particles
L_T	total length of cracks
l_d	development length required for reinforcing bar
l_e	embedded length
M	empirical factor for calculating development length
M_1, M_2, M_3	empirical equation for Eq. (5.6)
N	SAP particles number
P	pull-out failure mode
SR_M	maximum bond stress reduction due to the pre-cracking
S	slip of steel bar in pre-cracked concrete
S_r	spacing of periodical ribs
S_{r0}	effective length of crushed concrete between two adjacent ribs
S_{max}	slip corresponds to the maximum bond stress
$(S_m)_0$	slip corresponds to the maximum bond stress of intact bond-slip curve
$(S_m)_c$	slip corresponds to the maximum bond stress of reduced bond-slip curve
$(S_{res})_0$	slip corresponds to the residual bond stress of intact bond-slip curve
$(S_{res})_c$	slip corresponds to the residual bond stress of reduced bond-slip curve
w	initial crack width
$\acute{w}$	crack opening during the pull-out test of cracked specimens
w/c	water-to-cement ratio
w_e/c	additional water-to-cement ratio
w_T/c	total water-to-cement ratio
$w/(\Sigma p)$	ratio of crack width-to-the perimeter of reinforcing bar
w/p	water-to-powder ratio
X	total number of intersection in the area

τ	bond stress
$\bar{\tau}$	bond strength distributed over the spacing of periodical ribs:
τ_m	average bond stress recommended by RILEM
$\tau_{0.01}$	bond strength at slip of 0.01 mm
$\tau_{0.10}$	bond strength at slip of 0.10 mm
$\tau_{1.00}$	bond strength at slip of 1.0 mm
$\tau_{6.0}$	bond strength corresponding to slip of 6.0 mm
$(\tau_{max})_c$	maximum bond stress of cracked concrete, called bond strength
$(\tau_{max})_0$	maximum bond stress of uncracked concrete, called bond strength
$\tau_{Uncracked}$	maximum bond stress for uncracked concrete, called bond strength
$\tau_{Pre-cracked}$	maximum bond stress for pre-cracked concrete, called bond strength
τ_{Healed}	maximum bond stress of healed specimens after wet-dry cycles
τ_c	bond stress of steel bar in pre-cracked concrete
τ_{ave}	average bond stress along the embedded length, equal to the bond strength for the present thesis due to the small rebar embedded length
τ_{max}	maximum bond stress, called bond strength
τ_{res}	residual bond stress
τ_q	shear stress on the rib-front face
τ_n	shear stress over the bearing concrete block
τ_u	maximum bond stress, called bond strength
τ_r	residual bond stress
$(\tau_{res})_0$	residual bond stress of intact bond-slip curve
$(\tau_{res})_c$	residual bond stress of reduced bond-slip curve
${\tau_m}^*$	normalized average bond stress with concrete square root of compressive strength
${\tau_u}^*$	normalized maximum bond stress with concrete square root of compressive strength
${\tau_r}^*$	normalized residual bond stress with the concrete square root of compressive strength

Ψ_t	bar location factor
Ψ_e	epoxy coating factor
Ψ_s	bar size factor
λ	lightweight factor for concrete
υ	ratio of the experimental-to-the theoretical value
α	a coefficient related to the nonlinear shape of the initial ascending branch
α	rib–face angle (Chapter 3)
ρ_{nm}	reduction factor of maximum bond stress due to the pre-cracking
ρ_u	bond reduction ratio
β	bearing angle
σ_q	bearing stress on the rib-front face
σ_n	uniform distribution of radial pressure
μ_1	friction coefficient between concrete and steel
μ_2	friction coefficient between concrete and concrete
t_i, x_i, y_i	vertical and horizontal projection length
ψ	internal friction angle
φ	a factor for determining the portion of every side on bearing force
Δ_1	difference between bond strength of uncracked and pre-cracked concrete
Δ_2	difference between bond strength of healed and pre-cracked concrete

INTRODUCTION

The interaction between the reinforcement and the surrounding concrete, known as the "bond-slip" phenomenon, plays a crucial role in the structural behaviour of reinforced concrete (RC) members (Dehestani & Mousavi, 2015). This phenomenon strongly affects the behaviour of RC members in both fields of limit and ultimate states (Eligehausen et al., 1983; Haskett et al., 2008; Filip & Ahmad, 1988; Monti & Spacone, 2000). Bond-slip phenomenon affects the structural efficiency of different sub-elements in an RC frame (Figure 0.1) including column, foundation, interior, and exterior beam-column joint, beam (crack pattern, crack width, and failure mode), and RC slabs. In the case of RC columns subjected to bending at the beam-column joint or footing-column interface, significant-end rotations have been reported due to the anchorage slip (Papadrakakis et al., 2013; Saatcioglu et al., 1992). In addition to the rotation calculated from flexural analysis of an RC column, bond-slip phenomenon (or reinforcement slip), additive rotation of reinforcement slip outside the flexure length leads to the greater drift of columns, beams, and walls under lateral loads (Saatcioglu & Alsiwat, 1996; Sezen & Setzler, 2008). By ignoring this additive rotation, the predicted lateral deformations may be significantly underestimated (Saatcioglu & Ozcebe, 1989). Energy dissipation capacity of joint (Eom et al., 2015), strutural behaviour of interior and exterior beam-column joints as well as lateral deformation of RC frames (Fallah et al., 2013; Fernandes et al., 2013; Limkatanyu & Spacone, 2003), stiffness of RC frame (Limkatanyu & Spacone, 2003), beam-end rotation (Alva & de Cresce El, 2013; Coronelli & Mulas, 2001; Kwak & Kim, 2006; Kwak & Kim, 2010), and natural frequency of RC frame (Limkatanyu & Spacone, 2003) are affected by the bond-slip phenomenon. Bond reduction along with slip occurrence in the column rebars cause lower flexural moments of columns in interior joints as compared to the perfect bond conditions, leading to a predominantly brittle failure mechanism in the beam-column joints. Model without considering the bond-slip phenomenon has slightly lower natural frequency as compared to the model with bond-slip, showing a stiffer model. Lateral stiffness of the RC frame with considering the bond-slip phenomenon (rebar slippage) can be reduced. Moreover,

using the perfect bond link in the RC model can considerably increase the energy dissipation as compared to the model including rebars bond-slip interface. Additionally, in the case of RC beam-column joints, poor bond conditions may lead to insufficient anchorage of rebars within the joints so that important rebar slippage may happen and transfer the anchorage point outside the joint area. In this situation, the beam compression reinforcement on one side of the column could essentially be in tension, leading to a drastic reduction in flexural strength and ductility. Under cyclic loading, stress concentration is far steeper along the internal RC beam-column joints as compared to the bond stress concentration at the extremities of the beams framing into these joints. This indicates higher bond needs in the joints areas. So the bond strength is much important in joints than along the beams (Hakuto et al., 1999). In the case of crack pattern, as load increases, the depth and width of the cracks increase, while tensile stress in higher in the steel bonded to the concrete between the cracks. Insufficient bond results in the formation of much larger cracks and possible early failure of the beam.

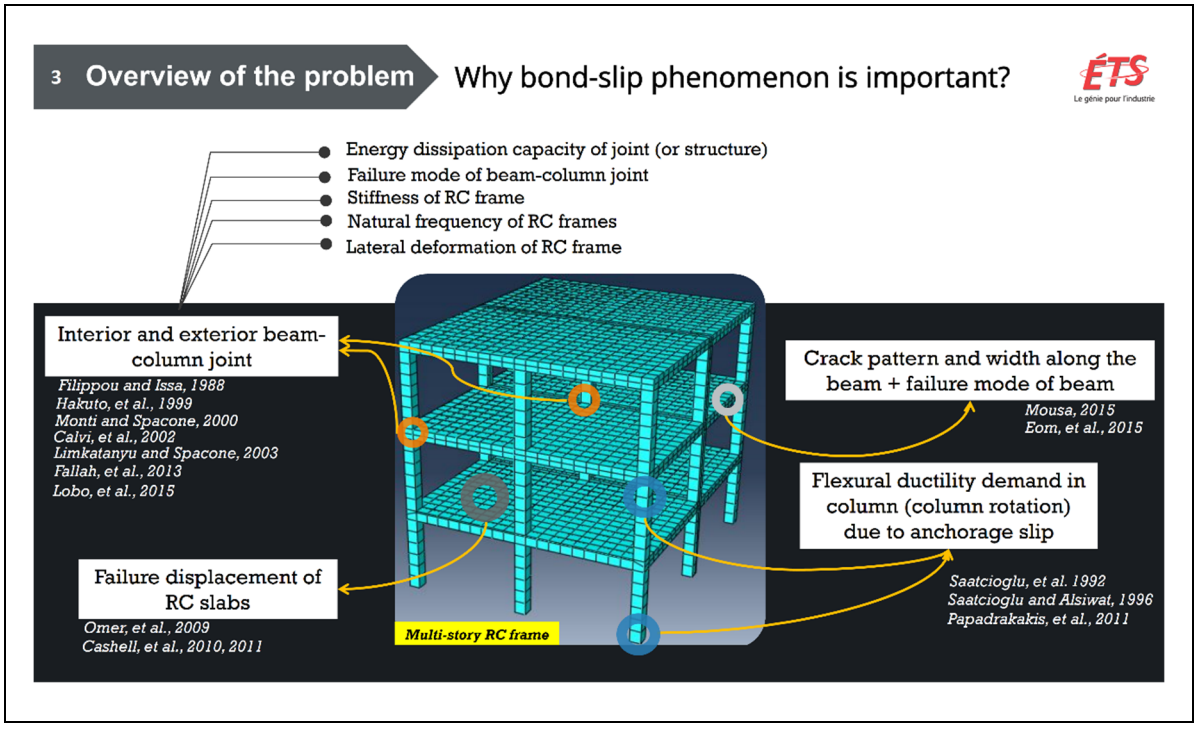

Figure 0.1 Effect of bond-slip phenomenon on structural performance of RC frame

0.1 Pre-cracking phenomenon and bond behaviour

The mechanism of load and stress transfer within the interface between reinforcing bar (rebar) and surrounding concrete is called “bond”, which is shear stress along the interface of rebar and surrounding concrete. Bond is, however, accompanied by a relative displacement between the rebar and surrounding concrete, called “slip”. This interaction is denoted as “bond-slip phenomenon”. The majority of the previous classic studies on rebar-concrete bonding characteristics in reinforced concrete (RC) members have been carried out based on pull-out tests, where rebar is pulled out from an uncracked specimen, which can be cylinder, prism or cube (Figure 0.2(a)). In the pull-out test, the bond is controlled by the concrete strength and rebar surface deformations (lugs) or by the tensile splitting strength of the concrete, denoted as concrete cover. In the latter case, bond failure occurs due to the uncontrolled cracking of the concrete specimen (Brantschen, 2016) (Figure 0.2(b)). Pull-out and splitting failures, as the two main bond failure modes, can fundamentally affect the structural performance of RC members. Enough concrete cover around the rebar and/or appropriate lateral confinement by stirrups leads to a pull-out failure mode. As concrete cover increases, local rebar-concrete bond strength increases. Effect of concrete cover can be characterized by the normalized ratio of concrete cover-to-rebar diameter (c/d_b). In the case of concrete without stirrups, the preventive value is $c/d_b \geq 3.0$ (Wu & Zhao, 2012). The bond splitting failure can occur at the locations where the concrete cover and lateral pressure are not enough or reduced by corrosion phenomenon and concrete spalling. Due to the brittle (and sudden) nature of bond splitting failure mode, design codes and regulations considered different specifications to maintain pull-out failure mode specially for RC joints and foundations, by using larger development length.

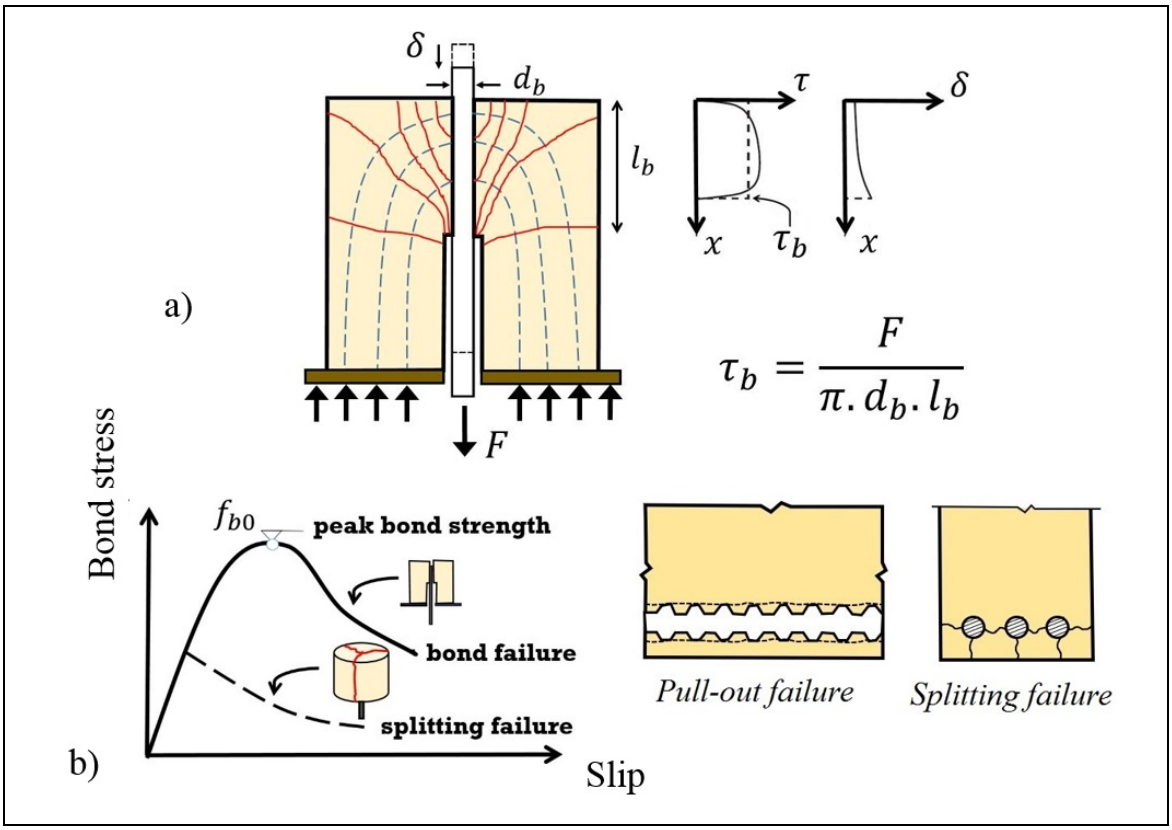

Figure 0.2 Schematic representation of bond in uncracked concrete
Taken from Brantschen (2016)

One of the most relevant problems of steel-congested concrete structures is undesirable cracking along with the reinforcing bar, denoted as the "pre-cracking phenomena" (Matsumoto et al., 2016). Despite classic test setups on the bond-slip phenomenon, bond in real structures frequently develops within cracked concrete, where cracks propagate in a plane where reinforcement is also located (Brantschen et al., 2016), such as joints, shear walls, and two-way slabs. Once cracking happens in the concrete near a bearing or joint, the performance of steel rebar-concrete is unclear (Figure 0.3). The bond characteristics of rebar in real RC members are consequently affected by the presence and propagating of these cracks and are different from those considered in classic pull-out tests.

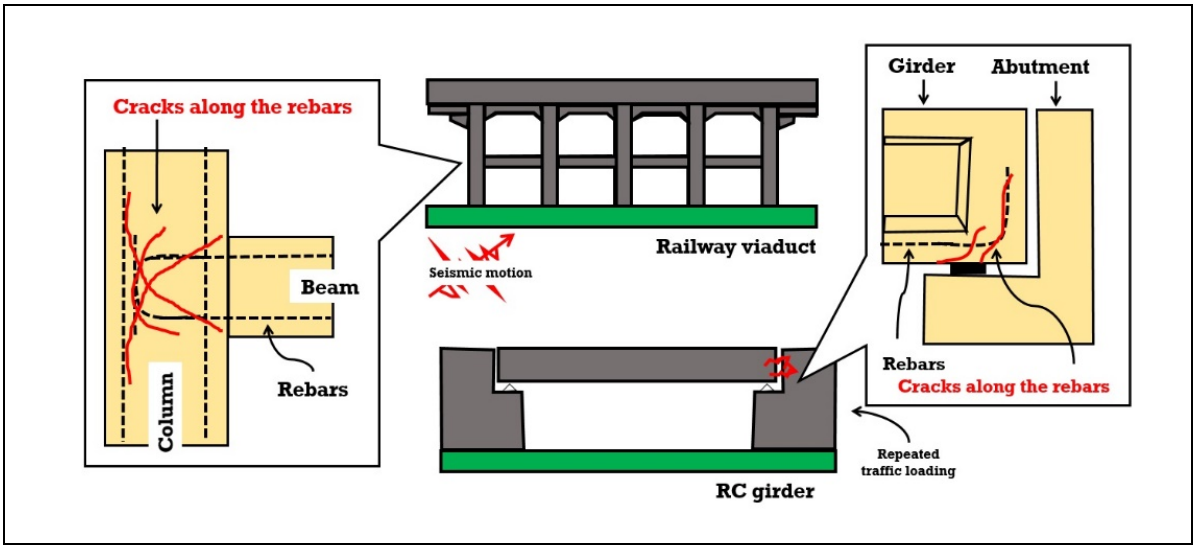

Figure 0.3 Possibility of initial damages in concrete structures
Taken from Matsumoto et al. (2016)

Many practical situations with a high potential of cracks developing in the plane of the reinforcement of structural concrete members are shown in Figure 0.4. Brantschen (2016) has divided these cracks (of constant or variable over the thickness of the element) into two categories (Brantschen et al., 2016). The first corresponds to structural members where the opening of the cracks is controlled such as the flexural reinforcement in slabs (Dawood & Marzouk, 2012) (Figure 0.4(a)), joints of precast elements with overlapping reinforcement (Joergensen and Hoang 2015) (Figure 0.4(b)), suspension reinforcements or fasteners (Lotze, 1987) (Figure 0.4(c)), retaining walls (Figure 0.4(d)) or the anchorage of the web reinforcement in flanged sections members (Rehm et al., 1978) (Figure 0.4(e)). The second corresponds to cases where the development of cracks is uncontrolled (Brantschen et al., 2016), such as delamination cracks at the level of the flexural reinforcement of arch-shaped members or members without transverse reinforcement (Ruiz et al., 2015) (Figure 0.4(f)), and as it has been observed in slabs due to environmental situations where the development of these specific cracks can lead to a premature failure. Controlling of these cracks can be performed by ribs of rebar (deformed rebar instead of plain rebar), sufficient concrete coverage around the rebar, and transverse reinforcement for controlling crack widths (Brantschen et al., 2016).

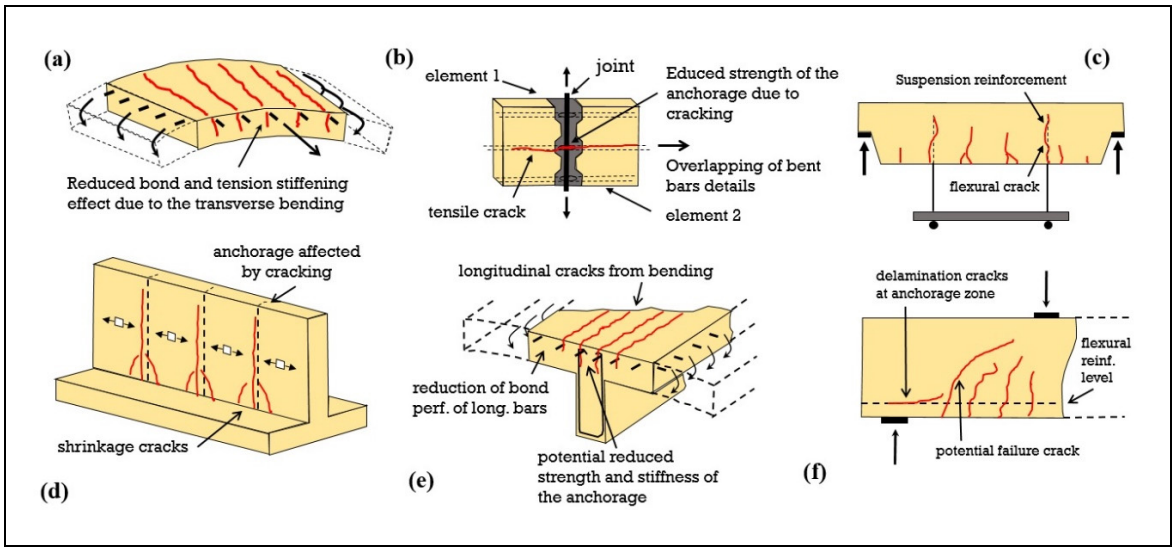

Figure 0.4 Schematic representation of practical cases for pre-cracked specimens
Taken from Brantschen (2016)

The presence (or propagating) of parallel cracks to reinforcement direction may considerably affect bond behaviour in critical zones and can propagate to affect the global performance and safety of reinforced concrete structures. For example, Kotsovos et al. (2013) carried out tests on beam-column assemblies. They reported that bond failure, especially by splitting cracks, leading to shear cracking shear cracking in the beam-column element (Kotsovos et al., 2013). Extension of this crack leads to brittle modes of failure so that some researchers have proposed to eliminate bond by use of polyvinyl chloride (PVC) pipe cover to the portion of steel bars within the critical regions of beam-column connections (Iemura et al., 2004; Kotsovos et al., 2013; Pandey & Mutsuyoshi, 2004). They used a rare approach to remove the plastic zone from the joint to provide a stable behaviour of critical plastic hinges. However, this can make discontinuity in the structural performance of the joints (Lobo & Almeida, 2015). As neglecting the pre-cracking phenomenon leads to unclear effects on the structural behaviour of steel-congested members, such as joints, it is essential to comprehensively study the residual performance of structures after an earthquake (or an overstress) and present a practical solution to recover a minimum level.

Researchers proposed some formulations to predict the reduced bond strength as a function of the crack width concerning the reference strength in uncracked conditions (see Chapter 2). However, as the test processes used in the literature were not uniform, the experimental database gathered from the literature is not enough accurate. An increase of the slip associated with the peak strength was also generally observed with the presence of a crack, and significant changes arise in the several phases of the behaviour (bond-slip curve) as compared to uncracked conditions including initial bond stress, bond strength, and residual bond stress (Figure 0.5) (Brantschen, 2016). Before the bond strength, the reduced contact area between rebar and surrounding concrete tends to limit the propagation of radial cracks as compared to the case without cracks, until a premature failure of the extremity of the concrete cantilevers takes place. The latter phenomenon generally results in a significantly smaller stiffness than for the reference case in these initial phases. The contraction of the concrete in the direct vicinity of the bar (associated with the partial closure of the mentioned radial cracks) then controls a friction mechanism up to the development of the maximum force defining the bond strength. With the increase of the relative displacement between the bar and the surrounding concrete, a progressive smoothening of the interface initiates the post-peak phase. The related stiffness is not strongly affected by the presence of a crack, independently of its opening (Brantschen, 2016). Once the slip reaches a value corresponding approximately to the distance between two consecutive ribs, the entire contact surface contributed to the force transfer and only a residual strength can be further provided. The latter is reduced proportionally with the embedment length available until the bar is entirely pulled-out of the concrete specimen (Iemura et al., 2004). Although this scenario was proposed based on the experimental results of Brantschen (2016), there is no specific analytical and empirical model to formulate the characteristics of the modified bond-slip curve of pre-cracked specimens. Moreover, more explanations are necessary to be described by researchers on the reduced contact pressure after the pre-cracking phenomenon.

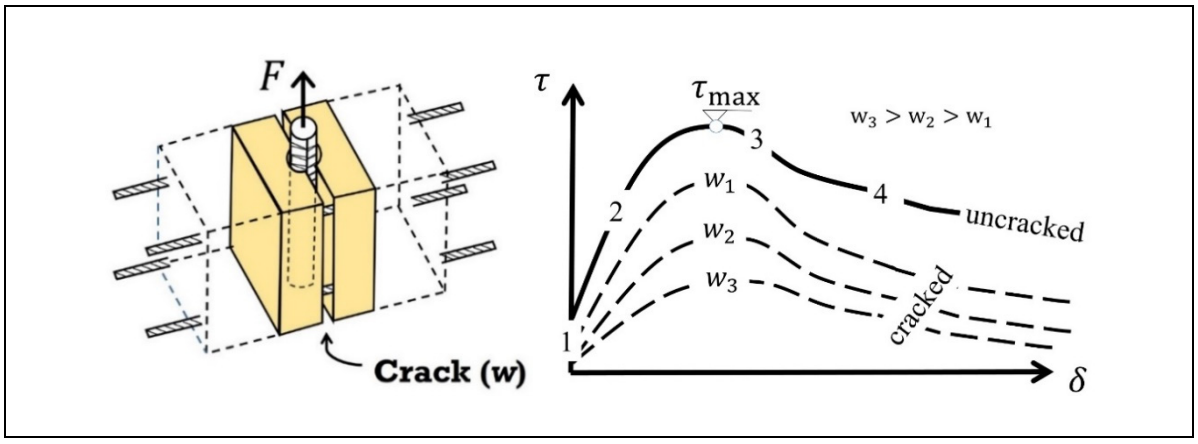

Figure 0.5 Effect of pre-cracking on rebar-concrete bond strength
Taken from Brantschen (2016)

Remarkably, few investigations were conducted on the influence of cracks on the bond and anchorage performance. Additionally, the methods of pre-cracking in the current literature vary considerably, which makes difficult the interpretation and direct comparison of results. Hence, the present thesis intends to conduct experimental and analytical investigations to comprehensively study the effect of the pre-cracking phenomenon on bond-slip curves of normal (NC) and self-consolidating concrete (SCC). This proposal concentrates on moderately confined concrete members without transverse reinforcement. However, enough concrete cover is considered to prevent premature bond failure of uncracked specimens (splitting failure).

0.2 Self-healing method by changing concrete composition

Based on the literature review (see Chapter 1), the concrete composition is a significant missing parameter in predicting the rebar-concrete interfacial properties and also can contribute to preventing the bond failures (splitting failure) or healing the cracks that can be used as an initial factor of deterioration. As shown in Figure 0.6, bond strength depends on different key parameters including concrete compressive strength, surrounding confinement by transverse reinforcement, concrete cover, embedded length, rebar type (plain, deformed, FRP,etc.), rebar rib geometry, and bond test type. Most of them have been considered in the regulations and

specifications as key parameters in the predicting formulas. However, the concrete composition has been neglected.

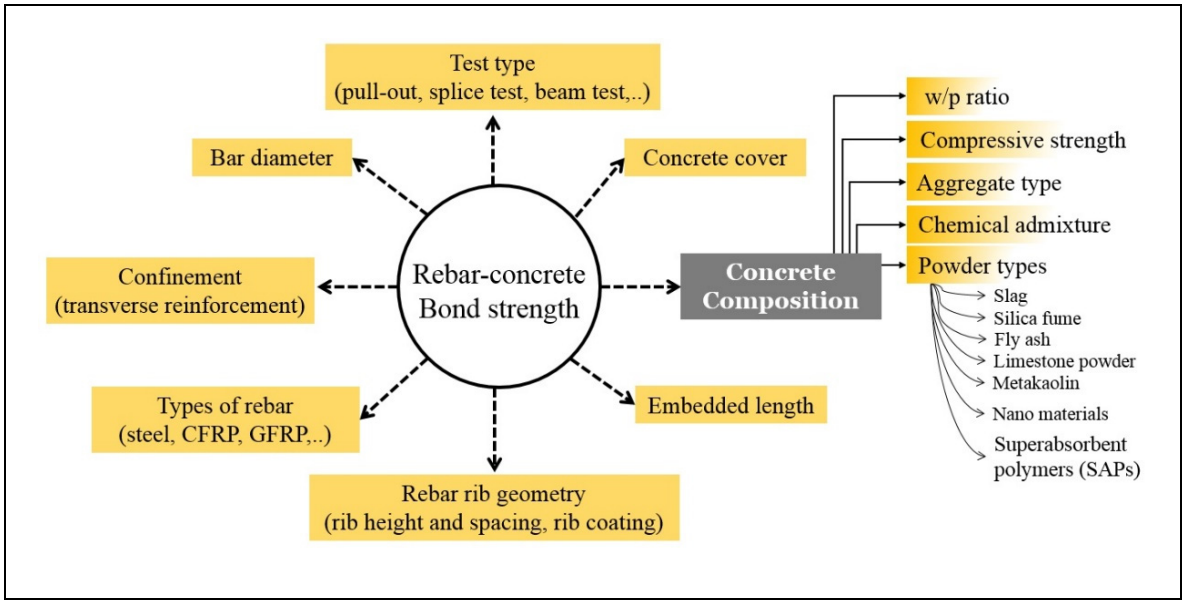

Figure 0.6 Key parameters in the rebar-concrete interaction

As already mentioned in the previous studies (Guizani et al., 2017; Mousavi et al., 2017), the compressive strength of concrete is the only parameter considered for determining bond strength, while the concrete composition is defined by four other important parameters including water-to-cementitious material ratio, powder content and type, admixtures, and aggregate (Figure 0.6). Changing each of these components can change the concrete type. Figure 0.7(a) summarizes the effects of using different concrete composition (type) on bond strength of steel rebar, from 2009 to 2019. Current concrete design codes (CSA A23.3, 2014; ACI-318R, 2014; ACI-408R, 2003) and existing predicting equations (Guizani et al., 2017; Wu & Zhao, 2012) for bond strength only considered compressive strength of concrete without considering the effect of concrete composition (Wu & Zhao, 2012). To make a direct comparison of results for each batch, the effect of concrete composition (including compressive strength) is isolated by comparing it to a reference concrete, which is illustrated in Figure 0.7(b). In some cases, a conflicting trend is reported as a result of using different concrete compositions such as SCC, fly ash concrete, and lightweight concrete. For instance,

pull-out results of silica fume concrete showed higher bond strength as compared to the normal concrete (NC) (Abadjiev et al., 1993; Bubshait & Tahir, 1997; Dybeł & Furtak, 2015; Fu & Chung, 1998; Gjorv et al., 1990; Helland et al., 1988; Hou & Chung, 2000; Khedr & Abou-Zeid, 1994; Monteiro et al., 1989; Mor, 1993; Sancak & Simsek, 2011; Sfikas & Trezos, 2013; Songpiriyakij et al., 2011; Tanyildizi, 2009; Trezos et al., 2014; Turk et al., 2010). Additions of silica fume to concrete caused a considerable impact on reducing the interface porosity up to a distance of 40 microns (Zayed, 1991). Hence, it can clearly indicate that concrete composition can affect rebar-concrete interfacial properties.

Influence of type and content of powders, used in the concrete mixture, on bond strength can be a good option for changing the structure of rebar-concrete interfacial behaviour and improve the damaged layers around the rebar caused by splitting cracks. There is no research on explaining a method for repairing the bond damages in the normal area of RC or even steel-congested concrete. Hence, this thesis intends to determine the possibility of an efficient method to improve the rebar-concrete interfacial properties considering splitting cracks, which results in bond failure. Although there has been a growing tendency to find an efficient way of the crack-healing in concrete structures to regain mechanical strength, no specific research has been concentrated on healing cracks at rebar-concrete interaction after initial damages. This thesis intends to apply a novel experimental and numerical study of the effect of concrete composition on bond behaviour (including notable strength) with pre-existing cracks. This study investigates also the effect of concrete composition on the healing of the internal cracks (and also external), through the recovery of bond properties in NC and SCC. Superabsorbent polymer (SAP) is considered as a healing agent inside concrete mixtures, denoted as SAP concrete, to accelerate the self-healing performance of concrete.

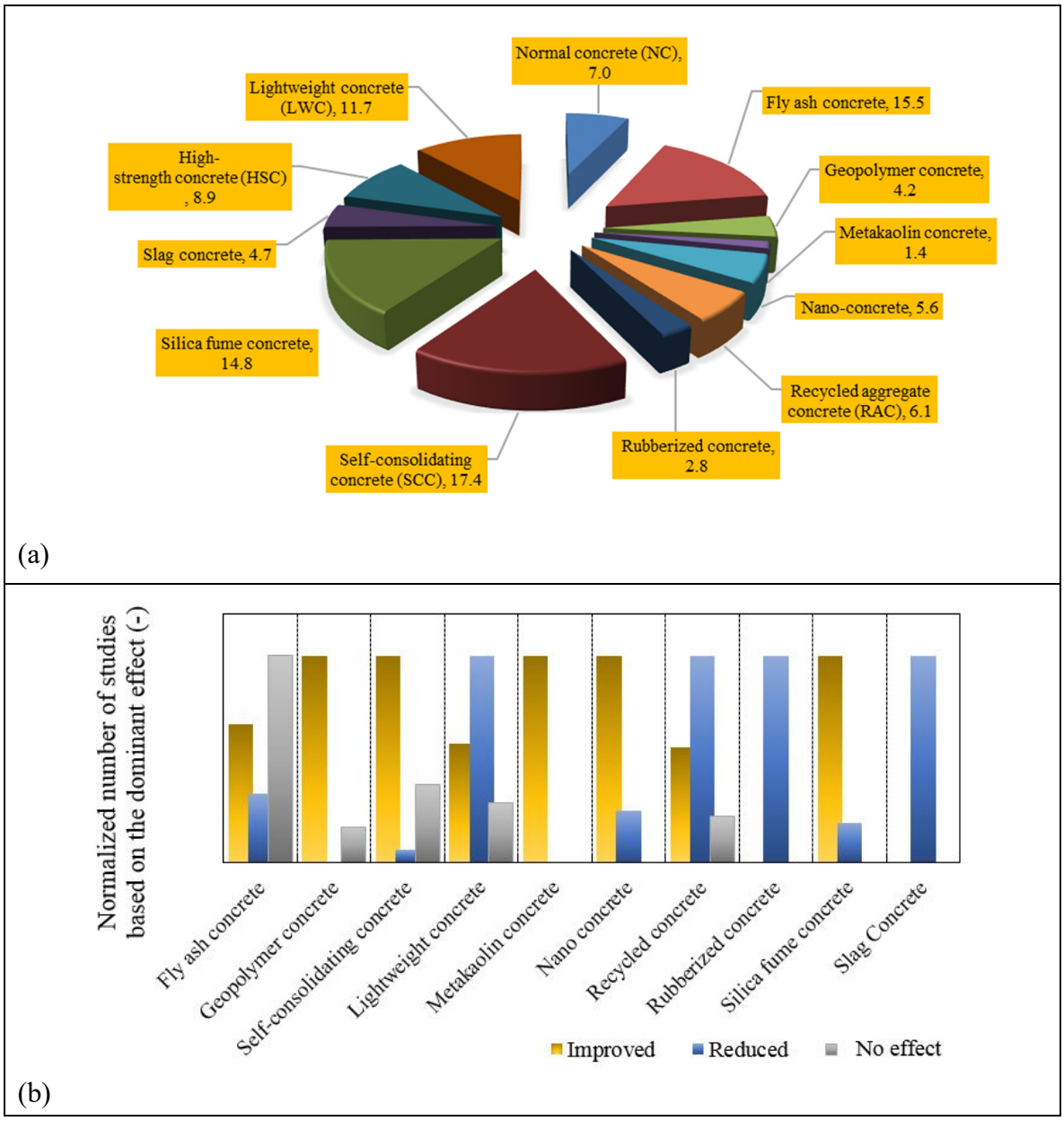

Figure 0.7(a) concrete types studied in bond studies (2009-2019);
(b) dominant impacts of concrete types
Taken from Mousavi et al. (2020)

Concrete has the ability to heal the internal or external cracks. Although extensive research has been performed to confirm the autogenous healing of concrete, there is no study specific to this phenomenon about rebar-concrete bond-slip behaviour. There is a limitation of crack width for using autogenous healing of concrete without any healing agents inside the mixture (Lee et

al., 2016; Snoeck et al., 2012). To accelerate this autogenous healing and increase the ability for healing larger crack widths, healing agents (such as superabsorbent polymers) have been introduced by researchers (Mignon et al., 2015; Snoeck & De Belie, 2015; Snoeck & De Belie, 2019; Snoeck et al., 2012; Snoeck et al., 2014). These healing agents have the ability to absorb the water and to release it after cracking accelerates the crack-healing inside the specimen. Both the unhydrated cement particles and water resources inside the concrete are necessary to provide appropriate conditions for the healing process (Figure 0.8). Selecting the healing agents for accelerating autogenous healing is an important part of this study. Previous research has proved that external curing is not efficient enough for providing water sources to continue the crack-healing by rehydrated un-hydrated cement particles inside the concrete (Bentz & Weiss, 2011; Castro et al., 2010). External water curing is only able to enter several millimetres into mixtures with a low water-to-cement ratio, while internal curing allows the water to be distributed more equally across the cross-section (Meng, 2019). Thus, healing agents inside the concrete can be used also as internal water resources for activating the rehydrating. So, this proposal aims to study the effect of both autogenous healings of NC with and without these healing agents (powder type) for healing the pre-cracked concrete.

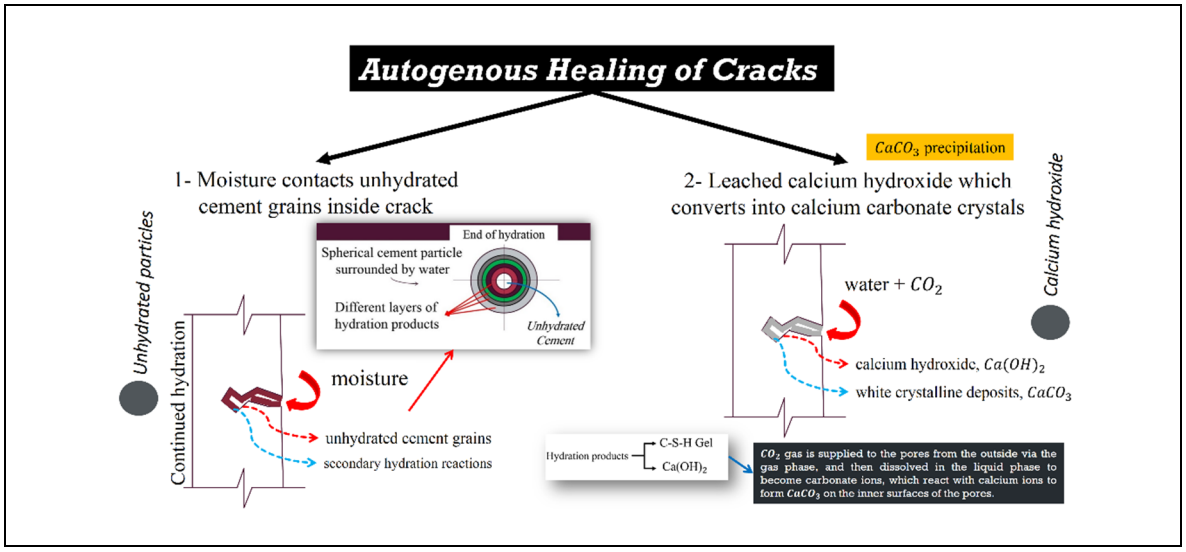

Figure 0.8 Mehcanisms of autogenous healing of cracks in concrete

CHAPTER 1

STATE-OF-ART AND RESEARCH METHODOLOGY

This chapter intends to review the previous studies on the effect of the pre-cracking pheonmnon on rebar-concrete bond properties, along with previous researches on self-healing method to identify gaps in previous works. Additionally, the research objectives of this thesis and the general methodoly followed to reach such objectives are presented in this chapter. Moreoer, effect of SAP particles on mechanical and self-healing peroperties of concrete mixtures are reviewed. As shown in Figure 1.1, there are three main sections in this chapter. In the first section 1.1, the fundamental properties of the bond-slip phenomenon are explained. Section 1.2 reviews the previous research on the effect of concrete composition on bond strength are explained. The focus of this subsection is on the effect of powder type on the bond strength. Section 1.3 determines the main difference between NC and SCC. In section 1.4, the effect of pre-cracking on bond strength has been determined. Section 1.5 gives a description of the self-healing process and the main different ways of self-healing in cementations material. Sections 1.6 to 1.10 present respectively research gaps, objectives, adopted methodoly, limitations, and original contributions of this thesis.

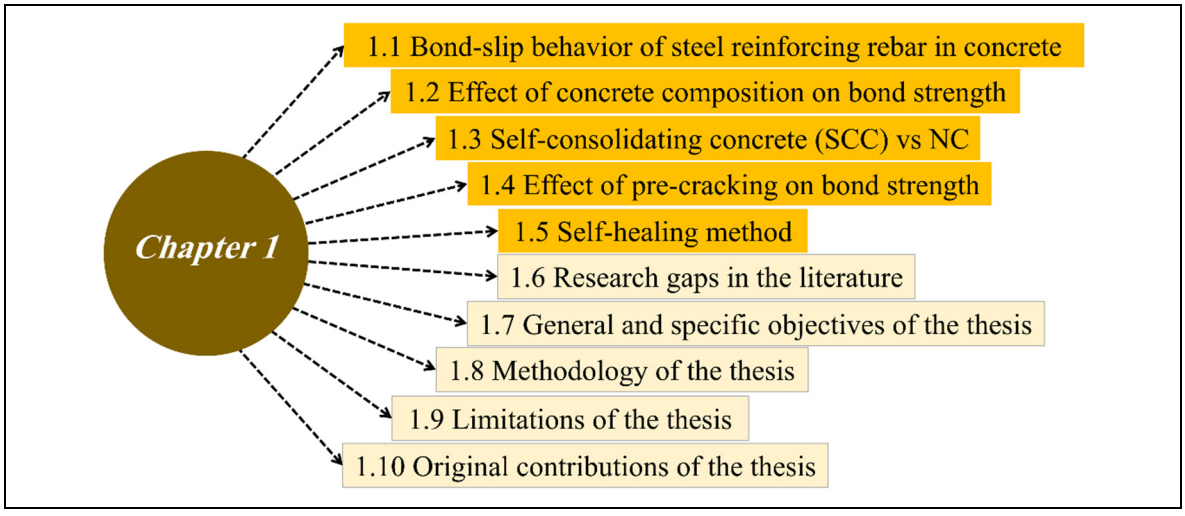

Figure 1.1 Overview of sections in Chapter 1

1.1 Bond-slip behaviour of steel reinforcing rebar in concrete

Interfacial bond stress between reinforcement and concrete allows longitudinal forces to be transferred from concrete to rebar and inversely. Consequently, the force varies along the rebar. Once steel strains vary from concrete strains, a relative displacement between the rebar and concrete, denoted as rebar "slippage", appears. As shown in Figure 1.2(a), the distance between two adjacent cracks in RC member is called by S_r (Dehestani & Mousavi, 2015). The concrete placed between the bending cracks contributes to the tensile strength of the cross-section, while in the cracked section, the concrete has no influence on the tensile strength and the tension force is transferred to the rebar. This can result in stress concentration in rebar at the cracked section (Figure 1.2(b)).

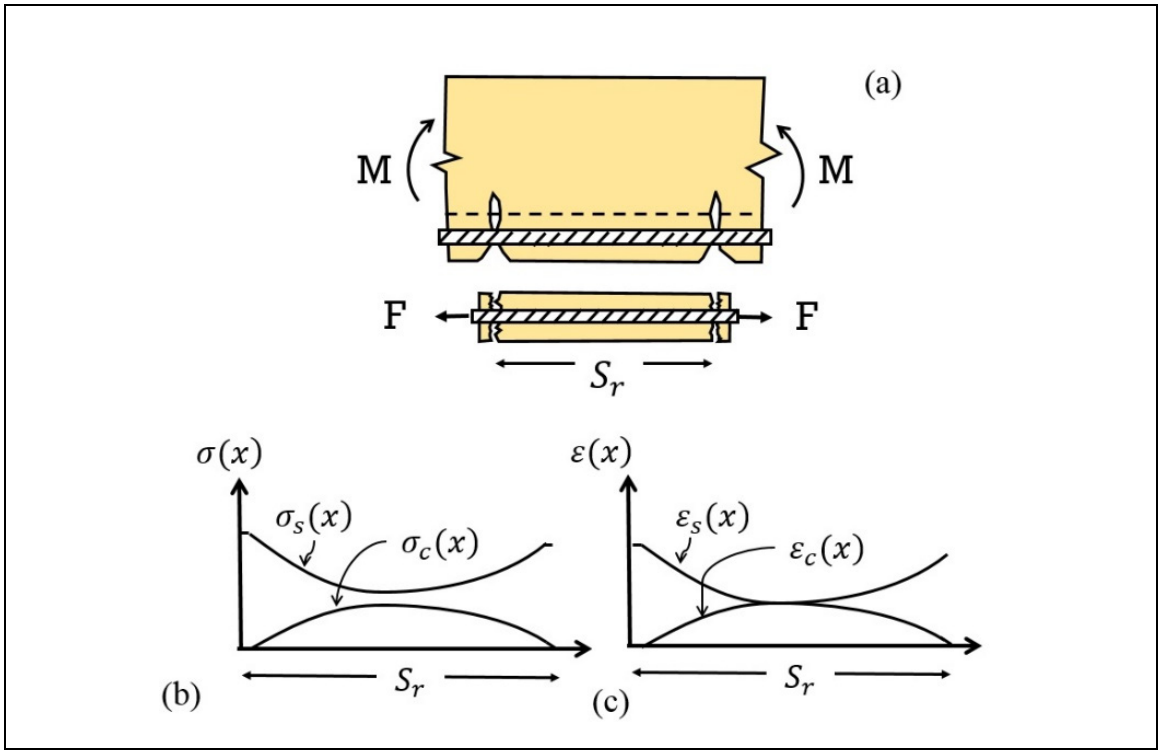

Figure 1.2 Local bond-slip phenomenon (a) cracked flexural RC member;
(b) stress distribution; (c) strain distribution
Taken from Dehestani & Mousavi (2015)

As illustrated in Figure 1.3, there are two main bond failure modes including pull-out failure and splitting failure. Inadequate confinement surrounds the rebar leads to a brittle and sudden bond fracture, called splitting failure mode, where splitting cracks propagate in the plane of the rebar (Figure 1.3(a)). Enough concrete coverage around the rebar, adequate lateral confinement by stirrups, and appropriate rebar lug pattern (rib height-to-spacing ratio) can provide good bond condition following by pull-out failure mode (Figure 1.3(b)). The pull-out failure mode is accompanied by concrete shearing off between adjacent ribs along with local concrete crushing at the rib front. Frictional bond strength can be activated after this failure, denoted as "residual bond stress". Concrete design codes and regulations intend to recommend critical specifications to provide pull-out bond failure instead of the sudden splitting failure. Rebar corrosion products (rusts) generate micro-cracks at the rebar-concrete interface, resulting in increasing the risk of splitting bond failure. So, design codes mostly concentrate on the rebar corrosion field.

Typical bond-slip curves of pull-out and splitting bond failures are shown in Figure 1.3(c). Initial bond stress ($\tau_{0.01}$), maximum bond stress (called bond strength, τ_{max}), residual bond stress (τ_{res}), average bond stress (τ_m), slip corresponding to the maximum bond (S_{max}), slip corresponding to the residual bond (S_{res}), and area under bond-slip curve till residual strength (bond energy, E) are the main bond characteristics, which should be considered for every bond-slip curve. Initial bond stress ($\tau_{0.01}$) shows the chemical adhesion between rebar and concrete and represents a small section of ascending branch till slip of 0.01 mm. After this section, the mechanical interlock phenomenon between rebar surface deformations (lugs) in contact with concrete (bulk matrix) starts till bond strength (τ_{max}). There is a plateau in this section for pull-out failure mode as compared to the splitting failure mode, in which a sudden drop happens. Descending branch of the bond-slip curve corresponds to the concrete shearing off between two adjacent ribs (for pull-out failure) and/or wedging of concrete combs and widening of splitting cracks (for splitting failure) till residual bond stress (τ_{res}). The latter corresponds to the frictional resistance between the sheared-off part of the concrete and the rebar. After reaching this characteristic strength (residual bond stress), the bond-slip curve follows a plateau, practically constant. In addition to these parameters, RILEM

(Recommendation RC 6, append to RILEM TC (1994)) defined arithmetic mean of bond stresses, denoted as "average bond stress, τ_m", formulated by the average of $\tau_{0.01}$, $\tau_{0.10}$, and $\tau_{1.00}$ bond strengths corresponding to bond stresses at slips of 0.01, 0.10, 1.00 mm respectively. Another important bond parameter is the area under the bond-slip curve until residual bond stress, called "bond energy", which is shown by "E" throughout the present thesis. The schematic figure shows that area under the bond-slip curve is significantly higher for pull-out failure ($E_{Pull-out}$), as compared to the splitting failure mode (($E_{Splitting}$). This can clearly show that pull-out failure mode is a ductile failure while brittle and sudden failure happens for splitting failure mode. Moreover, bond strength is significantly lower for splitting bond failure than pull-out failure. Regarding slip corresponding to the bond strength, S_{max}, different values were reported in the literature. Unified bond-slip model presented by Wu & Zhao (2012) obtained the domain of 0.14-3.0 mm, while the CEB-FIP Model Codes (fib Model Code 2010, 2013; MC90, 1993) proposed a range of 0.6-3.0 mm. A similar scattered data was obtained by the experimental results of Guizani et al. (2017). Regarding slip corresponds to the residual bond stress (S_{res}), Eligehausen et al. (1983) recommended the value equal to clear rib spacing which is logical and fully compatible with the physical explanation/mechanism of the bond. General results of the present thesis in the following chapters used values between 6-10 mm (less than the approximate value of clear rib spacing). By this speculation, bond energy can be calculated until 6 or 12 mm, depend on the study objectives.

1.2 Effect of concrete composition on bond strength

As explained in chapter of "INTRODUCTION", the concrete composition is a missing parameter in predicting bond-slip behaviour. To clarify this hypothesis, the general results of a detailed review are shown in Table 1.1. Concrete sedimentation (or bleeding) can significantly affect the bond, denoted as "top rebar effect", which is considered in design codes by considering a reduction factor for bond strength. However, the effect of other parameters is neglected. Powder types used in the literature (showed before in Figure 0.7) have considerable effects on bond strength.

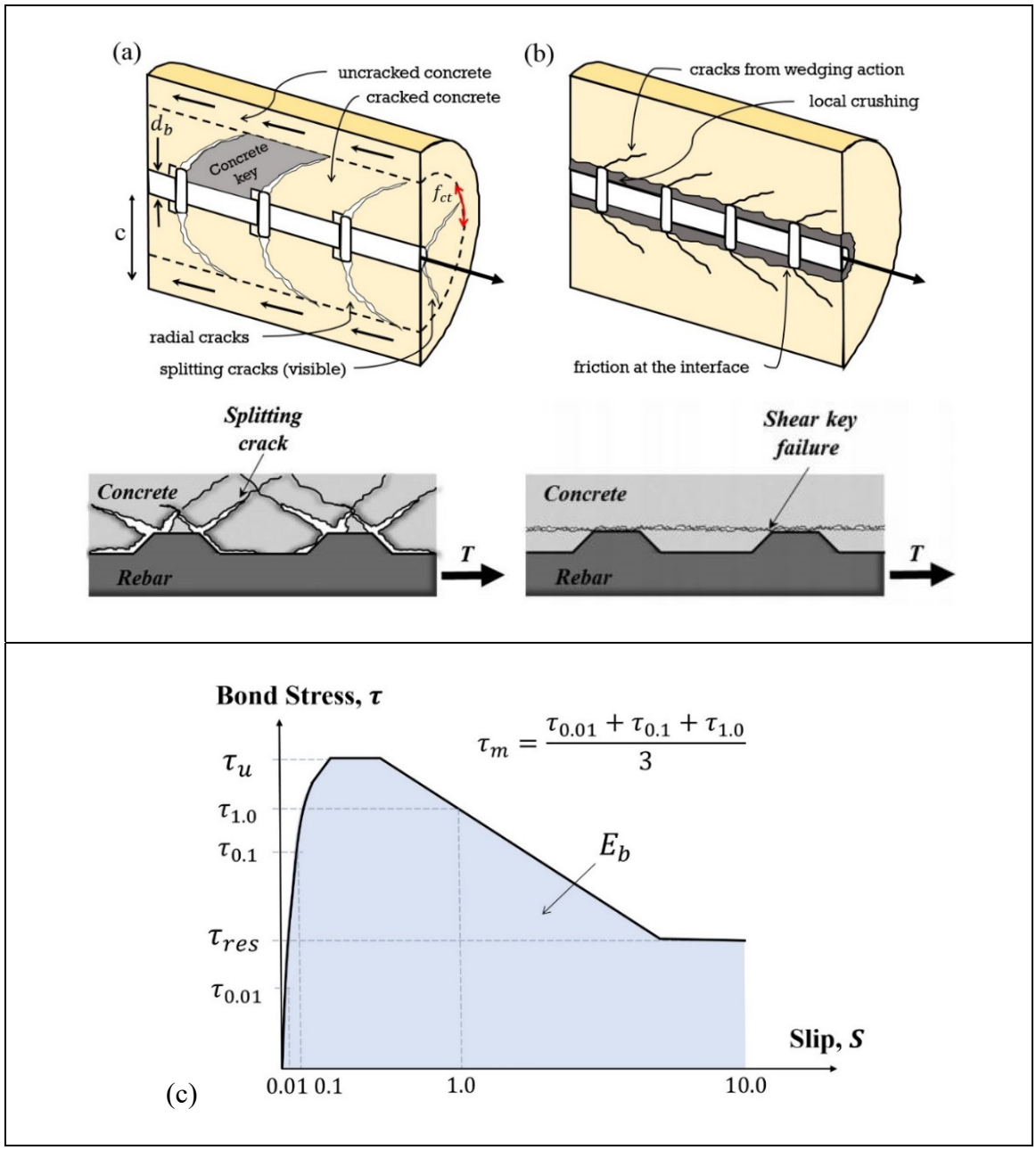

Figure 1.3 Schematic of local bond-slip envelope curves: (a) splitting failure; (b) pull-out failure mode and wedging action; (c) bond characteristics
Taken from Brantschen (2016) and Kim et al. (2018)

Table 1.1 Effect of concrete composition on bond
Taken from Mousavi et al. (2020)

Items	References			Parameters studied			
	Improved	Decreased	No effect	f'_c	C	d_b	L
Sedimentation or Slump	(Pop et al., 2015)	(Dakhil et al., 1975; Khayat & Guizani, 1997; Welch & Patten, 1965)	(Thrane et al., 2010)	×		×	
Chemical admixtures	(Collepardi & Corradi, 1979; Hossain & Lachemi, 2008; Musser et al., 1985; Sfikas & Trezos, 2013)	(Brettmann et al., 1986)	(Zilveti et al., 1985)	×	×		
Water/cement ratio	(Fu & Chung, 1998)	(Martí-Vargas et al., 2013; Martí-Vargas et al., 2012; Sfikas & Trezos, 2013; Zhu et al., 2004)	-	×	×	×	
Fillers (or binders)							
Fly Ash	(Arezoumandi et al., 2015; Naik et al., 1989)	(Cross et al., 2005)	(Arezoumandi et al., 2013; Gopalakrishnan et al., 2005; Volz et al., 2012)	×	×	×	×
Metakaolin	(Sancak et al., 2016)		(Karahan et al., 2012)	×		×	
Nano-material	(El-Feky et al., 2016; Hashemi & MirzaeiMoghadamb, 2014; Hashemi & Sedighi, 2016; Ismael et al., 2016; Sadawy & Elsharkawy, 2016; Serag et al., 2017; Tastani et al., 2015; Tastani et al., 2016; Zhang et al., 2015)	-	-	×	×	×	
Silica fume	(Abadjiev et al., 1993; Bubshait & Tahir, 1997; Burge, 1983; Gjorv et al., 1990; Karatas et al., 2010; Monteiro et al., 1989; Sancak & Simsek, 2011; Tanyildizi, 2009; Trezos et al., 2014)	(Hamad, 2000; Hamad & Machaka, 1999; Hamad & Itani, 1998; Hamad & Sabbah, 1998; Hwang et al., 1994)	-	×	×	×	
Slag	(Zhu et al., 2004)	(Xia et al., 2006)	(Mo et al., 2015)	×		×	
Limestone powder	(Zhu et al., 2004)	(Pop et al., 2013)	-	×		×	×

Although researchers have found conflicting results, the main findings can be summarized as follows:

- Concretes with a large settlement and bleeding characteristics could cause an appreciable loss of bond in practice.

- For a given slump, concrete mixtures containing superplasticizer have higher bond strength, as compared to those containing no superplasticizer.
- Lower water content in concrete reduces the accumulation of bleed water under rebar, which results in higher bond strength.
- Adding nanopowders have a great effect on bond strength.
- Conflicting results have been deduced from using powders or fillers to improve bond strength.

By reviewing the famous equations regarding development length in ACI, the importance of the concrete composition on bond strength would be highlighted. The minimum length of rebar embedded in concrete to develop the maximum tensile stress is called development length. Good bond conditions provide a condition in which shorter development length is required. Different normalized models are used in the specifications for formulating the development length of steel rebars in NC. ACI Code (ACI 318R, 2014) proposed Eq. (1.1) for the development length of tension-loaded straight steel rebar in normal intact concrete, l_d (in).

$$l_d = \frac{3}{40}\left(\frac{f_y}{\lambda\sqrt{f'_c}}\right)\left[\frac{\alpha\beta\gamma}{\left(\frac{c + K_{tr}}{d_b}\right)}\right]d_b \tag{1.1}$$

where f_y is the yield stress of the steel rebar in psi, and c is the concrete cover in inches. Factors α, β, and λ take into account the effects of rebar location, epoxy coating, and lightweight concrete respectively. A rebar location factor of 1.3 is used in American (ACI 318R, 2014) and Canadian standards (CSA Code A23.3, 2014) for rebar placed so that more than 12 in. (300 mm) of fresh concrete is cast below and 1.0 for other rebar locations. ACI Code (318R, 2014) defines different values for coating factor including 1.5 for epoxy-coated rebar with concrete cover less than $3d_b$ or clear spacing less than $6d_b$, 1.2 for other epoxy-coated rebars, and 1.0 for uncoated rebar. CSA Code (A23.3, 2014) and ACI Code (318R, 2014) standards specify 0.75 for lightweight concrete and 1.0 for normal-weight concrete. The term γ is a factor for rebar size in which the value of 0.8 has been considered for a rebar diameter of NO.6 (19.05

mm) or smaller and 1.0 for other diameters. In the Eq. (1.1), k_{tr} defines the effect of stirrups and confinement on the bond strength, which is ignored in this study. However, similar to confinement provided by stirrups, the concrete cover leads to an important influence on confinement around the rebar by resisting hoop stresses (Desnerck et al., 2015) leading to an increase in bond strength. The effect of concrete cover is considered in Eq. (1.1) by the term c normalized by rebar diameter, d_b. However, as shown in chapter of "INTRODUCTION" (Figure 0.7), along with Table 2.1, Eq. (1.1) is not applicable and efficient for different types of concrete. Only the effects of lightweight aggregate and concrete sedimentation are considered in Eq. (1.1), while there is no specific parameter for different types of powders. Besides, regarding lightweight aggregates, there is no direct trend. However, Eq. (1.1) just present a reduction factor for lightweight aggregate without determining the type of lightweight aggregate. Finally, this review indicates that contrary to the current formulations, the concrete composition can be a good option to improve rebar-concrete interfacial properties and control the damages at the rebar-concrete interface (Mousavi et al., 2017; Mousavi et al., 2016).

1.3 Self-consolidating concrete (SCC) vs NC

Self-consolidating or self-compacting concrete, often abbreviated SCC, would replace a significant portion of NC within the next decades especially in developed countries (Said & Nehdi, 2007). Higher content of fine aggregate along with using fillers makes it possible for SCC mixtures to have higher characteristic fresh properties so that this type of concrete has the potential to practical use in the steel-congested area in RC members. Different definitions of SCC have been used from researches and also industry associations across the world, for instance:

1- A concrete that "can be compacted into every corner of a formwork, purely by means of its weight and without the need for vibrating compaction." (Amura & Ouchi, 1999).
2- SCC is an advanced concrete mixture that does not need vibration for placing and compaction, which reduces the amount of formwork. It can flow under its weight, filling formwork and attaining complete compaction, even in the steel-congested area in RC

members. The hardened concrete is dense, homogeneous and has the same mechanical characteristics and durability properties, as compared to NC (Daczko, 2012).

3- SCC is an extremely flowable and non-segregating mixture that can spread into place, fill the formwork, and encapsulate the reinforcement without any mechanical consolidation (ACI 237R, 2007).

SCC is obviously recognized by its fresh properties. Portland cement, fine aggregate, coarse aggregate, water, chemical admixtures (superplasticizer and viscosity modifying admixture), and typically supplementary cementitious materials such as fly ash, slag, silica fume, and metakaolin are typical SCC composition. Moreover, mineral fillers such as limestone powder can be as filler in SCC mixtures. To have a high flowable SCC mixture, different types and dosages of superplasticizers are used along with viscosity modifying admixtures to keep the stability of mixture, prevent concrete segregation, and improve the mixture's consistency. Both mineral and chemical admixtures play a major role in producing SCC mixtures. Many researchers have proposed SCC mixture proportions, that usually have a higher cementitious or powder content, and having a lower per unit volume of coarse aggregate, as compared to NC (Figure 1.4) (Daczko, 2012; Jacobs & Hunkeler, 1999).

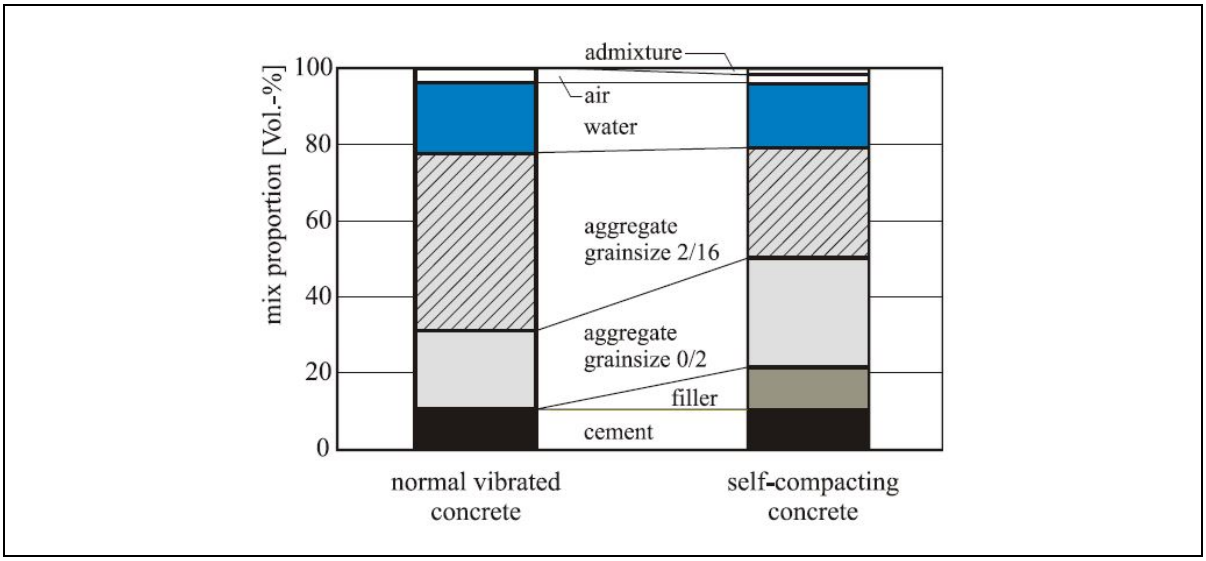

Figure 1.4 Difference of mixture composition between NC and SCC
Taken from Holschemacher & Klug (2002)

1.3.1 Fresh properties of SCC

As illustrated in Figure 1.5, SCC has considerably higher workability characteristics, as compared to NC. SCC mixtures need to have specific fresh properties including filling ability, passing ability, and stability. These new properties can be characterized by a slump flow test, T_{50} value, V-funnel test, J-ring, and L-box test. The slump flow test shows the filling ability of SCC mixture. The viscosity of SCC mixtures can be quantified by T_{50} and V-funnel tests. Passing ability also can be measured by L-box (height ratio) and J-ring step tests. Among these tests, slump flow and T_{50} values are obligatory to be reported in the studies. Slump flow value can be obtained by measuring average diameter (from two perpendicular directions) of concrete after the horizontal free flow of mixture in the absence of obstacles. Once the flow reaches the diameter of 50 cm, the time is recorded, denoted as T_{50}. Segregation phenomenon is critical in this test so that different trial mixtures are necessary to be performed before the main batch. Good segregation resistance can be obtained when the distributions of aggregate particles in SCC mixture are somewhat equal at all locations. Segregation resistance can be checked by a sieve segregation test (%), which is comprehensively explained by Euro-EFNARC Guidelines (EFNARC, 2002). Standard criteria recommended by the codes and the literature for the slump flow test and T_{50} of SCC mixtures are summarized in Table 1.2. Range of 500-800 mm for slump flow and $T_{50} \geq 2$ are accepted values.

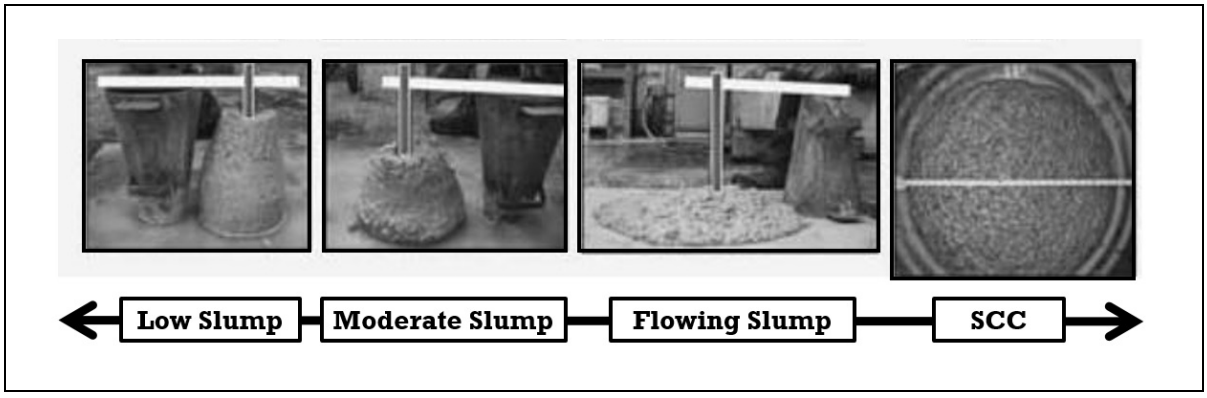

Figure 1.5 Workability Continuum from low slump NC to SCC
Taken from Daczko (2012)

Table 1.2 Standard criteria for slump flow and T50 of SCC mixture

Test	EFNARC (2002)	ASTM-C1611/C1611M (2009)	Domone (2006)	Nagataki & Fujiwara (1995)	CSA A23.1-14/A23.2 (2014)	JSCE (1999)
Slump flow (mm)	650-800	508-660.4	-	500-700	500-800	500-760
T_{50} (s)	-	-	1.8-12	-	-	3-15

1.3.2 Hardened properties of SCC

Compressive strength, splitting tensile strength, elastic modulus, shear strength, and bond strength are the main hardened properties of SCC. Different experimental studies were conducted to determine the mechanical characteristics of SCC, as compared to NC. Holschemacher & Klug (2002) reviewed the previous studies on SCC mixtures and reported that the compressive strength of SCC and NC is similar for the same water-to-cement ratio. However, there is scattered data for the same-water-to-powder ratio, since the amount of cement can be replaced by different types of filler such as limestone powder, fly ash, etc. effect of these fillers on hydration process is different. Regarding splitting tensile test, data analysis conducted by Holschemacher & Klug (2002) shows that splitting tensile strength of SCC is slightly higher than NC. It can be attributed to the lower porosity, good pore size distribution within the interfacial transition zone, and denser bulk matrix of SCC mixture due to the higher amount of fine particles, as compared to NC. In the case of elastic modulus, Persson (2001) reported that there is no considerable difference between elastic modulus of SCC and NC. In this field, Biolzi et al. (2014) showed that that large-scale SCC beams have similar shear strength accompanying by a more brittle behaviour, as compared to NC. Different water-to-cement and water-to-powder ratios were considered in their research. Also, different compressive strengths were obtained for NC and SCC. Similar results were obtained by Choi et al. (2012) for the shear strength of SCC members. Akinpelu et al. (2019) reported that higher powder content along with lower coarse aggregate in SCC has no impact on the mechanical properties, while Krishna et al. (2010) reported that size and content of aggregate in SCC have

considerable influences on the mechanical properties. Comprehensively explained models for predicting the compressive strength of SCC as a function of water-to-binder ratio were proposed by the recently published book of Kodeboyina (2018). Although many investigations showed higher bond strength of steel rebar embedded in SCC as compared to NC (de Almeida Filho et al., 2008; Mousavi et al., 2017; Sonebi & Bartos, 1999; Valcuende & Parra, 2009), Esfahani et al. (2008) reported that SCC mixtures have lower or the same bond strength, as compared to NC. Sfikas & Trezos (2013) attributed these inconsistent results to SCC mixtures and the experimental conditions. As different types of filler, aggregate type and aggregate dosage (fine-to-coarse ratio) can be used for producing SCC, conflicting results can be expected for mechanical strength. However, general results show that SCC has comparable mechanical characteristics with NC.

1.4 Effect of pre-cracking on bond strength

Cracks are inherent to reinforced concrete structures and develop when tensile stresses locally reaching the material strength. They can result either from external action (overload) or from the restraint of deformations (shrinkage, environment variations, and support settlements). The relatively low tensile strength of concrete requires the disposition of a material reinforcement to limit the propagation of the cracks and the related risk of collapse of the concrete members (Brantschen, 2016). As former code provisions generally define the maximum width of these cracks (Figure 1.6), current ones rather tend to prefer the limitations of the stresses in the reinforcement due to the uncertainties associated with the random nature of cracking in concrete. Indeed, this phenomenon is particularly complex to estimate and predict is structural elements due to a large number of parameters involved.

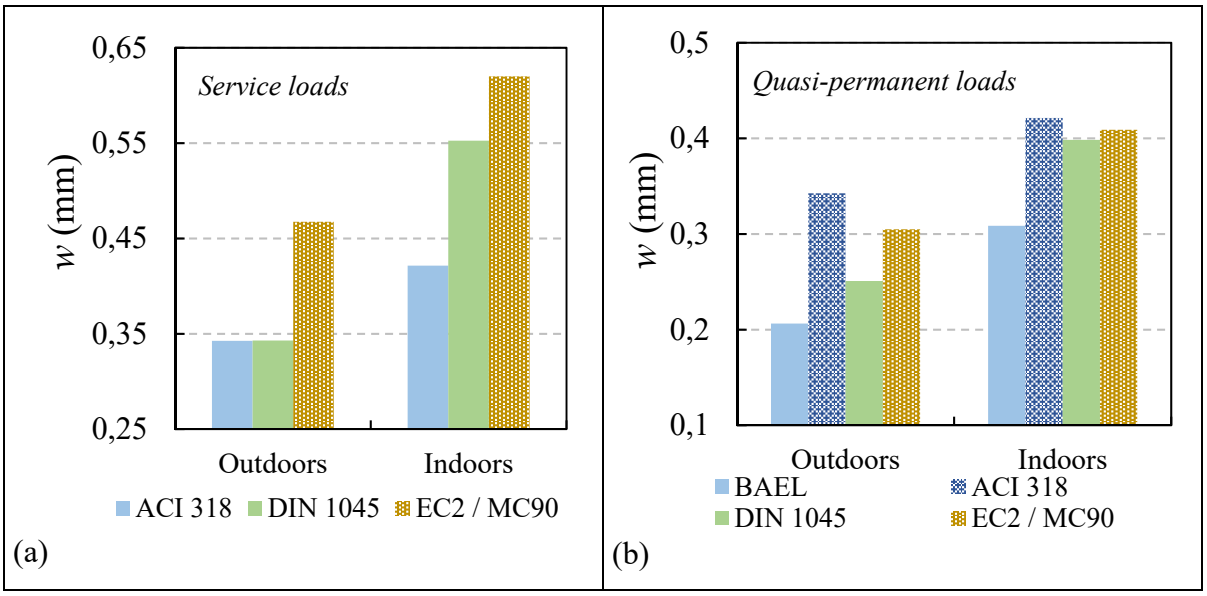

Figure 1.6 Allowable crack width according to codes:
(a) service loads; (b) quasi-permanent loads

In this field, Eligehausen & Bozenhardt (1989) have reported that the crack openings generally do not exceed 0.4 mm under quasi-permanent loads-associated to the durability of the structure and 0.6 mm under maximum permissible service loads, potentially affecting bond and anchorage performance to a considerable extent. Although it is possible to distinguish regions of a structure that might stay uncracked during its service life, it seems reasonable to assume that elements such as reinforcement rebars or anchorages have a higher probability to be situated in cracks. In fact, it has been observed that cracks tend to develop in these specific positions, as high tensile stresses are present resulting from the activation of several force transfer mechanisms between concrete and steel (Bergmeister, 1988; Lotze, 1987).

Until now, specific test setups have been introduced to experimentally study the effect of in-plane cracks on interfacial rebar-concrete characteristics (Desnerck et al., 2015; Gambarova & Karakoç, 1981; Gambarova et al., 1993; Gambarova & Zasso, 1985; Idda, 1999; Mahrenholtz, 2012; Simons, 2007). Based on these test results, several formulations were proposed by researchers to determine the reduced bond strength ($\tau_{cracked}$) as a function of crack width (w) with respect to the reference strength in uncracked conditions (τ_{normal}). An increase of the

slip associated to the peak strength is also generally observed with the presence of a crack, and significant changes arise in the several phases of the behaviour compared to uncracked conditions.

Gambarova & Karakoç (1981) and Gambarova & Zasso (1985) have performed a number of short pull-out tests on concrete specimens with performed cracks under active confinement on rebars of 18 mm diameter (Figure 1.7(a)). They have introduced the first empirical formulations to consider the effect of in-plane cracks on the bond performance (Eq. (1.2)). No limitations range of this empirically-calibrated formulation was clearly defined by the authors, but it was validated based on tests performed in a normal strength concrete and a short embedded length (L/d_b=3.0) for a maximum normalized crack opening (w/d_b) close to 0.02.

$$\frac{(\tau_{max})_c}{(\tau_{max})_0} = \frac{20}{9}\left[\frac{0.03}{\frac{w}{d_b}+0.05} - 0.15\right] \tag{1.2}$$

Based on the results of (Gambarova & Karakoç, 1981; Gambarova & Zasso, 1985), Biuriani and Plizzari (1985) proposed a general formulation in the frame of a more general work on the bond phenomenon after splitting of the surrounding concrete (Figure 1.7(b) (Giuriani et al., 1991; Giuriani & Plizzari, 1998)), which is linearly dependent on the normalized crack opening as follows:

$$\frac{(\tau_{max})_c}{(\tau_{max})_0} = 1 - \left(42\frac{w}{d_b}\right) \tag{1.3}$$

Although the value of the experimental coefficient proposed by the authors strongly limits the practical application of the formulation (crack width up to 0.10 mm, d_b=18 mm), Eq. (1.3) has the benefit of being relatively simple and pragmatic. Idda (1999) has performed a large experimental program of relatively short pull-out tests in pre-cracked reinforced concrete ties, varying parameters such as the bonded length (L/d_b=3.5-12.5), the rebar diameters (6, 10, 20,

28, and mainly 16 mm) and the type of concrete (normal and high-strength). Although the longitudinal reinforcement of the test specimen was locally unbonded to minimize the passive confinement during the pull-out of the rebar (Figure 1.7(c)), a variation of the crack width could not be totally avoided. The exponential expression proposed by Idda (1999) (the function of the ratio between the crack width and the maximum height of the rib) was empirically adjusted by a dimensional analysis thanks to the significant amount of tests conducted. Assuming $h_{r,max} \approx (4/3).f_R.d_b$ with $f_R = 0.056$, the effect of cracks on the ultimate bond strength can thus be derived from the original formulation as Eq. (1.4).

$$\frac{(\tau_{max})_c}{(\tau_{max})_0} = e^{-5.1\sqrt{\frac{w}{d_b}}} \tag{1.4}$$

Despite the fundamentally different approaches presented by Idda (1999) as compared to the model of Gambarova et al. (1981, 1985), it is interesting to mention that a similar trend can be observed in both formulations. Based on the results of Idda (1999), additional finite element analyses were conducted by Purainer (2005) to evaluate the importance of several parameters. Finally, a linear correction term (also function of the crack width and maximum rib height) was adopted and supported the negligible effect of the crack spacing and concrete strength on bond performance. Considering as previously $h_{r,max} \approx (4/3).f_R.d_b$ with f_R=0.056 and d_b=20 mm, it yields to Eq. (1.5), as follows:

$$\frac{(\tau_{max})_c}{(\tau_{max})_0} = e^{-5.1\sqrt{\frac{w}{d_b}}}(1 + 2\frac{w}{d_b}) \tag{1.5}$$

The trend of this expression reasonably follows Idda (1999) but the influence of the crack is slightly reduced due to the linear term considered. The range of application of the proposed formulation is however strictly limited to that of the additional numerical investigations performed by the author (crack openings from 0.05 to 0.5 mm, and rebars diameters 8, 14, and 25 mm).

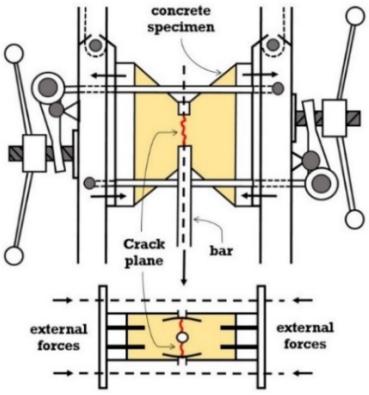

(a) (Gambarova & Karakoç, 1981; Gambarova & Zasso, 1985)

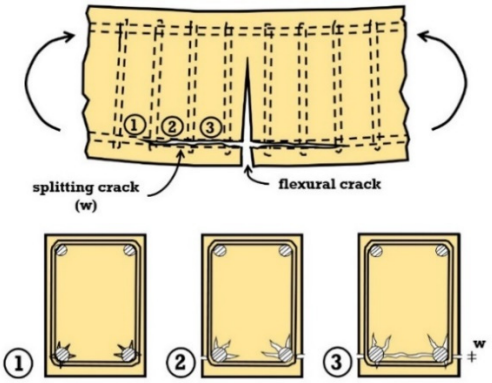

(b) (Giuriani et al., 1991; Giuriani & Plizzari, 1998)

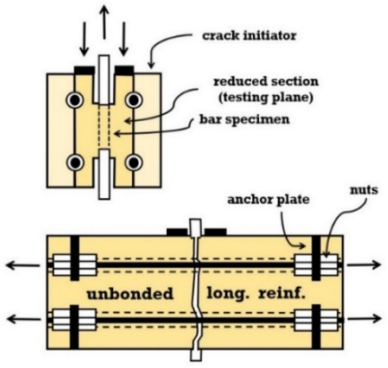

(c) (Idda, 1999)

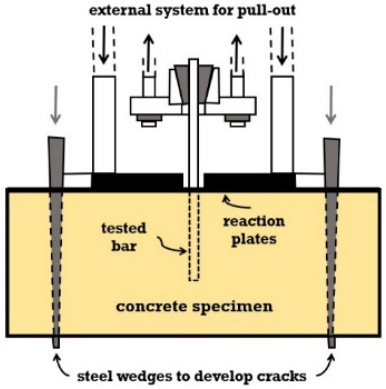

(d) (Simons, 2007)

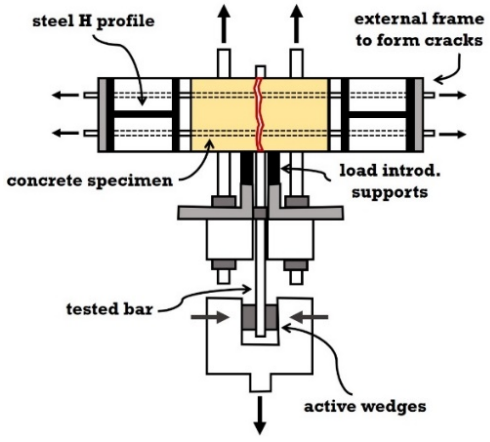

(e) (Purainer, 2005)

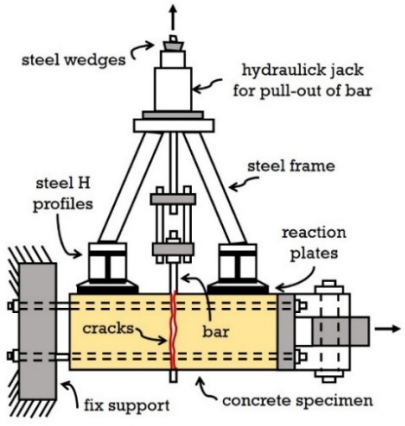

(f) (Mahrenholtz, 2012)

Figure 1.7 Bond tests in the pre-cracked concrete reported in the literature
Taken from Brantschen (2016)

In this context, pull-out tests in pre-cracked concrete performed by Simons (2007) in large reinforced concrete specimens (Figure 1.7(d)) on short embedded straight rebars (L/d_b=5-8) (in the frame of a more general study on the bond performance of various resins for post-installed systems under solicitation) lead to the derivation of Eq. (1.6).

$$\frac{(\tau_{max})_c}{(\tau_{max})_0} = 1 - 26.4\frac{w}{d_b} \tag{1.6}$$

This equation was obtained considering a maximum crack width of 0.4 mm (value at which the pull-out tests have been performed in the most severe cases) and d_b=20 mm as a reasonable average of the test diameters (12, 20, and 32 mm, with respectively $f_R \approx$ 0.091, 0.082 and 0.075). For filling the research gaps in bond fatigue in reinforced concrete under transverse tension, Lindorf (2011) performed experimental pull-out tests in pre-cracked conditions. Their test setup was composed of two perpendicular and independent frames aiming respectively at the development of cracks in the concrete specimen (horizontal direction) and then to process to the pull-out of the rebar (vertical direction) (Figure (1.7(e)). Although there is no specific equation in this study, the author still confirmed the reported observations and trends in the literature regarding bond reduction as a result of the pre-cracking phenomenon. Additionally, using only 16 mm diameter rebars ($f_R \approx$ 0.09) along with a wall-defined test procedure leads to very limited scatter in comparison to previous studies. Recently, some short pull out tests (L/d_b=5) on embedded rebars of diameter 16 mm ($f_R \approx$ 0.07) in pre-cracked sections were conducted by Mahrenholtz (2012) on reinforced concrete ties (Figure (1.7(f)). Based on reported results, and the aforementioned ones from the literature, a linear equation (Eq. (1.7)) was formulated for cracks smaller than the rib height ($w < h_R$) with a good correlation.

$$\frac{(\tau_{max})_c}{(\tau_{max})_0} = 1 - 10.0\frac{w}{d_b} \tag{1.7}$$

In this context, Desnerck et al. (2015) introduced a new test method to study the bond behaviour of rebar in cylindrical cracked reinforced concrete specimens. Number of cracks,

crack orientation, confinement and concrete cover are key parameters studied in their research. They reported that the even small range of crack widths, 0.03–0.04 mm, resulting in a major decrease of the bond strength. 44% and 54% bond strength reductions were obtained for specimens with a single crack and double cracked, respectively. Although there is a clear trend of decreasing the efficiency of the force transfer between steel and concrete in the presence of cracks, a significant scatter arose amongst the proposed equations. This can be justified by the fact that the existing formulations mainly have an empirical background, thus depending mostly on the performed tests and calibration range. These disparities might result from the consideration of several rebar types over the decades and a custom test setup for each of the investigations.

1.5 Self-healing method

Penetration of aggressive liquids and gasses in the cracks can significantly affect the durability characteristics of RC structures. Propagation of cracks through the RC member and growing crack width can cause a condition in which reinforcement can directly be exposed to the environment. When the reinforcement begins to corrode, the whole collapse of the RC structure may occur. In this context, even the existence of small crack width can be important for the life cycle of the RC structure. It appears clear that inspection, maintenance, and repair of concrete cracks are all crucial, while they are cost-effective approaches. Moreover, inspection methods are not completely efficient for finding internal cracks. Hence, researchers proposed a promising method to increase the life of RC members by the so-called “autogenous healing method” or “self-healing method”. Unhydrtaed cement particles in the bulk matrix (around the aggregate and rebar) play a major role in this method. Hydration of unhydrated cement particles and dissolution and subsequent carbonation of calcium hydroxide ($Ca(OH)_2$) are the main crack-sealing and -healing mechanisms in this method. There is some limitations in the autogenous healing method including providing water resources in the hardened mixture and crack width. Different methods were proposed to solve these limitations (Figure 1.8). Similar to the water-curing, the healing process needs water to be released gradually for producing more hydration products. Therefore, a smart agent is necessary inside the mixture to keep the

water and slowly release that. Moreover, to maintain cracks with small widths, fibers and enough lateral confinement are necessary to increase the performance of the self-healing method (Van Tittelboom & De Belie, 2013). Additionally, to increase the amount of unhydrated particles, different types of cementitious materials with different water-to-powder ratios can be used (Sahmaran et al., 2013). These modifications in the self-healing method are called “accelerated self-healing method”, which is depicted in Figure 1.9. In this context, self-healing in cementitious materials can be classified broadly into three groups of “intrinsic healing”, “capsule-based healing” and “vascular healing”. It is worth mentioning that there is a considerable difference between “crack-healing” and “crack-sealing”. Capacity of concrete to close crack for preventing the entrance of aggressive liquids and gasses is called “crack-sealing”, while the effect of these healing products for regaining mechanical strength is denoted by “crack healing”.

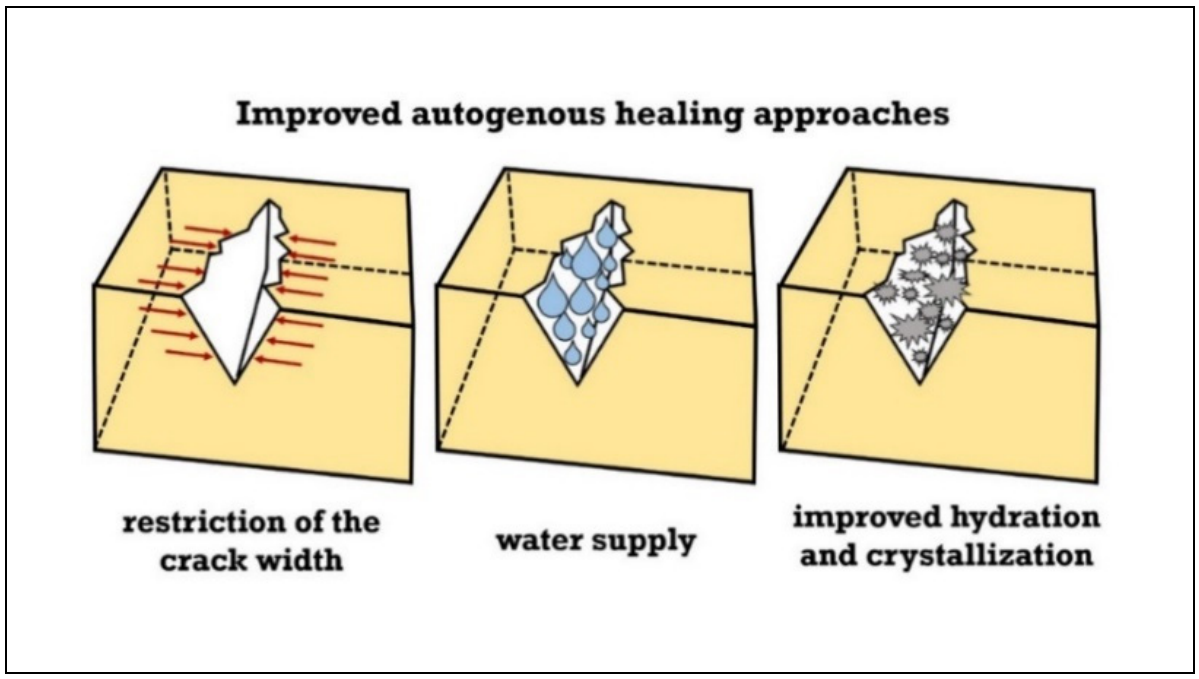

Figure 1.8 Overview of autogenous self-healing approach
Taken from Van Tittelboom & De Belie (2013)

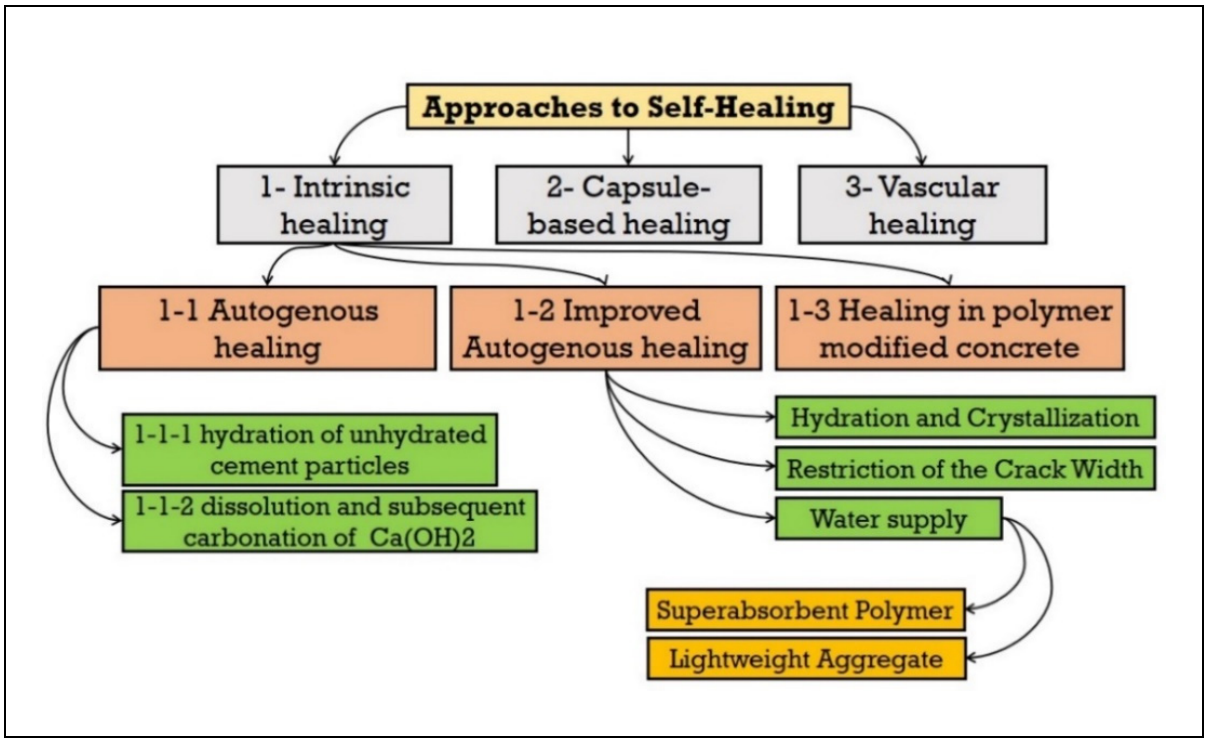

Figure 1.9 Overview of self-healing methods

1.5.1 Self-healing of SCC

Only a few studies determined the effect of the self-healing method in SCC. Şahmaran et al. (2008) experimentally studied self-healing of SCC incorporating high volumes of fly ash subjected to water exposure (water re-curing). They used fly ash replacement ratios of 0%, 35%, and 55% in SCC mixtures were prepared to have a constant water-to-binder ratio of 0.35. They used uniaxial compression loading to simulating pre-cracking (micro-cracks) in specimens up to 70% and 90% of the ultimate compressive load. Percentage of loss in mechanical properties was used as the damage index. Damaged specimens were kept in water for a month to healing cracks. Mechanical properties were recorded every two weeks by compressive strength test and ultrasonic pulse velocity (UPV) method. Their results showed that healing periods caused 7.0% strength reduction in fly ash-contained SCC as compared to the value 27.0% just after the pre-loading test, indicating considerable healing. However, the lower healing percentage was obtained for SCC mixtures without fly ash. This can be attributed

to the fact that fly ash has a low hydration process so that a large quantity of unhydrated fly ash particles is available in the bulk matrix. This can increase the performance of the self-healing method. In this context, Ramadan & Haddad (2017) investigated the self-healing method and potential regaining of the mechanical properties of SCC mixtures. A water-to-cement ratio of 0.45 was considered for SCC mixtures. To simulate pre-loading, different compressive stress levels ranging from 80.0% to 100% of their ultimate load capacity were applied to the specimens. Water and air re-curing process were considered to mitigate damages. UPV test and compressive strength were conducted to measure damage healing index. Their results indicated that re-curing (healing) in water is more efficient as compared to the air re-curing process for both the crack-sealing and crack-healing. Their results showed that pre-loaded SCC specimens, up to levels of 90% or less, were completely healed, while more than 90% damages lost considerable strength and re-curing could not mitigate the damages.

1.5.2 Effect of SAP on self-healing

Hydrogels, or superabsorbent polymers (SAP), can absorb an important volume of liquid from the nearby atmosphere (up to 500 times their weight) and keep the liquid within their structure. SAP particles swell due to the osmotic pressure variance between the hydrogel and the external solution (Snoeck et al., 2012). SAP particles improve the self-healing method by preparing water on the crack surface. This leads to a more sensible crack closure (crack-sealing) and more strength regaining (crack healing) (Figure 1.10). Details of SAP used in the previous studies are summarized in Table 1.3. Types of SAP, company name, dosage, and curing type are mentioned in this Table.

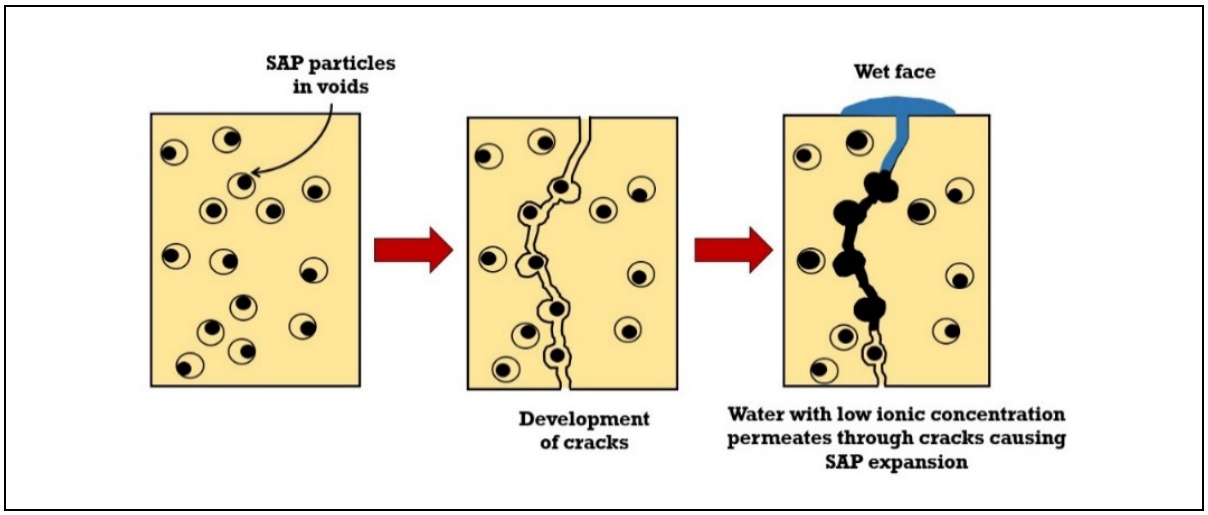

Figure 1.10 Mechanism of self-healing cracks using SAP
Taken from Lee et al. (2016)

Many previous researches studied the effect of SAP on the self-healing method. Snoeck & De Belie (2015) reported that SAP concrete can totally heal cracks up to 30 µm, while crack width $30 \leq w \leq 150$ µm was partially healed. Wet-dry cycles were considered for healing periods. They found that at a relative humidity (RH) of more than 90%, the performance of the self-healing method with SAP is significantly lower as compared to the wet-dry cycles. Moreover, at a relative humidity of 60%, only the mixtures with SAP show partial healing. So, they found $60\% < RH < 90\%$ as the best condition for the self-healing method in SAP mixtures. Snoeck & De Belie (2015) found that the macro-pores, generated by the shrinkage of SAP after releasing water, could play as the crack initiators. Pre-loading tests conducted by Lee et al. (2010) generated cracks with controllable width between 100-400 μm on SAP-modified cement paste and mortar. They studied the effect of SAP type on the crack-sealing and -healing. They reported that Poly(acrylate-co-acrylamide) is more effective, as compared to Poly(acrylate). Moreover, they found that larger SAP particle size shows more positive influences on crack-sealing. In this context, Snoeck et al. (2012) used neutron radiography, as a non-destructive test. Their monitoring technique found that by adding SAP inside the mixture, both capillary water absorption and permeability of cracked concrete decreases. They also observed that swelling of SAP at the crack faces leads to the crack blockage. SAP particles can keep the water within their structure and the crack is sealed autonomously.

Table 1.3 Details of SAP used in the previous studies

Reference	Type of SAP	Dosage	Remarks
Snoeck & De Belie (2015)	SAP A: Copolymer of acrylamide and sodium acrylate (particle size 100±21.5 µm) …….. SAP B: Cross-linked potassium salt polyacrylate (particle size 476.6±52.9 µm)	0, 0.5, and 1 (%) mass percent of SAP versus cement weight	SAP particles promote self-healing. The healed specimens are able to regain some of their mechanical properties (up to 75%).
Lee et al. (2010)	Poly(AA) Poly(AA) Poly(AA-co-AM)	3% SAP (by wt. of cement)	They compared three methods for estimating the swelling ratio of SAP in concrete.
Lee et al. (2010)	Poly(acrylate) (Poly(AA)) …… Poly(acrylate-co-acraylamide) (Poly(AA-co-AM))	5% Poly(acrylate) (Poly(AA)) or 4% Poly(acrylate-co-acraylamide) (Poly(AA-co-AM))	The cumulative flow through specimens containing SAP was significantly lower than for the control.
Schröfl et al. (2012)	-	-	SAP counteracted autogenous shrinkage during the acceleration period of cement hydration.
Snoeck et al. (2012)	SAP B: a crosslinked potassium salt polyacrylate (particle size 477±53µm (n=50)) ……. SAP C: a new synthetic vinyl-based superabsorbent polymer (particle size 420 ±148µm (n=50))	1 and 2% (m%) of cement weight	SAP particles are able to seal the crack, thus allowing a recovery of the water-tightness of the structure.
Al-Nasra & Daoud (2013)	Sodium polyacrylate	0.11 percent of the weight of cement	Adding SAP to the concrete mix makes the fresh concrete more plastic and uniform. This helps in placing and finishing the concrete.
Al-Nasra (2013)	Sodium polyacrylate	-	The use of sodium polyacrylate in concrete may increase the concrete strength due to internal curing process.
Lee et al. (2010)	cross-linked sodium polyacrylate , Poly(AA) …… potassium poly-(acrylate-co-acrylamide), Poly(AA-co-AM)	1% SAP (by weight percentage of cement)	Transport testing found that the flowrate through a 340 µm wide model crack is reduced substantially by using less than 1 vol.-% SAP.
Snoeck & De Belie (2013)	SAP A : being a copolymer of acrylamide and sodium acrylate …….. SAP B: a cross-linked potassium salt polyacrylate	0, 0.5, 1 mass-% (m%) of cement weight,	SAP hold the mixing water and do cause a densification of the matrix and reduce the water permeability. Additional water counteracts this effect and provides approximately the same capillary microstructure and transport properties compared to reference samples.
Snoeck et al. (2014)	SAP A: a copolymer of acrylamide and sodium acrylate (particle size 100.0 ± 21.5 µm (n= 50)) …….. SAP B: a cross-linked potassium salt polyacrylate (particle size 477 ± 53 µm (n= 50)).	0.5 or 1 m% by weight of cement	SAP particles reduce the flow, cause a densification of the matrix due to internal curing and reduce the strength due to macro-pore formation.
Mechtcherine et al. (2014)	monomer acrylic acid	0.30 % by mass of cement	SAP causes a considerable decrease in autogenous shrinkage attributable to internal curing.
Snoeck et al. (2014)	SAP A being a copolymer of acrylamide and sodium acrylate …….. SAP B, a cross-linked potassium salt polyacrylate.	0.5 or 1 m% by weight of cement	There was a regain in strength properties when specimens with SAP were allowed to heal in wet/dry cycles (75% after 28 days of healing).
Snoeck et al. (2014)	SAP A= a copolymer of acrylamide and sodium acrylate, and SAP B, a cross-linked potassium salt polyacrylate.	-	SAP can sustain hydration by yielding their absorbed water and provide water for the precipitation of $CaCO_3$.

Lee et al. (2016) reported that high alkalinity and ionic content of the pore solution in SAP cause swelling phenomenon. This absorbed water can help for cement hydration. Additionally, the SAP re-swelling phenomenon can be happened by the ingress of an external solution with low ionic concentration into the cracks. This was monitored by using a stereomicroscope. This swelling cycle can block the crack and thus water penetration decreases. They found that the crack-sealing can efficiently happened in width of 340 μm by using 1.0% (volume) SAP. In this field, Snoeck et al. (2014) reported that the smaller SAP is not efficient to seal a crack. They attributed this observation to the fact that small size of SAP cannot bridge a crack efficiently and may wash out.

In the view of compressive strength, adding SAP to concrete mixtures has two main influences including (Jensen, 2013) (1) SAP generates macro voids in the concrete, resulting in the reduction in compressive strength; (2) SAP acts as an internal water curing agent, which increases the degree of hydration. The dominant impact of these two phenomena depends on the water-cement ratio (w/c), the maturity of the concrete, the amount of SAP addition, and the type of SAP. Although most of the previous studies reported the reduction of compressive strength due to the SAP addition (see the section 1.5.3 of the present chapter), Al-Nasra & Daoud (2013) (Al-Nasra, 2013; Al-Nasra & Daoud, 2013) observed that using sodium polyacrylate, like SAP, leading to a slight increase in compressive strength. They attributed this result to the internal curing effect of SAP (low dosage) in the concrete mixture, while a higher dosage of SAP causes compressive strength reduction. There is no effect of SAP on cement hydration for water-to-cement ratio higher than 0.45), where the impact of the macro void on strength reduction is dominant in the SAP modified mixture. Some studies reported that SAP addition causes a slight increase in compressive strength for a low w/c (< 0.45) (Hasholt et al., 2012; Hasholt et al., 2010; Hasholt et al., 2010), as an internal curing agent. However, extensive experimental results provided by Mechtcherine et al. (2014) showed that generally, SAP leads to a reduction in compressive and flexural strengths. More experimental studies are thus necessary for future studies for finding an adjustment between internal curing effect and macro voids influences of SAP in the concrete mixtures.

Regarding the fresh properties of SAP concrete, Lee et al. (2010) showed that the swelling ratio of SAP affects the workability of the mixture by changing the water-to-cement ratio. Moreover, the porosity of the hardened cement paste is modified. That is why additional water along with appropriate superplasticizer needs to be used to compensate for the workability loss, especially for a higher dosage of SAP in NC. In this context, to check the accuracy of the water absorption capacity for a higher dosage of SAP, an approach proposed by Schröfl et al. (2012), in which water absorption capacity can be obtained by just gradually adding water during mixing to retain the slump constant. Regarding the workability of SAP concrete, Snoeck et al. (2014) confirmed that additional water is necessary to keep approximately the same global microstructure, which can be affected by the flowability and workability of mixture. However, they deduced a debatable conclusion that the additional water causes also further hydration for w/c=0.50 (Snoeck et al., 2014).

The properties and results of the experimental database are summarized in Table 1.4. More details of these studies are presented in Table APPENDIX I.1 (see page 299). SAP percentage, water-to-cement ratio (w/c), total water-to-cement ratio (w_T/c), additional water-to-cement ratio (w_e/c), concrete compressive strength (f'_c), curing days, SAP size, and strength reduction percentage are the main variables mentioned in Table 1.4. The author of this dissertation tried his best to gather all available databases from the primary studies to the recent ones. As mentioned in Table APPENDIX I.1 (see page 299), most of the previous research has confirmed strength reduction due to using SAP in concrete mixtures. Regarding SAP size, the maximum values of ranges reported in the literature were mentioned.

Table 1.4 Collected test specimens for SAP mixtures in the literature

References	SAP (%)	w/c	w_e/c	w_T/c	f'_c (MPa)
Lam & Hooton (2005)	0, 0.3, 0.6	0.35	0, 0.10	0.35, 0.45	34.51-56.86
Igarashi & Watanabe (2006)	0, 0.35, 0.7	0.25	0, 0.04, 0.09	0.25-0.34	67.00-97.40
Piérard et al. (2006)	0, 0.3, 0.6	0.35	0, 0.02, 0.04	0.35-0.39	76-107
Lura et al. (2006)	0, 0.40	0.31, 0.32	0, 0.05	0.31-0.37	70.19-117.22
Mechtcherine et al. (2006)	0, 0.40	0.25	0, 0.04	0.25, 0.29	129, 132
Esteves et al. (2007)	0, 0.20	0.25-0.35	0, 0.05	0.25-0.40	49.97-84.24
Dudziak & Mechtcherine (2008)	0, 0.40	0.24, 0.25	0.03, 0.05	0.28, 0.29	129-172
Craeye & De Schutter (2008)	0.04, 0.06, 0.08	0.32	0-0.10	0.32-0.42	75.0-108.69
Dudziak & Mechtcherine (2009)	0, 0.3, 0.4	0.22, 0.27	0-0.07	0.22-0.31	94-225
Wang et al. (2009)	0, 0.3, 0.5, 0.7	0.3, 0.34	0-0.06	0.30-0.38	56.60-71.80
Hasholt et al. (2010)	0-0.6	0.35-0.50	0-0.07	0.35-0.57	36.36-75.52
Craeye et al. (2011)	0-0.42	0.32	0-0.19	0.32-0.51	59.72-97.25
Schröfl et al. (2012)	0, 0.1, 0.2, 0.3	0.30	0-0.26	0.30-0.56	36.39-101.37
Olawuyi & Boshoff (2013)	0-0.6	0.25	0-0.19	0.25-0.44	49.38-106.12
Mechtcherine et al. (2014)	0, 0.3	0.30	0, 0.03, 0.04	0.30-0.34	79.10-103.20
Laustsen et al. (2015)	0, 0.07, 0.15, 0.3	0.45	0-0.13	0.45-0.58	43.0-63.0
Wang et al. (2013)	0-0.60	0.35	0	0.35	60.68-72.92
Snoeck et al. (2014)	0, 0.5, 1.0	0.50	0-0.3	0.50-0.80	20.36-61.98
Justs et al. (2015)	0, 0.21, 0.31	0.15, 0.2	0, 0.03	0.15-0.20	122.91-183.58
Kong et al. (2015)	0, 0.20, 0.40	0.29	0, 0.05, 0.1	0.29-0.39	32.29-84.19
Van Tittelboom et al. (2016)	0, 1.0	0.27	0, 0.07	0.27, 0.34	47.70-58.40
Shen et al. (2016)	0.05, 0.15, 0.26	0.33	0-0.05	0.33-0.38	57.30-64.0
Mechtcherine et al. (2017)	0-0.60	0.45	0, 0.05, 0.07	0.42-0.50	33.20-58.0

1.5.3 Effect of SAP on compressive strength (statistical analysis)

This section intends to propose regression models for 7 and 28 days compressive strengths of SAP concrete, based on the experimental database gathered from the literature (Table 1.3). As shown in Figure 1.11(a), there is a weak correlation between 7-day compressive strength and w/c ratio, while a good correlation is obtained for total w/c ratio (Figure 1.11(b), $R^2 = 0.81$).

This shows the critical role of additional water added to the mixture in compensating water loss due to SAP absorption capacity. Eq. (1.8) is obtained as follows:

$$(f'_c)_{7d} = 19.37\left(\frac{w_T}{c}\right)^{-1.2} \quad (1.8)$$

Regarding 28-day compressive strength, Figures 1.11(c, d) show a similar trend that the total water-to-cement ratio is more appropriate to predict the compressive strength of SAO modified concrete. Similarly, Eq. (1.9) is obtained as follows:

$$\left(f'_c\right)_{28d} = 18.75\left(\frac{w_T}{c}\right)^{-1.4} \quad (1.9)$$

Minitab software (Minitab, 2014) is used to statistically analyze the database regarding strength reduction of SAP concrete. Akima's polynomial method is used to measure the interfacial impacts of SAP percentage and w/c ratio. This method generates acceptable results in some cases, while it can produce misleading results in other cases. Because this method uses a fifth-order polynomial, it can estimate z-values at x-y positions beyond those you have sampled that are too large or small (Minitab, 2014). The results illustrated in Figure 1.12 indicate that SAP percentage has considerable impact on strength reduction for both 7 and 28-day strength especially for $w/c \leq 0.35$ in which SAP can cause considerable strength reduction (more than 50%). While for $w/c > 0.35$, a low dosage of SAP ($< 1.0\%$) has no significant influence on strength reduction. At a low water-to-cement ratio, there is no enough water in the matrix for internal curing, so the negative effects of macro voids generated by SAP particles are dominant. Hence, even for $w/c \leq 0.20$, value of 0.20% SAP leads to 50% strength reduction in SAP concrete. Accordingly, adding water to SAP concrete for having the same slump causes initiating internal curing by SAP particles along with the following impacts of macro voids after releasing water. These two phenomena have overlap on each other and in some cases play a major role in mechanical characteristics of SAP concrete. Hence, comparing the results of NC with SCC can show a constructive trend for future studies for working on SAP in construction industries.

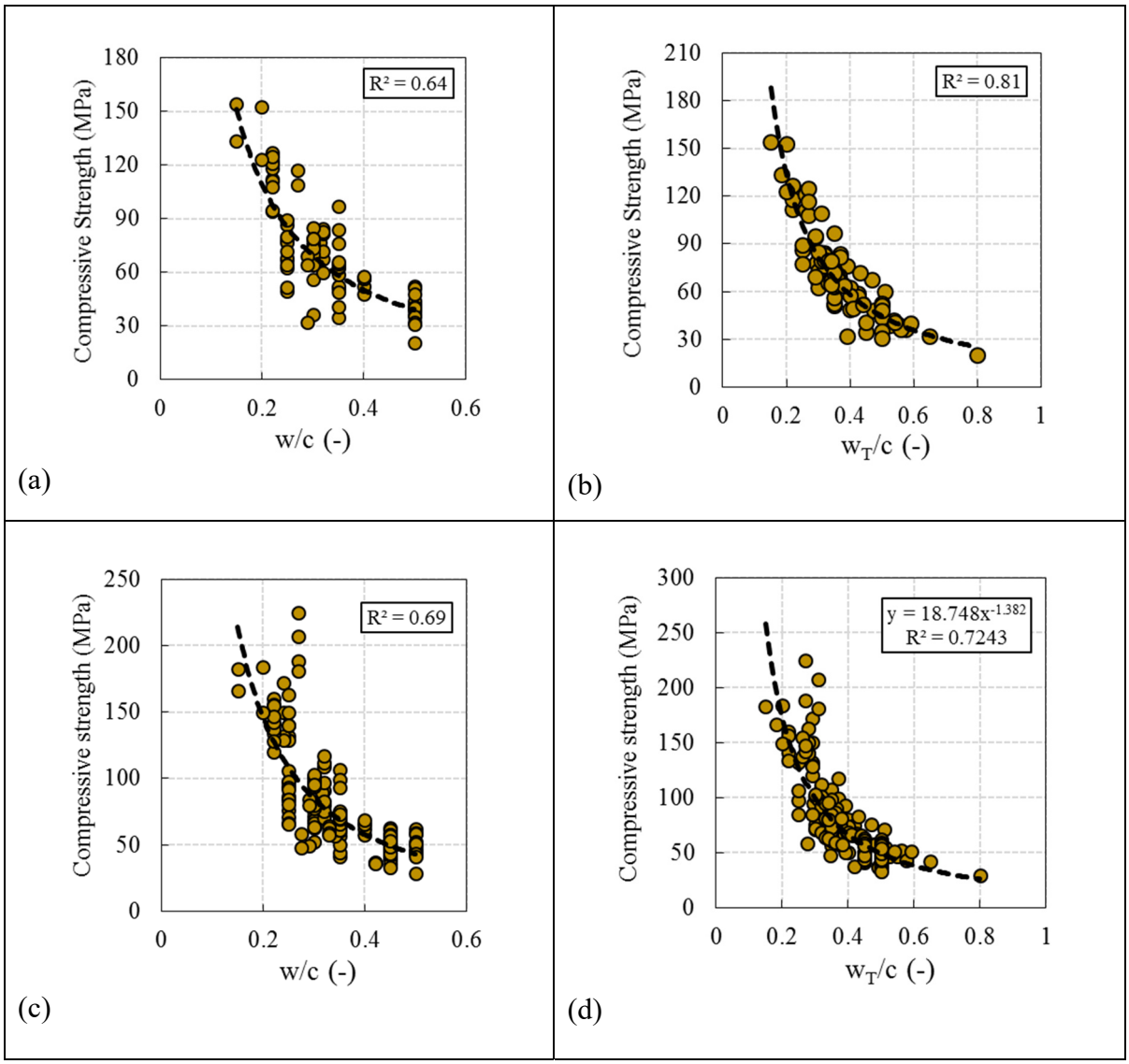

Figure 1.11 Compressive strength of SAP concrete:
(a) 7-day strength versus w/c; (b) 7-day strength versus w_T/c;
(c) 28-day strength versus w/c; (d) 28-day strength versus w_T/c

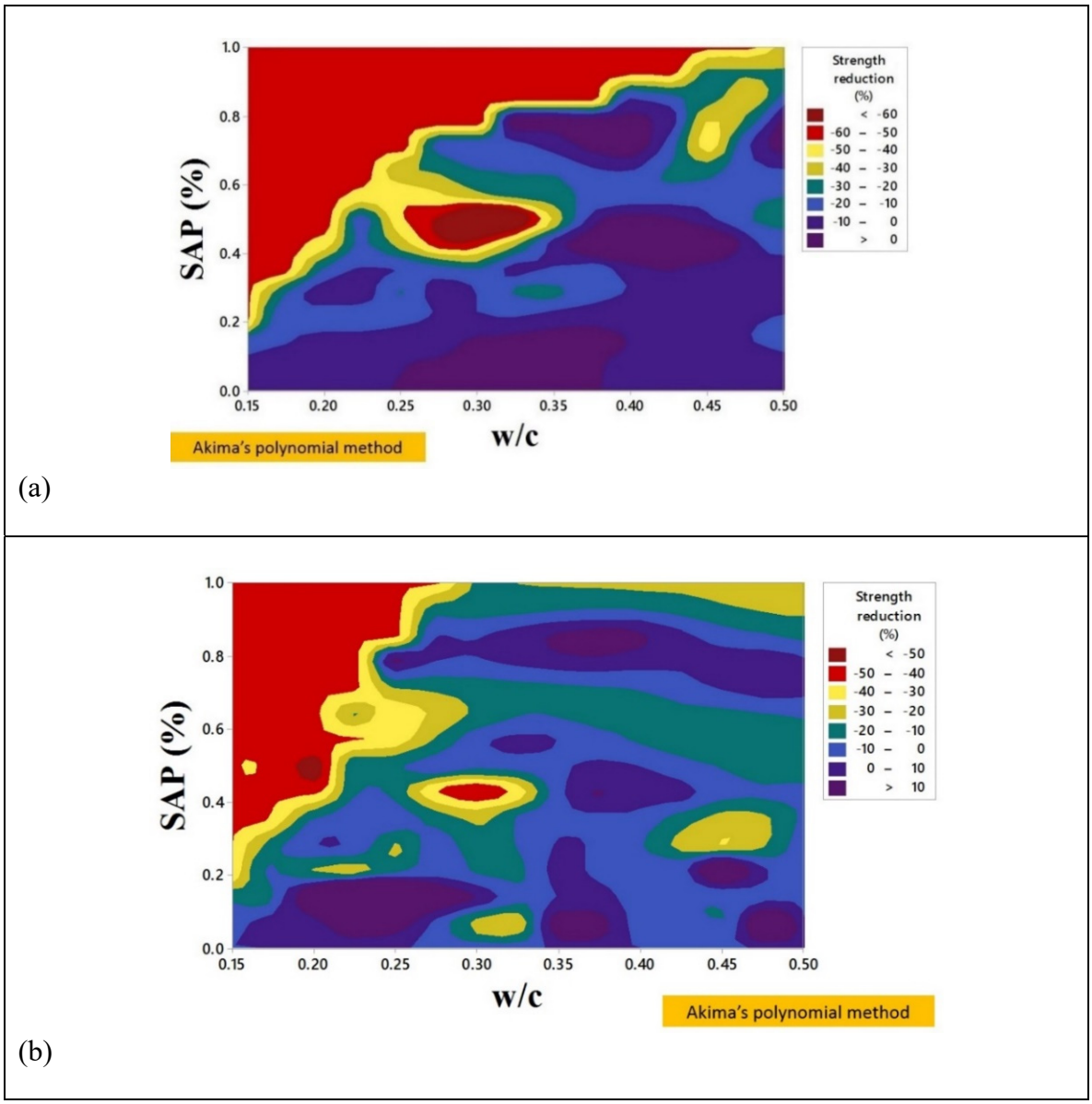

Figure 1.12 Contour plot of strength reduction versus SAP% for different w/c ratios: (a) 7-day; (b) 28-day

1.6 Research gaps in the literature

As comprehensiely revied in the present chapter, theres is some research gap, which needs to be filled by experimental studies including:

1. Only maximum bond stress (bond strength) reduction has been considered for the pre-cracking phenomenon without introducing a bond-slip envelope curve.
2. Crack widths limited to less than 0.30 mm have been proided in the literature.
3. No specific analytical method has been presented to clarify the pre-cracking phenomenon at rebar rib-front zone.
4. Only normal concrete (NC) has been used in the preivious experimental tests for studying the pre-cracking phenomenon..
5. There has been no practical solution to partly mitigate the internal damages of the pre-cracking phenomenon.

1.7 General and specific objectives of the thesis

To fill the current research gaps in the context of the pre-cracking phenomenon, the present thesis intends to perform a comprehensive experimental and analytical studies. The main objectives of the present thesi are to determine the effect of the pre-cracking phenomenon on bond behaviour and present a method to mitigate the internal damages at the rebar-concrete interface by using healing agent inside the concrete (Figure 1.14). Specific Objectives of the present Manuscript-based thesis are as follows:

- Quantify the effect of the pre-cracking phenomenon on bond behaviour and (a) present a modified bond-slip model; (b) introduce an analytical simplified model.
- Determine experimentally the effect of concrete type on bond behaviour of rebar in uncracked & cracked concrete by considering different types of concrete mixtures including concrete with different workabilities, concrete mixtures containing superabsorbent polymer (SAP), and concrete mixtures air-entraining admixture.
- Determine the efficiceny of using superabsorbent polymers (SAP) to mitigate the pre-cracking phenomenon by self-healing method with and without AE admixture.

- Measure the effect of concrete composition and SAP type on self-healing method at the rebar-concrete interface including (a) effect of SAP percentage; (b) effect of SAP type; (c) SCC vs NC for healing cracks; and (d) effect of air-entraining admixture

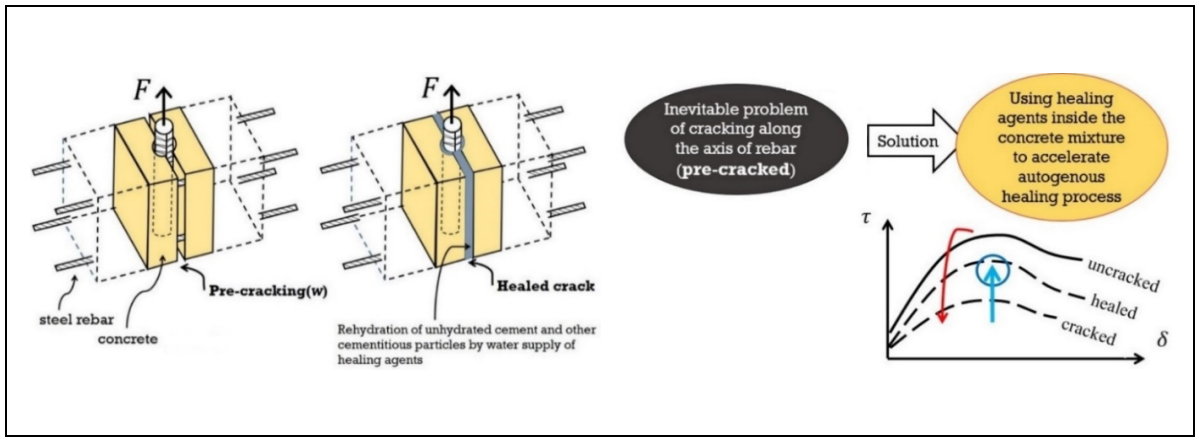

Figure 1.13 Schematic representation of the general objectives of the present thesis

As shown in Figure 1.15, this dissertation is organized into 7 chapters. These chapters can be classified into two main sections, named: “Explaining and investigating the problem” and “investigating some proposed solutions”. The first section consists of three main subsections of “description of pre-cracking”, “Presenting analytical model based on rebar geometry”, and “Effect of concrete composition (flowability) on the pre-cracking phenomenon”, presented in Chapters 2, 3, and 4 respectively. These chapters intend to describe and study the pre-cracking phenomenon by experimental and analytical approaches. After explaining and investigating different aspects of the problem (pre-cracking phenomenon), this thesis investigates the potentiel and effeciency of a possible solution that is the self-healing method by SAP in three main subsections of the “Self-healing method by SAP (Chapter 5)”, ”Effect of air-entraining admixture (AE) on self-healing method (Chapter 6)”, and “Self-healing method in SCC (Chapter 7)”. Chapter of “Conclusions” summarizes the experimental, numerical, and statistical results. Finally, the last Chapter proposes some recommendations for future research. Due to the schedule and limitations considered in the present thesis, some assumptions were

considered for the experimental and analytical works. Hence, more efforts are necessary for future studies, which are listed in the last Chapter, “Recommendations for future studies”.

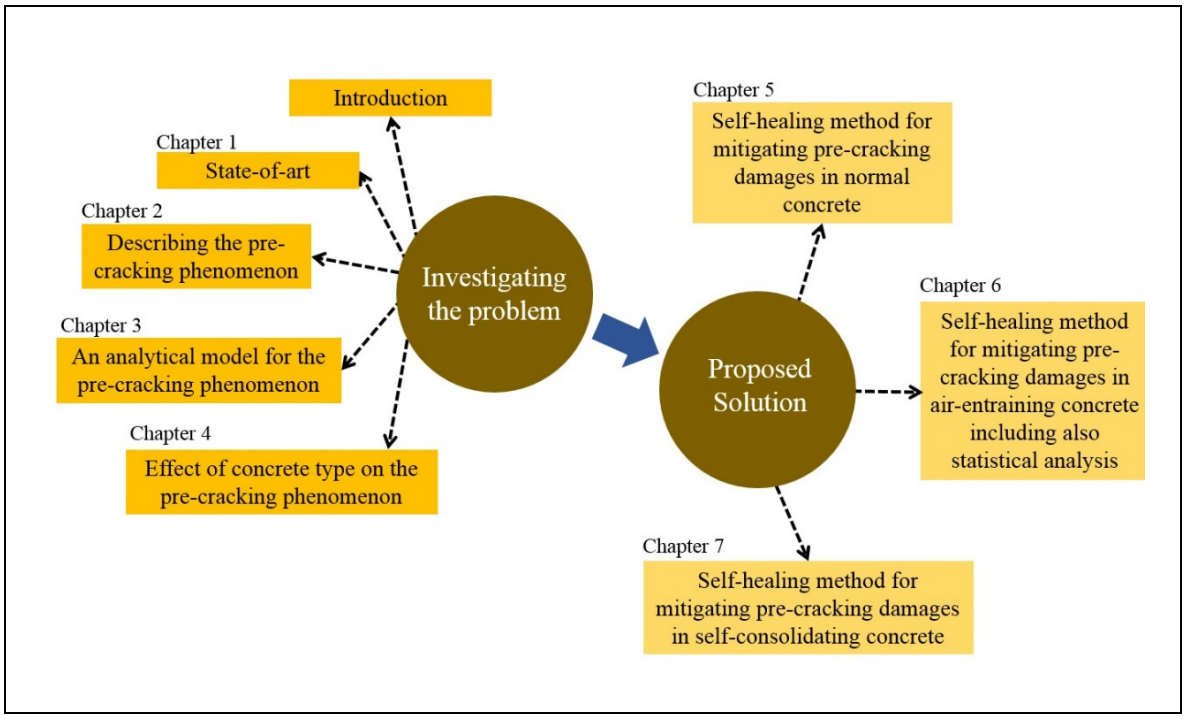

Figure 1.14 List of chapters considered for the present thesis

1.8 Methodology of the thesis

The overall plan of the present thesis is summarized in Figure 1.15 along with Figure 1.16. Three main statuses of uncracked, pre-cracked, and healed specimens are considered for the experimental program. To study the pre-cracking phenomenon, pull-out results of pre-cracked concrete are compared with the results of uncracked concrete. To simulate cracks, the splitting test (Brazilian) is used with a speed rate of 0.11-0.15 mm/min. Different crack openings are considered to determine the effect of crack width on bond-slip curves. Direct pull-out tests are considered for obtaining the bond-slip curve. As illustrated in Figure 1.16, comparing the results of uncracked with pre-cracked concrete should provide a new bond-slip model considering crack width to measure residual interfacial strength. The results of this section are

summarized in Chapter 2 for NC. For every concrete batch, it takes 7 and 28 days for preparing molds and curing time respectively. Along with the experimental program, an analytical model is also described to simply present bond failure damage after facing the pre-cracking phenomenon (Chapter 3). Along with NC with a slump of around 100 mm, NC with a slump of 200 mm and also SCC are considered. The results of this section can show the effect of concrete flowability on the pre-cracking phenomenon, which is presented in Chapter 4.

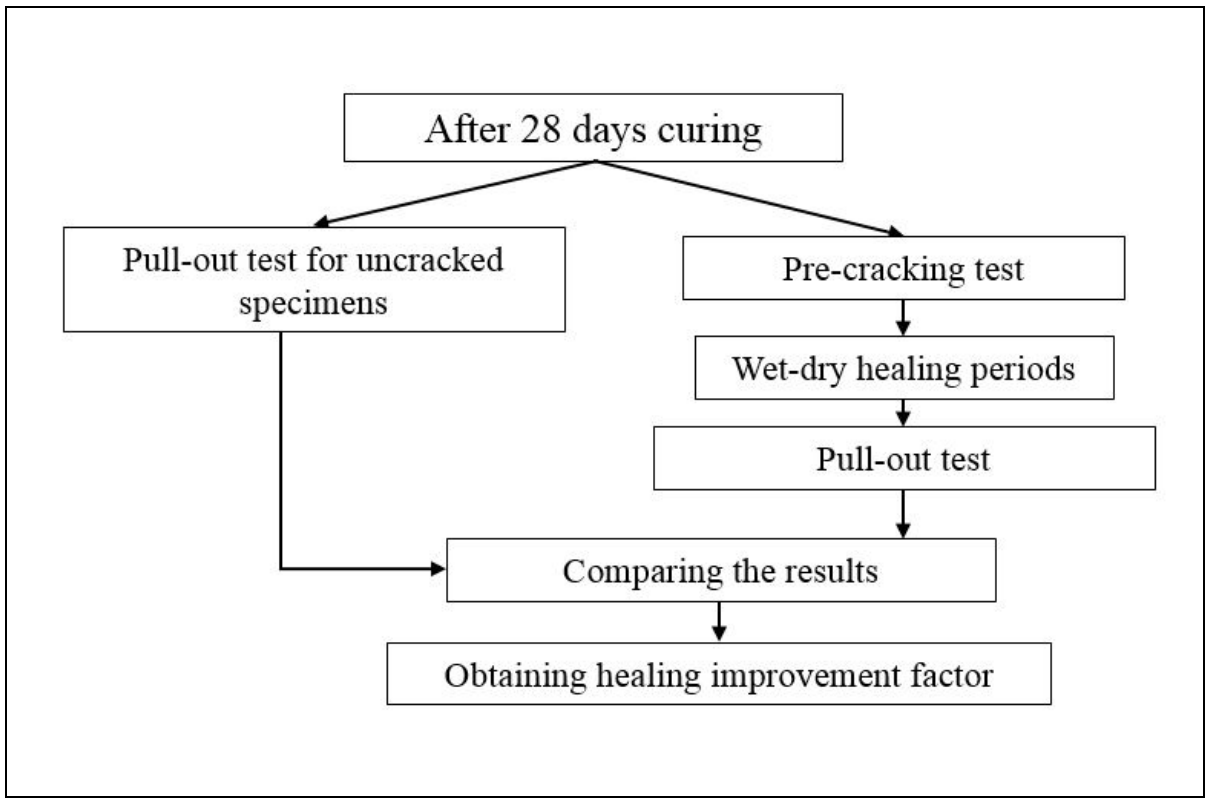

Figure 1.15 Simplified scheme of the present study

The second part of the present study concentrates on the self-healing method (Figure 1.16). This part intends to determine the efficiency of SAP on healing cracks due to the pre-cracking phenomenon. Two types of air- and non-air-entraining concretes are considered for concrete mixtures. Three dosages of 0.25%, 0.50%, and 1.0% SAP are used. Two types of SAP with different chemistries and sizes, but the same water absorption, are provided for the self-healing section. As shown in Figure 1.17, after pre-cracking specimens, some of them transferred to

the water tank for wet-dry cycles, including 24 hours inside the water tank and 24 hours outside. 14- and 28-day healing periods are considered. After finishing healing periods, direct pull-out tests should be conducted to compare the results with pre-cracked and intact concrete. Finally, the value of the improvement factor (IF) can show the performance of SAP concrete on healing damages. Every concrete mixture needs 56 days (without considering mold and material preparation) to finish this approach.

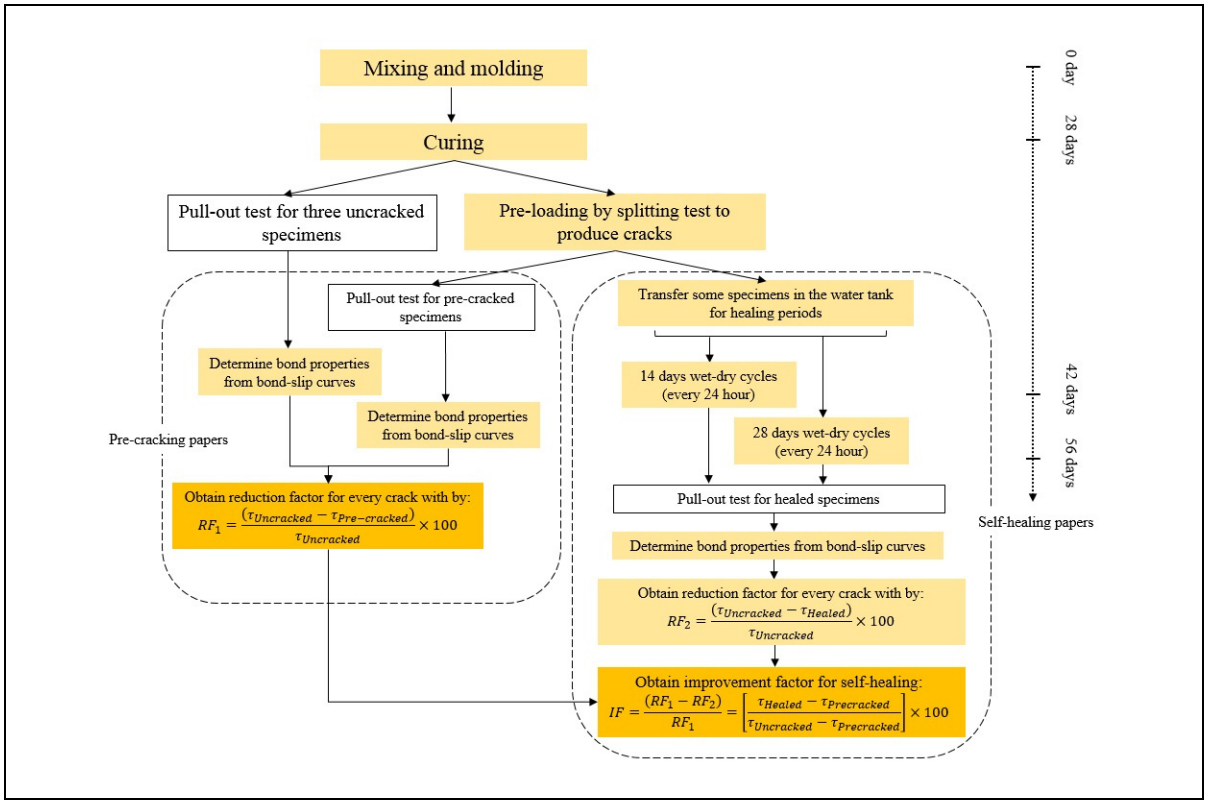

Figure 1.16 Thesis research framework and methodology

As shown in Figure 1.18, to measure the healing improvement factor (IF) different approaches are used in the present thesis including approaches A and B. In the approach A, used in Chapter 5, average bond properties of the healed specimens are compared with those of cracked ones to measure specific values of the IF. In the approach B, bond properties of each healing specimen are compared with the average values of the cracked ones. So, different values of the

"IF" are obtained in approach B, and the average value of these "IFs" is determined as the healing results.

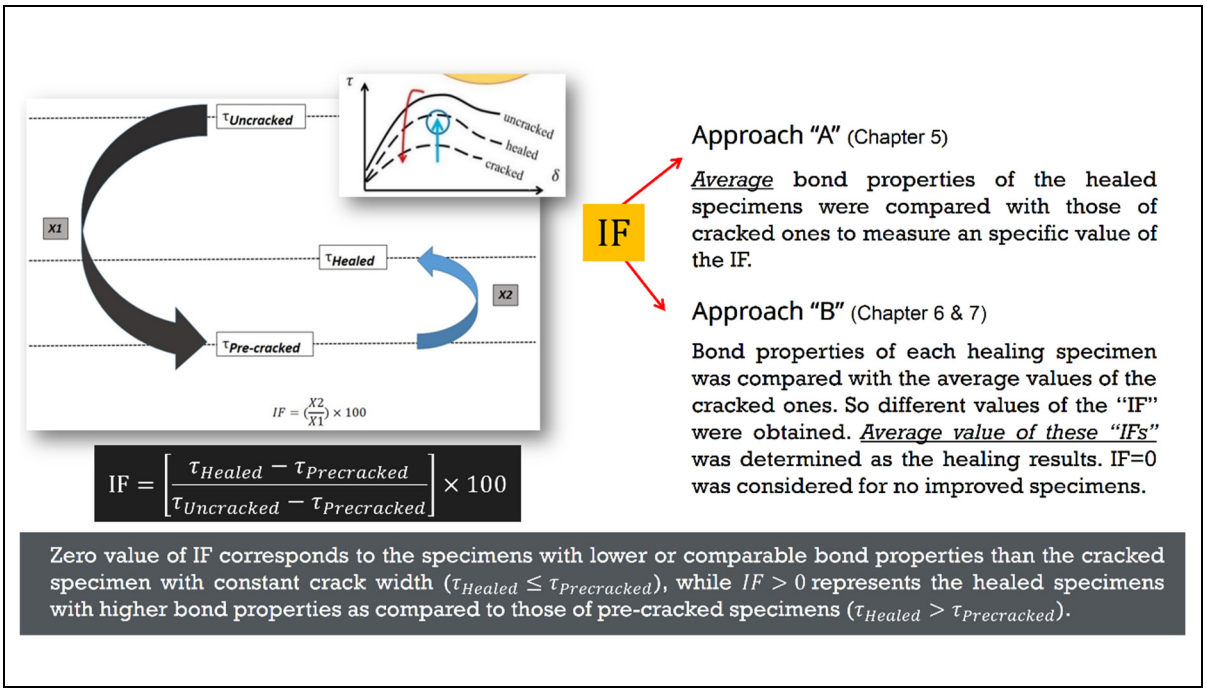

Figure 1.17 Analysis of healing improvement factor (IF) throughout the thesis

1.9 Limitations of the thesis

Due to the limitations in materials and schedule, some assumptions are considered in the experimental and analytical parts of the present thesis as follows:

- Only steel rebars of a nominal diameter of 10 mm are considered in the experimental section, to be embedded in cylindrical specimens;
- Embedded length of $5d_b$ (5 times the bar diameter) is considered;
- Only one healing regime, wet-dry cycles, is considered for the self-healing part. A maximum of 28 days is provided for the healing period. To increase this period, non-steel reinforcement maybe needed for use (such as GFRP) to prevent possible corrosion;

- Bar diameter and geometry are constant throughout the thesis. More experimental studies are needed for future studies to determine the effect of rebar parameters on the pre-cracking and the self-healing method;
- One dosage of air-entraining admixture (AE) is considered for air-entraining SAP concrete;
- The monotonic pull-out test is considered for the experimental program;
- Normal fine and coarse aggregates are used for both NC and SCC;
- Microscopic image analysis is performed with a distance of around 7.5 mm from the rebar edge;
- Vertical casting is considered for all cylindrical specimens;
- Three repetitions are considered for uncracked specimens. However, due to the brittle nature of splitting tests (to simulate the pre-cracking), less than 3 specimens are tested for the pre-cracked and the healed specimens. Although a displacement rate of 0.11-0.15 mm/min is considered for splitting tests, controlling cracks is not simple especially for concrete cylinders with rebar located at the center of the specimen;
- There is no transverse reinforcement in concrete cylinders. Concrete cover around the specimens is the only surrounding confinement considered for all the specimens;
- Normal water is considered for healing cracks;
- Constant room temperature and relative humidity (RH) were considered for healing.

1.10 Original contributions of the thesis

The present thesis, along with the recently published studies, intends to emphasize the importance of the pre-cracking phenomenon and presents a practical solution to mitigate damages. Only fib Model code 2010 considered this phenomenon in the design code, while there is no even a simple regulation in other codes. Additionally, the formulations suggested by the fib Model code 2010 are not practical and efficient (which is checked in Chapter 2). Hence, more considerations are necessary to prevent the side effect of unexpected cracks near the critical regions where rebar-concrete plays a major role such as joints, shear walls, and slabs. Also, more practical techniques need to be described by codes to measure cracks. To address this issue, the present thesis comprehensively studies the effect of the pre-cracking

phenomenon on the bond-slip curve of NC and SCC. New macro bond-slip models are also presented by modifying bond parameters as a function of initial crack width. Moreover, modified ACI formulation is also introduced for predicting development length of rebar in the cracked concrete. The efficiency of the regulation considered by the fib Model code 2010 is also checked by the experimental results. Moreover, a new bond micro-model for precracked concrete is also presented, as a function of rebar deformation. Finally, the effect of mixture workability on the pre-cracking phenomenon is also checked by using different concrete compositions with different slump flows. Generally, the present thesis investigates the effect of concrete composition on the pre-cracking phenomenon by considering NC normal slump flow (100 mm), NC with moderate slump flow (200 mm), and SCC with slump flow 600-700 mm. Briefly, the present thesis is an innovator effort, containing the mentioned novelties, to determine the influences of key factors on bond characteristics of steel rebar embedded in cracked concrete including crack width, concrete composition, and concrete workability. Additionally, the effect of concrete composition in NC is considered by using concrete mixtures with different water-to-cement ratios along with using air-entraining admixture.

After comprehensively describing the problem by different chapters, the present thesis, as a pioneer study, intends to present an efficient way of alleviating damages due to the pre-cracking phenomenon. Self-healing method is used, for the first time, to check the possibility of the crack-healing in the critical regions of the rebar-concrete interface. Superabsorbent polymer (SAP) is used to accelerate the self-healing method. Additionally, as until now, there is no study on bond properties of SAP concrete in both conditions of uncracked and cracked specimens, some parts of the present thesis dedicate to determine the effect of SAP dosage and type on uncracked specimens. The effect of SAP chemical composition on macro voids around the rebar edge is also investigated in the present thesis by microscopic images. This original contribution can help readers and researchers to find out the hardened properties of SAP concrete. Moreover, the self-healing method at the rebar-concrete interface by SAP is another novelty of the present thesis. Until now, there is no specific study on this topic. SEM analysis is also performed on healing products at crack surfaces. Three concrete types of NC, NC with air-entraining, and SCC are also considered for the self-healing section. Different types and

dosages of SAP are used in these mixtures. Comparing these results together is another novelty and collaboration of the present thesis. The results of the present study can be used in real RC structures to seal and heal cracks. However, the main question for future efforts is a practical technique to use the proposed approach. For exposed to humid weather, the results of the present study can be efficient. Different steel-congested regions exist in these structures, where the pre-cracking phenomenon can also be observed. Using SAP leads to mitigate some parts of damages. Additionally, the technique of wet-dry cycles exposure regime, used for the self-healing method, can be similar to the common repairing techniques in internal or external RC joints and slab sections near the column, which are more critical for the pre-cracking phenomenon.

CHAPTER 2

ON BOND-SLIP RESPONSE AND DEVELOPMENT LENGTH OF STEEL REBARS IN PRE-CRACKED CONCRETE

Seyed Sina Mousavi [a], Lotfi Guizani [b], and Claudiane Ouellet-Plamondon [c]

[a, b, c] Department of Construction Engineering, École de Technologie Supérieure, 1100 Notre-Dame West, Montreal, Quebec, Canada H3C 1K3

Paper published in *Construction and Building Materials*[1], February 2019

Abstract

Previous research on steel rebar-concrete bond behaviour has been concentrated mostly on the intact concrete without considering initial cracks induced by transverse tensile loading called pre-cracking phenomenon. There is no accurate model for evaluating bond behaviour and development length of steel rebar in pre-cracked concrete. This paper aims to characterize the bond-slip behaviour of steel rebars in pre-cracked concrete by direct pull-out tests and proposes a constitutive law as a function of the crack width. Results show that induced cracks notably cracks wider than 0.15 mm, cause a significant reduction in maximum and residual bond stress. Also, results indicate that larger crack widths result in considerably lower dissipated energy by the bond mechanism. The results obtained from both the experimental tests and the referenced database demonstrate that the pre-cracking phenomenon has a higher impact on the residual bond stress compared to the bond strength. Unlike existing equations, the proposed model accurately considers cracking effects on the steel rebar-concrete bond properties and shows a satisfactory fit with the experimental database. A predictive equation is also proposed for

[1] Mousavi, S. S., Guizani, L., & Ouellet-Plamondon, C. M. (2019). On bond-slip response and development length of steel bars in pre-cracked concrete. Construction and Building Materials, 199, 560-573. https://doi.org/10.1016/j.conbuildmat.2018.12.039

calculation of the development length in pre-cracked concrete, which is more conservative and prudent compared to existing regulations in design codes.

Keywords: Bond model; Slip; Development length; pre-cracked concrete

2.1 Introduction

Although extensive research has been accomplished in describing the bond-slip behaviour of steel rebars in intact concrete (Bompa & Elghazouli, 2017; Carvalho et al., 2018; Dehestani et al., 2017; Dehestani & Mousavi, 2015; Eligehausen et al., 1983; Mousavi et al., 2017; Wu & Zhao, 2012), very little and also scattered research has been devoted to the effect of induced localized cracks on bond properties. Corrosion-caused pre-cracking (Desnerck et al., 2015; Jiang et al., 2018), mechanical pre-loading (Brantschen et al., 2016), biaxial load transfer (Hadidi & Saadeghvaziri, 2005; Lindorf et al., 2009; Saadeghvaziri & Hadidi, 2005), multiaxial stress states (Cervenka, 1985; Purainer, 2005), and transverse tension (Lindorf, 2011) are different terms used in the literature referring to the induced initial cracking situations along the axis of the steel rebars in the surrounding concrete, hereafter called pre-cracking phenomenon. The mechanism of pre-cracking is similar to bond splitting cracking and mainly affects the bond-slip behaviour of the rebar. Potential anchorage problems of flexural in reinforced concrete (RC) members (Dawood & Marzouk, 2012), loop connections subjected to combined tension and bending (Joergensen & Hoang, 2015), arch-shaped members without transverse reinforcement (Ruiz et al., 2010), and reinforced concrete members without transverse reinforcement (Ruiz et al., 2015) are practical instances in which pre-cracking occurs along the axis of the rebar in concrete cover. Vecchio & Collins (1986) have studied the pre-cracking phenomenon by a particular set of in-plane shear and axial stress loading. They defined pre-cracked concrete as a new material with modified stress-strain characteristics. Their results show that transverse tensile strain after pre-cracking leads to a significant reduction in concrete compressive strength. Many researchers have reported similar findings (Belarbi & Hsu, 1991; Kollegger & Mehlhorn, 1990; Mikame et al., 1991; Shirai & Noguchi, 1989; Vecchio & Collins, 1993), showing that concrete compressive strength and

stiffness of reinforced panels are significantly affected by tension-compressive cyclic loading. Despite previous extensive research done on the compressive strength of pre-cracked concrete, there are not enough studies focusing on steel rebar/pre-cracked concrete bond behaviour.

Corrosion of steel rebars is one of the commonly detected problems of RC structures, which leads to multiple localized cracks in concrete cover along the axis of the rebar (fib-Bulletin10, 2000; Jiang et al., 2018). A practical case of this issue is a half-joint beam in which corrosion of longitudinal tensile reinforcement leads to an anchorage zone cracking (Desnerck et al., 2017). In the case of corrosion or severe exposure, it is concluded that cracks less than 0.20 mm have no significant effect on the role of concrete cover to prevent cracks along with the rebar (Okada & Miyagawa, 1980; Şahmaran, 2007; Seki & Maruyama, 1973), while crack widths between 0.20 mm to 0.40 mm cause reduction in concrete cover. However, the value of 0.10 mm has been suggested by other studies as a crack width limit for efficient protection against reinforcement corrosion (Kamiyama, 1972; Nakamura & Ogawa, 2000). A summary of the limitations of crack widths for normal and severe exposure in various standards is illustrated in Figure 2.1. Allowable crack widths related to different standards are in the range of 0.10-0.33 mm for severe exposure while a crack width up to 0.40 mm is allowed for normal exposure. These limits are practically the same crack width limits around tension steel reinforcement used for service limit states in the North American standards for interior and exterior exposures (CSA A23.3, 2014; ACI 318R, 2014), based on the pioneering work of Lutz & Gergeley (1967).

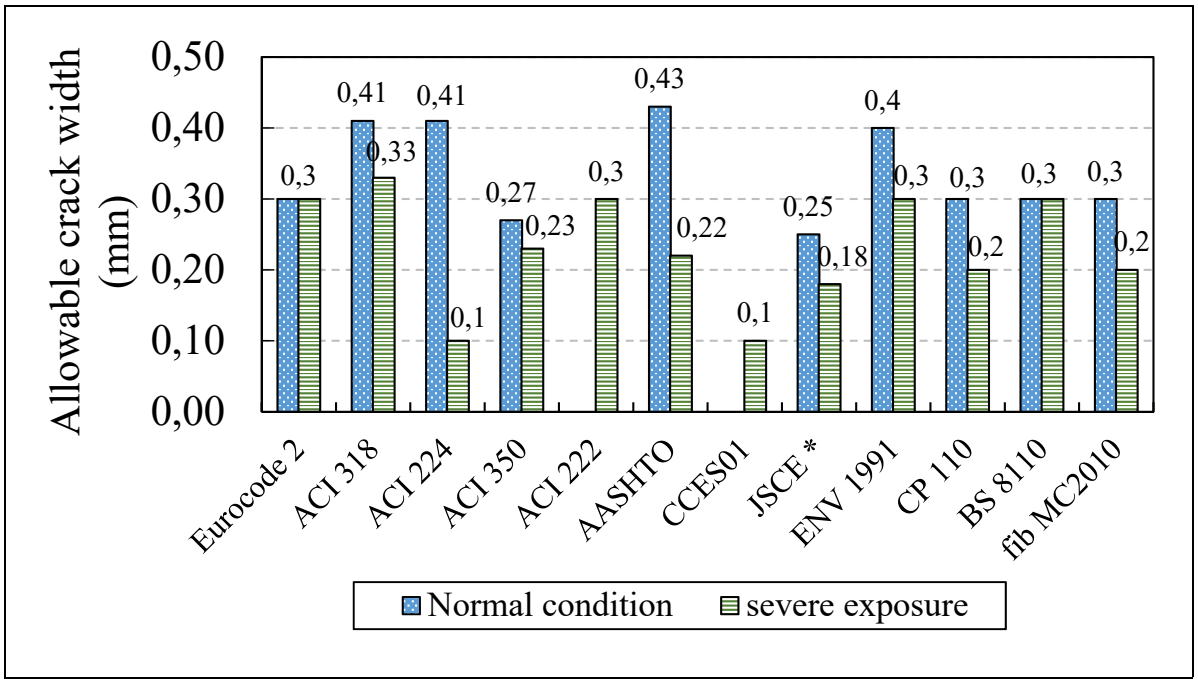

Figure 2.1 Allowable crack widths from different standards
(*: 0.005C for NC and 0.0035C for the severely corrosive condition, C is the concrete cover, C=50 mm is selected here)

Most of the previous research on pre-cracked concrete has concentrated on corrosion impact by considering the combination of the effects of cracking and the formation of a layer of corrosion products around the steel rebar (Desnerck et al., 2015). However, this approach is not efficient enough to accurately analyze the pre-cracking phenomenon in other situations such as plastic shrinkage cracks in congested reinforcement and accidental damages due to the previous overloading in which corrosion has no significant impact on pre-cracking. On the other hand, as different situations can cause pre-cracking, it is essential to analyze this issue by a general approach in which crack width should be considered as a critical parameter in the formulations. Hence, this study follows an approach presented by Desnerck et al. (2015) to cover most potential situations of pre-cracked concrete. Besides, previous research related to bond in pre-cracked concrete has only concentrated on the degradation of bond strength without introducing a specific bond-slip model for pre-cracked concrete (Brantschen et al., 2016; Gambarova et al., 1989; Idda, 1999; Mahrenholtz, 2012). Even in the case of bond strength, limited experimental results have been devoted to the pre-cracked concrete. A lack

of consensus on bond behaviour in pre-cracked concrete exists and can be attributed to the variety of experimental set-ups used for simulating pre-cracks. Despite the importance of the pre-cracking phenomenon, few unclear regulations, formulating reduced bond strength, have been considered in design codes. Consequently, the primary objective of this paper is to quantify the effect of the pre-cracking phenomenon on the steel rebar-concrete bond response curve and the development length under monotonic loading. This is achieved by a statistical analysis of the database extracted from the literature along with results obtained from an additional experimental test performed by the authors.

2.2 Experimental program

2.2.1 Materials, test setups, and specimens

A total number of 17 tests are carried out on monotonically loaded pull-out samples to (1) gain a better understanding of the rebar-concrete interface at pre-cracking conditions in comparison with the un-cracked concrete, and (2) develop a bond-slip model for reinforcing steel embedded in pre-cracked concrete under monotonic loading. Two types of concrete with 28-day cylinder strength (f'_c) of about 47.9 MPa and 58.8 MPa are used. The water-to-cement ratio of the mixture is 0.41, and the sand-to-aggregate ratio is 0.42. Mix proportions of both batches of concrete are summarized in Table 2.1. The aggregates are natural sand with a maximum grain size of 1.25 mm and a specific gravity of 2.68 and gravel with a nominal maximum size of 14 mm and a specific gravity of 2.68.

Table 2.1 Concrete composition for both test series A and B

Constituent	Quantity (kg/m^3)	
	NC1	NC2
Water	165	165
Cement (GU)	395	395
Fine aggregate (0-1.25 mm)	788	788
Coarse aggregate (5-10 mm)	822	822
Coarse aggregate (10-14 mm)	258	258
Superplasticizer	3.65	2.34
Air entraining	0.68	0.00
f'_c (MPa)	47.9 (1.41)	58.8 (1.39)

Note: Data inside the parentheses denote the standard deviation.

For the experimental program, the nominal steel rebars diameter (10M rebars, CAN/CSA-G30.18-09 2009) is about 10 mm. The rib pattern of steel rebars used in the experimental tests is shown in Figure 2.2. The yield stress f_y and ultimate tensile strength f_u of the steel rebars, obtained from mill tests, are 432 MPa and 620 MPa respectively.

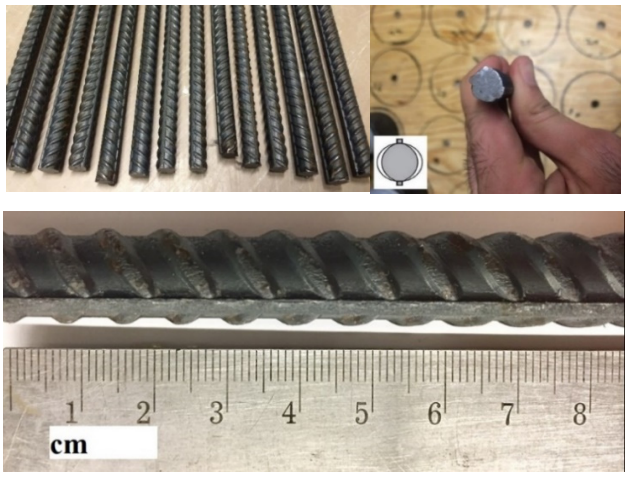

Figure 2.2 Rib pattern of steel rebars

To determine the effect of pre-cracking, the experimental program is divided into two series including 1- Pre-cracking tests by splitting the cylinders containing steel rebars, in the manner of the Brazilian test and; 2- Pull-out tests on the pre-cracked specimens. A displacement-controlled loading with a rate of 0.15 mm/min is applied to impede unexpected splitting failure during the pre-cracking loading. Two crack gauges are used on both sides of pre-cracked specimens for controlling crack widths (Figure 2.3(a)). A total of seventeen (17) specimens of 150×300 mm×mm are used, including six un-cracked specimens and 11 pre-cracked specimens with different crack widths. The pull-out test set-up is shown in Figure 2.3(b). The unloaded end slip is measured with a linear variable differential transformer (LVDT). An automatic data acquisition system is considered to record the data. A displacement-controlled pull-out force is applied at the rate of 0.5 mm/min. Embedded length (L) of $5d_b$ is placed at the center of cylindrical specimens to minimize extremities effects such as confinement from friction between the loaded end of specimens and the set-up plate. A ratio of concrete cover to rebar diameter equal to 7.5 is selected, which results in confined concrete conditions, preventing splitting bond failure modes for intact concrete specimens. As this paper aims to study the effect of pre-cracking on bond strength including strength and failure modes, it is tried to impede splitting bond failure. To provide pre-crack widths from 0.10 to 0.40 mm, two series of test specimens are used including 1- Series A with $f'_c = 47.9$ MPa and dimension of 150×306.5 mm×mm; and 2- Series B with $f'_c = 58.8$ MPa and specimens size of 150×113 mm×mm (Figure 2.3).

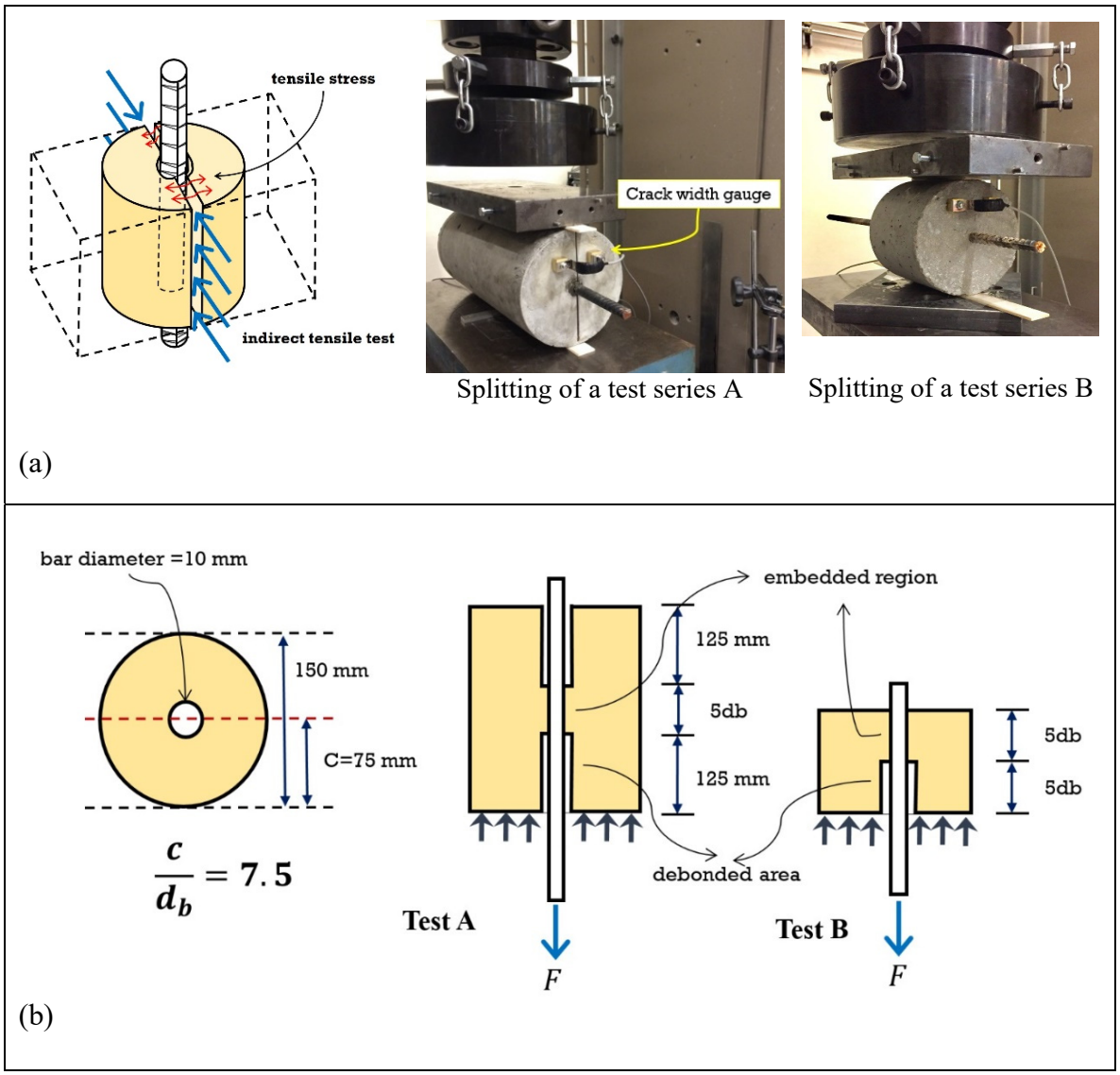

Figure 2.3 Test set-up: (a) pre-cracking by indirect tensile test; (b) pull-out tests

At the completion of a concrete cylinder splitting, the crack width is not instantaneously stabilized and continues to reduce noticeably for a few minutes. So, for uniformity of results, manual measurement of crack width is systematically made immediately after unloading (removal of the load). Photos of crack measurement are shown in Figure 2.4. Although crack gauges are considered for controlling cracks, the highly scattered nature of the concrete, especially in tension, generated different crack widths directly measured after the pre-cracking

test. Due to this scatter, five series of crack widths (w) of 0.10, 0.15, 0.20, 0.30, and one value larger than 0.40 mm are obtained.

$w \geq 0.40$ mm

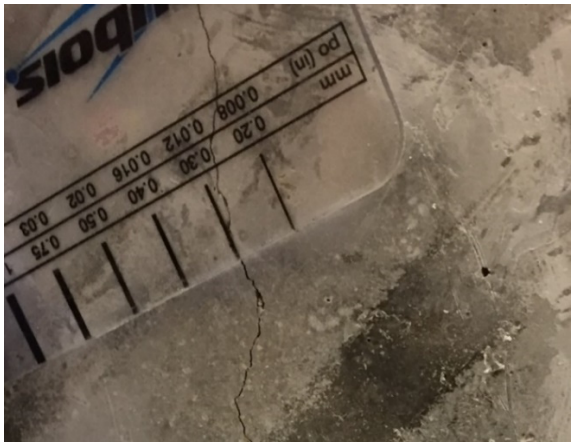

$w = 0.30$ mm

Figure 2.4 Crack measurement just after the pre-cracking test

2.2.2 Experimental results

Details and results of the experimental tests are listed in Table 2.2. Bond strength, τ_{max}, and the residual bond stress, τ_{res}, are reported from obtained experimental bond-slip curves. Normalized bond strength considering the compressive strength of concrete defined by the ratio of $\tau_{max}/\sqrt{f'_c}$ as well as the failure mode (pull-out or splitting) are also reported for each test. To determine the strength reduction due to the pre-cracking phenomenon, bond strength reduction due to the pre-cracking (SR_M) is defined as below:

$$SR_M = \left[\frac{(\tau_{max})_0 - (\tau_{max})_c}{(\tau_{max})_0}\right] \times 100 \qquad (2.1)$$

where $(\tau_{max})_0$ and $(\tau_{max})_c$ are the bond strength of steel rebar in intact and pre-cracked concrete respectively.

Table 2.2 Details of test specimens

Notation		w	d_b	L	f'_c	τ_{max}	$\tau_{max}/\sqrt{f'_c}$	SR_M[1]	τ_{res}	FM[2]
		mm	mm	mm	MPa	MPa	(-)	(%)	MPa	
Test series A	NC1-U	0.00	11.3	$5d_b$	47.90 (1.41)	22.38	3.23		6.04	P
						23.54	3.40		8.38	P
						22.22	3.21		5.80	P
						22.71 (0.71)	3.28 (0.10)	-	6.74 (1.42)	
	NC1-C10	0.10	11.3	$5d_b$	47.90	22.79	3.29		6.75	P
						20.99	3.03		4.90	P
						Failed	-		-	-
						21.89 (1.26)	3.16 (0.18)	3.61	5.83 (1.65)	
	NC1-C15	0.15	11.3	$5d_b$	47.90	18.11	2.62		4.41	P
						18.50	2.67		3.87	P
						Failed	-		-	-
						18.31 (1.57)	2.65 (0.04)	19.37	4.14 (0.38)	
	NC1-C20	0.20	11.3	$5d_b$	47.90	13.07	1.89		2.12	S
						16.28	2.35		0.39	S
						17.97	2.60		3.90	S
						15.77 (2.99)	2.28 (0.36)	30.54	2.14 (1.76)	
Test series B	NC2-U	0.00	11.3	$5d_b$	58.82 (1.39)	25.19	3.28		5.77	P
						25.07	3.27		5.55	P
						27.12	3.54		8.18	P
						25.79 (1.15)	3.36 (0.15)	-	6.50 (1.46)	
	NC2-C30	0.30	11.3	$5d_b$	58.82	12.87	1.68			S
						10.42	1.36			S
						Failed	-			-
						11.64 (1.74)	1.52 (0.23)	54.87	≈ 0	
	NC2-C40	≥0.40	11.3	$5d_b$	58.82	4.72	0.62			S
						4.52	0.59			S
						Failed	-			-
						4.62 (0.14)	0.61 (0.02)	82.10	≈ 0	

[1] Maximum bond stress (bond strength) reduction due to the pre-cracking phenomenon; [2] Modes of failure: P=pull-out; S=splitting; Note: Data inside the parentheses denote the standard deviation.

Two different types of failure modes are observed during the experiments including (1) pull-out of reinforcing rebar failure, and (2) splitting of surrounding concrete failure (Table 2.2). Although transverse reinforcement is ignored in the specimens, confinement provided by the concrete cover ($c/d_b = 7.5$) is enough for preventing splitting failure in intact concrete so that pull-out failures are observed for both NC1-U and NC2-U (Table 2.2). Similar to the un-cracked concrete, induced crack widths smaller than 0.15 mm ($w \leq 0.15$ mm) cause pull-out bond failures (Figure 2.5(a)). However, results show that pre-cracking for crack widths larger than 0.15 mm ($w > 0.15$ mm) changes the failure modes from the pull-out to splitting (Figure 2.5(b)).

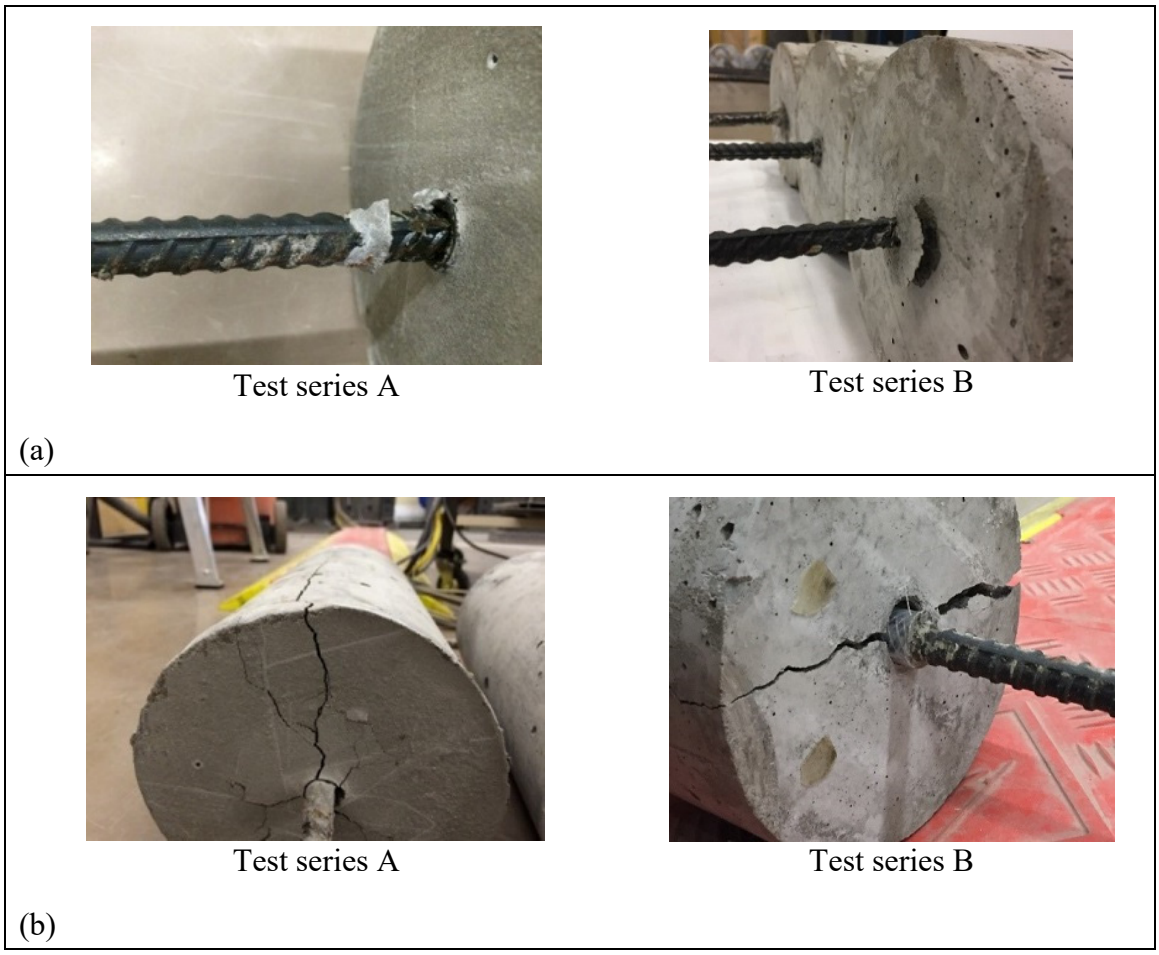

Figure 2.5 Failure modes: (a) pull-out failure; (b) splitting failure

The bond-slip behaviour of steel rebar is noticeably influenced by the presence of initial crack widths (Figure 2.6). Results show that induced cracks of 0.10, 0.15, 0.20, 0.30, and larger than 0.40 mm widths cause 3.61%, 19.37%, 30.54%, 54.87%, and 82.10% reduction in the bond strength, respectively (Figure 2.7(a)). Moreover, crack width larger than 0.15 mm results in more than 50% reduction in residual bond stress so that there is no significant residual strength of concrete with crack widths of 0.30 mm or larger (Figure 2.7(b)). Furthermore, as illustrated in Figure 2.6, a low characteristic energy value (area under the bond-slip curve) is due to the brittle bond behaviour associated with splitting failure modes, while a high energy value results from a ductile bond response associated with pull-out failure (Guizani et al., 2017). Similar to results reported by previous studies (Brantschen et al., 2016; Mahrenholtz, 2012), Figure 3.6 indicates that when cracking width increases, energy absorbed by the bond mechanism significantly decreases. Results also show that pre-cracking has no apparent effect on the slip at which the bond strength is observed. This is coherent and similar to the undefined trend obtained from the experimental literature database (Brantschen et al., 2016; Mahrenholtz, 2012).

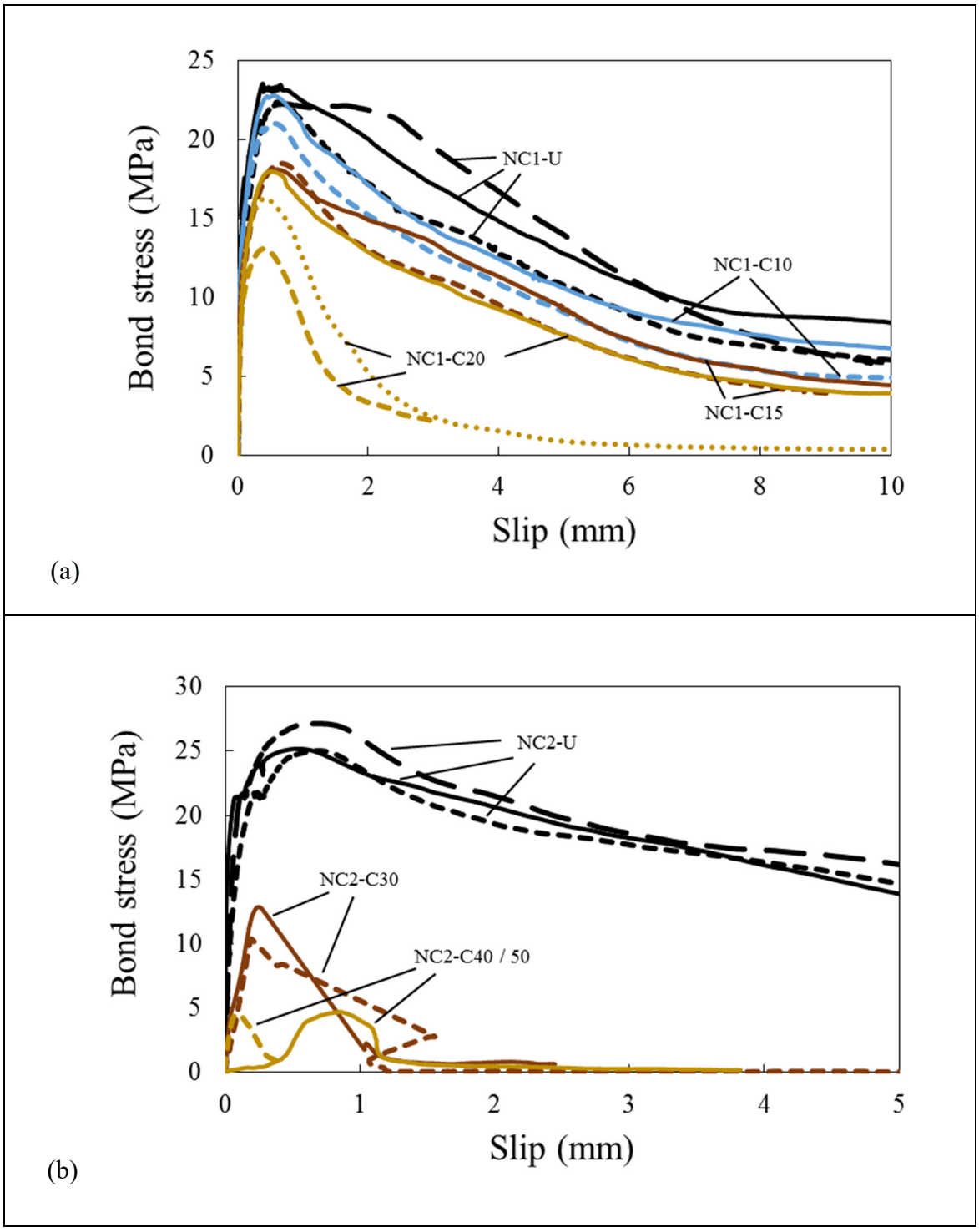

Figure 2.6 Experimental bond-slip curves: (a) test series A; (b) test series B

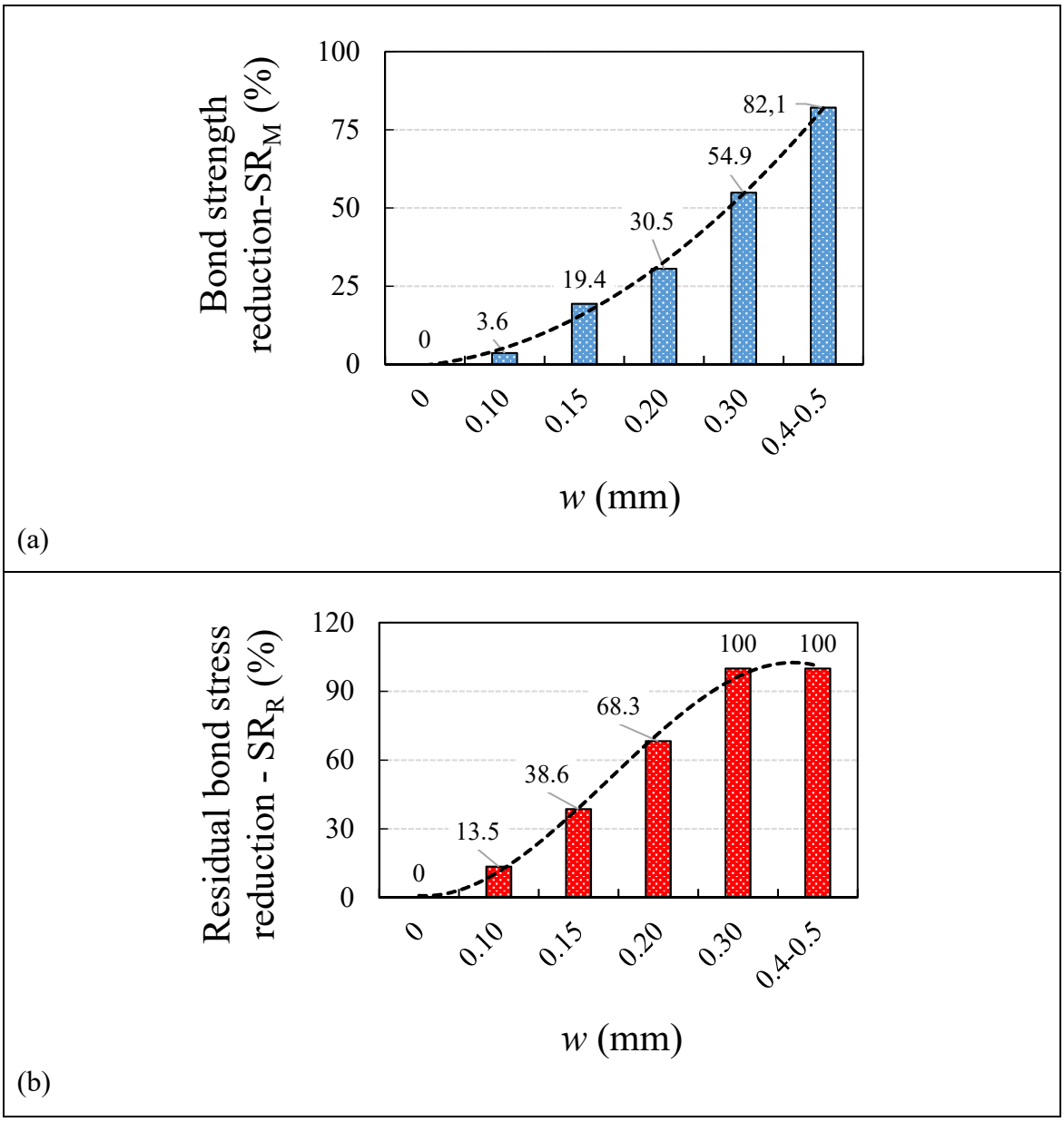

Figure 2.7 Strength reduction versus crack width: (a) bond strength; (b) residual bond stress

2.3 Models for bond strength and development length

In the field of the pre-cracking phenomenon, the bond strength of steel rebar in pre-cracked concrete, $(\tau_{max})_c$, is the only parameter considered by previous studies (Gambarova et al., 1989; Idda, 1999; Mahrenholtz, 2012). Table 2.3 lists existing equations and regulations

presented for predicting the bond strength of steel rebar in pre-cracked concrete. Degeneration of bond strength is introduced as a function of the crack width (w) and rebar diameter (d_b). Crack width-to-rebar diameter ratio, w/d_b, has been found to affect the normalized bond strength of steel rebar in pre-cracked concrete, $(\tau_{max})_c/(\tau_{max})_0$. A similar equation has been suggested by the Model Code 2010 for crack widths smaller than 0.50 mm. However, the effect of crack width-to-rebar diameter ratio, w/d_b, has been ignored in Italian National Code (NTC-08, 2008) and German National Code (DIN-1045-1, 2001) so that the normalized degraded bond strength, $(\tau_{max})_c/(\tau_{max})_0$, is limited to the constant value of $2/3$.

Table 2.3 Existing equations for bond strength in pre-cracked concrete

Reference	**Equation**	
Gambarova et al. (1989)	$\frac{(\tau_{max})_c}{(\tau_{max})_0} = \frac{20}{9}\left[\frac{0.03}{\frac{w}{d_b}+0.05} - 0.15\right]$	
Idda (1999)	$\frac{(\tau_{max})_c}{(\tau_{max})_0} = e^{-5.1\sqrt{\frac{w}{d_b}}}$	
Mahrenholtz (2012)	$\frac{(\tau_{max})_c}{(\tau_{max})_0} = 1 - (10\frac{w}{d_b})$	
German National Code (DIN-1045-1 2001)	$\frac{(\tau_{max})_c}{(\tau_{max})_0} = \frac{2}{3}$	$w \geq 0.20\ mm$
Italian National Code (NTC-08 2008)	$\frac{(\tau_{max})_c}{(\tau_{max})_0} \leq \frac{2}{3}$	$w \leq 0.20\ mm$
Model Code 2010 (fib 2013)	$\frac{(\tau_{max})_c}{(\tau_{max})_0} = 1 - (24\frac{w}{d_b})$	$w \leq 0.50\ mm$

Experimental results available in the related literature (Brantschen et al., 2016; Gambarova et al., 1989; Idda, 1999; Mahrenholtz, 2012) are used to introduce an efficient model for the bond strength of steel rebars in pre-cracked concrete. The properties and results of experimental databases are summarized in Table 2.4. Compressive strength of concrete, f'_c, rebar diameter,

d_b, crack width, w, maximum bond stress (bond strength), τ_{max}, residual bond stress, τ_{res}, slip at the maximum bond stress, s_m, and normalized dissipated energy, E_c/E_0, are the key parameters summarized in Table 2.4. Maximum and minimum crack widths of 0.10 and 1.0 mm respectively are reported for this database.

Table 2.4 Summarized test conditions and bond results from the literature

Reference	f'_c	d_b	w	τ_{max}	τ_{res}	s_m	E_c/E_0
	MPa	mm		MPa		mm	
Gambarova et al. (1989)	40.2	18	0.00	18.49	16.31	1.06	1.00
	40.2	18	0.10	15.00	13.14	0.90	0.82
	40.2	18	0.20	13.89	11.14	0.88	0.71
	40.2	18	0.30	13.10	10.58	0.78	0.67
Idda (1999)	19.2	16	0.00	12.10	4.81	1.45	1.00
	19.2	16	0.25	8.55	2.82	1.52	0.66
	19.2	16	0.50	7.38	2.04	1.55	0.49
	19.2	16	0.75	5.82	1.39	1.53	0.37
	19.2	16	1.00	4.99	1.08	1.88	0.31
Mahrenholtz (2012)	19.1	16	0.00	7.80	2.55	1.66	1.00
	19.1	16	0.10	7.40	2.69	1.89	0.93
	19.1	16	0.40	5.81	2.11	1.92	0.74
	19.1	16	0.80	3.78	1.14	1.98	0.44
Brantschen et al. (2016)	30.1	10	0.00	12.91	4.74	0.77	1.00
	30.1	10	0.20	7.67	2.22	1.05	0.52
	30.1	10	0.50	2.94	0.95	0.96	0.17
	30.1	10	1.00	1.53	0.19	0.08	0.05
	30.1	14	0.00	10.88	4.10	0.60	1.00
	30.1	14	0.20	6.06	1.87	1.13	0.50
	30.1	14	0.50	3.08	0.80	0.94	0.23
	30.1	14	1.00	1.83	0.27	0.12	0.08
Range	19-40	10-18	0-1	1-18	0.19-16	0.08-2	0.08-1

2.3.1 New model for bond strength in pre-cracked concrete

A modified local bond-slip model under monotonic loading is proposed, as illustrated in Figure 2.8. Five characteristic response parameters (CP), namely bond strength for pre-cracked

concrete, $(\tau_{max})_c$, residual bond stress for pre-cracked concrete, $(\tau_{res})_c$, slip corresponding to the bond strength of pre-cracked concrete, $(S_m)_c$, slip corresponding to the residual bond stress of pre-cracked concrete, $(S_{res})_c$, and a coefficient related to the nonlinear shape of the initial ascending branch, α, define the envelope curve of this model as expressed in Eq. (2.2).

$$\begin{cases} \tau_c = (S/(S_m)_c)^{\alpha}(\tau_{max})_c & for\ 0 \le S < (S_m)_c \\ \tau_c = (\tau_{max})_c - ((\tau_{max})_c - (\tau_{res})_c)(S - (S_m)_c)/((S_{res})_c - (S_m)_c) & for\ (S_m)_c \le S < (S_{res})_c \\ \tau_c = (\tau_{res})_c & for\ S \ge (S_{res})_c \end{cases} \quad (2.2)$$

where the bond stress of steel rebar in pre-cracked concrete is presented as a function of slip, $\tau_c = f(S)$. The subscripts "c" and "0" denote pre-cracked and un-cracked concrete respectively. In addition to these CPs, the characteristic energy absorbed by the bond mechanism, E, is used to compare the behaviour of steel rebars in intact and pre-cracked concrete (Guizani et al., 2017). The characteristic energy is defined as the area below the bond-slip curve between the origin, and the slip corresponding to the residual bond stress, that is S_{res} (Figure 2.8).

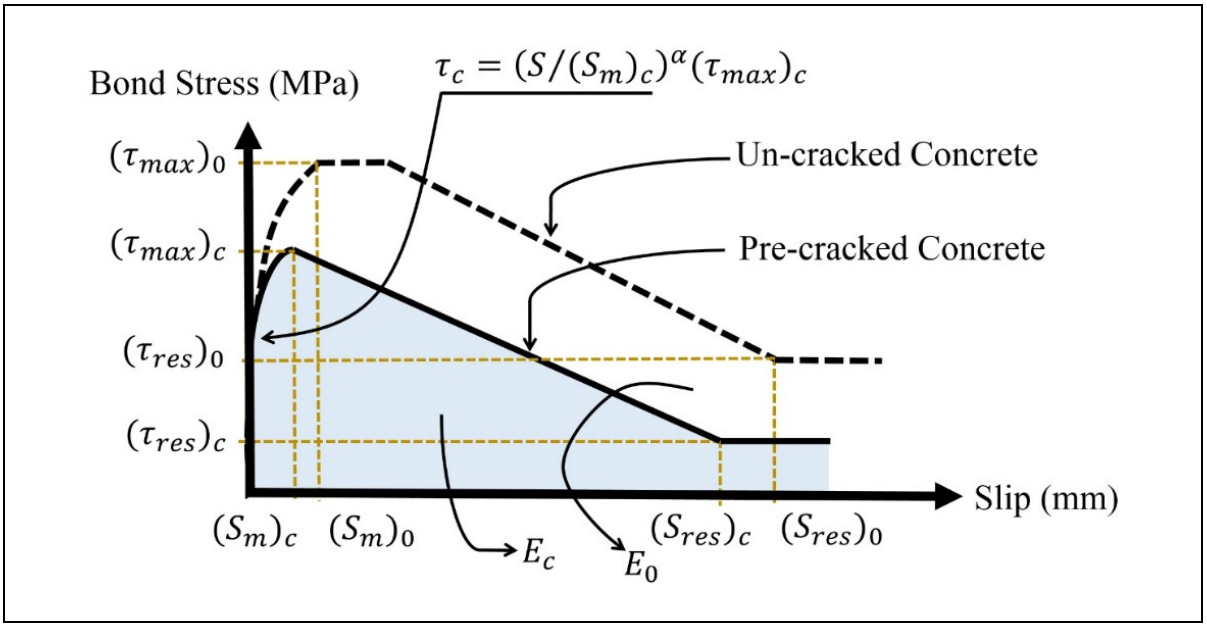

Figure 2.8 Proposed bond-slip model for pre-cracked concrete

Although there is a plateau after the bond strength for confined (by enough concrete cover) un-cracked concrete (Figure 2.6), a sudden drop is reported for pre-cracked concrete which is considered in the proposed local bond-slip envelope (Figure 2.8). Results also show that as crack width increases, the slope of the descending branch of the envelope increases, meaning a more rapid drop in bond stress with increasing slip.

As mentioned in Table 2.3, the ratio of crack width-to-rebar diameter (w/d_b) has been considered by previous studies (Gambarova et al., 1989; Idda, 1999; Mahrenholtz, 2012) as the main parameter for the derivation of the bond strength of rebar in pre-cracked concrete, $(\tau_{max})_c$, from those of un-cracked concrete, $(\tau_{max})_0$. A similar format is considered for obtaining CPs used in the proposed bond-slip envelope curve. Each of these parameters is accurately calibrated for pre-cracked concrete using regression analyses on the results of the literature database.

The obtained predictive equation for the absorbed energy under the bond-slip envelope for pre-cracked concrete, E_c, can be written as ($R^2 = 0.87$, Figure 2.9):

$$\frac{E_c}{E_0} = e^{-27.91\left(\frac{w}{d_b}\right)} \tag{2.3}$$

where E_0 is the area under the bond-slip curve of intact concrete. As the crack width increases, absorbed energy decreases which shows the more brittle behaviour of rebar-concrete bond response. For a given pre-crack width, more damage and less characteristic absorbed energy are expected as the rebar diameter decreases. Low normalized energy dissipated is associated with a brittle bond response associated with moderately and unconfined concrete, while a high energy value shows a ductile bond response tending toward confined concrete bond response (Guizani et al., 2017). The effect of this parameter has been included in the Eligehausen-Filippou model (Eligehausen et al., 1983), in which degradation of bonds under cyclic loading is considered by a damage index defined as a function of normalized dissipated energy.

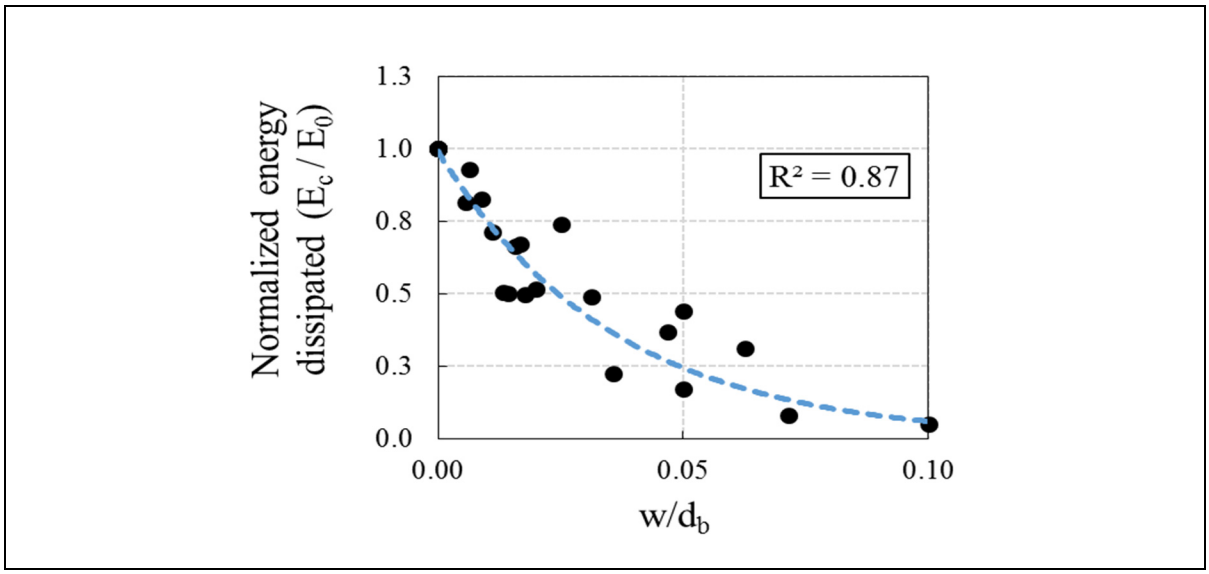

Figure 2.9 Normalized absorbed energy by the bond mechanism in Eq. (2.3)

Using the database extracted from the referenced literature and trial-and-error based algorithms, the obtained best-fitted equation for predicting the degraded bond strength of steel rebars in NC as a function of the crack width, w, unaltered concrete bond strength, $(\tau_{max})_0$, and rebar diameter, d_b, can be written as:

$$\frac{(\tau_{max})_c}{(\tau_{max})_0} = e^{-21.15\left(\frac{w}{d_b}\right)} \tag{2.4}$$

Figure 2.10 shows a good fit of Eq. (2.4) to the experimental database. The lower and upper values predicted by Eq. (2.4) are 1.0 and 0.12, respectively. The upper value applies for un-cracked concrete while the lower value corresponds to a crack width-to-rebar diameter ratio of 0.10. As the proposed equation for reduced bond strength, Eq. (2.4), is similar to the format of the equation presented by Idda (1999) in Table 2.3, a comparison is illustrated in Figure 2.10. Contrarily to the proposed equation, the model of Idda (1999) leads to a considerable overestimation of the reduced bond strength for all crack widths (Figure 2.10). Comparison of results also indicate that the predicting equation presented by Mahrenholtz (2012) overestimates the reduced bond strength for $w/d_b \leq 0.05$, while underestimated predictions are obtained for larger crack widths. Among the existing equations listed in Table 2.3, the one

presented by Gambarova et al. (1989) shows very similar results to Eq. (2.4), as illustrated in Figure 2.10.

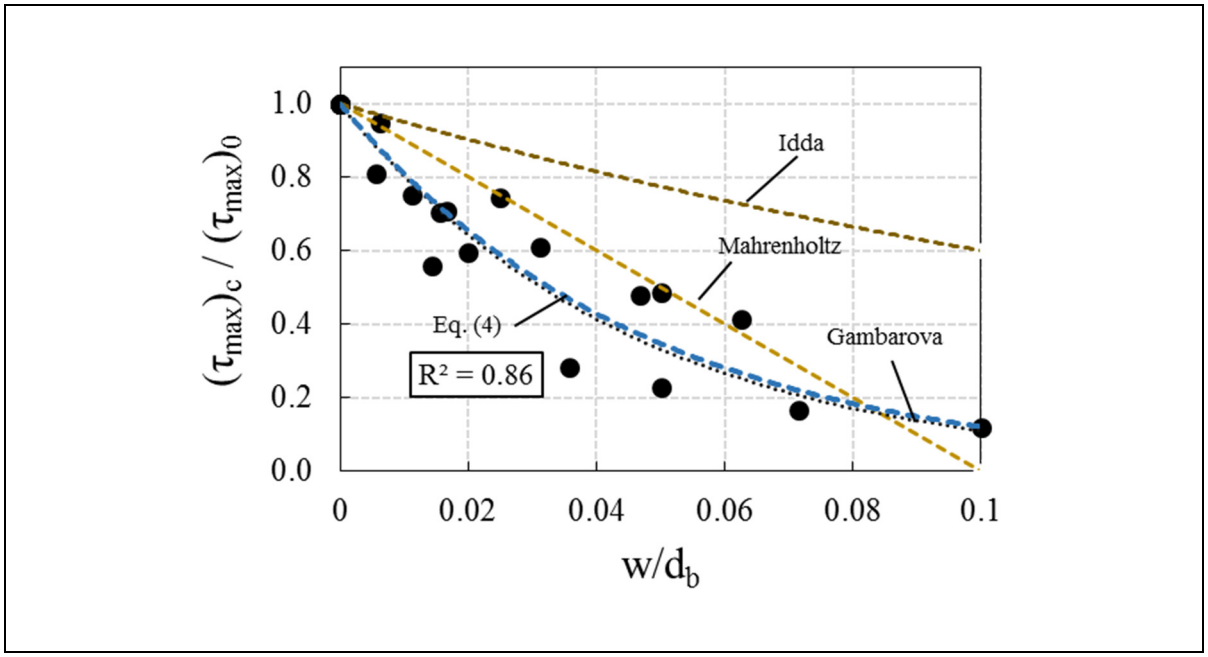

Figure 2.10 Decrease of bond strength in the presence of cracks according to Eq. (2.4) and existing models

The deviation of the predicting equations from the experimental database for bond strength is evaluated through the term of Integral Absolute Error (IAE) (Mousavi et al., 2017; Mousavi et al., 2016), and the conventional statistical analyses of the experimental-to-theoretical value ratio υ, as defined in Eq. (2.5) and Eq. (2.6) respectively. The IAE is more sensitive than υ to the deviation between the models and database (Mousavi et al. 2017; Wu and Zhao 2012). Models with lower IAE percent and υ factor close to unity indicate a better correlation with the test results.

$$\text{IAE} = \sum \frac{\sqrt{[Experimental((\tau_{max})_c/(\tau_{max})_0) - Theoretical((\tau_{max})_c/(\tau_{max})_0)]^2}}{\sum Experimental((\tau_{max})_c/(\tau_{max})_0)} \qquad (2.5)$$

$$\upsilon = \frac{Experimental((\tau_{max})_c/(\tau_{max})_0)}{Theoretical((\tau_{max})_c/(\tau_{max})_0)} \quad (2.6)$$

The evaluation of the degraded bond strength, Eq. (2.4), with the current experimental test results and all databases is shown in Figure 2.11. Results show that Eq. (2.4) has the lowest IAE compared to the other equations for both series of data including "Current Study" (12.81%) and "Database+Current Study" (11.08%). Also, Eq. (3.4) generates the closest value of υ to unity (υ=0.99) among the seven models studied for the entire experimental database (current tests and referenced literature). Among the existing equations for predicting degraded bond strength, predictions of the model presented by Gambarova et al. (1989) are very close to the Eq. (2.4) and show acceptable results. However, it generates a slightly larger derivation value from all experimental database compared to the proposed model. Similar to Figure 2.10, equation developed by Idda (1999) significantly overestimates the reduced bond strength so that IAE and υ are 18.68% and 1.15 respectively for all databases. The amount of experimental data with the variation of crucial parameters has a considerable effect on the performance of a model. When more data is available, the proposed model shows a better estimation of the bond strength of steel rebars in pre-cracked concrete.

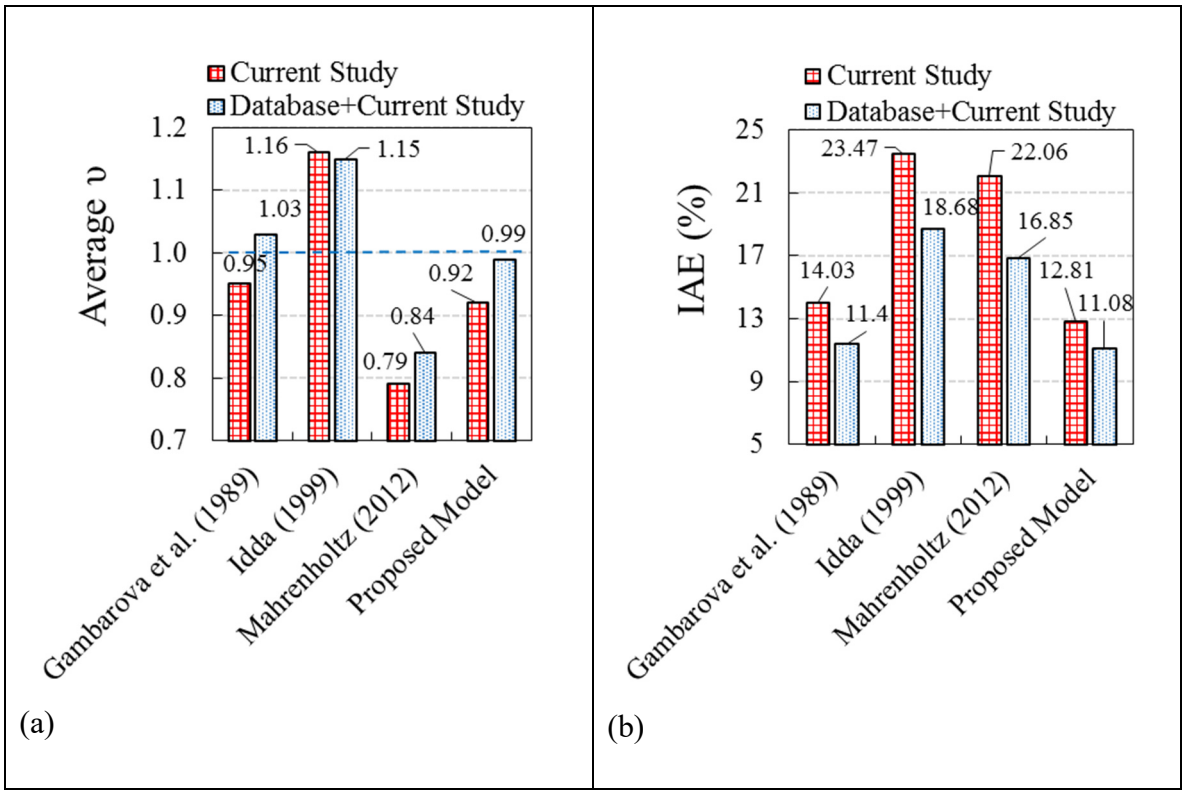

Figure 2.11 Performance of Eq. (2.4) for predicting bond strength of steel rebars in pre-cracked concrete compared to existing models: (a) Average υ; (b) IAE

A crack width of 1.2 mm for 12 mm diameter rebar, which corresponds to a $w/d_b = 0.10$, is expected to induce a 88% reduction in the bond strength (Eq. (2.4)). A smaller crack width of 0.50 mm results in a 59% reduction in the bond strength of such rebar. Eq. (2.4) also indicates a lower sensitivity of reinforced concrete to pre-cracking for larger rebar diameters. As mentioned in Eq. (2.4), crack width is related to the reduced bond strength by the rebar diameter, d_b. Hence, it can be deduced from the Eq. (2.4) that for a constant value of crack width, larger rebar diameter leads to lower damages due to the pre-cracking phenomenon. To explain this mechanism, the ratio of the crack width-to-the perimeter of reinforcing rebar in contact with surrounding concrete, $w/(\Sigma p)$ or $w/(\pi d_b)$. This parameter measures the unbonded portion of the rebar external surface area. As this ratio (or indicator) increases, reduction in bond strength increases indicating higher damage due to the pre-cracking phenomenon, as schematically illustrated in Figure 2.12.

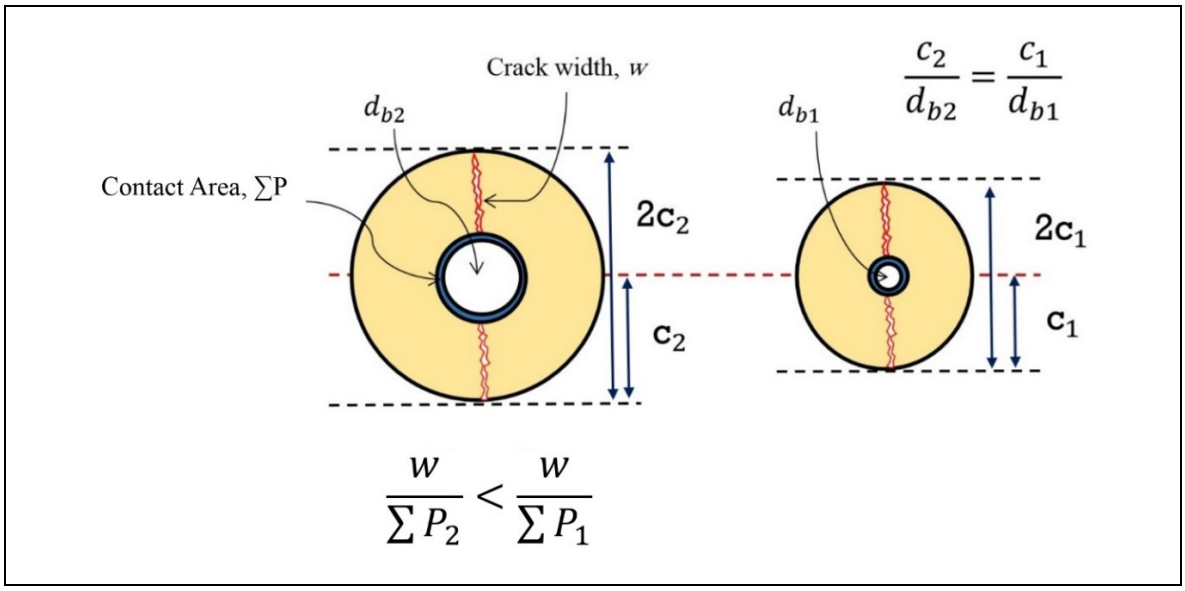

Figure 2.12 Schematic view of the effect of the rebar diameter on the pre-cracking phenomenon for a constant value of crack width

Using the experimental database for the normalized degraded residual bond stress, the following regression relationship is obtained:

$$\frac{(\tau_{res})_c}{(\tau_{res})_0} = e^{-30.43\left(\frac{w}{d_b}\right)} \tag{2.7}$$

Although Eq. (2.7) is physically reasonable and presents a satisfactory fit with database results ($R^2 = 0.89$, Figure 2.13), one out-of-trend point exists indicating higher residual bond stress of pre-cracked concrete in comparison with the intact concrete. Comparing the proposed equations of (2.4) and (2.7) shows that the pre-cracking phenomenon has a higher impact on the residual bond stress compared to the bond strength. For instance, crack width-to-rebar diameter 0.02 leads to 34.5% and 45.6% reduction in the bond strength and the residual bond stress, respectively. As illustrated in Figure 2.6, similar results are observed from the experimental tests of the current study so that a crack width of 0.20 mm results in 30.5% and 68.3% reduction in maximum and residual bond stress respectively.

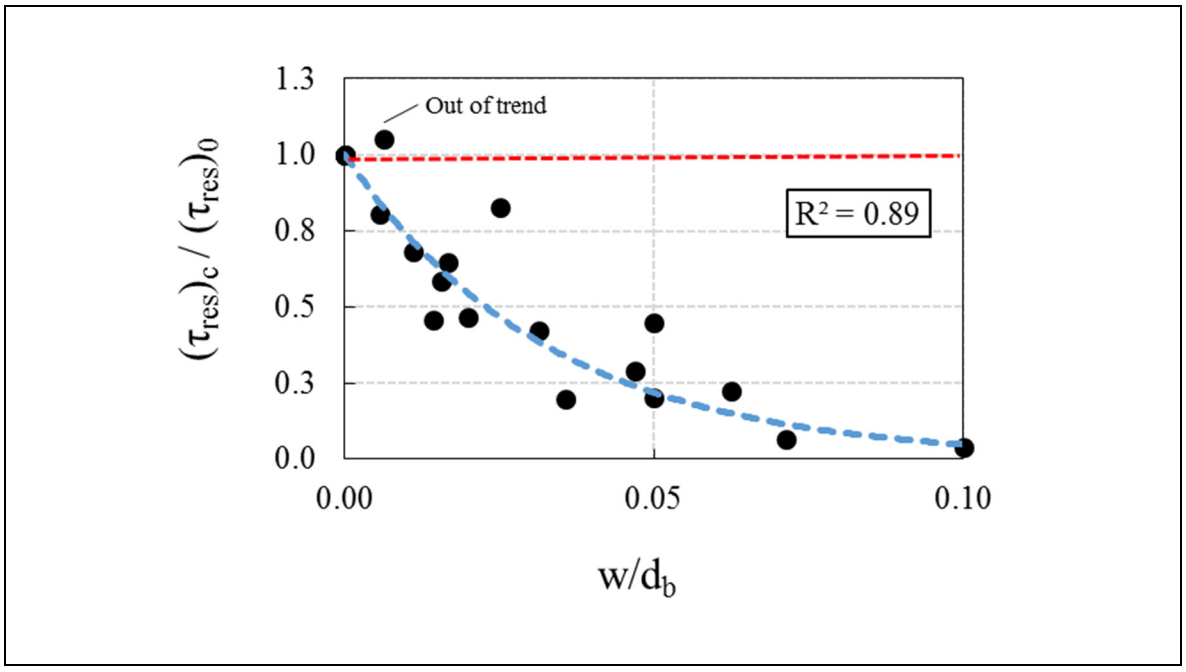

Figure 2.13 Efficiency of Eq. (2.7) for predicting the normalized residual bond stress

Contrarily to Eqs. (2.4) and (2.7), there is no clear trend for variation of the slip corresponding to the bond strength, S_m, with a crack width-to-rebar diameter ratio. The following regression ($R^2 = 0.49$, Figure 2.14) is proposed:

$$\frac{(S_m)_c}{(S_m)_0} = -256.18\left(\frac{w}{d_b}\right)^2 + 15.35\left(\frac{w}{d_b}\right) + 1 \qquad (2.8)$$

The regression of $(S_m)_c/(S_m)_0$ is more difficult because an appropriate function is difficult to obtain directly from the experimental database. Scrutiny of Figure 2.13 reveals that for the range of $w/d_b \leq 0.04$, $(S_m)_c/(S_m)_0$ seems to be slightly increasing as w/d_b increases. However, this trend is not manifested across the whole database so that for the range of $0.04 < w/d_b \leq 0.10$, an increase in w/d_b leads to a significant reduction of $(S_m)_c/(S_m)_0$. Similar difficulties have been pointed out by previous researches (Eligehausen et al. 1983; Guizani et al. 2017) to accurately predict this parameter for concrete. For large crack widths, $0.07 < w/d_b$, Eq. (2.8) gives a very small normalized slip, $(S_m)_c/(S_m)_0 \leq 0.25$, attributed to the short ascending branch of the bond-slip curve. As illustrated in Figure 2.14, two points are out

of the trend (Eq. (2.8)) in predicting the slip corresponding to the bond strength for pre-cracked concrete, $(S_m)_c$, including 1) $w = 0.20\ mm$, $d_b = 14\ mm$ in Brantschen et al. (2016); and 2) $w = 1.0\ mm$, $d_b = 14\ mm$ in Brantschen et al. (2016). They are probably due to the large scatter and the low correlation associated with the slip at maximum bond stress (Eligehausen et al., 1983; Guizani et al., 2017).

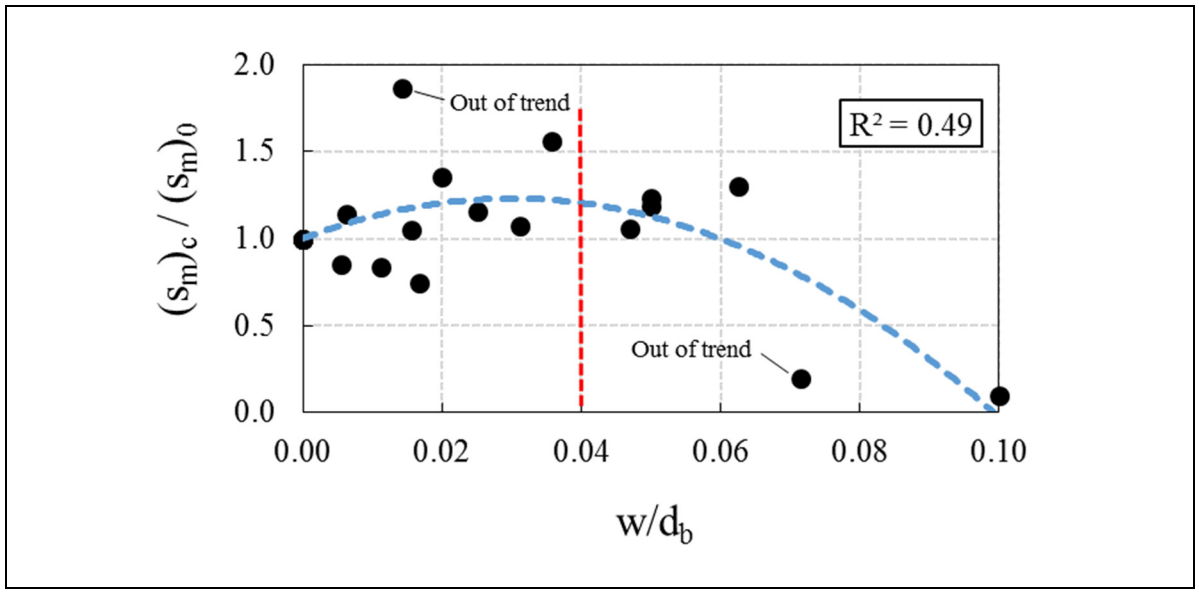

Figure 2.14 Efficiency of Eq. (2.8) for predicting normalized slip corresponding to the bond strength

The parameter α, defining the nonlinear shape of initial ascending branches of the bond-slip envelope is set equal to the value suggested by fib Model code 2010, $\alpha = 0.40$. The normalized slip corresponding to the residual bond stress,$(S_{res})_c$, is calculated regarding the w/d_b ratio by the following regression equation ($R^2 = 0.85$, Figure 2.15):

$$\frac{(S_{res})_c}{(S_{res})_0} = 85.31\left(\frac{w}{d_b}\right)^2 - 12.32\left(\frac{w}{d_b}\right) + 1 \qquad (2.9)$$

As crack width increases, the slope of the proposed model reduces so that for $w/d_b \geq 0.04$, the pre-cracking phenomenon has no impact on slip corresponding to the residual bond stress

(Figure 2.15). Lower $(S_{res})_c$ for $w/d_b < 0.04$ can be associated with lower energy absorbed by the bond mechanism as the crack width increases and the slip by wedging of the concrete key becomes predominant, as for unconfined concrete.

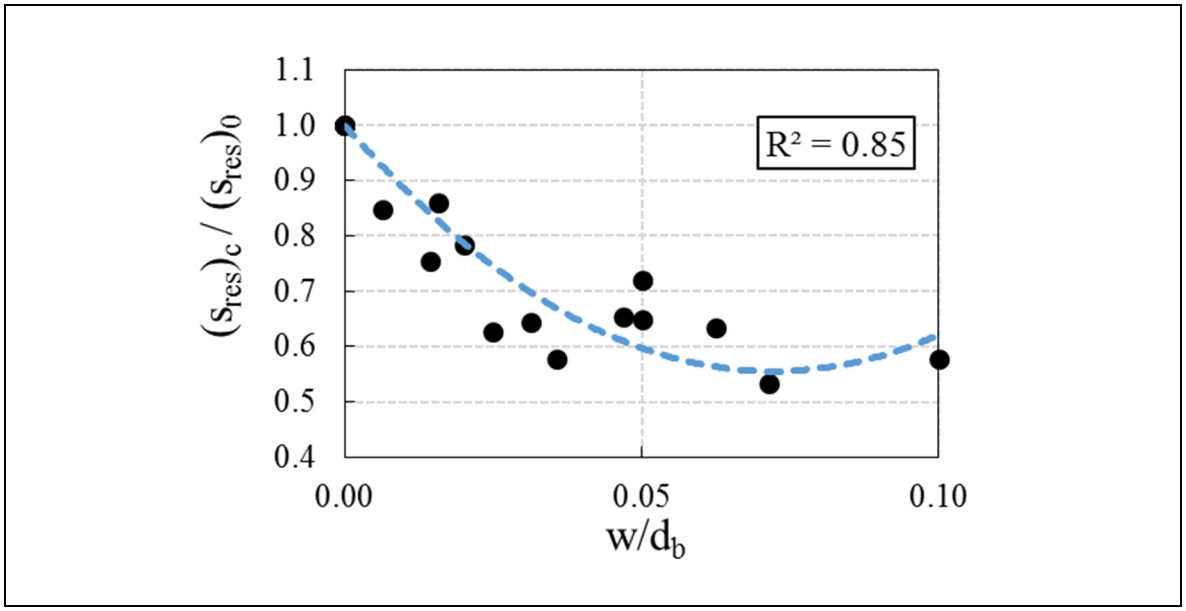

Figure 2.15 Efficiency of Eq. (2.9) for normalized slip corresponds to residual bond stress

2.3.2 New model for development length in pre-cracked concrete

The minimum embedded length of rebar in surrounding concrete to develop the maximum tensile stress, that is yield stress, f_y, is called development length. Reinforcement rebars with good bond conditions require shorter development lengths thanks to the higher bond strength that can be mobilized along the rebar. Different normalized equations are considered in the specifications for the development length of steel rebars in NC. ACI 318R (2014) introduces the general Eq. (2.10) to determine development length of tension-loaded straight steel rebar in normal intact concrete, l_d (mm).

$$l_d = \left[\frac{f_y}{1.1\lambda\sqrt{f_c}}\frac{\Psi_t\Psi_e\Psi_s}{\left(\frac{c+K_{tr}}{d_b}\right)}\right]d_b \tag{2.10}$$

where f_y is the yield stress of the steel rebar in MPa, and c is the concrete cover in mm. Factors Ψ_t, Ψ_e, and λ take into account the effects of rebar location, epoxy coating and lightweight concrete respectively. A rebar location factor of 1.3 is used in American (ACI 318R, 2014) and Canadian standards (CSA A23.3, 2014)) for rebar placed so that more than 300 mm of fresh concrete is cast below and 1.0 for other rebar location. ACI 318R (2014) defines different values for coating factors including 1.5 for epoxy-coated rebar with concrete cover less than $3d_b$ or clear spacing less than $6d_b$, 1.2 for other epoxy-coated rebars, and 1.0 for uncoated rebar. CSA Code (A23.3, 2014) and ACI Code (ACI 318R, 2014) standards specify 0.75 for lightweight concrete and 1.0 for normal-weight concrete. The term Ψ_s is a factor for rebar size in which the value of 0.8 has been considered for rebar diameter of No. 19 or smaller and 1.0 for other diameters. In the Eq. (2.10), K_{tr} defines the effect of stirrups and confinement on the bond strength, which is ignored in this study. However, similar to confinement provided by stirrups, the concrete cover leads to an important influence on confinement around the rebar by resisting hoop stresses (Desnerck et al., 2015) leading to an increase in bond strength. The effect of concrete cover is considered in Eq. (2.10) by the term c normalized by rebar diameter, d_b. As expressed in previous research (Mousavi et al., 2017), Eq. (2.10) can be written in the form of Eq. (2.11):

$$l_d = M\left(\frac{A_b f_y}{\sqrt{f'_c}}\right) \tag{2.11}$$

where A_b is the area of steel rebar and M is an empirical factor in 1/mm, which is deduced from Eqs. (2.10) and (2.11) based on ACI Code (ACI 318R, 2014):

$$M_{ACI} = \frac{4}{1.1\lambda\pi}\left[\frac{\Psi_t\Psi_e\Psi_s}{c+K_{tr}}\right] \quad (2.12)$$

By evaluating the equilibrium equation along the embedded length of the steel rebar, the following equation is obtained:

$$\frac{\pi d_b^2}{4} f_y = \tau_{ave}\pi d_b l_d \quad (2.13)$$

where τ_{ave} is the average bond stress around the steel reinforcing rebar at its interface with the surrounding concrete. Therefore, the development length is given alternatively by Eq. (2.14):

$$l_d = \frac{f_y d_b}{4\tau_{ave}} \quad (2.14)$$

The equilibrium Eq. (2.13) presumes that the bond stress is constant and equal to the average bond stress along the embedded length of the steel rebar, which is considered by previous research (Dehestani & Mousavi, 2015). For short embedded length (generally five times the rebar diameter or less such as the current study), bond stress is observed to be close to having a uniform distribution and can be used to get a better measure of local bond strength. Even for longer embedded lengths, this hypothesis leads to an acceptable result for analyzing reinforced concrete (RC) members such as two-way RC slab (Dehestani & Mousavi, 2015), anchorage bond strength in high-performance concrete (Yerlici & Ozturan, 2000), in-plane behaviour of masonry infilled concrete frames (Nasiri & Liu, 2017), and RC bridge deck slabs under cyclic moving loads (Deng & Matsumoto, 2018). In a long embedded length, concrete and steel rebar have the same strain at the middle distance between two adjacent cracks, especially for constant moment region (Mousavi et al., 2017; Mousavi et al., 2016). However, there is no bond stress in the pre-cracked section, which results in strain and stress concentration. The yield strain is obtained by $\varepsilon_y = f_y/E_s$ which is in the range of 0.002 to 0.003 for a f_y ranging from 400 MPa to 600 MPa. The cracking strain at cracking tensile stress of concrete is about 0.00008, which is more than 20 times lower than the yield strain of steel (Belarbi & Hsu, 1994). So, it is clear

that multiple cracks can take place in a long embedded length before steel yielding. The section experiences bond strength after generating deep cracks, which is associated with commencing stress concentration in steel. This leads to considering $\tau = f_y d_b / 4L$ as a controlling value at long embedded members (Mousavi et al., 2017). Hence, a constant value can be reasonably used for bond strength along the embedded length of steel rebars. By equating Eqs. (2.11) and (2.14), the empirical factor M can be expressed as:

$$M_{Exp} = \frac{\sqrt{f'_c}}{\pi d_b \tau} \tag{2.15}$$

The range of factor M can be obtained from the database of experimental tests. The efficiency of this approximate calculation of development length by Eq. (2.15) has been discussed and established by previous research (Mousavi et al., 2017; Mousavi et al., 2016). As shown in Figures 2.7(a) and 10, the bond strength of steel rebars in pre-cracked concrete is lower than for intact (un-cracked) concrete, which leads to larger development length. However, there is no consideration in ACI Code (ACI 318R, 2014) for crack width. Hence, this paper proposes an increase factor, K_I, for increasing the development length, $(l_d)_{Pre-cracked} = K_I \times (l_d)_{un-cracked}$, which can be obtained as:

$$\left(M_{Exp}\right)_{Pre-cracked} = K_I (M_{Exp})_{Un-cracked} \tag{2.16}$$

Finally, based on the experimental database of related references, the following equation fits the increase factor, K_I, as a function of the crack width:

$$K_I = e^{21.06\left(\frac{w}{d_b}\right)} \tag{2.17}$$

Figure 2.16 shows the correlation of Eq. (2.17) to the value of w/d_b fitted from the experimental database ($R^2 = 0.87$). Practical use of Eq. (2.17) is a member exposed to a severe exposure condition. Figure 2.1 illustrates that when a reinforced concrete member exposed to a severe exposure condition, crack width should be limited to the value of 0.33 mm based on the ACI Code (ACI 318R, 2014) recommendation. This crack width only prevents

accelerated and/or rapid corrosion phenomenon while bond behaviour would be significantly affected by the existence of that crack at the steel rebar-concrete interface. Eq. (2.17) suggests that for this environmental condition, development length should be increased by 78.0% (for $d_b = 12$ mm) to provide reliably embedded length when such cracks can run parallel to the rebars.

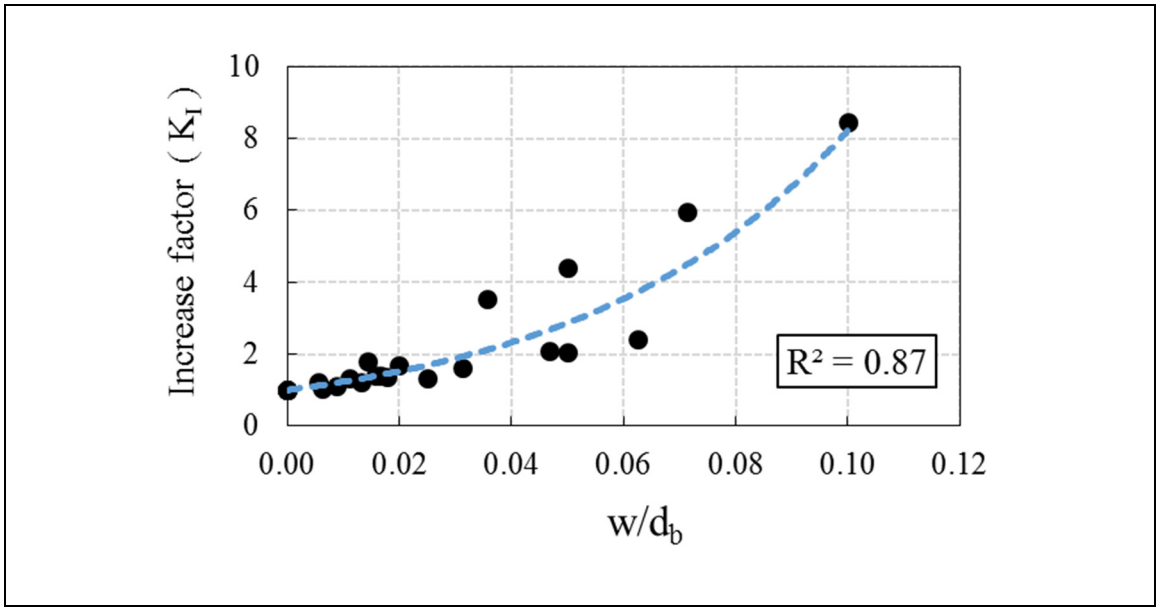

Figure 2.16 Performance of Eq. (2.17) for the increase factor of development length in pre-cracked concrete

By applying increase factor (K_I) from Eq. (2.17) or using the ratio of $(M_{Exp})_{Pre-cracked}/(M_{Exp})_{Un-cracked}$, Eq. (2.12) can be rewritten as follows:

$$M_{Modified-ACI} = \frac{4}{1.1\lambda\pi}\left[\frac{\Psi_t\Psi_e\Psi_s}{c + K_{tr}}\right]K_I \tag{2.18}$$

Finally, based on the accuracy of Eq. (2.18), modified ACI formulation for development length of steel rebars in pre-cracked concrete is given by Eq. (2.19):

$$l_d = \left[\frac{f_y}{1.1\lambda\sqrt{f'_c}}\frac{\Psi_t\Psi_e\Psi_s}{\left(\frac{c+K_{tr}}{d_b}\right)}\right] d_b e^{21.06\left(\frac{w}{d_b}\right)} \tag{2.19}$$

2.4 Validation of the proposed model

To verify the efficiency of the proposed bond-slip model for un-cracked concrete, its predictions are compared to some envelope curves from the experimental database. As shown in Figure 2.17, results indicate that the proposed model is in good agreement with the experimental database for small crack width ($w < 1.0$ mm). In terms of maximum and residual bond stress, the proposed model gives a more conservative prediction but with a slower descending slope in comparison with test results of Mahrenholtz (2012) (Figure 2.17(a)), whereas a nearly exact match with the test curve of Idda (1999) is observed for the proposed model (Figure 2.17(b)).

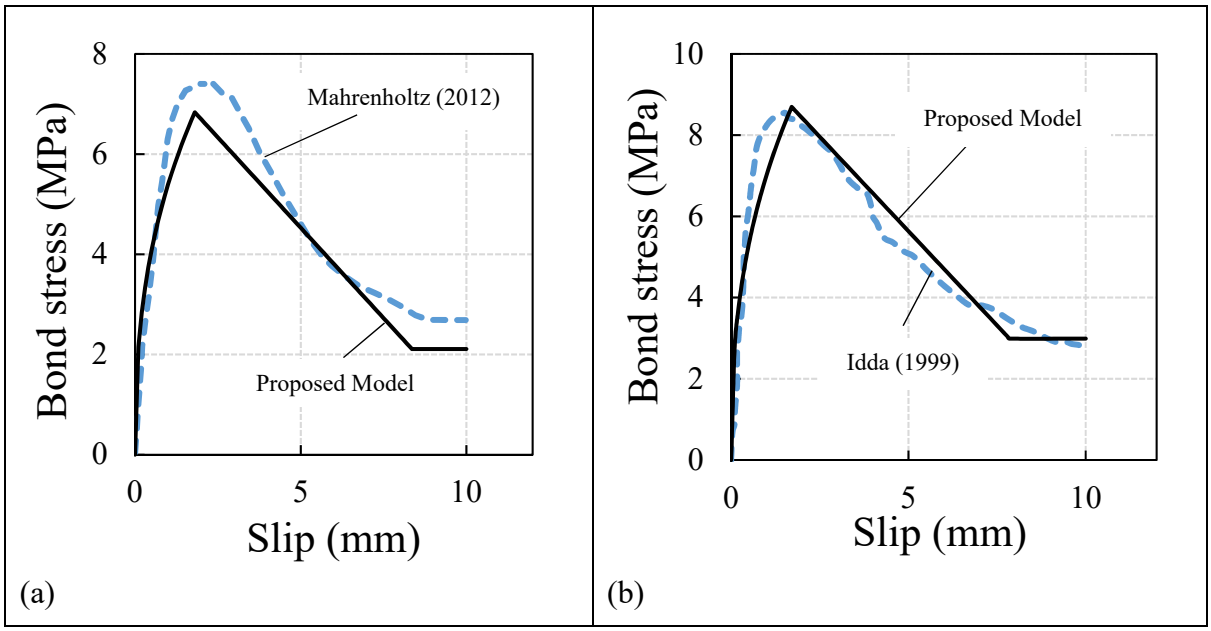

Figure 2.17 Validation of proposed bond-slip model for small crack width by:
(a) Mahrenholtz (2012), w=0.10 mm ($c/d_b \approx 12.5,\ E_c/E_0 = 0.93$);
(b) Idda (1999), w=0.25 mm ($c/d_b \approx 6.25,\ E_c/E_0 = 0.66$)

The differences are mainly attributed to the highly scattered nature of the concrete bond-slip response, which can be exacerbated by the presence of initial cracks. Such deviations between predictive models and experimental results have been reported by many researchers who introduced different bond-slip models for intact concrete (Guizani et al., 2017; Wu & Zhao, 2012). Figure 2.18 examines the performance of the proposed model for a large crack width (w=1.0 mm). Although the bond strength and residual bond stress are accurately predicted, the proposed model overestimates the absorbed energy (area under the curve) which can be attributed to the limit of the current database for a large crack width. There is a limit value of the characteristic energy ratio, E_c/E_0, about 0.37, below which the proposed model is not efficient as the bond stress decreases more quickly, indicating a brittle behaviour. This is explained by the fact that for lower values, slip mechanism is radically different and takes place by wedging of the concrete key around the reinforcing rebar. Considering the most significant importance of bond strength in standards rather than absorbed bond energy, the proposed model performs very well in the case of large crack width. However, more experimental test results are deemed necessary to validate and increase the precision of the model.

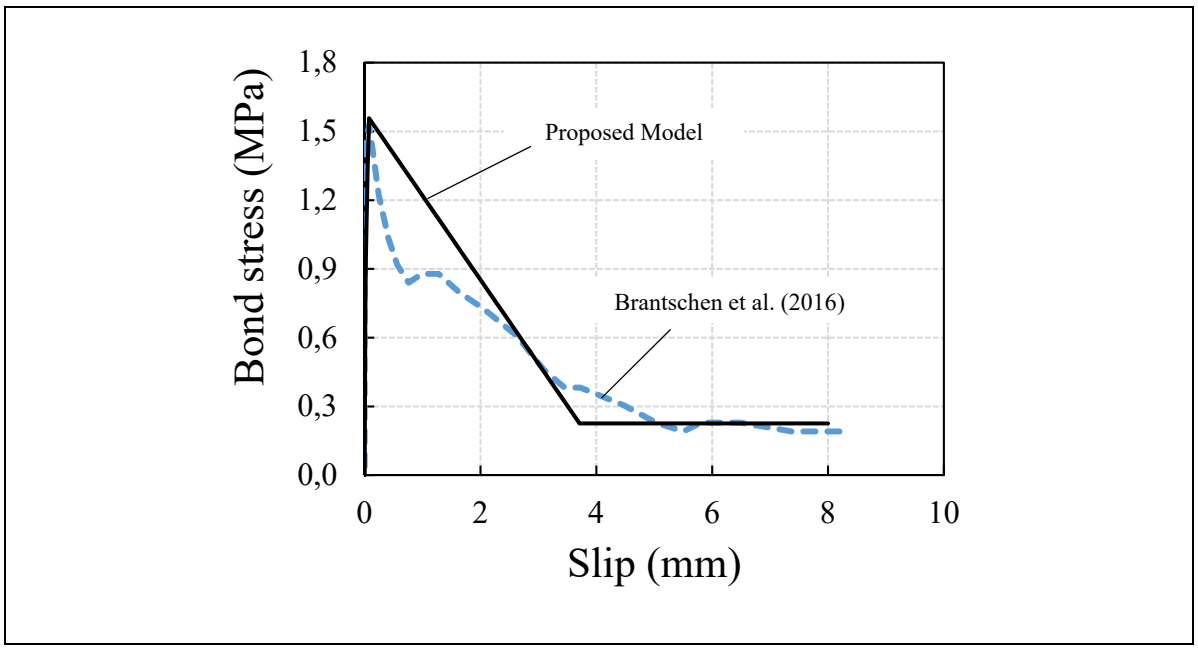

Figure 2.18 Proposed bond-slip model versus experimental database (Brantschen et al. (2016) for large crack width (w=1.0 mm, $c/d_b \approx 15, E_c/E_0 = 0.05$, four 18 mm diameter longitudinal rebars for controlling cracks)

Validation of the proposed model with experimental results obtained in this study is illustrated in Figure 2.19. Results show that the proposed bond-slip model for pre-cracked concrete is in good agreement with experimental curves of the current pull-out tests for crack widths up to 0.20 mm (Figure 2.19(a-c)). Generally, the bond strength predicted by the proposed model is slightly lower than the measured bond strength obtained from the current pull-out tests so that 13.96%, 6.33%, and 0.96% reductions are found for crack widths of 0.10 mm, 0.15 mm, and 0.20 mm respectively (Figure 2.19(a-c)). The proposed model is found to accurately estimate the residual bond stress for all crack widths (Figure 2.19) but overestimates the dissipated energy by the bond mechanism for large crack widths so that 68.0% and 79.8% reduction of the area under the bond-slip curves are obtained for crack widths of 0.20 mm and 0.30 mm respectively. This can be attributed to the large slip corresponding to the residual bond stress in the proposed model compared to the experimental bond-slip curves (Figure 2.19(c-d)) due to the moderate confinement provided for some specimens in the experimental database (such as Gambarova et al. (1989) and Brantschen et al. (2016)). As shown in Figures 2.18 and 2.19(d), for large crack widths, the bond-slip curves show abrupt reductions of the bond beyond the bond strength point. This is a result of the brittle nature of the bond failure of pre-cracked concrete, governed by a rapid degradation of the tensile resistance (mainly by aggregate interlock) of concrete through the splitting crack. As there are not enough studies focusing on purely unconfined pre-cracked concrete, more experimental tests are necessary to adjust or calibrate the proposed bond-slip models.

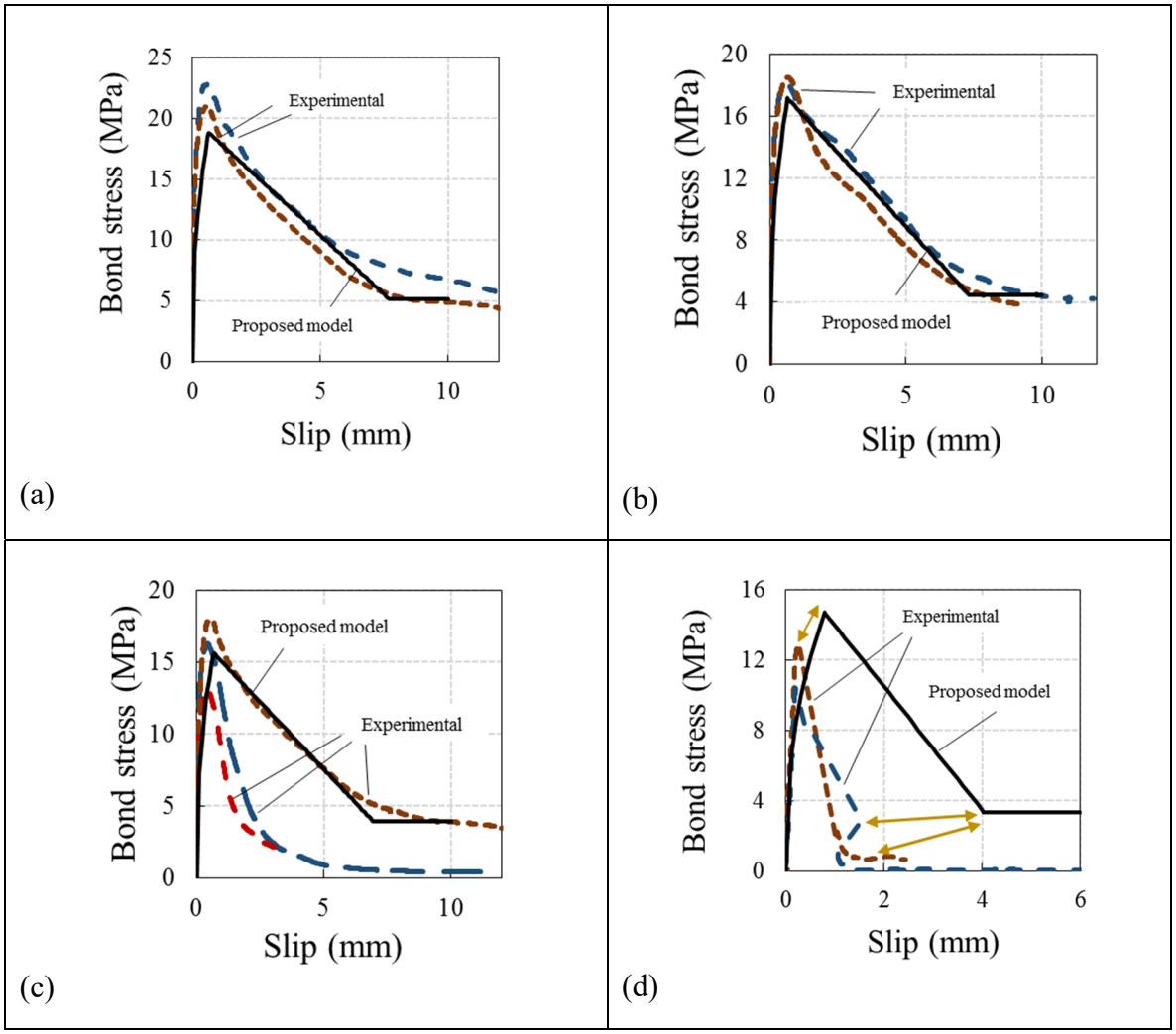

Figure 2.19 Validation of the proposed bond-slip model for pre-cracked concrete with experimental results of this study:
(a) w=0.10 mm; (b) w=0.15 mm; (c) w=0.20 mm; (d) w=0.30 mm

Overall, results of this study indicate that the existence of crack around the rebar leads to a significant change in rebar-concrete interaction properties, especially in the bond strength. Hence higher development length should be considered for reinforced concrete members exposed to the pre-cracking phenomenon. However, as crack width increases, the performance of Eq. (2.12) presented by ACI Code (ACI 318R, 2014) decreases resulting in a less prudent regulation where the development length predicted is smaller than the required length based on the experimental database (non-safety region). However, adjusting the development length in pre-cracked concrete by the increase factor, K_I, results in a conservative prediction while

maintaining a reasonably small deviation from the pull-out tests, even for large crack widths. It is interesting to note that although pull-out tests have limitations in model development and simulating realistic conditions, acceptable results can be achieved for comparative purposes such as the current study. The limitations of pull-out tests are mainly attributed to the fact that the stress state and crack pattern are different from the realistic conditions of splice zones (Cairns, 2015; Guizani et al., 2017; Tastani & Pantazopoulou, 2009) so that pull-out tests generate an arching action of compression struts that causes an additional confining action of the bonded zone. Hence more investigations are necessary to study the bond-slip response of rebar in pre-cracked concrete by other test specimen configurations such as beam-end, beam anchorage, and splice specimens.

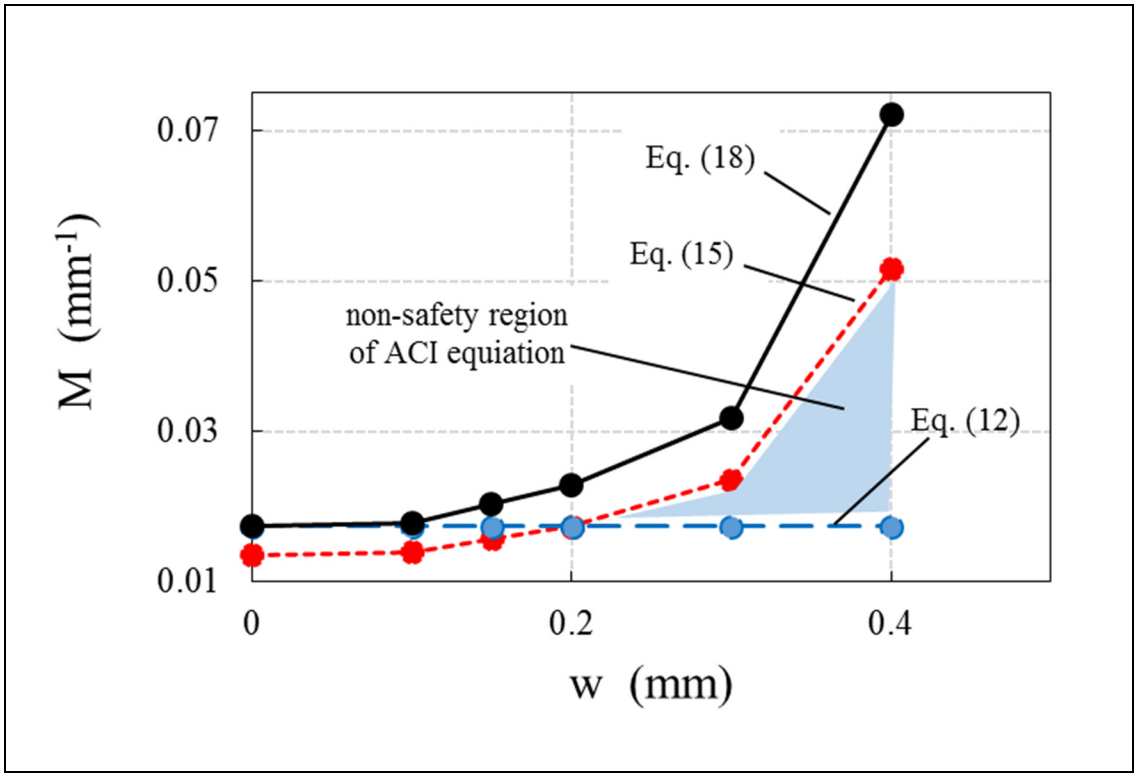

Figure 2.20 Validation of the Eq. (2.18) with pull-out tests of this study (ratio of $(M_{Exp})_{Cracked}/(M_{Exp})_{Un-cracked}$ is used here for increase factor)

2.5 Performance of standards

As mentioned in Table 2.3, there are some considerations in codes for reducing the bond strength due to the pre-cracking phenomenon. German National Code (DIN-1045-1, 2001) and Italian National Code (NTC-08, 2008) have considered the value of 2/3 (0.67) for the ratio of pre-cracked to un-cracked bond strength. They have determined the crack width of 0.20 mm for this regulation. The performance of this specification concerning the used database and the obtained experimental results are shown in Figure 2.21. Results indicate that for crack widths smaller than 0.20 mm, the regulations considered by German and Italian national codes are conservative enough while they largely underestimate the degradation of bond strength for larger crack width ($w \geq 0.20$ mm). Despite the other national codes, the predicting model presented by the fib Model Code 2010 (Table 2.3) considers rebar diameter by the ratio of w/d_b in the reduced bond strength formulation which leads to more conservative prediction up to the crack width of 0.50 mm. This underestimation is appropriate for design codes in which the safety factor is considered. However, no regulation has been determined for $w >$ 0.50 mm in the fib Model Code 2010. As shown in Table 2.3, only very few design codes have considered the effect of the pre-cracking phenomenon and more regulations are necessary.

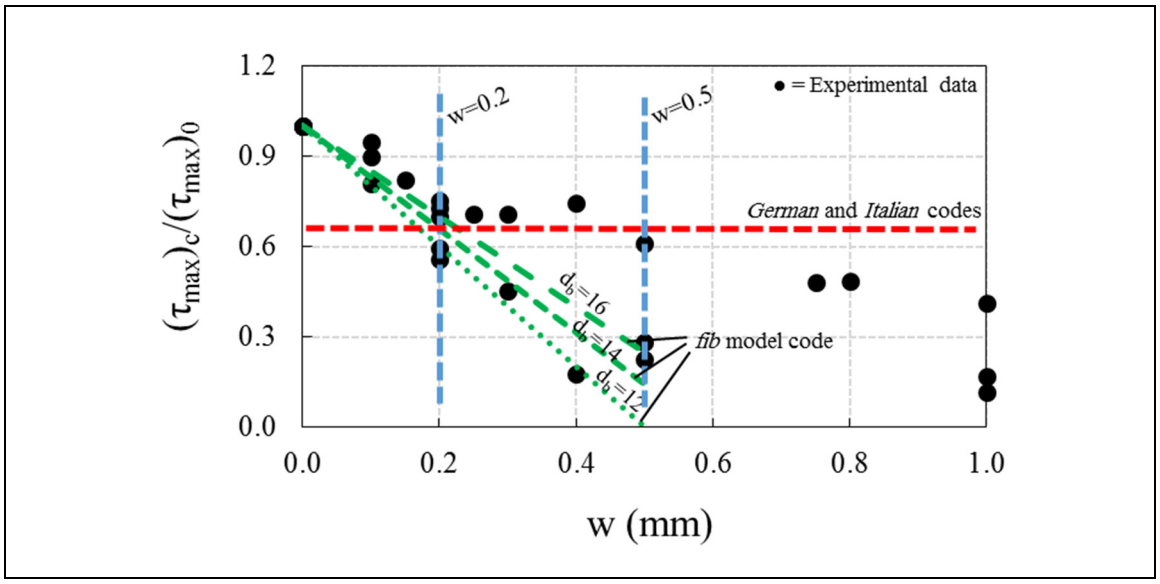

Figure 2.21 Performance of existing standards for predicting the effect of pre-cracking on bond strength (all databases)

To separately compare the results of tests from the current study with the available standards, the reduction factor (RF) is defined as below:

$$\mathrm{RF} = \left[1 - \left(\frac{\tau_{Cracked}}{\tau_{Uncracked}}\right)\right] \times 100 \tag{2.20}$$

Similar to Figure 2.21, results of the pull-out tests illustrate that these codes are conservative enough for cracks lower than 0.20 mm so that there is a significant difference between reduction factors of codes compared to the experimental results (Figure 2.22). Despite the Italian (NTC-08, 2008) and German National Codes (DIN-1045-1, 2001), the fib Model Code 2010 shows a prudent estimation of the degraded bond strength of pre-cracked concrete which similarly illustrated in Figure 2.21. Hence, more regulations are necessary for standards to reflect more accurately degradation of bond strength due to the pre-cracking phenomenon caused by corrosion or past overloading especially for crack width larger than 0.50 mm.

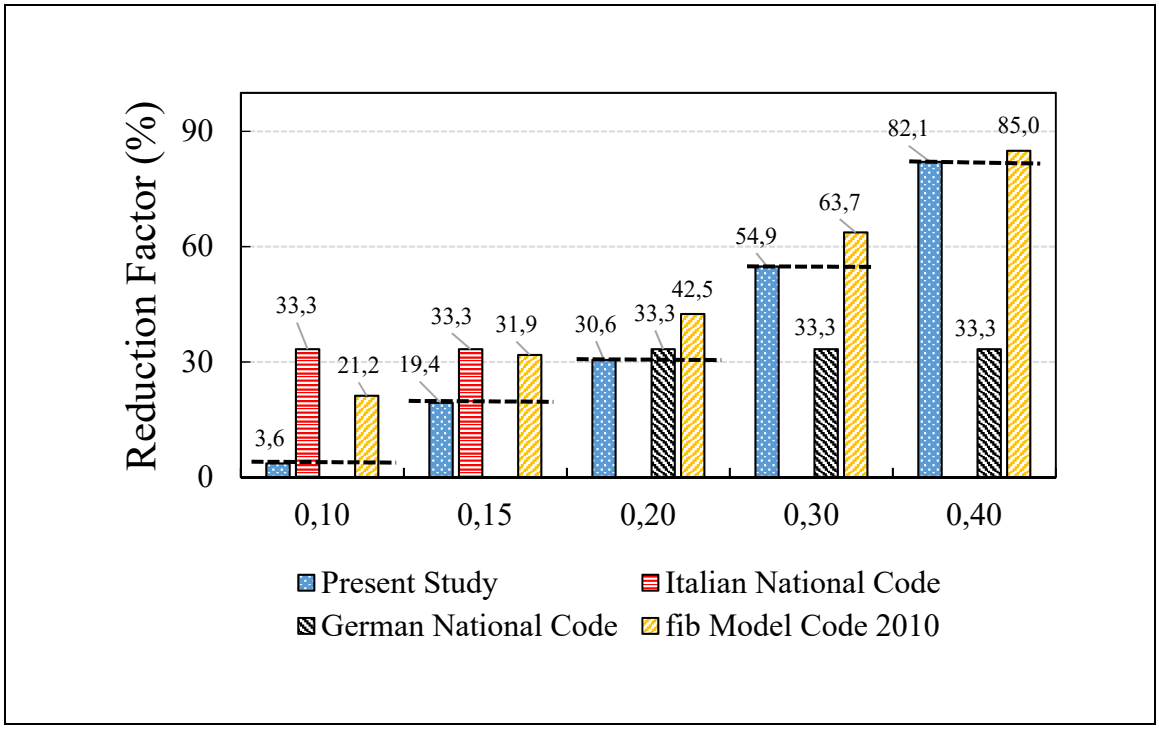

Figure 2.22 Performance of the standards for predicting the effect of pre-cracking on bond strength (pull-out test)

2.6 Summary and concluding remarks

This study presents a detailed explanation of a highly ignored issue in rebar-concrete interface properties, the pre-cracking phenomenon. Along with an experimental test, a database of previous research has been used to propose a modified bond-slip model as a function of the crack width. The following important concluding remarks are drawn:

- Induced cracks cause significant reduction in rebar-concrete interface strength so that crack widths of 0.10 mm, 0.15 mm, 0.20 mm, 0.30 mm, and larger than 0.40 mm result in 3.61%, 19.37%, 30.54%, 54.87%, and 82.10% reduction in bond strength respectively. Even though there is no corrosion, for crack width less than 0.30 mm based on standard recommendations, there is a significant reduction in bond strength. Thus, standards should take into account bond reduction due to the pre-cracking phenomenon in reinforced concrete caused by other sources than corrosion.
- The pre-cracking phenomenon has an adverse effect on energy dissipated by the bond mechanism so that larger crack widths result in considerably lower energy absorbed value, which is an illustration of the brittle behaviour.
- The proposed local bond stress-slip law for steel rebar embedded in pre-cracked concrete, Eq. (2.2), reasonably reproduces the monotonic experimental local bond stress-slip response for both experimental database and results obtained by the current study.
- An adjustment factor of the development length in pre-cracked concrete is proposed in Eq. (2.17) as a function of crack width. Results show that the application of this factor leads to a conservative prediction of the required development length showing small deviation from the pull-out tests, even for large crack widths.
- Considering the pre-cracking phenomenon, codes are conservative for crack width smaller than 0.20 mm so that there is an acceptable difference between the reduction factors of codes compared to the experimental results while they largely underestimate the degraded bond strength for larger crack widths ($w \geq 0.20$ mm).

As a limited set of parameters are considered in the experimental database such as compressive strength ($f'_c < 60$ MPa), rebar diameter ($d_b \leq 18$ mm), and rebar-concrete interfacial test

(pull-out test), more experimental studies are necessary to determine the efficiency of the proposed model for pre-cracked concrete.

CHAPTER 3

SIMPLIFIED ANALYTICAL MODEL FOR INTERFACIAL BOND STRENGTH OF DEFORMED STEEL REBAR EMBEDDED IN PRE-CRACKED CONCRETE

Seyed Sina Mousavi [a], Lotfi Guizani [b], and Claudiane Ouellet-Plamondon [c]

[a, b, c] Department of Construction Engineering, École de Technologie Supérieure, 1100 Notre-Dame West, Montreal, Quebec, Canada H3C 1K3

Paper published in *ASCE Journal of Structural Engineering*[2], August 2020

Abstract

Although extensive bond models have been developed for use in the numerical simulation of an uncracked reinforced concrete, no simplified method exists providing satisfactory accuracy and efficiency for pre-cracked concrete. This paper intends, therefore, to explain bond failure mechanisms in pre-cracked concrete - as compared to intact concrete - using a simplified theoretical model. The main bond failure mechanisms considered in this study involve: 1) crushing a wedge-shaped concrete block using reinforcing rebar ribs, and 2) tearing off the concrete between two adjacent ribs. Based on these scenarios, analytical expressions are derived to predict the average bond stress for uncracked concrete, in which the bearing angle, the rib face angle, the rib height, the rib spacing, and the friction coefficient between surfaces are the key parameters. A modified version of this model is proposed to predict the bond strength of rebars embedded in pre-cracked concrete by introducing a reduction factor of surrounding confinement caused by the pre-cracking phenomenon. An experimental program is also conducted to validate the proposed models. Experimental results emphasize the crucial

[2] Mousavi, S. S., Guizani, L., & Ouellet-Plamondon, C. M. (2020). Simplified Analytical Model for Interfacial Bond Strength of Deformed Steel Rebars Embedded in Pre-cracked Concrete. Journal of Structural Engineering, 146(8), 04020142. DOI: https://doi.org/10.1061/(ASCE)ST.1943-541X.0002687

impact of the pre-cracking phenomenon on both the bond strength and the failure pattern. Analysis results show that the bearing angle and surrounding confinement by concrete cover are crucial parameters controlling bond failure of rebars in pre-cracked concrete. The results also indicate that as the crack width corresponding to the low confinement increases, rib sliding is expected to occur as an illustration of weak interfacial strength. The proposed bond mechanism models are also in good agreement with the experimental observations.

Keywords: bond mechanism model; pre-cracked concrete; rib geometry; bearing angle.

3.1 Introduction

Pull-out failure develops under conditions of sufficiently thick concrete cover (moderately confined) or well confined by transverse steel reinforcement. High concrete cover-to-rebar diameter ratio confinement ($c_C/d_b \geq 2$ and ≈ 3.00 (Esfahani & Rangan, 1998; Turk et al., 2005; Walker et al., 1997)), without transverse steel, is defined as a moderate confinement condition. A similar trend has been suggested by ACI Code (ACI 318R, 2014), in which for confinement term $(c_C + k_{tr})/d_b$ higher than 2.5, a pull-out failure is likely to occur. Shear mechanics dominate the bond strength of rebar in pull-out failure mode, which is directly affected by the rib geometry of deformed rebar (Choi & Yang, 2010; Choi et al., 2010; Choi & Lee 2002). The ratio of rib spacing-to-rib height (S_r/h_r) has been used to consider the influence of rib pattern on possible failure modes (Rehm, 1957). Possible pull-out failure mechanics for a low and medium rib spacing-to-height ratios include (1) concrete shear-off between two adjacent ribs along the key line for well or moderately confined concrete (Wu & Chen, 2015), and (2) crushing of wedge-shaped concrete blocks on the rib-front face for weak confinement (Choi et al., 2010). It is worth emphasizing that rib spacing is more crucial in this classification (S_r/h_r) so that small rib spacing corresponds mainly to shear off, while the second failure mode is dominant for the cases of large rib spacing (Fernández Ruiz et al., 2005). However, previous studies have confirmed the impact of rib height on the experimental results of the second mode of failure (Darwin & Graham, 1993; Han et al., 2018). The second failure mode accompanies crack opening at the tip of the ribs, denoted as splitting cracks. Propagation

of splitting cracks along with the concrete crushing depends on the surface roughness so that in some cases, concrete crushing angle is equal to the rib face angle (Cairns & Abdullah, 1996). Extensive research has been performed to study the effect of ribs' geometry on local bond strength (Han et al., 2018; Lutz & Gergely, 1967; Rehm, 1957). Ribs' geometries include rib-face angle, rib height, and rib spacing. Several studies have reported that the rib face angle ranging from 45º to 57º (Menzel, 1939) and also 48.5º to 57.8º (Skorobogatov & Edwards, 1979) imposed a similar effect on bond-slip behaviour. However, results have indicated that a small rib-face angle (less than 15º (Soretz & Holzenbein, 1979), less than 30º (Lutz & Gergely, 1967; Rehm, 1957), and also less than 40º reported by Murata and Kawai (1984)) results in weak bond strength. To determine the effect of rib geometry on bond strength, bond index (also called relative rib area, f_R), which is the ratio between the area of the projection of a single rebar and the cross-section of a deformed rebar, has been defined by previous researches as the ruling criterion (Cairns & Jones, 1995; Darwin & Graham, 1993; Hong & Park, 2012; Rehm, 1957). Approximate relation of $f_R \approx h_r/S_r$ can be considered for bond index. Darwin and Graham (1993) have shown that as bond index varies between 0.05 and 0.20, bond strength increases about 10%. In this field, Cairns and Jones (1995) have reported a 30% increase in bond strength for bond index variation from 0.05 to 0.10. As a confirmation of this trend, experimental results presented by Metelli and Plizzari (2014) have shown that bond strength is strongly dependent on the relative rib area so that 40% increase has been obtained for bond index variation from 0.04 to 0.10. Hence, it can be deduced from the mentioned literature that, overall, analysis of previous studies confirms the fact that rib geometries have important roles in bond mechanism and bond strength.

Although extensive studies have concentrated on characterizing bond properties in uncracked or intact concrete (Eligehausen et al., 1983; Mahrenholtz & Eligehausen, 2017), further investigations are needed to study the structural significance of bond decay in induced cracked concrete, denoted as the "pre-cracking phenomenon (Mousavi et al., 2019)", especially based on different mechanisms of bond failure. In bond-slip research, pre-cracked concrete triggers a situation in which cracks develop through a plane containing a rebar axis before the rebar is pulled out from concrete blocks (Mousavi et al., 2019). Different situations can cause the pre-

cracking phenomenon including corrosion (Desnerck et al., 2015), mechanical pre-loading (Brantschen et al., 2016; Mousavi et al., 2019), biaxial load transfer (Hadidi & Saadeghvaziri, 2005; Lindorf et al., 2009; Saadeghvaziri & Hadidi, 2005), multi-axial stress states (Cervenka, 1985; Purainer, 2005), and transverse tension (Lindorf, 2011). These cases do not necessarily imply a bond failure before the maximum capacity of rebar-concrete interaction, besides the contact surface between rebar and concrete-through the ribs- is reduced (Brantschen et al., 2016). Whereas some research has been done to determine the effect of the pre-cracking phenomenon on bond strength (Brantschen et al., 2016; Gambarova et al., 1989; Idda, 1999; Mousavi et al., 2019), there is no specific study on the formulation of bond strength of steel rebar in moderately confined pre-cracked concrete as a function of the rib pattern and failure mode. The mechanism of pre-cracking is similar to bond splitting cracking and mainly affects the bond-slip behaviour of the rebar (Mousavi et al., 2019). Previous studies on pre-cracked concrete have been mainly concentrated on the residual bond stress of steel rebar as a function of crack width in pre-cracked concrete (Gambarova et al., 1989; Idda, 1999; Matsumoto et al., 2016). Different test setups with active or passive confinement have also been developed to experimentally simulate the pre-cracking phenomenon. Recently, Brantschen et al. (2016) have studied the phenomenon of bond in pre-cracked concrete by presenting the results of an experimental investigation with 89 monotonic pull-out tests. Crack openings ranging from 0.20 mm to 2.0 mm are considered in their pre-cracking tests. They showed that in-plane cracking has a significant effect on both the strength and bond-slip stiffness. Moreover, they used the aggregate interlock approach to analytically study the effect of in-plane cracking on bond behaviour, considering the bond index. However, they reported that the bond index, in its current form, could not adequately characterize bond properties in cracked concrete. They recommended that other rib geometry parameters, such as rib orientation, lug width, and spacing, be used separately for different rebar types for future studies related to the pre-cracking phenomenon (Brantschen et al., 2016). Although Mousavi et al. (2019) presented a specific bond-slip model, as well as a development length formulation for steel rebar embedded in pre-cracked concrete, they only used the crack width (ranging from 0.10 mm to 0.4 mm) in their formulations in a bid to consider induced cracked effects, and not the rib geometries.

Hence, a more specific bond model is needed to take into consideration the rib geometries of rebar embedded in pre-cracked concrete.

To numerically simulate the internally-damaged reinforced concrete (RC) members (such as elevated temperature (Khalaf et al., 2016), freeze-thaw damage (Petersen et al., 2007; Wang et al., 2019), corrosion (Feng et al., 2015; Jiang et al., 2018; Lin et al., 2017), etc.), modified analytical models are presented by considering damage-dependent parameters. Similarly, the pre-cracking phenomenon can generate internal damages in concrete bridge decks due to the changes in the volume of a restrained mass of concrete (Saadeghvaziri & Hadidi, 2005), transverse reinforcement in two-way slabs (Dawood & Marzouk, 2012; Einpaul et al., 2016), joints of precast elements (Joergensen & Hoang, 2015), and cracks in punching phenomenon (Brantschen, 2016; Brantschen et al., 2016). Accordingly, a modified bond model is necessary to (a) apply in numerical simulation of the mentioned RC members with the high risk of cracking parallel to the reinforcement direction; (b) use in structural evaluation of existing structures, more specifically predicting anchorage performance or capacity of a member subject to observed existing cracks. Hence, the present study intends to pursue the following questions:

1. How much does the crack width affect the bond strength of steel rebar in pre-cracked concrete?
2. How can the bond strength of steel rebar embedded in pre-cracked concrete be predicted by a specific bond mechanism as a function of the rib geometries of rebar?

With regard to the first question, an experimental program is conducted in this paper to introduce a reduction factor for bond strength as a function of crack width-to-rib height ratio. For the second question, a simplified theoretical model is presented to formulate the bond strength as a function of two distinct failure modes, which depend directly on the rebar ribs geometries and the crack width.

3.2 Experimental program

A total of 18 monotonically loaded pull-out tests are carried out using uncracked and pre-cracked specimens to (1) obtain a better understanding of the rebar-concrete interface exposed to the pre-cracking phenomenon, and (2) validate and calibrate the analytical procedure on the formulation of local bond strength proposed in this paper. Direct pull-out tests are carried out by applying a tensile force directly on the rebar by gripping the rebar from one side of the specimen (Figure 3.1(a)). The unloaded end slip is measured with a linear variable differential transformer (LVDT). An automatic data acquisition system is used to record the data. A displacement-controlled pull-out force is applied at a rate of 0.5 mm/min. To simulate the pre-cracking, an indirect tensile test (Brazilian splitting test) is used and calibrated for cylindrical concrete blocks with rebar placed at the center of specimens (Figure 3.1(b)). A displacement-controlled loading at a rate of 0.15 mm/min is applied to impede splitting failure during the pre-cracking loading. To measure the crack width, two crack gauges are installed on both sides of the concrete cylinders. The ultimate crack width is directly measured after the pre-cracking procedure is stopped. Because this paper focuses on the effect of the pre-cracking phenomenon on bond behaviour, including interfacial strength and failure modes, an attempt is made to prevent splitting bond failure by providing enough concrete cover around the rebar ($c_c/d_b = 7.5$). To accurately control crack widths, especially for those larger than 0.20 mm, a smaller-size NC2 is also considered in the experimental program. The embedment length of the rebars is $5d_b$ for all specimens. A summary of the experimental program and its main results are presented in this study. Further details can be found in Mousavi et al. (2019).

As the brittle nature of concrete makes some difficulties on simulating the pre-cracking phenomenon in unconfined concrete (without transverse reinforcement) (Desnerck et al., 2015; Mousavi et al., 2019), two types of specimens with different cylindrical dimensions and concrete strength are tested in the experimental program including NC1 specimen dimensions of 150 mm × 306.5 mm and $f'_c = 47.9$ MPa; and NC2 with dimensions of 150 mm × 113 mm and $f'_c = 58.8$ MPa. Further details of concrete composition and materials can be found in a recently published paper by Mousavi et al. (2019). In all cases, the rebar is positioned at

the center of cylinders. The used steel rebars have a diameter of 10 mm in conformity with the CSA-G30.18-400W (CAN/CSA-G30.18-09 2009) with a specified yield strength and ultimate tensile strength of 432 and 620 MPa respectively. The surface characteristics and rib pattern of the rebars used are shown in Figure 3.2. The average value of a rib–face angle for rebars used in the experimental program is about 55 degrees. The ratio of rib spacing-to-rib height (S_r/h_r) is about 7.0.

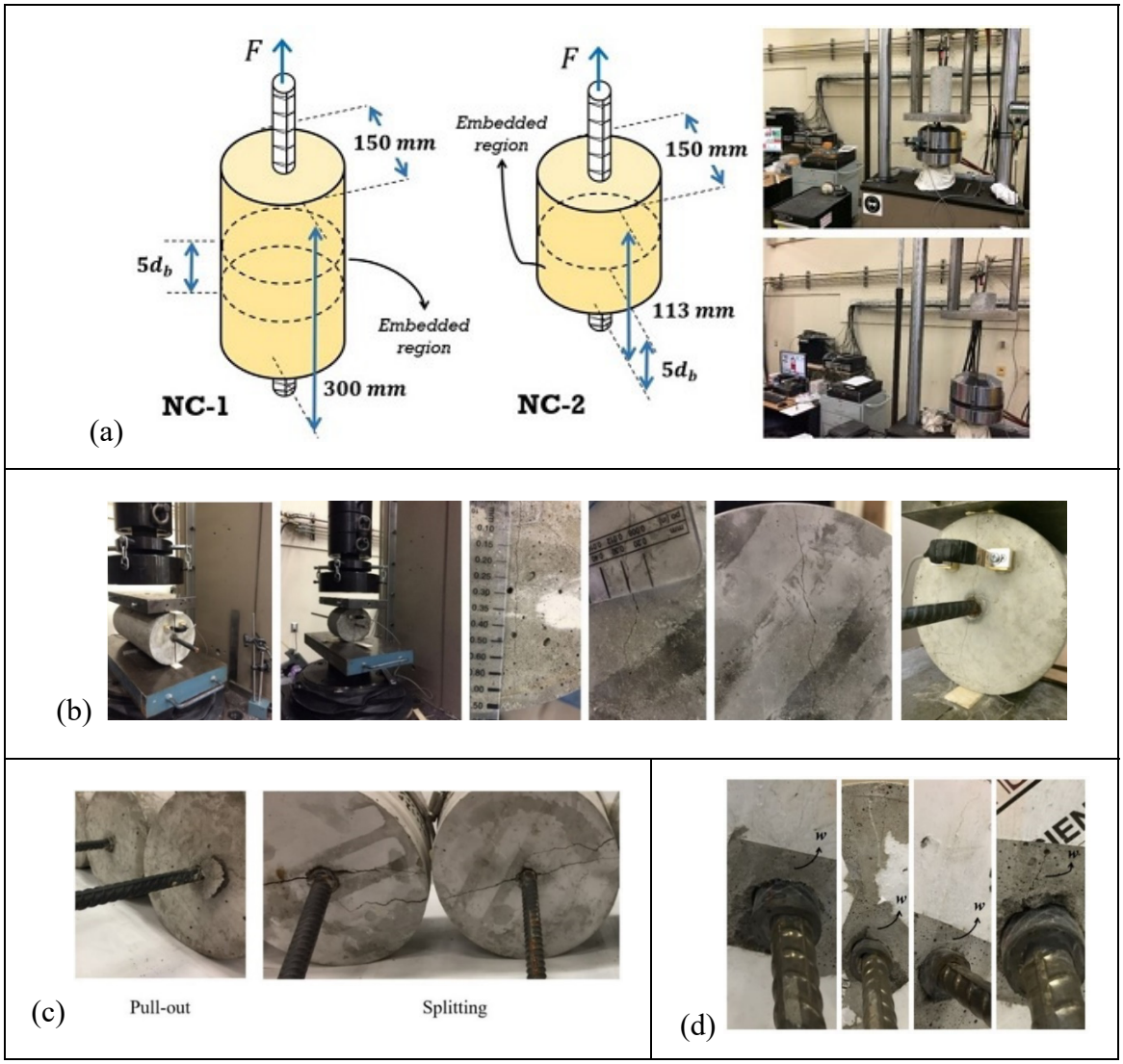

Figure 3.1 Experimental program: (a) test set-up; (b) pre-cracking test;
(c) failure modes for uncracked concrete;
(d) pull-out failure of pre-cracked concrete with $w < 0.15$ mm

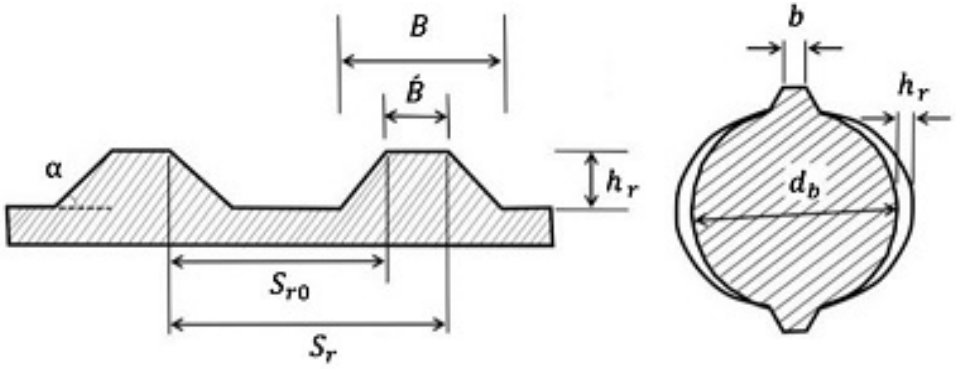

d_b (mm)	h_r (mm)	B (mm)	b (mm)	S_r (mm)	S_{r0} (mm)	α (degree)
10	1.89	4.86	2.70	13.22	12.14	55

Figure 3.2 Rebar geometry used in the experimental tests

3.2.1 Experimental results and observations

The effect of the crack width on the bond behaviour is analyzed in this section. Maximum bond stress (called bond strength, τ_{max}) and the reduction factor (ρ_n) caused by the pre-cracking phenomenon are the critical mechanical properties extracted from the results. As mentioned widely in the literature (Guizani et al., 2017; Wu & Zhao, 2012), for the short bond region (generally five times the rebar diameter), bond stress is close to uniform distribution and can be used to get a better measure of local bond strength by the average bond stress. Hence, in the pull-out test, average bond stress is used as:

$$\tau = \frac{F}{\pi d_b l_e} \tag{3.1}$$

where F is the tensile load, d_b is the rebar diameter, and l_e is the embedded length. A summary of results obtained from the bond tests, as well as the failure modes are given in Table 3.1. Crack width, w, maximum bond stress (bond strength), τ_{max}, and residual bond stress, τ_{res} ,

are reported as the main parameters. The normalized bond strength considering the compressive strength of concrete, defined by the ratio $\tau_{max}/\sqrt{f'_c}$, as well as the failure mode (pull-out or splitting), are reported for each test (Figure 3.1(c)). The identification of the specimens listed in Table 3.1 is patterned as follows: "NCx" for specimen type (x=1 or 2); "U" for uncracked reference concrete; and "Cx" for pre-cracked concrete with a crack width equal to x/100 mm. After pre-cracking, samples with crack widths of 0.10, 0.15, 0.20, 0.30, and 0.4 mm are obtained for both types of concrete specimens (Table 3.1). General observations show that cracked specimens with $w > 0.15$ mm failed following the splitting of concrete surrounding the rebar, while pull-out failure modes are observed for small crack widths (Figure 3.1(d)).

Table 3.1 Experimental results

Specimen Id.	w	τ_{max}	τ_{res}	**Strength reduction**	$\tau_{max}/\sqrt{f'_c}$	**n**[1]	**Failure mode**[2]
	mm	**MPa**	**MPa**	**(%)**			
NC1-U	0.00	22.71 (0.71)	6.74 (1.42)	-	3.28	3	P,P,P
NC1-C10	0.10	21.89 (1.26)	5.83 (1.65)	3.61	3.16	2	P,P
NC1-C15	0.15	18.31 (1.57)	4.14 (0.38)	19.37	2.65	2	P,P
NC1-C20	0.20	15.77 (2.99)	2.14 (1.76)	30.54	2.28	3	S,S,S
NC2-U	0.00	25.79 (1.15)	6.50 (1.46)	-	3.36	3	P,P,P
NC2-C20	0.20	18.05	0.00	30.03	2.35	1	S
NC2-C30	0.30	11.64 (1.74)	0.94 (0.21)	54.87	1.52	2	S,S
NC2-C40/50	0.40-0.50	4.62 (0.14)	0.41 (0.59)	82.10	0.60	2	S,S

[1]number of specimens tested for every test series.[2] P=pull-out failure; S=splitting failure.
Note: data inside the parentheses denote the standard deviation

As the results reported by Brantschen et al. (2016) and Mousavi et al. (2019) showed the crucial role of the rebar diameter on the behaviour of cracked specimens, the dimensionless ratio of

crack width-to-rebar diameter (w/d_b) is used in describing the bond properties in cracked concrete. The normalized bond strength versus the w/d_b ratio is illustrated in Figure 3.3. A good correlation ($R^2 = 0.95$) exists between the experimental data and the w/d_b ratio, as expressed by Eq. (3.2). A value of 3.40 is obtained for uncracked concrete (based on Eq. (3.2)), while the pre-cracking phenomenon had a considerable impact on the normalized bond strength.

$$\frac{\tau_{max}}{\sqrt{f'_c}} = -63.82\frac{w}{d_b} + 3.40 \tag{3.2}$$

Based on the proposed equation for the normalized bond strength of rebar in pre-cracked concrete, cracks larger than about 0.60 mm resulted in zero bond strength ($\tau_{max}/\sqrt{f'_c} \approx 0$). General observations show that the crack width significantly changes the interfacial bond behaviour, leading to bond failure changes for crack widths larger than 0.15 mm (Figure 3.1(c)). A crack width of 0.10 mm (NC1-C10) had no significant (less than 5% reduction) effect on the bond strength (Figure 3.3) or the bond-slip behaviour. Furthermore, steel rebar embedded in NC1-C10 is pulled out of concrete without splitting crack (Figure 3.1(d)), which is the same as for uncracked concrete (NC1-U). However, in the $0.10\ mm < w \leq 0.15\ mm$ case, there is a fairly high reduction in the bond strength (Figure 3.3). Crack widths larger than 0.15 mm caused a significant reduction in bond strength along with a change in failure mode (Table 3.1). The results summarized in Table 3.1 and Figure 3.3 clearly demonstrate that the bond behaviour of pre-cracked concrete for $w \geq 0.15$ mm is governed by the splitting failure mode similarly as for uncracked concrete, in which a sudden drop in bond resistance can be observed until an equilibrium is reached between the radial component of the post-splitting bond stresses and the post-splitting confining action (tensile resistance of the concrete) (Harajli, 2009; Mousavi et al., 2019). This can be attributed to the change in failure mode, which is analyzed analytically by the following sections.

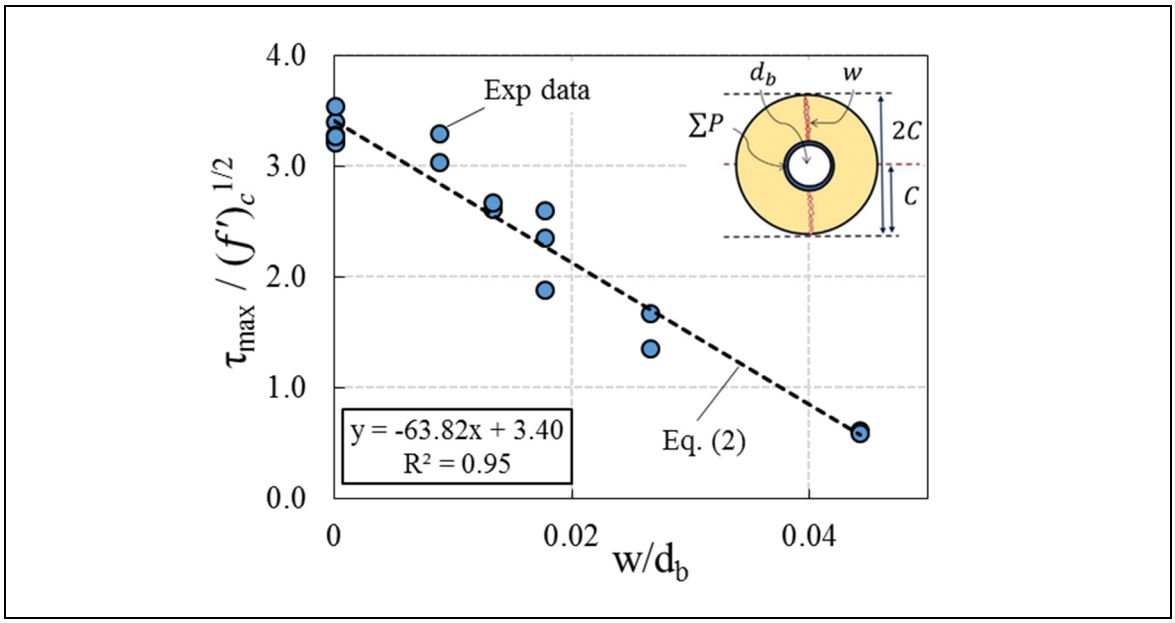

Figure 3.3 Normalized bond strength concerning w/d_b ratio

Bond failure mechanisms in uncracked concrete are followed by the surface separations in both parallel and perpendicular directions. Induced cracks due to the pre-cracking phenomenon result in a similar surface separation, but with more significant impacts (Mousavi et al., 2019). Murcia-Delso & Benson Shing (2014) presented the only bond-slip model in the literature considering surface separations for uncracked concrete. They related bond reduction to rib height without concentrating on the pre-cracking phenomenon. Accordingly, a reduction factor (ρ_{nm}) can be obtained for pre-cracked concrete by the experimental results, as a function of surface separation, as follows:

$$\rho_{nm} = \frac{(\tau_{max})_{\text{pre-cracked}}}{(\tau_{max})_{\text{uncracked}}}$$

$$\rho_{nm} = \begin{cases} 1 & w/2 \le 0.026h_r \\ 1.58e^{(-8.14\frac{w}{h_r})} & 0.026h_r < w/2 < 0.15h_r \\ 0 & w/2 \ge 0.15h_r \end{cases} \quad (3.3)$$

where ρ_{nm} is a reduction factor of bond strength that considers the opening of cracks due to the pre-cracking phenomenon in concrete. The performance of the proposed model is shown

in Figure 3.4. The dependence of the reduction factor on the ratio of crack width-to-rib height (Eq. (3.3)) can be attributed to the fact that the loss of bond strength is related to a reduction in the contact surface between the steel ribs and the concrete. For well-confined situation (uncracked concrete and $w \leq 0.10$), the interface separation is very small; consequently, the reduction ratio will be equal or very close to one ($\rho_{nm} \approx 1$). Based on the experimental results, the domain of $w/2 \leq 0.026 h_r$ is considered in the Eq. (3.3) for the reduction factor equal to 1.0. Based on the model presented by Murcia-Delso & Benson Shing (2014), if the interface separation is larger than the rib height, the contact between ribs and the concrete is lost, and the bond resistance disappears ($\rho_{nm} = 0$). However, the value of $0.15 h_r$ is obtained based on Eq. (3.2) ($w \approx 0.60$ mm) as a critical separation value for complete loss in bond strength. This can be attributed to the significant reduction in compressive strength of surrounding concrete due to the pre-cracking phenomenon, which has been reported by several works (Belarbi & Hsu, 1991; Kollegger & Mehlhorn, 1990; Mikame et al., 1991; Shirai & Noguchi, 1989; Vecchio & Collins, 1993). Considerable effect of compressive strength on the rebar-concrete interfacial strength has been frequently confirmed (Guizani et al., 2017; Mousavi et al., 2017).

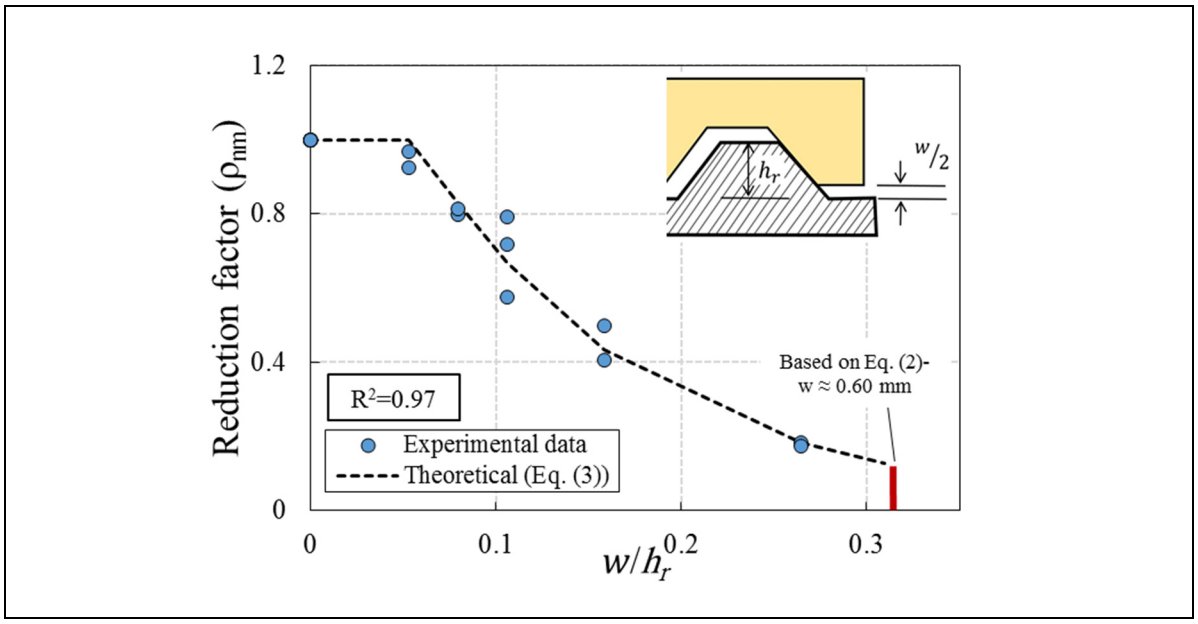

Figure 3.4 Performance of the bond reduction factor defined by Eq. (3.3)

3.3 Proposed models for bond strength formulation

Most previous research works on the bond behaviour of rebar in pre-cracked concrete have ignored the impact of separation on the rib front face. They just consider the effects of transverse tensile strain after pre-cracking by reducing the concrete compressive strength, and not the surface separation (Cervenka, 1985; Vecchio & Collins, 1993). Hence, this section intends to propose a simplified theoretical model for local bond strength formulation, considering the contact separation between the rebar and the surrounding concrete. As shown in Table 3.1, the pre-cracking phenomenon changes the failure mechanism at the rebar-concrete interface. Possible failure mechanisms of uncracked and pre-cracked concrete can be observed at rebar surfaces, as illustrated in Figure 3.5. The main bond failure mechanisms of deformed rebar embedded in uncracked and pre-cracked surrounding concrete are respectively the tearing off the concrete keys on the rib front (Figure 3.5(a)) and crushing of the concrete in shear due to the wedging action of the ribs (Figure 3.5(b)). Enough concrete cover around the rebar provides moderate confinement to impede splitting failure, resulting in the first failure mechanism (shear-off concrete). In the latter failure mechanism, the opening of primary cracks, caused by the pre-cracking phenomenon, occurred simultaneously with the crushing of a wedge-shaped concrete (Figure 3.5(c)), preventing concrete shear-off between two adjacent lugs. A sudden clearance could occur in the cases of large crack widths. Given these classifications and assumptions, simplified theoretical models are expressed for each of the failure modes in the following subsections. In the case of splitting failure modes in “uncracked” and “pre-cracked” concrete, the resultant movement of the concrete relative to the rebar (RMvt) is considered in the present study (Figures 3.8 and 3.12). Horizontal (tangent) component of RMvt corresponds to the relative slippage of concrete to the rebar, while its radial component corresponds to the crack opening occurring simultaneously with the slippage, which is confirmed by Guizani et al. (2017) and Murcia-Delso & Benson Shing (2014). Hence, as crack opening varies during the test, it is worth mentioning that the w referred in the paper represents the initial crack width.

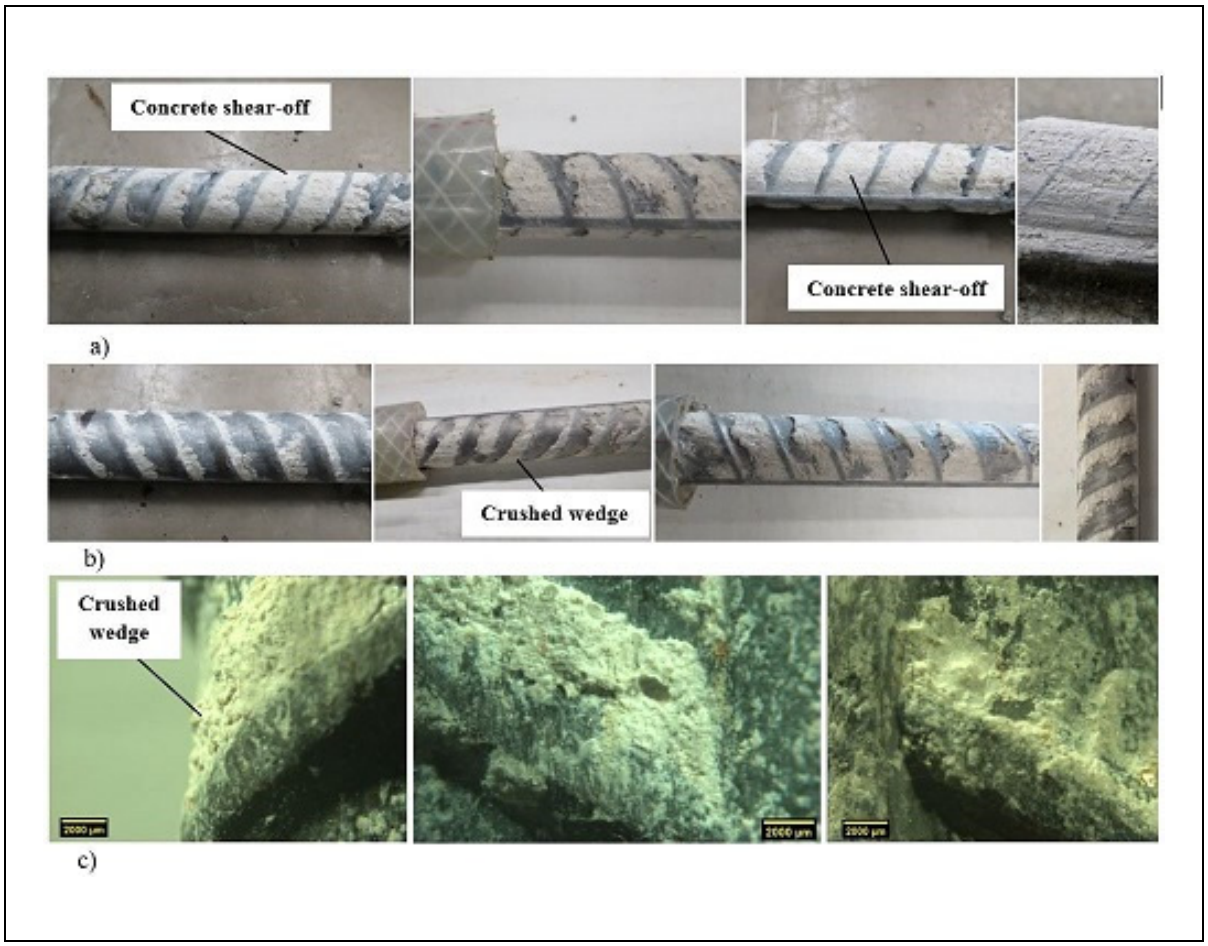

Figure 3.5 Failure mechanism: (a) sheared-off concrete in uncracked specimens; (b, c) crushed wedge-shaped concrete blocks in pre-cracked specimens

3.3.1 Uncracked concrete

Although the classification of bond failure mechanisms was presented before by theoretical models developed by Wu & Chen (2015) and Choi et al. (2010), more experimental proof is needed to validate their theories. Hence, this study uses both types of failure mode mechanisms to test the validity of these theories by experimental results for uncracked and pre-cracked concrete separately. For both failure mechanisms, frictional force, cohesion strength of steel-concrete and concrete-concrete interfaces along with rib–face angle, α, and bearing angle, β, are the main resistance parameters described in the following subsections. Bearing stress on the rib-front face, σ_q, and shear stress on the rib-front face, τ_q, are the two interfacial stress

between rebar-concrete surface interaction. Both flat and non-flat portions of the rebar-concrete interfaces are considered in this paper. Wu & Chen (2015) and Dehestani et al. (2017) introduced different analytical and empirical equations for bearing stress on the rib-front face at the rebar-concrete interface, σ_q, at bond failure which are shown in Eqs. (3.4) and (3.5) respectively:

$$\sigma_q = f'_c \tag{3.4}$$

$$\sigma_q = \frac{\sqrt{f'_c}}{\mu_1}\left(\frac{2.88}{1 + 2.7e^{-0.75(c_c/d_b)}}\right) \tag{3.5}$$

where compressive strength of the surrounding concrete (f'_c) is the main parameter for defining bearing stress. Neglecting cohesion at the steel rebar-concrete interface, shear stress on the rib-front face at the rebar-concrete interface can be defined by the Mohr-Coulomb model making use of the friction coefficient between concrete and steel, μ_1:

$$\tau_q = \mu_1 \sigma_q \tag{3.6}$$

Different values have been used in the literature for the coefficient of friction between concrete and steel, μ_1. Baltay & Gjelsvik (1990) suggested the value of 0.47 under stress levels between 0.007 MPa and 469 MPa (1 and 68000 psi). Also, Rabbat & Russell (1985) reported values in the range of 0.57–0.68 under normal compressive stresses ranging from 0.14 MPa to 0.69 MPa. Further, a targeted method of discrete element model (DEM) considering key parameters of bond strength between concrete and steel rebar, reported by Dehestani et al. (2017), has shown that a friction coefficient ranging from 0.61 to 0.64 is appropriate for steel-concrete interface modeling in DEM used in the pressure-overclosure relationship. Zhao & Zhu (2017) have reported the value of 0.28 for average static friction coefficients of the steel-to-concrete interface. However, Zhao & Zhu (2018) have used the value of 0.45 as a best-fit formulation for their proposed local bond-slip model. Hence, the results of the literature define the static friction coefficient in the wide range of approximately 0.28-0.65. To derive more accurate

friction coefficients for the concrete used in the experimental program (Mousavi et al., 2019), the results of uncracked concrete are used, as introduced in the following subsections. By substituting Eq. (3.5) into Eq. (3.6), the effect of friction coefficient will vanish in the formulation. Hence, for the current study, the use of Eq. (3.4) is deemed more appropriate than Eq. (3.5), since the friction coefficient is separately considered in shear stress on the rib-front face. To define normal and shear stresses on the crushed and shorn-off part of the concrete-concrete interface, Mohr-Coulomb (MC) failure theory criterion suggests:

$$\tau_n = C + \mu_2 \sigma_n \tag{3.7}$$

where μ_2 and C are friction coefficient and cohesion strength between two layers of concrete respectively. Zhao & Zhu (2017) reported the values of 0.52 and 0.54 for static and dynamic friction coefficients between two layers of concrete, respectively. The average value of 0.53 is used in this study. According to the study presented by Cairns & Abdullah (1996), the cohesion of concrete is estimated to be $0.25f'_c$. Cela (1998) used the visco-plastic Drucker and Prager (DP) criterion to derive Eq. (4.8) for concrete cohesion strength:

$$C = f'_c\left(\frac{1 - \sin\psi}{2\cos\psi}\right) \tag{3.8}$$

where ψ is the internal friction angle. Montoya et al. (2001) constituted a MC failure criterion with a constant internal friction angle of 37 degrees. Arslan (2004) stated that the range of ψ is between 30 and 37 degrees for conventional concrete and $\psi = 37$ degrees for high-strength concrete. Although Eq. (3.8) is used for this study, similar values are obtained for cohesion models; for example, in the case of $f'_c = 47.9\ MPa$, cohesion strengths of 11.97 MPa and 11.94 MPa are predicted by Cairns & Abdullah (1996) and Cela (1998) respectively (also 14.70 MPa and 14.66 MPa for $f'_c = 58.8$ MPa). The following subsections present formulations of three bond failure mechanisms models for uncracked and pre-cracked concrete. Experimental results of this study are also used to determine the performance of the proposed models.

3.3.1.1 Mode-1 of uncracked concrete (UM1)

The mode-1 failure mechanism is defined by shearing-off the concrete key between two adjacent ribs (Figure 3.8). The frictional force of the rebar-concrete interface at the flat portion of rebar is considered in mode-1. Previous research has reported a classification in which this type of bond failure mechanism corresponds to steel rebar with the rib ratio of $S_r/h_r \leq 7.0$ (Choi et al., 2010; Wu & Chen 2015). Strong rebar-concrete interaction can be deduced from the complete shear failure, dominating this mechanism (Figures 3.5(a) and 3.6), which can be attributed to the high tensile strength of concrete used and large rib height. On the other hand, mode-1 of bond failure mechanism is a sustained status (particular case) of the mode-2 (section 3.3.1.2), in which several unsuccessful attempts by different transverse internal cracks occurred to crush the concrete ($\beta = 0$).

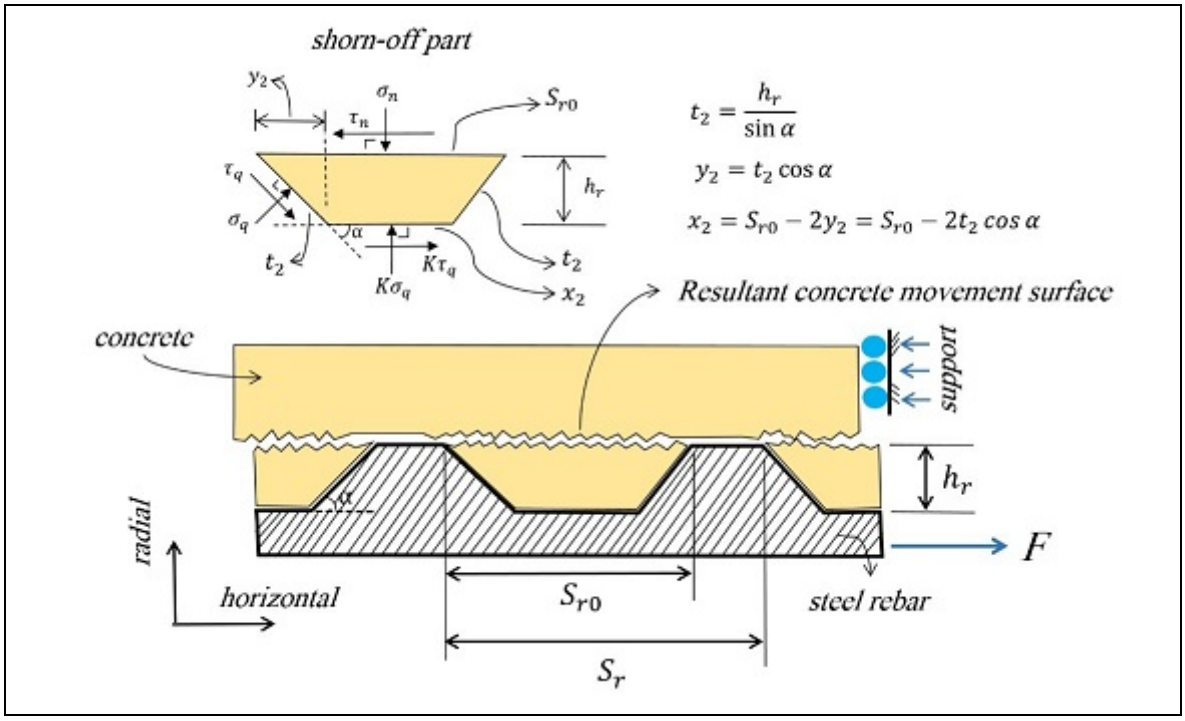

Figure 3.6 Failure mechanism of uncracked concrete at rib-front area (unit thickness out of plane)

Equilibrium of the main crushed concrete in the horizontal direction (Figure 3.6) gives:

$$-\tau_n S_{r0} + K\tau_q x_2 + \tau_q t_2 \cos\alpha + \sigma_q t_2 \sin\alpha = 0 \tag{3.9}$$

where K is a reduction factor for horizontal steel-concrete interfacial pressure due to the pure shear failure in this bond failure mechanism. $K = 1$ corresponds to the high contact pressure similar to the first bond failure, while $K = 0$ indicate no contact pressure between horizontal steel-concrete interfacial surfaces. Although, there is no specific experimental and theoretical study concerning contact pressure at different points of steel-concrete interfacial surfaces, the pure shear key line illustrated in Figure 3.6 shows that this reduction factor, $0.0 < K < 1.0$, should be calibrated for obtaining the bond strength. Substituting τ_q from Eq. (3.6) into Eq. (3.9) and utilizing calculation illustrated in Figure 3.6 for x_2 and t_2, Eq. (3.10) is obtained for the shear stress over the bearing concrete block:

$$\frac{\tau_n}{\sigma_q} = K\mu_1 + \left[\frac{h_r}{S_{r0}}(\mu_1 \cot\alpha\,[1-2K]+1)\right] \tag{3.10}$$

Introducing the average bond stress, τ_{ave}, and integration of stresses into forces along the rebar-concrete interface allows:

$$\tau_{ave}\pi d_b l_e = \tau_n S_{r0}\pi d_b \frac{l_e}{S_r} \tag{3.11}$$

Finally, by substituting Eq. (3.10) into Eq. (3.11), the average bond stress over the embedded length can be obtained:

$$\frac{\tau_{ave}}{\sigma_q} = \frac{S_{r0}}{S_r}K\mu_1 + \left[\frac{h_r}{S_r}(\mu_1[1-2K]\cot\alpha+1)\right] \tag{3.12}$$

Eq. (3.12) uses a hypothesis in which bearing force on concrete keys for different lugs activates at the same time so that the term of l_e/S_r, number of stucks concrete in front of lugs for different rib spacings along the embedded length have no effect on average bond stress.

Regarding Eq. (3.12), the average bond stress along the embedded length of rebar is a function of:

$$\tau_{ave} = f(\sigma_q, \mu_1, h_r, S_r, S_{r0}, \alpha, K) \tag{3.13}$$

Sensitivity analysis of Eq. (3.12) to the variation of parameters is shown in Figure 3.7. Compressive strength of concrete, friction coefficients between rebar and concrete, rib–face angle, rib pattern of rebar (height and rib spacing), and reduction factor for horizontal steel-concrete interfacial pressure are the main parameters of average bond stress of mode-1. Rebar-concrete interface frictional force is the only surface-surface strength parameter in mode-1 of failure mechanism. It can be attributed to the quantity of the surface of rebar in contact with surrounding concrete in the first bond failure mechanism. Compressive strength of concrete (or normal stress at the rebar-concrete interface) and rib spacing (S_r) are the most effective parameter for mode-1 (Figure 3.7(a)). As rib spacing increases, bond index (f_R) or distance between two adjacent ribs decreases, which results in lower bond strength. However, the length of concrete key between two adjacent ribs shows different trends so that higher value of S_{r0} results in higher bond strength. This can be attributed to the relation between S_r and S_{r0} which can approximately determine by:

$$S_r - S_{r0} = \acute{B} \tag{3.14}$$

where $\acute{B} < B$ is the length of the top horizontal section of ribs (Figure 3.2) which has no significant impact on interfacial bond strength. As $\acute{B}$ increases, efficient interfacial surfaces between rebar and concrete decreases, so that reduces the bond strength.

Rib-face angle has the lowest impact on the average bond stress compared to other variables. Similar results have been reported in the literature (Lutz & Gergely, 1967; Menzel, 1939; Skorobogatov & Edwards, 1979). Figure 3.7(b) precisely shows the effect of the rib-face angle on bond strength for different values of friction coefficients. Parametric results indicate that the rib-face angle higher than 45º has no considerable impact on bond strength. A similar result has been reported by Murata & Kawai (1984) that the rib-face angle smaller than 40 degrees

has a considerable effect on bond reduction. Concrete-concrete friction coefficient has no impact on this failure mode. As mode-1 of bond failure mechanism is an ultimate limit of mode-2 for well-confined condition (or intact concrete cover), failure would occur at the strain corresponds to the pure shear strength of concrete. In this condition, the friction coefficient of the concrete-concrete interface, denoted as the aggregate interlock, is less important than the strength of concrete and the friction coefficient of the steel rebar-concrete interface. Figure 3.7 also shows that the reduction factor for horizontal steel-concrete interfacial pressure, K, has a considerable impact on predicting bond strength corresponds to this failure mechanism.

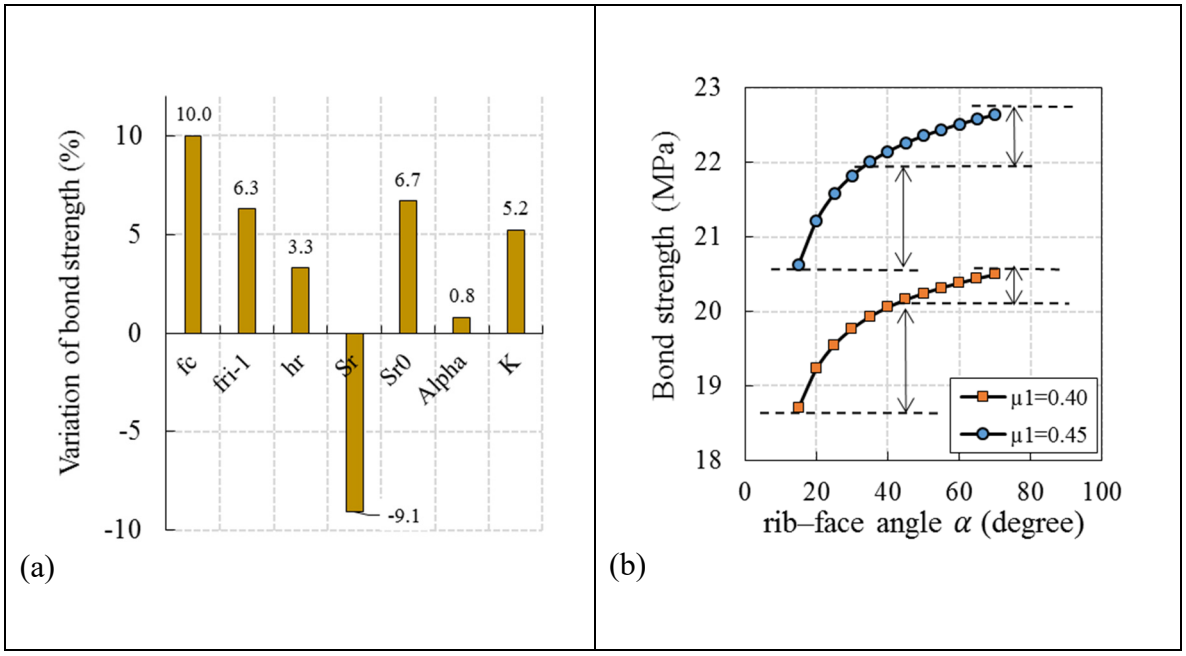

Figure 3.7 Sensitivity analysis of bond strength proposed by UM1:
(a) for a 10% increase in every variable (reference: $\alpha = 55$ degrees, $f'_c = 40$ MPa, $\mu_1 = 0.4$, $h_r = 1.89\ mm$, $S_r = 13.22$ mm, $S_{r0} = 12.14$ mm, and K $= 0.7$);
(b) effect of rib-face angle

3.3.1.2 Mode-2 of uncracked concrete (UM2)

The second mode of bond failure mechanism for uncracked concrete corresponds to the concrete crushing by a wedge block of concrete at the rib-front face, as illustrated in Figure

3.8. Previous studies classified this type of bond failure mechanism for steel rebar with the rib ratio of $S_r/h_r > 10.0$ (Choi et al., 2010; Wu & Chen, 2015). In this bond failure mechanism, separation of surfaces after concrete crushing causes sliding up the surrounding concrete. Although there is no fact of the hypothesis in which concrete crushing with a wedge block of concrete is weaker than the shearing-off concrete between two adjacent ribs, the shape of the first failure mechanism shows an unexpected failure. This behaviour of bond failure may be attributed to the incorrect surface interlocks due to rib height, rib spacing, the tensile strength of concrete, and probably initial contact separation due to pre-cracking caused by previous earthquakes or corrosion products (Brantschen et al., 2016; Desnerck et al., 2015; Matsumoto et al., 2016; Mousavi et al., 2019).

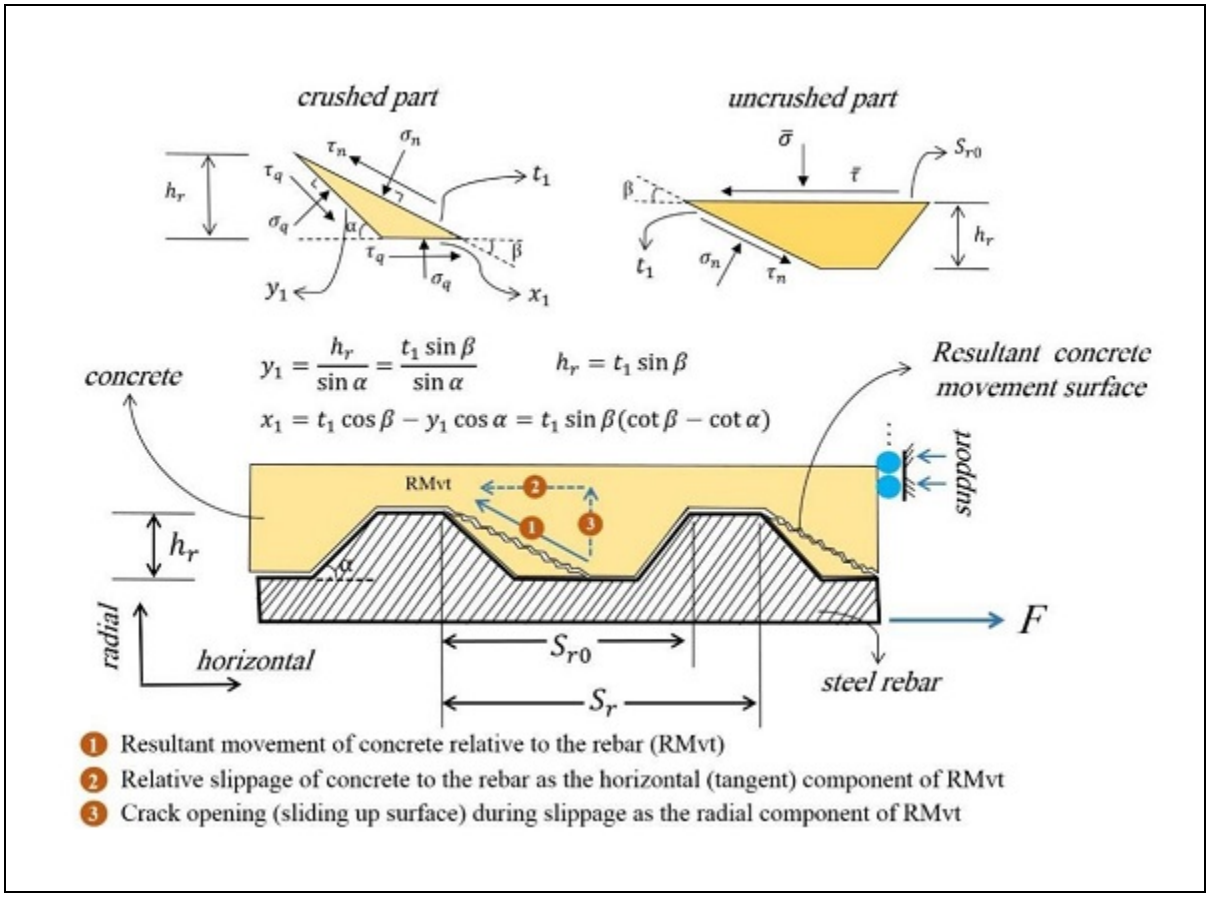

Figure 3.8 Failure mechanism of mode-2 (concrete crushing) at rib-front area (unit thickness out of plan)

To present a simplified formulation for this mode, two directions of relative displacement between steel rebar and surrounding concrete are considered including radial separation due to the sliding up the movement of crushed concrete, and vertical caused by the slippage of the crushed concrete parallel to the rebar axis. The horizontal force equilibrium of the crushed part of the rib-front area (Figure 3.8) allows:

$$\tau_q x_1 + \tau_q y_1 \cos\alpha + \sigma_q y_1 \sin\alpha - \tau_n t_1 \cos\beta - \sigma_n t_1 \sin\beta = 0 \tag{3.15}$$

where x_1, y_1, and t_1 are vertical and horizontal projection area (unit thickness out of planes), as shown in Figure 3.8. Substituting τ_q and τ_n from Eqs. (3.6) and (3.7) respectively into Eq. (3.15) gives:

$$\sigma_n = \frac{\sigma_q(1 + \mu_1 \cot\beta) - C \cot\beta}{(1 + \mu_2 \cot\beta)} \tag{3.16}$$

which relates the uniform distribution of radial pressure at the crushed area of the concrete-concrete interface, σ_n, to the normal stress on the rib-front face at the rebar-concrete interface, σ_q. Similar to the approach presented by Wu & Chen (2015), the compressive strength of concrete is considered in the current study for σ_q for both flat and non-flat portions of the rebar-concrete interfaces. Substituting the Eq. (3.16) into Eq. (3.7), the shear stress along the wedging surface of the crushed concrete block is obtained as:

$$\tau_n = \frac{C + \mu_2 \sigma_q (1 + \mu_1 \cot\beta)}{(1 + \mu_2 \cot\beta)} \tag{3.17}$$

For determining the horizontal component of the shear stress, an uncrushed part of concrete is considered. As shown in Figure 3.8, force equilibrium of the uncrushed part of concrete in contact with the crushed block gives:

$$-\bar{\tau}\, S_{r0} + \tau_n t_1 \cos\beta + \sigma_n t_1 \sin\beta = 0 \tag{3.18}$$

which results in the Eq. (3.19) for determining bond strength distributed over the spacing of periodical ribs:

$$\bar{\tau} = \frac{h_r}{S_{r0}}\left[\frac{\tau_n(1+\mu_2\cot\beta)-C}{\mu_2}\right] \tag{3.19}$$

By utilizing the force equilibrium along the rebar:

$$\tau_{ave}\pi d_b l_e \cong \bar{\tau}\pi d_b S_{r0}\frac{l_e}{S_r} \tag{3.20}$$

where l_e and S_r are rebar embedded length and periodical ribs spacing, respectively. Note that the term of l_e/S_r in Eq. (3.20) represents the number of ribs in which crushed concrete stuck to the front of lugs. To convert the shear stress over the rib spacing ($\bar{\tau}$) to the average bond stress over the embedded length (τ_{ave}), the term S_{r0} is considered in Eq. (3.19). By substituting Eq. (3.17) into Eq. (3.19) and rewriting Eq. (3.20), the average bond stress over the embedded length can be expressed as:

$$\frac{\tau_{ave}}{\sigma_q} = \frac{h_r}{S_r}[1+\mu_1\cot\beta] \tag{3.21}$$

Hence, the average bond stress over embedded length for failure mode-2 can be expressed as a function of:

$$\tau_{ave} = f(\sigma_q, \mu_1, \beta, h_r, S_r) \tag{3.22}$$

Compressive strength of concrete, the friction coefficient between rebar-concrete, bearing angles, and rib deformations are the main parameters of average bond stress. Concerning the bearing angle, β, different ranges of 30-40º by Lutz & Gergely (1967), 17-40º by Darwin & Graham (1993), and 26-33º by Choi & Lee (2002) were reported for different rib-face angles. So the value of 17 degrees is used in this study for the minimum bearing angle. Sensitivity analysis of the Eq. (3.22) to different variables is shown in Figure 3.9(a). Results indicate that

the compressive strength of concrete (or normal stress at the rebar-concrete interface) (Figure 3.9(b)), and rib height are the most effective parameter for Eq. (3.21), which has similarly been reported by previous studies (Darwin & Graham 1993; Han et al., 2018). It can be deduced from Eq. (3.21) that the proposed formulation is independent of the rib–face angle and can be used for different types of rebar with rib pattern variation. Based on the sensitivity analysis (Figure 3.9), a smaller bearing angle indicates a higher bond strength which was similarly reported by Wu et al. (2012) for bond strength between enamel-coated rebar and concrete. Similar to the bearing angle, Eq. (3.21) shows that as rib spacing increases, bond strength reduces which can be attributed to the lower bond index ($f_R \approx h_r/S_r$). Similar trend has been stated by previous research (Fernández Ruiz et al. 2005; Metelli and Plizzari 2014).

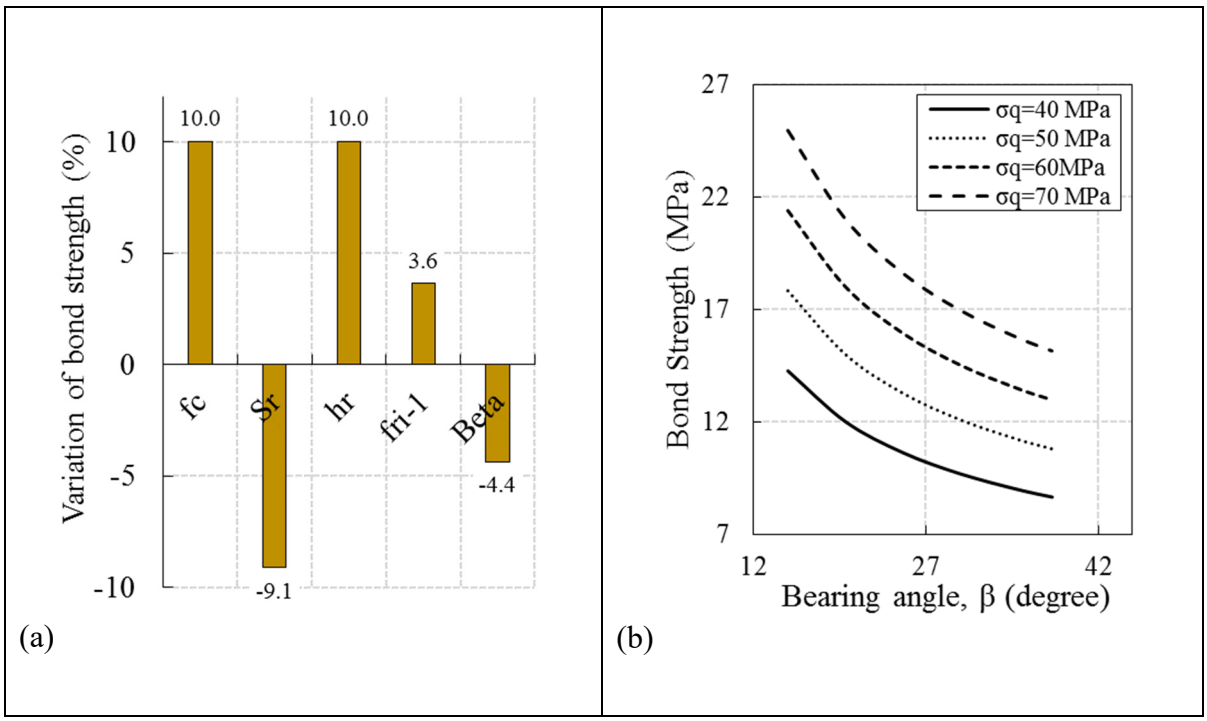

Figure 3.9 Sensitivity analysis of bond strength proposed by UM2:
(a) for a 10% increase in every variable (reference: $= 35$ degrees, $f'_c = 40$ MPa, $\mu_1 = 0.4, h_r = 1.89\ mm, S_r = 13.22$ mm);
(b) effect of bearing angles with respect to the bearing stress on the rib-front face

3.3.1.3 Performance of the proposed model for uncracked concrete

To determine the efficiency of the proposed model, the experimental results of uncracked concrete are used in this section. The proposed model of the first failure mechanism for uncracked concrete (UM1) shows obtainable results to be adjusted with the experimental results especially for models with friction coefficient higher than or equal to 0.40 (Figure 3.10(a, b)). The friction coefficient of the rebar-concrete interface has a considerable impact on bond strength. However, as shown in Figure 3.10(c, d), the proposed model for Mode-2 of uncracked concrete considerably underestimate the bond strength compared to the experimental results for both specimens of NC1-U and NC2-U. This can be attributed to the fact that the ratio of rib spacing-to-height of rebar used in the experimental program is equal to 7.0 which is lower than the range reported by Wu and Chen (2015) ($S_r/h_r > 10.0$) for crushing a wedge-shape concrete. The parametric study shown in Figure 3.10 indicate that as bearing angle increases, bond strength decreases so that bearing angle equal to the rib-face angle ($\beta = \alpha = 55$) represents the lowest interfacial strength, denoted as "rib sliding failure mechanism". In this case, the friction coefficient of the rebar-concrete interface (μ_1) has no impact on bond strength while μ_1 has a decisive role for a lower value of bearing angle.

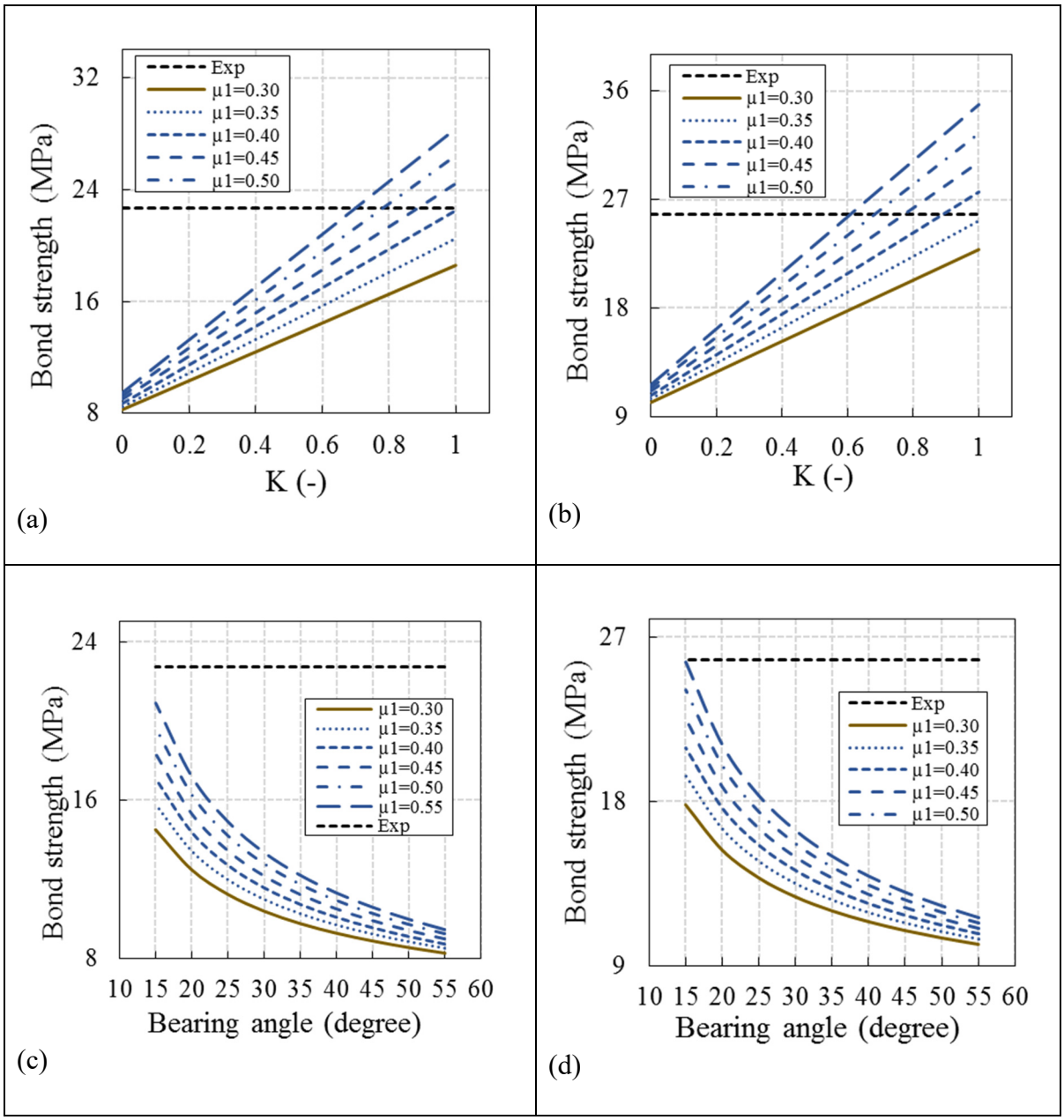

Figure 3.10 Performance of the proposed model for uncracked concrete:
(a) UM1, specimen NC1-U; (b) UM1, specimen NC2-U; (c) UM2, specimen NC1-U;
(d) UM2, specimen NC2-U

The parametric study illustrated in Figure 3.10(a, b) shows that the effect of friction coefficient on UM1 significantly reduces for a lower value of K while friction coefficient has a crucial role in the performance of UM1 with higher contact pressure. Also, the results of the proposed

model indicate that the reduction factor for contact pressure, K, has a critical role in the performance of UM1. A reduction factor lower than 0.6 considerably underestimates the bond strength especially for lower friction coefficient (Figure 3.10(a, b)), while UM1 model with a reduction factor of $0.61 < K < 0.7$ and a friction coefficient of 0.55 has the lowest deviation from experimental results for both compressive strengths (Table 3.2). In the case of $\mu_1 = 0.45$ (reported by Baltay & Gjelsvik (1990) and Zhao & Zhu (2018)), values of 0.89 and 0.78 are obtained for the reduction factor of contact pressure (Table 3.2).

Table 3.2 Results of UM1 for bond strength of steel rebar in uncracked concrete

Friction Coefficient (μ_1)	**Reference used**	**Best-fitted K [-]**	
		$f'_c = 47.9$	$f'_c = 58.8$
0.30	(Fernández Ruiz et al., 2005; Zhao & Zhu, 2017)	1.0 (18.1%)	1.0 (11.4%)
0.35	-	1.0 (9.4%)	1.0 (2.1%)
0.40	-	1.0 (0.82%)	0.89 (0.04%)
0.45	(Baltay & Gjelsvik, 1990; Zhao & Zhu, 2018)	0.89 (0.32%)	0.78 (0.37%)
0.50	-	0.78 (0.22%)	0.68 (0.29%)
0.55	-	0.7 (0.08%)	0.61 (0.11%)
$\mu_1 \approx 0.60$	(Dehestani et al., 2017; Rabbat & Russell, 1985; Wu & Chen, 2015)	0.63 (0.07%)	0.55 (0.35%)

* data inside the parentheses indicate the deviation between predicted bond strength of UM1 with the experimental results.

3.3.2 New model for pre-cracked concrete (CM)

Despite the observed failure modes for cracked specimens with $w \leq 0.15$ mm (pull-out, Figure 3.1(d)), no decisive observation is recorded for shearing-off the concrete for small crack widths. Hence, one scenario is followed in this section to present a modified version of UM2 for pre-cracked concrete, in which the normal stress on the rib-front face at the rebar-concrete

interface (σ_q) is reduced due to the reduction in the surrounding confinement by concrete. As reported by Murcia-Delso and Benson Shing (2014), 70% of bond strength can be provided by the bearing action between the rebar lugs and the surrounding concrete, while only 30% of bond strength is included by the friction action. After the pre-cracking phenomenon, this 70% portion of bearing force should be increased due to the separation of surfaces so that increases the critical role of surrounding confinement by concrete. As shown in Figure 3.11, different separation mechanisms can be occurred for pre-cracked concrete, including one-side and both-side separations. Parameter of φ can be defined for determining the portion of every side on bearing force. The value of $\varphi_1 = \varphi_2 = 0.5$ corresponds to the crack width of $w/2$ at every side which is suggested by Brantschen et al. (2016) as an idealized pre-cracking phenomenon.

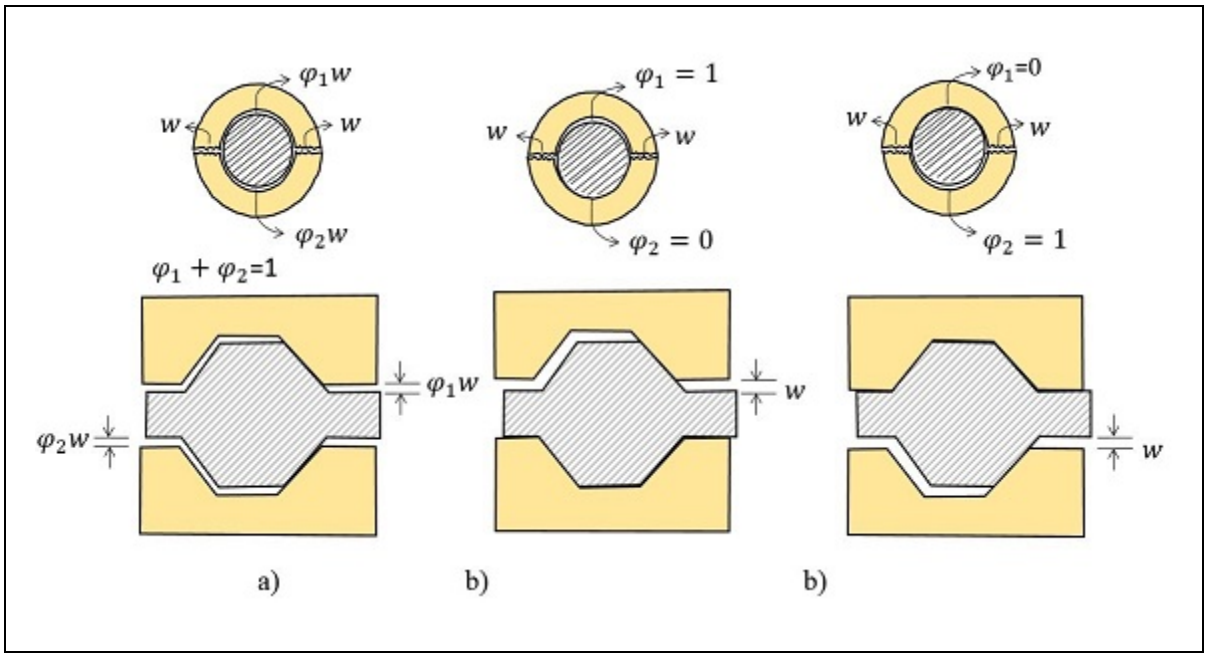

Figure 3.11 Different separation scenarios for cracked concrete:
(a) both-side separation; (b) one-side separation

Configuration of failure mechanism for pre-cracked concrete is presented in Figure 3.12. As mentioned for uncracked concrete, weak rebar-concrete bond strength causes concrete crushing in the front of the tip of rebar lugs. Hence, as illustrated in Figure 3.5(b), this failure mechanism is more appropriate for determining bond strength. There is no need for gripping

action of surfaces in uncracked concrete while for activating bearing force and gripping contact, an initial slip of between rebar and pre-cracked concrete is necessary. The horizontal force equilibriums of the crushed part of the rib-front area in Figure 3.12 can be expressed as:

$$L\tau_q x_1 + \tau_q y_1 \cos\alpha + \sigma_q y_1 \sin\alpha - \tau_n t_1 \cos\beta - \sigma_n t_1 \sin\beta = 0 \qquad (3.23)$$

where t_1 , x_1, and y_1 are derived from Figure 3.12. L is a reduction factor for contact pressure due to the pre-cracking phenomenon. As determining the contact areas around the rebar after pre-cracking is challenging and also inapplicable (illustrated in Figure 3.11), this reduction factor approximately demonstrates the confinement pressure of interfacial surfaces. The value of L =1.0 corresponds to uncracked concrete (Eq. 3.21) while $L \approx 0$ can be used for large separation due to the pre-cracking phenomenon.

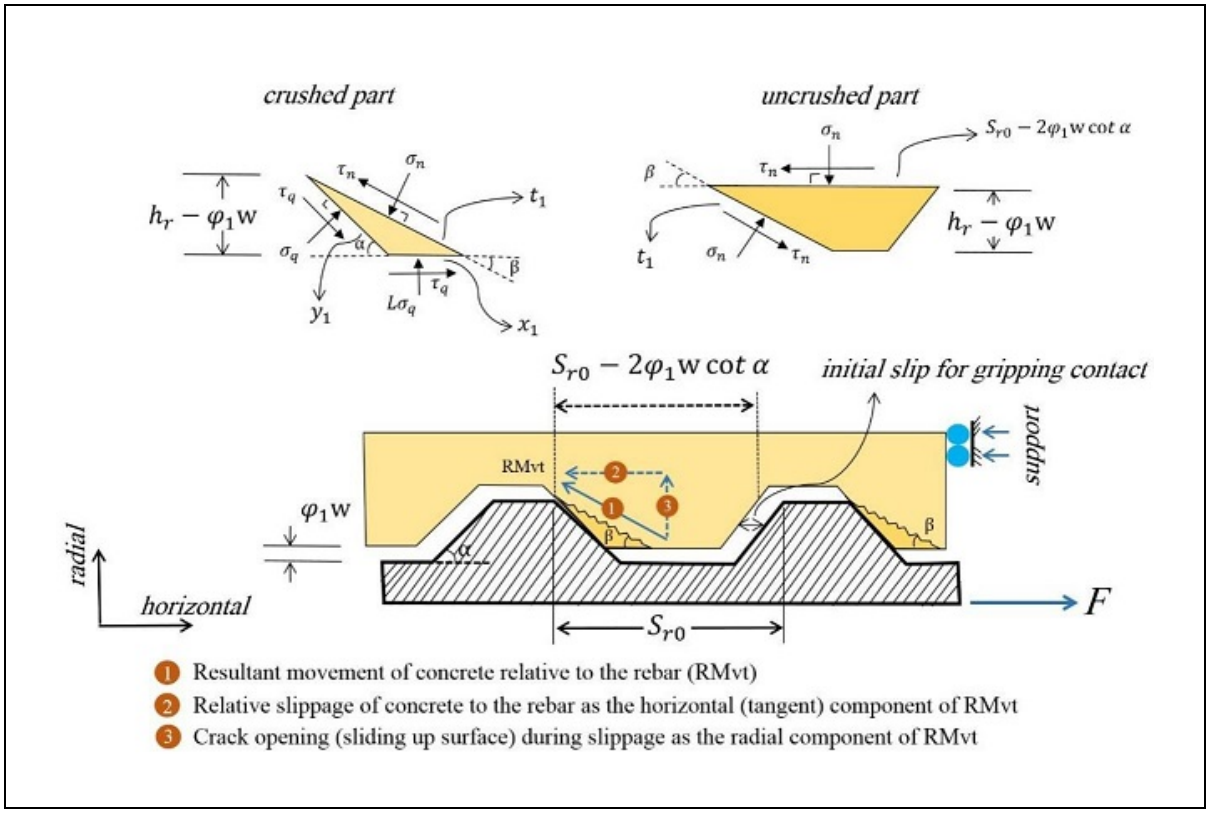

Figure 3.12 Failure mechanism of pre-cracked concrete at rib-front area
(unit thickness out of plane)

Substituting the Eqs. (3.6) and (3.7) into Eq. (3.23), the shear stress over the bearing concrete block is obtained as:

$$\tau_n = \frac{C + \mu_2\sigma_q(1 + \mu_1\,(1 - \mathrm{L})\cot\alpha + L\mu_1\cot\beta)}{(1 + \mu_2\cot\beta)} \tag{3.24}$$

Similarly, to the uncracked concrete, force equilibrium of the uncrushed part of concrete in contact with the crushed block gives (Figure 3.12):

$$-\bar{\tau}\,(S_{r0} - 2\varphi_1 w\cot\alpha) + \tau_n t_1\cos\beta + \sigma_n t_1\sin\beta = 0 \tag{3.25}$$

which results in the Eq. (3.26) for obtaining bond strength distributed over the spacing of periodical ribs:

$$\bar{\tau} = \frac{(h_r - \varphi_1 w)}{(S_{r0} - 2\varphi_1 w\cot\alpha)}\left[\frac{\tau_n(1 + \mu_2\cot\beta) - C}{\mu_2}\right] \tag{3.26}$$

By using the force equilibrium along the rebar:

$$\tau_{ave}\pi d_b l_e \;\cong\; \bar{\tau}\pi d_b(S_{r0} - 2\varphi_1 w\cot\alpha)\frac{l_e}{S_r} \tag{3.27}$$

Finally, rewriting Eq. (3.27) allows obtaining the average bond stress over the embedded length by:

$$\frac{\tau_{ave}}{\sigma_q} = \frac{(h_r - \varphi_1 w)}{S_r}[1 + L\mu_1\cot\beta + (1 - L)\mu_1\cot\alpha] \tag{3.28}$$

Hence, the average bond stress over the embedded length of pre-cracked concrete can be expressed as a function of:

$$\tau_{ave} = f(\sigma_q, \mu_1, h_r, S_r, \alpha, \beta, w, L, \varphi_1) \tag{3.29}$$

The parameter of $\varphi_1 w$ considered in Eq. (3.28) determine the geometry impact of crack width on bearing concrete blocks while the factor of L mainly determines the effect of pre-cracking on surrounding confinement due to the separation of the surface. As confinement increases due to the lower crack width, the factor of L increases so that the impact of β will be higher than α (Eq. (3.28)). However, for a lower confinement condition corresponding to a lower value of L, the effect of α on bond strength is dominant compared to the bearing angle. Sensitivity analysis of parameters on Eq. (3.28) is shown in Figure 3.13 for a 10% increase in the value for every parameter. Results indicate that concrete compressive strength, along with rebar geometries (rib height and spacing) play a significant role in the bond strength of rebar in pre-cracked concrete (Figure 3.13(a)). Parametric study of Eq. (3.28) shows that the contact reduction factor due to the pre-cracking phenomenon has a significant impact on bond strength, especially for lower values of bearing angles (Figure 3.13(b)). In the case of lower confinement (lower value of L), the bearing angle has no significant impact on bond strength compared to the case of high confinement (Figure 3.13(b)).

Cracks propagate after reaching the bond strength (crushing of concrete or contact sliding) which generates a higher impact of the pre-cracking phenomenon on the residual bond stress compared to the bond strength (Mousavi et al., 2019). Results for the splitting cracks measured by Guizani et al. (2017) indicate that cracks mostly propagate after reaching the bond strength for unconfined concrete and crack widths at bond strength are about 0.37 and 0.51 mm for unconfined and confined concrete respectively. So, low residual bond stress and additional slippage due to the crack-opening phenomenon leads to a lower slip of rebar corresponding to the final stage of residual bond stress, which is similarly reported by Mousavi et al. (2019). A lower slip at the residual bond stress phase is associated with a sudden drop in the bond-slip curve as an illustration of a brittle bond failure mechanism. Hence, in the case of pre-cracked concrete, initial crack width induced by the preloading can be used for calculating the bond strength, as considered in description of L and φw in Eq. (3.28).

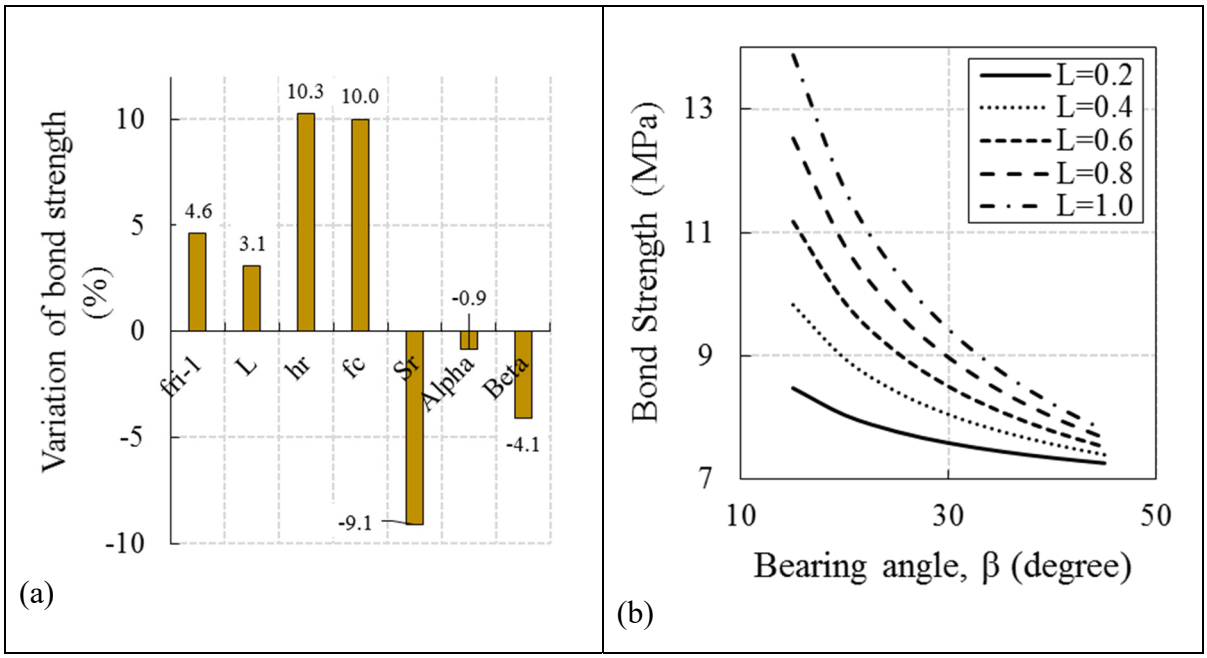

Figure 3.13 Sensitivity analysis of bond strength proposed for cracked concrete: (a) for a 10% increase in every variable (reference: $\alpha = 55°$, $f'_c = 40$ MPa, $\mu_1 = 0.4$, $h_r = 1.89\ mm$, $S_r = 13.22$ mm, $\beta = 20°$, w $= 0.1$, L $= 0.7$, and $\varphi = 0.5$); (b) effect of bearing angles concerning the reduction factor (L)

3.3.2.1 Performance of the pre-cracked concrete model (CM)

To determine the efficiency of the proposed model for bond strength of steel rebar in pre-cracked concrete, experimental tests of this study are used in this section. Best-fitted values obtained to accurately predict the bond strength are summarized in Table 3.3 for different crack widths. An adjustment between bearing angle, β, and the reduction factor of contact pressure due to the pre-cracking phenomenon, L, is conducted to obtain the lowest deviation from the experimental results. As confirmed by the proposed model for uncracked concrete (Figure 3.10 and Table 3.2), a value of 0.55 is used here for friction coefficient between steel rebar and surrounding concrete (μ_1) to study the efficiency of CM with experimental specimens. Overall, results indicate that for crack widths smaller than 0.40 mm, the proposed model can accurately predict the bond strength of steel rebar in pre-cracked concrete (Table 3.3). However, the proposed model overestimates the bond strength for crack widths larger than 0.40 mm.

Although this conservative and prudent prediction can be a good option for using in design codes, some simplified coefficient could be defined for both bearing angle and contact reduction factor.

Table 3.3 Results of CM for bond strength of steel rebar in cracked concrete

Crack width	**Best-fitted values**		$(\tau_{max})_{Eq.\ (3.27)}$	$(\tau_{max})_{Exp}$	**Deviation (%)**
	β **(degree)**	L **(-)**			
0.10	14	1.0	21.37	21.89	2.36
0.15	14	0.77	18.33	18.31	0.1
0.20	17	0.74	14.70	15.77	6.8
0.20	18	0.67	18.01	18.05	0.23
0.30	37	0.35	11.66	11.64	0.15
0.40-0.5	55	≈ 0	8.57	4.62	Overestimation

From Eq. (3.28) and Figure 3.14, it can be deduced that a good correlation exists between the reduction factor of contact pressure and the reduction factor of bond strength (defined by Eq. (3.3)). Hence, parameter L can be directly replaced by the factor ρ_{nm}, as follows:

$$L = -0.27{\rho_{nm}}^2 + 1.29\rho_{nm} \tag{3.30}$$

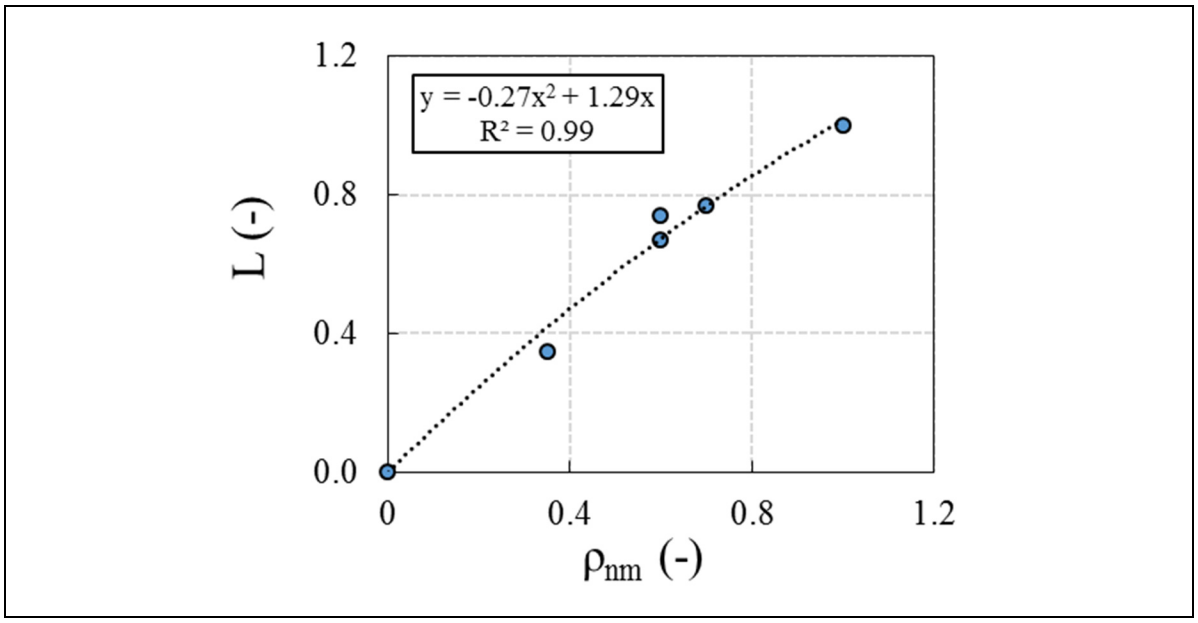

Figure 3.14 Reduction factor of contact pressure relative to the reduction factor of bond strength due to the pre-cracking phenomenon

Overall, results summarized in Table 3.3 indicate that as crack width increases, the bearing angle of crushed concrete, β, increases in the pre-cracked concrete. A good correlation exists between the normalized bearing angle (β/α) and crack width (R^2=0.92, Figure 3.15). Cracking at the rebar-concrete interface changes the confinement condition. As shown in Figure 3.15, high confinement condition attributes to the uncracked concrete or pre-cracked with low crack width. Large crack widths cause a reduction on the rebar-concrete surface and results in a low confinement condition. This weak rebar-concrete interface results in a rib sliding failure mechanism with a bearing angle (β) close to the rib-face angle, α. It is worth emphasizing that concrete cover is the only surrounding confinement for experimental specimens tested in this study. All reported results are based on this determined condition. Hence, more experimental studies are necessary to determine the effect of the pre-cracking phenomenon in concrete confined by transverse reinforcement, different non-ferrous rebars, and also calibrate the different coefficients presented in this study for predicting bond strength as a function of rib geometries for more extensive conditions.

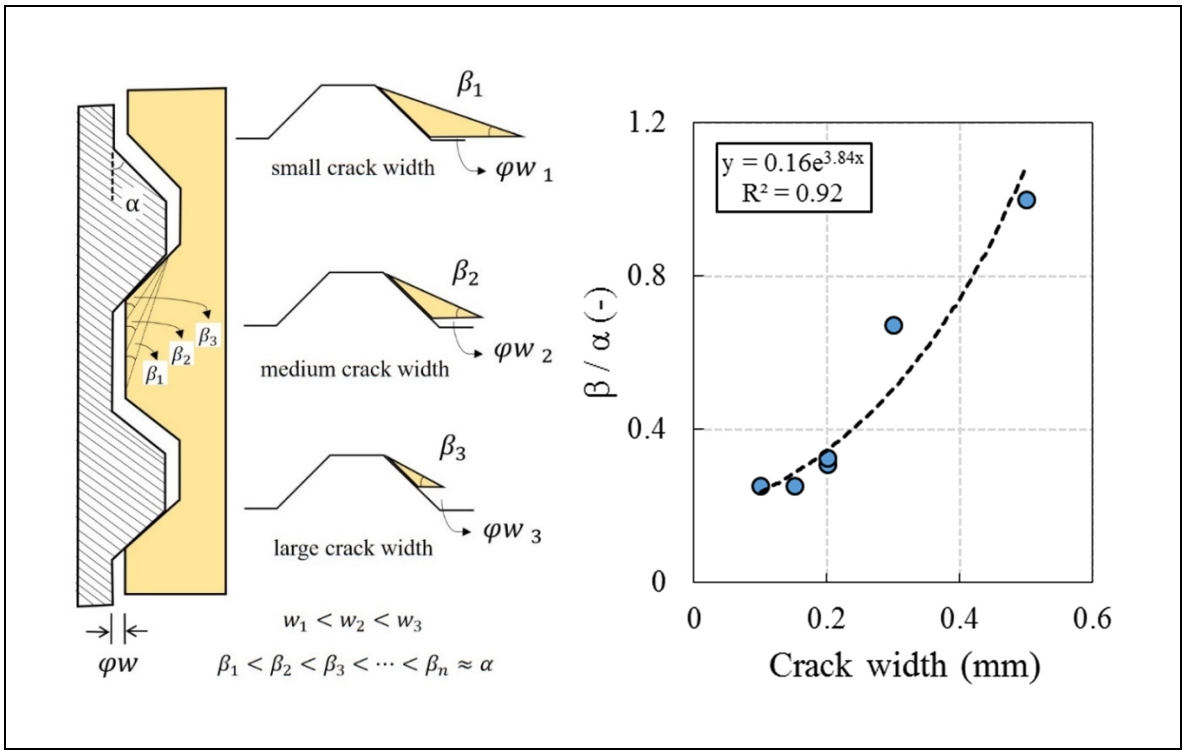

Figure 3.15 Normalized bearing angel versus crack width for pre-cracked concrete

3.4 Conclusion

As there is no specific investigation on the prediction of the bond strength of steel rebar in pre-cracked concrete, an experimental program is performed in this study to present a simplified analytical model for the pre-cracking phenomenon. Further, this paper introduces a simplified model for uncracked concrete, as well as a modified version by adjusting parameters for pre-cracked concrete. Degradation of the surrounding confinement is considered as a function of surface separation variables.

Regarding the main objective of this study, which is to present a practical and simplified bond model for use in numerical simulations of reinforced concrete members, the proposed model for uncracked concrete satisfactorily predicts the bond strength of steel rebar in moderately confined uncracked concrete. Fundamental properties of the rebar geometries and contact characteristics are considered in the proposed model. A frictional coefficient of about 0.55 is

obtained as a best-fitted value of the rebar-concrete interface property based on the experimental results. Regarding the rib geometries of rebar used in this study, mode-2 of uncracked concrete (crushing a wedge-shaped concrete block) significantly underestimates the bond strength, which is confirmed by several previous studies. The pre-cracking phenomenon changes the bond failure mechanism so that by increasing the crack width, a weak rebar-concrete interface leads to “rib sliding failure”. Although proposed models accurately predict the bond strength of rebar in pre-cracked concrete of moderately confined concrete, overestimate prediction is obtained for large crack widths ($w \geq 0.40$ mm).

Regarding the efficiency of the proposed model for pre-cracked concrete, very encouraging and satisfactory results are obtained. However, more experimental studies are needed to adjust the parameters of the proposed model for the high confinement condition, where the impact of crack width opening can be controlled by transversal reinforcement. Moreover, only a simplified model is presented in this study, while more experimental tests and verifications are needed to achieve a perfect bond model for pre-cracked concrete.

CHAPTER 4

EFFECT OF CONCRETE WORKABILITY ON BOND PROPERTIES OF STEEL REBAR IN PRE-CRACKED CONCRETE

Seyed Sina Mousavi [a], Lotfi Guizani [b], Chandrasekhar Bhojaraju [c], and Claudiane Ouellet-Plamondon [d]

[a, b, c, d] Department of Construction Engineering, École de Technologie Supérieure, 1100 Notre-Dame West, Montreal, Quebec, Canada H3C 1K3

Paper submitted for publication in *Proceedings of the Institution of Civil Engineers: Structures and Buildings,* April 2020

Abstract

Although previous research has shown a considerable influence of the pre-cracking phenomenon on steel-congested concrete structures, only normal concrete (NC) has been considered in the literature. Hence, this paper intends to study the effect of the pre-cracking phenomenon on the bond response of pre-cracked NC, concrete with moderate slump flow, and self-consolidating concrete (SCC). Initial crack widths ranging from 0.0 to 0.5 mm are studied. Results show that initial crack widths larger than 0.10 mm have a significant influence on bond properties so that higher than 30% and 50% reduction factors are obtained for the maximum bond strength of concrete specimens exposed to the initial crack widths of 0.2 mm and 0.4 mm respectively. Results show that concrete mixtures with higher workability are less sensitive to the pre-cracking phenomenon as compared to NC mixtures. The average bond stress of steel rebar in the pre-cracked SCC is found to be similar to that of the NC with a slump flow of 200 mm, which is considerably better than for NC with 97 mm slump flow. Moreover, results show that 65.8%, 80.6%, 88.5%, and 93.1% fracture energy reductions are obtained for crack widths of 0.20, 0.30, 0.40, and 0.50 mm, respectively, as compared to small crack width of 0.15 mm.

Keywords: bond strength; self-consolidating concrete; pre-cracked concrete; steel rebar; flowability.

4.1 Introduction

Recently, there has been a growing tendency of studying bond responses of steel rebar embedded in cracked concrete, denoted as "pre-cracking phenomena", in which cracks develop through a plane containing a rebar axis (Brantschen et al., 2016; Lindorf, 2011; Matsumoto et al., 2016; Mousavi et al., 2019; Mousavi et al., 2020). Until now, different expressions have been used in the literature for describing the pre-cracking phenomenon including mechanical pre-loading (Brantschen et al., 2016), biaxial load transfer (Lindorf et al., 2009; Saadeghvaziri & Hadidi, 2005), multiaxial stress states (Purainer, 2005), and transverse tension (Lindorf, 2011). These situations provide the propagation of cracks parallel to the rebar direction, which generates internal damages at the rebar-concrete interface. Unlike the corrosion-induced cracking at the rebar-concrete interface, plastic shrinkage cracks in steel-congested concrete structures (Hadidi & Saadeghvaziri, 2005; Saadeghvaziri & Hadidi, 2005) and accidental damages due to the previous overloading (such as earthquakes and/or overstress situations) (Matsumoto et al., 2016) can cause pre-cracking phenomenon, in which corrosion has no significant impact.

Recently, Brantschen et al. (2016) studied the bond behaviour of rebars in pre-cracked concrete by presenting the results of an experimental investigation including 89 monotonic pull-out tests with initial crack openings ranging from 0.20 mm to 2.0 mm. They have shown that in-plane cracking has a significant influence on the maximum bond strength and bond-slip envelope curve. Moreover, they have used the aggregate interlock approach for analytical modeling the effect of in-plane cracking on bond behaviour, considering bond index. However, they have reported that the bond index, in its current form, could not adequately characterize bond properties in cracked concrete. They recommended other rib geometry parameters such as rib orientation, lug width, and spacing for different rebar types for future studies related to the pre-

cracking phenomenon (Brantschen et al., 2016). In this field, Mousavi et al. (2019) presented a specific bond-slip model and also development length formulation for steel rebar embedded in pre-cracked NC. They have considered crack width (ranging from 0.10 mm to 0.40 mm) in their formulations. Recently, Mousavi et al. (2020) proposed a simplified model for bond-slip response in pre-cracked NC. They used rebar deformations (rib height and distance) and crack width to introduce an analytical model for predicting the bond strength of rebar embedded in the pre-cracked concrete.

As reported by the previous research, steel-congested concrete members have been mostly affected by pre-cracking phenomenon (Matsumoto et al., 2016), such as the typical surface crack pattern of a slab specimen reinforced with transverse elements (cracks in punching area around column) (Brantschen et al., 2016), flexural reinforcement in slabs (Dawood & Marzouk, 2012), and joints (Joergensen & Hoang, 2015). However, only NC has been considered in the previous researches, while relatively new generations of concrete mixture have been used to relieve the steel-congested regions and maintain desired structural behaviour, such as NC with a high slump (higher than 150 mm) and/or SCC with slump values higher than 500 mm (Mousavi et al., 2017; Mousavi et al., 2016).

Few studies have investigated the effect of concrete workability on mechanical properties of reinforced concrete members especially bond strength. They presented some conflicting results. The addition of a higher amount of water, using different types of superplasticizer, using a high amount of fine aggregates, using air-entraining (AE) admixture, and addition of fillers are different approaches used for increasing the workability of concrete mixtures. Most of these studies have concentrated on “the top bar effect” in which concrete mixtures with a higher slump increase the risk of the bleeding phenomenon and tend to crack more easily. This increases the porosity of the hydrated cement paste surrounding the lower parts of horizontally placed rebar (Khayat & Guizani, 1997). However, despite the “top bar effect”, few studies have determined the effect of concrete workability on normally-positioned rebar without bleeding phenomenon. In this field, Collepardi & Corradi (1979) reported that the addition of chemical admixtures (naphthalene-sulfonated polymer-based superplasticizers) improves the

rebar-concrete bond strength for both ordinary and lightweight mixtures along with the flowability of concrete mixtures. Similarly, Fu & Chung (1998) and Pop et al. (2015) reported that with an increase in the fluidity of concrete mixture, the interfacial void content decreases causing higher bond strength. However, Brettmann et al. (1986) showed that high slump NC made with a high-range water-reducer (HRWR) has a lower bond strength as compared to a low slump concrete of equal strength. In this field, Zilveti et al. (1985) reported that high slump concrete has bond strengths comparable to that of low slump mixture, which was similarly confirmed by Thrane et al. (2010). Some previous studies discussed these conflicting and scattered results on the effect of concrete workability on the bond strength (Mousavi et al., 2017, Mousavi et al., 2016).

Hence, the present study intends to determine the effect of concrete workability (or flowability) on the bond response of steel rebar embedded in pre-cracked concrete. To address this issue, the results of an experimental program are provided in the current study. Three different concrete mixtures with different slump values are considered for this experimental program, where the bond response of pre-cracked concrete is studied through pull-out tests. A comparison study is performed on test results to determine the influence of using concrete with high flowability in steel-congested concrete members exposed to the pre-cracking phenomenon.

4.2 Experimental program

4.2.1 Materials

Three different concrete mixes are considered for this experimental program made of a general use Portland cement (CSA A3001 type GU or ASTM C150 type I) with a density of 3.15 g/cm^3, natural sand with a maximum grain size of 1.25 mm and a specific gravity of 2.68, and gravel with a particular gravity of 2.68 and a nominal maximum diameter of 14 mm and 20 mm for normal (NC) and self-consolidating concrete (SCC) respectively. Limestone powder is used as a filler in SCC mixtures with a relative density of 2.68 and a maximum particle size of about

200 μm. The particle size distribution of the cement and limestone powder is illustrated in Figure 4.1. Mixture proportions, fresh properties, and compressive strength are given in Table 5.1. NC1, NC2, and SCC correspond to NC with a slump of 97 mm, moderate flowable concrete with a slump of 200 mm, and SCC with a slump flow of 709 mm respectively. Water-to-total powder ratios of 0.41, 0.43, and 0.41 are considered for mixtures of NC1, NC2, and SCC.

Table 4.1 Mixture proportions, fresh properties, and compressive strength

Constituent	**Quantity (kg/m^3)**		
	NC1	**NC2**	**SCC**
Water	165	170	215
Cement (GU)	395	395	420
Limestone powder	-	-	105
Fine aggregate	788	788	940
Coarse aggregate (5-10 mm)	822	822	352
Coarse aggregate (10-14 mm)	258	258	219
Coarse aggregate (14-20 mm)	-	-	270
Superplasticizer	2.34	5.2	5.0
Viscosity modifying admixture	-	-	2.5
Air entraining admixture	-	0.83	-
w/c	0.41	0.43	0.51
w/p[1]	0.41	0.43	0.41
Fresh mix temperature (ºC)	20.9	21.8	22.7
Slump (mm)	97	200	709
T_{50} (s)	-	-	2.37
Hardened density (kg/m^3)	2453.80	2390.08	2375.70
f'_c (MPa)	58.82 (1.39)[2]	38.80 (0.95)	40.34 (0.72)

[1] water-to-powder ratio, p=weight of powder (cement+limestone).
[2] data inside the parentheses denote the standard deviation.

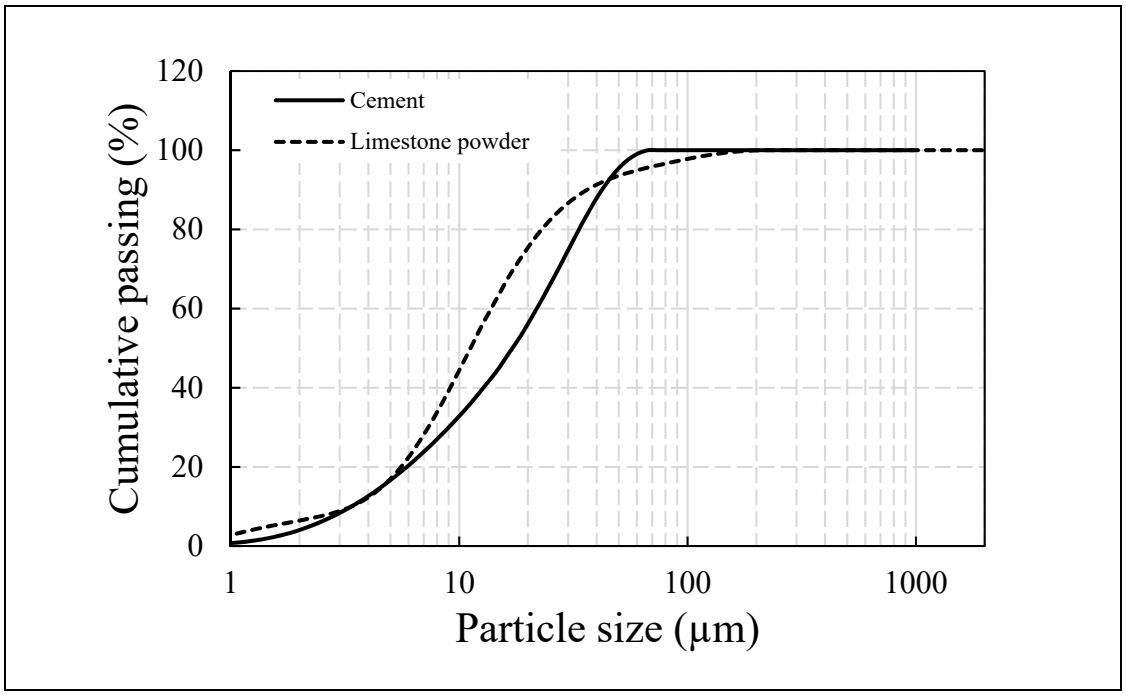

Figure 4.1 Particle size distribution of the powders used in the present study

4.2.2 Specimens and test set-ups

For each mixture, 3 cylindrical specimens with a diameter of 100 mm and a height of 200 mm are prepared to measure compressive strength. A total number of 26 cylindrical specimens with a diameter of 150 mm and a height of 113 mm are also considered for pull-out tests under monotonic loading including 9 uncracked and 17 cracked specimens (Figure 4.2(a)). All specimens are cured for 28 days in a moisture room at 97.3% relative humidity (RH) and 23 ºC temperature. To simulate the pre-cracking phenomenon, an indirect tensile test (Brazilian splitting test) is considered for generating cracks in the plane of the rebar placed at the center of cylindrical specimens (Figure 4.2(b)). A displacement-controlled loading with a rate of 0.15 mm/min is applied to prevent unexpected splitting failure during the pre-cracking loading. To measure the crack width, two crack gauges are installed at both sides of concrete cylinders. As crack width changes with unloading, the ultimate crack width is directly measured after stopping the pre-cracking procedure (Figure 4.2(c)). Direct pull-out tests are carried out by applying tensile force directly to the rebar by gripping the rebar from one side of the specimen.

The unloaded end slip is measured with a linear variable differential transformer (LVDT). To provide a relatively uniform distribution of bond stresses, the embedment length of the rebar is 50 mm (five times the nominal diameter of rebar) in all specimens. This short embedded length provides a better measurement of local bond strength by the average bond stress. Plastic sleeves are used for unbonded length (Fig. 4.2(a)). An automatic data acquisition system is used to record the data. A displacement-controlled pull-out force is applied at the rate of 0.5 mm/min. As the main focus of this paper is on the effect of pre-cracking on bond strength including strength and failure modes, it is tried to impede splitting bond failure by providing enough concrete cover around the rebar ($c_c/d_b = 7.5$). In all cases, the rebar is positioned at the center of cylinders. The used steel rebars have a diameter of 10 mm with a specified yield strength and ultimate tensile strength of 432 MPa and 620 MPa respectively. The surface characteristics and rib pattern of the rebars used are shown in Figure 4.2(d). The average value of rib–face angle for rebars used in the experimental program is about 55 degrees. The ratio of rib spacing-to-rib height (S_r/h_r) is about 7.0.

4.3 Experimental results

As mentioned widely in the literature (Guizani et al., 2017; Wu & Zhao, 2012), for the short bond region (generally five times the rebar diameter), bond stress is close to uniform distribution and can be used to get a better measure of local bond strength by averaging the bond stress along the anchored length. Hence, in the pull-out test, average bond stress, τ (N/mm^2), can be calculated by Eq. (4.1), where F is the tensile load, d_b is the rebar diameter, and l_e is the embedded length. Also, the average bond stress can be plotted as a function of slip (mm), measured by LVDTs.

$$\tau = \frac{F}{\pi d_b l_e} \tag{4.1}$$

As recommended by RILEM TC (1994), arithmetic mean of bond stresses (denoted as "average bond stress") is calculated by Eq. (4.2), in which variables $\tau_{0.01}$, $\tau_{0.10}$, and $\tau_{1.00}$ corresponding to bond stresses at slips of 0.01 mm, 0.10 mm, 1.0 mm respectively.

$$\tau_m = \frac{\tau_{0.01} + \tau_{0.10} + \tau_{1.00}}{3} \quad (4.2)$$

Based on the literature (Mousavi et al., 2019; Trezos et al., 2014), maximum (or ultimate) bond stress, τ_u, average bond stress, τ_m, residual bond stress corresponding to a slip of 10.0 mm, τ_r, and area under the bond-slip curve (denoted as bond energy, E_b) are considered as representative variables for the comparison of bond responses of different mixtures. All representative bond stresses are normalized to the square root of the concrete strength of each mixture, $\tau/\sqrt{f_c}$, to eliminate the effect of concrete compressive strength for.

Overall, results of uncracked and pre-cracked concrete, as well as the failure modes, are summarized in Table 4.2 including bond strength, average bond stress, and residual bond stress. Crack widths ranging from 0.0 (uncracked) to 0.5 mm are obtained following the pre-cracking tests. Specimens are designated by the type of concrete (NC1, NC2, and SCC) followed by the letter "C" and crack width in mm for pre-cracked concrete, or only "U" for uncracked concrete. Although three specimens are considered for every crack width, only two repetitions are obtained in some cases due to the brittle nature of the pre-cracking test and to the difficulty of controlling the target crack width. The pull-out failure mode is observed for uncracked specimens (Figure 4.3(a)). Similarly, pre-cracked specimens with crack widths smaller than 0.15 mm (w < 0.15 mm) failed by pulling out the rebar without splitting the surrounding concrete coverage. Similar results for NC have been reported by Mousavi et al. (2019), in which small crack width has no impact on bond failure mechanisms. However, large crack widths significantly affect the bond strength and also failure modes i.e., splitting failure mode is obtained for pre-cracked specimens with $w \geq 0.15\ mm$ (Figure 4.3(b)).

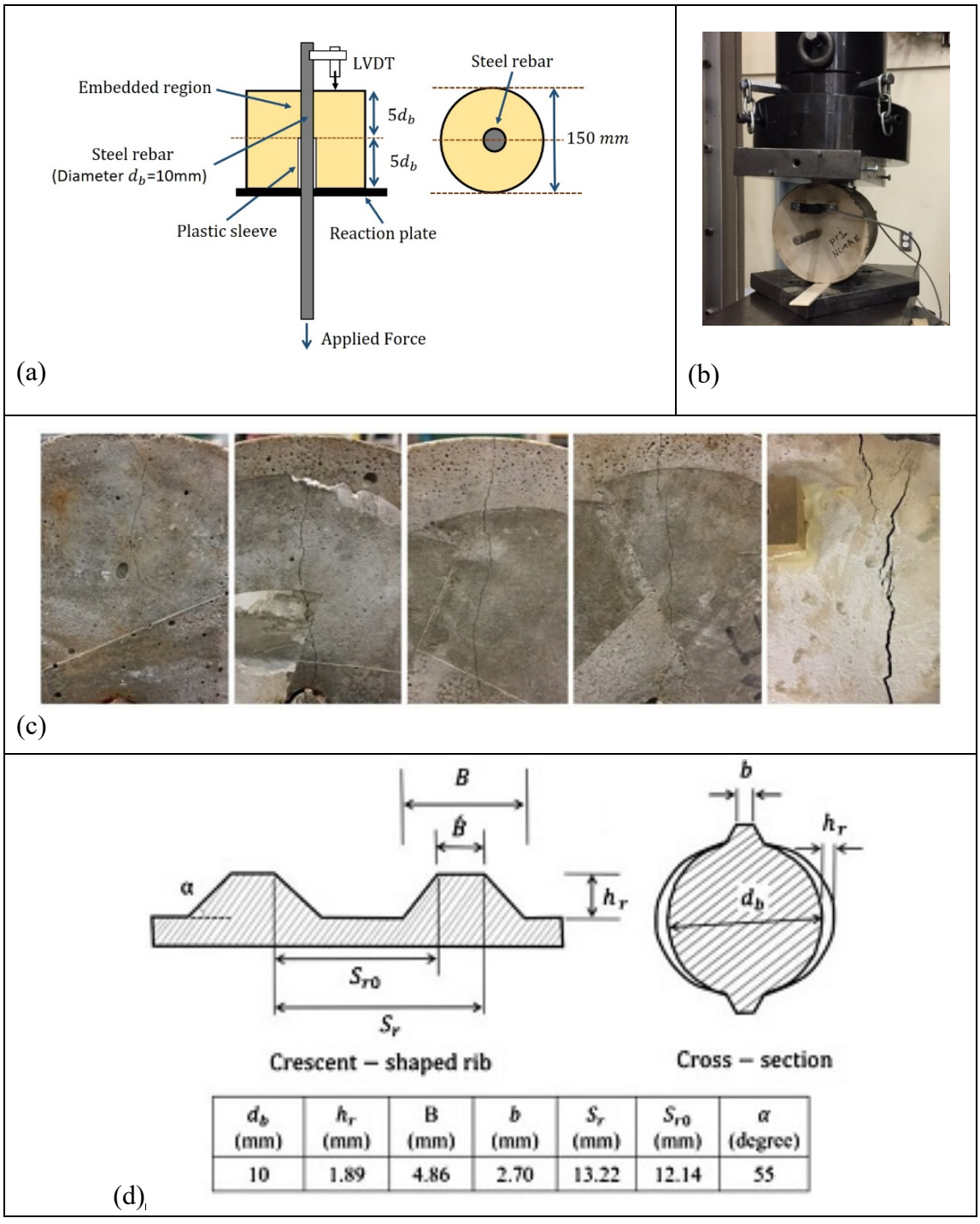

d_b (mm)	h_r (mm)	B (mm)	$\dot{b}$ (mm)	S_r (mm)	S_{r0} (mm)	α (degree)
10	1.89	4.86	2.70	13.22	12.14	55

Figure 4.2 Test set-up: (a) specimen dimensions and pull-out test setup; (b) pre-cracking test; (c) pre-cracked specimens; (d) rebar geometry

Table 4.2 Bond characteristics of mixture

Specimens	w	τ_m	$\tau_m/\sqrt{f'_c}$	τ_u	$\tau_u/\sqrt{f'_c}$	τ_r	$\tau_r/\sqrt{f'_c}$	E_b	**Failure***
NC1-U	0	19.48	2.54	25.19	3.28	5.77	0.75	146.0	P
	0	15.35	2.00	25.07	3.27	5.55	0.72	147.9	P
	0	17.36	2.26	27.12	3.54	8.18	1.07	163.6	P
	average	17.40 (2.07)	2.27 (0.27)	25.79 (1.15)	3.36 (0.15)	6.50 (1.46)	0.85 (0.19)	152.5	-
NC1-C0.2	0.20	7.32	0.95	18.05	2.35	0.00	0.00	12.6	S
NC1-C0.3	0.30	3.59	0.47	12.87	1.68	0.66	0.09	9.1	S
	0.30	3.85	0.50	10.41	1.36	0.01	0.00	8.8	S
	average	3.72 (0.18)	0.49 (0.02)	11.64 (1.74)	1.52 (0.23)	0.34 (0.46)	0.05 (0.06)	8.9	-
NC1-C0.4	0.40	1.46	0.19	4.71	0.61	0.17	0.02	4.0	S
	0.40	1.92	0.25	4.51	0.59	0.00	0.00	1.1	S
	average	1.69 (0.33)	0.22 (0.04)	4.61 (0.14)	0.60 (0.01)	0.09 (0.12)	0.01 (0.01)	2.6	-
NC2-U	0	14.37	2.31	24.74	3.97	14.60	2.15	180.1	P
	0	14.75	2.37	26.68	4.28	14.25	2.29	203.3	P
	0	18.18	2.92	27.47	4.41	17.75	2.85	221	P
	average	15.77 (2.10)	2.53 (0.34)	26.30 (1.40)	4.22 (0.23)	15.53 (1.93)	2.43 (0.37)	201.5	-
NC2-C0.1	0.10	13.30	2.13	21.85	3.51	0.0	0.0	117.0	S-P
NC2-C0.15	0.15	9.89	1.59	18.48	2.97	0.0	0.0	82.5	S
NC2-C0.5	0.50	2.75	0.44	5.51	0.88	0.56	0.09	8.11	S
	0.50	2.33	0.37	4.09	0.66	0.09	0.01	3.47	S
	average	2.54 (0.30)	0.41 (0.05)	4.80 (1.00)	0.77 (0.16)	0.33 (0.33)	0.05 (0.06)	5.79	-
SCC-U	0	14.61	2.30	23.95	3.77	12.95	2.04	180.6	P
	0	15.81	2.49	24.71	3.89	12.17	1.92	176.7	P
	0	15.53	2.45	25.16	3.96	11.52	1.81	171.3	P
	average	15.32 (0.63)	2.41 (0.10)	24.61 (0.61)	3.87 (0.10)	12.21 (0.72)	1.92 (0.12)	176.2	-
SCC-C0.1	0.10	16.38	2.58	23.20	3.65	4.97	0.78	108.0	P
SCC-C0.2	0.20	7.19	1.13	18.43	2.90	0.41	0.06	16.7	S
	0.20	4.98	0.78	16.83	2.65	0.0	0.0	9.8	S
	0.20	8.15	1.28	19.68	3.10	1.66	0.26	49.3	S
	average	8.77 (1.63)	1.06 (0.26)	18.31 (1.43)	2.88 (0.23)	0.69 (0.86)	0.11 (0.14)	25.3	-
SCC-C0.3	0.30	2.84	0.45	15.11	2.38	0.08	0.013	5.9	S
	0.30	7.89	1.24	14.33	2.26	0.35	0.06	17.4	S
	average	5.37 (3.57)	0.85 |(0.56)	14.72 (0.55)	2.32 (0.08)	0.22 (0.19)	0.04 (0.03)	11.7	-
SCC-C0.4	0.40	4.74	0.75	10.31	1.62	0.23	0.04	11.8	S
	0.40	5.29	0.83	9.90	1.56	0.10	0.02	7.7	S
	average	5.02 (0.39)	0.79 (0.06)	10.11 (0.29)	1.59 (0.04)	0.17 (0.09)	0.03 (0.01)	9.8	-

* Modes of failure: P=pull-out; S=splitting.
Note: data inside the parentheses denote the standard deviation.

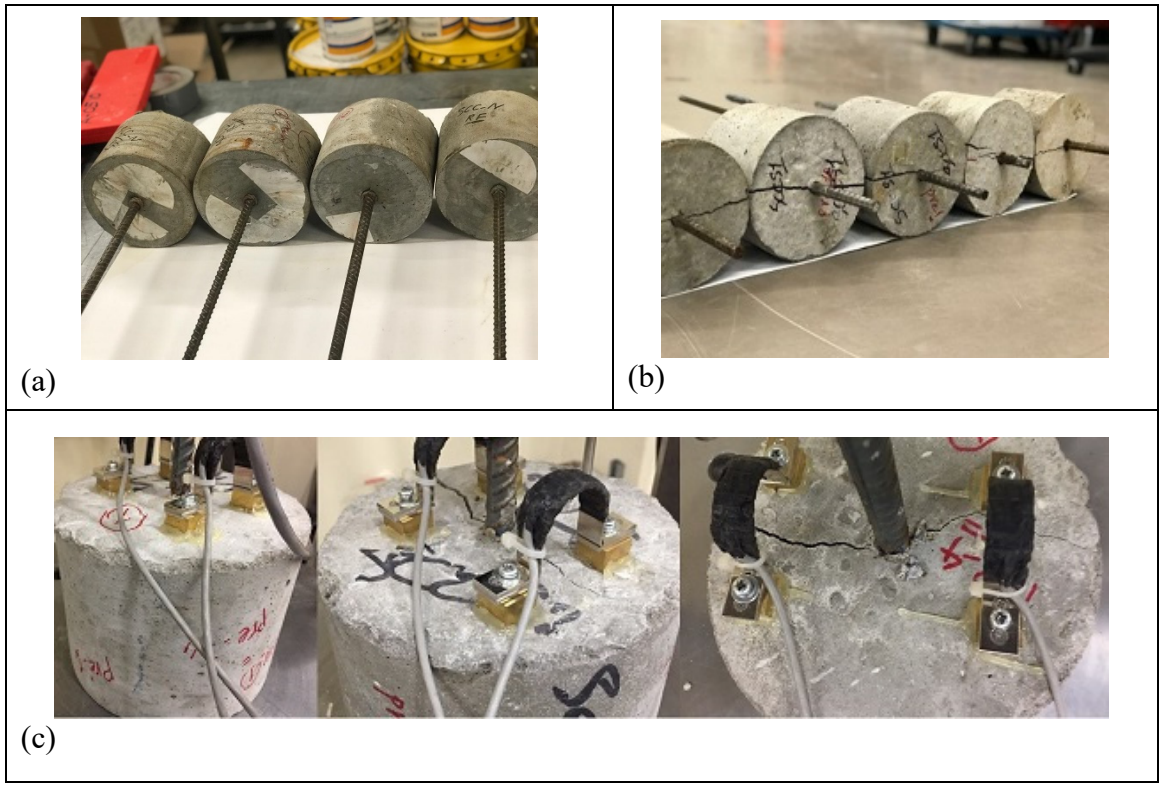

Figure 4.3 Failure modes: (a) pull-out; (b) splitting; (c) crack opening during pull-out tests

4.3.1 Uncracked concrete

Bond-slip curves of uncracked concrete for different mixtures along with the normalized bond properties are illustrated in Figure 4.4(a). Although comparable results are obtained for the normalized average bond stress, general results indicate that NC2 mixture has the highest interfacial maximum bond strength and NC1 has the lowest values (Fig. 4.4(b)). Although SCC and NC2 mixtures have an approximately similar compressive strength of 38.80 MPa and 40.34 MPa respectively (Table 4.1), SCC has lower bond properties as compared to NC2. However, bond strength and residual bond stress of SCC are higher than NC1 with the same water-to-powder ratio of 0.41. Although many studies have reported the higher amount of bond strength of steel rebar in SCC than NC (de Almeida Filho et al., 2008; Desnerck et al., 2010; Mousavi et al., 2017; Sabău et al., 2016; Valcuende & Parra, 2009; Zhu et al., 2004), some studies have shown SCC to have either lower or the same bond strength compared to NC

(Castel et al., 2006; Esfahani et al., 2008; Gibbs & Zhu, 1999; König et al., 2001; Lorrain & Daoud, 2002; Pandurangan et al., 2010; Schiessl & Zilch, 2001). Different reasons have been listed for these inconsistent results including concrete mixtures and the experimental conditions (Sfikas & Trezos, 2013). Comparing mixtures with the same average bond stress (τ_m), as recommended by RILEM, is appropriate in the section of pre-cracked concrete as this parameter is meaningful notably about on both bond strength and the initial stiffness.

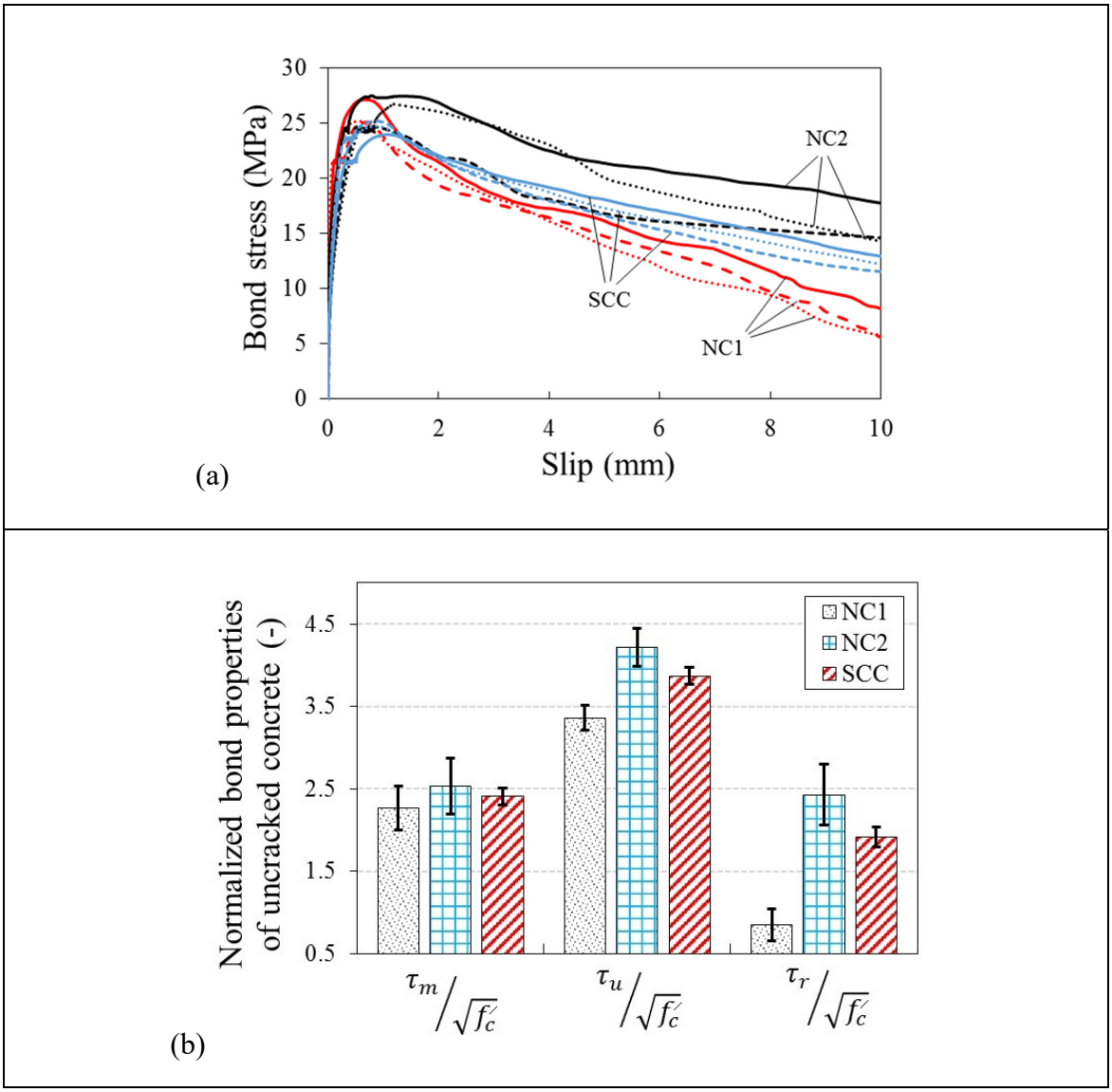

Figure 4.4 Uncracked concrete results: (a) bond-slip curves; (b) normalized bond properties

4.3.2 Pre-cracked concrete

Bond-slip curves of pre-cracked concrete for the studied concrete mixtures are shown in Figure 4.5. General results show that the pre-cracking phenomenon has a significant impact on bond-slip curves so that a high reduction is observed for bond energy in pre-cracked concrete. In the case of uncracked concrete, there is a plateau after the bond strength, while a sudden drop is observed for pre-cracked concrete in all mixtures. As crack width increases, the slope of the descending branch of the bond-slip curve increases, which shows a more rapid drop in bond stress with increasing slip (Figure 4.5). Although specimens with small initial crack widths (w<0.15 mm) have similar plateau at the peak, the pre-cracking phenomenon affects the residual bond strength so that the slope of the descending branch of the bond-slip curve is higher compared to uncracked concrete (Fig. 4.5(a, c)). This leads to around 39.0% and 42.0% reductions in the area under the bond-slip curves (characteristic bond energy, E_b) (Table 2). A low characteristic energy value corresponds to the brittle bond behaviour, while a high energy value results from a ductile bond response (Mousavi et al., 2019). To determine the bond strength reduction due to the pre-cracking phenomenon, a reduction factor is defined as below:

$$RF = \left[\frac{\tau_{Uncracked} - \tau_{Pre-cracked}}{\tau_{Uncracked}}\right] \times 100 \tag{4.3}$$

where $\tau_{Uncracked}$ and $\tau_{Pre-cracked}$ are bond strengths of uncracked and pre-cracked concrete respectively, which are listed in Table 4.2. Reduction factor corresponds to the bond strength of mixtures is illustrated in Figure 4.6(a). Results indicate that SCC has the lowest reduction factor, corresponding to the maximum bond strength, among the other mixtures. On the other hand, results of the maximum bond strength indicate that SCC mixture is less sensitive to the pre-cracking phenomenon among the concrete mixtures. This can be attributed to the high paste content in SCC mixture compared to NC mixtures. Regarding NC, a higher value of slump has a positive impact on the sensitivity of concrete to the pre-cracking phenomenon, so that NC2 has a lower reduction factor compared to NC1 for the bond strength. Regarding uncracked concrete, Fu & Chung (1998) and Pop et al. (2015) reported that with increase in

the slump (fluidity) of concrete mixture, the interfacial micro voids around the rebar decreases causing a higher bond strength. Uniform distribution of matrix and aggregate surrounding the rebar, due to the higher slump of concrete, may increase the probability of the aggregate interlocking phenomenon across the initial cracks. This phenomenon causes an increase in the maximum and average bond strength of concrete mixtures with a high slump. As shown in Figure 4.6(a), the reduction factor of the bond strength has a good empirical correlation with crack width (w) for all mixtures as follows:

$$RF_{NC1} = 163.36w \qquad R^2 = 0.99 \qquad (4.4)$$

$$RF_{NC2} = 193.68w \qquad R^2 = 0.96 \qquad (4.5)$$

$$RF_{SCC} = 138.30w \qquad R^2 = 0.95 \qquad (4.6)$$

Similarly, in the case of average bond stress, NC1 has the highest reduction factor (Figure 4.6(b)), while SCC and NC2 mixtures have approximately similar reduction factor. Although there is no precise trend for the reduction factor of the residual bond stress (Figure 4.6(c)), the general tendency indicates that SCC mixture has the lowest reduction factor.

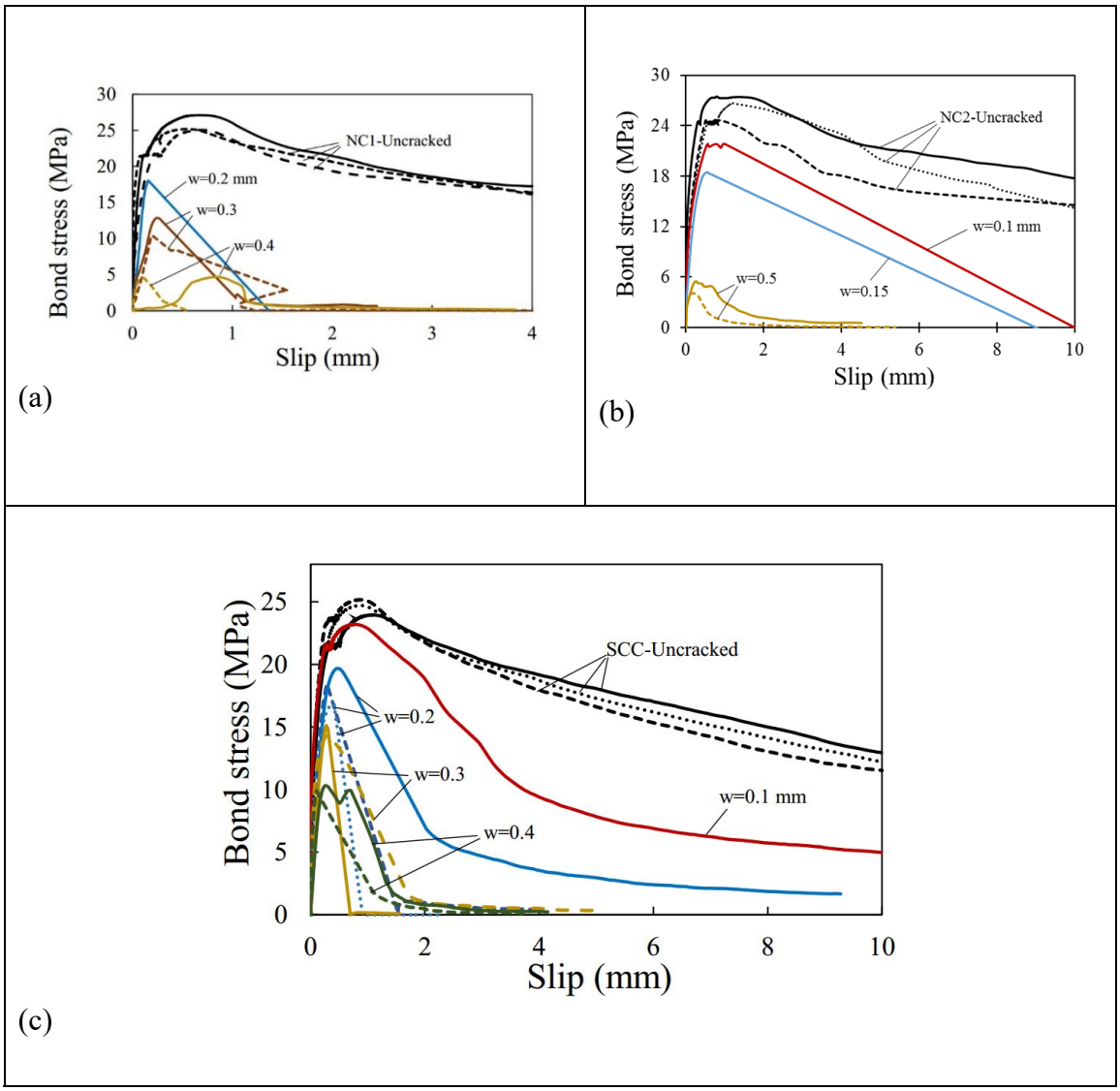

Figure 4.5 Bond-slip curves of uncracked and cracked specimens:
(a) NC1; (b) NC2; (c) SCC

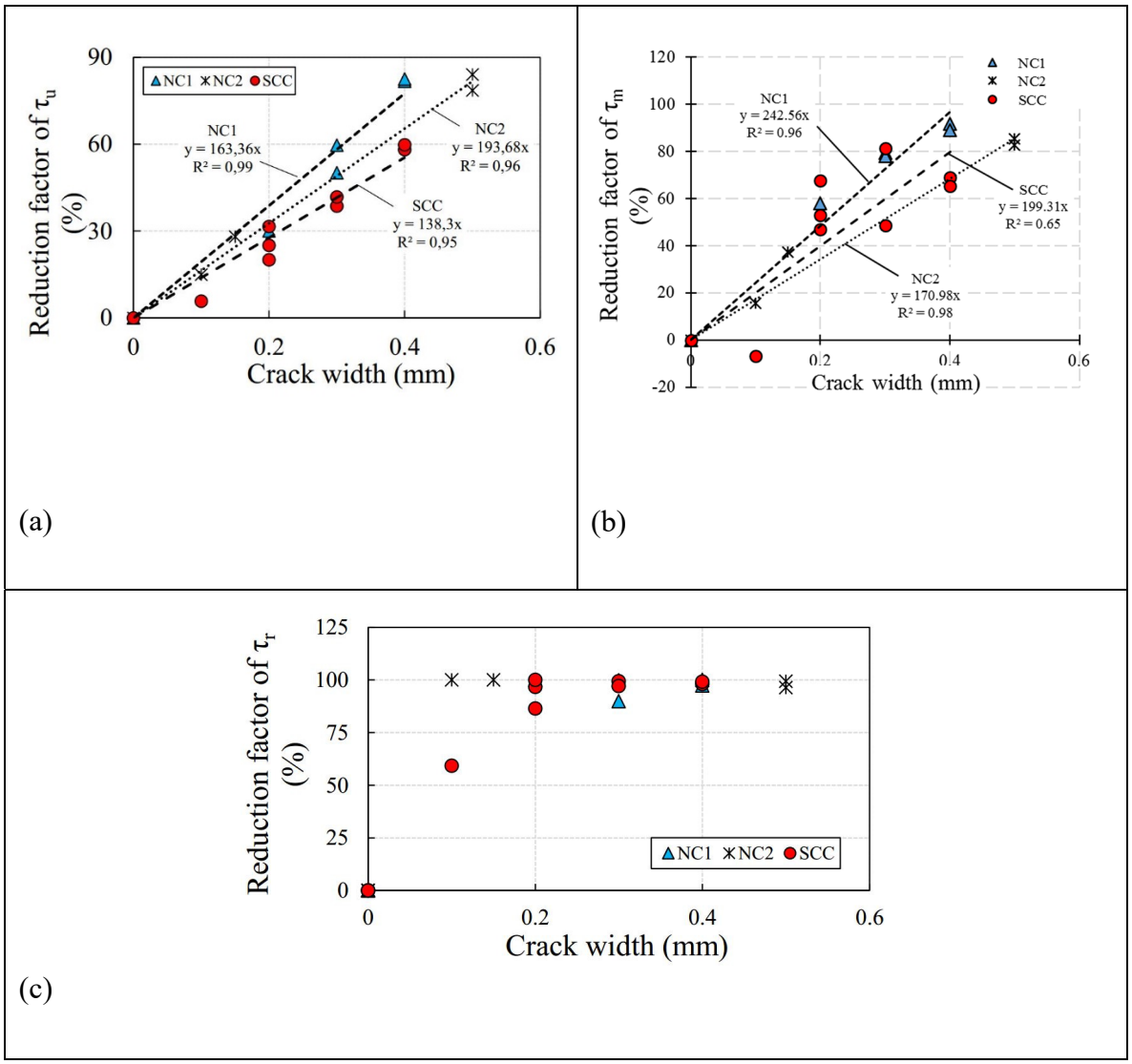

Figure 4.6 Reduction factors of bond response due to the pre-cracking:
(a) bond strength; (b) average bond stress; (c) residual bond stress

4.4 Discussion

As reported by Mousavi et al. (2019), rebar diameter has a considerable impact on the influence of the pre-cracking phenomenon, so that normalized bond stress is related to crack width-to-rebar diameter ratio (w/d_b). Similar trend is illustrated in Figure 4.7. Mixtures of NC2 and SCC approximately have same trend, while NC1 mixture follows different trends. Good

correlations exist between the experimental results and the w/d_b ratio for all mixtures, as expressed by Eqs. (4.7)-(4.9). Values of 3.41, 4.18 and 3.97 are obtained for normalized bond strengths of uncracked concrete mixtures of NC1, NC2, and SCC respectively, which reduce linearly with initial crack width as shown by these equations:

$$\left[\frac{\tau_u}{\sqrt{f'_c}}\right]_{NC1} = -73.41\frac{w}{d_b} + 3.41 \qquad R^2 = 0.97 \qquad (4.7)$$

$$\left[\frac{\tau_u}{\sqrt{f'_c}}\right]_{NC2} = -77.69\frac{w}{d_b} + 4.18 \qquad R^2 = 0.99 \qquad (4.8)$$

$$\left[\frac{\tau_u}{\sqrt{f'_c}}\right]_{SCC} = -64.15\frac{w}{d_b} + 3.97 \qquad R^2 = 0.97 \qquad (4.9)$$

Based on the proposed equations for normalized bond strength of rebar in pre-cracked concrete, cracks larger than values of 0.52 mm, 0.61 mm, and 0.70 mm results in zero bond strength ($\tau_{max}/\sqrt{f'_c} \approx 0$) for mixtures of NC1, NC2, and SCC respectively. This higher value of crack width corresponding to SCC mixture shows considerable resistance to the pre-cracking phenomenon. General observations show that crack width significantly changes the interfacial bond behaviour so that bond failure mode is changed for crack widths larger than 0.15 mm. The results summarized in Table 2 and Fig. 10 demonstrate that bond behaviour of pre-cracked concrete for $w \geq 0.15$ mm is governed by splitting failure modes, where a post-peak sudden drop in bond stress can be observed until reaching an equilibrium between the radial component of the post-splitting bond stresses and the post-splitting confining action (tensile resistance of the concrete) (Harajli, 2009; Mousavi et al., 2019). This can be attributed to the change in failure mode, which is the main objective of the following sections related to the theoretical analysis.

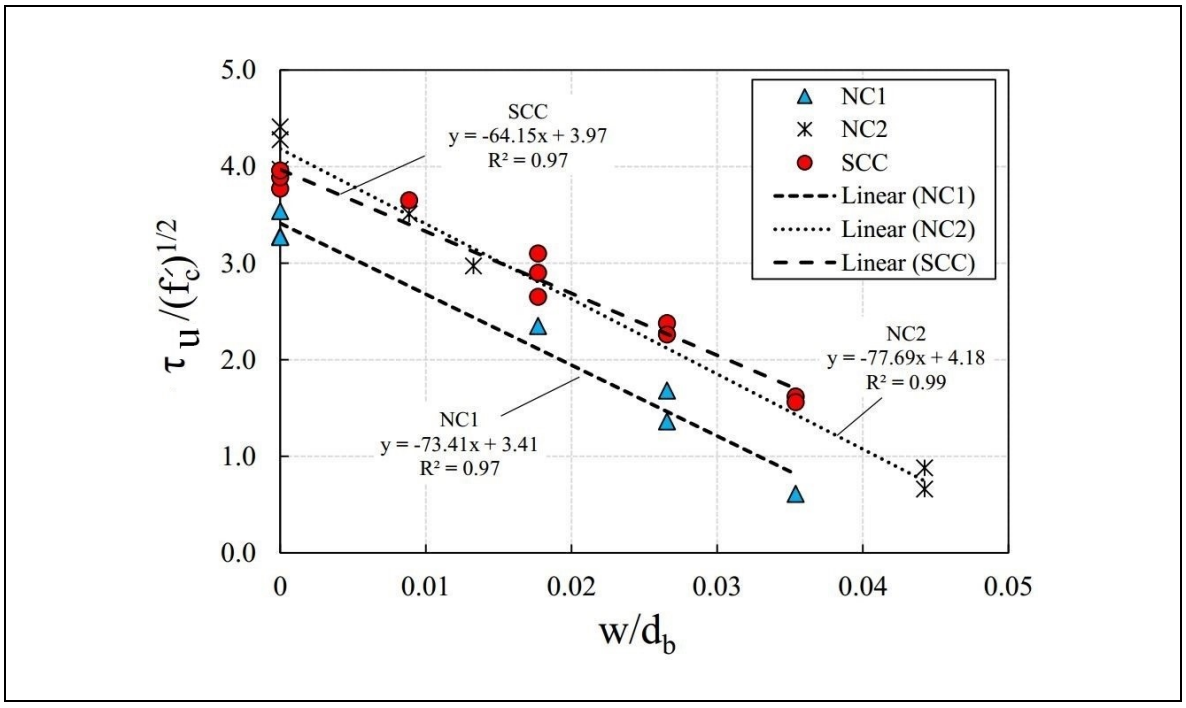

Figure 4.7 Correlation of normalized bond strength to w/d_b ratio

As reported by Murcia-Delso & Benson Shing (2014), surface separations (in both directions of parallel and normal) between rebar and surrounding concrete plays a significant role in the bond-slip phenomenon, which can significantly affect the interface strength. Initial cracks generated by the pre-cracking phenomenon causing similar surface separation with more significant impacts (Mousavi et al., 2020, Mousavi et al., 2019). As comprehensively described by Mousavi et al. (2020), the height of the rib above the surface of the rebar plays a major role in rebar-concrete interface separation due to the pre-cracking phenomenon. Thus, the ratio of crack width-to-rib height can be used to present the bond reduction factor. Murcia-Delso & Benson Shing (2014) have presented the only bond-slip model considering surface separation. They have related bond reduction to rib height without concentrating on the pre-cracking phenomenon. Accordingly, a reduction factor (ρ_{nm}) can be achieved based on the obtained experimental results, as a function of surface separation, as follows:

$$\rho_u = \frac{(\tau_u)_{\text{pre-cracked}}}{(\tau_u)_{\text{uncracked}}} \tag{4.10}$$

$$\rho_u = \begin{cases} 1 & w/2 \le M_1 h_r \\ f(w/h_r) & M_1 h_r < w/2 < M_2 h_r \\ 0 & w/2 \ge M_2 h_r \end{cases} \tag{4.11}$$

where ρ_u is a reduction ratio of bond strength that considers the opening of cracks due to the pre-cracking phenomenon in concrete. M_1 and M_2 are empirical coefficients for different concrete compositions, which are summarized in Table 4.3. Value of rib height used in Eq. (4.11) is presented in Figure 4.2(d).

Table 4.3 Empirical coefficients used in Eq. (4.11) for different concrete compositions

Mix	$\boldsymbol{f(w/h_r)}$ **in Eq. (4.11)**	$\boldsymbol{M_1}$	$\boldsymbol{M_2}$
NC1	$f(w/h_r) = -5.11\frac{w}{h_r} + 1.26$	0.026	0.14
NC2	$f(w/h_r) = 1.41e^{(-7.79\frac{w}{h_r})}$	0.026	0.16
SCC	$f(w/h_r) = 1.34e^{(-5.46\frac{w}{h_r})}$	0.026	0.19

The performance of the proposed model is shown in Figure 4.8. The dependence of the reduction ratio (ρ_u) on the ratio of crack width-to-rib height (Eq. (4.11)) can be attributed to the fact that the loss of bond strength is related to a reduction in the contact surface between the steel ribs and the concrete. For a well-confined situation (uncracked concrete and $w \le 0.10$), the interface separation is very small; consequently, the reduction factor will be equal or very close to one ($\rho_u \approx 1$). Different separation mechanisms can be occurred for pre-cracked concrete, including one-side and both-side separations. The value of 0.50 corresponds

to the crack width of $w/2$ at every side is considered in this section, which is suggested by Brantschen et al. (2016) as an idealized pre-cracking phenomenon. Based on the experimental results (Table 4.3), the domain of $w/2 \leq 0.026h_r$ is obtained (for all mixtures) in the Eq. (4.11) for the reduction factor equal to 1.0. Based on the model presented by Murcia-Delso & Benson Shing (2014), if the interface separation is larger than the rib height, the contact between ribs and the concrete is lost, and the bond resistance disappears ($\rho_u = 0$). However, the values of $0.14h_r$, $0.16h_r$, and $0.19h_r$ are obtained for NC1, NC2, and SCC respectively, as the critical separation values for complete loss in bond strength. These values are based on Figures 4.6 and 4.7 correspondings to crack widths of $w \approx 0.61$, 0.52, and 0.70 mm for NC1, NC2, and SCC respectively. This can be attributed to the significant reduction in compressive strength of surrounding concrete due to the pre-cracking phenomenon, which has been reported by several works (Belarbi & Hsu, 1991; Kollegger & Mehlhorn, 1990; Mikame et al., 1991; Shirai & Noguchi, 1989; Vecchio & Collins, 1993). Considerable effect of compressive strength on the rebar-concrete interfacial strength has been frequently confirmed by the literature (Guizani et al., 2017; Mousavi et al., 2017).

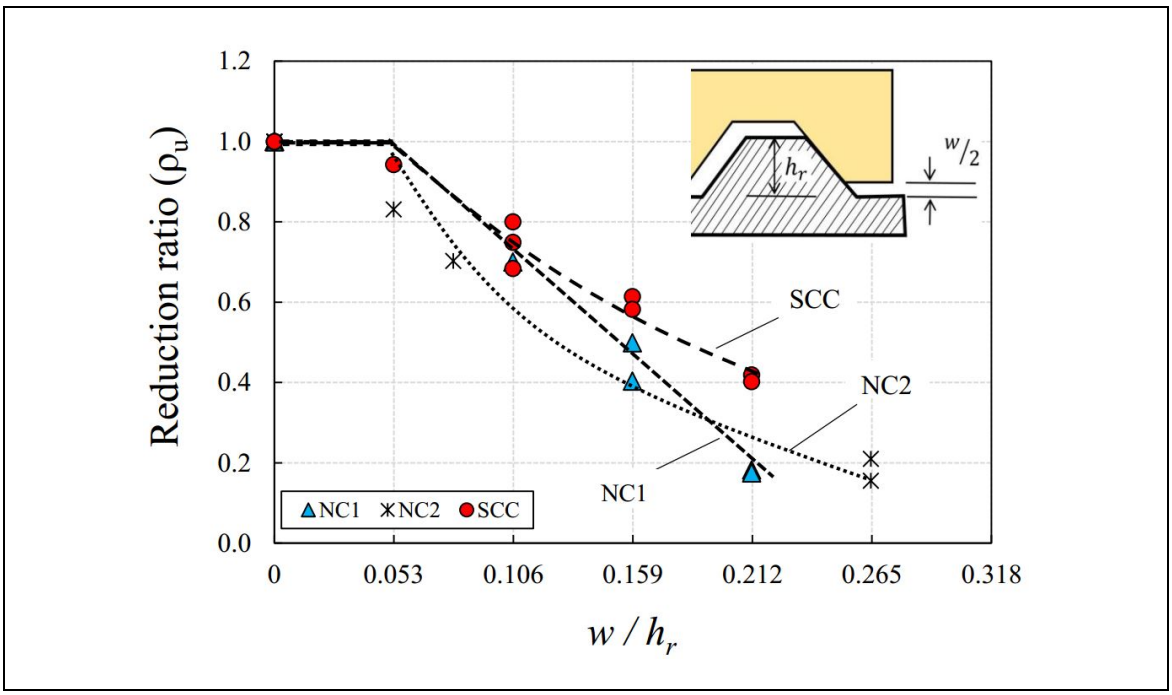

Figure 4.8 Reduction ratio of bond strength versus w/h_r ratio for concrete mixtures

Regarding small initial crack widths ($w \leq 0.10$ mm), as mentioned in Table 4.2, pull-out failure mode was observed for SCC specimen, while the failure was sudden for NC2 specimen causing concrete splitting along with pulling-out the rebar. As shown in Figure 4.9(a), initial crack widths cause 16.92% and 5.73% maximum bond stress reduction in NC2 and SCC mixtures respectively. Similar observations are obtained for average bond stress (τ_m) and residual bond stress (τ_r). However, comparable bond energy (E_b) is obtained for both mixtures. Regarding average bond stress, even improvement bond strength is observed for cracked SCC specimen as compared to the uncracked ones (Figure 4.9(a)), which can be due to the aggregate interlock at the crack surfaces. Crack opening of specimens was also recorded for NC2 and SCC mixtures. Two crack gauges were installed at both sides of rebar during the pull-out tests. As illustrated in Figure 4.9(b), for cracked SCC specimen, similar crack width opening is happened during the tests for two gauges, while different values of crack width opening are observed for NC2 mixture. Moreover, results show that an approximate linear ascending branch is observed for both mixtures prior to a plateau, before reaching to the maximum bond stress. The initial stiffness of this branch of curve is higher for NC2 specimen as compared to SCC specimen. The length of this plateau is longer for SCC specimens as compared to NC2, which means that higher sustained bond strength is obtained. The area under the bond-crack opening curve demonstrates the fracture energy. Similar to the bond energy shown in Figure 4.9(a), cracked SCC specimen has slightly higher/comparable fracture energy until the bond strength (Figure 4.9(b)), as compared to NC2 specimen, for small initial crack width.

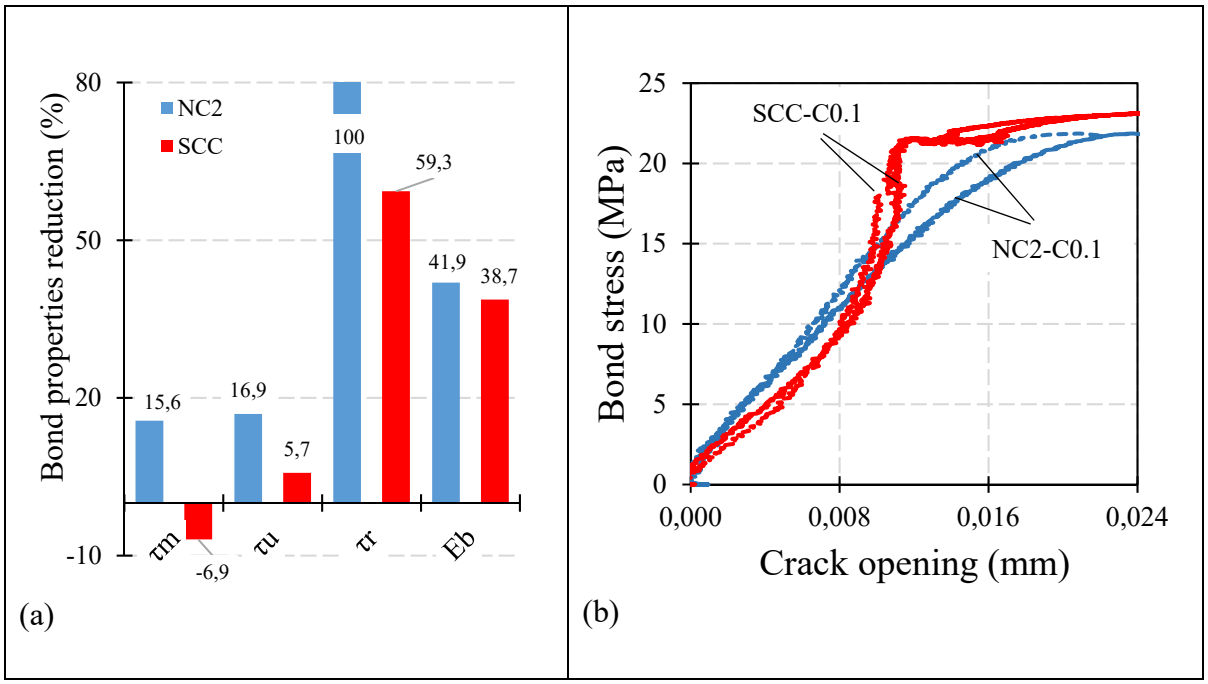

Figure 4.9 Effect of small initial crack widths (0.10 mm) on:
(a) bond properties; (b) crack opening during pull-out test

Bond stress-crack opening curves of the pre-cracked specimens with large initial crack widths are illustrated in Figure 4.10. Results show that the unsymmetrical crack opening phenomenon happened during pull-out tests, which is also illustrated in Figure 4.3(c). Results presented in Figure 4.10 show that this phenomenon is more crucial for NC2 specimens as compared to SCC ones, causing different bond stress-crack opening curves for two crack gauges installed at both sides of the steel rebar. Comparing the results shown in Figures 4.9 and 4.10 indicates that the crack opening growth of large initial cracks is different from the small ones. Crack opening more than 6.0 mm is observed for large crack widths. Crack opening is very low for the initial bond stress (bond strength, τ_u), while considerable crack opening values and also sudden drops in curves are observed after the maximum bond stress (bond strength, τ_u).

Area under the bond stress-crack opening curve can be used as the "fracture energy, F_{energy}" of the bond mechanism in cracked concrete. The maximum, minimum, and average values of fracture energy of NC2 and SCC mixtures are shown in Figure 4.11, with respect to the initial crack widths. Results show that as the initial crack width increases, the average fracture energy

decreases so that 40.7%, 13.9%, 7.9%, and 2.8% values are obtained for fracture energies of specimens exposed to 0.15, 0.2, 0.3, 0.4, and 0.5 mm initial crack widths. Similar results are observed for the minimum and maximum values of the fracture energy. Finally, Eq. (4.12) is achieved for predicting fracture bond energy of cracked specimens as a function of crack opening ($\acute{w}$) with a good correlation of $R^2 = 0.99$, as follows:

$$F_{energy} = 42.45w^{-1.62} \tag{4.12}$$

It is worth mentioning that the proposed equations are validated for the current experimental database. More experimental investigations are necessary to determine the efficiency of the proposed equations and to generalize them for different concrete mixtures.

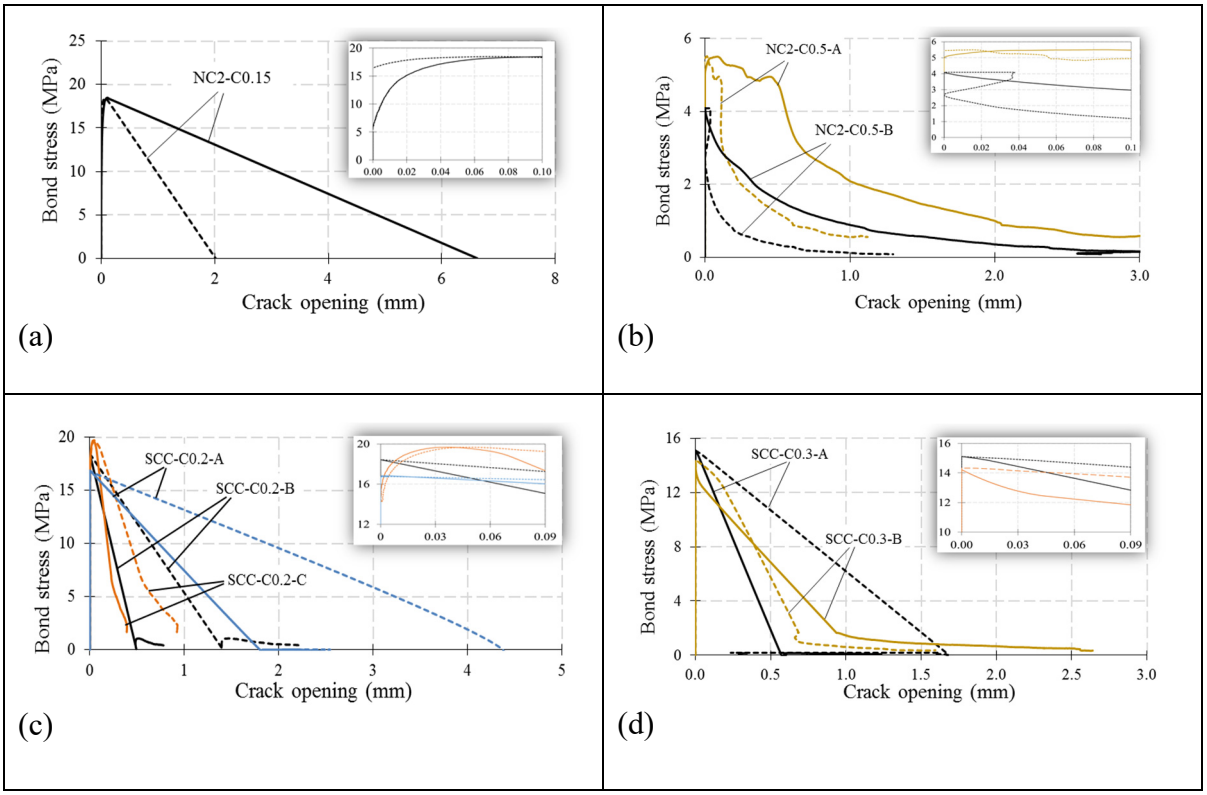

Figure 4.10 Effect of large initial crack widths on bond stress-crack opening curve: (a) NC2 with $w = 0.15$ mm; (b) NC2 with $w = 0.50$ mm; (c) SCC with $w = 0.20$ mm; (d) SCC with $w = 0.30$ mm; (e) SCC with $w = 0.40$ mm (Note: continuous and dashed lines denote results of crack gauges installed at both sides of rebar during pull-out test)

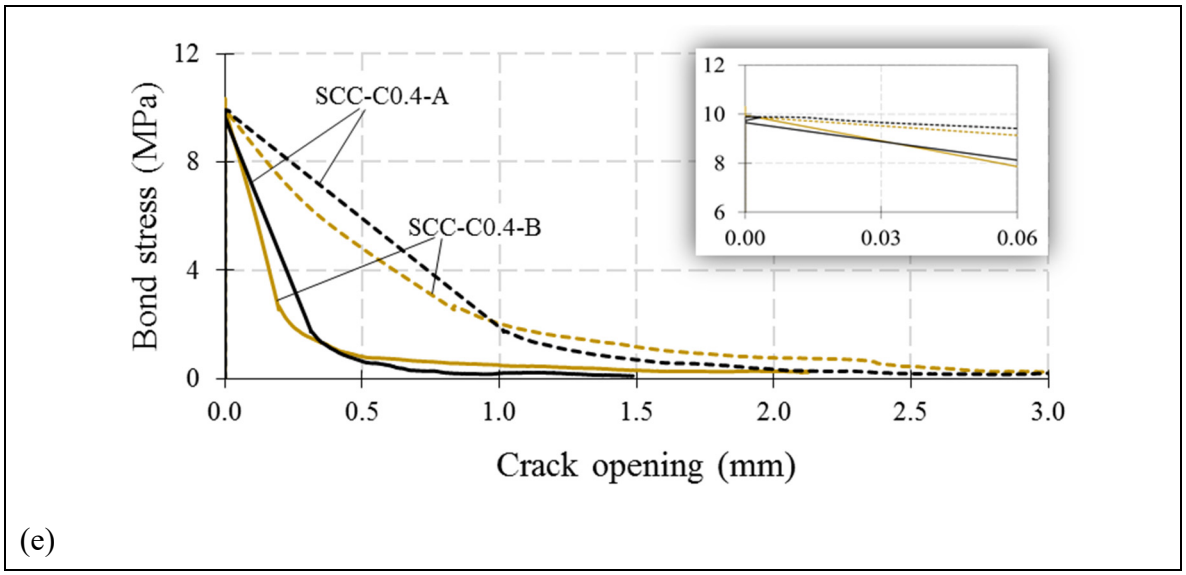

Figure 4.10 Effect of large initial crack widths on bond stress-crack opening curve: (a) NC2 with $w = 0.15$ mm; (b) NC2 with $w = 0.50$ mm; (c) SCC with $w = 0.20$ mm; (d) SCC with $w = 0.30$ mm; (e) SCC with $w = 0.40$ mm (continued)

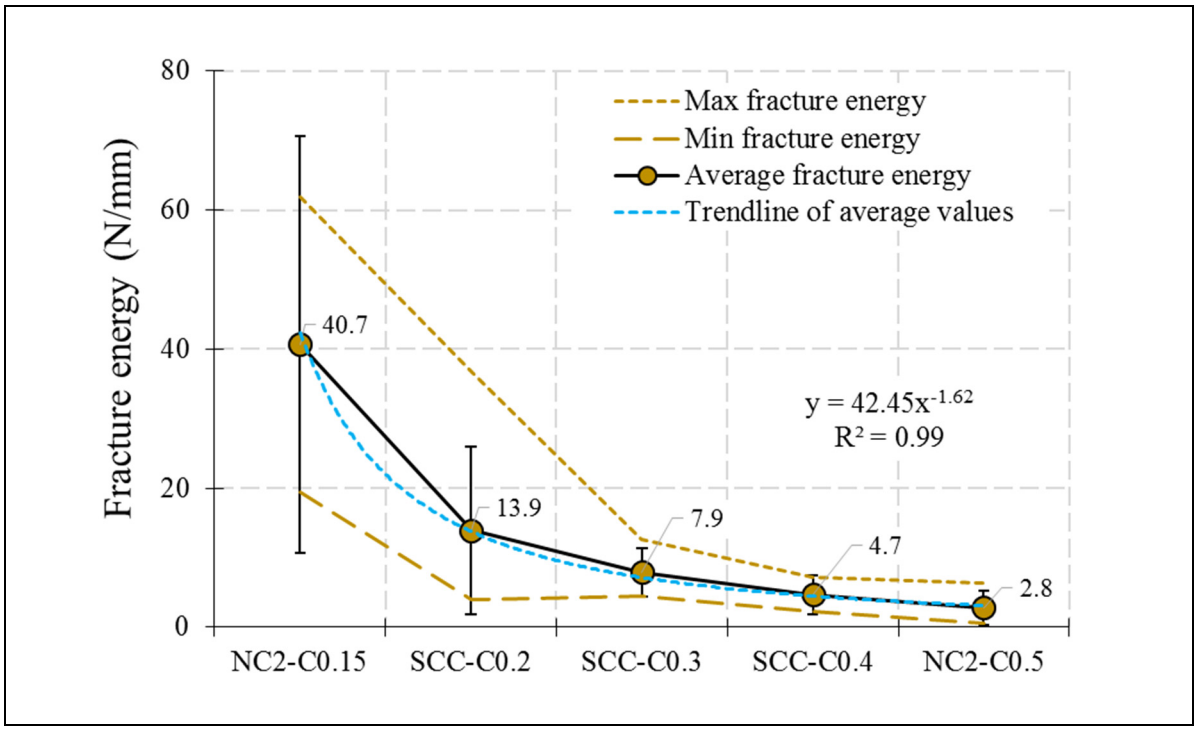

Figure 4.11 Fracture energy of cracked specimens from the bond stress-crack opening curve with respect to the initial crack width

4.5 Conclusions

An experimental program is conducted in this study to determine the effect of concrete workability (or flowability) on the pre-cracking phenomenon. Three concrete mixes with normal, moderate, and high flowability are considered. Specimens with different initial crack widths are obtained through the Brazilian test (splitting) on reinforced cylindrical concrete block. Pull-out results of pre-cracked specimens are compared with uncracked ones. According to the experimental results obtained in the present study, the following conclusions can be drawn:

- In the case of uncracked specimens, general results show that SCC has 13.2% higher normalized maximum bond strength as compared to NC1 mixture (normal concrete with a high slump flow of 97 mm) with the same water-to-powder ratio (0.41). However, SCC has 20.4% lower normalized maximum bond strength than NC2 (normal concrete with slump flow of 200 mm) with approximately the same compressive strength. This trend is more significant in normalized residual bond strength among the other interfacial bond parameters.
- Overall, results corresponding to the pre-cracked specimens show that SCC is less sensitive to the pre-cracking phenomenon as compared to the other NC mixes so that the slope of the maximum bond strength-crack width curves are 163.36, 193.68, and 138.30 for NC1, NC2, and SCC mixtures respectively. Moreover, NC2 mixture shows better performance (lower reduction factor) for all initial crack widths than NC1 mixture. A higher value of slump flow can be the main reason for this observation.
- Empirical equations are presented for all pre-cracked specimens (Eq. (12)). They show that despite the existing scenario of the total bond reduction till surface clearance of $w = h_r$, values of $0.14h_r$, $0.16h_r$, and $0.19h_r$ are obtained for NC1, NC2, and SCC respectively as the critical separation values for complete loss in bond strength.
- Results of the present study indicate that more specifications should be considered in the current concrete design codes for considering the effect of the pre-existing cracks on bond strength, especially in steel-congested concrete members such as interior and exterior joints,

slabs, and shear walls. Generally, the critical value of the initial crack width of 0.15 mm should be specified in codes for preserving the bond properties.

Due to the variety of mixtures in producing SCC, more experimental studies are necessary to determine the effect of the pre-cracking phenomenon on the bond of cracked concrete, especially for cement replacement dosage and types of fillers. Also, regarding Eq. (12), relating the reduction factor to crack width, more experimental studies with different geometries of rebar are suggested for future works to accurately determine the performance of the proposed model for different types of concrete mixtures and confining conditions, such as the presence of transverse confining reinforcement.

CHAPTER 5

ON MITIGATING REBAR–CONCRETE INTERFACE DAMAGES DUE TO THE PRE-CRACKING PHENOMENA USING SUPERABSORBENT POLYMERS

Seyed Sina Mousavi [a], Claudiane Ouellet-Plamondon [b], Lotfi Guizani [c], Chandrasekhar Bhojaraju [d], and Victor Brial [e]

[a, b, c,d, e] Department of Construction Engineering, École de Technologie Supérieure, 1100 Notre-Dame West, Montreal, Quebec, Canada H3C 1K3

Paper published in *Construction and Building Materials*[3], August 2020

Abstract

This study intends to determine the effect of superabsorbent polymer (SAP) on bond properties of steel rebar in un-cracked, pre-cracked, and healed concrete as a smart generation of concrete for autogenous healing its cracks. An experimental program is conducted to check the performance of SAP as a healing agent inside concrete to mitigate internal damages at rebar-concrete interfacial surfaces. Two types of SAP with different particle sizes (0.15 mm and 0.5 mm) and chemistries are considered in the experimental program. Results show that comparable and also better results are obtained for bond properties of steel rebar embedded in un-cracked and healed concrete containing a lower dosage of SAP. However, bond strength is lower in concrete containing a high dosage of SAP compared to normal concrete (NC) thanks to the presence of macro voids. A considerable healing effect is observed for initial bond stress, bond strength, and energy absorbed by bond mechanism, within the cracks of pre-cracked SAP concrete subjected to wet-dry cycles. SAP can significantly increase the autogenous healing

[3] Mousavi, S. S., Ouellet-Plamondon, C. M., Guizani, L., Bhojaraju, C., & Brial, V. (2020). On mitigating rebar–concrete interface damages due to the pre-cracking phenomena using superabsorbent polymers. Construction and Building Materials, 253, 119181. DOI: https://doi.org/10.1016/j.conbuildmat.2020.119181

capacity of concrete at rebar-concrete interfacial damages. Results also indicate that 24 days healing period is more efficient as compared to 14 days.

Keywords*:* bond strength; superabsorbent polymer (SAP); self-healing; pre-cracked concrete

5.1 Introduction

Pre-cracking phenomenon, the appearance of cracks along the axis of the steel rebar in the surrounding concrete, is a common issue in reinforced concrete structures, especially in steel-congested regions such as beam-column joints and shear walls (Matsumoto et al., 2016). Various situations can lead to the pre-cracking phenomenon, which include corrosion-caused pre-cracking (Desnerck et al., 2015; Jiang et al., 2018), mechanical pre-loading (Brantschen et al., 2016; Mousavi et al., 2019), biaxial load transfer (Hadidi & Saadeghvaziri, 2005; Lindorf, et al. 2009; Saadeghvaziri & Hadidi, 2005), multiaxial stress states (Cervenka, 1985; Purainer, 2005), and transverse tension (Lindorf, 2011). The pre-cracking mechanism is similar to bond-splitting cracking and mainly affects the bond-slip behaviour of the rebar. However, no fully efficient solution is available to tackle this inherent problem in reinforced concrete members (anchorage problems of flexural reinforcement in slabs (Dawood & Marzouk, 2012), loop connections subjected to combined tension and bending (Joergensen & Hoang, 2015), arch-shaped members without transverse reinforcement (Ruiz et al., 2010), and reinforced concrete members without transverse reinforcement (Ruiz et al., 2015)), which leads to a significant reduction in bond strength and residual bond stress (Brantschen et al., 2016; Mousavi et al., 2019). Hence, one of the main objectives of this study is to consider an accelerated self-healing method to mitigate damages due to the pre-cracking phenomenon. This proposal could provide new insight into a strategy of healing damages due to the pre-cracking phenomenon at critical interlayer sections of reinforced concrete members.

There is a developing propensity for the use of self-healing or autogenous healing methods in concrete structures, as an internal and active mitigation treatment, to entirely or partially alleviate damage (Mignon et al., 2017). Self-healing in concrete can be mainly attributed to

two mechanisms: hydration of unhydrated cement particles (Pérez et al., 2015) and the dissolution and subsequent carbonation of $Ca(OH)_2$ (Van Tittelboom et al., 2012). However, only a limited range of crack widths can be cured by the autogenous healing method (Lee et al., 2010). To accelerate autogenous healing and enhance the ability to heal large crack widths, different mechanisms have been used, including healing agents and water resources (Mihashi & Nishiwaki, 2012). As the water is a fundamental requirement for autogenous healing, it can be provided by different techniques, such as the cross-linked hydrogel network method, to accelerate the healing process. Superabsorbent polymer (SAP), as a hydrogel-forming polymer, can absorb a significant amount of water from the surrounding environment, which they retain within their structure (Figure 5.1). SAP is already used in high-performance concrete to mitigate self-desiccation and autogenous shrinkage (Beushausen & Gillmer, 2014; Mechtcherine et al., 2009; Shen et al., 2016; Snoeck et al., 2018; Song et al., 2016; Tu et al., 2019). Additionally, SAP promotes self-healing by enabling a crack closure mechanism that restores the mechanical properties of the material (Snoeck, 2018; Snoeck et al., 2014).

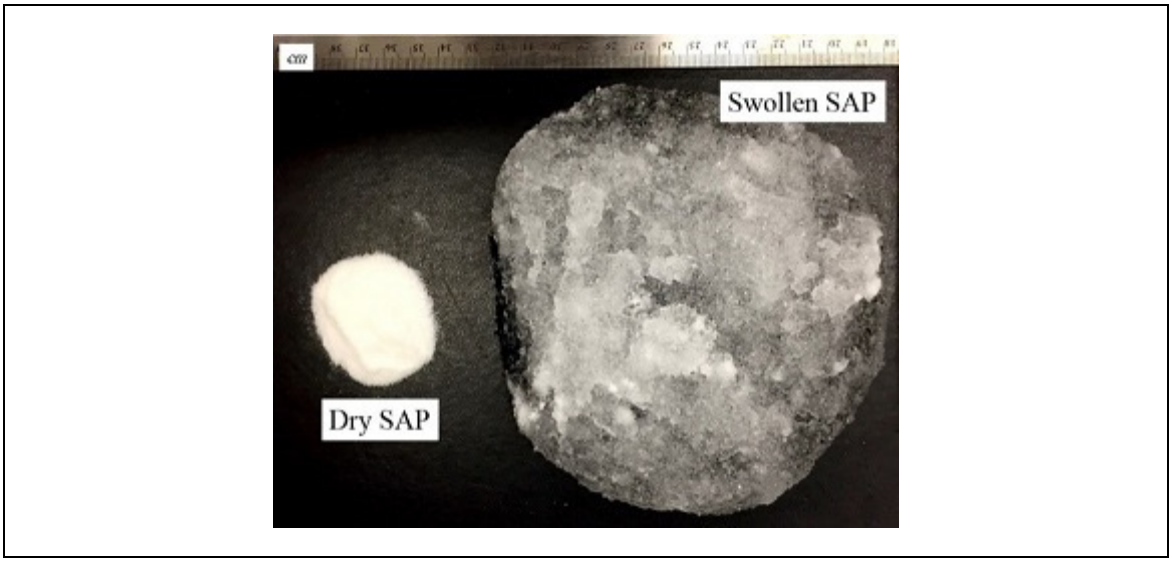

Figure 5.1 Swollen SAP particles (with a diameter of 0.5 mm) due to water absorption (the same weight is used for both dry and swollen SAP, 5 gr)

SAP-modified concrete research can be divided based on the targeted healing mechanism into two main groups: crack-sealing and crack-healing. Crack-sealing mainly focuses on closing

cracks to prevent water penetration, which increases the durability of the concrete (Al-Nasra, 2013; Hong & Choi, 2017; Lee et al., 2010; Lee et al., 2010; Snoeck & De Belie, 2013; Snoeck et al., 2012). Cracks up to 30 μm could heal entirely by SAP at the crack lip, and those up to 150 μm heal partially when specimens are subjected to wet-dry cycles (Snoeck & De Belie, 2015). It has also been reported that cracks up to 130 μm could be closed entirely in wet-dry cycles due to the precipitation of calcium carbonate in SAP-based concrete (Lee et al., 2016). Apart from these studies, another investigation clearly shows that with a 300 μm crack width, SAP particles can reduce the peak flow rate and total flow of penetrating water by up to 85% and 98%, respectively (Snoeck et al., 2012). However, there is little consistency in these results, a fact that can be attributed to the varying SAP particle size, w/c ratio, and healing period (time and procedure) between studies. Many research studies have also been carried out to examine the restoration of the mechanical characteristics of a damaged structure (Abdel-Jawad & Haddad, 1992; Dhir et al., 1973; Granger et al., 2007; Jacobsen & Sellevold, 1996; Jensen, 2013; Lauer & Slate, 1956; Van Tittelboom et al., 2016). However, there has not been an investigation to determine the effect of SAP on steel rebar-concrete bond behaviour and healing cracks at interfacial surfaces. Research conducted by Kim & Wang (2016) is the only reference that discussed the interfacial behaviour of glass fiber-reinforced polymer (GFRP) rebar embedded in concrete mixed with three types of internal curing agents using two mineral-based agents and a superabsorbent polymer. However, the authors only considered the effect of internal curing on GFRP rebar-concrete bond strength. There is no discussion on the healing of damages related to locally-induced cracks.

Most previous research on the effect of SAP on mechanical properties of concrete has been concentrated on compressive strength (Beushausen et al., 2014; Dudziak & Mechtcherine, 2009; Justs et al., 2015; Laustsen et al., 2015; Mechtcherine et al., 2014; Shen et al., 2016; Snoeck et al., 2014), which is traditionally considered to be one of the most important parameters for predicting steel rebar-concrete bond strength (fib Model Code 2010; Guizani et al., 2017; Harajli et al., 1995; Mousavi et al., 2017; Wu & Zhao, 2012). A reduction in compressive strength of SAP-modified concrete is severally reported by previous studies, which is attributed to the larger pores of SAP particles after hardening (Als & Beton, 2005;

Craeye, 2006; Justs et al., 2015; Piérard et al., 2006; Wyrzykowski et al., 2012). Quantifying the strength reduction as a function of SAP types is still challenging for researchers as different types of SAP have been used in the literature. Some studies have also shown the strength of SAP mixture to be generally equal to or only slightly lower than in the reference mixtures (Bentz et al., 2002; Geiker et al., 2004; Lura et al., 2006; Schröfl et al., 2012; Wang et al., 2013), which can be attributed to the choice of SAP dosage, size, and other concrete mix parameters. Despite these extensive efforts on the compressive strength of SAP-modified concrete, there is no specific investigation for bond strength of steel rebar embedded in uncracked, pre-cracked, and healed concrete. Hence, the present investigation begins by tackling the following general questions:

1. How does the bond behaviour between steel rebar and SAP concrete compare to that of NC for uncracked and pre-cracked concrete?
2. How effective are SAP particles for healing cracks related to the pre-cracking phenomenon at the steel rebar-concrete interface?

To answer these questions, this investigation presents an experimental program to determine the bond behaviour of steel rebar in these three states of concrete (intact, pre-cracked, and healed). The regular splitting test is considered to simulate pre-damage in the plane of the steel rebar. Two series of healing periods, 14 and 28 days, under wet-dry cycles, are considered for healing the cracks. Initial stiffness, maximum strength, and energy absorbed by the bond mechanism are the main bond characteristics considered to assess the performance of SAP concrete.

5.2 Experimental program

5.2.1 Materials

Five different concrete mixes are considered for this experimental program to compare results objectively to the reference mix (R) made of general use cement with a density of 3.15 g/cm^3, a natural sand with a maximum grain size of 1.25 mm and a specific gravity of 2.68, and a

gravel with a nominal maximum diameter of 14 mm and a particular gravity of 2.68. A water-to-cement ratio of 0.42 is considered for the reference mix (R). Despite using lower w/c, which is appropriate for healing cracks, the value of w/c=0.42 is selected to control cracks mechanically in pre-cracking tests. The challenges to control crack width are also reported by Desnerck et al. (2015) in simulating pre-cracking in cylindrical reinforced concrete specimens and a w/c of 0.60 is selected for their experiments. The SAP is added at a range of 0-1.0 wt.% of cement. To adjust the flowability of concrete, a polycarboxylate-based superplasticizer is added, at different proportions as detailed in Table 5.1. General mix proportions of concrete composites are given in Table 5.1. All specimens are initially cured 28 days in the moisture room at 97.3% RH and 23 ºC. Those specimens, which are subjected to wet-dry cycles, remained in the curing tank for longer periods of 14 and 28 days (20 ºC, 60% RH). One wet-dry cycle represents 24 hours in water followed by 24 hours in dry condition. Consequently, 7 and 14 cycles took 14- and 28-day of wet-dry cycles respectively.

Table 5.1 Concrete composition of mixtures (SAP% = wt.% of cement)

Mix	Cement	Sand	Gravel 5/10	Gravel 10/14	Water	Add water	SP	SAP	Slump	W_T/C
	(kg/m^3)							%	mm	(-)
R	395	788	822	258	165	0	2.5	0	97	0.41
25S1	395	788	822	258	165	24.8	3.5	0.25	104	0.48
25S2	395	788	822	258	165	24.8	3.3	0.25	109	0.48
50S1	395	788	822	258	165	49.5	3.8	0.50	95	0.54
100S1	395	788	822	258	165	98.8	5.6	1.00	91	0.66

* Note: Add=additional water, SP=superplasticizer, W_T/C=total water to cement ratio, SAP= % wt. of cement.

Two different approaches have been considered by the previous studies regarding using SAP in concrete mixture (Snoeck & De Belie, 2013; Snoeck & De Belie, 2019) including (1) using as an agent for internally curing into the mixtures together with the extra water; and (2) water reducing application without extra water. The first approach is considered in the current study. To determine the exact amount of water added to the mixture for SAP particles, three different ratios can commonly be used, including initial water-to-cement ratio (W/C, without SAP, 0.41

for this study), extra water (W_e/C, or entrained water-to-cement ratio (Hong & Choi, 2017; Van Tittelboom et al., 2016), and total added water-to-cement ratio (W_T/C) as follows:

$$\frac{W_T}{C} = \frac{W}{C} + \frac{W_e}{C} \tag{5.1}$$

In the case of $W_e/C > 0$, SAP is used as an agent for internally curing into the mixtures together with the extra water, while the water reducing application is intended for $W_e/C = 0$ (without extra or entrained water). The latter is different from the common practice in which the amount of extra water is directly proportioned to the SAP concentration (Mechtcherine & Reinhardt, 2012). To use the first procedure for producing SAP concrete, it is essential to accurately determine the water absorption of SAP. Overestimation of extra water required for the first procedure of using SAP inevitably reduces the strength of SAP concrete (Mechtcherine & Reinhardt, 2012).

Two different types of SAP are considered in this experimental study: SAP-1, a cross-linked copolymer of acrylamide and potassium acrylate (obtained from SNF CANADA), and SAP-2, a cross-linked anionic polyacrylamide (obtained from BASF company). A laser granulometry instrument (Mastersizer/E Malvern) is used to measure the particle size distributions of SAP samples along with cement in the dry state, which is illustrated in Figure 5.2. Table 5.2 gives the corresponding d10, d50, and d90 values. The d50 value for SAP-1 is 260 μm, whereas SAP-2 has a value of 47 μm. The shape of the SAP particles is investigated using SEM (Figure 5.3). SAP was produced through bulk polymerization technique, in which blocks of polymers were shredded into particles of irregular shapes.

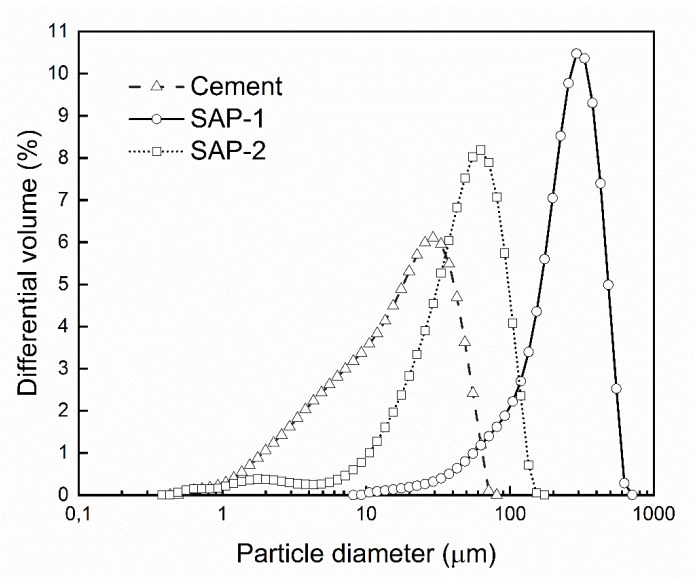

Figure 5.2 Particle size distributions of the SAP used along with cement in the dry state

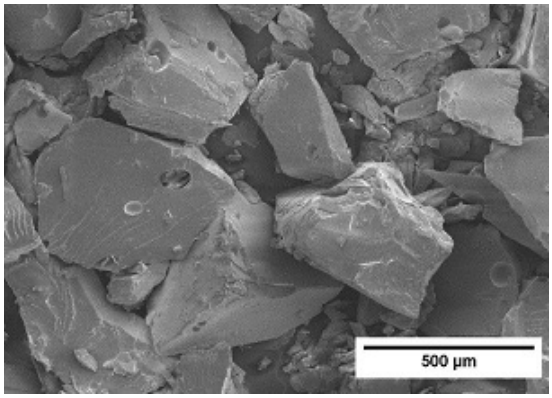

(a)

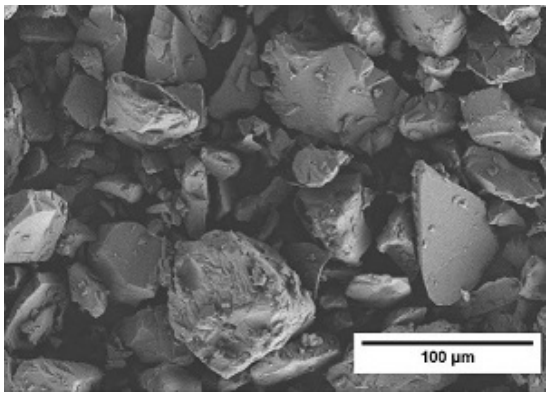

(b)

Figure 5.3 Scanning electron microscope (SEM) image of SAP particles:
(a) SAP-1; (b) SAP-2

Water absorption of SAP particles inside the concrete mixture is different from pure water due to the pH of concrete. To determine the amount of additional water necessary for SAP concrete, three separate methods are considered including the tea bag method, the concrete slump

method, and the water desorption. In the tea bag method, as explained by the RILEM technical committee (Mechtcherine et al., 2018; Snoeck et al., 2018), a tea bag is pre-wetted in the test fluid (centrifuged cement pore solution or deionized water) and then a specific amount of SAP is inserted to the tea bag. The ratio of the difference between the initial and final weight of water absorption to the initial weight provides water absorption capacity. The results are summarized in Table 5.2. For the higher dosage of SAP, to confirm the water absorption in centrifuged cement pore solution which is a crucial parameter for concrete mixtures, slump test is also performed, suggested by Schröfl et al., (2012) and RILEM (Mechtcherine et al., 2018; Snoeck et al., 2018). Details of these methods are reported in the Supplementary file (Figure-A II-1, Table-A II-1 and Table-A II-2). Regarding the desorption method, a specific amount of water and cement are mixed. Then liquid-solid separation by centrifuge is used to extract the water from pore solution (pH=12.8, measured). A specific amount of SAP is added to this water for about one hour. After weighing, a mix of water and SAP is kept in the oven at 105ºC. After 24 h, the difference between the initial and final weights of the mix is used to determine the water absorption of the SAP particle. The tea bag and the water desorption method provided similar results. Finally, as mentioned in Table 5.1, the value of 25 g water per g of dry SAP is considered for water absorption of both SAP particles.

Table 5.2 Properties of superabsorbent polymers (SAP) used in tests

Items	**SAP-1**	**SAP-2**
Chemical name	Cross-linked copolymer of acrylamide and potassium acrylate	Cross-linked anionic polyacrylamide
Company	SNF	BASF
Particle size (μm)	< 500	< 150
d10	92	13
d50	260	47
d90	450	92
Specific gravity	1.51	1.49
Bulk density	0.82	0.84
Mean absorption and desorption of SAP (g water per g SAP)		
deionized water, pH=6.5 (Tea bag method)	249	170
pore solution, pH=12.8 (Tea bag method)	26.7	25.4
desorption, pH=12.8 (centrifuge method)	26.1	25.0

5.2.2 Test set-ups

Three main states of the specimen are considered in the experimental program including un-cracked, pre-cracked and healed samples (Figure 5.4). Controlled splitting test, also known as the Brazilian test, is used to simulate pre-cracking. After pre-cracking, two sets of samples are exposed to wetting and drying cycles for periods of 14 and 28 days to heal the cracks at the interface of rebar-concrete.

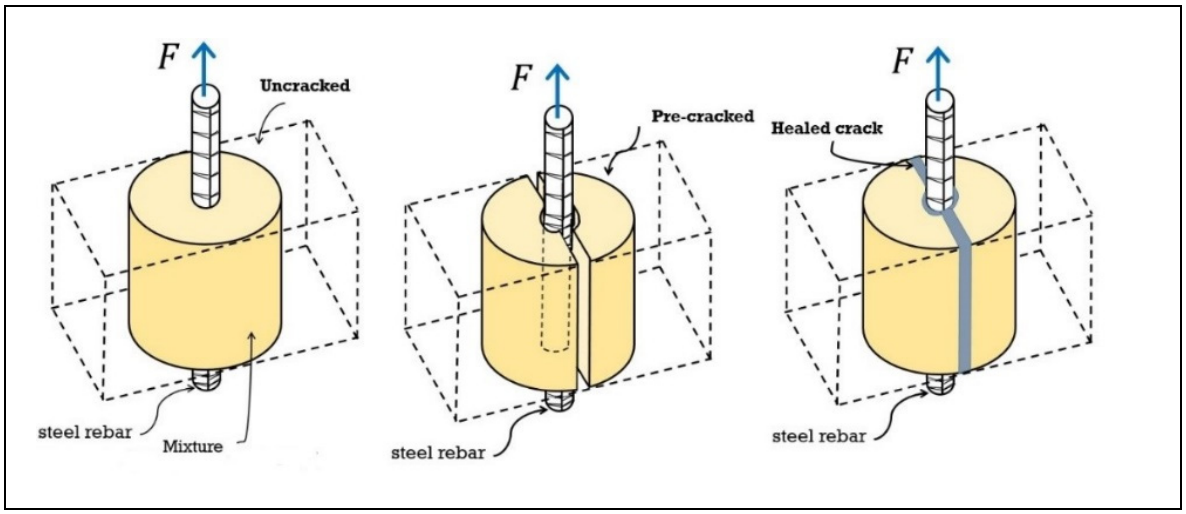

Figure 5.4 Types of specimens used in the experimental program

A total number of 68 specimens including 15 un-cracked and 53 pre-cracked with different crack widths are tested. Embedded length of $5d_b$ is considered for concrete cylinders (Figure 5.5). Long embedment length increases the non-linearity along the bond region so that the value of average bond stress cannot be an accurate measure of bond strength. However, as mentioned widely in the literature (Dehestani & Mousavi, 2015; Guizani et al., 2017), for short bond region (generally five times the rebar diameter, $5d_b$), average bond stress is close to uniform distribution and can be used to get a better measure of bond strength. The used steel rebars have a nominal diameter of 10 mm in conformity with the CSA-G30.18-400W (CAN/CSA-G30.18-09 2009). A ratio of concrete cover to rebar diameter equal to 7.5 is selected, which results in confined concrete conditions, preventing splitting bond failure mode

for intact concrete specimens. The yield stress f_y and ultimate tensile strength f_u of the steel rebars are 432 MPa and 620 MPa respectively. Deformation rates of 0.5 and 0.15 mm/min are considered for pull-out and splitting tests respectively (Figure 5.5).

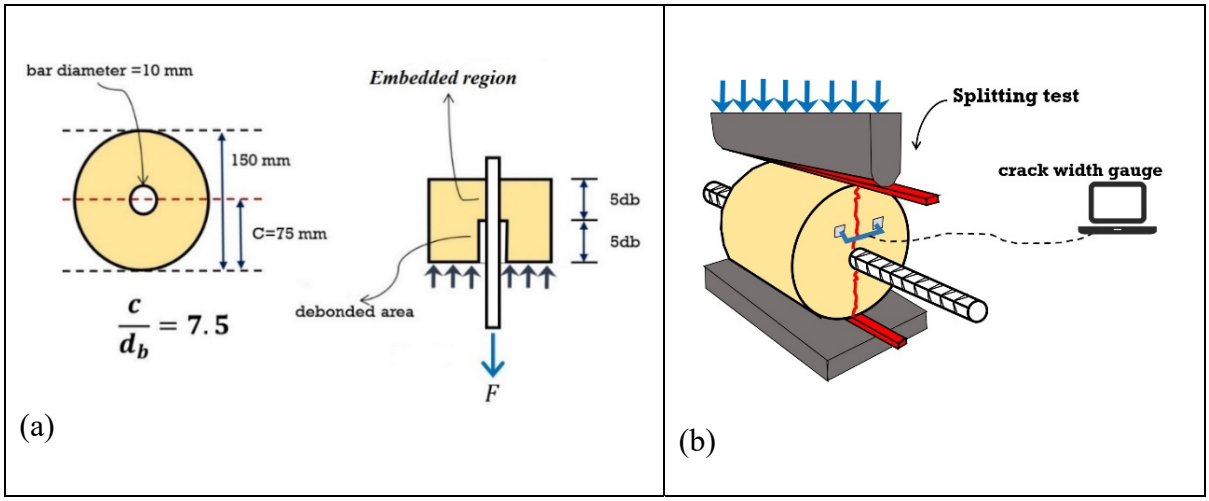

Figure 5.5 Test set-up: (a) pull-out test; (b) splitting test for providing pre-cracking damage (using crack gauges at both side of specimens)

In previous studies, different approaches have been implemented for simulating initial cracks at the rebar-concrete interface (Brantschen et al., 2016; Desnerck et al., 2015; Gambarova et al., 1989; Mahrenholtz, 2012). In this study, a controlled pre-loading approach introduced by Desnerck et al. (2015) was used to induce initial crack before conducting the pull-out test (Figure 5.5(b)). Two crack gauges are installed at both sides of concrete cylinders. At the completion of a concrete cylinder splitting, the crack width is not instantaneously stabilized and continues to reduce noticeably for a few minutes. So, for uniformity of results, manual measurement of crack width is systematically made immediately after unloading (removal of the load) (Figure 5.6).

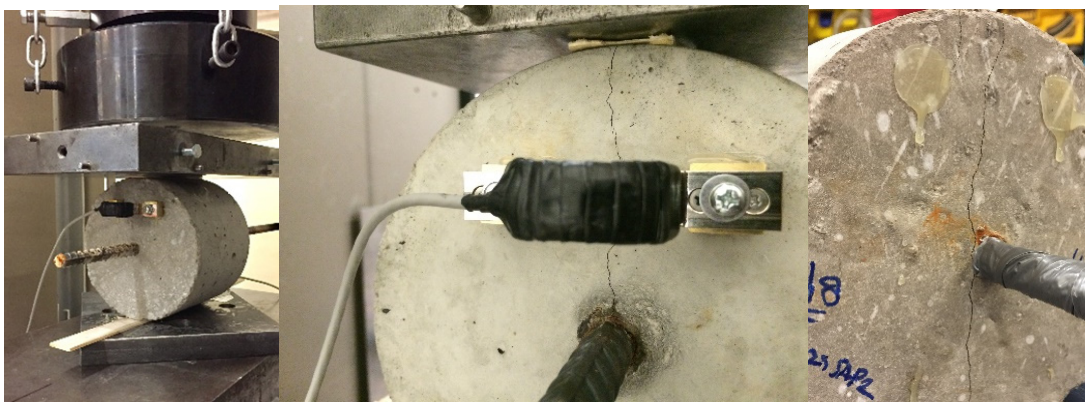

Figure 5.6 Induced cracks at rebar-concrete interface by controlled splitting test

5.3 Experimental results

5.3.1 Compressive strength

Figure 5.7 presents compressive strength of concrete mixtures with and without SAP. A lower percentage of SAP with larger diameter (25S1) has a lower influence on compressive strength (7.5% reduction) when compared with the smaller diameter SAP (25S2) (20.4% reduction). Similar results corresponding to SAP particle size effect are reported by some previous studies (Mechtcherine et al., 2017; Schröfl et al., 2012; Snoeck et al., 2014). Moreover, the chemistry of the SAP used seems to play an important role, the SAP-1 made of cross-linked copolymer of acrylamide and potassium acrylate and the SAP-2 made of cross-linked anionic polyacrylamide. However, a higher dosage of polymers causes a considerable reduction in concrete strength i.e, 23.8%, and 44.2% reduction are observed for 50S1 and 100S1 mixtures respectively. Generally, the compressive strength of SAP concrete compared to NC depends on curing conditions, age, and material composition (Mechtcherine & Reinhardt, 2012). However, similar strength reductions have been reported in previous investigations for different SAP dosages, which are attributed to the number of large pores (macro) of SAP particles after hardening (Craeye, 2006; Justs et al., 2015; Piérard et al., 2006; Wyrzykowski et al., 2012). Although the interpretation of the effect of SAP addition on compressive strength

is not clear enough, capillary porosity and degree of hydration have been considered as the main reasons for explaining this effect (Piérard et al., 2006).

Formation of macro voids, generated by initially filling of entraining pores with extra water and then gradually drying out, significantly changes the equivalent porosity and microstructure, which was strongly confirmed by a model presented by Powers & Brownyard (1946). This impact of SAP on compressive strength is significantly dependent on the amount of solid matrix of mixtures which results in different impacts on cement paste, mortar, and concrete (Lura et al. 2006). However, the internal curing of concrete using SAP particles has a positive impact on the hydration degree of cement grains which can affect the long-term compressive strength of SAP concrete (Esteves et al., 2007). In the case of 0.25% SAP-1, the negative effect of generated voids induced by the SAP particles is compensated by the improved degree of hydration so that only 7.5% reduction is observed in compressive strength (Figure 5.7(a)). However, higher bulk density of SAP-2 compared to SAP-1 increases the number of SAP particles in the same volume, which results in a significant reduction in the concrete compressive strength. Comparable results are observed by others (Schröfl et al., 2012; Snoeck et al., 2014). Snoeck et al. (2014) have noticed considerable reductions of 4.4% and 15.7% in compressive strength of mortars for 0.48 mm and 0.10 mm size particles respectively with 0.5% SAP (W/C=0.5, W_e/C=0). They have also reported a similar trend for 1.0% SAP so that 5.5% and 30.2% strength reductions are obtained for particle sizes of 0.48 and 0.1 mm respectively. Schröfl et al. (2012) have reported that concrete with 0.3% SAP (W/C=0.30, W_e/C=0.06) of 0.63 mm and 0.90 mm particle sizes have 23.7% and 21.3% strength reductions respectively. However, conflicting results have been reported by other studies (Mechtcherine et al., 2014; Olawuyi & Boshoff, 2013; Wang et al., 2009), in which larger SAP particle size leads to higher strength reduction. Hence, more experimental investigations are necessary to clarify these inconsistent results, which could be attributed to the chemistry of the SAP. Results of the splitting tensile strength (indirect test) are illustrated in Figure 5.7(b). Similar to the compressive strength, a lower dosage of SAP has a limited effect on tensile strength so that the addition of 0.25% SAP leads to only 5.0% reduction in tensile strength. However, 32.5% and 47.5% reductions are observed for 0.5 and 1.0% SAP, respectively (Figure 5.7(b)). General

results of Figure 6.7 shows that tensile strength is more sensitive to the SAP particle as compared to compressive strength so that, for instance, 23.8% reduction is observed for compressive strength of 0.5% SAP-contained concrete, while 32.5% reduction is obtained for tensile strength. This may attributed to the existence SAP macro voids inside the matrix bulk which can affect the pore network, causing changes in crack path and propagation. Crack width opening is also measured by the splitting tensile test, which is shown in Figure 5.7(c). Results show that crack width corresponding to the maximum tensile force is higher for SAP mixtures as compared to the reference mixture. This can shows that concrete specimens containing SAP have a more ductile behaviour under splitting tensile test, as compared to reference mixture. This is confirmed in the experimental results reported by Snoeck et al. (2018) under impact loads using a drop-weight machine. The relationship between splitting tensile strength and compressive strength of SAP concrete is shown in Figure 5.7(d). Eq. (5.2) is found as the best-fit correlation function for this relationship as follows:

$$f_{st} = 0.90e^{0.03\, f_c'} \tag{5.2}$$

where f_{st} is splitting tensile strength and f_c is the compressive strength of SAP concrete. As shown in Figure 5.7(d) correlation of $R^2 = 0.94$ shows the performance of this equation.

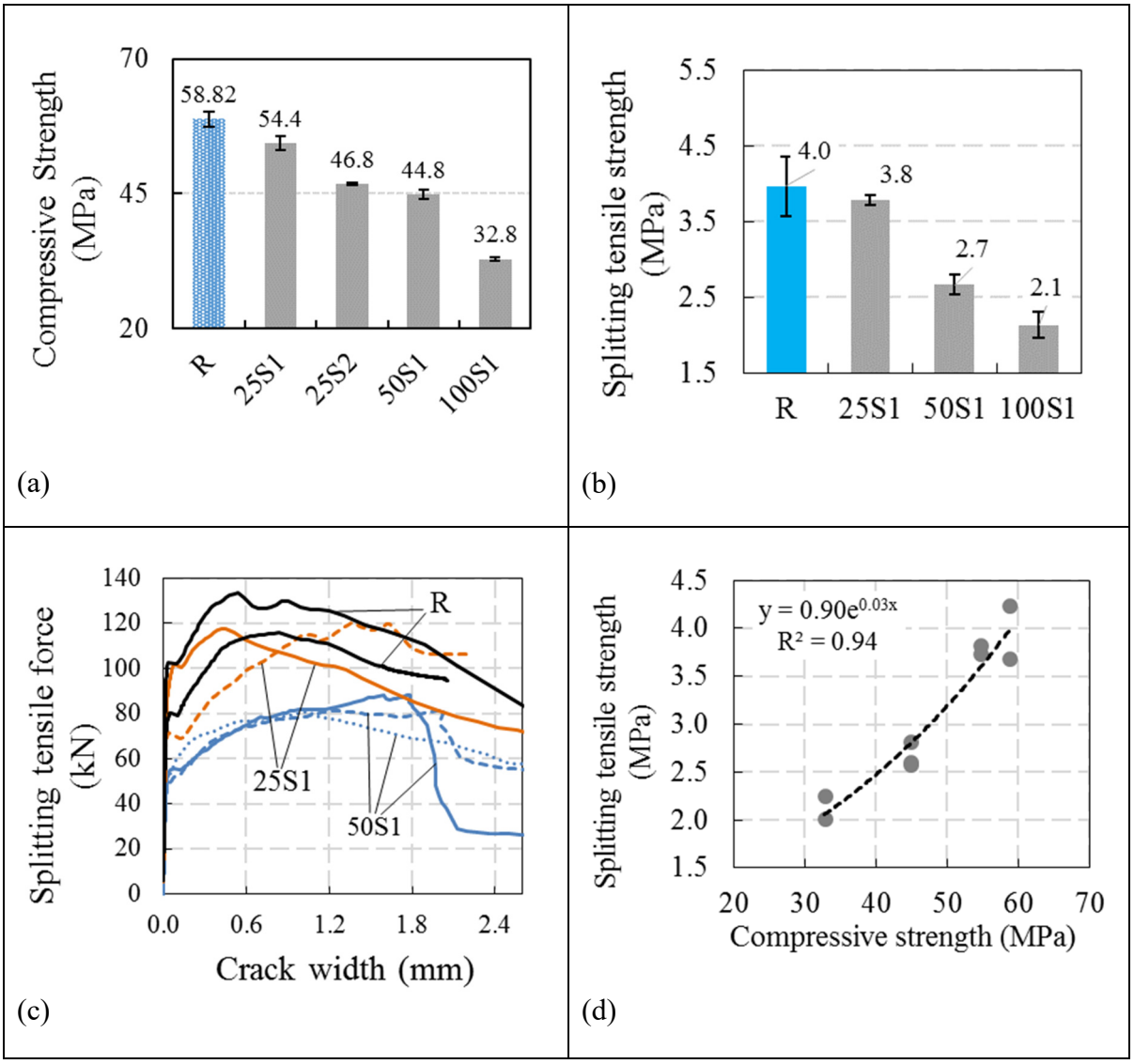

Figure 5.7 Mechanical properties of SAP concrete for different mixes:
(a) compressive strength; (b) splitting tensile strength; (c) tensile force-crack width curve;
(d) relationship between splitting tensile strength and compressive strength

5.3.2 Interfacial transition zone (ITZ)

To investigate the effect of SAP particle size on hardened properties of concrete, the results of a study conducted on the interfacial transition zone (ITZ) are summarized in Figure 5.8. Although the size of macro voids generated by SAP-2 is smaller compared to SAP-1, the results of image analysis show that the use of a small SAP particle size leads to a high number of

voids around the aggregate (in the matrix). As illustrated in Figure 5.7, this high number of voids leads to a high reduction in compressive strength. Results presented in Figure 5.8(b) show that the shape of macro voids in SAP-2 modified concrete is very close to the air void shape of NC, which is very different from the irregular shape of macro voids generated in SAP-1 modified concrete.

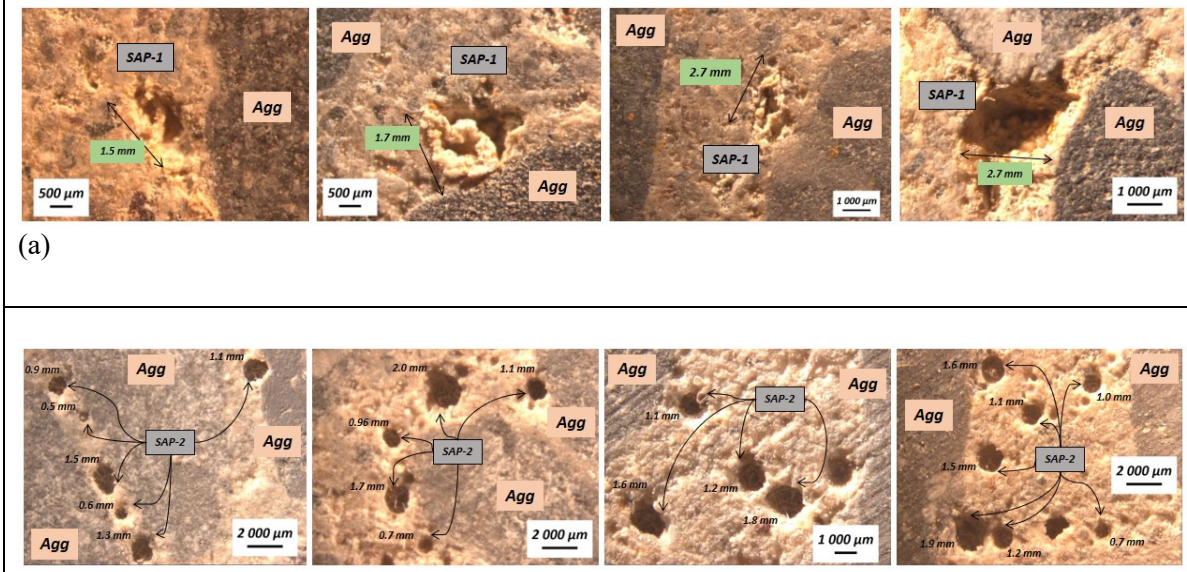

Figure 5.8 Image analysis of SAP particles around aggregate (ITZ): (a) SAP-1; (b) SAP-2

5.3.3 Pull-out tests

Results of pull-out tests are presented by the following subsections. Detailed results of pull-out tests for un-cracked, pre-cracked, and healed concrete are summarized in Table 5.3. The specimen identification is defined in Figure 5.9. Three nominally identical samples for un-cracked concrete are tested. Although more repetition tests have been considered for pre-cracked concrete, manual crack width measurement (immediately after unloading) provided less identical specimens for some cases. The main parameters of experimental results

summarized in Table 5.3 are crack width, w; compressive strength of concrete, f_c; initial bond stress of steel rebar-concrete interaction corresponding to a slip of 0.10 mm, $\tau_{0.1}$; bond strength, τ_{max}; residual bond stress corresponding to a slip of 6.0 mm, $\tau_{6.0}$; slip corresponding to the bond strength, S_{max}; and area under the bond-slip curve till a slip of 1.0 mm, $E_{1.0}$ (energy absorbed by bond mechanism). Besides, number of the specimens considered for every concrete mix and failure modes are mentioned in Table 5.3.

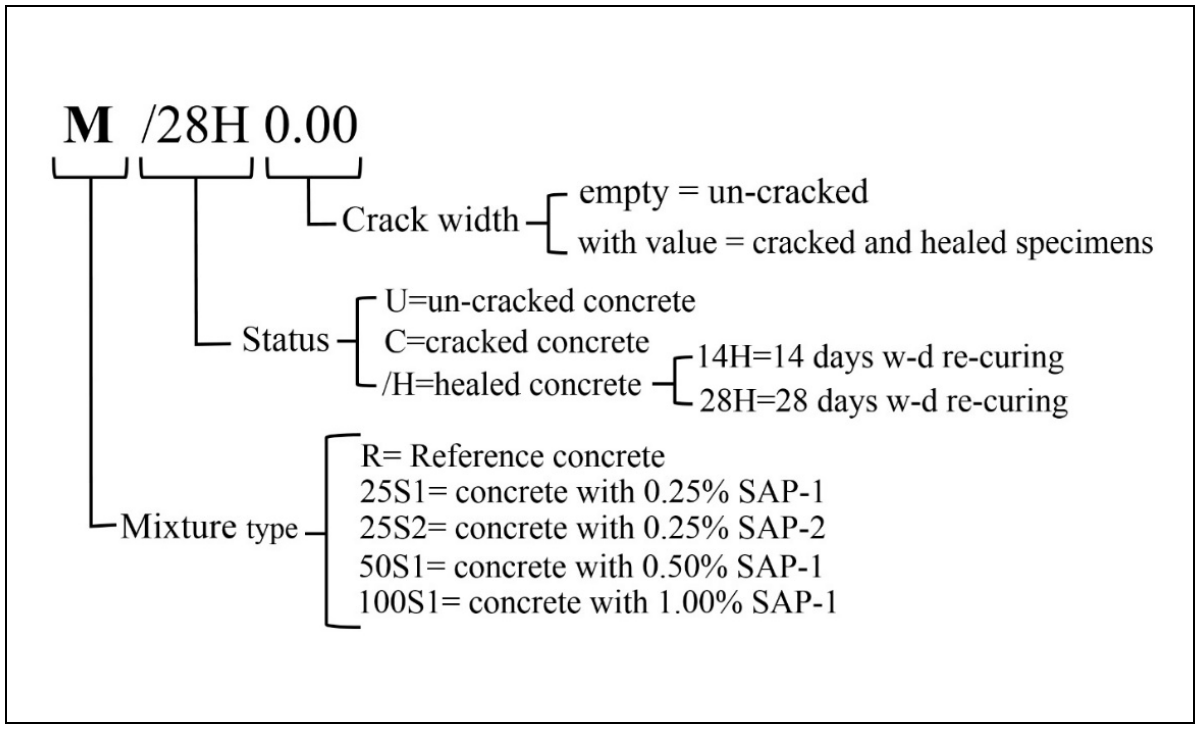

Figure 5.9 Specimen identification description

Table 5.3 Experimental results and failure modes

Specimen[1]	w	f'_c	$\tau_{0.1}$	τ_{max}	$\tau_{6.0}$	S_{max}	$E_{1.0}$	RF^2	IF^3	Failure Mode[6]
	(mm)	(MPa)				(mm)	(N/mm)	%	%	
RU	0.00	58.82 *(1.39)*	19.67 (*2.75*)	25.79 (*1.14*)	13.83 *(1.07)*	0.64 (*0.09*)	23.98 (*1.20*)	-	-	PO
RC0.2	0.20	58.82	13.96	18.05	-	0.16	11.57	69.99	-	S
RC0.3	0.30	58.82	5.98 (*1.22*)	11.64 (*1.74*)	-	0.22 (*0.04*)	8.66 (*1.16*)	45.14	-	S
RC0.4	0.40	58.82	2.37 (*3.01*)	4.61 (*0.14*)	-	0.48 (*0.53*)	1.79 (*0.92*)	17.89	-	S
R/14H0.3	0.30	58.82	4.99 (*1.66*)	9.35 (*2.77*)	-	0.22 (*0.07*)	4.24 (*1.09*)	36.25	-16.18	S
R/28H0.3	0.30	58.82	11.30 (*1.02*)	11.84 (*0.60*)	-	0.12 (*0.03*)	7.23 (*1.49*)	45.92	+1.41	S
R/28H0.4	0.40	58.82	4.33	5.82	-	0.22	3.45	22.57	+5.71	S
25S1U	0.00	54.36 *(1.20)*	11.98 (*2.50*)	24.37 (*0.31*)	12.19 *(1.63)*	0.63 (*0.04*)	21.44 (*0.45*)	-	-	PO
25S1C0.3	0.30	54.36	6.62 (*2.09*)	9.85 (*0.18*)	-	0.24 (*0.15*)	5.35 (*1.24*)	40.42	-	S
25S1C0.4	0.40	54.36	3.09 (*0.06*)	5.56 (*0.03*)	-	0.67 (*0.18*)	4.68 (*0.04*)	22.81	-	S
25S1C0.5	0.50	54.36	0.12	2.58	-	1.24	0.98	10.59	-	S
25S1/14H0.3	0.30	54.36	5.24 (*1.17*)	10.44 (*4.46*)	-	0.24 (*0.09*)	5.42 (*1.82*)	42.84	+4.03	S
25S1/14H0.4	0.40	54.36	3.49 (*0.43*)	4.26 (*0.73*)	-	0.11 (*0.09*)	2.39 (*0.13*)	17.48	-6.94	S
25S1/28H0.3		54.36	7.13 (*1.94*)	12.20 (*2.08*)	-	0.35 (*0.05*)	7.87 (*0.55*)	50.06	+16.2	S
25S1/28H0.4	0.40	54.36	2.65	7.06	-	0.59	4.79	28.97	+7.98	S
25S2U	0.00	46.83 *(0.17)*	8.41 (*1.36*)	25.02 (*0.15*)	13.81 *(3.15)*	1.32 (*0.15*)	18.01 (*0.52*)	-	-	PO
25S2C0.15	0.15	46.83	5.10 (*3.47*)	13.97 (*2.80*)	-	0.51 (*0.20*)	10.49 (3.02)	55.84	-	S
25S2C0.3	0.30	46.83	3.55 (*0.49*)	5.70 (2.37)	-	0.33 (*0.26*)	3.80 (*1.65*)	22.78	-	S
25S2/14H0.2	0.20	46.83	5.34 (*1.61*)	7.99 (*1.07*)	-	0.23 (*0.13*)	4.17 (*0.36*)	31.93	-28.0 [5]	S
25S2/14H0.3	0.30	46.83	4.14 (*1.30*)	7.03 (*0.01*)	-	0.24 (*0.03*)	3.41 (*0.18*)	28.1	+6.88	S
25S2/28H0.3	0.30	46.83	2.65 (*1.01*)	7.89 (*0.01*)	-	0.38 (*0.03*)	4.53 (*0.08*)	31.53	+11.3	S
25S2/28H0.35	0.35	46.83	1.58	6.58	-	0.40	2.91	26.3	+20.7[5]	S
50S1U	0.00	44.84 *(0.77)*	5.85 (*1.39*)	15.30 (*0.70*)	2.29 *(3.60)*	1.16 (*0.18*)	11.85 (*0.22*)	-	-	PO, S
50S1C0.1	0.10	44.84	7.55	14.41	-	0.40	11.24	94.18	-	S
50S1C0.3	0.30	44.84	2.69 (*0.05*)	4.16 (*0.09*)	-	0.22 (*0.00*)	1.96 (*0.32*)	27.19	-	S
50S1/14H0.3	0.30	44.84	2.31 (*1.10*)	5.59 (*2.27*)	-	0.51 (*0.32*)	2.76 (*0.27*)	36.54	+12.8	S
50S1/28H0.3	0.30	44.84	2.66 (*0.87*)	7.46 (*0.88*)	-	0.39 (*0.09*)	4.33 (*0.11*)	48.76	+29.6	S
100S1U	0.00	32.83 *(0.27)*	2.32 *(0.44)*	10.73 (*1.11*)	3.51 *(0.58)*	1.39 (*0.25*)	6.75 (*0.94*)	-	-	PO
100S1C0.3	0.30	32.83	1.40 (*1.11*)	3.32 (*2.24*)	-	0.71 (*0.39*)	2.28 (*1.50*)	30.94	-	S

Table 5.3 Experimental results and failure modes (continued)

Specimen[1]	w	f'_c	$\tau_{0.1}$	τ_{max}	$\tau_{6.0}$	S_{max}	$E_{1.0}$	RF^2	IF^3	Failure Mode[6]
	(mm)	(MPa)				(mm)	(N/mm)	%	%	
100S1/14H0.3	0.30	32.83	1.34 (*0.35*)	4.76 (*1.64*)	-	0.53 (*0.24*)	2.88 (*1.30*)	44.36	+19.42	S
100S1/28H0.3	0.30	32.83	1.60 (*0.31*)	5.18 (*1.10*)	-	0.52 (*0.07*)	3.34 (*0.95*)	48.28	+25.13	S
All specimens										$n = 68$

[1] Specimen identification according to Figure 5.9; [2] Reduction factor according to Eq. (5.5);
[3] Improvement factor according to Eq. (5.6); [4] number of specimens; [5] obtained by regression analysis of pre-cracked concrete; [6] PO=pull-out; S=splitting. Note: Data inside the parentheses denotes the standard deviation.

The final modes of failure are shown by notations of PO and S indicating pull-out and splitting respectively in Table 5.3. The general mode of failure for un-cracked specimens is pull-out (Figure 5.10(a)). Moreover, pre-cracked specimens of NC (RU) for crack widths of 0.10 mm and 0.15 mm experienced pull-out failure modes. Splitting failure modes are observed for pre-cracked concrete in which crack widths are larger than 0.20 mm (Figure 5.10(b)). Similar to pre-cracked concrete, splitting failure modes are observed for all healed specimens.

(a)

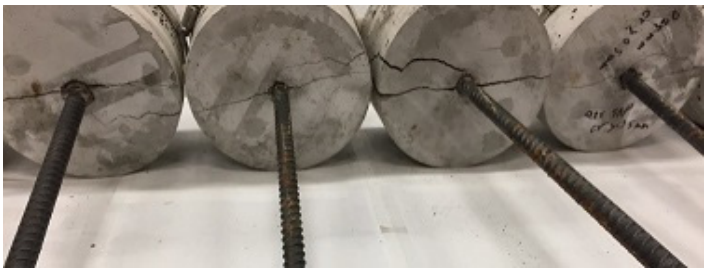

(b)

Figure 5.10 Failure modes: (a) pull-out (PO); (b) splitting (S)

5.3.3.1 Bond-slip response of un-cracked SAP concrete

Bond-slip curves of un-cracked concrete are provided in Figure 5.11. Obtained results indicate that mixtures with 0.25% SAP have comparable bond strengths to the reference mixture (RU) (Figure 5.11(a-c)). Similar results are obtained for the compressive strength of SAP-1 (Figure 5.7). Moreover, for uncracked specimens, the bond strength of mixture with 0.25% of SAP-2 is similar to the bond strength of 25S1U (Figure 5.11(b)). This contrasts with the results reported for compressive strength (Figure 5.7), where the compressive strength of 25S2U is lower than the reference mixture (RU). A lower percentage of SAP with larger diameter (25S1) has a lower influence on compressive strength, 7.5% reduction when compared with the smaller diameter SAP (25S2), which gives a 20.4% reduction. Similar results corresponding to SAP particle size effect are reported by previous studies (Mechtcherine et al., 2017; Schröfl et al., 2012; Snoeck et al., 2014). The chemistry of the SAP also seems to play an important role: the SAP-1 made of cross-linked copolymer of acrylamide and potassium acrylate and the SAP -2 made of cross-linked anionic polyacrylamide. Although the interpretation of the effect of SAP addition on compressive strength is not clear, capillary porosity and degree of hydration have been considered as the main reasons for explaining this effect (Piérard et al., 2006). Formation of macro voids, generated by initially filling of entraining pores with excess water, which then gradually dries out, significantly changes the equivalent porosity and microstructure. This theory is strongly confirmed by a model presented by Powers and Brownyard (1946). The impact of SAP on compressive strength is significantly dependent on the amount of solid matrix in mixtures which results in different impacts on cement paste, mortar, and concrete (Lura et al., 2006). However, the internal curing of concrete using SAP particles has a positive impact on the hydration degree of cement grains which can affect the long-term compressive strength of SAP concrete (Esteves et al., 2007). In the case of 0.25% SAP-1, the negative effect of generated voids induced by the SAP particles is compensated by the improved degree of hydration so that only 7.5% reduction is observed in compressive strength (Figure 5.7). However, the higher bulk density of SAP-2 compared to SAP-1 increases the number of SAP particles in the same volume yielding a significant reduction in the concrete compressive strength. Comparable results were reported by other authors, confirming this

phenomenon (Schröfl et al., 2012; Snoeck et al., 2014). Snoeck et al. (2014) have reported reductions of 4.4% and 15.7% in compressive strength of mortars for 0.48 mm and 0.10 mm SAP size particles respectively with 0.5% SAP (W/C=0.5, W_e/C=0). They have reported a similar trend for 1.0% SAP with 5.5% and 30.2 % strength reductions observed for particle sizes of 0.48 mm and 0.10 mm, respectively. Consistent with these results, Schröfl et al. (2012) have reported that concrete with 0.3% SAP (W/C=0.30, W_e/C=0.06) of 0.63 mm and 0.90 mm particle sizes have 23.7% and 21.3% strength reductions, respectively. However, conflicting results have been reported by other studies (Mechtcherine et al., 2014; Olawuyi & Boshoff, 2013; Wang et al., 2009) in which larger SAP particle size leads to higher strength reduction. Results show that a higher dosage of SAP considerably reduces the bond strength and residual bond stress (Figures 5.11(c) and 5.12). Initial stiffness of bond-slip curve is lower for concrete with a smaller particle size (Figure 5.12) compared to large particle size, which directly affects the slip corresponding to the bond strength (Figure 5.11(d)). Hence, it can be deduced from Figures 5.11 and 5.12 that high number of macro voids generated by the small size of SAP particles (Figure 5.8) seems to mostly affect the initial bond stress, while the size of macro voids seems to affect the bond strength and also bond stress corresponding to a slip of 6.0 mm, $\tau_{6.0}$ (Figure 5.12).

As illustrated in Figure 5.12, similar to bond strength and residual bond stress, energy absorbed by the bond mechanism of the un-cracked specimens (shown by $E_{1.0}$) is also affected by SAP dosage. Regarding energy absorption in SAP-contained cementitious materials, only Snoeck et al. (2018) conducted experimental tests on the self-healing characteristics under impact loads using a drop-weight machine. They found that the specimens containing SAP have a more ductile behaviour, as compared to reference mixture. However, the ductility mechanism in bond behaviour could be different from the impact behaviour. Overall, the results of Figures 5.11 and 6.12 show that SAP concrete with SAP dosage higher than 0.25% (wt.% of cement) has significantly lower dissipated energy by the bond mechanism which is associated with a weak paste that crushed more easily under concrete compression in front of the rebar lugs. Although most of the SAP-modified concrete test specimens failed by a pull-out bond mechanism, two specimens tested for 0.5% SAP failed by splitting failure modes, which may

be attributed to the specific random distribution of macro voids generated by SAP particles. However, the standard deviation reported for bond strength of 0.50 % SAP is in the range of accepted value (Figure 5.11(c)).

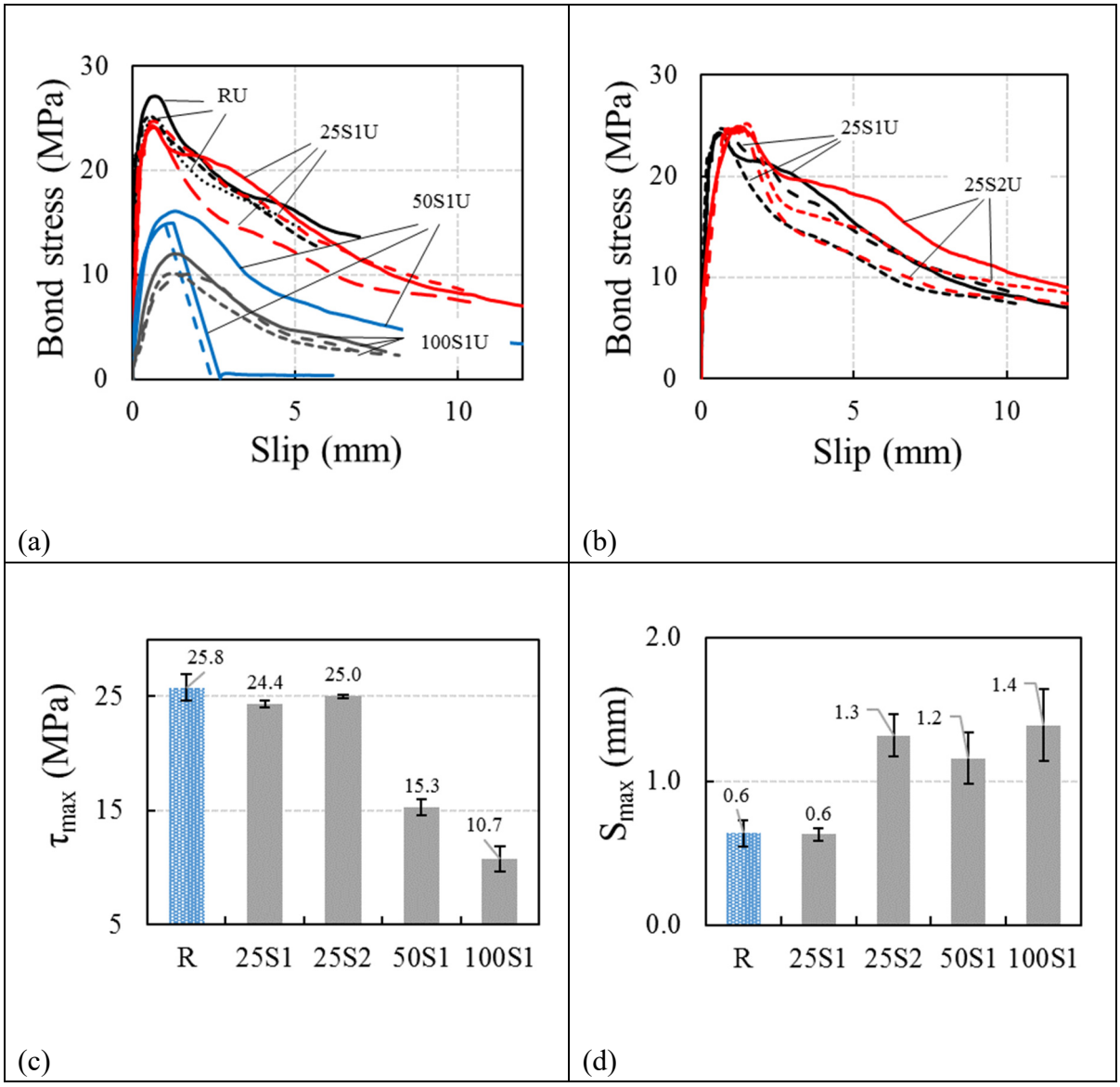

Figure 5.11 Results of un-cracked SAP concrete:
(a) bond-slip curves for different SAP percentages;
(b) bond-slip curves for different SAP particle sizes; (c) bond strength;
(d) slip corresponding to the maximum bond stress

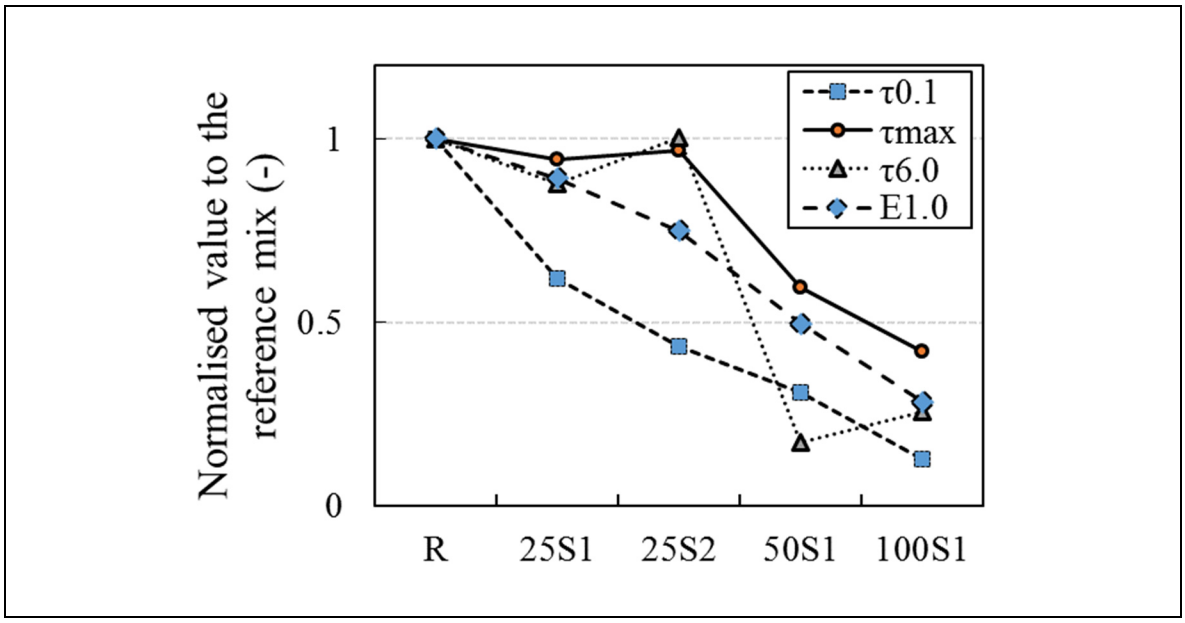

Figure 5.12 Normalized results of un-cracked SAP concrete to the reference mix

Most previous studies have approved that the bond strength is closely related to the square root of the concrete compressive strength as normalized bond strength, $\tau_{max}/\sqrt{f'_c}$ (Esfahani & Kianoush, 2005; Mousavi et al., 2017; Wu & Zhao, 2012). Effect of compressive strength and also SAP dosage on the bond strength of SAP concrete is formulated by Eqs. (5.3) and (5.4) respectively. Normalized bond stress by compressive strength of SAP concrete, is used in Eq. (5.3).

$$\tau_{max} = 8.2\sqrt{f'_c} - 37.2 \tag{5.3}$$

$$\frac{\tau_{max}}{\sqrt{f'_c}} = 3.48e^{(-0.64\mathrm{SAP}_{\%})} \tag{5.4}$$

As shown in Figure 5.13(a), good correlation is achieved for Eq. (5.3) in predicting the bond strength as a function of the square root of compressive strength for $f'_c > 20$ MPa (R^2=0.94). Also, to follow the proposed normalized ratio presented in the literature, Eq. (5.4) shows a

good correlation for relating the normalized bond strength of SAP concrete, as a function of SAP weight ratio used (R^2=0.87, Figure 5.13(b)).

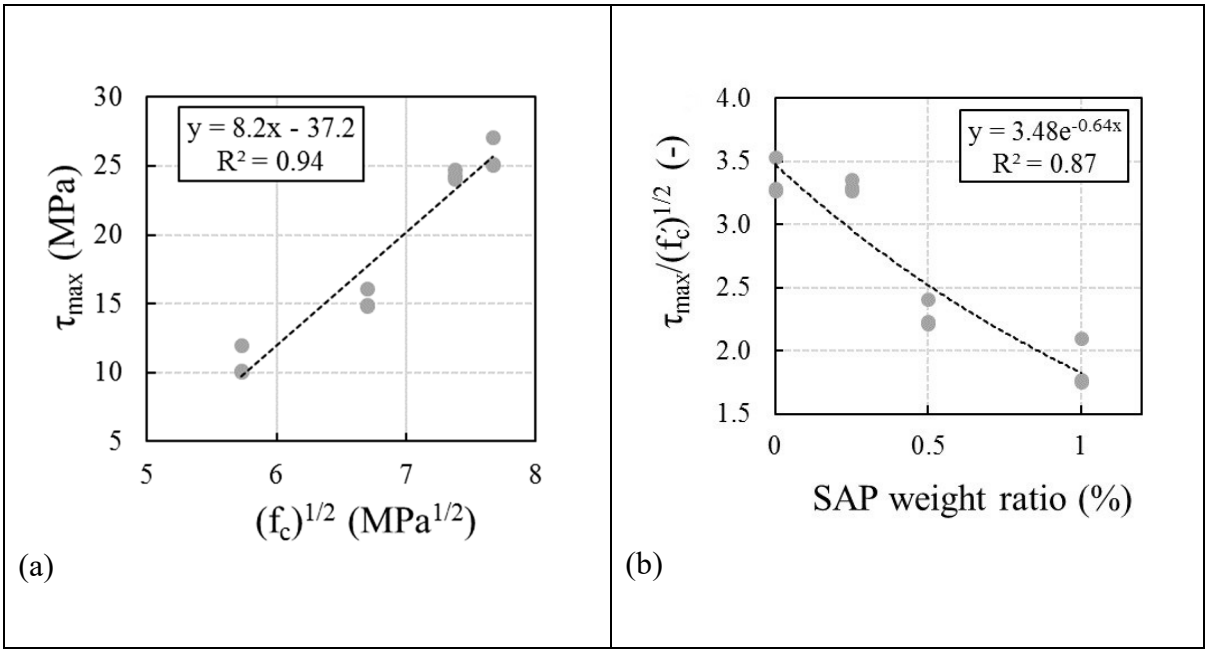

Figure 5.13 Bond strength of SAP concrete: (a) versus compressive strength; (b) normalized bond strength versus SAP weight ratio

To compare the size of the void around the rebar edge, disk-shaped layers of concrete cylinders are cut from tested specimens and analyzed under the microscope. Voids generated due to the SAP particles inside the concrete mixture are illustrated in Figure 5.14 for different SAP dosage ratios. SAP particles make much larger voids inside the concrete than air voids. In addition, the shape of the voids is changing in comparison with the reference concrete without SAP. The analysis shows that SAP percentage leads to a significant increase in the maximum diameter of the macro voids inside the mixture. The number of macro voids is increased for a higher percentage of SAP inside the concrete mixture.

5.3.3.2 Bond-slip response of pre-cracked SAP concrete

Although one of the most relevant problems of steel-congested concrete structures (such beam-column joint) is the pre-cracking phenomenon due to the plastic shrinkage cracks and accidental damages (previous earthquakes or over-loading), limited and also scattered studies have been devoted to address this issue (Brantschen et al., 2016; Matsumoto et al., 2016; Mousavi et al., 2019). Results of pre-cracked SAP concrete show that the bond-slip behaviour of steel rebar is noticeably influenced by the presence of initial crack widths (Figure 5.15). Bond strength and area under bond-slip curves are significantly affected by initial cracks induced by the pre-cracking phenomena. Similar results have been reported in the literature for NC (Brantschen et al., 2016; Mousavi et al., 2019). However, results show that crack width smaller than 0.15 mm has no significant effect on bond strength and failure mode of NC (Table 5.3). As the crack width increases, absorbed energy decreases which shows a more brittle behaviour of rebar-concrete bond response. Low normalized energy dissipated is associated with a brittle bond response associated with moderately and unconfined concrete, while a high energy value shows a ductile bond response tending toward confined concrete bond response (Guizani et al., 2017). Overall, observations indicate that the percentage and size of SAP directly affect the structural behaviour of the pre-cracked concrete. To accurately compare the results of pre-cracked and healed concrete with un-cracked concrete, a reduction factor is defined hereafter as follows:

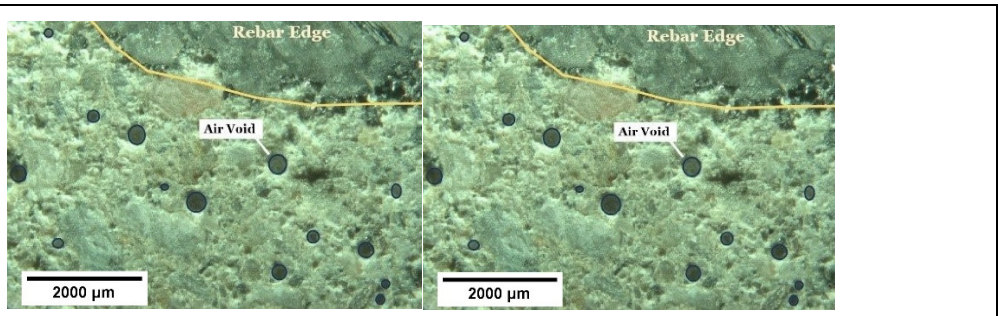

(a)

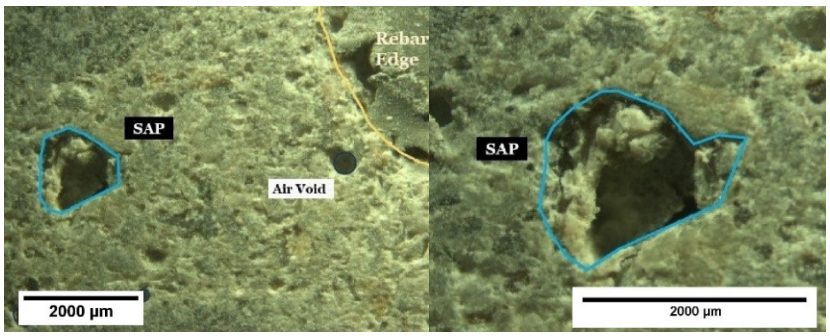

(b)

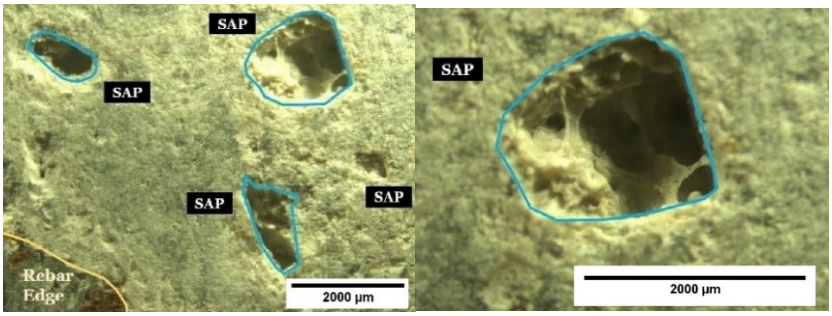

(c)

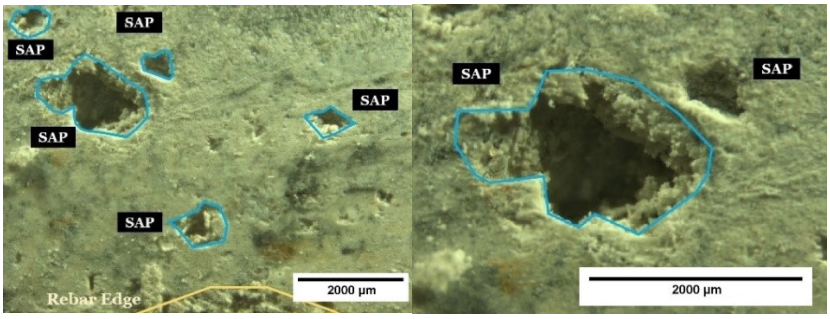

(d)

Figure 5.14 Voids generated in concrete containing SAP-1: (a) 0% SAP; (b) 0.25% SAP; (c) 0.50% SAP; (d) 1.0% SAP

$$\mathrm{RF} = \left[\frac{\tau_{Precracked}}{\tau_{Uncracked}}\right] \times 100 \tag{5.5}$$

A higher RF corresponds to lower damage due to the pre-cracking phenomenon so that, as the reduction factor increases, bond strength of rebar in pre-cracked concrete increases compared to the reference mixture (without crack). RFs of bond strength for pre-cracked concrete concerning different concrete mixtures, SAP percentage, are illustrated in Figure 5.15(f). Although the similar limited value of crack is defined for a pre-cracking recording device, different values of crack widths are measured at the end of the test called "ultimate crack width" which are in the range of 0.0-0.50 mm. A similar extent of scattering in the test results is observed and reported before in the literature related to the simulation of pre-cracking in the rebar-concrete interface (Desnerck et al., 2015; Mousavi et al., 2019). Consistent with the failure modes (Table 5.3), the trend shows that cracks having widths smaller than 0.15 mm (w < 0.15) have a limited impact on the bond strength, with a reduction factor close to unity (50S1C0.1). This is conforming to results reported by previous research (Mousavi et al. 2019). The results show that among the concrete mixes, 25S1 shows acceptable (25S1C0.3) and also a higher reduction factor (25S1C0.4) compared to the reference mixture (RC). This can be attributed to the fact that a lower dosage of SAP-1 improves the sensitivity of concrete mixtures to the pre-cracking phenomenon for larger crack widths (Figure 5.15). However higher dosage of SAP in the mixture leads to a considerable reduction in bond strength of rebar in pre-cracked concrete, due to the increased porosity which is similarly reported for compressive strength (Figure 5.7). A similar explanation has been reported by Powers & Brownyard (1946) in which porosity (pore volume) plays a critical role in hardened properties of cement paste. Higher dosage of SAP results in higher porosity (Figure 5.11(d)), due to the shrinking particles exposed to the surrounding dry environment. A similar explanation can also be used for a mixture containing 0.25SAP-2, in which despite the lower compressive strength compared to the 0.25SAP-1, similar bond strength is obtained for both SAP particle sizes (Figure 5.10(b)). Furthermore, the effect of higher porosity can be clearly observed in the initial stiffness of bond strength ($\tau_{0.1}$), so that a higher slip corresponding to the bond strength (S_{max}) is reported for 0.25SAP-2 compared to 0.25SAP-1.

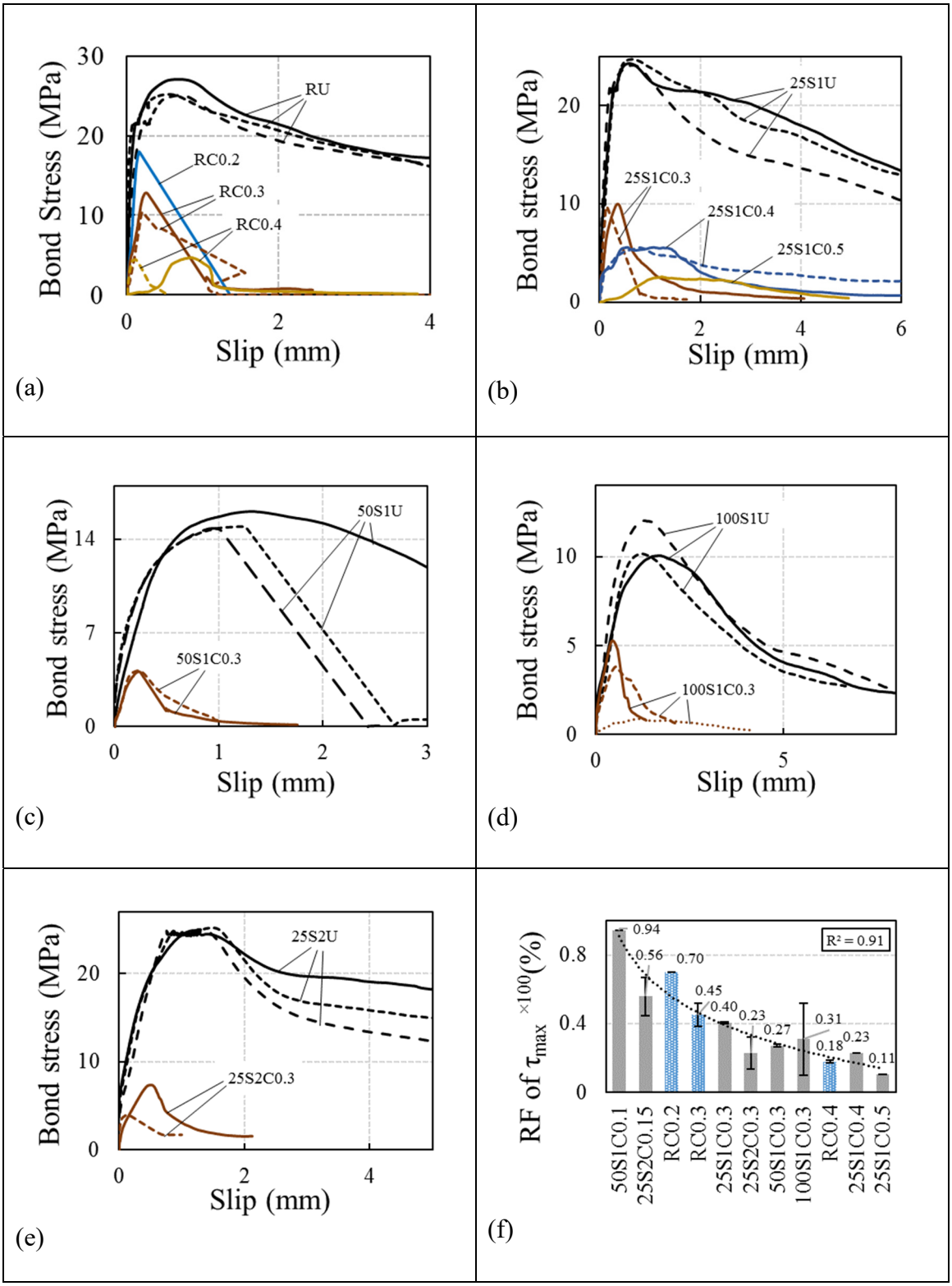

Figure 5.15 Bond-slip curves of pre-cracked concrete: (a) R; (b) 25S1; (c) 50S1; (d) 100S1; (e) 25S2; (f) reduction factor ordered by crack width for bond strength

Figure 5.16 shows the reduction factors as a function of the ratio of crack width-to-rebar diameter, w/d_b, for bond strength. General results show a significant impact of the pre-cracking phenomenon on bond strength of all mixtures. Concrete containing 0.25% SAP-1 shows the same and higher reduction factors (good performance for the pre-cracking phenomenon) in some cases compared to the reference concrete (Figures 5.15 and 5.16(a)). However, a higher dosage of SAP results in lower reduction factors caused by macro voids (Figure 5.16(a)). Moreover, it can be deduced from Figure 5.16(b) that concrete with SAP-2 (smaller size) has a lower reduction factor for the same w/d_b ratio compared to the concrete with SAP-1. This can be attributed to the higher bulk density of SAP-2, which increases the number of voids in the matrix.

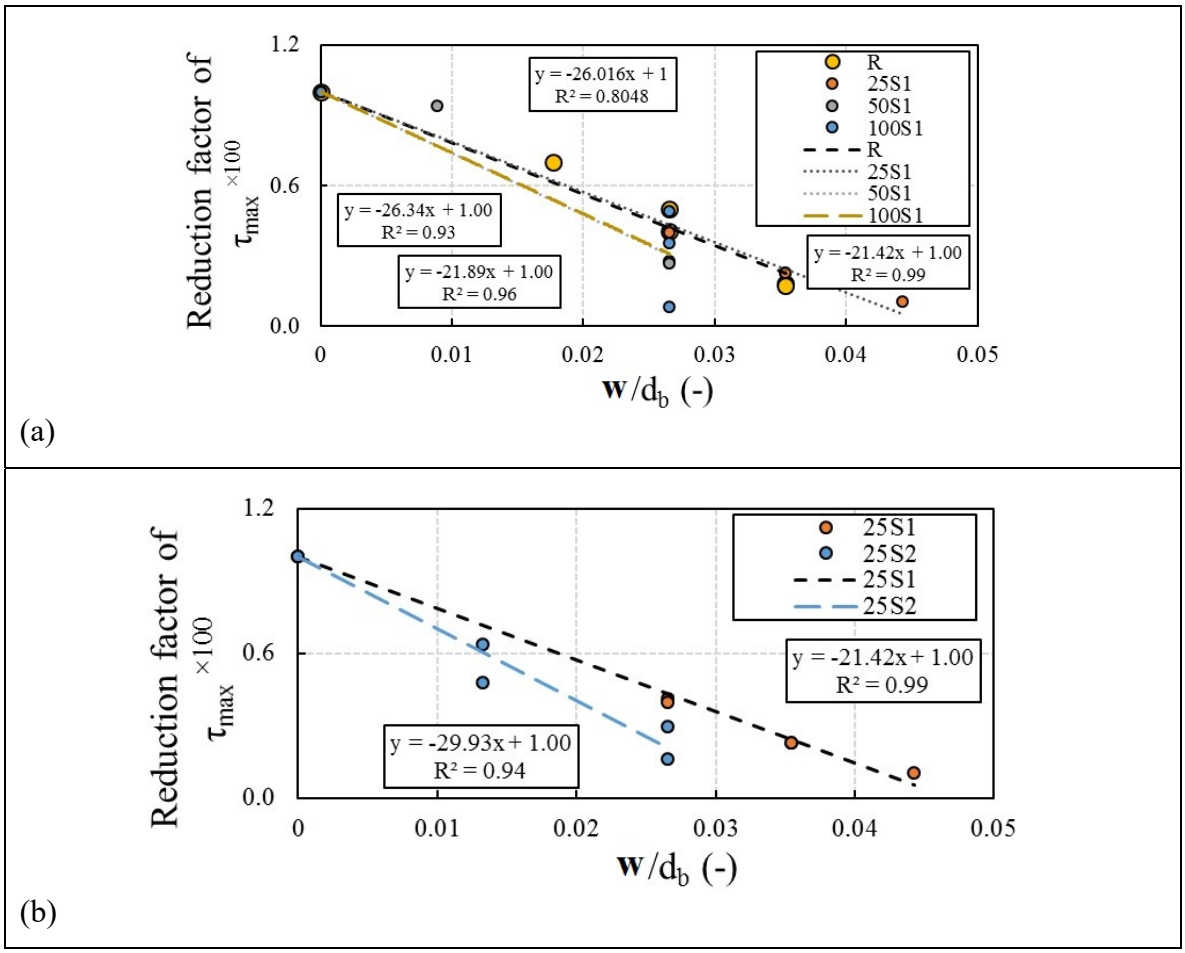

Figure 5.16 Reduction factor of bond strength of SAP concrete:
(a) according to the percentage of SAP; (b) for different SAP types

5.3.3.3 Bond-slip response of healed SAP concrete

Bond-slip curves of healed concrete are shown in Figure 5.17. Overall, results indicate that a higher percentage of SAP inside concrete leads to more autogenous healing compared to other mixtures. Moreover, observations confirm that 28-day healing periods resulted in higher healing, compared to 14-day healing periods. SAP concrete with larger crack widths shows considerable improvement factor (healing effects) than smaller size for crack widths of 0.30 mm (Figure 5.17(f)). Bond-slip curves of healed concrete show that the healing periods could not change the bond failure mechanism, splitting failure are observed for all healed concrete. However, the bond properties are improved which includes bond strength, residual bond stress, and absorbed energy by the bond mechanism (Figure 5.17 and Table 5.3). It is worth mentioning that if the crack width is closer to 0.15 mm, the bond failure mode could change due to healing with SAP especially after a long period of healing. Hence, more experimental studies are necessary for smaller crack widths and also for more extended periods of healing. To check the efficiency of SAP on the healing of cracks at the rebar-concrete interfacial surface, the improvement factor is defined as follows:

$$\text{IF} = \left[\frac{\tau_{Healed} - \tau_{Precracked}}{\tau_{Uncracked} - \tau_{Precracked}}\right] \times 100 \tag{5.6}$$

Improvement factor (IF) for SAP concrete is illustrated in Figure 5.18. Although SAP significantly increases the self-healing capacity of concrete for bond strength (τ_{max}), scattered results are obtained for initial bond stress ($\tau_{0.1}$) (Figure 5.18(a)). Moreover, promising results are observed for the energy absorbed by the bond mechanism until 1.0 mm (Figure 5.18(a)). In the case of reference concrete (R, without SAP), although considerable healing is observed after 28-day healing periods for initial bond stress, only 5.7% IF (R/28H0.4) is obtained for bond strength (R/28H0.4). However, similar to un-cracked (Figure 6.11) and pre-cracked (Figure 5.15) concrete, 0.25% SAP concrete shows good healing effect compared to the reference concrete so that maximum values of 16.2% and 20.6% IF is obtained for SAP-1 and SAP-2 concretes respectively after 28-day healing periods (Figure 5.18(a)).

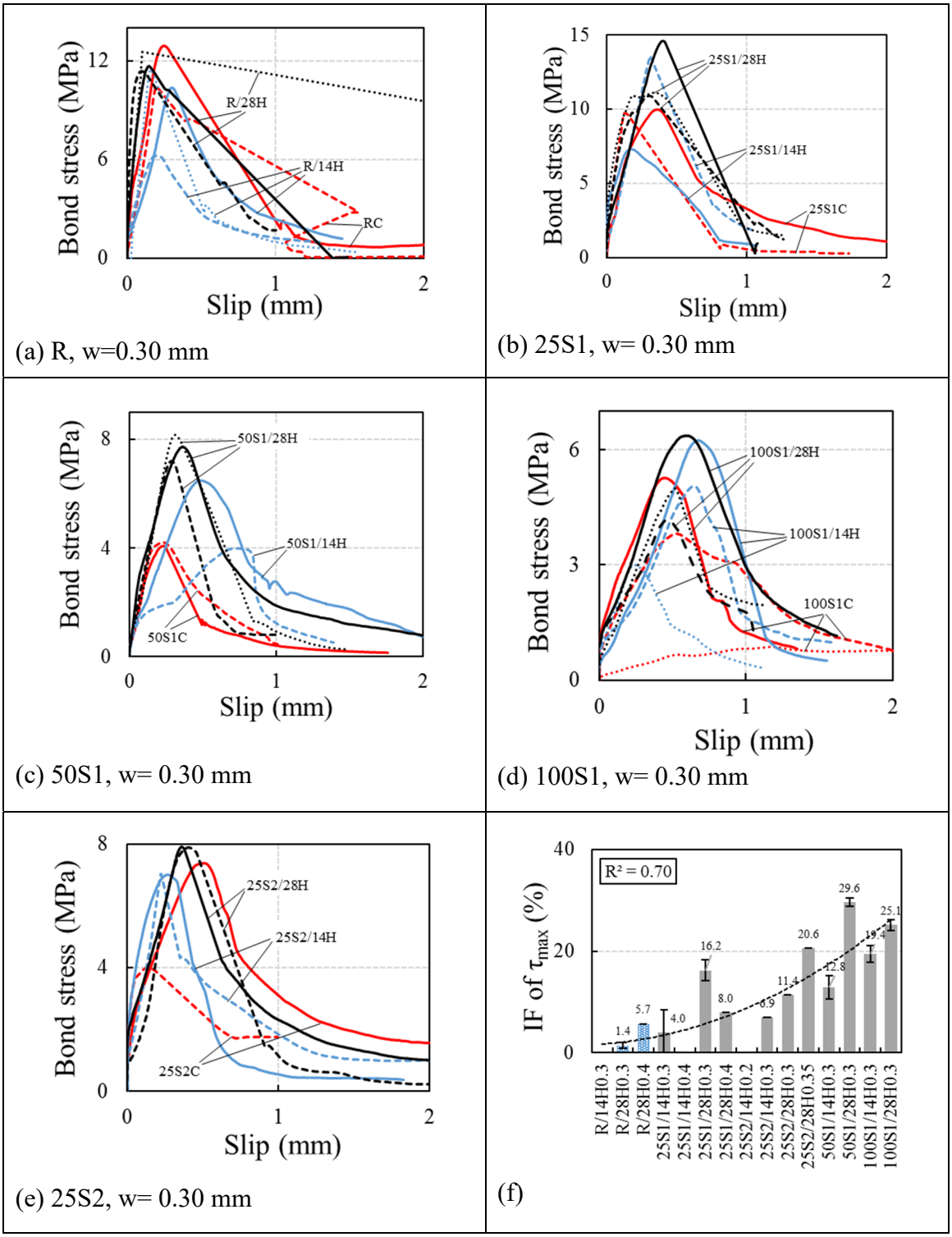

(a) R, w=0.30 mm

(b) 25S1, w= 0.30 mm

(c) 50S1, w= 0.30 mm

(d) 100S1, w= 0.30 mm

(e) 25S2, w= 0.30 mm

(f)

Figure 5.17 Bond-slip curves of healed concrete for: (a) R; (b) 25S1; (c) 50S1; (d) 100S1; (e) 25S2; (f) improvement factor (IF) of bond strength for all mixes ordered according to SAP concentration, healing period, and crack width
(red line=cracked, blue line=14-day healing, black line=28-day healing)

For crack width of 0.30 mm, concrete with large SAP particles (25S1/28H0.3) has a higher healing effect with IF of 16.2% compared to the concrete with small SAP particles (25S2/28H0.3, 11.4% IF). Even though 0.50% SAP leads to about 35% healing effect after 14-day healing periods, results indicate that this healing period is not sufficient (Figure 5.18(b)). Although higher SAP dosage reduces the bond strength of un-cracked concrete (Figure 5.11), the healing capacity is increased. The mixtures 50S1 and 100S1 heal the crack width of 0.30 mm with IF of 29.6% and 25.1% respectively after 28-day healing periods (Figure 5.18(a)). As mentioned in Table 6.1, a high amount of polycarboxylate-based superplasticizer is used for both 0.50% and 1.0% SAP to have appropriate slump flow. The same issue is reported by Van Tittelboom et al. (2016) for 0.50% SAP. This high amount of superplasticizer may affect the amount of remaining unhydrated cement particles in SAP concrete. Experimental results reported by Heikal et al. (2006) showed that the high content of superplasticizer causes slightly lower free lime content, showing a lower degree of hydration. The higher content of unhydrated cement particles inside the mixture may slightly affect the self-healing improvement factor. In some cases, initial bond stress is the only critical parameter improved by healing periods including R/28H0.3 and 25S1/14H0.4, these require more healing periods. Also, in some cases, the healing percentage of initial bond stress is significantly more than the other bond properties such as R/28H0.4, 25S2/14H0.3, and 25S1A/14H0.3 (Figure 5.18(a)).
Overall, results confirm that 0.25% SAP is the most effective on steel rebar-concrete interfacial properties in all statuses of un-cracked, pre-cracked, and healed concrete. The main advantages of 0.25% SAP concrete are comparable bond strength to un-cracked concrete, less or comparable sensitivity to the pre-cracking phenomenon (especially SAP-1), and higher healing effect compared to the reference concrete. General trends show that 14-day healing periods is approximately enough for healing the initial bond stress $\tau_{0.1}$, while longer healing periods are necessary to heal the bond strength. This can be explained by the fact that for the initial bond-ascending branch, it is the paste in contact with rebar ribs stiffness that governs the interfacial behaviour.

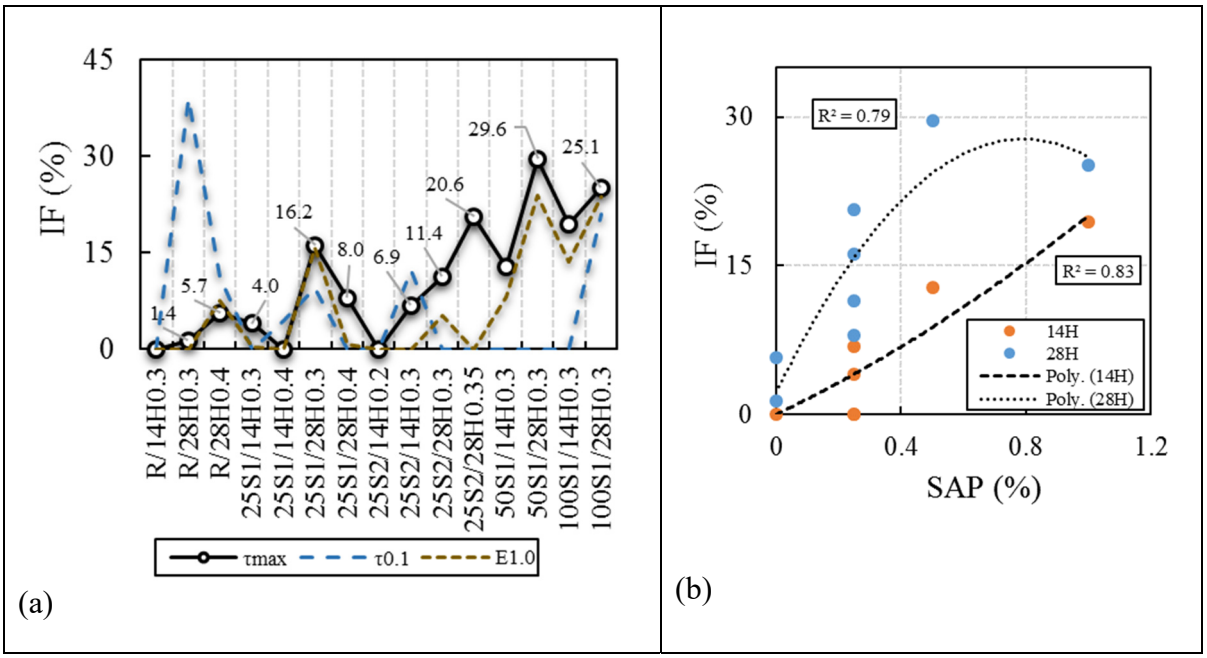

Figure 5.18 Improvement factor (IF) for the self-healing capacity of SAP concrete; (a) comparing bond properties; (b) for various healing periods

The external surface of the crack lip in the healed specimens after wet-dry cycles shows a large quantity of stalactites (Figure 5.19(a)), which is similarly reported by Snoeck et al. (2014). They have stated that the stalactites consist of a significant amount of $CaCO_3$ and washed out hydration products (Snoeck et al., 2014). Also, to visualize the hydration products at the interior of cracks healed by SAP, disk-shaped pre-cracked concrete specimens without steel rebar are considered in the current study. Microscopic images of the interior cracks of these specimens at the crack lip are presented in Figure 5.19(b-c). Abundant crystal formation can be seen for both SAP-1 and SAP-2. On the interior part of crack widths, white materials are observed, which could be attributed to the participation of $CaCO_3$ (Snoeck & De Belie, 2015; Snoeck et al., 2014). It is clearly visible in Figure 5.19(b-c) that crystallization starts from the closer parts of crack tips and then propagates to the interior parts of the crack to provide a bridge between the crack lips. To confirm the previous results of $CaCO_3$ participation, SEM analysis on healed products are conducted in the present study, which is illustrated in Figure 5.20. Six points are selected in map analysis from the healed products specimen to determine the most important element. The average value of mass percentage is shown in Figure 5.20.

Results clearly show a considerable mass percent of Calcium (the average value of 53.6%) in the healed products. Moreover, Map analysis of SEM image shows that elements of Oxygen and Carbon have 34.4% and 8.7% of mass percent of healed products respectively.

Figure 5.19 Healing products after wet-dry cycles: (a) on external surface of the crack lip; (b) on interior of cracks for SAP-1 modfified concrete; (c) on interior of cracks for SAP-2 modfified concrete

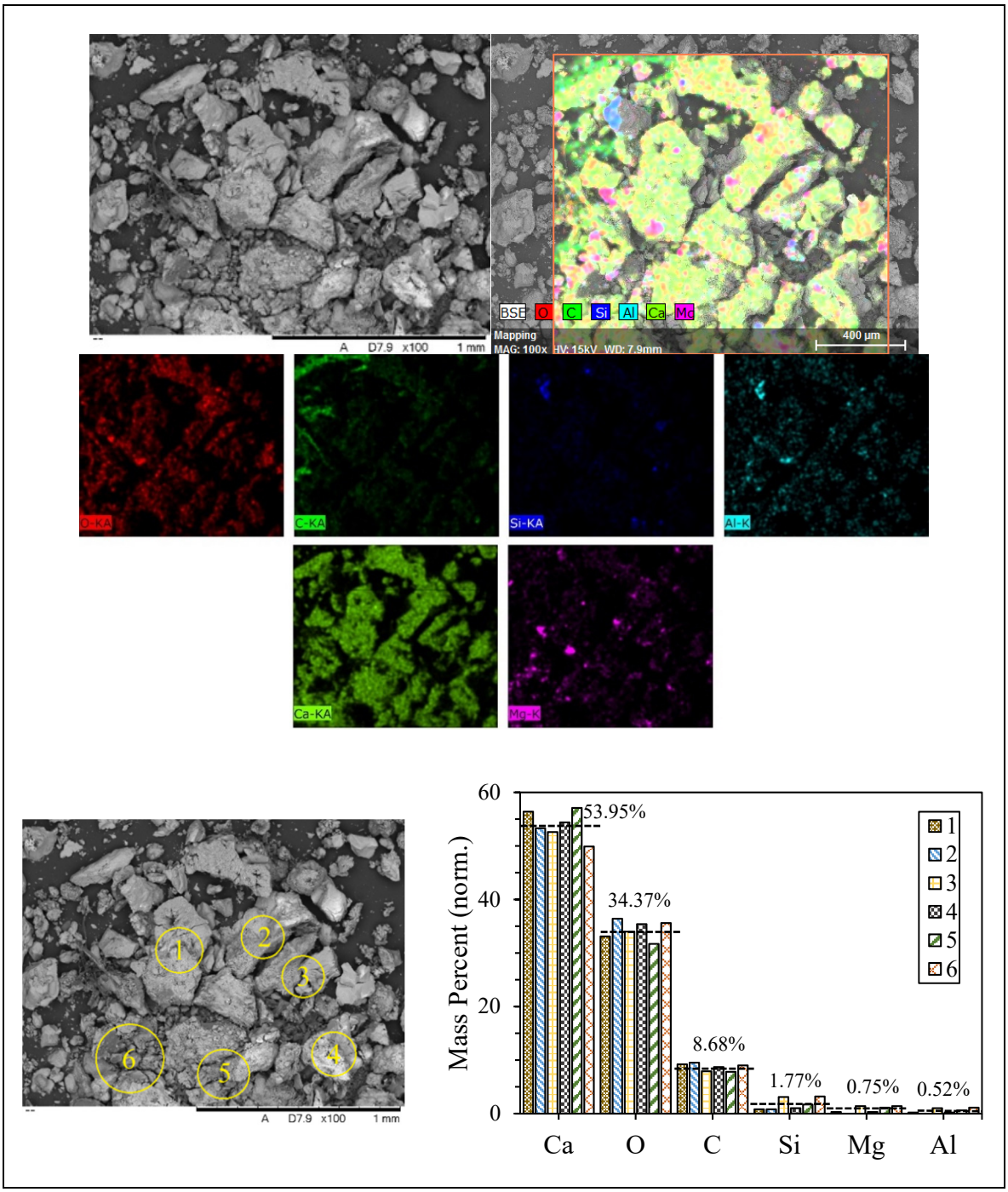

Figure 5.20 SEM image analysis of healed products
(average values of six points are presented for mass percent)

As SAP particle is needed at the crack surface for increasing the possibility of the crack-healing process, it is essential that cracks pass the locations in which SAP is located. This can provide water resources for producing healing products. Figure 5.20 shows that the position and the irregular shape of SAP voids has a significant impact on the crack path so that it provides an appropriate condition for healing. On the other hand, cracks propagate from the location of SAP particles. As the SAP percentage increases, the number of macro void increases (Figures 5.14(c) and (d)) providing more possible links for cracking path. Similar results of the role of SAP as a crack initiator are reported for SAP-modified engineered cementitious composites (ECC) (Kim & Schlangen, 2010; Yao et al., 2012). It is worth emphasizing that "unconfined" concrete (without transverse reinforcement) is only considered for the current study and more experimental works are necessary to confirm the observations for confined concrete with surrounding stirrups in which crack widths are controlled by transverse reinforcement.

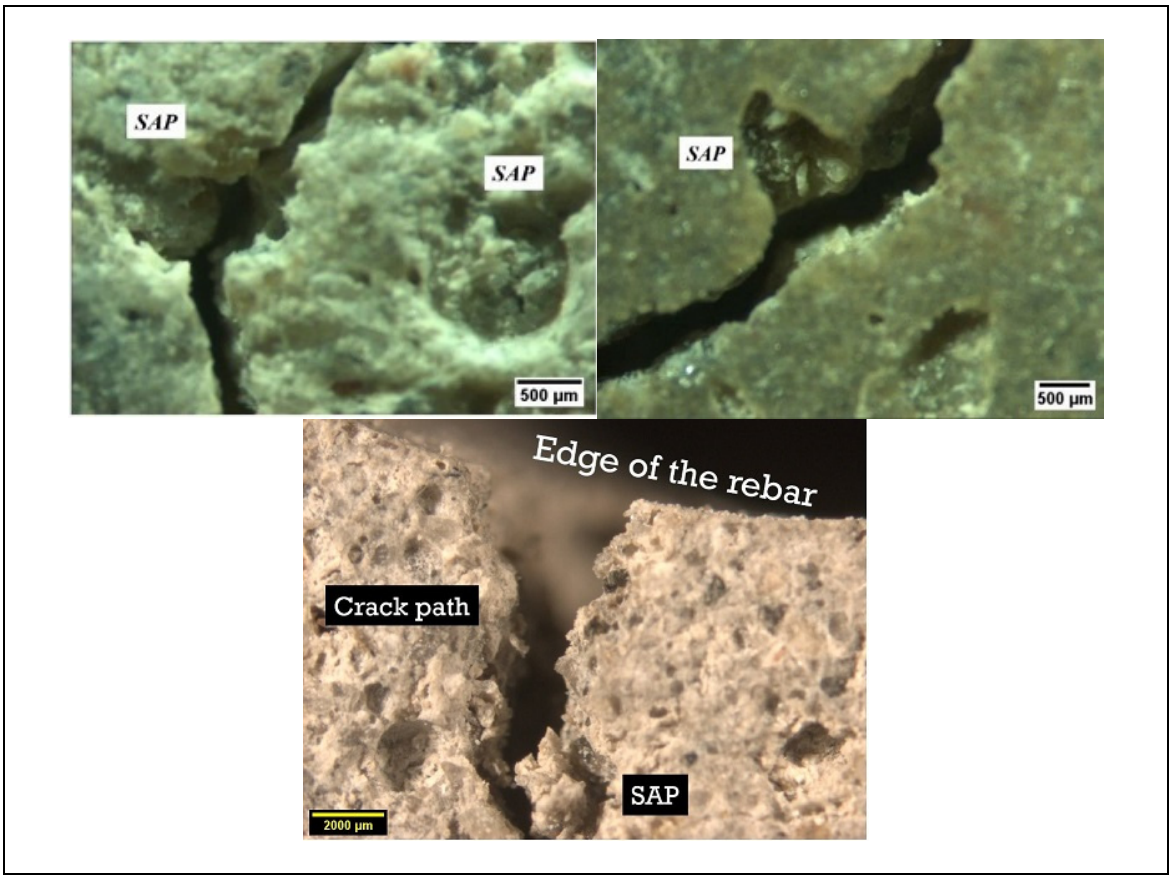

Figure 5.21 Cracks pathing through SAP locations

5.4 Macro voids around the rebar

Voids generated due to SAP particles inside concrete mixture around the rebar are illustrated in Figure 5.22. SAP particles generate larger voids inside concrete in comparison with the size of the air void. In addition, the shape of the voids is changed in comparison with concrete without SAP, which is precisely illustrated in Figure 5.14.

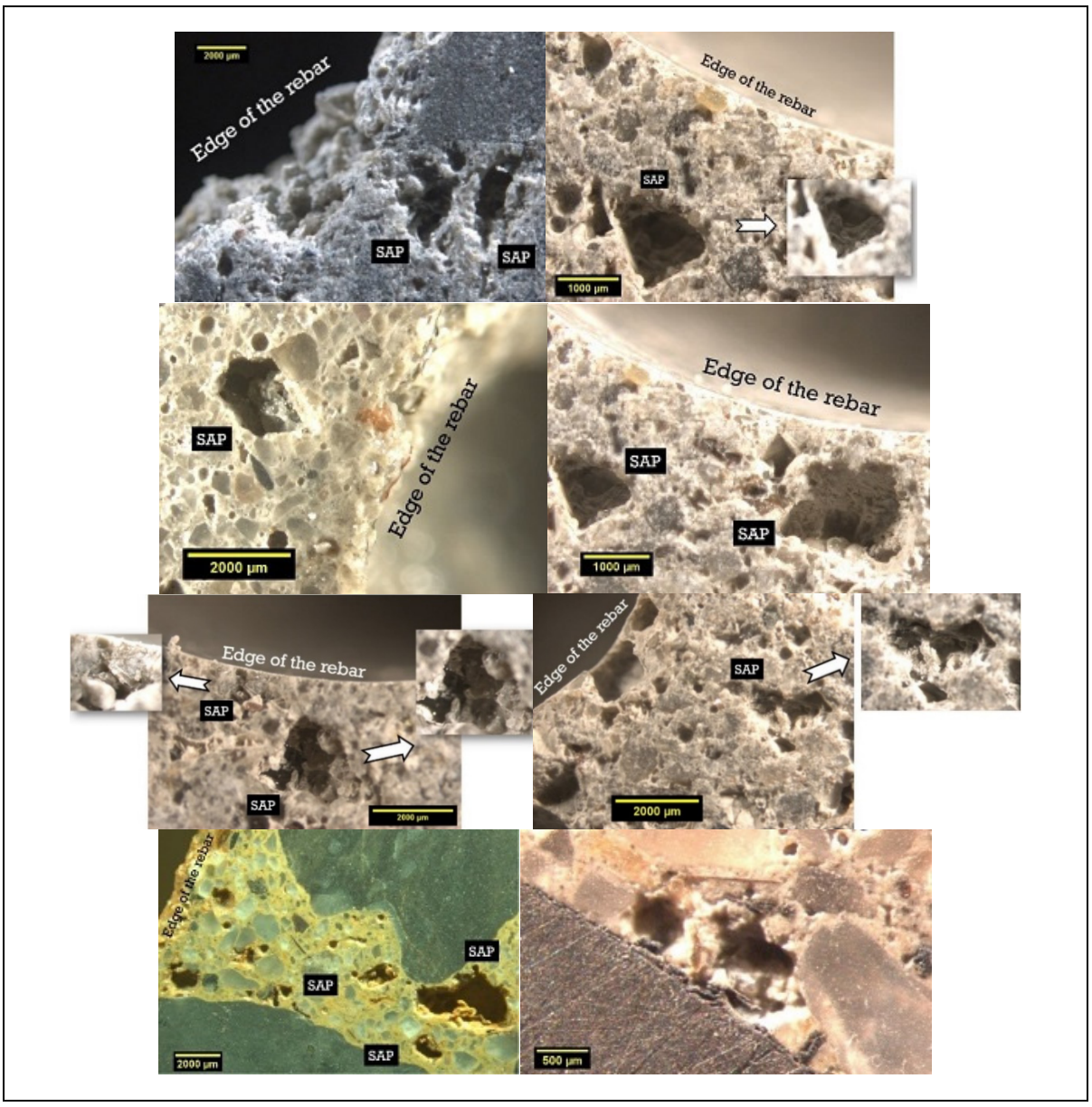

Figure 5.22 Voids generated around the rebar in concrete containing SAP

To compare the void size around the rebar edge, disk-shaped layers of concrete cylinders after 28 days curing are cut, polished and analyzed by the microscope. Six specimens are analyzed for every type of concrete, which is summarized in Table APPENDIX IV.1 (see page 313). The analysis is performed for a distance of about 7.5 mm from the edge of rebar. Analyze shows that SAP percentage causes a significant increase in the maximum diameter of the void inside the mixture (Figure 5.23(a)). The average maximum size of SAP particles existed in the mixture around rebar is about 1.30 mm, 1.88 mm, 2.28 mm, and 2.78 mm for SAP percentages of 0, 0.25%, 0.50%, and 1.0% respectively. Effect of SAP percentage on the maximum diameter of voids is formulated as follows by average values:

$$Max\ diameter = -998.95(SAP\%)^2 + 2468.1(SAP\%) + 1309.3 \qquad (5.7)$$

Additionally, the distance of the macro voids generated in SAP concrete is also measured for these six disk-shaped specimens. Results indicate that concrete containing SAP higher than 0.25% has macro voids closer to the rebar edge with maximum distances of 4.56-4.95 mm. The closest distance of 0.22 mm is observed for macro voids (Figure 5.23(b)). However, the average values of distances do not change between the mixtures. As severally reported in the literature, the rebar-concrete interface is largely composed of calcium hydroxide (CH), and that there is, therefore, a larger amount of CH present at the steel–cement paste interface than in the bulk cement paste (Al Khalaf & Page, 1979; BS-8110, 1997; Page, 1975; Yue & Shuguang, 2001). Having more macro voids occupied by SAP particle closer to steel edge, enriched by calcite, can significantly increase the possibility of calcium carbonate precipitation. Hence, more experimental studies are necessary for future works. It is essential to emphasize that this microscopic analysis only shows the distance of the maximum size macro voids to the rebar edge. Distribution of the macro voids around in the paste surrounding the rebar is previously studied in Figure 5.18, the interfacial transition zone (ITZ). Also, it is worth mentioning that more experimental studies are necessary to precisely concentrate on the effect of these macro voids on compressive strength and other mechanical strength of SAP concrete.

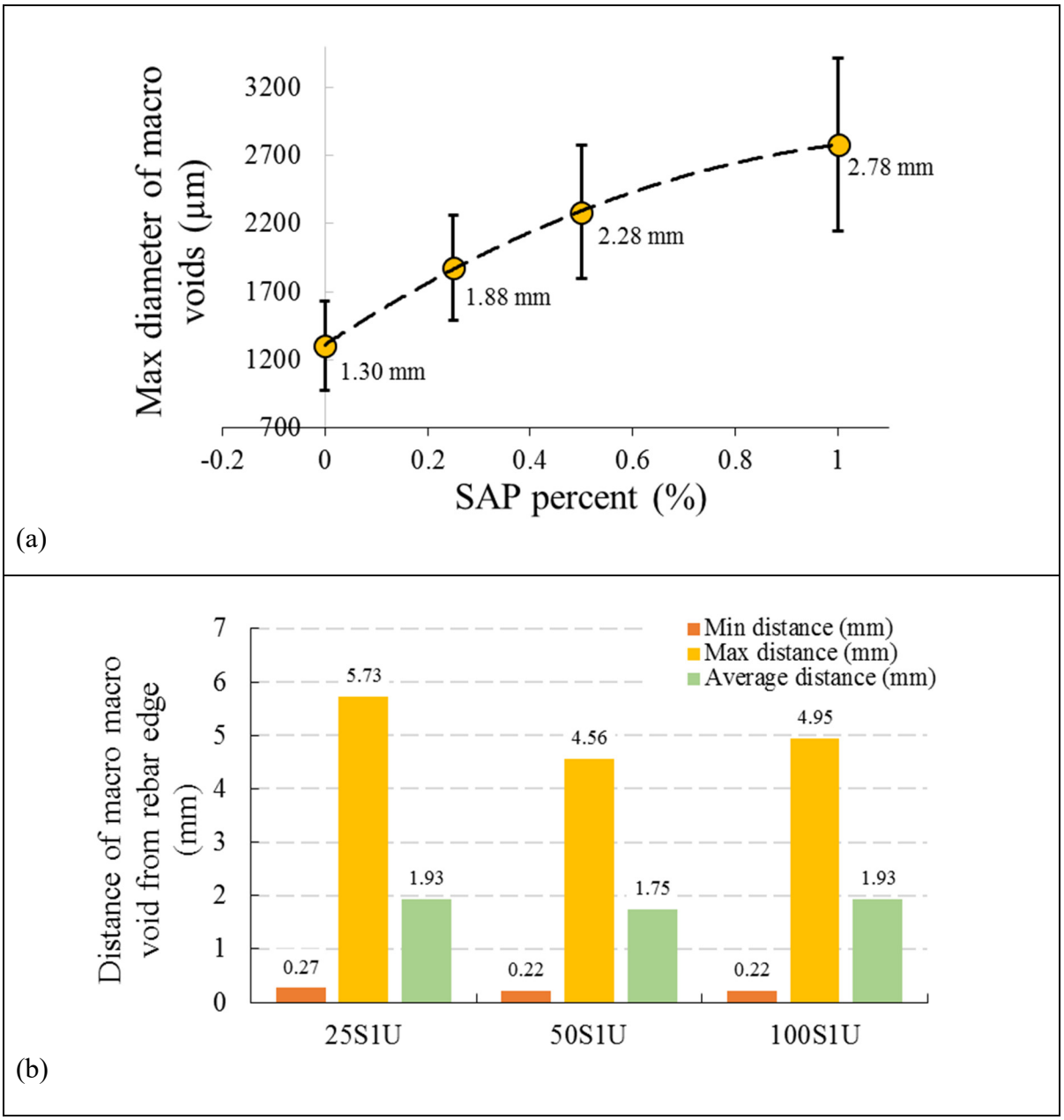

Figure 5.23 Results of the microscopic analysis till 7.5 mm from rebar edge: (a) maximum diameter of macro voids with respect to different SAP dosages; (b) distance of the macro voids from rebar edge

5.5 Summary and concluding remarks

This study evaluates the interfacial properties between the steel rebar and SAP-modified concrete. Findings support the hypothesis that concrete composition could be a critical parameter for controlling cracks at rebar-concrete interfacial surfaces. The following concluding remarks are drawn from the experimental program results:

- The addition of SAP accelerates the healing process in the concrete mixture. The self-healing ability of concrete containing SAP improved the initial bond stress, the bond strength, and the energy absorbed related to the bond response ductility.
- Overall, results confirm that 0.25% SAP is the most effective on steel rebar-concrete interfacial properties in all statuses of uncracked, pre-cracked, and healed concrete. It allows a comparable bond strength to uncracked concrete, lower sensitivity to the pre-cracking phenomenon, and a more pronounced healing effect compared to the reference concrete (without SAP).
- Despite reductions in the bond strength and residual bond stress for uncracked concrete with 0.50% and 1.0% SAP, a higher dosage of SAP inside the concrete mixture significantly increases the healing ability at the steel rebar-concrete interface.
- The results for the uncracked, pre-cracked, and healed concrete demonstrate that large SAP particle size is more effective than smaller particle size on steel rebar-concrete interfacial properties. However, concrete containing smaller particle sizes of SAP showed comparable bond strength of steel rebar in uncracked concrete.
- Results indicate that 14-day healing periods are not enough to heal cracks at the steel rebar-concrete interface, especially for bond strength recovery. However, promising results are obtained for 28-day healing periods.

It is worth emphasizing that “unconfined” concrete (without transverse reinforcement) is only considered for the present study, and more experimental works are necessary to confirm and/or adjust the observations for confined concrete with surrounding stirrups, in which crack widths are controlled by transverse reinforcement.

CHAPTER 6

THE EFFECT OF AIR-ENTRAINING ADMIXTURE AND SUPERABSORBENT POLYMER ON BOND BEHAVIOUR OF STEEL REBAR IN PRE-CRACKED AND SELF-HEALED CONCRETE

Seyed Sina Mousavi [a], Claudiane Ouellet-Plamondon [b], Lotfi Guizani [c], and Chandrasekhar Bhojaraju [d]

[a, b, c,d] Department of Construction Engineering, École de Technologie Supérieure, 1100 Notre-Dame West, Montreal, Quebec, Canada H3C 1K3

Paper submitted for publication in *Construction and Building Materials*, August 2020

Abstract

This paper investigates the effect of air-entraining admixture on self-healing method at the rebar-concrete interface. Pull-out tests are conducted on uncracked, pre-cracked, and healed specimens. 14 and 28 days are considered for healing periods. Two types of SAP with different chemical compositions and particle sizes are considered for the experimental tests. Scanning electron microscopy/energy dispersive X-ray spectrometry along with microscopic analysis is performed to study the healing products at crack surface and SAP macro voids around the rebar. 0.25% and 1.0% SAP dosages are considered for tested concrete mixtures, and air-entraining (AE) admixture with a dosage of 0.83 kg/m^3 is also used. Pull-out test results of mixtures containing AE admixture are compared with those in non-AE concrete. Overall, results indicate that AE admixture has a considerable impact on the performance of the self-healing method at the rebar-concrete interface especially for higher dosage of SAP (1.0%). This can be attributed to the internal voids networks around the rebar generated by AE admixture, which can ease the water transfer between SAP macro voids to participate in healing cracks after wet-dry cycles. SEM analysis shows that stalactites, healing products at the external surface of crack, are composed of a large amount of calcium and oxygen.

Additionally, a comprehensive statistical analysis is conducted in the present study to find out the most important parameter affecting the self-healing results.

Keywords*:* bond strength superabsorbent polymer; self-healing; air-entraining concrete

6.1 Introduction

Air-entraining (AE) admixtures are organic surfactants which entrain a controlled quantity of air in concrete is uniformly dispersed discrete bubbles of predominately between 0.25-1.0 mm diameter (Ramachandran, 1996; Usher et al., 1980). AE agents reduce the surface tension of water and facilitate bubble formation. Uniform dispersion and appropriate stability are obtained by the mutual repulsion of the negatively charged air-entrainer molecules and the attraction of the air-entrainer molecules for the positive charges on the cement particles (St John et al., 1998). AE increases the workability and consistency of concrete (Dolch, 1996), so that mixtures with AE admixture have a higher slump as compared to NC at the same water content. High workability of AE concrete is attributed to some sort of "ball bearing action" of the air bubbles, kept spherical by surface tension (Bruere, 1967; Mielenz, 1968). On the other hand, the presence of microscopic air bubbles acts as a lubricant. AE concrete is less sensitive to bleeding and segregation than is non-AE concrete (Ramachandran, 1996). AE admixtures have no noticeable impact on the hydration rate of cement or on the heat evolved by that process. The strength of the hardened concrete is decreased as the amount of air is increased.
Most of the previous studies on the field of AE concrete concentrated on the resistance of mixtures exposed to low temperatures (winter exposure) and freeze-thaw cycles in water-saturated RC members such as outdoor slabs, pavements and bridges (Dhir et al., 1999; Shang et al., 2009), i.e., durability problem in cold climates. Perenchio et al. (1990) postulated that the diffusion of gel water to capillary pores encompassing ice causes the growth and expansion of ice lenses, results in generating micro cracks. The freezing cycle increases the width of these micro-cracks, which afterward filled with water during thawing cycles. This cycle causes a rapid deterioration of concrete. Hill et al. (2008) found that frost damage of concrete can be attributed to the osmotic pressure, in which unfrozen water is compelled to capillary pores

under a salt concentration gradient. The growth of ice growth in such locations causes considerable degradation. The resistance of hardened concrete to this type of damage is considerably improved by the use of AE admixtures (Hang & Zhang, 2011; Łaźniewska-Piekarczyk, 2013; Molero et al., 2012; Peng et al., 2007; Şahin et al., 2007; Shang & Yi, 2013; Soutsos, 2010; Yuan et al., 2011; Zheng et al., 2014; Ziari et al., 2017). This is achieved by the entrained-air bubbles acting as expansion chambers to accommodate the ice formed within the capillaries (Dhir et al., 1990; Dhir et al., 1991). Moreover, for a given workability, AE concrete is more durable, as compared to the non-AE concrete by providing lower w/c (Aïtcin, 2016). Furthermore, in AE concrete, a network of closely "spaced air bubbles" (10–100 μm in diameter) provides a release for additional pressure caused by freezing-thawing cycles (Hazaree et al., 2011; Litvan, 1988). The AE admixture, as a surfactant, helps in bubble stabilization by reducing the surface tension of water (Łaźniewska-Piekarczyk, 2013). Total volume of the entrained air, average volumic surface, and spacing of the air bubbles are the fundamental characteristics of this "air bubble network", which is comprehensively discussed by Gagné (2016). These air bubbles need to be homogeneously dispersed in the mix, which can be characterized by what is called the "spacing factor of the bubbles network". There is a general agreement that this stabilized bubble network generated by AE admixture increases frost resistance and durability properties of both NC and high performance concrete (HPC) such as self-consolidating concrete (SCC) and high strength concrete (HSC) (Aitcin & Lessard, 1994; Bassuoni & Nehdi, 2005; Beaupré et al., 1999; Crouch et al., 2000; Dhir et al., 1999; Gagne et al., 1991; Gardner et al., 1986; Peng et al., 2007; Ziaei-Nia et al., 2018).

Similar to the AE admixtures, superabsorbent polymers (SAP) enhance freeze-thaw resistance of concrete (Craeye et al., 2018; Falikman, 2019; Jensen & Hansen, 2002; Jones & Weiss, 2014; Laustsen et al., 2015; Reinhardt et al., 2008; Sikora & Klemm, 2014; Tan et al., 2019; Wang et al., 2014) by producing a concrete with predefined size and spacing of air inclusions. Accordingly, Falikman (2019) showed that SAP voids can improve frost resistance with lower impact, as compared to the AE admixtures. Reinhardt et al. (2008) reported that this effect can be attributed to the densification of the concrete mixtures by the absorption of pore water by the SAP. Sikora & Klemm (2014) observed that SAP with high water absorption capacities

can mitigate flexural strength reduction caused by frost action. They confirmed the fact that SAP modified mixture is suitable for ice expansion during freeze-thaw cycles by the formation of larger pores suitable for ice expansion so that SAP may perform similarly to AE admixtures. Both the dosage and particle size of the SAP has a considerable effect on the freeze-thaw resistance of concrete (Craeye et al., 2018). Jones & Weiss (2014) showed that both air-entraining admixture and SAP are needed for concrete exposed to freeze-thaw cycles, while air-entrained concrete without SAP cannot provide sufficient freeze-thaw durability. However, there is no detailed study on the effect of AE-SAP combination on concrete characteristics.

As reviewed, despite the extensive studies of the effect of stabilized air bubble network, provided by AE admixture, on durability properties of concrete, there is no specific study on the impact of this spaced air bubble network on fracture mechanic and self-healing properties of concrete. Hence, the present study aims to continue the research presented in the previous chapters by adding AE admixture for improving the sensitivity of concrete exposed to the pre-cracking phenomenon and the self-healing method at the rebar-concrete interface. Main objectives of the present study are as follows:

1- How much does the AE admixture affect the bond strength of steel rebar in pre-cracked concrete?

2- How much AE admixture is efficient for the self-healing method by SAP at the steel rebar-concrete interface?

To address these questions, an extensive experimental plan is conducted in the present study. Different dosages of SAP and AE admixture are considered. Three main statuses of specimens are used including uncracked, pre-cracked, and healed specimens. Statistical analysis of obtained results is carried out on combined results from this experimental plan and from earlier chapters plan, to identify the most significant factors affecting the self-healing method performance.

6.2 Experimental program

6.2.1 Material properties and experimental plan

Ten different concrete mixes are considered for this study to compare the results between AE concrete (5 mixes) and non-AE concrete (5 mixes). Mixtures are designed to determine the effect of different parameters including (a) SAP percentages; (b) SAP size and chemistry; (c) concrete flowability; and (d) AE admixture on bond strength of uncracked, pre-cracked, and healed concrete. The concrete composition of AE mixtures is illustrated in Table 6.1. Details of non-AE mixtures for both NC and SAP-modified NC are mentioned in Chapter 5. General use (GU) cement is used for all mixtures with a density of 3.15 g/cm^3. Natural sand with a maximum grain size of 1.25 mm and a specific gravity of 2.68, and gravel with a nominal maximum diameter of 14 mm and a particular gravity of 2.68 are considered for mixtures. The SAP is added at a range of 0.0-1.0 wt.% of cement for non-AE concrete and only 0.25% and 1.0% for AE-contained mixtures. Details of SAP used including particle size, particle shape, and water absorption capacity are detailed in Chapter 5. To adjust the flowability of concrete mixtures, superplasticizer (MasterGlenium 1466 and EUCON PLASTOL 341) is added, at different proportions. AE concrete mixtures contain an aqueous solution compound of synthetic chemicals by 0.83 kg/m^3 of concrete mixture, with a specific gravity of 1.006, 7.5% of solids by weight, and a pH of 11.0.

Table 6.1 Concrete composition of AE concrete mixtures

Mix	Cement	Sand	Gravel 5/10	Gravel 10/14	Water	Add. water	SP	AE	SAP
	(kg/m^3)								%
RA-1	395	788	822	258	165	0	3.98	0.83	0
RA-2	395	788	822	258	165	0	5.23	0.83	0
25S1A	395	788	822	258	165	24.7	3.27	0.83	0.25
25S2A	395	788	822	258	165	24.7	2.23	0.83	0.25
100S1A	395	788	822	258	165	98.8	4.15	0.83	1.0

* Note: Add=additional water, SP=superplasticizer by MasterGlenium 1466 for all mixture except mixes RA-1 and 100S1A which used EUCON PLASTOL 341, SAP= % wt. of cement, AE=air entraining by Eucon air mac 6 (0.21% wt. of cement).

Specimens are initially cured 28 days in the moisture room at 97.3% RH and 23 ºC. Those specimens, which are subjected to wet-dry cycles, remained in the curing tank for longer periods of 14 and 28 days (20 ºC, 60% RH). One wet-dry cycle represents 24 hours in water followed by 24 hours in dry condition. Consequently, 7 and 14 cycles took 14- and 28-day wet-dry cycles respectively. Configurations of concrete mixtures studied in the present study are illustrated in Table 6.2. Reference mixes are designated by "R", "RA-1", and "RA-2". Character "A" in the names of some mixtures determines AE mixtures. "S1" and "S2" correspond to mixtures containing SAP-1 and SAP-2 respectively. Numbers of 25, 50, and 100 in some mixtures show 0.25%, 0.50%, and 1.0% SAP by weight of cement respectively.

Table 6.2 Configurations of mixtures used in the present study (with mixtures of Chapter 5)

Mixture	AE		Polymer		SAP percentage (%)				w_T/c	Slump (mm)	Density[1] (kg/m^3)
	With	Without	SAP-1	SAP-2	0	0.25	0.50	1.00			
R		×			×				0.41	97	2453.80
RA-1	×				×				0.41	110	-
RA-2	×				×				0.43	200	2390.08
25S1		×	×			×			0.48	104	2416.79
25S1A	×		×			×			0.48	170	2368.02
25S2		×		×		×			0.48	109	2419.22
25S2A	×			×		×			0.48	191	2283.30
50S1		×	×				×		0.54	95	2335.76
100S1		×	×					×	0.66	91	2256.72
100S1A	×		×					×	0.66	100	2219.85

* Note: w_T/c= total water-to-cement ratio.[1] average hardened density of mixtures after 28 days curing.

6.2.2 Experimental procedure

The pre-cracking test is carried out as detailed in Mousavi et al. (2019). Controlled Brazilian tests (splitting), recommended by Desnerck et al. (2015), are used to produce different crack widths parallel to the rebar direction (Figure 6.1(a)). To control crack opening, crack gauges are installed at both sides of specimens, along with manual measurement of crack widths. Based on empirical observations, the displacement rate of 0.11-0.15 mm/min is considered for

splitting tests. Then, direct pull-out tests are conducted after three stages of uncracked (without splitting test), pre-cracked, and healed (after 14 and 28 days re-curing) specimens with a displacement rate of 0.50 mm/min (Figure 6.1(b)). To prevent corrosion influences for 28-day healing periods, the heat-shrinkable tube is used along with using is at both end sides of tubes (Figure 6.1(c)).

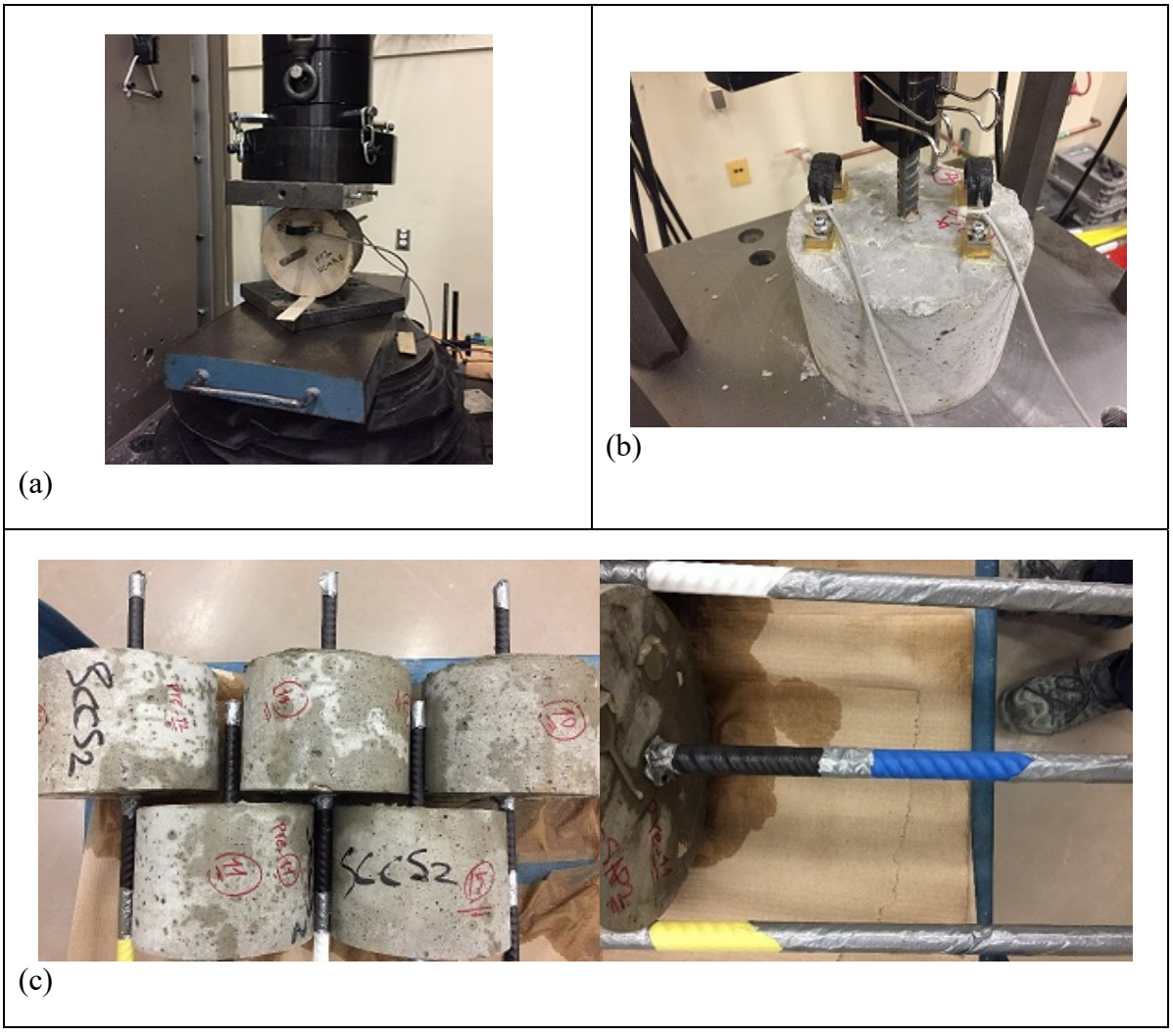

Figure 6.1 Experimental procedure :
(a) pre-cracking test; (b) pull-out test; (c) heat-shrinkable tube

6.3 Experimental results

This section intends to compare AE concrete mixtures with non-AE mixtures for three statuses of uncracked, pre-cracked, and healed concrete. As mentioned in the previous chapters and recently published companion paper (Mousavi et al., 2019), three main characteristics of average bond stress (τ_m), maximum bond stress called bond strength (τ_u), and residual bond stress (τ_r) are considered in the following subsections. Overall, results show that two main failure modes of pull-out (Figure 6.2(a)) and splitting (Figure 6.2(b)) are observed for uncracked and pre-cracked specimens, respectively. General observations show that uncracked and cracked specimens with $w < 0.15$ mm experience pulling out the rebar from concrete cylinder without propagating cracks in the plane of the rebar, while $w > 0.15$ mm leads to splitting specimens.

(a)

(b)

Figure 6.2 Failure modes for pull-out test specimens: (a) pull-out failure; (b) splitting failure

Compressive strength of concrete mixtures is shwon in Figure 6.3. Generally, results indicate that 25S1A is the optimum mixture among other air-entrained mixtures. Results show that using AE causes considerable reduction effect on compressive strength so thstrength

reductions of 18.6%, 7.0%, 16.5%, and 33.2% are obtained for mixtures of RA-1, 25S1A, 25S2A, and 100S1A repectively (Figure 6.3(a)). Moreover, results show that AE has lower impact on compressive strength of concrete containing SAP with larger particle size (25S1A) as compared to the smaller size SAP (25S2A). Besides, results show that AE has higher devastating impact on compressive strength of mixture contaning higher dosage of SAP (100S1A) as compared to the lower dosage (25S1A). As illustrated in Figure 6.3(b), the present study proposes Eqs. (6.1) and (6.2) for the 28 days compressive strength of non-air-entraining and air-entraining SAP concrete mixtures respectively, as a function of totall water-to-cement ratio (w_T/c), as follows :

$$f'_c = 152.7e^{-2.31(w_T/c)} \tag{6.1}$$

$$f'_c = 163.62e^{-3.0(w_T/c)} \tag{6.2}$$

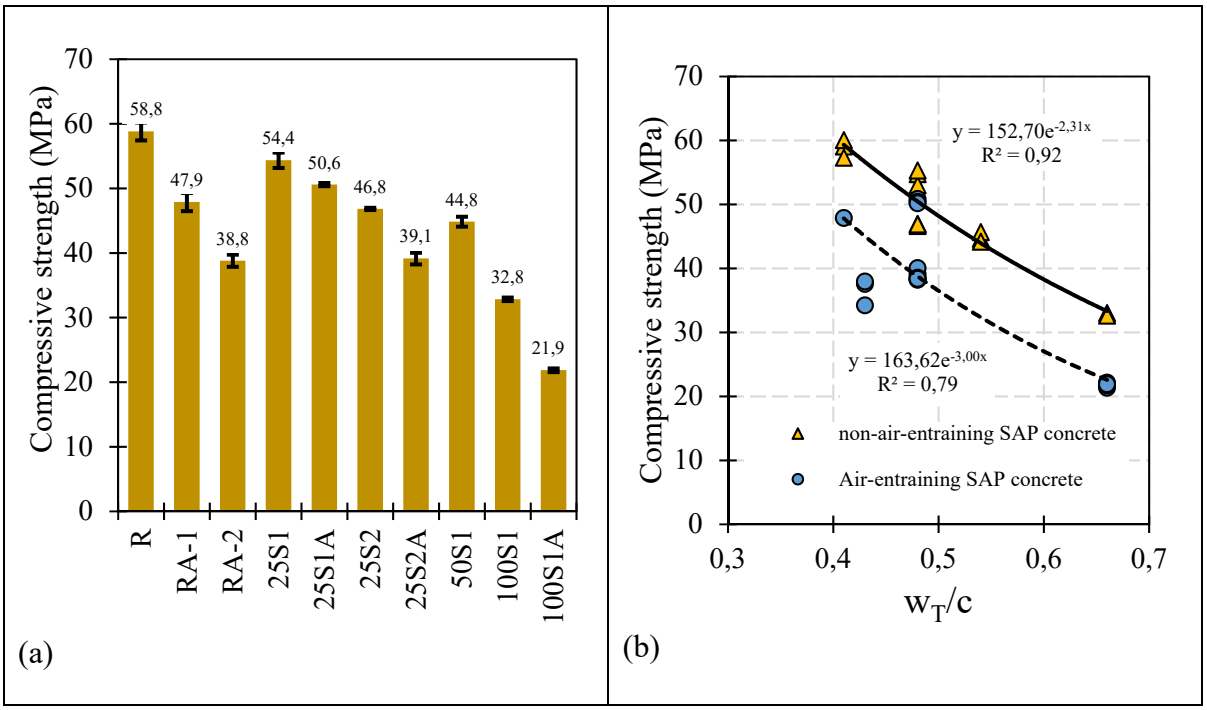

Figure 6.3 Compressive strength of concrete mixtures containing SAP and AE

6.3.1 Uncracked concrete

Results of uncracked concrete are shown in Figure 6.4 for all mixtures. To compare all mixtures, the effect of concrete compressive strength is eliminated by normalization. Bond characteristics of characteristic bond stresses. This is achieved by dividing these stresses by the square root of concrete compressive strength including normalized average bond stress, $\tau_m{}^* = \tau_m/\sqrt{f'_c}$, normalized bond strength, $\tau_u{}^* = \tau_u/\sqrt{f'_c}$, and normalized residual bond stress, $\tau_r{}^* = \tau_r/\sqrt{f'_c}$. Results indicate that RA-2 and R mixtures have the highest normalized average bond stress among other mixtures (Figure 6.4(a)). In the case of normalized bond strength, RA-2 has higher values (4.2), as compared to other mixtures (Figure 6.4(b)). Similar results are observed for normalized residual bond stress (Figure 6.4(c)) and energy dissipated by bond mechanism (Figure 6.4(d)). A detailed discussion of these observations is provided in Chapter 4. This can be attributed to the higher slump value of RA-2, which affects the rebar-concrete bond strength. A limited number of studies have noticed this observation (Mousavi et al., 2017; Sfikas & Trezos, 2013). The following subsections discuss the effect of SAP percentage, AE admixture, and SAP type on bond characteristics of steel rebar embedded in uncracked concrete.

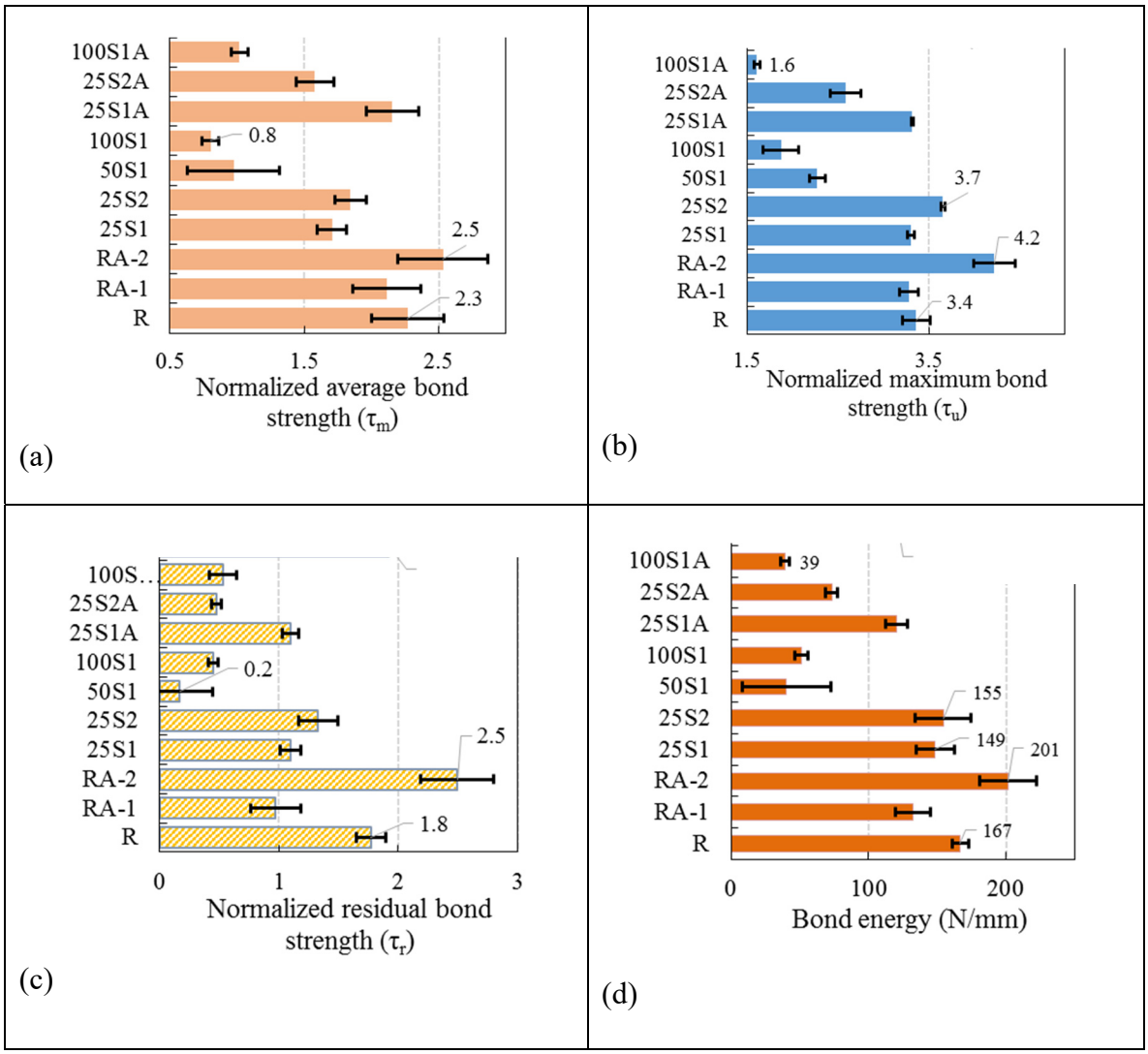

Figure 6.4 Normalized bond properties of mixtures: (a) average bond stress; (b) bond strength; (c) residual bond stress; (d) bond energy

6.3.1.1 Effect of SAP percentage on bond strength of AE and non-AE concrete

Figure 6.5 shows the effect of SAP percentage on the bond response of uncracked concrete. General results show that SAP percentage higher than 0.25% leads to a significant reduction in normalized bond strength.

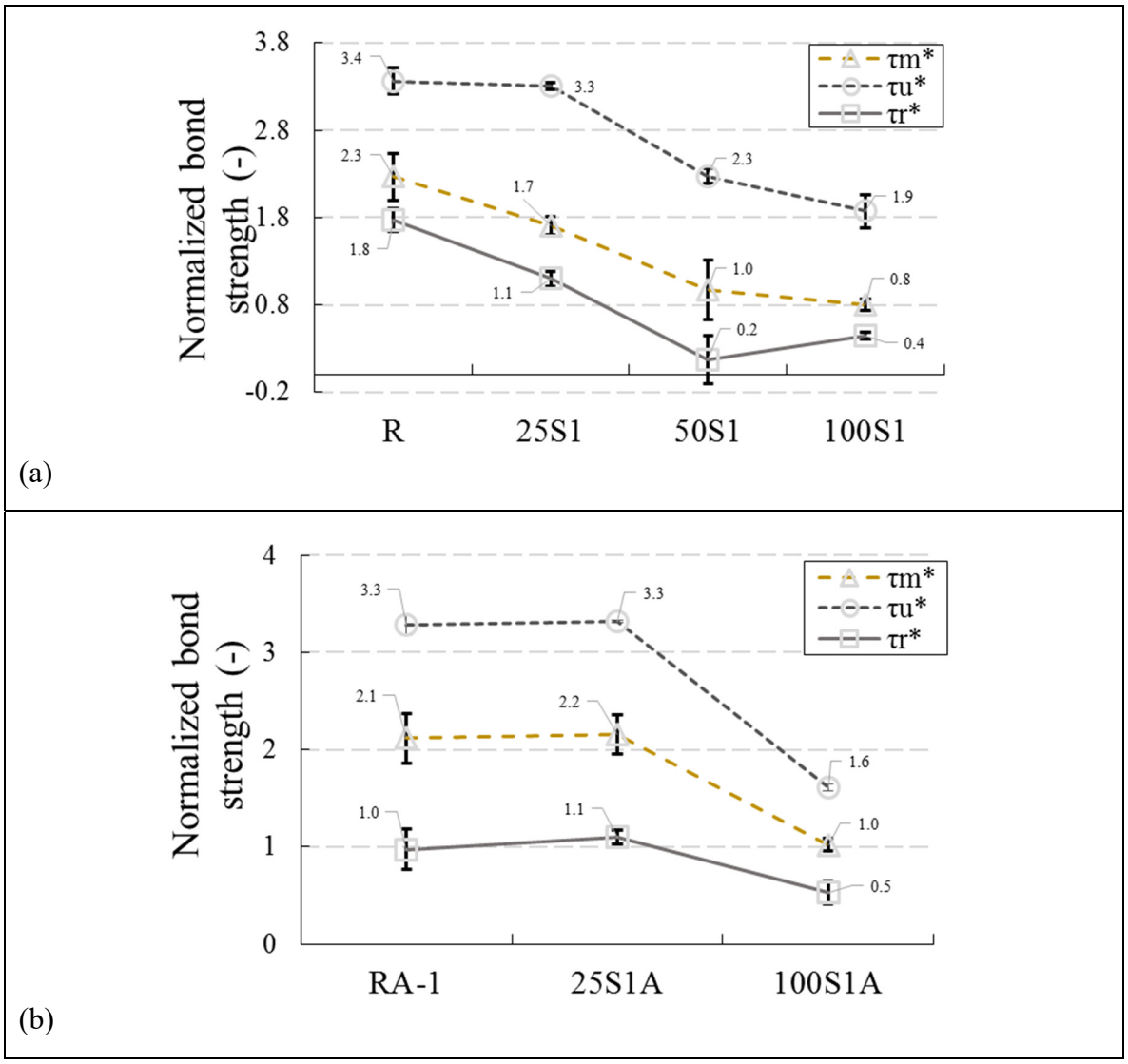

Figure 6.5 Effect of SAP percentage on normalized bond properties of uncracked concrete: (a) non-AE concrete; (b) AE concrete

In the case of non-AE concrete, general results show that a higher dosage of SAP causes a considerable reduction in bond properties, especially for residual bond stress (Figure 6.5(a)). Among the bond properties, SAP dosage has higher and lower influences on maximum (44.1%) and residual (77.8%) bond strength respectively for non-AE concrete. However, different trends are followed by AE concrete, so that approximate reduction of 50.0% is observed for all bond properties of mix 100S1A (Figure 6.5(b)). The optimal dosage of 0.25% is obtained for both AE and non-AE mixtures by 2.9% and 0.0% strength reductions on bond

strength respectively (Figure 6.5). Moreover, in the case of 0.25S1A, 4.8% and 10% increases are recorded for average and residual bond stress respectively. This finding can confirm the fact that AE admixture is in good combination with 0.25% SAP for using in concrete mixtures. Despite the findings of the present section, more experimental studies are necessary for future works to confirm the obtained results.

6.3.1.2 Effect of AE admixture on bond strength of AE and non-AE concrete

In the case of reference mixes, AE admixture has no considerable effects on maximum and average bond stress (Figure 6.6(a)), while 44.0% reduction is obtained for the AE-contained mixture (RA-1). For 0.25% SAP-1, maximum and residual bond stress are the same for both AE and non-AE mixtures, while the average bond stress of 25S1A is 29.0% more than 25S1 (Figure 6.6(b)). Similar results are obtained for 1.0% SAP-1 (Figure 6.6(d)). However, results show that AE admixture has negative impacts on bond properties of SAP-2 so that 22.0%, 30.0%, and 62.0% reductions of average bond stress, bond strength, and residual bond stress are obtained respectively for using AE admixture (Figure 6.6(c)), which is similar to the trend of reference mixture ("R" mixture, Figure 6.6(a)). Hence, comparable and higher bond properties of SAP-1 presented in Figures 6.5(b), and 6.6(b and d) show the fact that SAP-1 is more adaptable with AE admixture when compared with SAP-2.

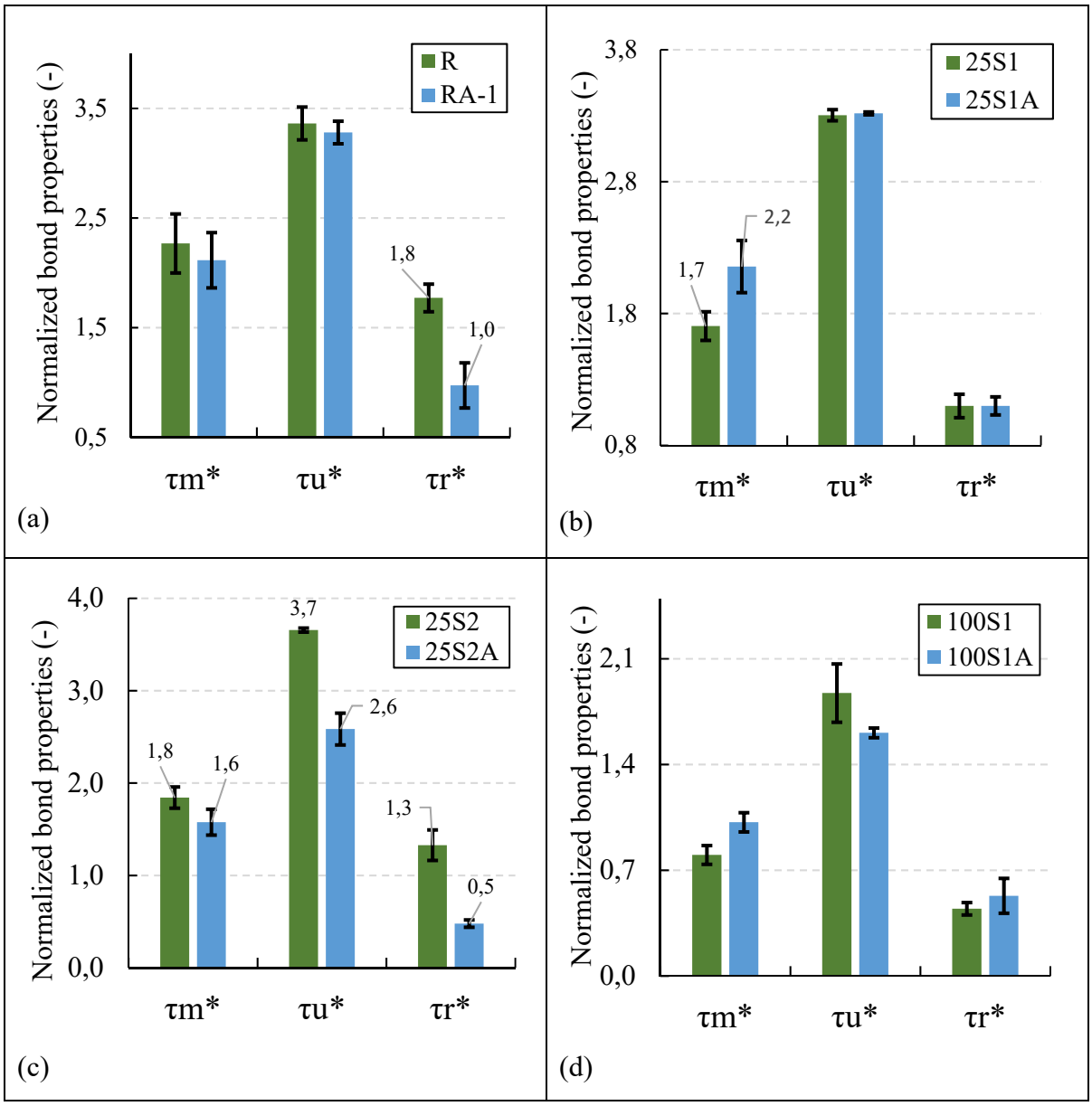

Figure 6.6 Effect of AE admixture on normalized bond properties of uncracked concrete: (a) reference mixtures (0% SAP); (b) 0.25% SAP-1; (c) 0.25% SAP-2; (d) 1.0% SAP-1

6.3.1.3 Effect of SAP particle size and type on bond strength of AE and non-AE concrete

The effect of SAP particle size (and/or chemistry) is shown in Figure 6.7. Results show that the mixture containing SAP-2 has higher average bond stress, bond strength, and residual bond

stress compared to those of SAP-1. This can be a conflicting result with the results presented in Chapter 5, in which SAP-2 has lower compressive strength compared with SAP-1. Figure 5.8 (Chapter 5) shows that SAP-2 produces a higher number of pores in paste around the rebar with a smaller void size. Therefore, the porosity pattern of SAP-2-contained concrete is different from SAP-1-contained concrete. A similar trend is reported by Sfikas & Trezos (2013) and Ahmad et al., (2018), which can be explained by a hypothesis that concrete compressive strength cannot be only used for predicting bond strength instead of water-to-cement ratio (w/c) and also mixture porosity. The effect of these parameters should be separately considered in bond strength field of study. For instance, due to the higher amount of porosity in lightweight aggregate concrete, recent findings show that concrete compressive strength has no significant effects on bond strength (Ahmad et al., 2018), which is different from the existing design codes where a safety factor is considered along with the concrete compressive strength. Different chemistries of SAP may affect the observed trend in uncracked concrete. However, the chemical part of SAP used is out of the scope of the present study and more studies are necessary for future studies.

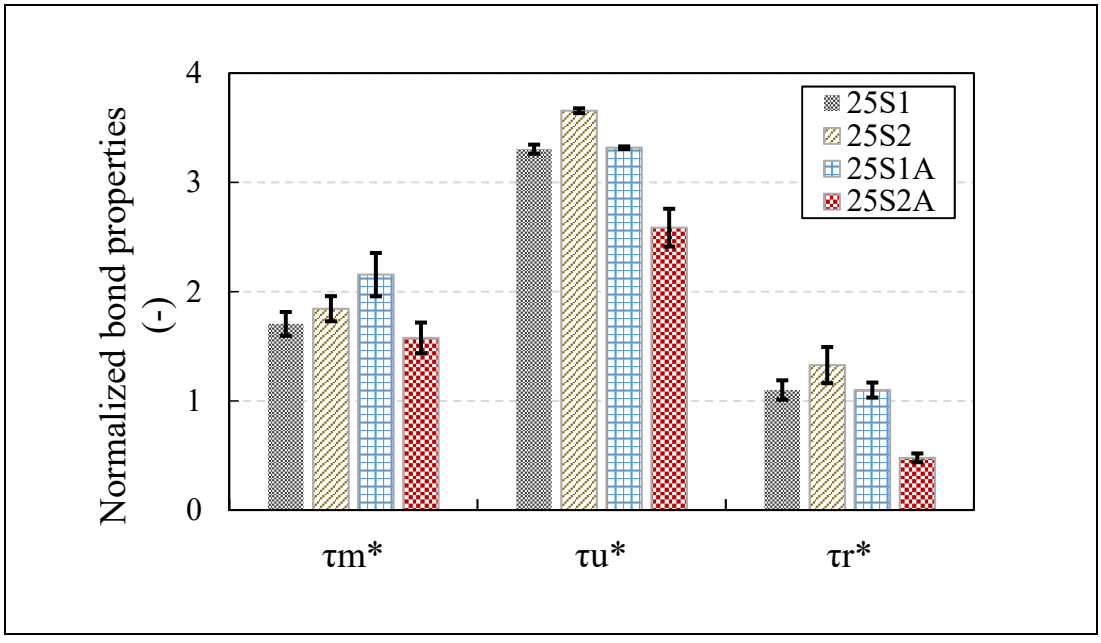

Figure 6.7 Effect of SAP type and particle size on normalized bond properties of AE and non-AE uncracked concrete

6.3.1.4 Performance of the proposed models for uncracked concrete

To determine the efficiency of the proposed models, introduced in Chapter 3 for predicting the bond strength, experimental results of uncracked concrete for all mixtures are used in this section. As shown in Figure 6.8, the proposed model for Mode-2 of uncracked concrete considerably underestimate the bond strength of the reference and mixtures containing low content of SAP (R, 25S1, 25S2, 25S1A, and 25S2A). This can be attributed to the fact that the ratio of rib spacing-to-height of rebar used in the experimental program is equal to 7.0, which is lower than the range reported by Wu and Chen (2015), $S_r/h_r > 10.0$, for crushing a wedge-shape concrete. Moreover, this clearly shows good concrete confinement around the rebar. In the case of mixtures containing SAP content higher than 0.25 % (50S1, 100S1, and 100S1A), even though UM2 model can achieve acceptable results, low value of bearing angle calibrated to the experimental results ($\beta \approx 20\,°$), showing that the first model presented for uncracked concrete containing shear-off bond failure mechanism is more accurate and reliable for predicting the bond strength of rebar in un-cracked specimens with appropriate concrete cover. Overall, results show that that UM2 underestimate the bond strength of steel rebar in concrete mixtures with the normalized bond strength higher than the value of 2.30 ($\tau_{max}/\sqrt{f'_c} > 2.30$). The parametric study conducted in Figure 6.8 indicates that as bearing angle increases, bond strength decreases so that bearing angle equal to the rib-face angle ($\beta = \alpha = 55$) represents the lowest interfacial strength, denoted as “rib sliding failure mechanism”. In this case, the friction coefficient of the rebar-concrete interface (μ_1) has no impact on the bond strength, while μ_1 has a decisive role for a lower value of bearing angle. Additionally, results show that the effect of friction coefficient on UM1 significantly reduces for a lower value of K while the friction coefficient has a key role in the performance of UM1 with a higher contact pressure. Also, the results of the proposed model indicate that the reduction factor of contact pressure (K) has a critical role in the performance of UM1.

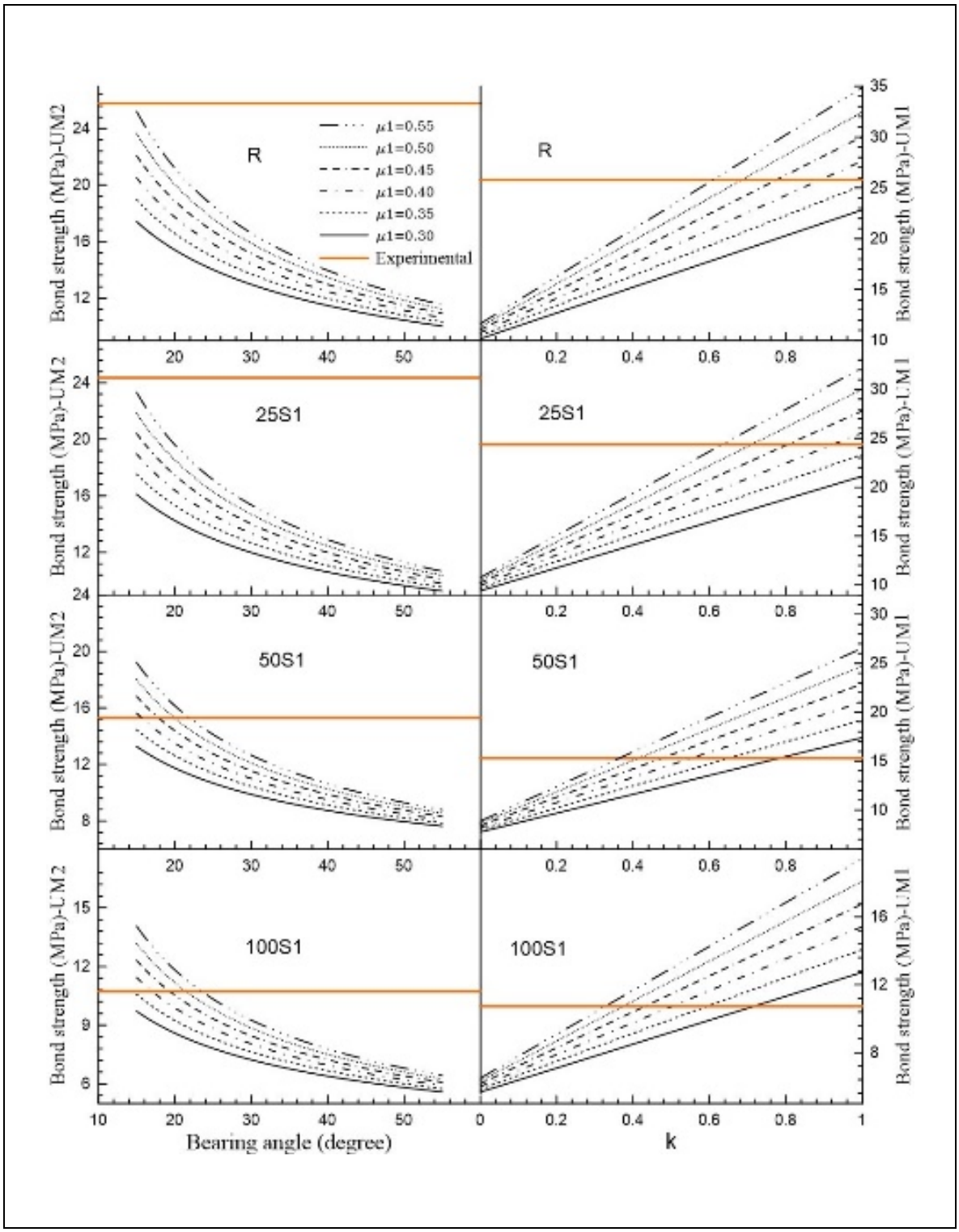

Figure 6.8 Performance of the proposed models in Chapter 3 for uncracked concrete with respect to different SAP percentages

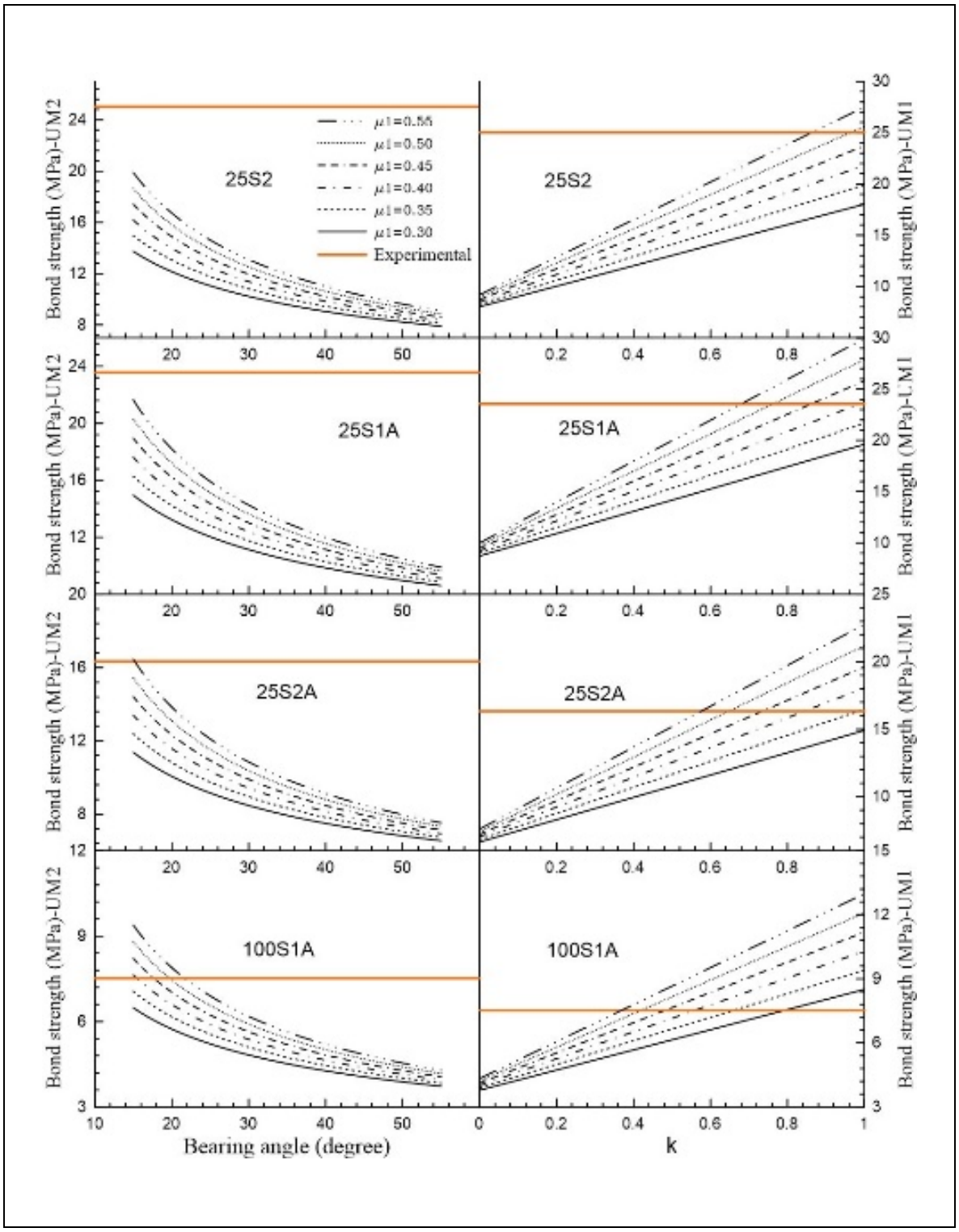

Figure 6.8 Performance of the proposed models in Chapter 3 for uncracked concrete with respect to different SAP percentages (continued)

Calibration of key parameters required for UM1 (friction coefficient and contact pressure) for all mixtures are summarized in Table 6.3. It can be shown that UM1 model with a higher friction coefficient needs lower contact pressure to accurately predict the bond strength. As reported by Dehestani et al. (2017), different interfacial properties are obtained for different types of concrete mixtures. Although different friction coefficients have been used by the literature, Zhao & Zhu (2018) confirmed the value of 0.45 for the static friction coefficient of normal concrete. In this case, the reduction factor for contact pressure in UM1 model is in the range $0.44 \leq K \leq 0.86$, where lower and higher reduction factors correspond to 100S1 and 25S1A mixtures respectively.

Table 6.3 Results of UM1 for all mixtures

μ_1	Reference	Best-fitted K [-]							
		R	**25S1**	**25S2**	**50S1**	**100S1**	**25S1A**	**25S2A**	**100S1A**
0.30	(Fernández Ruiz et al. 2005; Zhao and Zhu 2017)	-	-	-	0.78	0.72	-	-	0.79
0.35	-	-	-	-	0.65	0.60	-	0.98	0.66
0.40	-	0.89	0.92	-	0.56	0.50	0.98	0.84	0.56
0.45	(Baltay and Gjelsvik 1990; Zhao and Zhu 2018)	0.77	0.81	-	0.48	0.44	0.86	0.74	0.48
0.50	-	0.69	0.71	0.96	0.42	0.38	0.76	0.65	0.42
$\mu_1 \geq 0.55$	(Dehestani et al. 2017; Rabbat and Russell 1985; Wu and Chen 2015)	0.61	0.63	0.86	0.36	0.32	0.68	0.58	0.37

6.3.2 Pre-cracked concrete

Results of 100 pre-cracked pull-out specimens (excluding healed specimens) are summarized in Figure 6.9 by the normalized reduced bond ratio, $(\tau)_c/(\tau)_{un}$, versus w/d_b ratio. Parameters of $(\tau)_c$ and $(\tau)_{un}$ corresponding to the bond properties of cracked and uncracked specimens,

respectively. The significant impact of the pre-cracking phenomenon on average bond stress, bond strength, and residual bond stress is clear. Results show that residual bond stress is considerably affected by induced cracks so that even small crack widths cause more than 50.0% reduction in bond strength. However, three out of trend data is recorded for residual bond stress with $\tau_c > \tau_u$.

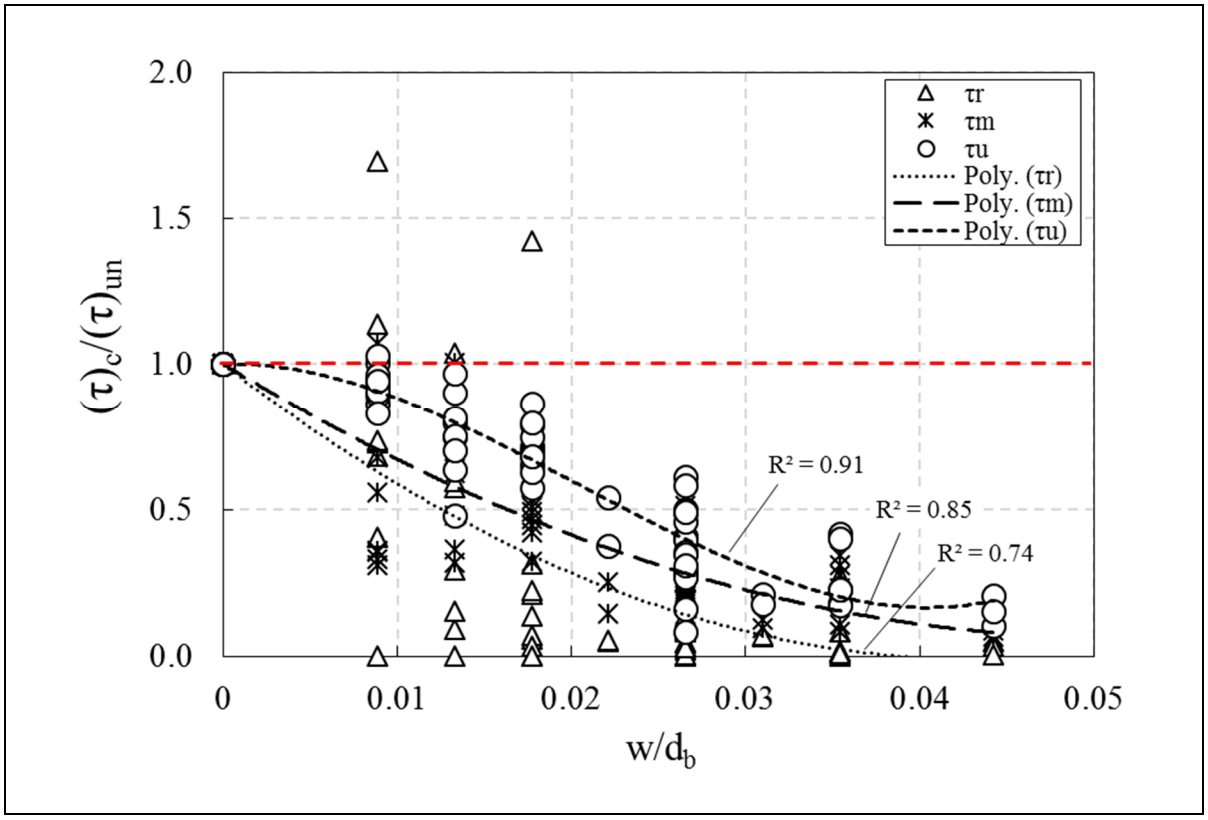

Figure 6.9 Effect of the pre-cracking phenomenon on bond properties for all mixtures

The following equations are proposed for reduced bond ratio after induced crack width:

$$\left(\frac{(\tau)_c}{(\tau)_{un}}\right)_m = 352.3\left(\frac{w}{d_b}\right)^2 - 36.4\frac{w}{d_b} + 1.0 \qquad (6.3)$$

$$\left(\frac{(\tau)_c}{(\tau)_{un}}\right)_u = 26160.4\left(\frac{w}{d_b}\right)^3 - 1609.2\left(\frac{w}{d_b}\right)^2 + 1.67\frac{w}{d_b} + 1.0 \quad (6.4)$$

$$\left(\frac{(\tau)_c}{(\tau)_{un}}\right)_r = 533.74\left(\frac{w}{d_b}\right)^2 - 46.5\frac{w}{d_b} + 1.0 \quad (6.5)$$

To determine the effect of AE on the pre-cracking phenomenon, the results presented in Figure 6.9 is divided in two separate groups of mixtures with AE and mixtures without AE for average bond stress, bond strength, and residual bond stress (Figure 6.10). Overall, trends obtained for AE-contained mixtures show that AE causes a higher bond reduction factor, leading to being less sensitive to the internal damages due to the pre-cracking phenomenon (Figure 6.10(a)). Similar results are obtained for bond strength and residual bond stress (Figures 6.10(b) and (c)). As crack width increases, this deviation increases. Proposed equations for predicting bond reduction factors are illustrated in Figure 6.10. A comprehensive discussion regarding this result is presented in the following subsections.

Similar to the analysis procedure used in the study carried out by Mousavi et al. (2019), the performance of the current existing equations on predicting bond strength of cracked concrete is illustrated in Figure 6.11. To use an equation for concrete codes, a conservative domain is necessary for providing a safety zone. In the case of the pre-cracking phenomenon, reduced bond ratio ($(\tau)_c/(\tau)_{un}$) predicted by an idealized equation should be lower than the experimental database to provide a safe region. However, Figure 6.11 shows that the only model presented by Eibl et al. (1999) and Idda (1999) is efficient till a crack width-to-rebar diameter of 0.025, while a higher bond ratio is predicted by this model, which provides the non-safety region.

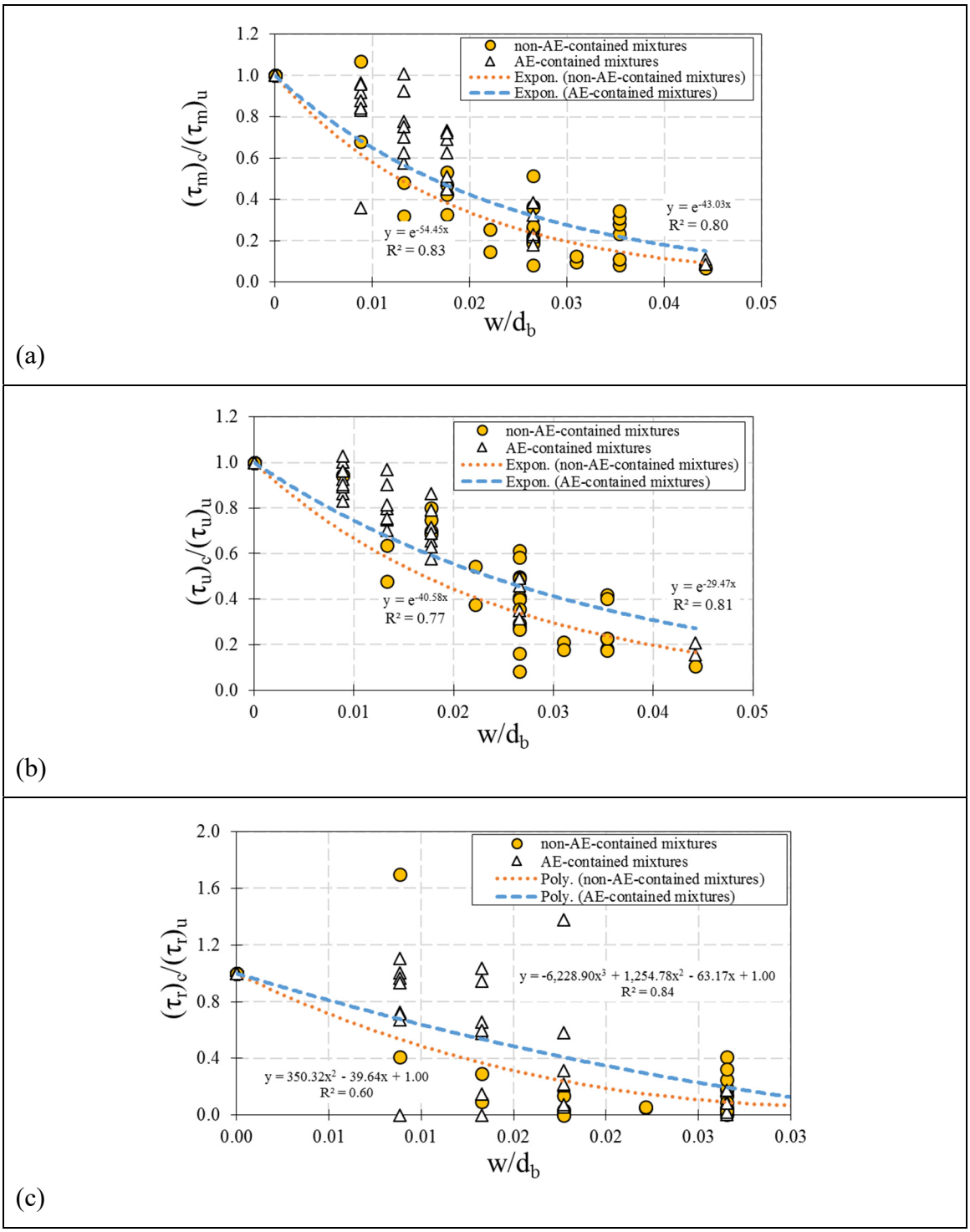

Figure 6.10 Effect of the pre-cracking phenomenon on bond properties with respect to AE admixture: (a) average bond stress; (b) bond strength; (c) residual bond stress

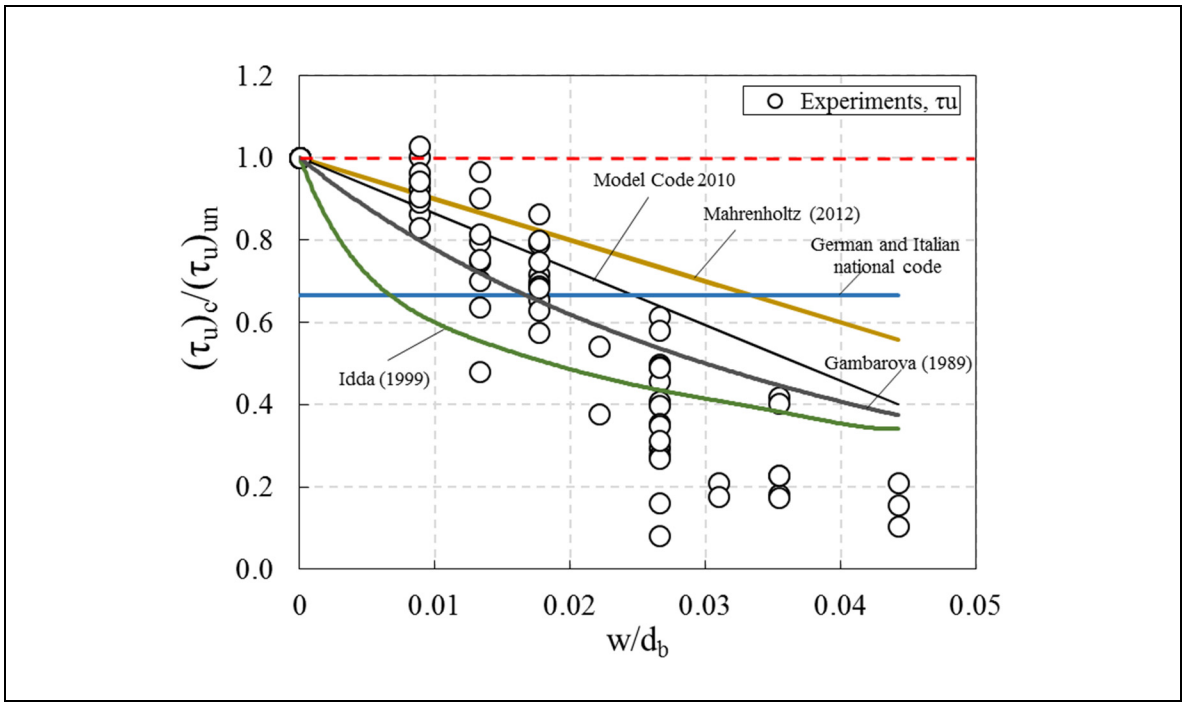

Figure 6.11 Performance of existing equations and standards for predicting bond strength of pre-cracked concrete for both AE- and non-AE-contained mixtures

Accordingly, the present study intends to propose an efficient equation for average and bond strengths (Figure 6.12), which are the lower bounds of the experimental database (Figure 6.9). The effect of mixtures types is ignored in this section to present a general equation for all types of concrete mixtures with concrete compressive strength ranging from around 21 MPa to 60 MPa. In the case of bond strength, the following equation is obtained as a best-fitted formulation which 95.0% of the experimental database is higher than this lower bound:

$$\left(\frac{(\tau)_c}{(\tau)_{un}}\right)_u = e^{-36.2\frac{w}{d_b}} \qquad w \leq 0.30 \text{ mm}$$

$$\left(\frac{(\tau)_c}{(\tau)_{un}}\right)_u = 0.00011\left(\frac{w}{d_b}\right)^{-2.1} \qquad w > 0.30 \text{ mm} \tag{6.6}$$

The efficiency of the proposed equation is shown in Figure 6.12(a) with an average correlation of around $R^2 = 0.97$ for both sections. Variation of bond reduction due to the pre-cracking phenomenon is higher in average bond stress compared to the bond strength (Figure 6.9). Following the conservative equation is proposed:

$$\left(\frac{(\tau)_c}{(\tau)_{un}}\right)_m = 0.002\left(\frac{w}{d_b}\right)^{-1.06} \tag{6.7}$$

The performance of the proposed model is shown in Figure 6.12(b). All the 100 experimental points have a higher reduced bond ratio than Eq. (6.7), which shows the sufficient safety region of the proposed model. However, no efficient model is obtained for residual bond stress, as significant bond reductions are recorded even for small crack width. As commonly bond strength is important for design codes, Eq. (6.6) can be used instead of the current equations for predicting bond strength of steel rebar embedded in pre-cracked concrete.

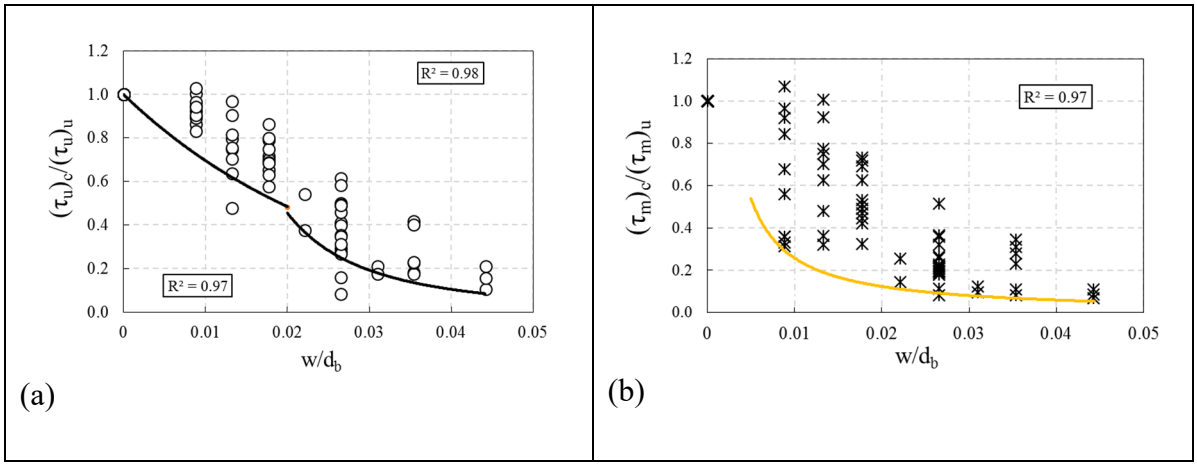

Figure 6.12 Proposed lower bound conservative equations for pre-cracked concrete: (a) bond strength; (b) average bond stress

The effect of AE admixture on the pre-cracking phenomenon (i.e. bond properties) is illustrated in Figures 6.13, 6.14, and 6.15 for average bond stress, bond strength, and residual bond stress respectively. General results of average and bond strength show that concrete mixtures containing AE admixtures are less sensitive to the pre-cracking phenomenon, as compared to

the non-AE mixtures. This can be attributed to the high flowability (slump flow) of AE mixtures, which is shown in Table 6.2. Similar results are obtained for SCC as compared to NC, which is summarized in Chapter 4.

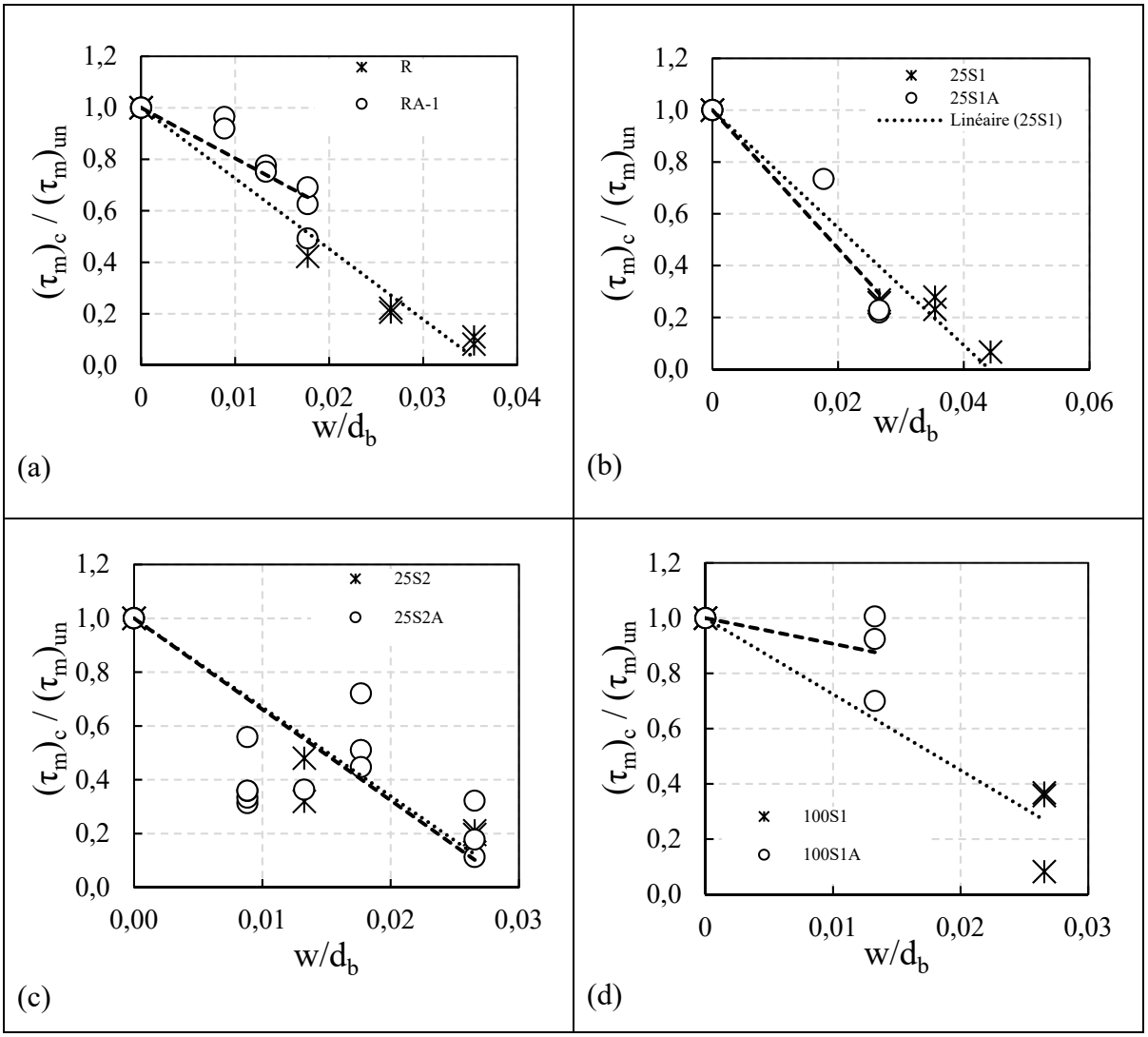

Figure 6.13 Effect of AE admixture on the average bond stress of pre-cracked concrete with respect to different SAP percentages: (a) 0% SAP; (b) 0.25% SAP-1; (c) 0.25% SAP-2; (d) 1.0% SAP-1

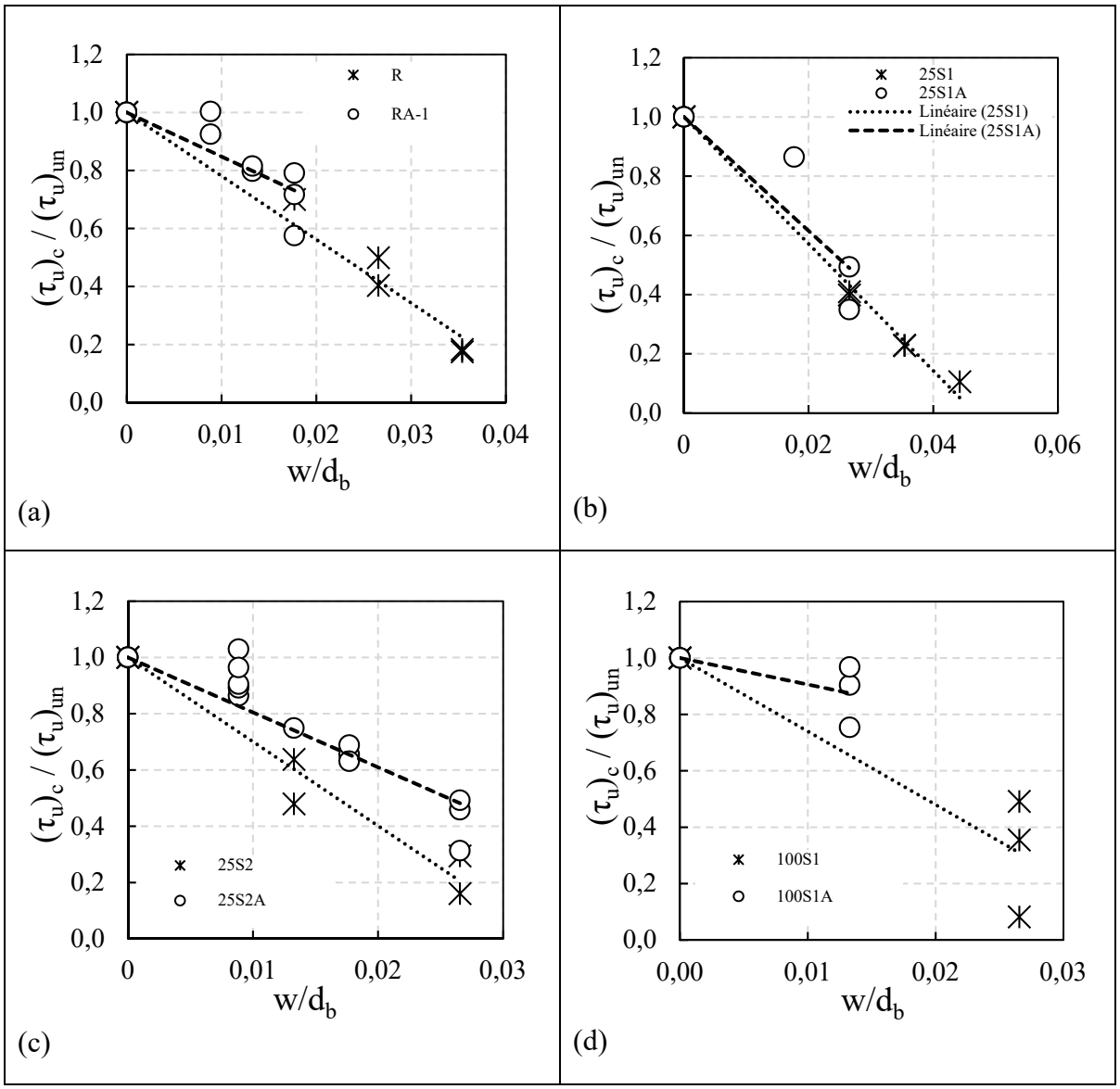

Figure 6.14 Effect of AE admixture on the bond strength of pre-cracked concrete with respect to different SAP percentages: (a) 0% SAP; (b) 0.25% SAP-1; (c) 0.25% SAP-2; (d) 1.0% SAP-1

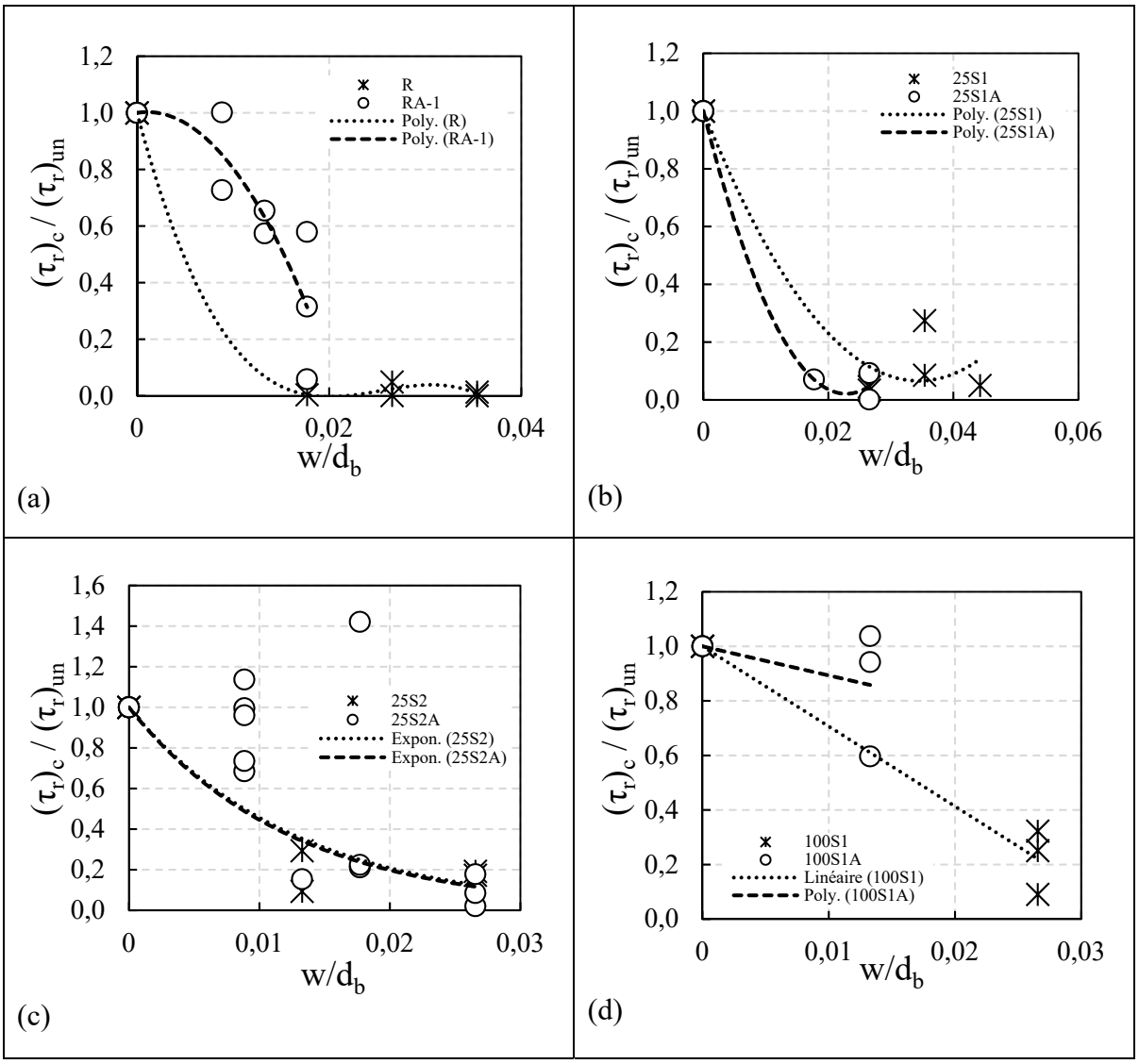

Figure 6.15 Effect of AE admixture on the residual bond stress of pre-cracked concrete with respect to different SAP percentages: (a) 0% SAP; (b) 0.25% SAP-1; (c) 0.25% SAP-2; (d) 1.0% SAP-1

6.3.3 Healed concrete

An improvement factor (IF) is defined in this section by Eq. (6.8) to measure the performance of SAP and AE for healing cracks at the rebar-concrete interface in different mixtures. As *IF* increases, the healing efficiency of the mixture increases. Zero value of IF corresponds to the specimens with lower or comparable bond properties than the cracked specimen with constant

crack width ($\tau_{Healed} \leq \tau_{Precracked}$), while $IF > 0$ represents the healed specimens with higher bond properties as compared to those of pre-cracked specimens ($\tau_{Healed} > \tau_{Precracked}$). It is necessary to emphasize that due to the brittle nature of concrete in tension, different crack widths are obtained by splitting tests. Hence, to compare bond results of healed specimens with cracked ones, bond reduction-crack width curves are used to predict bond properties of cracked specimens, in the case that different cracks are generated. Examples of these curves are presented in Figure 5.16 (Chapter 5) and Figure 6.10.

$$IF = \left[\frac{\tau_{Healed} - \tau_{Precracked}}{\tau_{Uncracked} - \tau_{Precracked}}\right] \times 100 \quad (6.8)$$

A total number of 63 healed specimens for 14- and 28-day healing periods (in the water tank) are tested in the present study. All results are summarized in Table 6.4 for average bond stress, bond strength, and residual bond stress. Similar to the cracked specimens (Figure 6.9), crack widths of $0.15\ mm \leq w \leq 0.40\ mm$ are considered in the healed specimens. The designation of specimens is as follows: first character in specimen identification describes mixture type including R=reference; RA2=reference mix with AE admixture; 25S1=0.25% SAP-1; 25S2=0.25% SAP-2; 50S1=0.5% SAP-1; 100S1=1.0% SAP-1; 25S1A=0.25% SAP-1 with AE admixture; 25S2A=0.25% SAP-2 with AE admixture; and 100S1A=1.0% SAP-1 with AE admixture. The second character shows an initial crack width before healing; For instance, C0.3= crack width of 0.30 mm. The last character determines the healing period so that 14H and 28H show specimens after 14- and 28-day healing periods respectively. Also, the number of repetitions (n) for each category is mentioned in Table 6.4.

Table 6.4 Healing improvement factors of bond properties

Specimens	IF of τ_m (%)	IF of τ_u (%)	IF of τ_r (%)	n
RC0.3-14H	2.73 0 0	0 0 0	0.15 6.30 4.81	3
RC0.3-28H	37.01 15.49 13.57	6.18 0 0.24	2.16 10.22 0	3
RC0.4-28H	8.40	5.69	11.47	1
RA2C0.35-14H	0	0	0	1
RA2C0.15-14H	0	0	1.25	1
RA2C0.2-14H	0 0	0 0	1.08 2.03	2
25S1C0.3-14H	0 2.30	25.77 0	18.15 6.09	2
25S1C0.4-14H	0 0	0 0	0 0	2
25S1C0.3-28H	0 16.96 6.23	32.72 8.76 7.13	8.23 15.11 12.01	3
25S1C0.4-28H	0	7.97	0	1
25S2C0.2-14H	0 0.23	0 0	0 0	2
25S2C0.3-14H	0.93 0	6.87 6.94	0 0	2
25S2C0.3-28H	0.07 0	11.42 11.33	0 0	2
25S2C0.35-28H	0	20.6	0	1
50S1C0.3-14H	4.37 0	27.48 0	61.29 26.32	2
50S1C0.3-28H	9.82 14.50 2.49	21.03 32.23 36.28	0 0 0	3
100S1C0.3-14H	0 0.68 8.25	0 23.27 39.45	0 21.14 0	3
100S1C0.3-28H	21.96 2.38 8.02	41.01 22.64 11.73	29.53 69.86 28.99	3
25S1AC0.2-14H	0	12.80	0	1
25S1AC0.25-14H	0	57.97	0	1
25S1AC0.3-14H	9.92	7.32	0	1
25S1AC0.3-28H	51.08 17.01 21.49 12.20	22.79 4.57 5.61 23.23	0 0 3.16 7.82	4
25S2AC0.2-14H	0 0 0 0	0 0 0 0	0 0 0 0	4
25S2AC0.3-28H	1.03 24.07 16.19	3.61 23.34 4.70	12.44 7.61 5.75	3

Table 6.4 Healing improvement factors of bond properties (continued)

Specimens	IF of τ_m (%)	IF of τ_u (%)	IF of τ_r (%)	n
25S2AC0.4-28H	27.81 18.16	17.33 25.98	7.31 14.85	2
25S2AC0.25-28H	12.10 11.66	18.94 5.68	8.92 0	2
25S2AC0.2-28H	10.29	4.18	0	1
100S1AC0.15-14H	0 100.31 0	0 30.93 45.46	0 356.14 303.29	3
100S1AC0.15-28H	0 321.39 167.52 121.46	0 164.36 145.18 136.67	124.74 0 372.76 386.55	4
All specimens	-	-	-	63
Range (%)	0-321.39	0-164.36	0-386-55	-
Average IF (%)	18.70	20.77	31.23	-

Improvement factor for average bond stress (IF_{τ_m}) with a determined standard deviation (SD) is illustrated in Figure 6.16 for all mixtures. Considerable healing of 0.15 mm crack widths after 28-day healing periods by 100S1A mixture is clearly depicted in Figure 6.16, which is higher than 100% (IF_r=152.6%). However, a high SD is obtained for this case. In this field, the reference mixture improved the average bond stress (τ_m) by 22.0% and 8.4% for crack widths of 0.30 mm and 0.40 mm, respectively. Moreover, mixtures of 25S1, 50S1, 100S1, 25S1A, and 25S2A improved self-healing capacity up to $IF_{\tau_m} \leq 25.4\%$ for average bond stress.

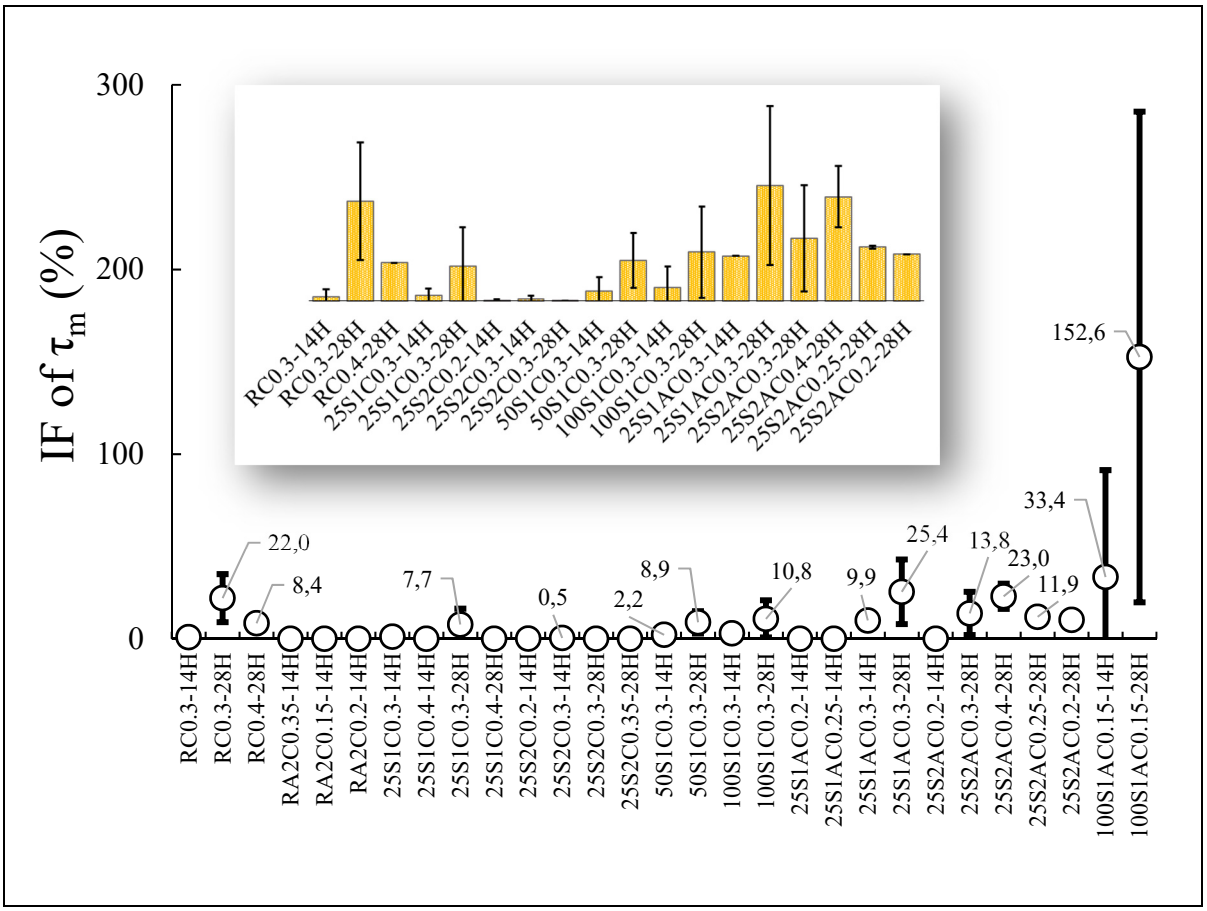

Figure 6.16 Determination of IF for average bond stress

Results of bond strength are more important as compared to other results, as this parameter affects directly structural and anchorage capacity. Similar to the average bond stress, concrete mixtures containing 1.0% SAP (100S1A and 100S1A) have significant improvement factor of bond strength (Figure 6.17). General results of IF_{τ_u} indicate that a reference mixture without a healing agent has a low improvement factor (5.7%), as compared to SAP mixtures. In this field, mixtures of 25S1, 50S1, 25S1A, and 25S2A show $IF_{\tau_u} \leq 58.0\%$. It is clearly observed that SAP has a real potential of self-healing capacity and mitigating damage due to the pre-cracking phenomenon at the rebar-concrete interface.

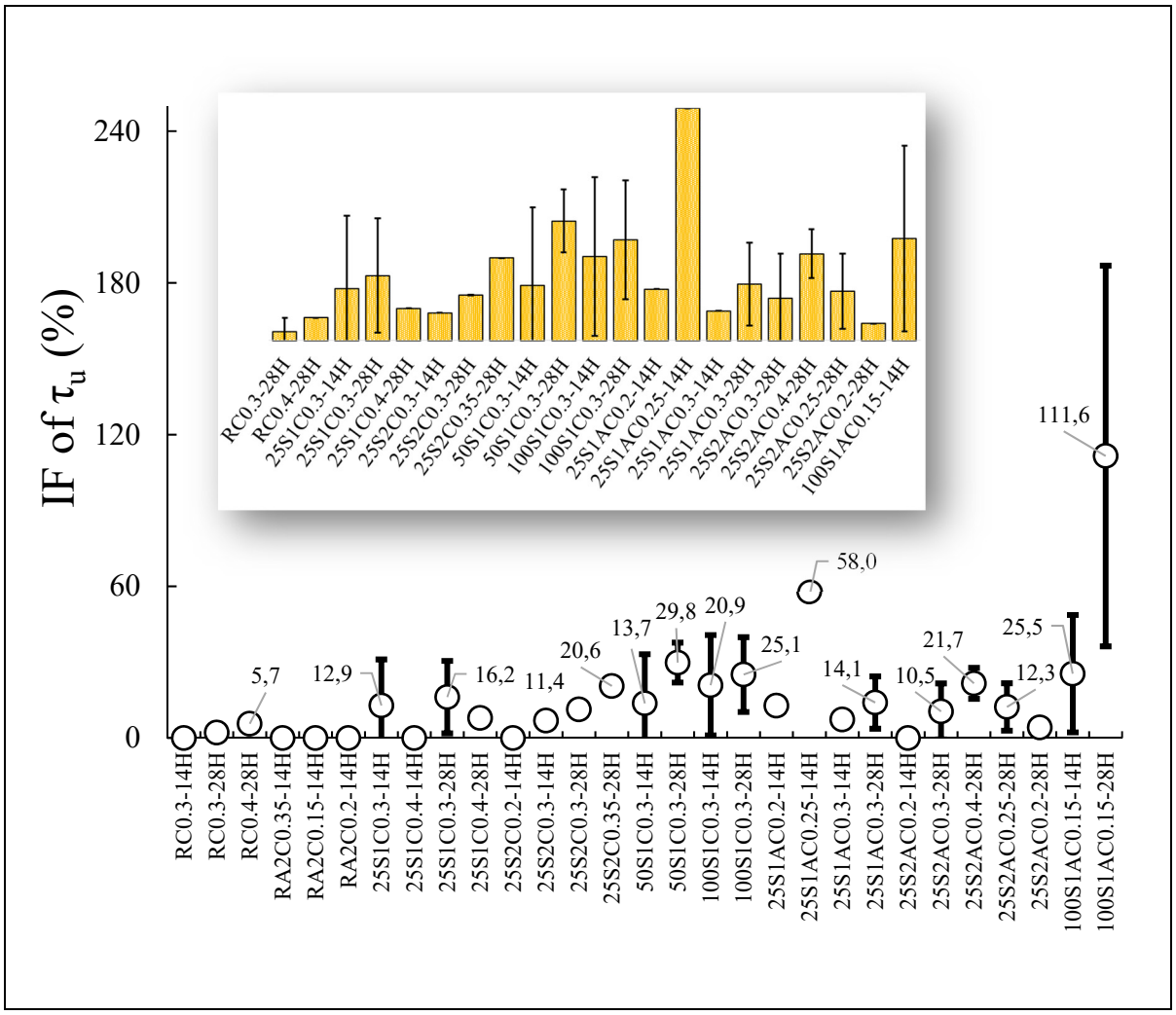

Figure 6.17 Determination of IF for bond strength

Similar results of residual bond stress healing (IF_{τ_r}) are obtained for mixtures of 50S1, 100S1, and 100S1A (Figure 6.18). Compared to the bond strength and average bond stress, a lower improvement factor is observed for residual bond stress of other mixtures. The general trend observed in Figures 6.16-6.18 shows that SAP has considerable influences on healing cracks for mitigating damages, especially for mixtures of 50S1, 100S1, and 100S1A.

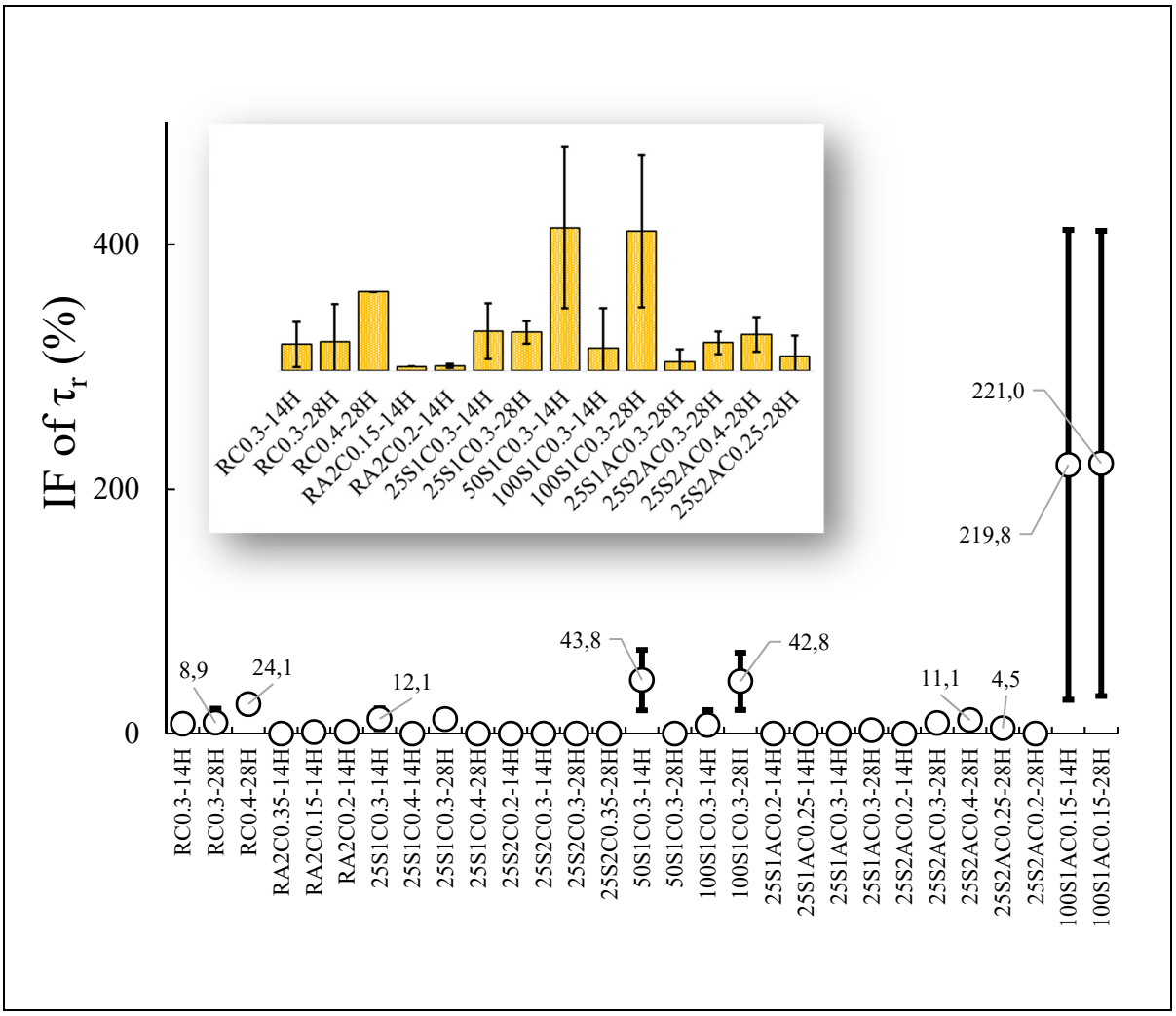

Figure 6.18 Determination of IF for residual bond stress

Bond-slip curves of 100S1A mixtures are illustrated in Figure 6.19 for the cracked and the healed specimens. As mentioned in Table 6.4, due to the low tensile strength of mixtures containing 1.0% SAP and AE, crack width of 0.15 mm is considered in the splitting test for this type of mixture. Pull-out failure modes are observed for this small crack width, which is obvious from the bond-slip curves, where no sudden drop presence after the maximum bond stress (Figure 6.19(a)). Results show that the bond strength is considerably increased after both 14- and 28-day healing periods (Figure 6.19(b)). Moreover, slip corresponds to the maximum bond stress is also increased along with strength recovery. Initial ascending parts of the bond-slip curve for different specimens are shown in Figure 6.19(c). Results show that the healed

specimens have higher initial stiffness as compared to the cracked specimens. A similar observation is achieved for the residual bond stress (Figure 6.19(d)). Energy absorbed (dissipated) by bond mechanism is also measured by the area under the bond-slip curve up to the slip of 10 mm, which is illustrated in Figure 6.19(e). Results show that the self-healing method by 1.0% SAP significantly increased the absorbed energy, as compared to the cracked specimens. Overall, results show that a crack width of 0.15 mm can be mostly recovered by 1.0% SAP and AE.

Bond-slip curves of 25S1A mixtures are illustrated in Figure 6.20 for cracked and healed specimens. Crack widths of 0.20, 0.25, and 0.30 mm are generated in the splitting test for this type of mixture. Splitting failure modes are observed for these crack widths. Sudden drops in the bond-slip curves are obtained for cracked specimens (Figure 6.20(a)). Scattering results are obtained for this type of mixture with a low dosage of 0.25% SAP. Results clearly show that the 14-day healing period is not enough to recover bond properties. As shown in Figure 6.20(b), higher bond strength is obtained for the healed specimens with crack widths of 0.30 mm after 28-day healing periods. Healed specimens have higher initial stiffness of bond-slip curves, as compared with cracked specimens (Figure 6.20(c)). However, there are no promising results for residual bond stress of mixtures containing 0.25% SAP with AE (Figure 6.20(d)), which is different from 1.0%SAP mixtures (Figure 6.19(d). Absorbed energy (dissipated) by the bond mechanism in 25S1A mixture is significantly affected b 28-day healing periods so that even higher area is observed as compared with uncracked specimens (Figure 6.20(e)). However, splitting failure modes are observed for all healed specimens. Overall, results indicate that healing specimens cannot change the failure mode.

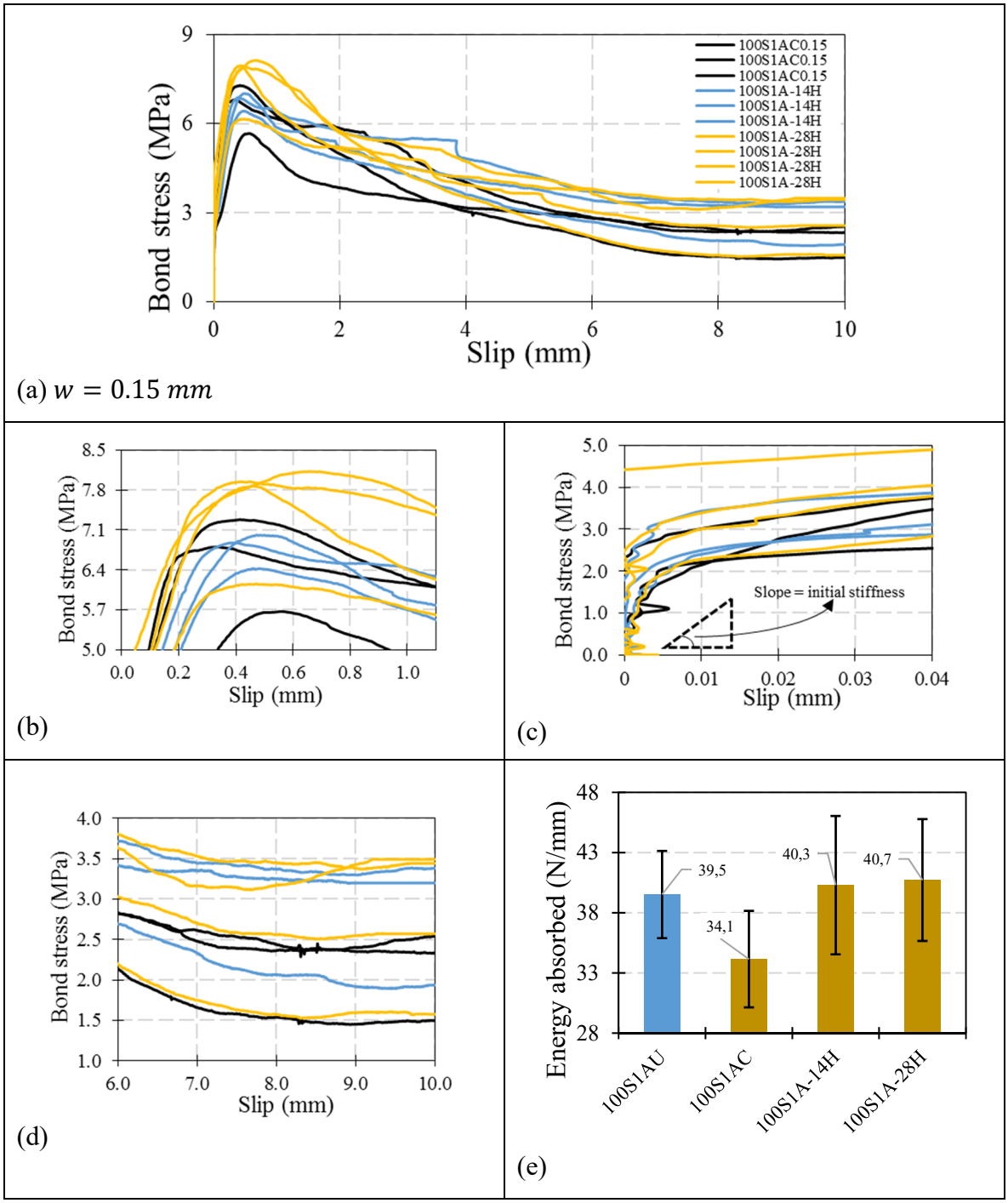

Figure 6.19 Results of 100S1A mixtures: (a) bond-slip curves; (b) bond strength; (c) initial bond stiffness; (d) residual bond stress; (e) energy absorbed by bond

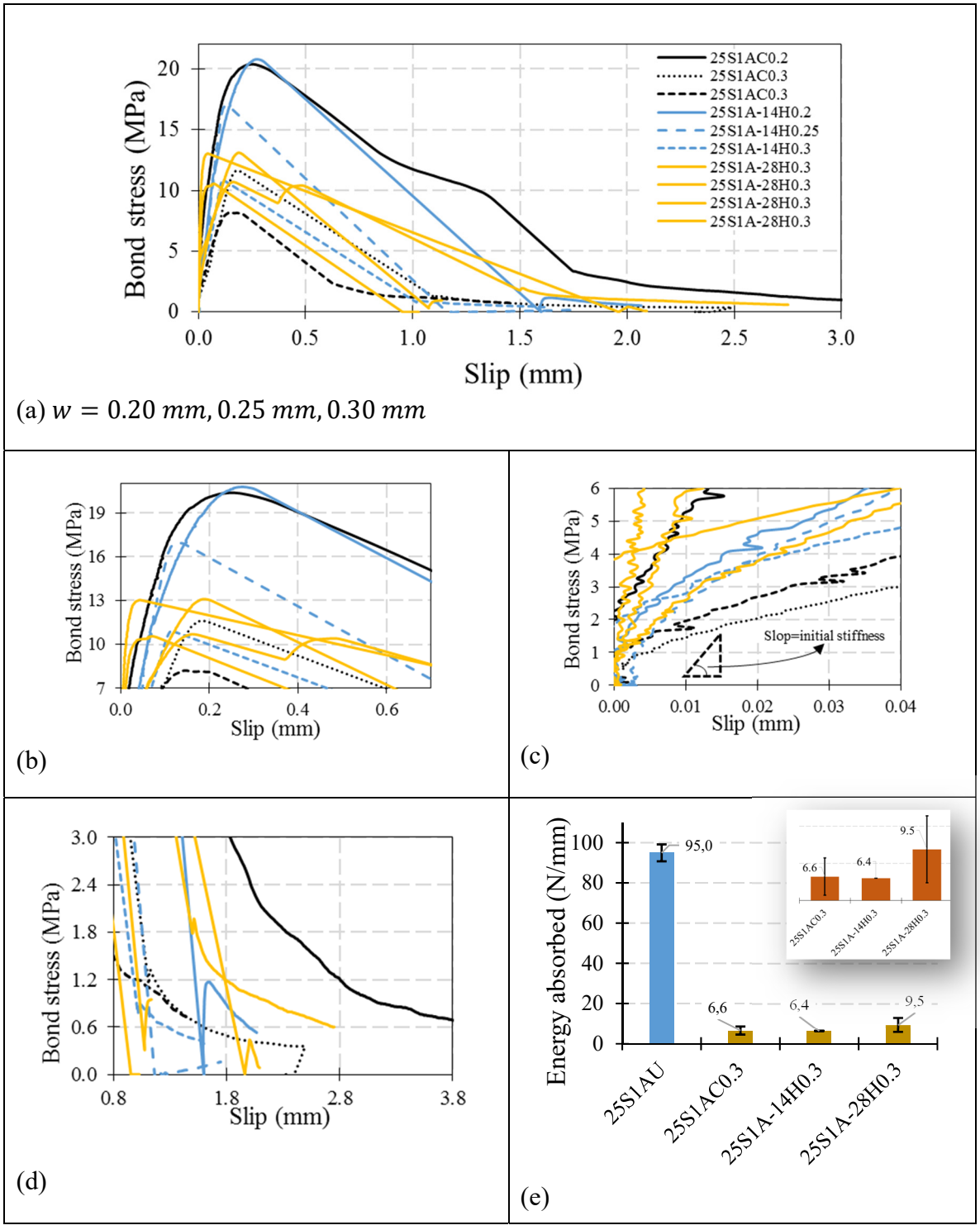

Figure 6.20 Results of 25S1A mixtures: (a) bond-slip curves; (b) bond strength; (c) initial bond stiffness; (d) residual bond stress; (e) energy absorbed by bond

Bond-slip curves of 25S2A mixtures are illustrated in Figure 6.21 for cracked and healed specimens. Crack widths of 0.20-0.40 mm are generated in the splitting test for this type of mixture. Splitting failure modes are observed for these crack widths. Sudden drops in the bond-slip curves are observed for cracked specimens (Figure 6.21(a)). For crack width of 0.30 mm, results for 28-day healing periods show higher bond strength as compared to the cracked specimens (Figure 6.21(b)). Also, two cracked specimens with $w = 0.40$ mm are considered for 28-day healing periods. As there are no cracked specimens with this width to compare the results, a bond reduction trend is used similar to the approach followed by Figure 6.9 and Figure 6.10. The results are summarized in Table 6.4. General results of the initial stiffness (slop) of bond-slip curve show that healed specimens have slightly higher slop as compared to the cracked specimens, while the trend is weaker for 0.25% SAP (Figure 6.21(c)) than 1.0% SAP (Figure 6.19(c)). This may be attributed to the small crack width generated (by splitting test) for 1.0% SAP. Similar to 25SAP1A mixture, there is no clear trend for residual bond stress in 25SAP2A mixture (Figure 6.19(d)). Despite the previous mixture containing SAP and AE, 25SAP2A mixture could not drastically improve the absorbed energy, especially for crack width of 0.25 mm (Figure 6.21(e)). Close photos of the healed specimens are shown in Figures 6.22 and 6.23 (white crystals). Scanning electron microscopy/energy dispersive X-ray spectrometry (SEM/EDS) microanalysis method is conducted to identify and quantify all elements of healed products. A considerable amount of calcium deposits are mostly abundant close and at crack lips, which may be an illustration of calcium carbonate precipitation for healing cracks (Figure 6.22). SEM/EDS results of one sample are illustrated in Figure 6.24, while more samples are shown in APPENDIX III (see pages 308-311). To compare the results of SEM/EDS analysis between healing products obtained from internal and external surfaces of cracks, 16 samples are provided, which is illustrated in Table APPENDIX III.1 (see page 312). The summary of the results is shown in Figure 6.25. Results indicate that healing products at the external surfaces of cracks have a considerably lower content of calcium (Ca), as compared to the internal ones. However, higher content of oxygen (O), carbon (C), and especially magnesium (Mg) are observed for external healing products, as compared to the internal ones. Snoeck et al. (2014) have reported that the external healing products consist of $CaCO_3$ and washed out hydration products. However, there is no accurate description of the

differences between elements of the internal and the external products, which is shown by the present study (Figure 6.25).

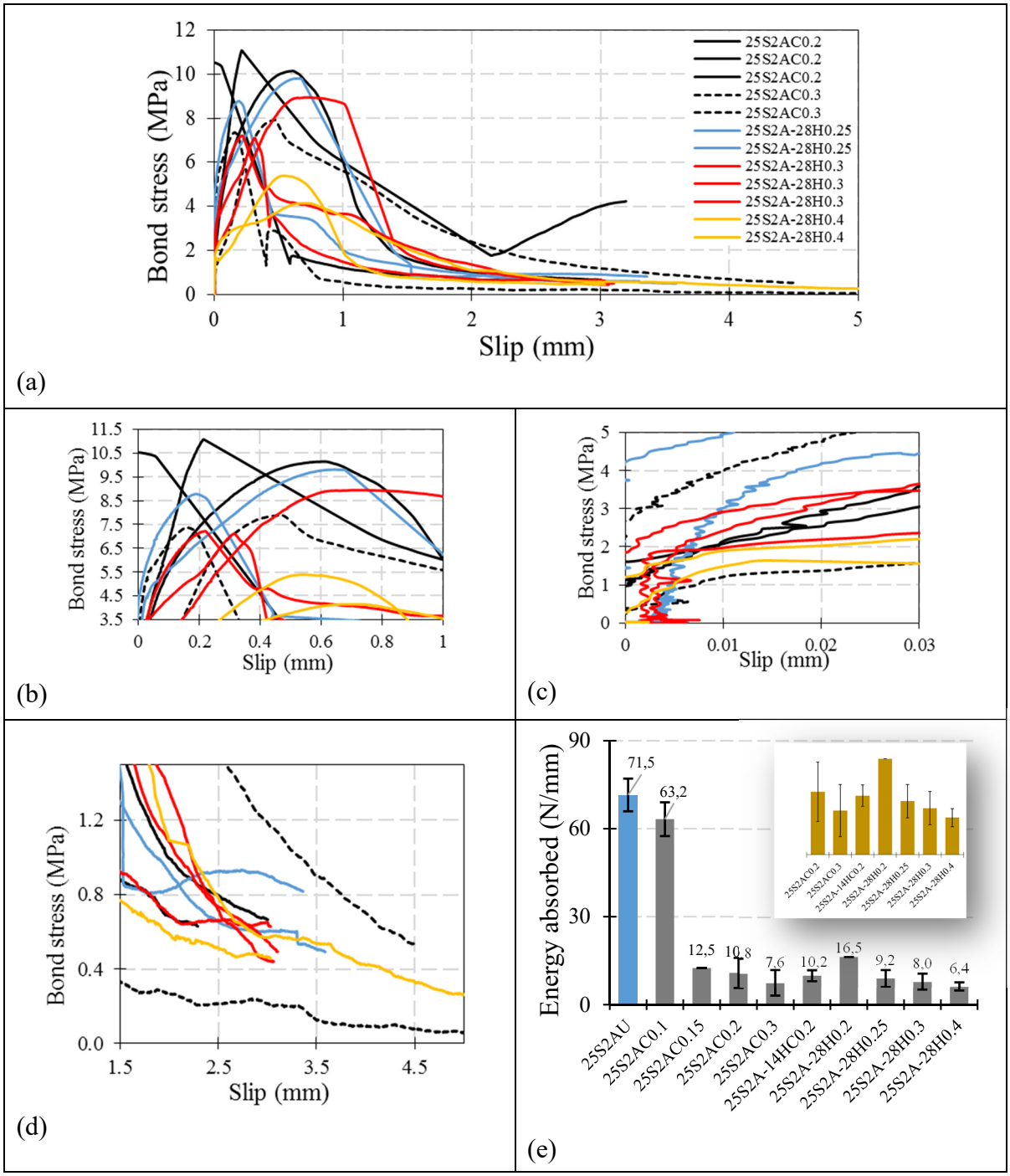

Figure 6.21 Results of 25S2A mixtures: (a) bond-slip curves; (b) bond strength; (c) initial bond stiffness; (d) residual bond stress; (e) energy absorbed by bond

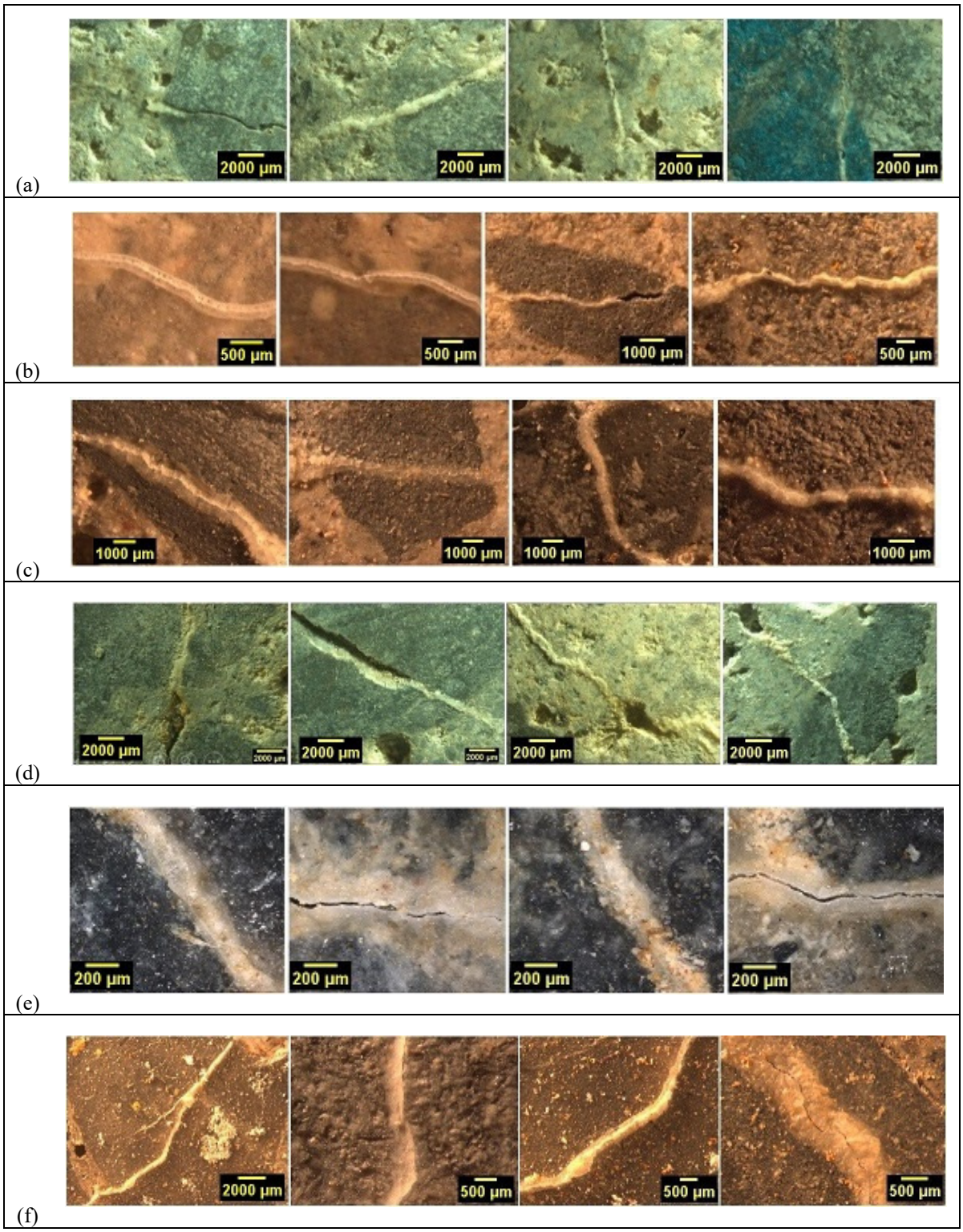

Figure 6.22 Self-healing (and/or sealing) products on crack surface after wet-dry cycles: (a) 25S1; (b) 25S2; (c) 25S2A; (d) 50S1; (e) 100S1; (f) 100S1A

Figure 6.23 Healing products at the external crack surface of pull-out specimens of SAP-based NC mixtures with and without AE

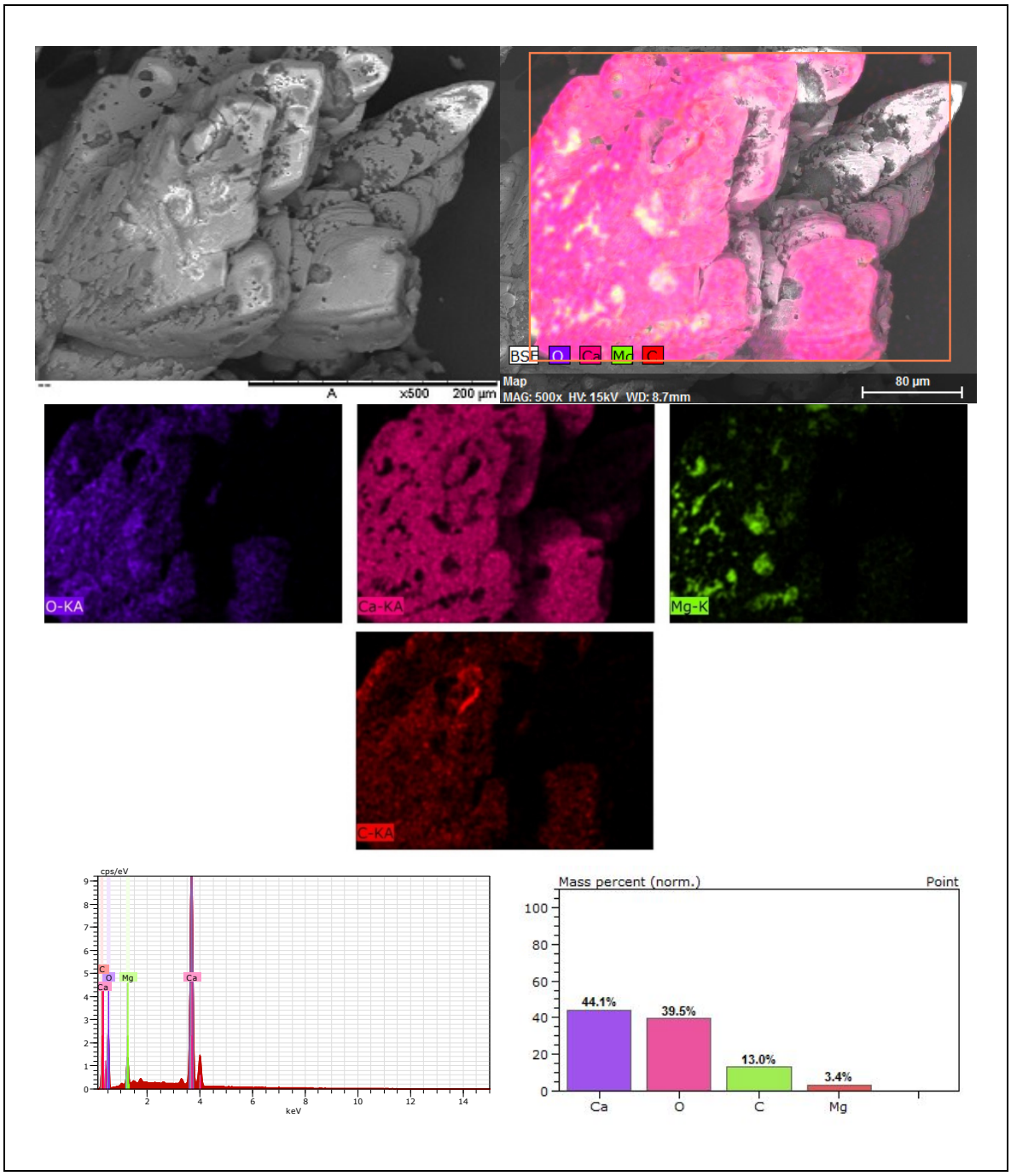

Figure 6.24 SEM image analysis of healed products at the external lip of cracks

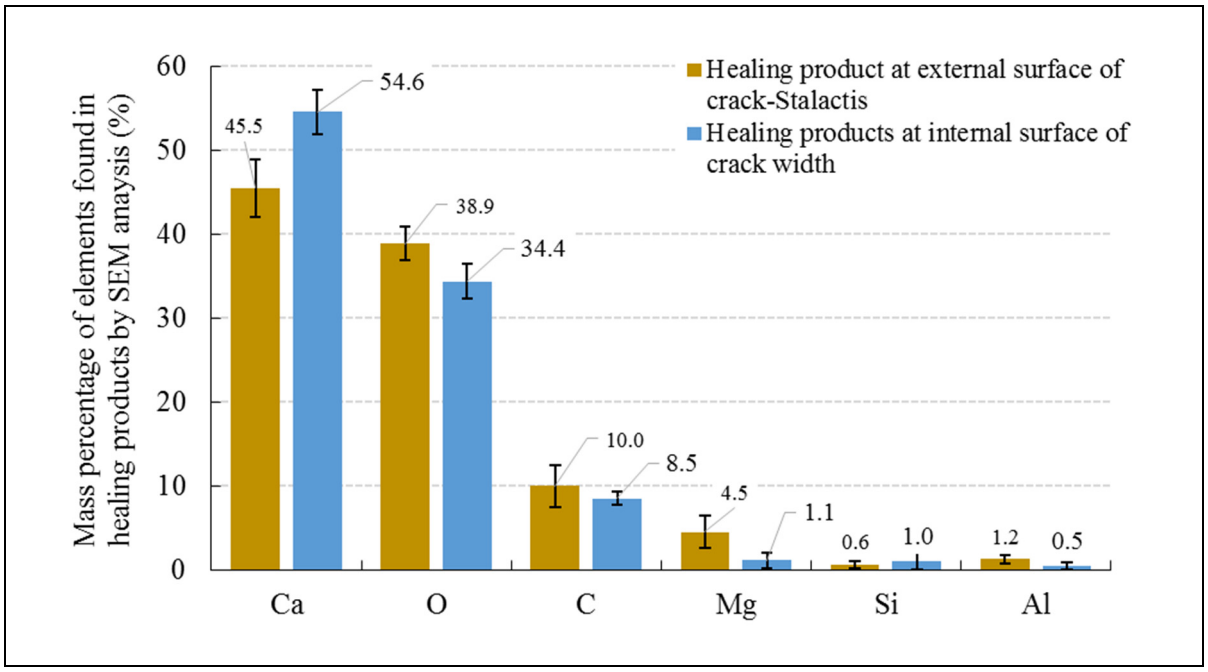

Figure 6.25 Comparison of mass percentage of elements found in the healing products at the internal and external surfaces of cracks

At the end of this section, different healing (or sealing) products, as compared to before starting healing periods, are illustrated. Disk-shaped specimens are prepared to capture the healing products. Specimens of SAP-2 and SAP-2+AE are considered in this section for Figures 6.26 to 6.33.

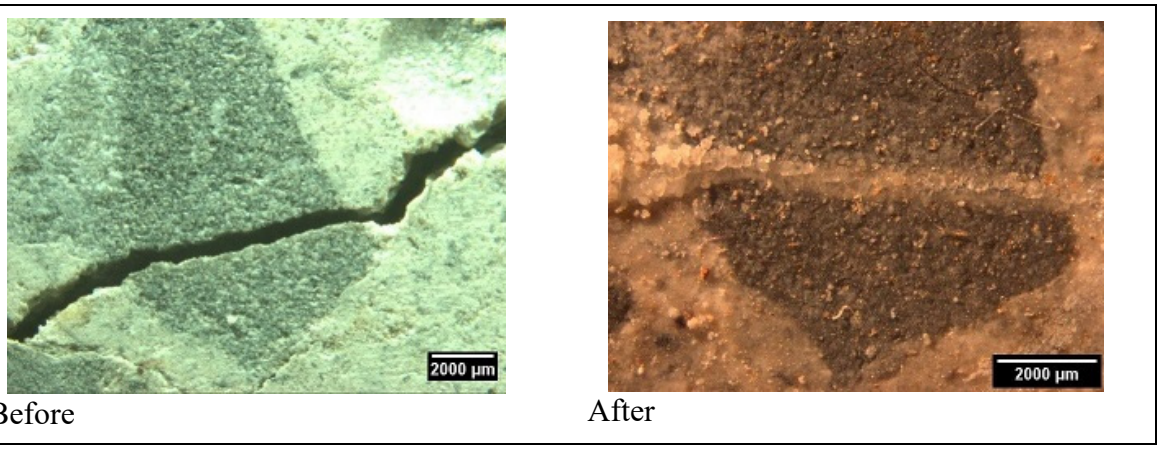

Figure 6.26 Pre-cracked specimens before and after healing periods (0.25SAP2+AE)

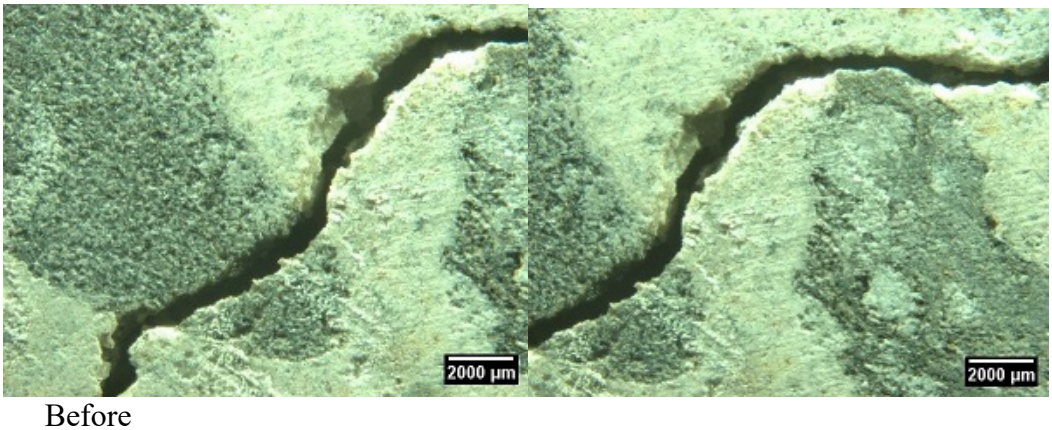

Before

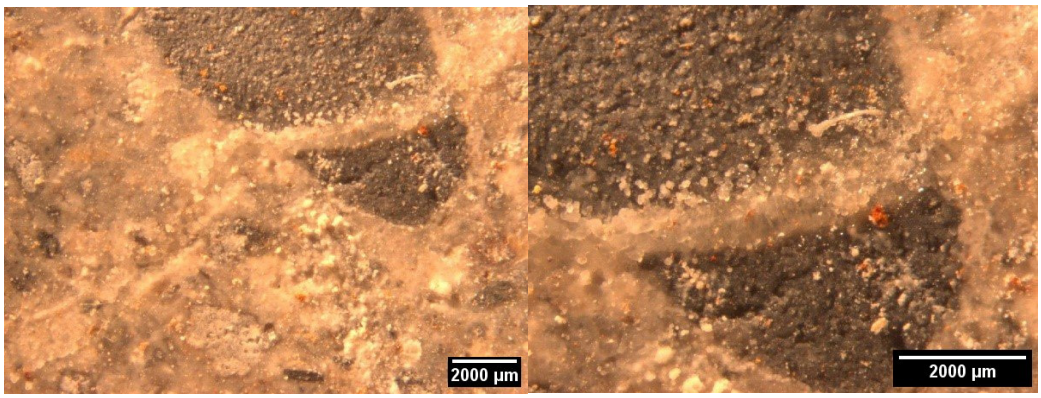

After

Figure 6.27 Pre-cracked specimens before and after healing periods (0.25SAP2+AE)

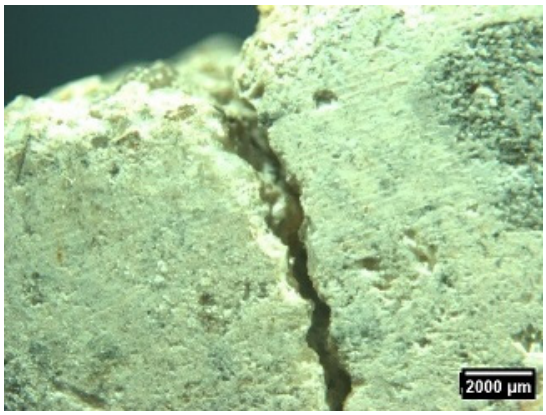

Before

After

Figure 6.28 Pre-cracked specimens before and after healing periods (0.25SAP2+AE)

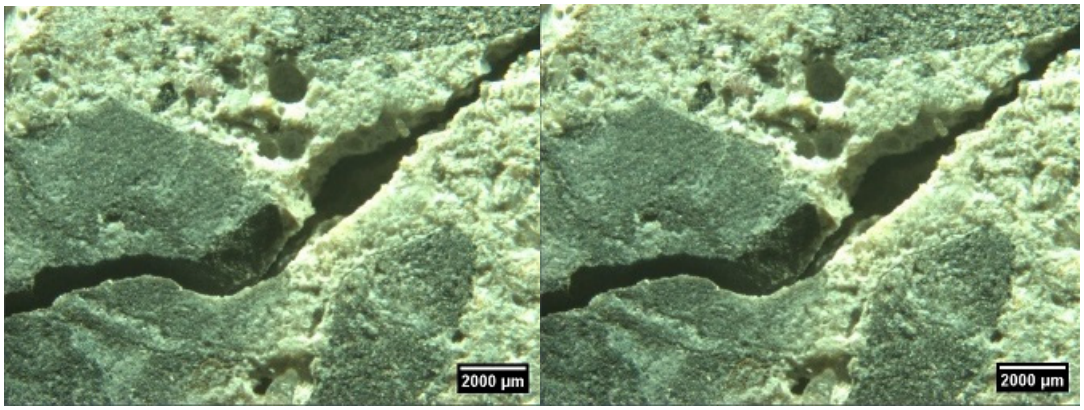

Before

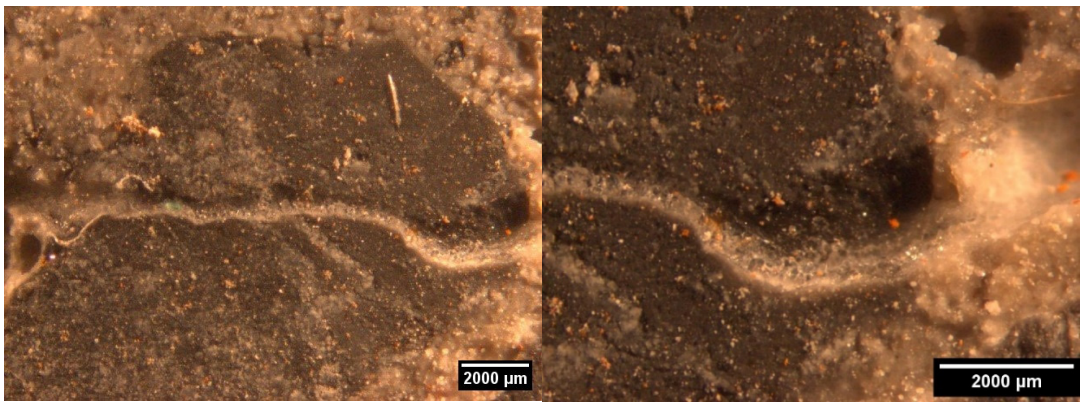

After

Figure 6.29 Pre-cracked specimens before and after healing periods (0.25SAP2+AE)

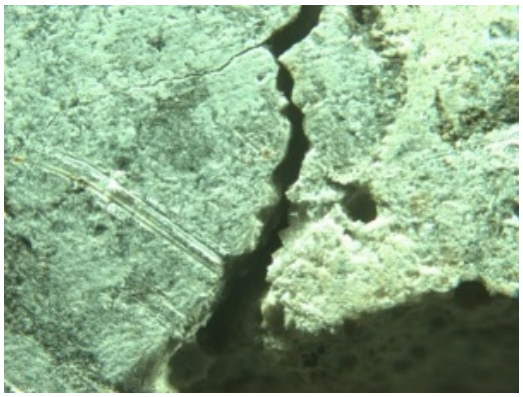

Before

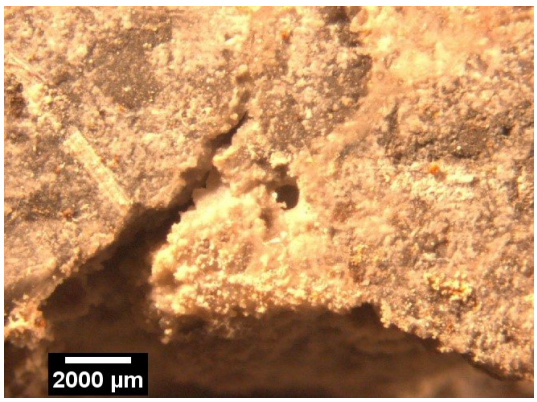

After

Figure 6.30 Pre-cracked specimens before and after healing periods (0.25SAP2+AE)

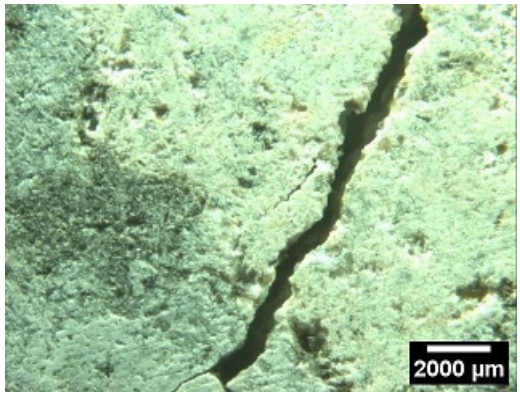

Before

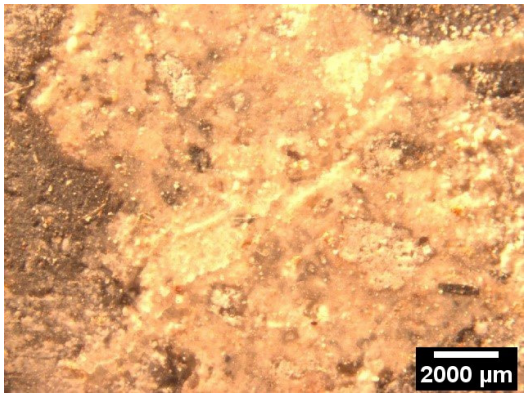

After

Figure 6.31 Pre-cracked specimens before and after healing periods (0.25SAP2+AE)

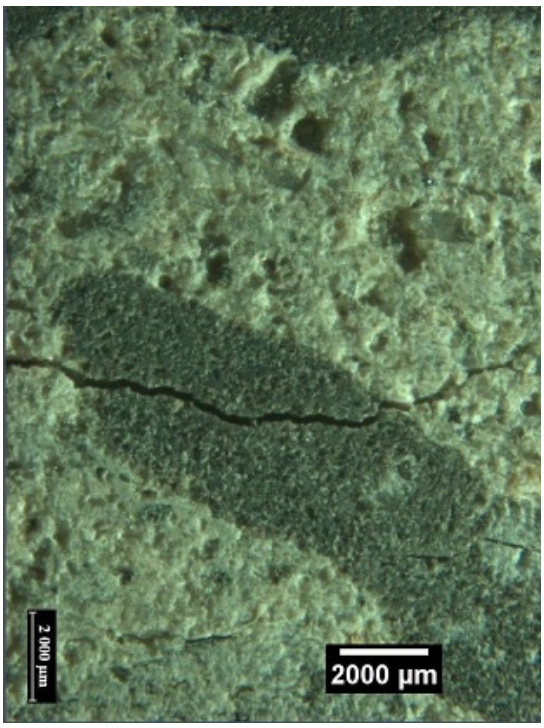

Before

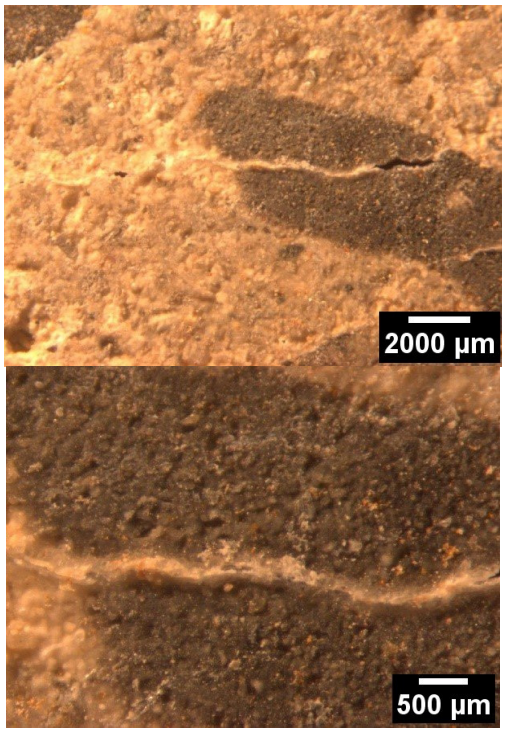

After

Figure 6.32 Pre-cracked specimens before and after healing periods (0.25SAP2)

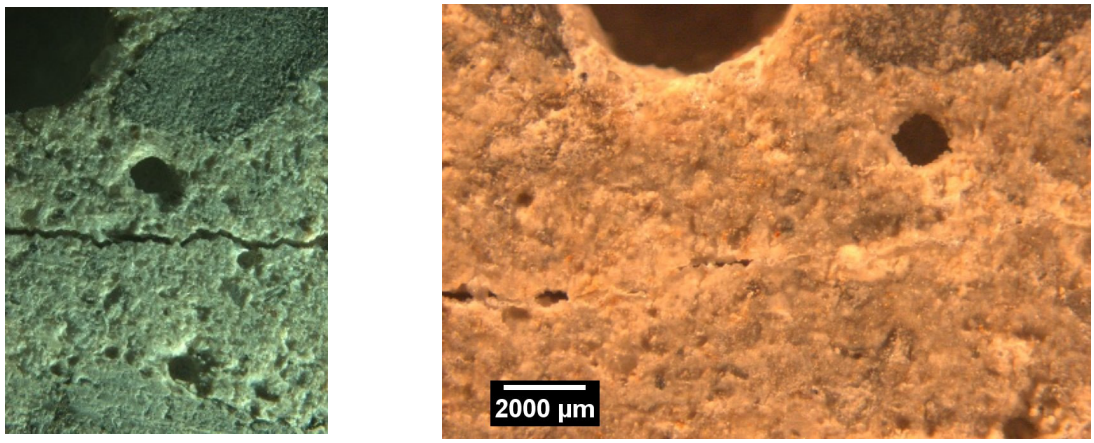

Figure 6.33 Pre-cracked specimens before and after healing periods (0.25SAP2)

6.4 Statistical analysis of healing improvement factor (IF)

After presenting and discussing results of the self-healing method for non-AE and AE concrete in Chapter 5 and 6 respectively, this section intends to perform a comprehensive statistical analysis to find out (1) the most important parameter affecting the self-healing results; (2) interaction plots of improvement factors with respect to different key variables. To follow this statistical approach, two statistical software of "Minitab" and "Statistica" are used. Crack width (w), healing period (H), SAP percentage, SAP type, and AE percentage are the main variables considered for the input of analysis. Improvement factors of maximum (IF_u), average (IF_m), and residual (IF_r) bond strength are the output results. Additionally, the average values of these three improvement factors (IF_{ave}) is also considered in the analysis. Analysis of variance is conducted to explain the interaction between variables and also output. ANOVA results clearly confirm the significant impact of SAP percentage on self-healing performance. Statistical results indicate that as crack with increases, efficiency of the self-healing method at the rebar-concrete interface decreases. Results also show that 28-day healing periods are more effective than 14-day healing periods. Finally, a multilinear regression model is presented to formulate average improvement factor (IF_{ave}) as a function of the healing period, SAP% and

AE percentage. However, due to the unclear trend of the effect of SAP type, this parameter is ignored in the model.

6.4.1 Main effects by ANOVA method in Minitab 17

As mentioned in the present and previous Chapters, the number of 193 specimens are tested in the present study to determine the efficiency of the proposed approach of mitigating rebar-concrete damages due to the pre-cracking phenomenon using SAP. Different parameters of concrete type, crack width, healing period, SAP dosage, SAP type, and AE admixture are considered in the previous sections. To present the general trend observed in this experimental investigation, analysis of variance (ANOVA) by statistical software of Minitab (Minitab, 2014) is used in the present section. Healing improvement factors of average bond stress (IF_{τ_m}), bond strength (IF_{τ_u}), and residual bond stress (IF_{τ_r}) are considered as output parameters (Figure 6.34). Average value of these improvement factors is also measured (IF_{ave}).

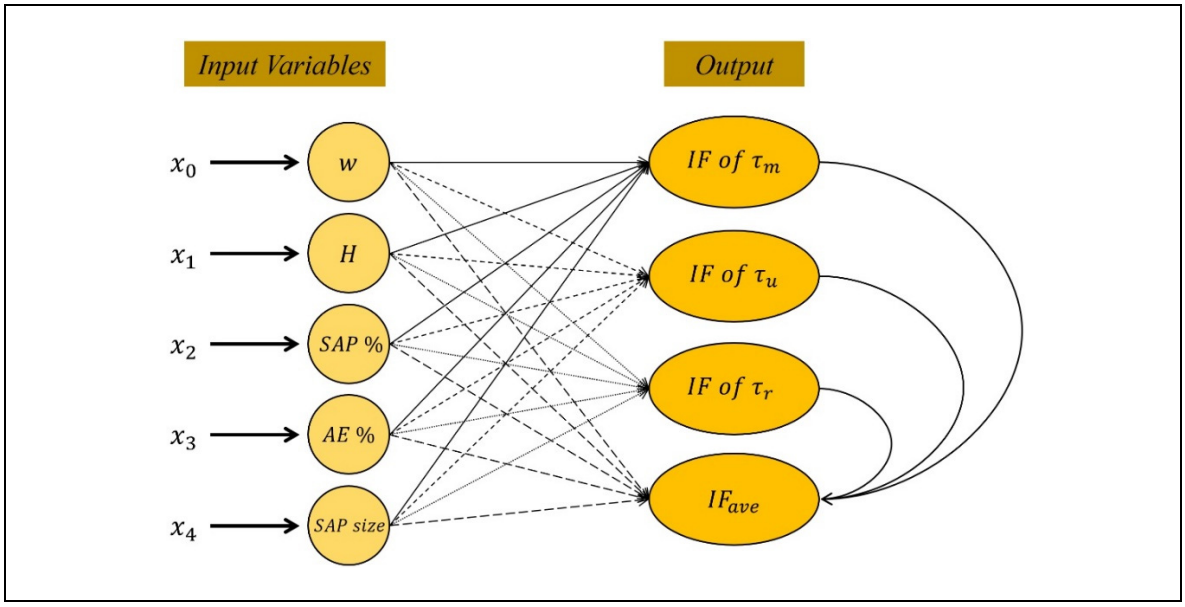

Figure 6.34 Schematic representation of input variables and output parameters for ANOVA analysis

Results of ANOVA for the average improvement factor (IF_{ave}) is shown in Table 6.5. Results show that crack width (w) has the most significant influence on the self-healing performance of mixtures, as compared to other variables, with the lowest P-value of 0.003. While high P-value of 0.509 for AE shows the low influence of this parameter on the average improvement factor. Moreover, ANOVA could not obtain any value for SAP size. Residual plot for average IF is shown in Figure APPENDIX V.1 (see page 314).

Table 6.5 Summary of analysis of variance (ANOVA) for IF_{ave}

Source	**DF**	**Adj SS**	**Adj MS**	**F-Value**	**P-Value**
w	5	20548	4109.5	4.06	0.003
H	1	3062	3061.7	3.02	0.088
$SAP\%$	3	5366	1788.6	1.77	0.165
$SAP\ size$	-	-	-	-	-
AE	1	448	447.7	0.44	0.509
Model Summary					
S	R-sq		R-sq(adj)	R-sq(pred)	
31.8173	62.67%		55.49%	45.18%	

The main effects of variables obtained by ANOVA are illustrated in Figure 6.35 for average bond stress, bond strength, and residual bond stress improvement factor. Moreover, the average values of theses improvement factors are also measured and compared. Results indicate that crack width smaller than 0.20 mm is fully recovered by wet-dry healing cycles (higher than 50%), while there is around 20% to 25% IF for $w > 0.20$ mm (Figure 6.35(a)). A similar range of around 0.14 mm is reported by Snoeck et al. (2014) to completely seal cracks by SAP. Regarding healing periods, ANOVA results show that an average value of 20% is obtained for 14-day wet-dry cycles, while the average value of 35% is obtained for 28-day wet-dry cycles (Figure 6.35(b)). As the healing period increases, enough time is available to provide more $CaCO_3$ participation at crack surfaces, which is similarly reported by Snoeck et al. (2018, 2019) (Snoeck, 2018; Snoeck & De Belie, 2019). The effect of SAP size (and type) on healing improvement factors is shown in Figure 6.35(c). The analysis shows that SAP with larger size (0.50 mm, SAP-1) has considerably higher improvement factor as compared to the smaller

SAP (0.15 mm, SAP-2). As comprehensively discussed in Chapter 5, concrete containing SAP-1 generates larger macro voids as compared to SAP-2 (Figure 5.8 in Chapter 5), which may provide more possibility to pass the crack line. However, there is no fact regarding this difference in the literature. Different chemistry types of SAP used may affect the obtained results. The effect of AE admixture on the self-healing capacity of concrete is illustrated in Figure 6.35(d).

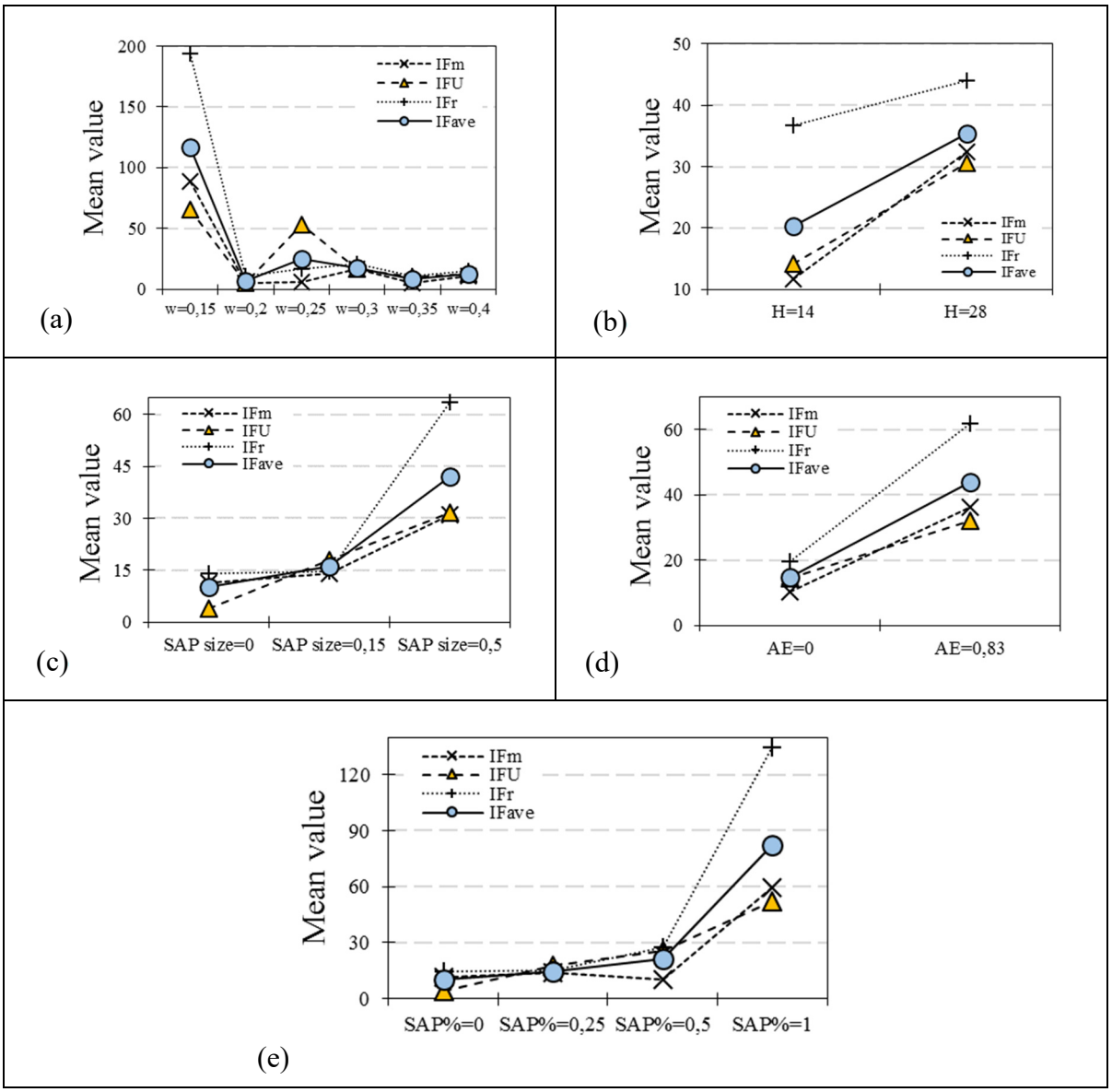

Figure 6.35 Main effects plot obtained by ANOVA with respect to: (a) crack width; (b) healing period; (c) SAP size; (d) AE dosage; (e) SAP percentage

Results show that AE admixture has considerable influences on self-healing capacity so that improvement factor higher than 60% is obtained for the maximum improvement factor of AE mixtures. Figure 6.35(e) shows that SAP percentage has considerable influence on improvement factors. Although NC without SAP obtained less than 10% IF, SAP concrete mixtures have a range of $20\% \leq IF < 150\%$ for 1.0% SAP. Average improvement factor (IF_{ave}) has a range 60%-90% for 1.0% SAP percentage. Regarding NC without SAP, IF_u has the lowest value among the improvement factors, while this parameter is increased for 0.25% and 0.50% SAP (Figure 6.35(e)). However, in the case of 1.0% SAP which small crack widths are tested, still lower healing capacity is observed as compared to other improvement factors. Moreover, results show that 28-day healing period is enough for regaining residual bond stress, as compared to the bond strength. It seems that more healing periods are necessary to regain bond strength after the pre-cracking phenomenon.

6.4.1.1 Influence of crack width by ANOVA

Interaction plots of average improvement factor (IF_{ave}) with respect to crack width is shown in Figure 6.36. Results indicate that higher dosage of SAP has a positive impact on IF_{ave}, especially 0.5% and 1.0% SAP (Figure 6.36(a)). Figure 6.36(b) shows that SAP-1 has better performance as compared to SAP-2 for $w < 0.30$ mm. AE admixture has a considerable impact on average improvement factor after healing periods even for crack width of 0.40 mm (Figure 6.36(c)). The 28-day healing period is more efficient as compared to the 14-day healing period for all crack widths (Figure 6.36(d)).

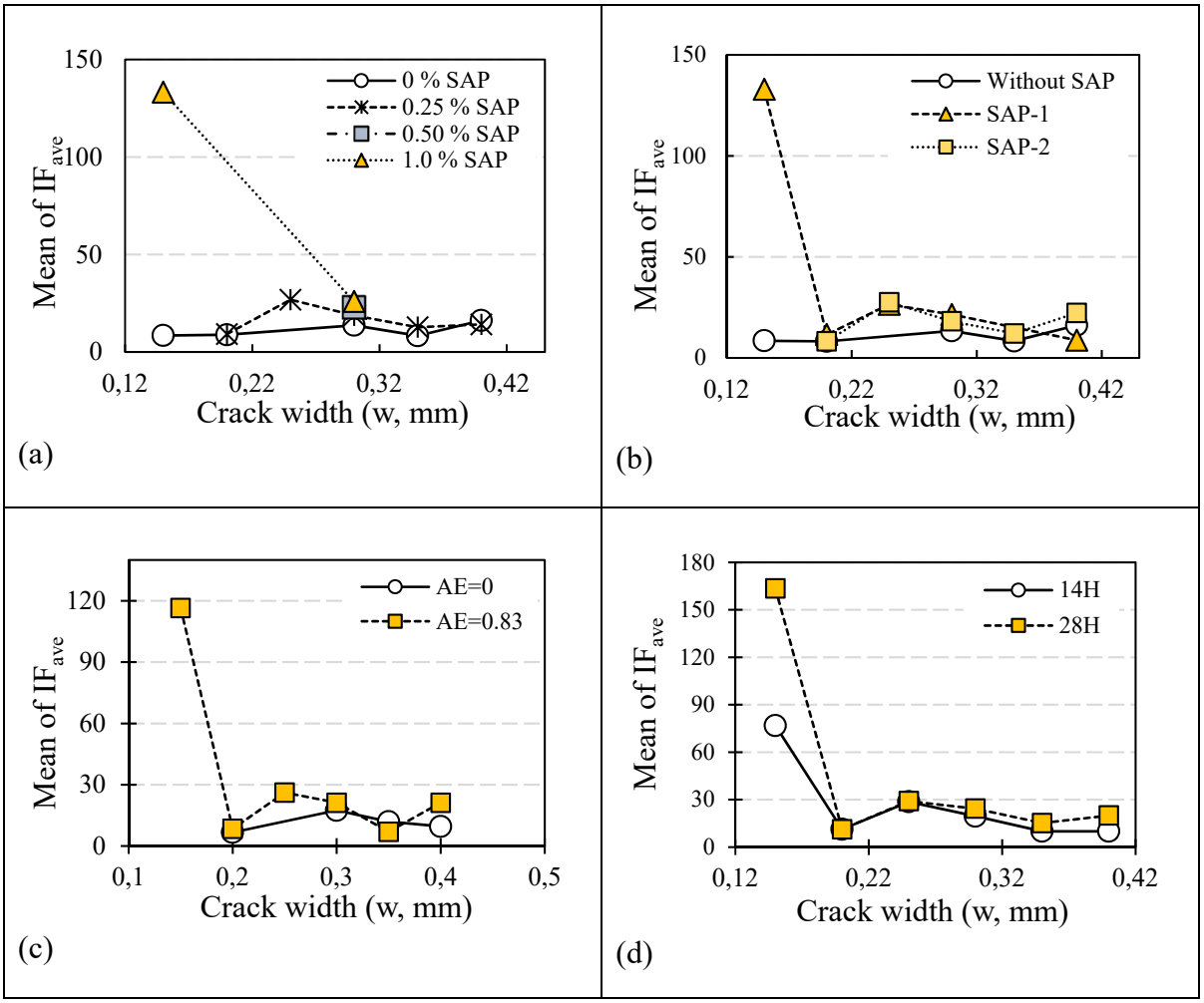

Figure 6.36 Interaction plots of improvement factors with respect to crack width: (a) *w* versus SAP%; (b) *w* versus SAP type; (c) *w* versus AE; (d) *w* versus healing period

6.4.1.2 Influence of the healing period by ANOVA

Interaction plots of average improvement factor (IF_{ave}) with respect to the healing period is shown in Figure 6.37. Results indicate that the self-healing capacity of mixtures containing 1.0% SAP considerably increases after 28 days. However, a longer healing period is necessary for a lower dosage of SAP (Figure 6.37(a)). Considerable healing results are obtained for mixtures containing AE admixture after 28-day healing periods (Figure 6.37(b)). Self-healing capacity is higher for SAP-1 modified concrete as compared to SAP-1, especially for smaller

crack widths (Figure 6.37(c and d). Interval plots are shown in Figure APPENDIX V.2 (see page 315) to confirm the general results of this section.

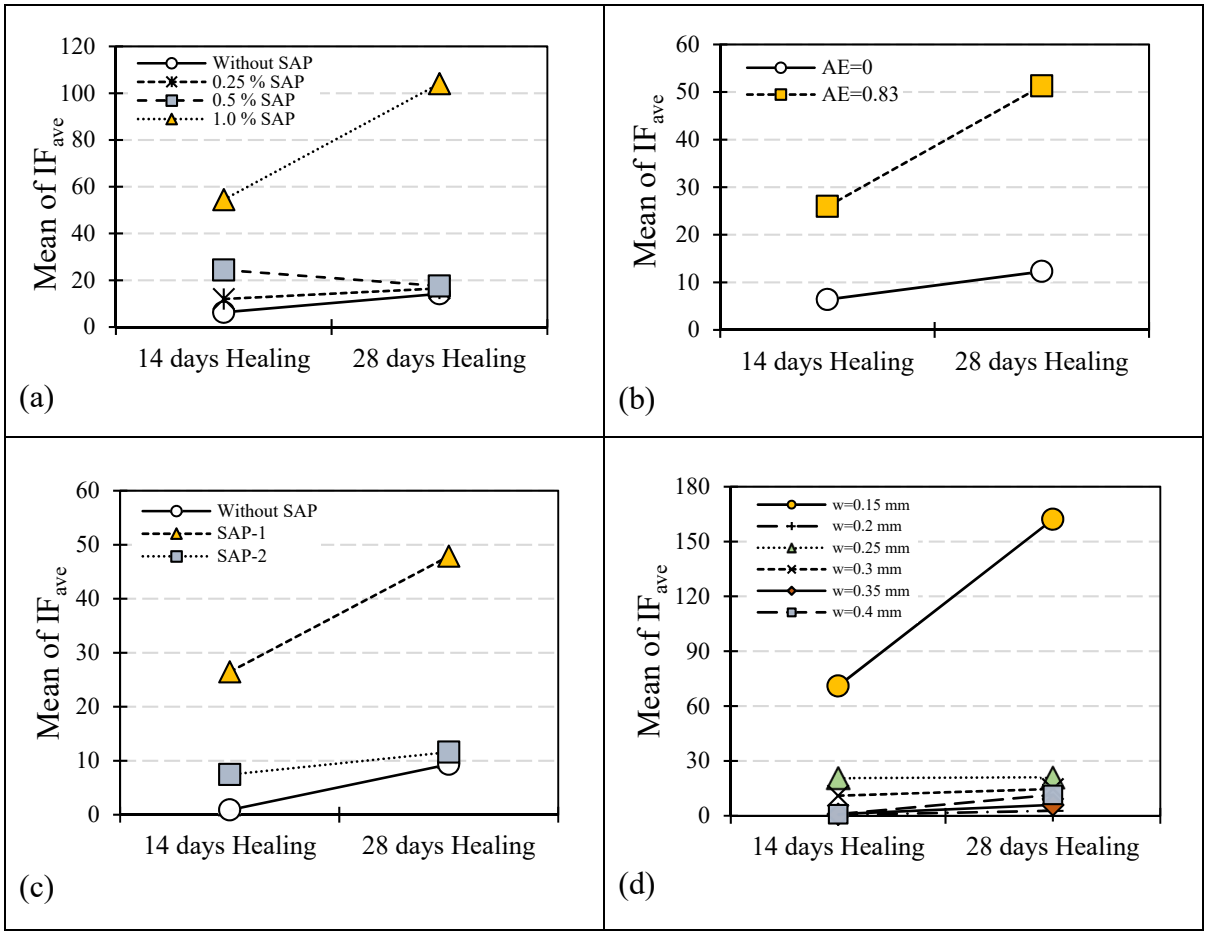

Figure 6.37 Interaction plots of improvement factors with respect to healing period: (a) *H* versus SAP%; (b) *H* versus AE; (c) *H* versus SAP type; (d) *H* versus crack width

6.4.1.3 Influence of AE admixture by ANOVA

Figure 6.38 clearly confirms the results of the previous subsection regarding AE admixtures. Results indicate that AE admixture has a positive impact on self-healing capacity for both dosages of 0.25% and 1.0% SAP. About the mean value of 40% IF is recorded for AE-contained mixtures (Figure 6.38). This impact is higher for residual bond stress as compared to the bond strength.

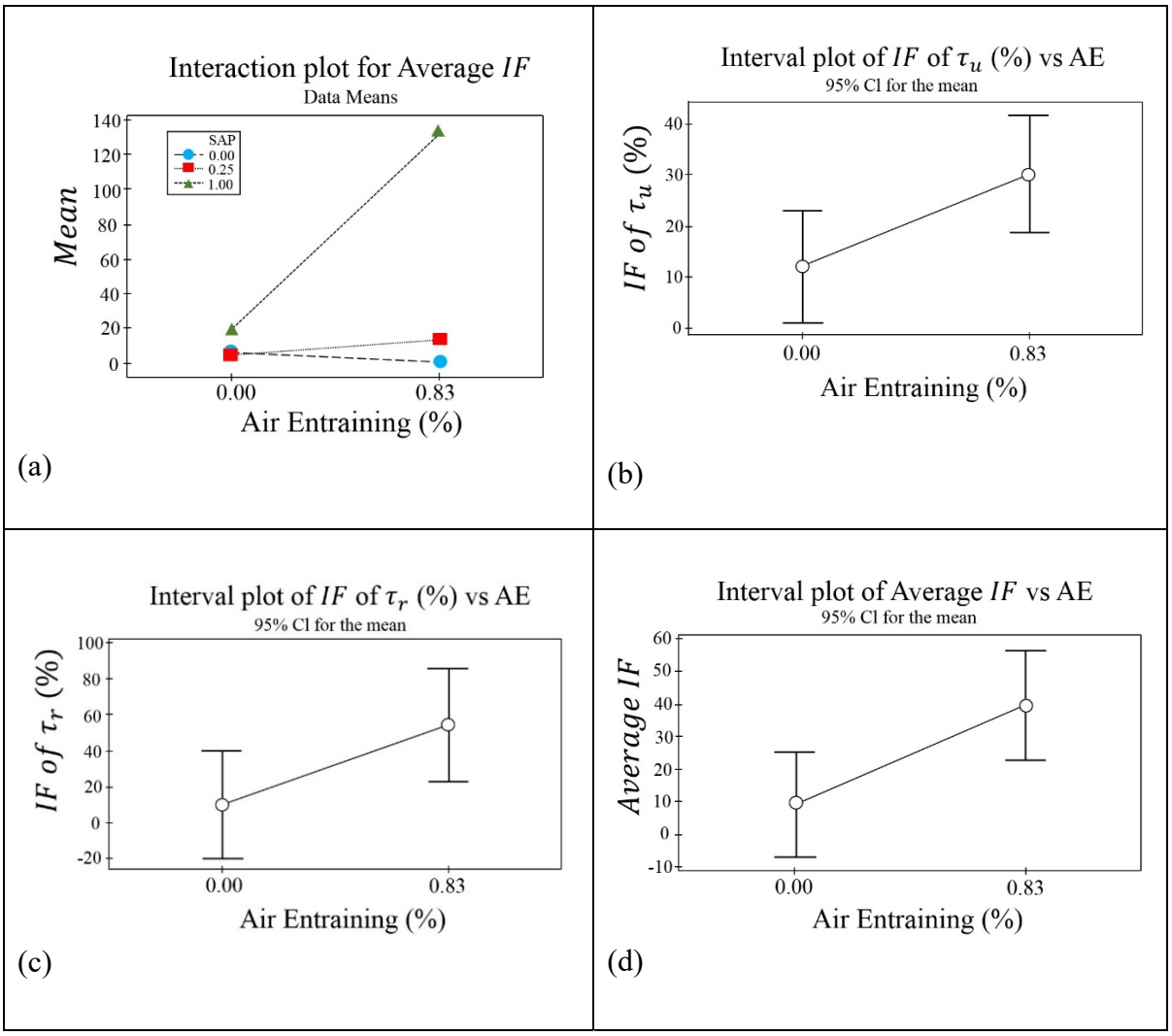

Figure 6.38 Influence of AE admixture based on ANOVA:
(a) interaction plot with respect to SAP%; (b) interval plot of $IF_{\tau u}$; (c) interval plot of $IF_{\tau r}$;
(d) interval plot of average improvement factor (IF_{ave})

6.4.1.4 Influence of the SAP percentage

Figure 6.39 clearly confirms the results of the previous subsection regarding SAP percentage. Results indicate that a higher dosage of SAP has a significant impact on self-healing capacity, especially after 28-day healing periods and in concrete containing AE admixture.

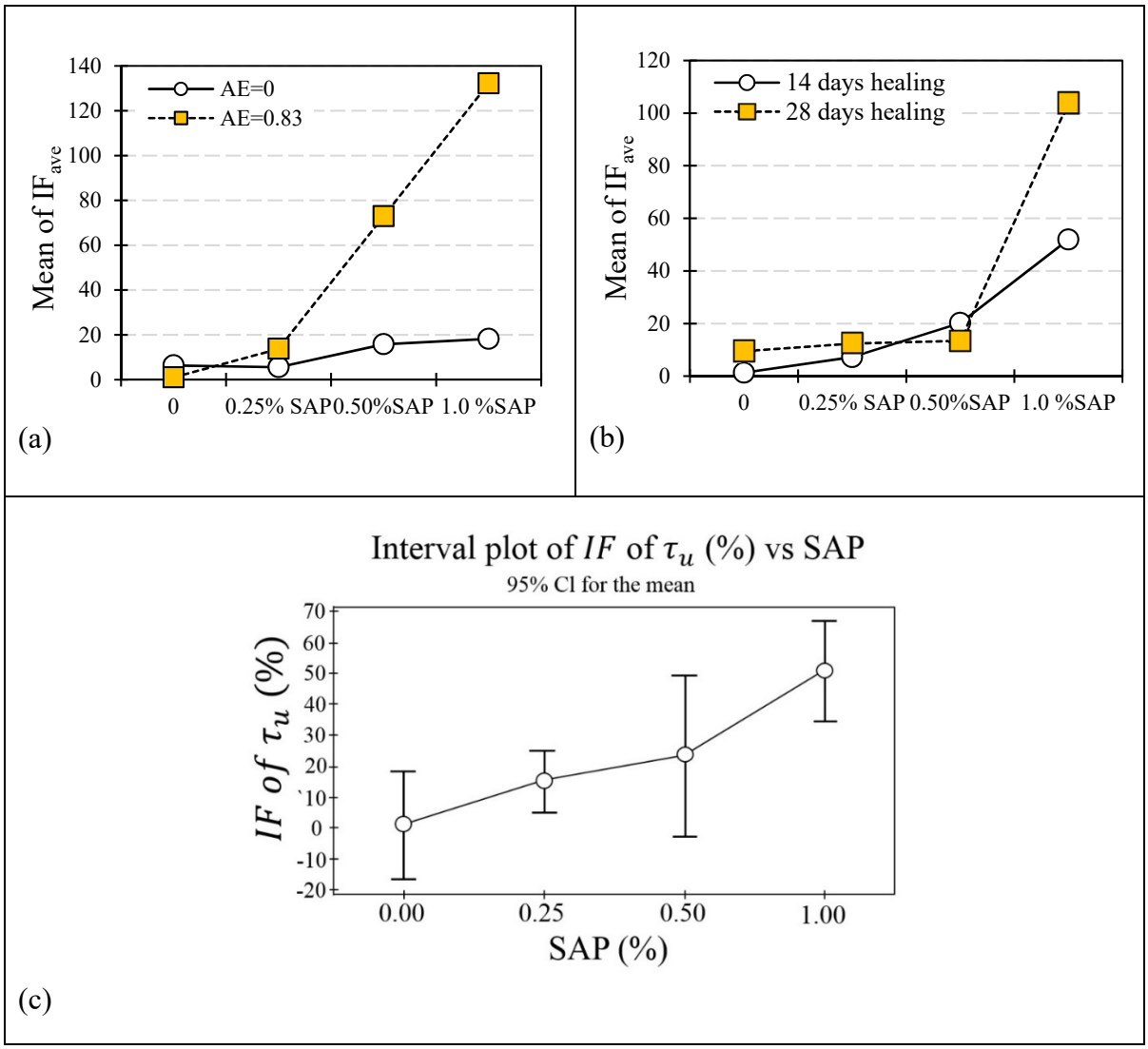

Figure 6.39 Influence of SAP percentage based on ANOVA:
(a) interaction plot with respect to AE; (b) interaction plot with respect to healing period;
(c) interval plot of IF_u

6.4.1.5 Influence of the SAP size (or type)

Statistical results show that SAP-1 (0.50 mm size) has a higher influence on self-healing capacity as compared to SAP-2 (0.15 mm), especially for AE-contained mixtures (Figure 6.40(a)). Moreover, the effect of the healing period is more important for SAP-1 modified concrete mixtures (Figure 6.40(b)). General results confirm that SAP-1 is more efficient for

use as a healing agent, even for uncracked, pre-cracked, and healed concrete. Details of this observation are comprehensively presented in Chapter 5.

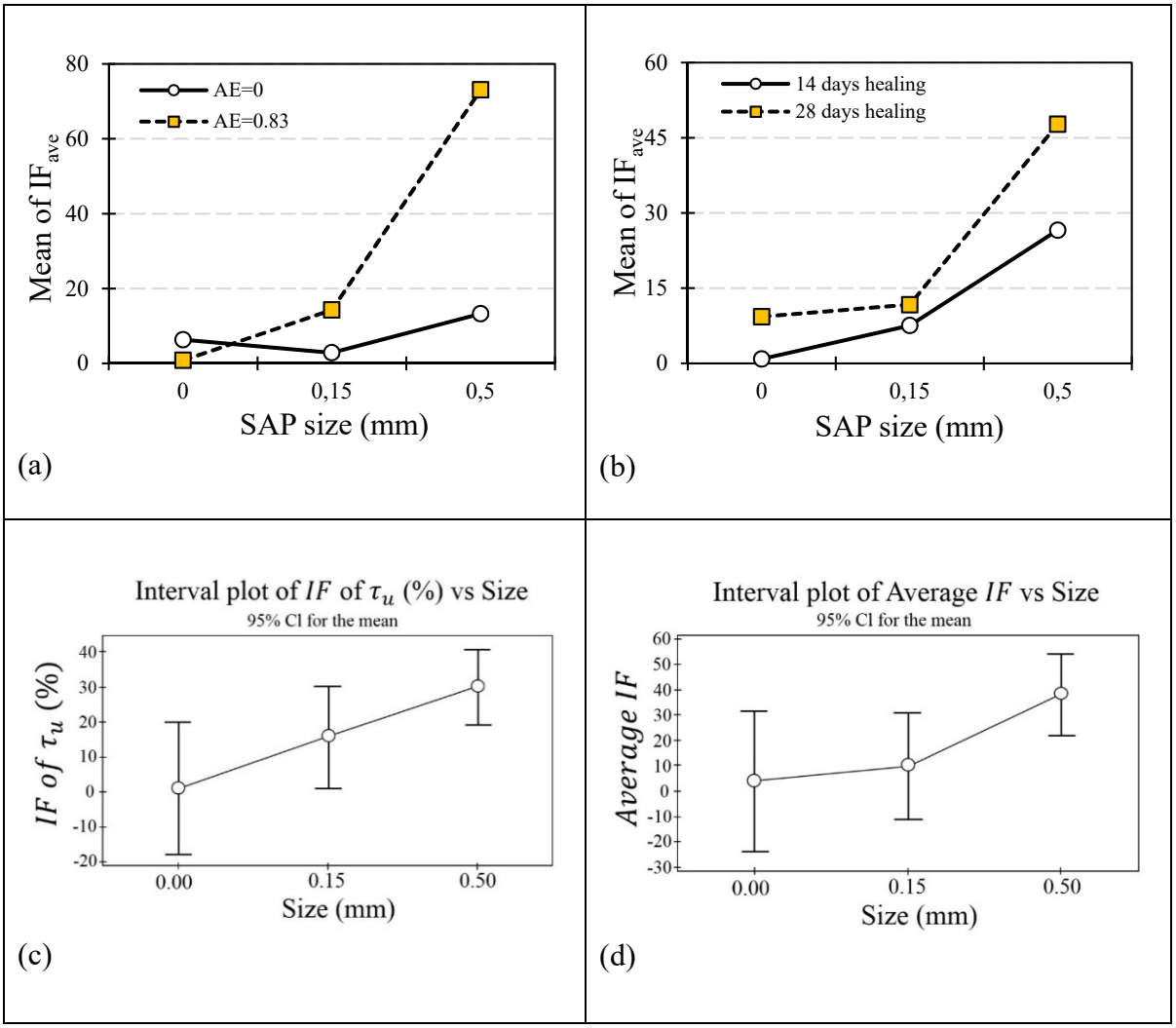

Figure 6.40 Influence of SAP size based on ANOVA:
(a) interaction plot with respect to AE; (b) interaction plot with respect to healing period;
(c) interval plot of IF_u; (d) interval plot of IF_{ave}

6.4.2 Multilinear regression results by STATISTICA

Based on statistical results obtained in the previous subsections, this section intends to propose a statistical equation to predict average improvement factor (IF_{ave}). Similar to the ANOVA

method summarized in Table 6.6, the multilinear regression model by STATISTICA software (STATISTICA, 2011) shows that crack width plays a critical role in the self-healing method which has severally confirmed by Snoeck et al. (2014, 2019) (Snoeck & De Belie, 2019; Snoeck et al., 2014). Moreover, SAP% and the healing period have considerable effects on average improvement factors (Table 6.6). However, SAP size has the lowest impact on IF_{ave}, as compared to other variables. Hence, the proposed model ignore this parameter.

Table 6.6 Summary of multilinear regression for IF_{ave}

Source	**P-Value**
w	0.014763
H	0.059884
$SAP\%$	0.001885
$SAP\ size$	0.906894
AE	0.125392
Model Summary	
R-sq	R-sq(adj)
51.0%	46.0%

Finally, the statistical equation of Eq. (6.9) is obtained to predict average improvement factor (IF_{ave}), as follows:

$$IF_{ave} = -0.30 + 0.18H + 0.46SAP\% + 0.17AE \quad (6.9)$$

where H is the healing period, $SAP\%$ is polymer percentage replacement by cement weight, and AE is AE percentage replacement by cement weight. Performance of Eq. (6.9) is shown in Figure APPENDIX V.3 (see page 316). Based on the extensive experimental tests and various parameters, an acceptable correlation is obtained ($R^2 = 0.51$) which is summarized in Table 6.6. To cross-check the results obtained by the ANOVA method in Minitab, the results of predicted trends obtained by the multilinear regression model in STATISTICA software are illustrated in Figure APPENDIX V.4 (see page 317) for all variables. Figure APPENDIX V.4(a) shows that the statistical trend confirms the positive impact of SAP percentage on the

self-healing capacity of concrete. Figure APPENDIX V.4(b) shows the importance of crack width on the healing process. So, microfibers or transverse reinforcement is necessary for regions exposed to the pre-cracking phenomenon so that the self-healing method can practically heal cracks. It is essential to mention here that simulating induced cracks by splitting tests are done based on the tensile strength of every mixture. On the other hand, some difficulties in the pre-cracking tests made it difficult to have various crack widths for every mixture. Based on these difficulties, the displacement rate of 0.11-0.15 mm/min is applied to the splitting device. Although Figure APPENDIX V.4(c) shows a positive impact on healing periods on the self-healing capacity of concrete, this figure cannot accurately shows the impact of healing periods, as different mixtures using different variables. P-value mentioned in Tables 6.5 and 6.6 can illustrate this influence. Figure APPENDIX V.4(d) shows a considerable impact of AE on the self-healing capacity of concrete. More experimental tests are necessary for the field of "healing chemistry" to clarify the main reason for the phenomenon. These promising results can be so interesting for the cold region, in which using AE is essential for concrete mixtures.

6.5 Discussion of the results

As mentioned in the previous sections, SAP percentage, AE, and healing periods have considerable impacts on the crack-healing at the rebar-concrete interface, which is summarized in Eq. (6.9). This section intends to explain the main reasons for these findings by using Buffon needle problem and the probability of crack-hitting by SAP particles (Figure 6.41). Buffon's problem considers a grid of parallel lines with spacing C and a needle length of d. When the needle is dropped "at random", so that its position and orientation are random (Chung, 1981), the needle intersects at least one line of the grid by the probability of P_T (Lin et al., 2018). Regarding SAP-modified concrete, we assume that SAP particles are randomly dispersed in the concrete mixture. As shown in Figure 6.41, crack pattern is constant in the case of the pre-cracking phenomenon. The process of tossing SAP onto the crack network generates two scenarios including: (1) SAP particles intersecting the cracks; (2) SAP are far from the crack edges. Hence, these scenarios reminds the "*Buffon needle problem*".

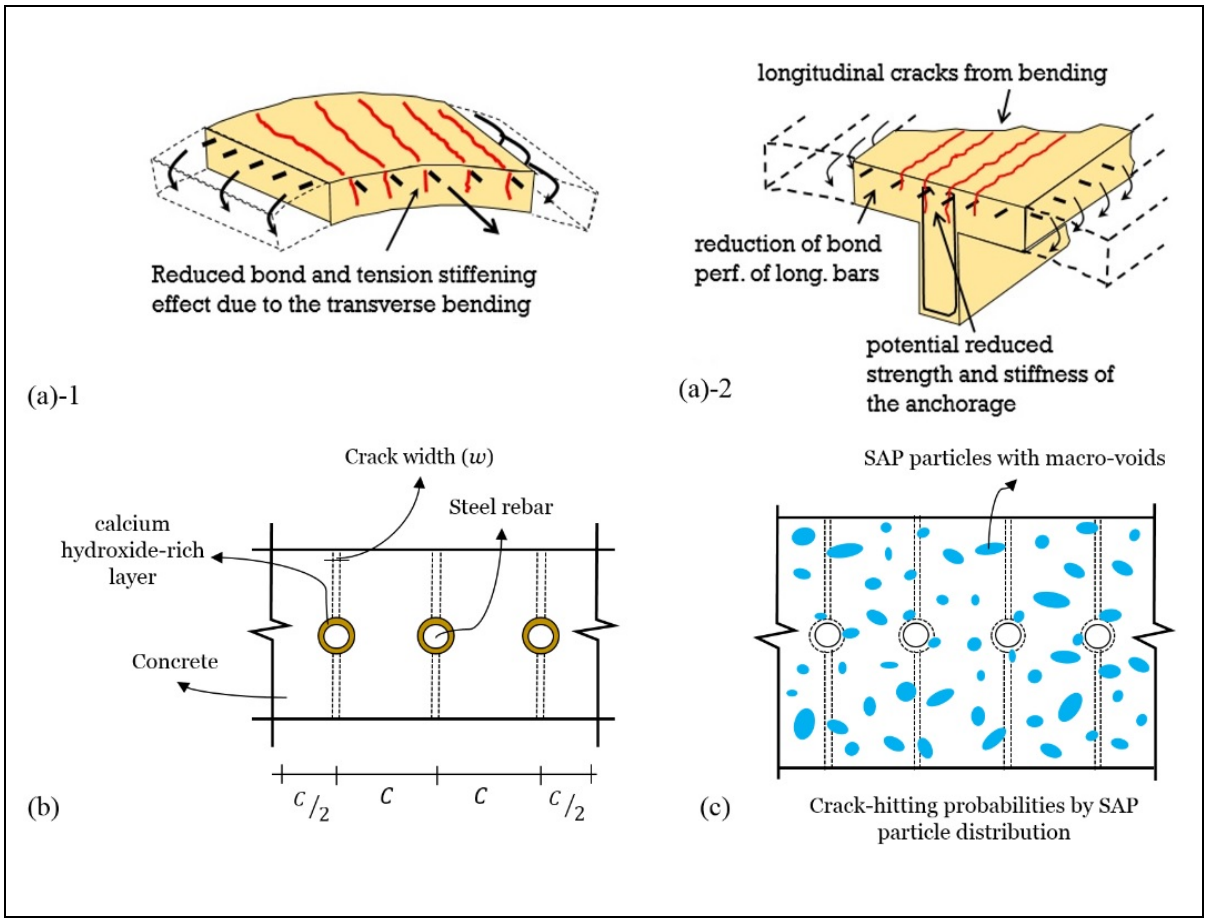

Figure 6.41 Crack-hitting probabilities in the pre-cracked concrete containing SAP: (a) practical case of pre-cracking phenomenon (Dawood & Marzouk, 2012; Rehm et al., 1978); (b) existence of $Ca(OH)_2$ around rebar for increasing the probability of crack healing; (c) application of Buffon needle problem in crack intersection by SAP particles

For SAP particles, if there are N SAP particles and the crack-hitting probabilities by the SAP (P) are considered the same, the random variable X meaning the total number of intersection in the area, and the mean of X, denoted as $E(X)$, can be given by Lin et al. (2018):

$$E(X) = N \times P_T \tag{6.10}$$

If each SAP has the ability to repair cracks of length equal to the threshold L_{heal}, the expected length of repairing the crack by N number of SAP can be written by $L_{heal} \times E(X)$. The total

length of cracks in the material is L_T. If those cracks can be completely healed, the following formulation should be fulfilled:

$$L_{heal} \times E(X) \geq L_T \tag{6.11}$$

Hence, using Eq. (6.10) into Eq. (6.11), healing capacity of SAP intersected the crack lines (L_H) can be given by Lin et al. (2018):

$$L_H = L_{heal} \times N_A \times A_T \times P_T \tag{6.12}$$

where N_A is the ratio of N/A_T. Regarding P_T of buffon needle, several studies reported Eq. (6.13) (Chung 1981; Johannesen 2008):

$$P_T = \frac{2l}{\pi C} \tag{6.13}$$

where C is the distance between cracks and l is the maximum dimension of SAP particles around the rebar. As showed in Figure 5.23(a) (Chapter 5), this length is between 1.88 mm to 2.78 mm for 0.25% and 1.0% SAP respectively. Higher values for higher SAP% can be attributed to the accumulation of SAP which is similar to higher dosages of nanoparticles. Finally, results of the present chapter can be justified by Eq. (6.12), as follows:

a) Higher SAP percentage causes a considerable impact on the healing improvement factor. This can be related to the parameter of $N \times P_T$. By increasing the SAP percentage, the Intersection probability of crack-hitting will be increased so that it causes higher healing possibilities at the rebar-concrete interface.

b) Statistical results indicate that 28-day healing periods are more efficient as compared to the 14-day healing periods. This can be attributed to the L_{heal}. Additionally, as crack width increases, self-healing capacity decreases which similarly can affect the L_{heal}. There is no specific research on studying the expected crack-repairing length by each SAP particle.

Regarding the pre-cracked concrete surrounding the rebar, there are two main potential zones including (1) zone I around the rebar with a distance of $w/2$; and (2) zone II far from the rebar as compared to zone I (Figure 6.42). Zone I is more dominant for starting the healing process due to the existence of the calcite layer around the rebar, which is essential for $CaCO_3$ precipitation as follows:

$$CaO + H_2O \rightarrow Ca(OH)_2 \qquad pH = 12.4 \tag{6.14}$$

$$Ca(OH)_2 + CO_2 \rightleftarrows CaCO_3 + H_2O \qquad pH = 9.4 \tag{6.15}$$

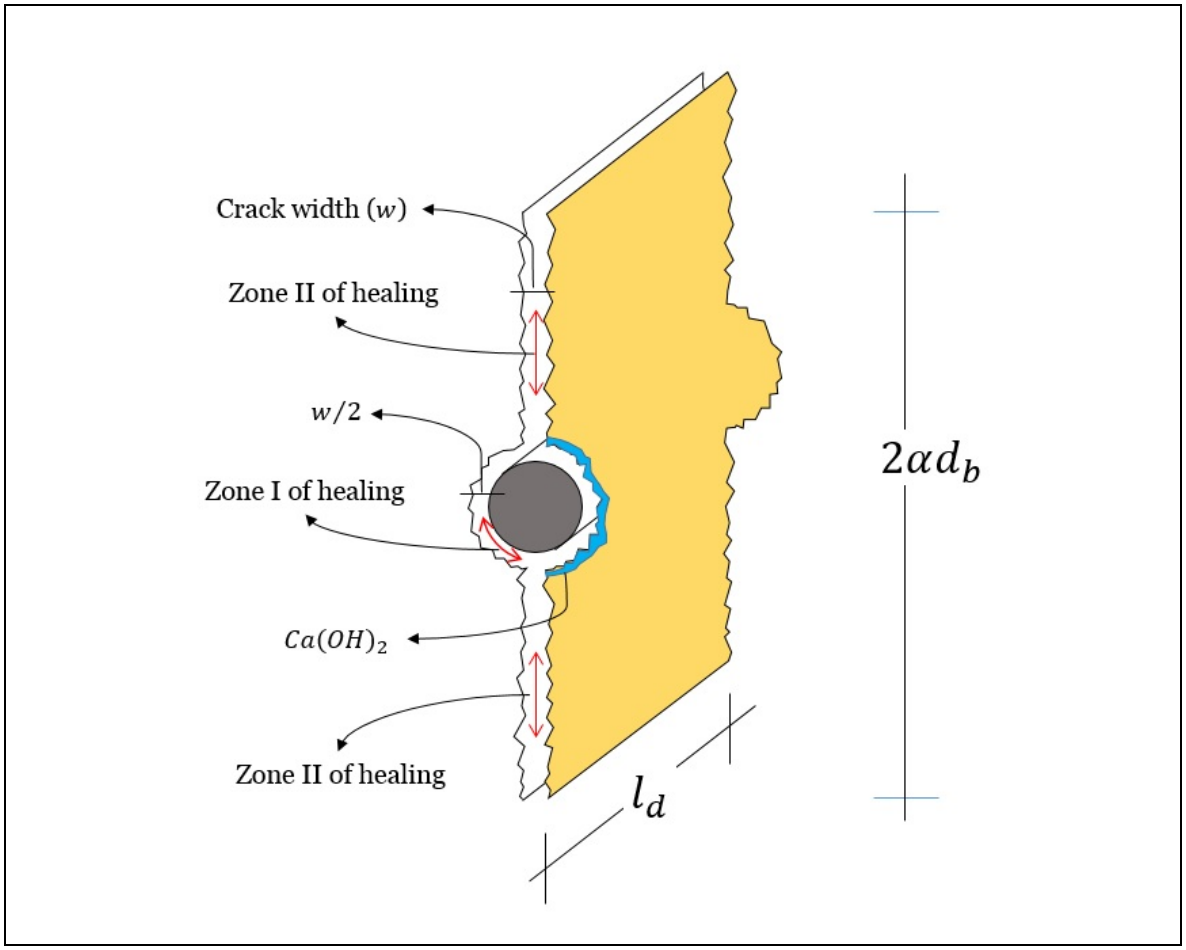

Figure 6.42 Schematic representation of different potential zones for healing

Many studies reported the enriched quantity of calcium hydroxide at the rebar-concrete interface, as compared to the bulk cement paste (Al Khalaf & Page, 1979; Chen et al., 2019; Horne et al., 2007; Page, 1975; Page & Treadaway, 1982; Sagoe-Crentsil & Glasser, 1990; Yue & Shuguang, 2001; Zayed, 1991), observed by the SEM images as well as the EDS analysis (Arya et al., 2019). To explain this phenomenon, Moreau (1973) reported that the cement particles inclined to separate from the matrix, generating a slender zone around the rebar with fewer cement particles and thus more water. This provides a layer in which Ca^{2+} ions can diffuse from outside the interface region, resulting in the formation of the considerable content of calcium hydroxide (Moreau, 1973). As shown in Figure 6.42, the domain of zone II is determined by αd_b. This distance is a controlled zone in which concrete cover has a considerable impact on bond strength and failure modes. For concrete without stirrups, the limiting value is reached when $c/d_b \geq 3.0$ (Wu & Zhao, 2012), while for concrete with a $0.4f'_c$ lateral pressure, the normalized ratio $\tau_{max}/\sqrt{f'_c}$ tends to stop increasing after $c/d_b \geq 2.0$ (Walker et al., 1997). Finally, the present chapter suggests the simplified following equations for the first potential healing volume around the rebar (Zone I), and the second scenario which is the developed version of the first scenario (zone I and zone II):

$$(V_{healed})_{zone\ I} = 3.93wd_b[2d_b + w] \tag{6.16}$$

$$(V_{healed})_{zone\ I+zone\ II} = 5wd_b[5.57d_b - 0.21w] \tag{6.17}$$

$$(V_{healed})_{zone\ I+zone\ II} > (V_{healed})_{zone\ I} \tag{6.18}$$

$(V_{healed})_{zone\ I}$ corresponds to the concrete mixtures with medium healing improvement factor, while $(V_{healed})_{zone\ I+zone\ II}$ corresponds to a high healing improvement factor. For instance, for rebar diameter of 10 mm and crack width of 0.20 mm, values of 158.77 mm^3 and 556.58 mm^3 are obtained for $(V_{healed})_{zone\ I}$ and $(V_{healed})_{zone\ I+zone\ II}$ respectively. As shown in samples after healing periods in Figure 7.43, white powders around the rebar and also at rebar

rib places are clear and the content is higher than the bulk matrix. This can clearly confirm the hypothesis presented in Figure 6.42, in which healing probability at Zone I is higher as compared to Zone II.

Figure 6.43 Healed products (white powder) content around the rebar as compared to the bulk matrix (AE concrete containing 0.25% SAP)

c) Regarding AE, the statistical results of the present chapter indicated that AE admixture has a positive impact on the healing improvement factor at the rebar-concrete interface. As shown in Figure 6.44, AE admixture provides a pore network in the matrix, which makes it easy to transfer water between SAP particles. This clearly increases the parameter L_{heal} in the Eq. (6.12). The distribution of SAP particles along with AE pores is illustrated in Figures 6.45 and 6.46 for pre-cracked and healed samples, respectively.

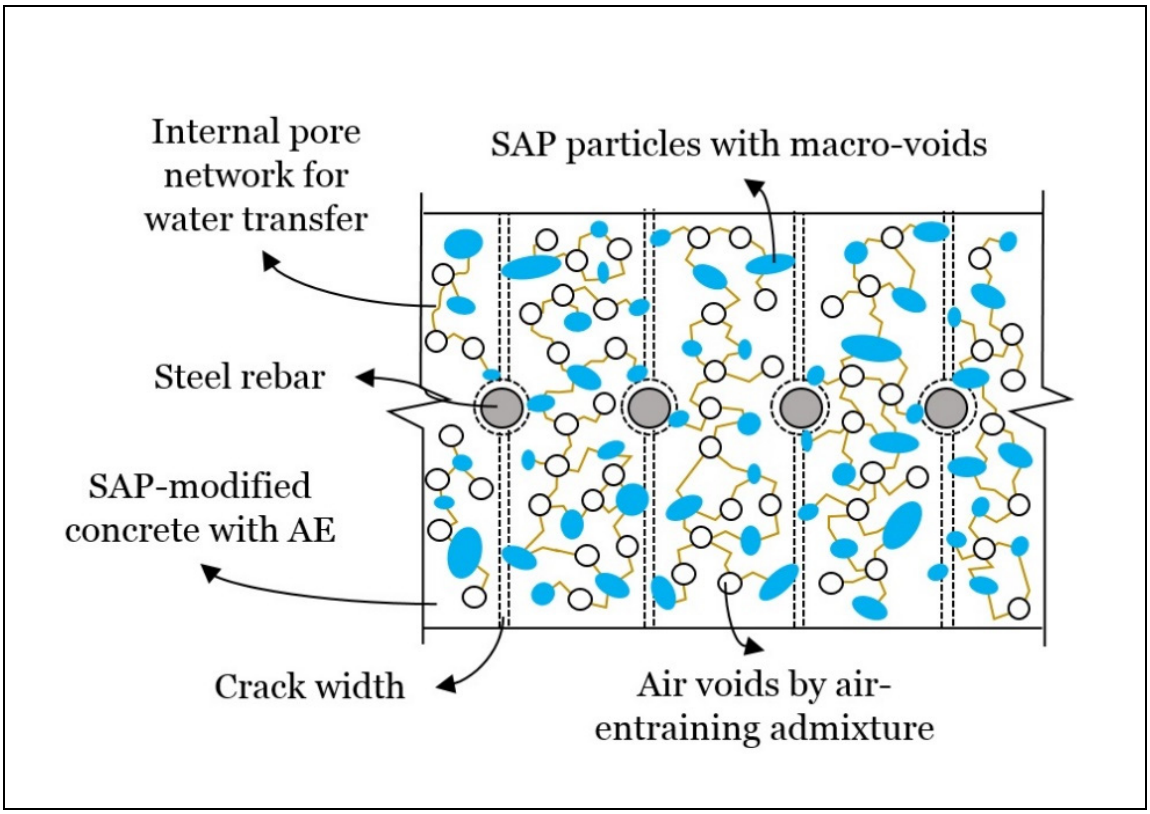

Figure 6.44 Schematic representation of the internal pore network for water transfer in self-healing method of SAP concrete containing AE admixture

It is worth mentioning that the present study is only an initial effort to determine the effect of AE admixture on the self-healing method at the rebar-concrete interface. Obviously, more research is needed to understand the optimum structure of the bubble network (volume and spacing) for different dosages of AE admixture and SAP. Moreover, different types of SAP (varied chemical composition) with different water absorptions are necessary to be tested for obtaining optimum SAP+AE-contained concrete. Furthermore, as mentioned in Eq. (6.12), results showed that L_{heal} of SAP concrete can be improved by the AE network. However, more studies are needed to quantify this parameter as a function of SAP percentage and AE dosage.

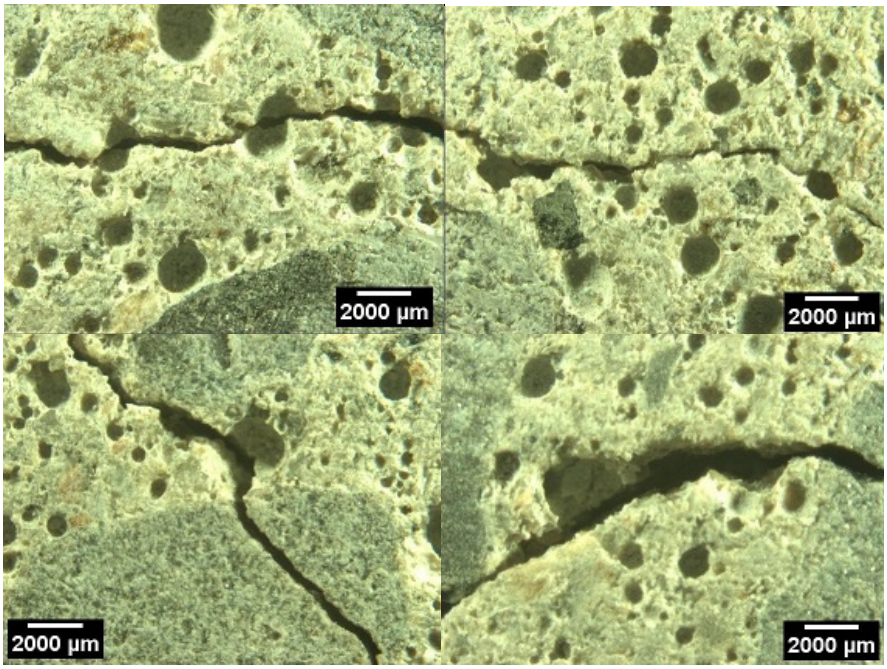

Figure 6.45 Distribution of SAP and AE pores around the crack path (0.25SAP2AE-unhealed)

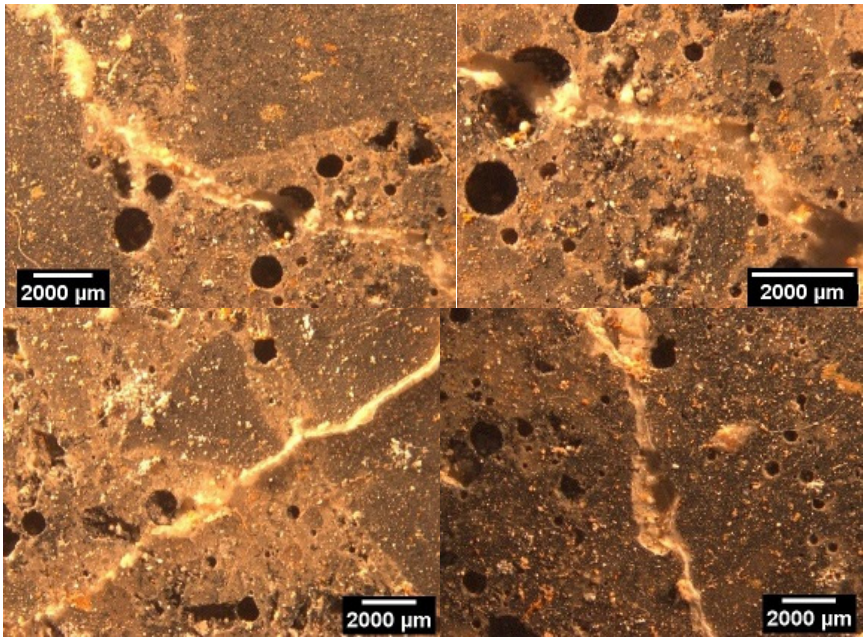

Figure 6.46 Distribution of SAP and AE pores around the crack path (1.00SAP1AE-healed)

6.6 Summary and concluding remarks

This study evaluates the effect of air-entraining admixture on interfacial properties between the steel rebar and un-cracked, pre-cracked, and healed concrete by extensive experimental tests. A comparison study is conducted between AE and non-AE concrete. Two dosages of 0.25% and 1.0% SAP and one dosage of 0.21% AE are considered for the experimental program. Additionally, a statistical approach is performed to comprehensively analyze the results. The following critical concluding remarks are drawn from the experimental and statistical results:

- The optimum dosage of 0.25% SAP is obtained for both AE and non-AE mixtures.
- AE admixture is more adaptable with SAP-1 as compared to SAP-2 for uncracked specimens so that AE concrete mixtures containing both 0.25% and 1.0% SAP-1 have similar normalized maximum and residual bond stress, and even higher average bond stress, as compared to the non-AE mixtures.
- Results of uncracked specimens show that SAP type has a significant impact on porosity patterns of AE and non-AE mixtures so that there are some conflicting results between compressive strength results and bond strength results.
- Overall, the results of the pre-cracked specimens show that the pre-cracking phenomenon has higher and more impacts on residual bond stress, as compared to the bond strength.
- AE concrete mixtures are less sensitive to the pre-cracking phenomenon, as compared to the non-AE mixtures.
- Results of the healed specimens show that SAP can improve the self-healing capacity of AE concrete for mitigating damages at the rebar-concrete interface.
- SEM results show that healing products at the external surface of crack have a considerable content of calcium (Ca), while the content is lower than the internal surfaces of cracks.
- It can be deduced from both experimental and statistical results that AE admixture can provide a stabilized bubble network along with SAP locations for improving the self-healing method.

CHAPTER 7

SELF-HEALING METHOD FOR MITIGATING PRE-CRACKING DAMAGES IN SELF-CONSOLIDATING CONCRETE USING SUPERABSORBENT POLYMER

Seyed Sina Mousavi [a], Claudiane Ouellet-Plamondon [b], Lotfi Guizani [c], and Chandrasekhar Bhojaraju [d]

[a, b, c,d] Department of Construction Engineering, École de Technologie Supérieure, 1100 Notre-Dame West, Montreal, Quebec, Canada H3C 1K3

Paper submitted for publication in *Journal of Materials in Civil Engineering*, June 2020

Abstract

Accelerated self-healing of concrete is used in the present study, by adding superabsorbent polymer (SAP) to concrete mixtures, to present an efficient approach for mitigating damages between steel rebar and self-consolidating concrete (SCC). Two different healing regimes of 14 and 28-day healing periods are considered for the experimental program. Initial bond stress, average bond stress, bond strength, and residual bond stress are considered for evaluating the results in three conditions of uncracked, pre-cracked, and healed specimens. Regarding the healed specimens, an improvement factor of bond strength healing is defined and studied. Additionally, a comparison study is conducted between the results for normal concrete (NC) and those for SCC mixtures. Two SAPs with different particle sizes and chemical compositions are considered in the experimental program. Results show that despite the higher reduction effect of SAP with smaller particle size on compressive strength, SCC containing this type of SAP has the highest bond strength in uncracked specimens, as compared to SAP with larger particle size, for both SAP-modified NC and SCC mixtures. Moreover, regarding the healed specimens, results show that SCC and NC containing SAP considerably have higher healing improvement factors for large crack widths ($w \geq 0.30$ mm) as compared to mixtures without

polymers so that almost 46%, 30%, and 24% healing improvement factors are obtained for average bond stress, bond strength, and residual bond stress of SAP-contained mixtures respectively. Although mixtures without polymer show very little improvement factor for large crack widths, complete strength recovery (100% healing improvement factor) is obtained for SCC mixture with $w = 0.10$ mm, exposed to 28-day healing periods.

Keywords*:* bond strength; superabsorbent polymer (SAP); self-consolidating concrete; self-healing

7.1 Introduction

In recent years, there is a growing interest in studying the influence of cracked concrete on bond characteristics of reinforcing bar (rebar) in reinforced concrete (RC) structures. Pre-cracking phenomenon, propagating cracks parallel to the rebar direction, cause a considerable reduction in bond strength of steel rebar in normal concrete (NC) (Brantschen et al., 2016; Mahrenholtz, 2012; Mousavi et al., 2019). Moreover, only NC was considered in their researches so that there is no specific study on the effect of the pre-cracking phenomenon in different types of concrete mixtures such as self-consolidating concrete (SCC). Additionally, very few studies concentrated on finding a practical solution to mitigate damages due to the pre-cracking phenomenon. In this context, Mousavi et al. (2019) used superabsorbent polymers (SAP) in NC mixtures (denoted as NCSAP), as a healing agent. They obtained promising results for healing cracks at the steel rebar–concrete interface after exposure to the pre-cracking phenomenon by promising healing improvement factor in NCSAP mixtures as compared to NC without polymers. However, more experimental studies are necessary to determine the effect of SAP on bond characteristics of uncracked and cracked specimens in different types of concrete mixtures. Hence, the present study intends to study the effect of the pre-cracking phenomenon in SCC mixtures as compared to NC. Also, different types of SAPs are used in SCC mixtures, denoted as SCCSAP mixtures, to mitigate damages by the self-healing method. Regarding SCC mixture containing SAP, most of the previous researches only focused on autogenous shrinkage (Han et al., 2014; Mechtcherine et al., 2006; Shi et al., 2016), drying

shrinkage (Han et al., 2014), fresh properties and passing ability (AzariJafari et al., 2016), tensile strength (Al-Hubboubi et al., 2018; Mechtcherine et al., 2006), compressive strength (Al-Hubboubi et al., 2018; Alex, 2019; AzariJafari et al., 2016; Baloch et al., 2019; Han et al., 2014; Mechtcherine et al., 2006), chloride ion permeability (Shi et al., 2016), and self-sealing and –healing cracks (Van Tittelboom et al., 2016). However, there is no specific research on the effect of SAP on interfacial properties between steel rebar and uncracked SCC specimens. As compressive strength is a crucial parameter in the bond-slip phenomenon, previous results of compressive strength of SCC mixtures containing SAP can be interesting and considerable. Generally, SAP has two main influences on the microstructure of concrete mixtures including (1) it develops the hydration reaction by internal curing, which causes strength improvement, and (2) it generates macro voids (pores) in the mixtures causing a considerable increase and reduction in the porosity and strength respectively. Most of previous studis on SCCSAP mixtures show that the existence of macro voids generated by SAP particles is the main reason for the strength reduction. To compensate the formation of macro pore with SAP adding. Mechtcherine et al. (2006) reported that using 0.40% SAP (by mass weight of cement) with a particle size of 200 μm in high-performance concrete (HPC), with a water-to-cement ratio of 0.24, causes 12.8%, 18.8%, and 25% strength reduction in compressive strength, tensile strength, and flexural strength respectively. Experimental results conducted by Han et al. (2014) showed that addition of 4.0% SAP (by mass weight of cementitious materials) with particle size ranging from 180 μm to 420 μm results in 7.1% and 11.1% reduction in compressive strength and elastic modulus of high strength SCC mixtures ($f'_c > 100\,MPa$) with a water-to-binder ratio of 0.20. AzariJafari et al. (2016) studied the characteristics of lightweight SCC mixtures containing 1.5% pre-soaked SAP (by mass weight of binder). They found strength reduction in SCCSAP mixtures ranging from 27% to 53% in mixtures with water-to-binder ratios of 0.36 and 0.39 respectively. Van Tittelboom et al. (2016) reported that addition of 0.50% SAP (particle sizes below 600 μm) in SCC mixtures causes 18.3% strength reduction in a water-to-powder ratio of 0.30. However, contrary to these studies, Al-Hubboubi et al. (2018) reported that addition of 0.50% SAP (by weight of cement) causes comparable and/or higher compressive strength as compared with reference SCC mixture so that 1.7% strength reduction, 5.2% strength improvement, and 6.5% strength improvement were obtained

for water curing, moist curing, and air curing methods respectively. A slight increase in the mechanical properties due to the SAP addition in the SCC mixture was also reported by Alex (2019). Generally, experimental observations of the previous studies indicate that the chemical composition of SAP, the particle size of SAP, and the initial water-to-cement ratio of the mixture have significant effects on the probability of occurrence strength reduction or improvement in SCCSAP mixtures.

Only a few studies determined the autogenous healing capacity of SCC mixtures with and without any polymer. Şahmaran et al. (2008) studied the effect of the self-healing method in SCC mixtures incorporating high volumes of fly ash (35% and 55%). After the pre-loading process, they kept specimens in water for 28 days and subsequently, the mechanical and permeation properties were measured. Promising self-healing results were observed in their results. Fly ash-based SCC had a significant content of unhydrated fly ash particles available in its microstructure which was efficient for healing the pre-existing cracks by the formation of C–S–H gels. In this field, Ramadan & Haddad (2017) investigated the potential of the self-healing method and strength recovery in SCC pavement. Their results showed that re-curing (healing) in water is more efficient as compared to only air curing to heal cracks so that damaged SCC specimens recovered compressive strength by 58% (Ramadan and Haddad 2017). Takagi et al. (2015) reported that the mechanical strength recovery is higher in SCC mixtures containing blast furnace slag cement (up to 55%) as compared to other Brazilian types of cement. They also recommended that the wet-dry cycle is more efficient than only wet conditions for the self-healing method in SCC. Sasi (2018) investigated the effect of sodium silicate (Na_2SiO_3) and polyurethane on the self-healing capacity in SCC inserted by the pharmaceutical capsule and cementitious hollow tubes. They found that the self-healing ability of SCC can be effectively improved by using self-healing agents such as sodium silicate and polyurethane by the optimum dosage of about 4.0%. However, a limited number of previous efforts worked on the self-healing methods in SCC using SAP. In this context, Van Tittelboom et al. (2016) used encapsulated polyurethane and SAP in SCC mixtures to achieve self-healing concrete by monitoring the crack-sealing of RC beams. Their results show that the crack-sealing ratio for the SCC mixture containing SAP particles is significantly higher as compared

to mixtures with encapsulated polyurethane. However, there is no specific study for determining the effect of SAP on strength recovery after exposure of initial damages.

Thus, the present study concentrates on determining the effect of using SCC on the pre-cracking phenomenon at the steel rebar-concrete interface and checking the efficiency of using SAP, as a healing agent, on mitigating damages. Accordingly, the present study intends to address the following objectives:

1. Determine the influence of crack width on bond characteristics of steel rebar embedded in cracked SCC specimens as compared to NC.
2. Study the effect of 0.25% SAP-1 and SAP-2 on bond properties of steel rebar embedded in uncracked and cracked SCC specimens, as compared to NC.
3. Check the performance of SAP particles in healing cracks and mitigating damages at the rebar-concrete interface.

To address these objectives, an extensive experimental program is performed in the present study. A number of 94 pull-out specimens are prepared and tested in three different statuses of uncracked, pre-cracked, and healed specimens are considered in the experimental program. Two concrete types of SCC and NC mixtures are provided containing two different SAPs with different particle size and chemical composition. Consequently, a comparison study is conducted between NCSAP and SCCSAP mixtures.

7.2 Experimental program

7.2.1 Material properties

Six different concrete mixtures are considered for this study to determine the effect of SAP on bond characteristics of NC and SCC in three statuses of uncracked, pre-cracked, and healed specimens. Initial water-to-cement ratios of 0.41 and 0.51 are considered for reference NC and SCC respectively, while a constant initial water-to-powder ratio of 0.41 is considered for both mixtures. General use (GU) cement is used for all mixtures with a density of 3.15 g/cm^3 and maximum particle size about 70 μm. Limestone powder is used as a filler with a relative density

of 2.68 and a maximum particle size of about 200 μm. The particle size distribution of the cement and limestone powder is illustrated in Figure 7.1. Natural sand with a maximum grain size of 1.25 mm and a specific gravity of 2.68, and gravel with a nominal maximum diameter of 20 mm and a particular gravity of 2.68 are considered for mixtures. Two types of SAP are considered for the experimental program including (1) SAP1: a cross-linked copolymer of acrylamide and potassium acrylate with maximum particle size and d50 of 500 μm and 260 μm respectively. SAP1 has water absorption capacities of 249 g/g and 25 g/g/ in deionized water and pore solution respectively; (2) SAP2: a cross-linked anionic polyacrylamide with maximum particle size and d50 of 150 μm and 47 μm respectively. SAP1 has water absorption capacities of 170 g/g and 25 g/g/ in deionized water and pore solution respectively. Both SAPs have average specific gravity and bulk density of around 1.50 and 0.83 respectively. The tea bag method, slump test method, and water desorption method (the absorption of a centrifuged cement pore solution) were used to measure the water absorption capacity of SAPs. The SAP is added by 0.25 wt.% of cement. Particle size distributions of SAP samples are illustrated in Figure 7.1. Also, SEM images of SAP particles are shown in Figure 7.2. SAP particles were produced through the bulk polymerization technique, in which blocks of polymers are shredded into particles of irregular shapes. To adjust the flowability and stability of SCC mixtures, superplasticizer and viscosity-modifying admixture are used, respectively. A constant proportion of superplasticizer is used for both SCC and SAP-modified SCC mixtures to keep the slump above 500 mm, as recommended by JSCE (1999), ASTM-C1611/C1611M (2009), and Nagataki & Fujiwara (1995). The concrete composition of mixtures is illustrated in Table 7.1. NC mixtures containing 0.25% SAP1 and 0.25%SAP2 are identified by NC SAP1 and NCSAP2 respectively throughout the paper. Similar mix identification is considered for SCC mixtures. Additional water is added to mixtures containing SAP with a dosage of 25 grams of water per gram of dry SAP to adjust the fresh state of mixtures with reference NC and SCC. Fresh properties of mixtures are also mentioned in Table 7.1.

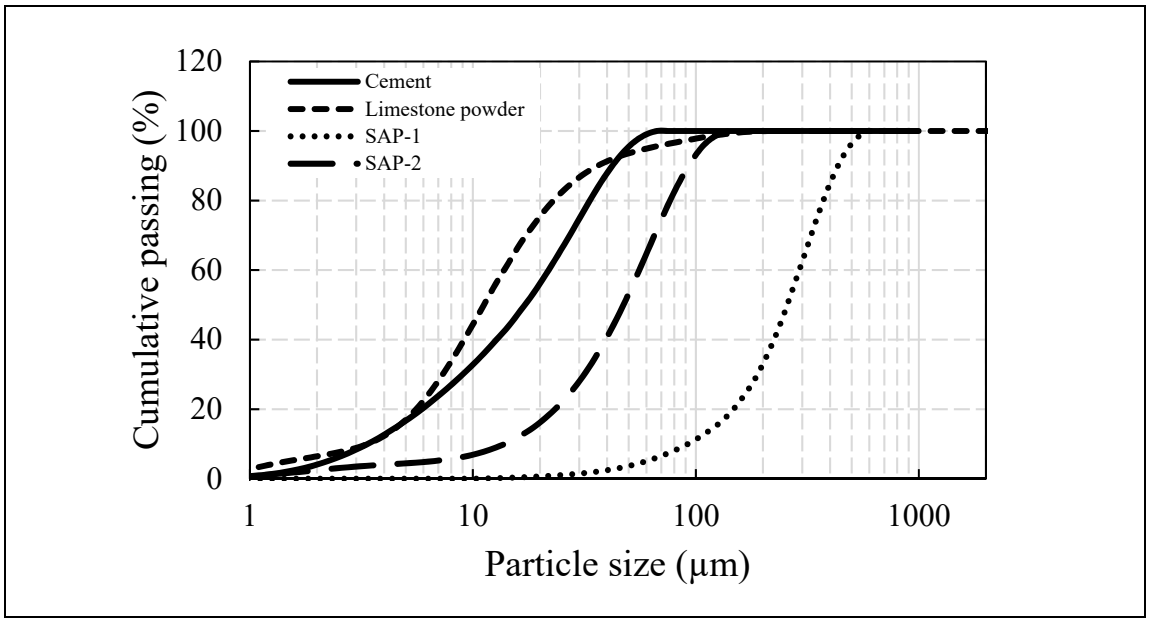

Figure 7.1 Particle size distribution of the powders used in the present study

Table 7.1 Mix proportions of concrete mixtures (parentheses denote standard deviation)

Constituent	Quantity (kg/m^3)					
	NC	**NCSAP1**	**NCSAP2**	**SCC**	**SCCSAP1**	**SCCSAP2**
Water (w)	165	165	165	215	215	215
Cement (GU) (c)	395	395	395	420	420	420
Limestone powder	-	-	-	105	105	105
Total powder	395	395	395	525	525	525
Superabsorbent polymer [1]	-	0.99	0.99	-	1.31	1.31
Fine aggregate	788	788	788	940	940	940
Coarse aggregate (5-10 mm)	822	822	822	352	352	352
Coarse aggregate (10-14 mm)	258	258	258	219	219	219
Coarse aggregate (14-20 mm)	-	-	-	270	270	270
Superplasticizer	2.34	3.5	3.3	5.0	5.0	5.0
Additional water	-	24.8	24.8	-	32.8	32.8
VMA	-	-	-	2.5	2.5	2.5
Total w/c	0.41	0.48	0.48	0.51	0.59	0.59
Total w/p [2]	0.41	0.48	0.48	0.41	0.47	0.47
Slump (mm)	97	104	109	709	618	675
T_{50} (s)	-	-	-	2.37	3.80	2.30
Hardened density (kg/m^3)	2453.8	2416.8	2419.2	2375.7	2330.6	2346.0
Compressive strength (MPa)	58.82 (1.39)	54.36 (1.20)	46.83 (0.17)	40.34 (0.72)	43.63 (0.54)	37.24 (0.46)

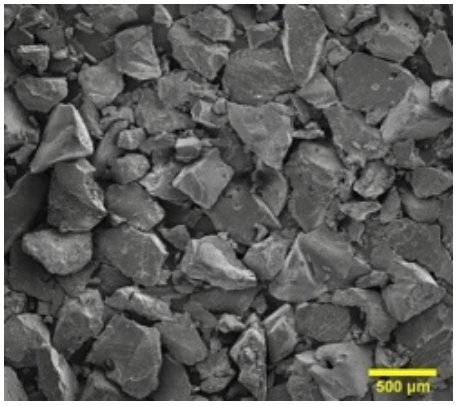

(a)

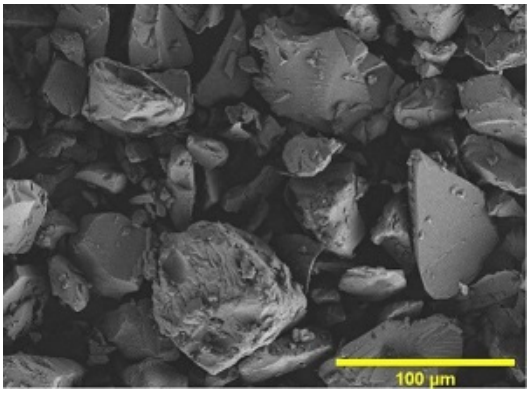

(b)

Figure 7.2 SEM image of SAP particles: (a) SAP-1; (b) SAP-2

7.2.2 Test set-up and analyze procedure

Cylindrical specimens with dimensions of 150 mm × 113 mm are considered for specimens (Figure 7.3) with a concrete cover of 75 mm. Steel rebars are positioned at the center of cylinders for all specimens with a nominal diameter of 10 mm, average rib–face angle of 55 degrees, rib height of 1.89 mm, rib spacing of 13.22 mm, and rib spacing-to-rib height ratio of 7.0. Specified yield strength and ultimate tensile strength of steel rebars are 432 and 620 MPa respectively. Pre-cracking simulation is applied to the specimens by controlled splitting tests. Crack gauges are installed to control the crack width. However, due to the brittle behaviour of concrete, direct measurement of crack width is considered instantly after finishing the splitting test. Then direct pull-out tests, with a displacement rate of 0.50 mm/min, are conducted after three stages of uncracked (without splitting test), pre-cracked, and healed (after 14 and 28 days re-curing) specimens. Based on empirical observations, the displacement rate of 0.11-0.15 mm/min is considered for splitting tests. Experimental test set-ups are shown in Figure 7.3.

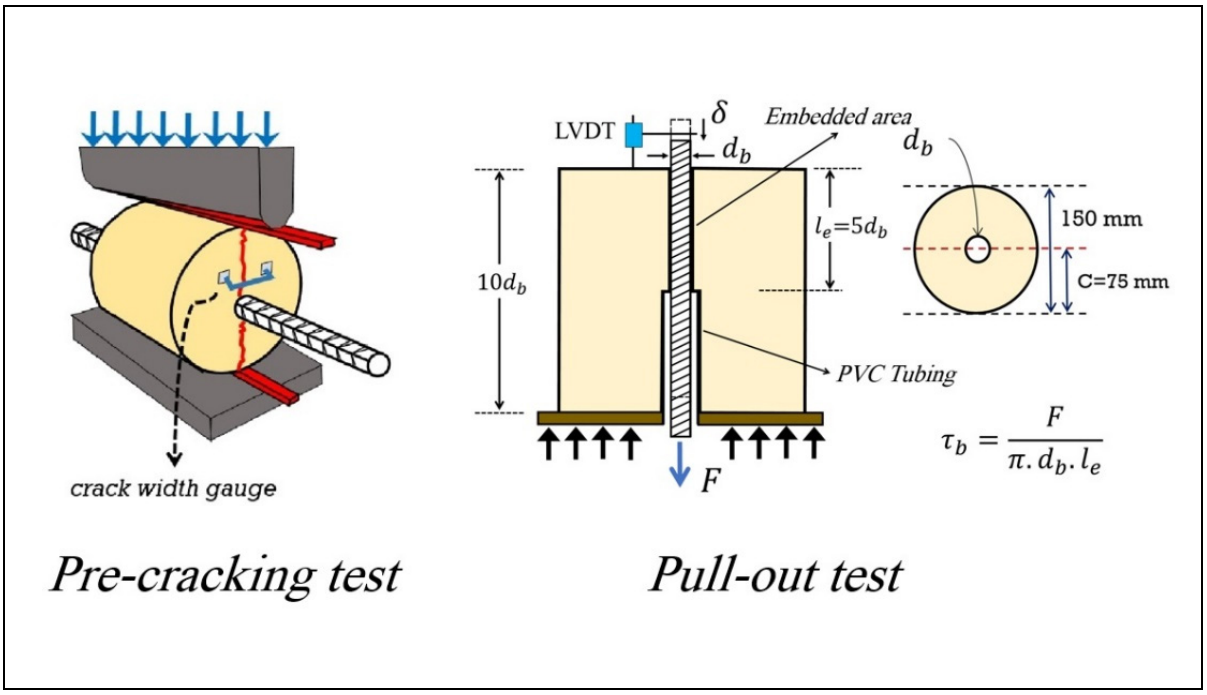

Figure 7.3 Experimental test set-ups

To prevent corrosion influences for 28-day healing periods, the heat-shrinkable tube is used along the rebar at both end sides of specimens. To analysis the results of SCC and compare them with NC, different bond parameters are considered, as shown in Figure 7.4, including bond strength (τ_u), average bond stress (τ_m), residual bond stress (τ_r), and bond energy which is the area under bond-slip curve till rebar slippage of 10 mm (E). Average bond stress (τ_m) is recommended by RILEM (Recommendation RC 6, append to RILEM TC (1994)) as the arithmetic mean of bond stresses of $\tau_{0.01}$, $\tau_{0.10}$, and $\tau_{1.00}$ corresponding to slips of 0.01 mm, 0.10 mm, 1.00 mm respectively, which is illustrated in Figure 7.4.

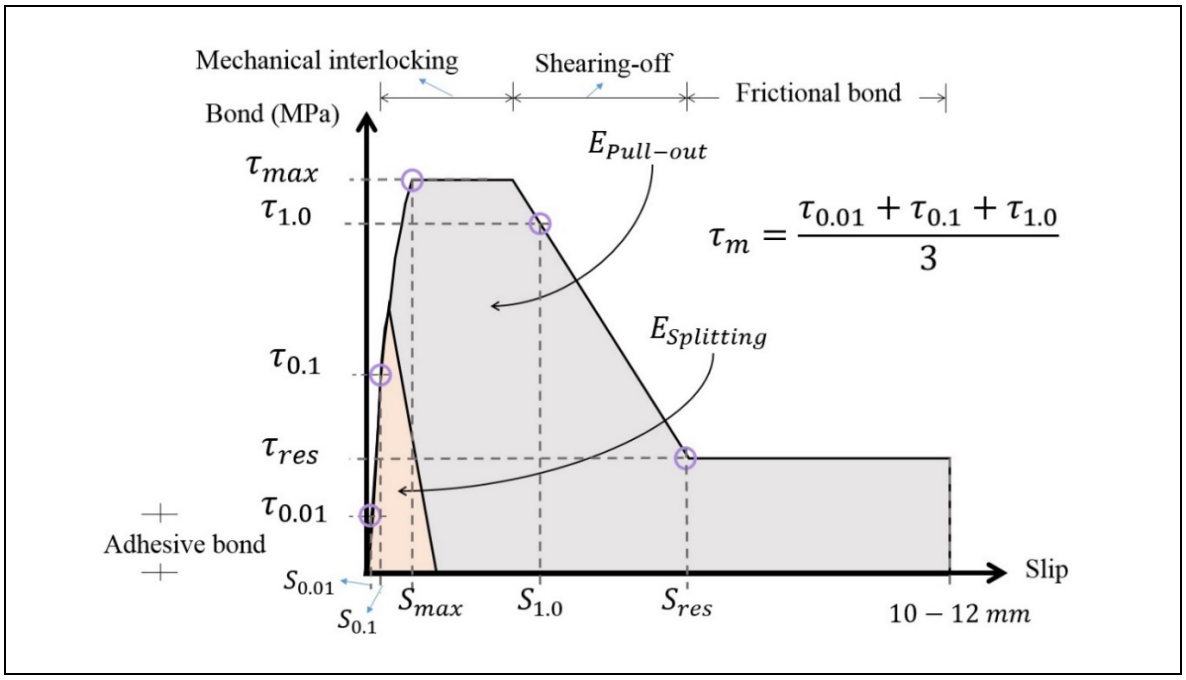

Figure 7.4 Bond parameters of bond-slip curves considered for the present study

7.3 Results and discussions

7.3.1 Uncracked specimens

Results of uncracked, pre-cracked, and healed SCC are summarized in Table 7.2. Crack width, compressive strength, average bond stress, maximum bond stress (bond strength), residual bond stress, bond energy, number of specimens, and failure modes are mentioned in Table 7.2. A total number of 94 pull-out specimens are tested in the present study. As shown in Figure 7.5(a), results show that pull-out failure mode is observed for uncracked specimens. Concrete cover-to-rebar diameter ratio of around 7.5 and rib spacing-to-rib height ratio of 7.0 provide enough confinement surrounding the steel rebar preventing splitting failure mode.

Table 7.2 Experimental results and failure modes

Specimen	w	τ_m	τ_u	τ_r	E	IF_m	IF_u	IF_r	n	Failure mode
	(mm)	MPa			(N/mm)	%				
NC	0.00	17.40 (2.07)	25.79 (1.15)	6.50 (1.46)	152.51 (9.66)	-	-	-	3	P, P, P
NCC0.2	0.20	7.35 (-)	18.05 (-)	0.043 (-)	12.57 (-)	-	-	-	1	S
NCC0.3	0.30	3.72 (0.19)	11.64 (1.74)	0.33 (0.46)	8.92 (0.19)	-	-	-	2	S, S
NCC0.4	0.40	1.68 (0.35)	4.61 (0.14)	0.087 (0.12)	2.56 (2.02)	-	-	-	2	S, S
NC/14H0.3	0.30	2.98 (0.97)	9.35 (2.77)	0.83 (0.43)	4.70 (1.31)	+0.91 (1.58)	0	+8.07 (6.90)	3	S, S, S
NC/28H0.3	0.30	6.73 (1.78)	11.84 (0.60)	0.80 (0.82)	20.96 (23.81)	+22.02 (13.01)	+2.14 (3.50)	+8.87 (11.58)	3	S, S, S
NC/28H0.4	0.40	3.0 (-)	5.82 (-)	1.64 (-)	3.77 (-)	+8.40 (-)	+5.69 (-)	+24.14 (-)	1	S
NCSAP1	0.00	12.57 (0.80)	24.37 (0.31)	8.11 (0.65)	148.66 (13.97)	-	-	-	3	P, P, P
NCSAP1C0.3	0.30	3.29 (0.09)	9.85 (0.19)	0.32 (0.07)	7.10 (3.35)	-	-	-	2	S, S
NCSAP1C0.4	0.40	3.20 (0.42)	5.56 (0.03)	1.46 (1.08)	17.85 (4.45)	-	-	-	2	S, S
NCSAP1C0.5	0.50	0.83 (-)	2.58 (-)	0.40 (-)	7.25 (-)	-	-	-	1	S
NCSAP1/14H0.3	0.30	3.04 (0.65)	10.44 (4.46)	1.26 (0.66)	5.49 (1.86)	+1.149 (1.63)	+12.89 (18.22)	+12.12 (8.53)	2	S, S
NCSAP1/14H0.4	0.40	2.05 (0.04)	4.26 (0.73)	0.44 (0.03)	2.62 (0.22)	0	0	0	2	S, S
NCSAP1/28H0.3	0.30	3.73 (1.20)	12.20 (2.08)	1.24 (0.27)	8.14 (0.34)	+7.73 (8.58)	+16.20 (14.33)	11.78 (3.45)	3	S, S, S
NCSAP1/28H0.4	0.40	1.73 (-)	7.06 (-)	1.13 (-)	5.06 (-)	0	+7.97 (-)	0	1	S
NCSAP2	0.00	12.61 (0.79)	25.02 (0.15)	9.08 (1.13)	154.60 (20.31)	-	-	-	3	P, P, P
NCSAP2C0.15	0.15	5.04 (1.43)	13.97 (2.80)	1.76 (1.29)	13.22 (1.46)	-	-	-	2	S, S
NCSAP2C0.3	0.30	2.57 (0.12)	5.69 (2.37)	1.66 (0.12)	4.90 (3.21)	-	-	-	2	S, S
NCSAP2/14H0.2	0.20	3.34 (1.16)	7.98 (1.06)	1.03 (0.92)	4.70 (0.58)	+0.11 (0.16)	0	0	2	S, S
NCSAP2/14H0.3	0.30	2.39 (0.38)	7.03 (0.01)	0.67 (0.45)	4.35 (1.03)	+0.47 (0.66)	+6.91 (0.05)	0	2	S, S
NCSAP2/28H0.3	0.30	1.95 (0.88)	7.89 (0.01)	0.47 (0.28)	6.07 (1.27)	+0.033 (0.047)	+11.37 (0.07)	0	2	S, S
NCSAP2/28H0.35	0.35	0.82 (-)	6.58 (-)	0 (-)	2.92 (-)	0	+20.60 (-)	0	1	S
SCC	0.00	15.32 (0.63)	24.61 (0.61)	12.21 (0.72)	176.18 (4.69)	-	-	-	3	P, P, P
SCCC0.1	0.10	16.38 (-)	23.20 (-)	4.97 (-)	107.96 (-)	-	-	-	1	P
SCCC0.2	0.20	6.79 (1.64)	18.31 (1.43)	0.69 (0.86)	25.24 (21.12)	-	-	-	3	S, S, S
SCCC0.3	0.30	5.37 (3.57)	14.72 (0.55)	0.22 (0.19)	11.66 (8.08)	-	-	-	2	S, S
SCCC0.4	0.40	5.14 (0.57)	10.11 (0.29)	0.17 (0.09)	9.78 (2.92)	-	-	-	2	S, S
SCC/14H0.3	0.30	4.65 (1.76)	9.12 (4.33)	0.13 (0.06)	7.40 (7.38)	+2.61 (3.70)	0	0	2	S, S
SCC/28H0.1	0.10	13.17 (-)	25.32 (-)	2.41 (-)	49.70 (-)	0	+100 (-)	0	1	P
SCC/28H0.25	0.25	8.99 (-)	16.80 (-)	0.36 (-)	18.86 (-)	+17.09 (-)	+0.91 (-)	+1.22 (-)	1	S
SCC/28H0.4	0.40	1.71 (-)	6.60 (-)	0.13 (-)	2.60 (-)	0	0	0	1	S
SCCSAP1	0.00	13.21 (0.69)	24.50 (1.19)	11.02 (0.17)	166.36 (7.19)	-	-	-	2	P, P
SCCSAP1C0.3	0.30	4.29 (0.04)	10.44 (2.65)	0.33 (0.02)	12.41 (2.64)	-	-	-	2	S, S

Table 7.2 Experimental results and failure modes (continued)

Specimen	w	τ_m	τ_u	τ_r	E	IF_m	IF_u	IF_r	n	Failure mode
	(mm)	MPa			(N/mm)	%				
SCCSAP1C0.4	0.40	2.07 (0.13)	4.39 (0.54)	0.42 (0.02)	8.33 (2.27)	-	-	-	2	S, S
SCCSAP1/14H0.3	0.30	5.44 (0.42)	11.08 (1.82)	0.18 (0.03)	9.32 (0.55)	+12.93 (4.67)	+7.14 (9.61)	0	3	S, S, S
SCCSAP1/14H0.4	0.40	1.46 (0.40)	3.27 (0.59)	0.10 (0.06)	2.15 (0.69)	0	0	0	2	S, S
SCCSAP1/28H0.3	0.30	5.0 (1.89)	13.05 (3.43)	0.30 (0.04)	11.39 (4.67)	+11.55 (17.87)	+18.55 (24.41)	+0.047 (0.09)	4	S, S, S, S
SCCSAP1/28H0.4	0.40	2.89 (-)	7.33 (-)	0.10 (-)	5.89 (-)	+7.36 (-)	+14.62 (-)	0	1	S
SCCSAP2	0.00	16.45 (1.87)	25.20 (0.56)	6.75 (1.50)	125.91 (13.59)	-	-	-	3	P, P, P
SCCSAP2C0.3	0.30	6.23 (0.86)	13.40 (0.52)	0.095 (0.01)	9.46 (2.99)	-	-	-	2	S, S
SCCSAP2C0.4	0.40	4.13 (0.40)	8.12 (0.21)	0.11 (0.08)	5.18 (0.91)	-	-	-	2	S, S
SCCSAP2/14H0.3	0.30	8.40 (1.00)	16.75 (2.35)	0.64 (0.45)	17.67 (7.47)	+21.23 (9.83)	+28.56 (19.60)	+8.19 (6.75)	4	S, S, S, S
SCCSAP2/14H0.4	0.40	3.65 (-)	7.39 (-)	0.17 (-)	4.35 (-)	0	0	0.90 (-)	1	S
SCCSAP2/28H0.3	0.30	9.81 (2.82)	16.90 (2.63)	0.35 (0.25)	17.10 (8.29)	+35.07 (2.82)	+29.66 (22.22)	+3.97 (3.64)	5	S, S, S, S, S
Range of parameter	0.10 $\leq w \leq$ 0.50	0.8-19.5	2.6-27.1	0.0-14.5	1.1-180.6	0.0 to +45.50	0.0 to +100.0	0.0 to +24.14	All specimens $n = 94$	

Figure 7.5 Failure modes of SCC specimens: (a) pull-out in uncracked concrete; (b) pull-out in cracked concrete with $w = 0.10$ mm; (c) splitting in healed specimens and cracked concrete with $w > 0.10$ mm

Bond-slip curves of uncracked specimens for NC and SCC mixtures are illustrated in Figure 7.6. In the case of NC mixtures, although similar bond-slip curves are obtained for NCSAP mixtures, SAP1 and SAP2 cause an initial reduction in ascending branch of the bond-slip curve after 10 MPa and 5 MPa bond stress respectively (Figure 7.6(a)). This corresponds to the mechanical interlocking effect before the maximum bond stress (bond strength), as schematically shown in Figure 7.4. This is the stage of first cracking where rebar lugs induce large bearing stresses in the surrounding concrete and transverse micro-cracks originate at the tips of the lugs allowing the rebar to slip. Observation shows the higher impact of SAP2 on initial bond reduction as compared to SAP1. However, as shown in Figure 7.6(b), contrary to NC, SAP2 has no effect on the initial stiffness of the ascending part, while SAP1 causes a

considerable reduction in the initial stiffness of the ascending part. These observations clearly indicate that type of SAP can affect bond stiffness in different concrete compositions. Moreover, Figure 8.6 shows that this effect initiates at specific bond stress ranging from 5 MPa to 10 MPa.

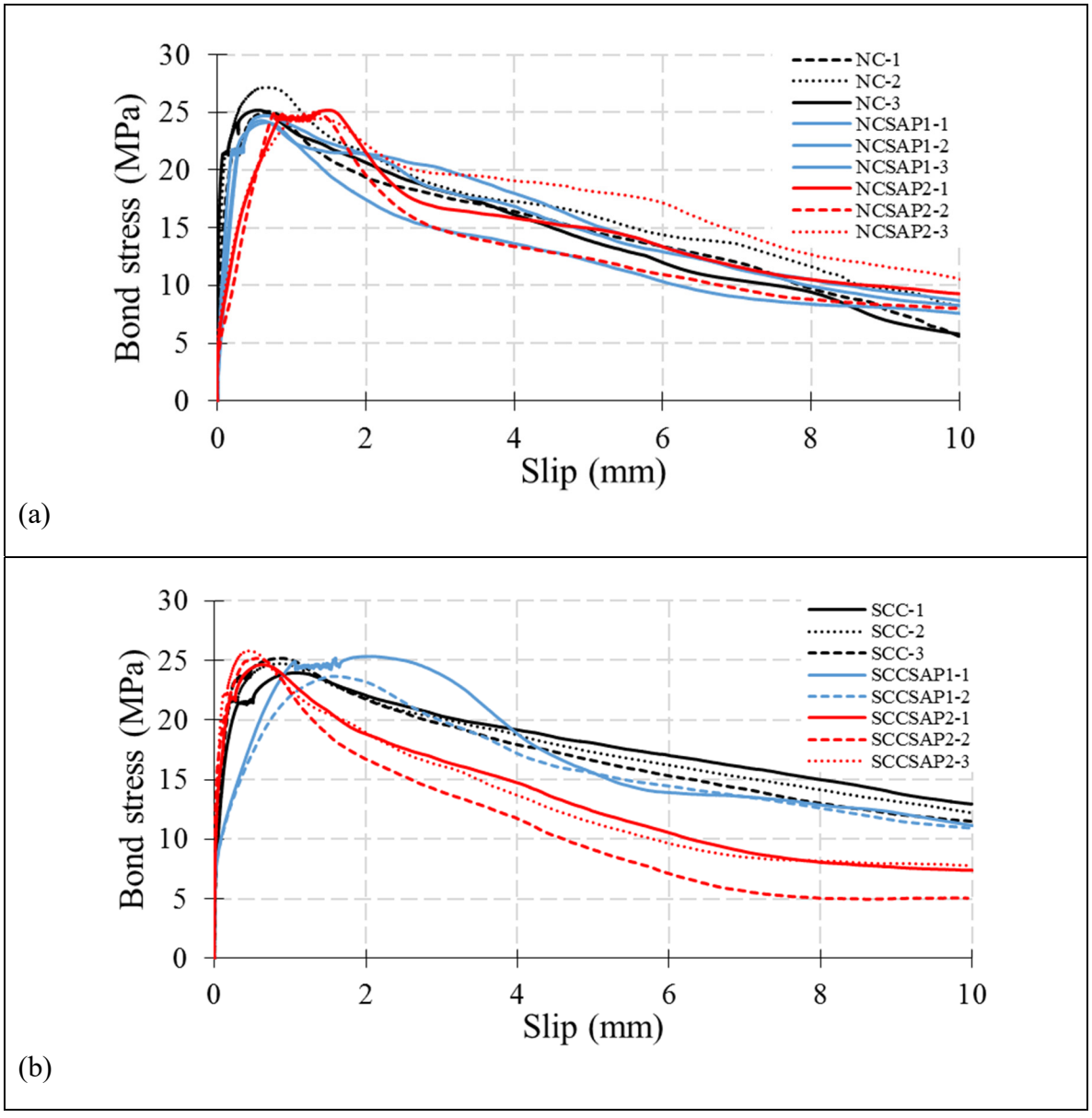

Figure 7.6 Bond-slip curves of uncracked specimens:
(a) NC mixtures containing SAP; (b) SCC mixtures containing SAP

Compressive strength of mixtures is shown in Figure 7.7(a). Results show that SCC mixture has lower compressive strength as compared to NC with the same water-to-powder ratio. Results indicate that mixtures containing SAP1 have comparable and slightly higher compressive strength as compared to reference mixtures, while SAP2 causes a considerable reduction in compressive strength. This reduction effect is more crucial for NC mixtures (20.4% reduction) than SCC mixtures (8.3% reduction). This may be attributed to the smaller particle size of SAP2 as compared to SAP1, which produces more macro-voids in the bulk matrix. Bond parameters of uncracked specimens are extracted from bond-slip curves, shown in Figure 7.7(b). Average bond stress, bond strength, and residual bond stress of mixtures are extracted from bond-slip curves. Also, bond stress corresponds to the slip of 0.01 ($\tau_{0.01}$) is obtained to show the primary stiffness of the curves before the initial stiffness explained in Figure 7.6. Results show that SCC has lower primary bond stress ($\tau_{0.01}$) and average bond stress (τ_m), while comparable and higher bond strength (τ_u) and residual bond stress (τ_r) are obtained for SCC respectively. Higher bond strength of SCC than NC was reported by the literature (Mousavi et al., 2017; Mousavi et al., 2016). As shown in Figure 7.7(b), even though SAP1 and SAP2 cause similar bond strength of mixtures to the reference mixtures, SAP2 is more efficient by having higher bond strength, average bond stress, and primary bond stress as compared to SAP1. However, there is no clear trend for the residual bond stress of mixtures. Results show that SAP causes higher residual bond stress in NC mixtures while it has a contradictory impact on SCC mixtures. By comparing Figures 7.6(a) and (b) it can be deduced that although SAP2 produces more macro-voids in the bulk matrix of both NC and SCC mixtures resulting in lower compressive strength while providing a better interface between steel rebar and surrounding concrete. For explaining this phenomenon, normalized bond properties are shown in Figure 7.7(c) with the square root of compressive strength. Previous researches along with concrete design codes used normalized value of bond strength to concentrate on the rebar-concrete interface than the bulk matrix (Wu & Zhao, 2012).

Generally, normalized results indicate that SCC mixtures have higher normalized bond properties as compared to NCC mixtures, especially SAP2 so that SCCSAP2 is the optimum mixture among all concrete mixtures of the present study. This can be attributed to the filling

and passing abilities of SCC mixtures with high workability, which reduces the porosity at the rebar-concrete interface. Using lower content of coarse aggregate and higher content of filler material can affect this phenomenon in SCC mixtures. In the case of normalized bond strength ($\tau_u{}^* = \tau_u/\sqrt{f'_c}$), results show that SAP2 is considerably more efficient as compared to SAP1. NCSAP1 and SCCSAP1 mixtures have comparable normalized bond strength as compared with reference mixtures.

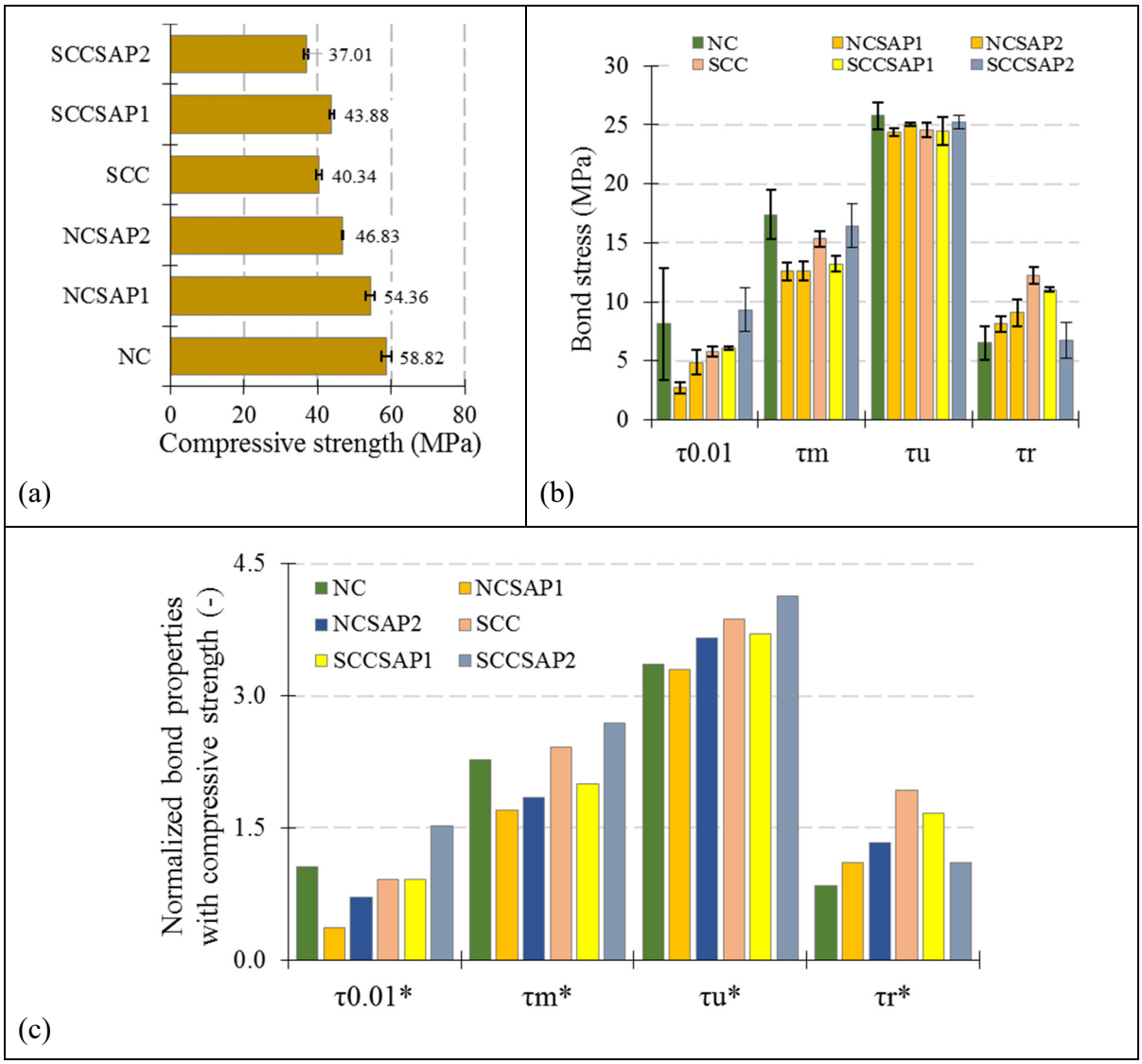

Figure 7.7 Comparison of uncracked concrete results:
(a) compressive strength; (b) bond characteristics;
(c) normalized bond properties with the square root of compressive strength

To study the adhesive bond of mixtures, primary bond stress ($\tau_{0.01}$) is defined in the present study. This can clearly be deduced from bond-slip curves of mixtures until the slip of 0.05 mm (Figure 7.8). This low bond stress at a low slip range corresponds to chemical adhesion between the rough steel surface and the surrounding concrete (Tassios, 1979). Highly localized stress is existed close to lug tips (elastic behaviour) at the end of this stage. Regarding primary normalized bond stress in NC ($\tau_{0.01}{}^{*} = \tau_{0.01}/\sqrt{f'_c}$), Figure 7.7(c) shows that both NCSAP1 and NCSAP2 have lower bond stress as compared with NC, which continues until the slip corresponds to the maximum bond stress (Figure 7.6(a)). Although NCSAP2 has higher primary bond stress as compared to NCSAP1 (Figure 7.8(a)), lower initial stiffness at the ascending branch of bond-slip curve is observed in Figure 7.6(a). Changing interfacial behaviour happens from the chemical adhesive bond stage to the mechanical interlocking bond stage. In the case of SCC mixtures, SAP2 causes reduction in the initial stiffness in ascending branch (Figure 7.6(b)), while has no effect on primary bond stress (chemical adhesive bond, Figure 7.8(b)).

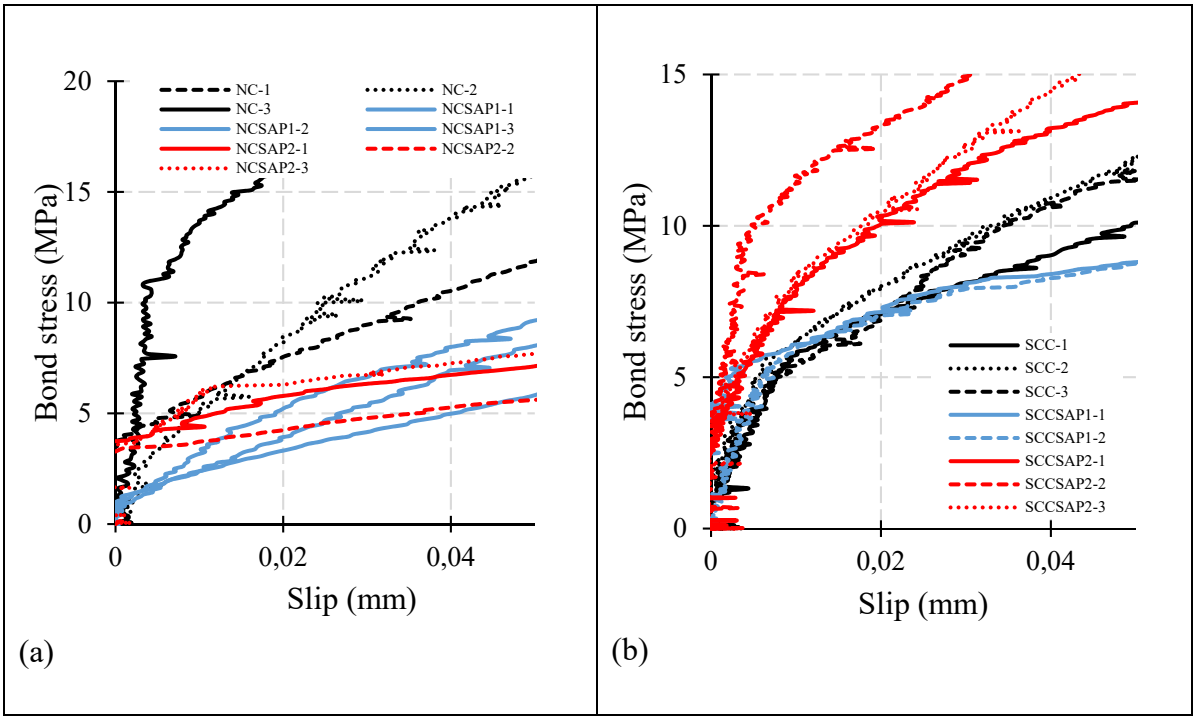

Figure 7.8 Bond-slip curves of uncracked specimens until slip of 0.05 mm:
(a) NC mixtures containing SAP; (b) SCC mixtures containing SAP

The area under bond-slip curves of uncracked specimens, denoted as “absorbed energy by bond mechanism”, is illustrated in Figure 7.9. Results show that the SCC reference mixture has higher absorbed energy (the average value of 176.2 N/mm) as compared to the NC reference mixture. The maximum value of 180.59 N/mm is recorded for SCC samples. In the case of NC mixtures, SAP has no considerable impact on absorbed energy so that NCSAP1 and NCSAP2 mixtures have comparable and slightly higher absorbed energy respectively as compared to NC reference mixture. However, in the case of SCC mixtures, SAP1 and SAP2 cause 5.6% and 28.5% reduction in absorbed energy (Figure 7.9). Regarding energy absorption in cementitious materials containing SAP, only Snoeck et al. (2018) have conducted experimental tests on the self-healing characteristics under impact loads using a drop-weight machine. They found that specimens containing SAP have a more ductile behaviour, as compared to the reference mixture. However, the bond energy absorption mechanism is different from the impact behaviour. SAP can act as a stress initiator to cause multiple cracks, which increases the ductility of the specimen exposed to the impact loading (Snoeck et al., 2018). However, in the present study, a lower area under the bond-slip curve represents lower bond ductility, resulting in a brittle and sudden bond drop after the maximum bond stress (bond strength). This leads to lower residual bond stress, which is clearly shown in Figure 7.6(b) for SCCSAP2 mixture. High bond strength of SCCSAP2 mixtures along with the low absorbed energy by this mixture results in a challenging issue on designing concrete mixtures containing SAP particles. It is worth emphasizing that more experimental tests are needed for future studies to figure out the effect of SAP types (particle size and chemical composition) on mechanical strength and microstructure (bulk matrix and rebar-concrete interface) of concrete mixtures.

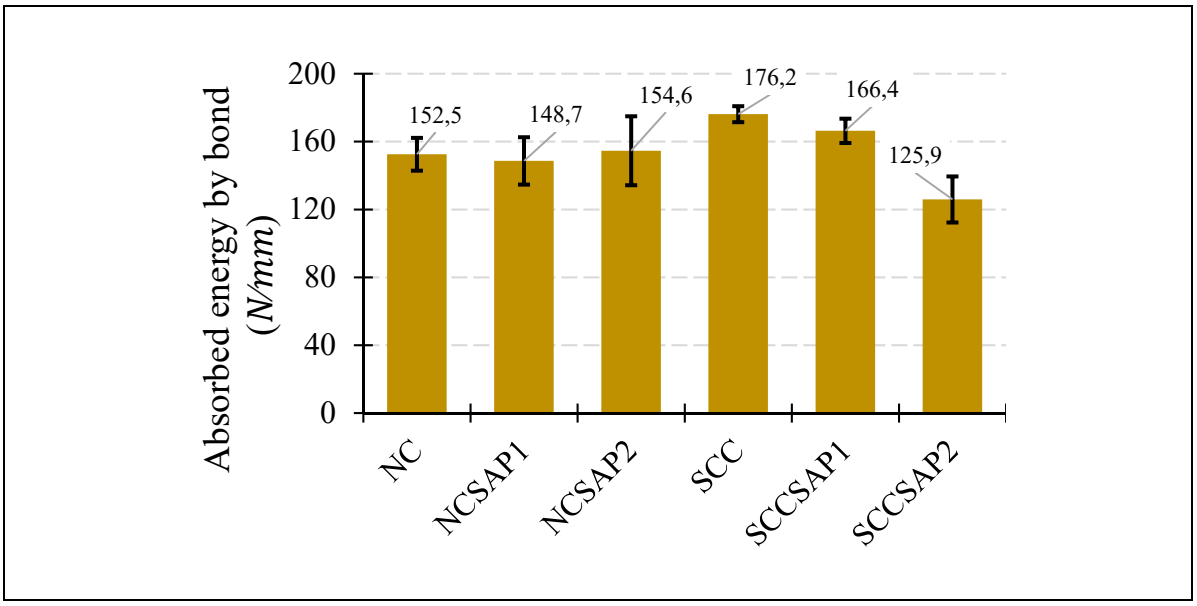

Figure 7.9 Bond absorbed energy of NC and SCC mixtures

7.3.2 Pre-cracked specimens

As shown in Table 7.2 and Figure 7.5(b), cracked specimen with $w = 0.10$ mm failed by pull-out failure mode while splitting failure modes are observed for larger crack widths (Figure 7.5(c)). Bond strengths of steel rebar embedded in cracked specimens with respect to the initial crack width is shown in Figure 7.10. Results show that small crack width has no considerable impact on bond strength so that only 5.7% bond reduction is observed for SCCC0.1 specimen. However, large crack width causes significant reduction in bond strength insofar as crack widths of 0.15, 0.20, 0.30, 0.40, and 0.50 mm cause around 36-52%, 21-33%, 40-84%, 59-84%, and 90% bond strength reduction respectively. Generally, results show that SCC mixtures are less sensitive to the pre-cracking phenomenon than NC mixtures so that SCC and SCCSAP2 mixtures have higher bond strength for different crack widths as compared to NC and NCSAP2 mixtures respectively. However, NCSAP1 and SCCSAP1 mixtures have similar behaviour regarding cracked samples so that similar trend lines are obtained for them for bond strength as a function of crack width (Figure 7.10). Moreover, initial crack width has considerable influence on the absorbed energy so that a minimum value of 1.14 N/mm is

recorded for NC mixture with 0.40 crack width (NCC0.4, the average value of 2.56 N/mm for two repetitions).

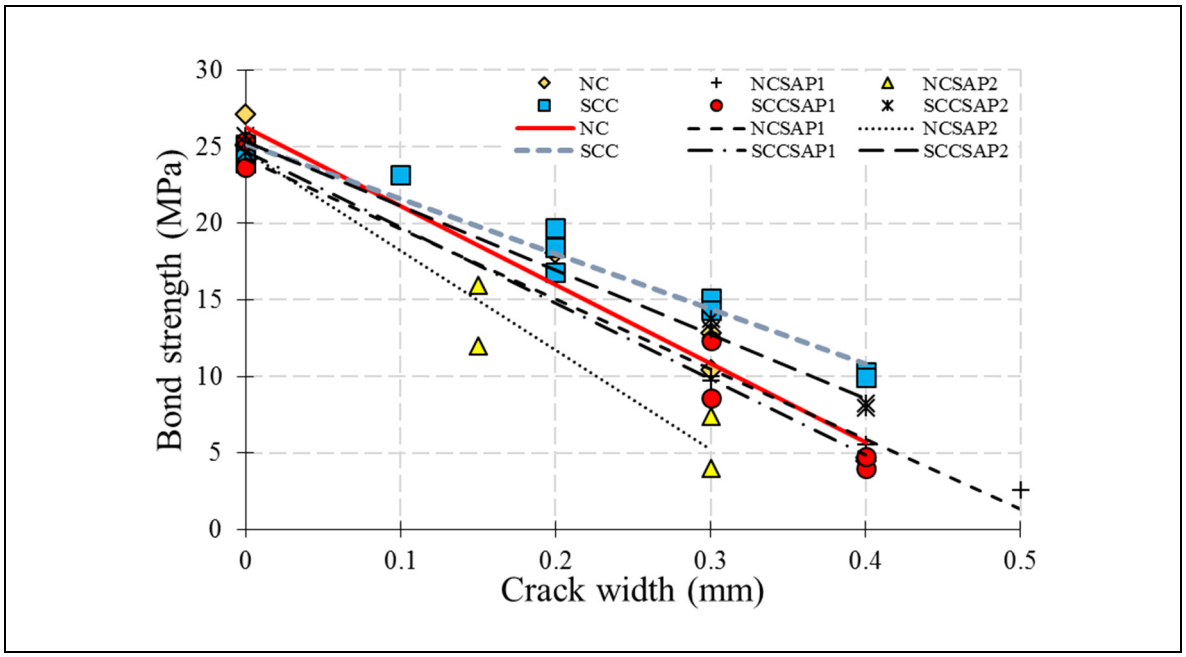

Figure 7.10 Effect of crack width on bond strength of cracked specimens

7.3.3 Healed specimens

As illustrated in Figure 7.5(c), healed specimens with $w > 0.10$ mm failed by splitting of surrounding concrete. However, as mentioned in Table 7.2, pull-out failure is observed for the healed specimen of SCC/28H0.1 after 28-day healing periods. A healing improvement factor (IF) is defined in the present study, shown in Eq. (7.1), to determine the efficiency of concrete mixtures for healing cracks passing the steel rebar, and mitigating damages. As IF increases, the healing efficiency of the mixture increases. Zero value of IF corresponds to the specimens with lower or comparable bond properties than the cracked specimen with constant crack width ($\tau_{Healed} \leq \tau_{Precracked}$), while $IF > 0$ represents healed specimens with higher bond properties as compared to those of pre-cracked specimens ($\tau_{Healed} > \tau_{Precracked}$). As different crack widths are obtained by splitting tests due to the brittle nature of concrete in

tension, bond reduction-crack width curves are used in few cases to predict bond properties of cracked specimens. These predicted values are used for measuring the IF.

$$IF = \left[\frac{\tau_{Healed} - \tau_{Precracked}}{\tau_{Uncracked} - \tau_{Precracked}}\right] \times 100 \quad (7.1)$$

Average healing improvement factors (IF) for all mixtures (with different repetitions) and crack widths are shown in Figure 7.11 in which IF_m, IF_u, and IF_r are healing efficiency of average bond stress, bond strength, and residual bond stress respectively. Range of these values is summarized in Table 7.2. As illustrated in Figure 7.11, in the case of the average bond stress (τ_m), the maximum value of $IF_m = 45.50\%$ is obtained for SCCSAP2/28H0.3 (the average value of 35.07% for 5 repetitions). In the case of the bond strength (τ_u), the maximum value of $IF_u = 100.0\%$ is obtained for SCC/28H0.1. High healing performance for SCC/28H0.1 corresponds to the small crack width of 0.10 mm, which makes it easy to entirely regain bond strength. NCSAP1/14H0.3 mixture has the highest healing $IF_r = 18.15\%$ of residual bond stress (the average value of 12.12% for 2 repetitions). Generally, results show that SAP has a significant influence on increasing the healing performance of bond strength in large initial crack widths ($w > 0.10$ mm) so that the average maximum $IF_u = 29.7\%$ is obtained for SCCSAP2/28H0.3, while the maximum value of 5.7% is recorded for mixtures without SAP (Figure 7.11). Similarly, in the case of the average bond stress, the maximum average value of $IF_m = 35.07\%$ is obtained for SCCSAP2/28H0.3. Moreover, results presented in Figure 7.11 show that SCC mixtures containing SAP particles are more efficient for healing damages (and/or bond strength regaining) as compared to NC mixtures containing SAP particles. This may be attributed to the fact that the existence of limestone in SCC mixtures affect cement hydration so that more unhydrated cement grains remain in the hardened concrete samples, which provides a better situation for healing damages in both the bulk matrix and the rebar-concrete interface. Additionally, results show that 14-day healing periods are not enough to heal crack especially for regaining bond strength, while promising results are obtained for 28-day healing periods. Moreover, Figure 7.11 indicates that healing of large crack width ($w >$ 0.40 mm) is totally difficult so that $IF_u < 10.0\%$ is observed for bond strength of healed

samples with 0.40 mm initial crack width. Besides, results show that SAP2 is slightly more efficient than SAP1 for improving healing IF, especially in SCC mixtures.

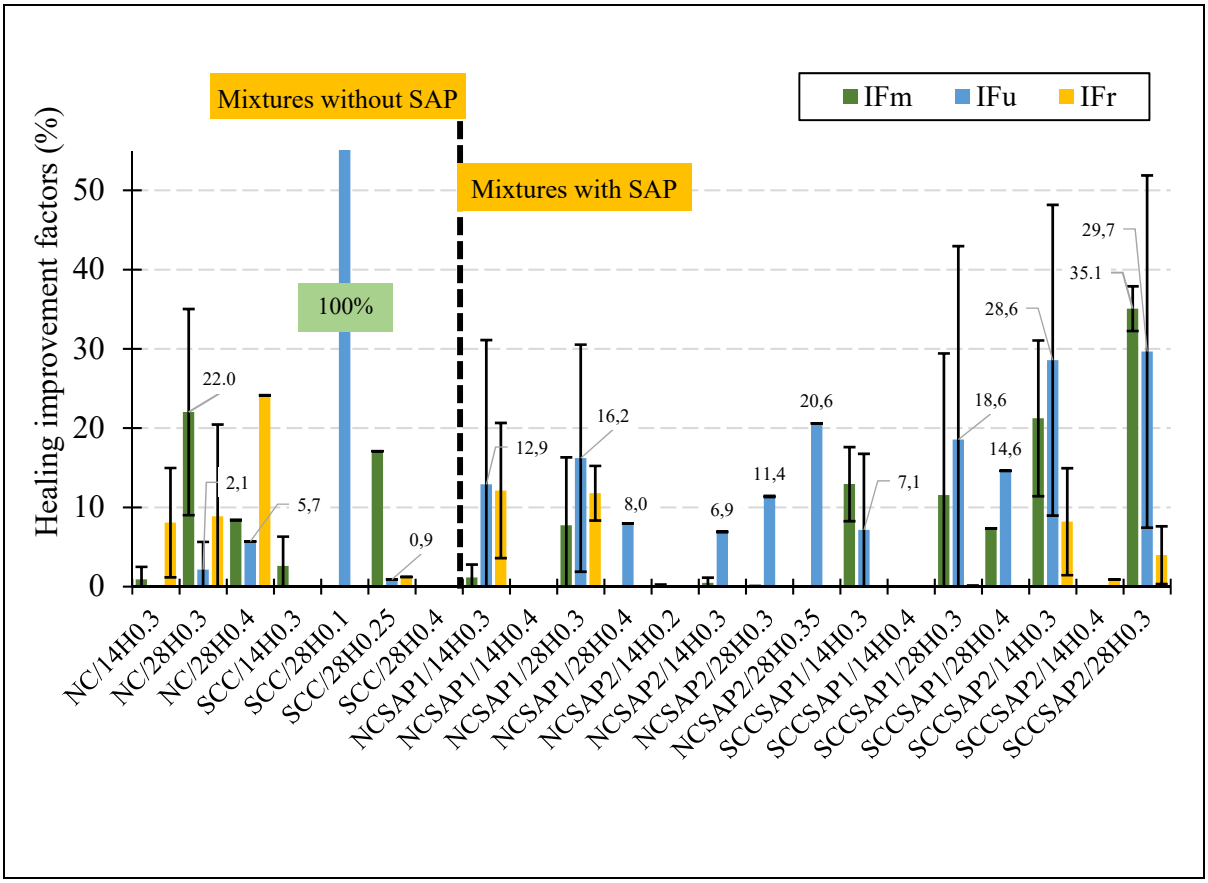

Figure 7.11 Healing improvement factors of bond properties for all mixtures

Bond-slip curves of the healed specimens are shown in Figure 7.12. Regarding w=0.10 mm for SCC mixture, results indicate that even though maximum bond stress (bond strength) is completely recovered (regained) after healing periods, residual bond stress and bond energy are still significantly degraded (Figure 7.12(a)). The pull-out failure mode is observed for this small crack (SCC/28H0.1) after 28-day healing periods (Table 7.2). Results also show that splitting failures, sudden drops in bond-slip curves after reaching maximum bond stress, are observed for all healed specimens ($w > 0.10$ mm). As shown before in Figure 7.6, the presence

of SAP particles near rebar and at the crack path leads to higher healing improvement factors for both NCSAP and SCCSAP.

As reported in Figures 7.11 and 7.12, SAP-contained mixtures have higher healing IF as compared with reference mixtures. There is a strong hypothesis for explaining this phenomenon. The reaction between calcium ions (Ca^{2+}), available in the matrix, and bicarbonates (HCO_3^-) and carbonates (CO_3^{2-}), available due to water ingress in the crack surface along with carbon dioxide in the air, generate calcite. These precipitates increase the ability of concrete to seal and heal the cracks (Aliko-Benítez et al., 2015). Hence, the content of calcite precipitates can directly affect the strength- and stiffness-recovery. Due to the heterogeneity at the rebar-concrete interface, a transition zone exists by a physical barrier of calcium hydroxide. Enhanced quantity of calcium hydroxide at the rebar-concrete interface, as compared to the matrix, have been confirmed in the literature (Arya et al., 2019; Horne et al., 2007; Yue & Shuguang, 2001). Due to the internal shear force, cement grains tend to separate from the matrix, causing a thin area around the rebar with fewer cement particles and more water, where calcium ions can diffuse from outside the interface zone to form areas filled by calcium hydroxide (Arya et al., 2019; Moreau, 1973). Results of the present study confirm that the presence of this reach calcite layer around the rebar is useful to partly/entirely heal cracks and regain bond strength.

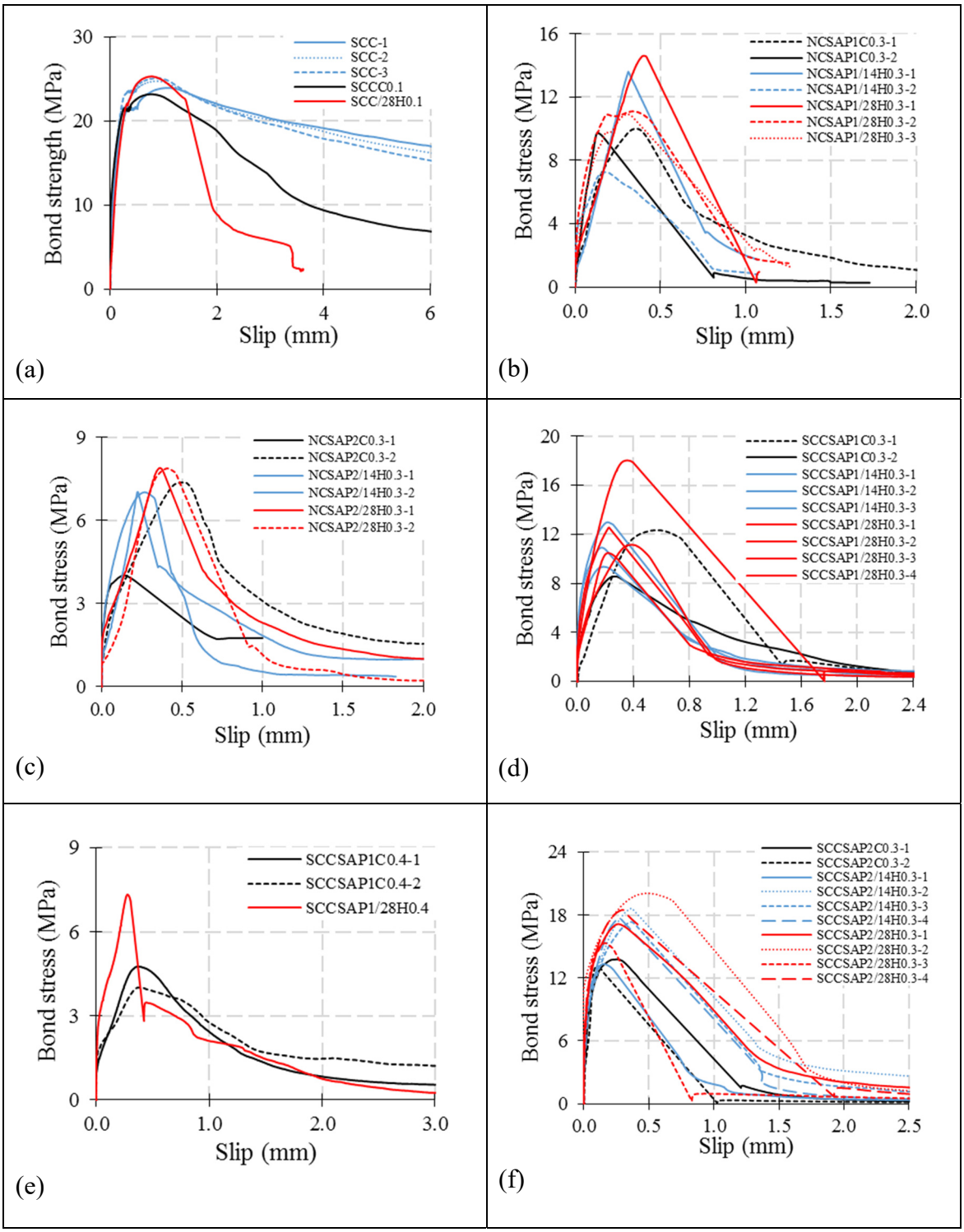

Figure 7.12 Bond-slip curves of healed specimens as compared with the cracked ones: (a) SCC with w=0.10 mm; (b) NCSAP1 with w=0.30 mm; (c) NCSAP2 with w=0.30 mm and 0.35 mm; (d) SCCSAP1 with w=0.30 mm; (e) SCCSAP1 with w=0.40 mm; (f) SCCSAP2 with w=0.30 mm

The existence of SAP particles in the mixtures increases the possible consumption of calcite for sealing/healing cracks. Moreover, macro-voids generated by SAP particles provide a condition in which the crack path passes through the SAP particle locations. This improves the performance of the self-healing method. Even in the case of concrete without polymers, almost 5.7% healing improvement factor is obtained for large crack width (Figure 7.5). However, due to the complicated pattern and distribution of healing products at the rebar-concrete interface, a sudden jump is observed in some bond-slip curves, indicating different efforts made between surfaces of rebar and healed surrounding concrete, called “strength regain” (Figure 7.13). A similar observation is shown in Figure 7.12(e) for SCCSAP1/28H0.4 mixture.

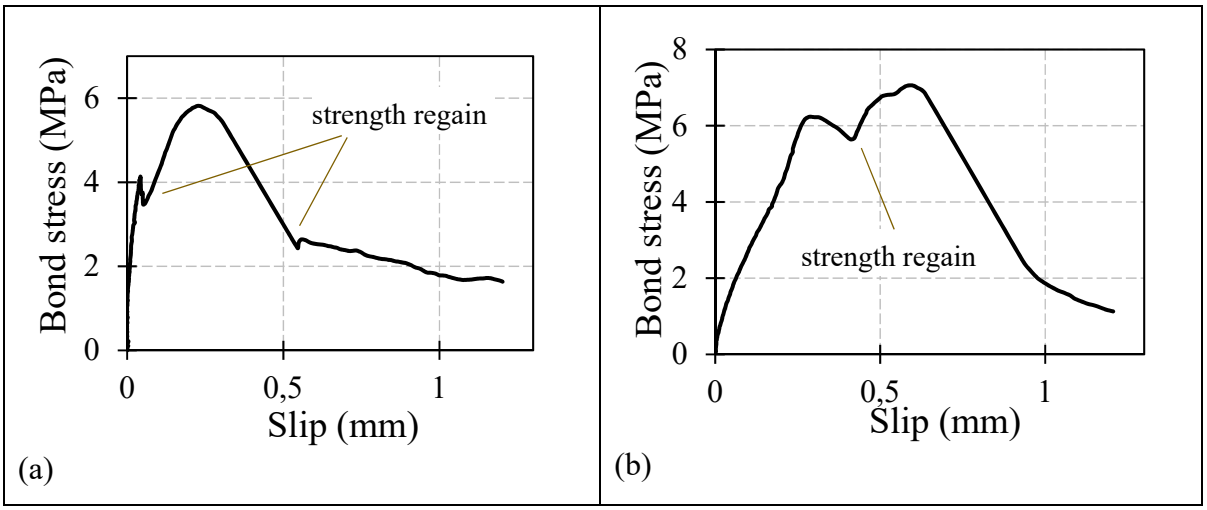

Figure 7.13 Phenomenon of strength regain occurred in the healed specimens:
(a) NC/28H0.4; (b) NCSAP1/28H0.4

A large quantity of stalactites is observed in the external surface of mixtures containing SAP (Figure 7.14). Snoeck et al. (2014) reported that the stalactites consist of a significant amount of $CaCO_3$ and washed out hydration products. Crystallization starts from the closer parts of crack tips and then propagates to the interior parts of the crack to provide a bridge between the crack lips. It is worth emphasizing that the crack-healing phenomenon is different from the crack-sealing phenomenon. To highlight this fact, crack-sealing monitoring of two concrete samples after one month healing period is considered in the present study by micro-computed tomography (micro-CT) scanning. Similar to the pull-out specimens, splitting test is

considered to simulate the pre-cracking phenomenon. However, to monitor crack closing by micro-CT scanning, larger cracked widths ($w > 0.50$ mm) are considered as compared to the pull-out specimens (Figure 7.15). As shown in Figure 7.11, SAP2 shows good healing performance. Hence, NCSAP2 mixture is used for samples of micro-CT scanning. Different locations considered in the concrete sections to compare the crack widths before and after the healing periods. Similar to pull-out specimens, wet-dry cycles are used to seal cracks.

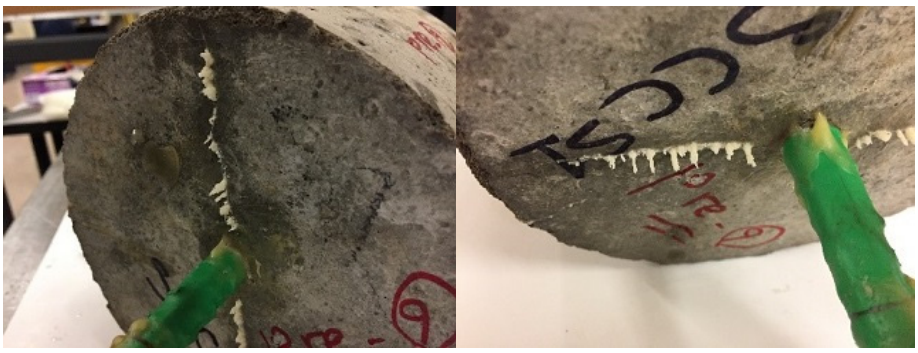

Figure 7.14 Healing products at the external crack surface of pull-out specimens of SCCSAP1 mixture

As shown in Figure 7.15, crack widths provided by splitting tests are not constant along the crack pass. The average value is considered for this section. This can explain some high standard deviations that existed in Figure 7.11 for different crack widths in the pull-out specimens. Sealing improvement factors (IF) of locations (A, B, C, D, and E) are illustrated inside Figure 7.15. Results show that SAP2 causes a maximum of 50.4% sealing IF for the average crack width of $w = 1.20$ mm (Figure 7.15(a)), while maximum of 62.7% sealing IF is obtained for the average crack width of $w = 0.95$ mm (Figure 7.15(b)). Similar to the crack-healing IF (Figure 7.11), SAP2 is efficient for sealing cracks. However, the range of sealing even for so large crack widths is significantly higher than the maximum crack-healing IF_u (29.7% for SAP2). Different mechanisms can help for closing (sealing) cracks including hydration of unhydrated particles and participation of calcium carbonate. The strength of sealed products to maintain similar mechanical properties of uncracked specimens is a challenging issue. Healing IF (bond strength recovery) should be lower than sealing IF.

Comparing the results presented in Figures 7.11 and 7.15 confirms this fact. It is worth mentioning that due to the continuous hydration in the bulk matrix of mixtures throughout the wet-dry cycles, transparency of images of micro-CT scanning after healing periods is lower than the first stage.

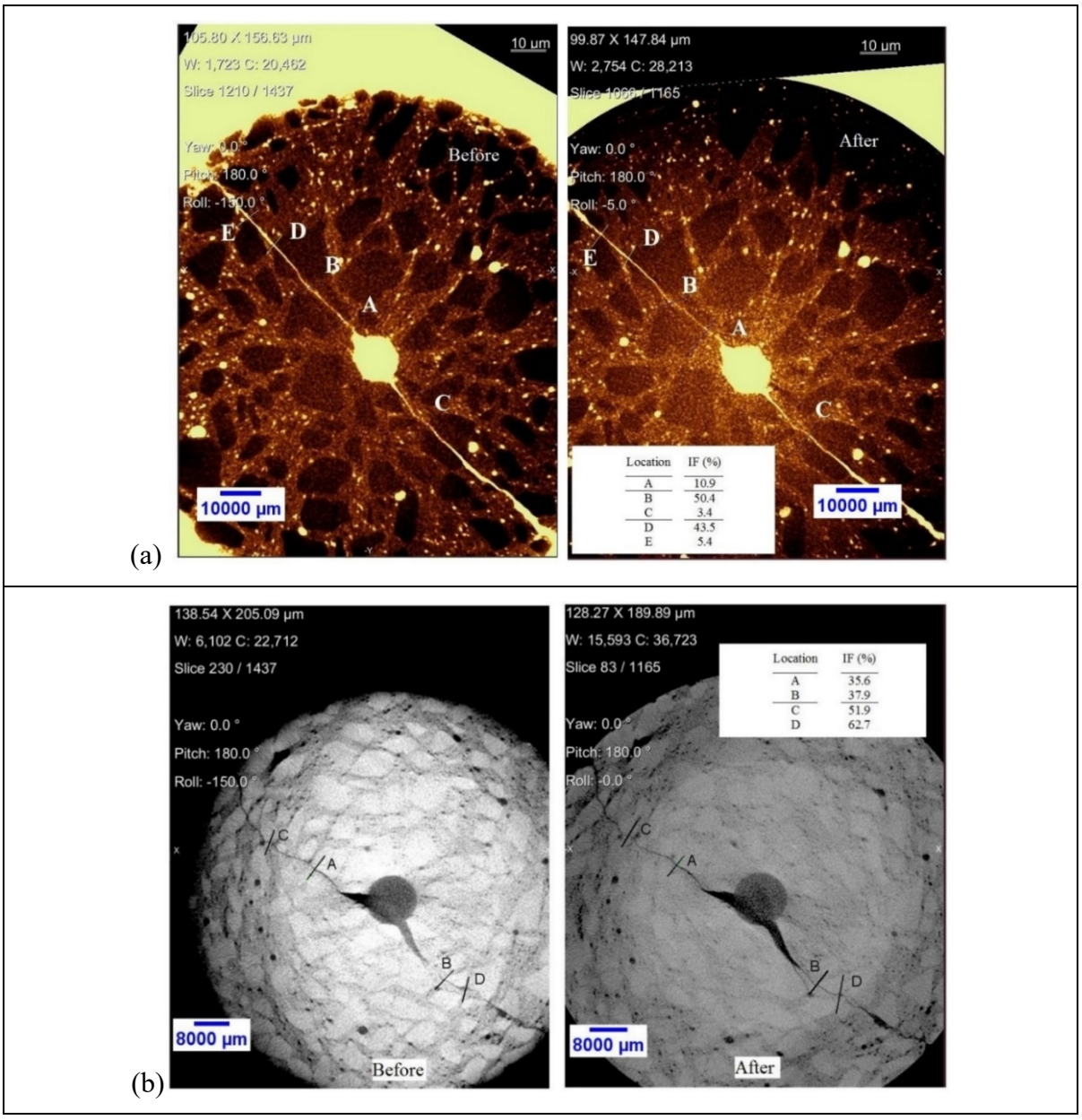

Figure 7.15 Crack-sealing monitoring in NCSAP2 samples after 1 month healing period by micro-computed tomography (micro-CT) scanning for average crack widths of:
(a) 1.20 mm; (b) 0.95 mm

7.4 Summary and concluding remarks

This paper determines the effect of SAP on the self-healing of bond damages in NC and SCC mixtures. An experimental program is carried out in three separate statuses of uncracked, pre-cracked, and healed specimens. Moreover, as there is no specific study on SAP-modified SCC mixtures, a comprehensive discussion is performed in the present study on uncracked mixtures. A comparison study is also performed on the results of NC and SCC mixtures. From the experimental results, the following main conclusions can be drawn:

- It is found that crack width smaller than 0.15 mm in SCC has no impact on failure mode so that pull-out failure is observed for pre-cracked specimens with $w = 0.10$ mm.
- Mixtures containing SAP1 have comparable and also slightly higher compressive strength as compared to the reference NC and SCC mixtures respectively, while SAP2 causes a considerable reduction in the compressive strength. This reduction effect is more crucial for NC mixtures (20.4% reduction) than SCC mixtures (8.3% reduction).
- Generally, results show that the bond strengths of steel rebar embedded in NC and SCC mixtures are not affected by a lower dosage of SAP (0.25%). Although SAP2 (smaller particle size) causes a considerable reduction in compressive strength, higher bond properties are obtained for this type of SAP as compared to SAP-1 with larger particle size in both NC and SCC mixtures. This clearly shows that the chemical composition of SAP plays a major role in the mechanical characteristics. More experimental studies are needed for the future to comprehensively clarify this important finding.
- Regarding the cracked specimens, SCC mixtures are less sensitive to the pre-cracking phenomenon as compared to NC mixtures.
- Promising healing results are obtained for NC and SCC mixture containing SAP particles as compared to the reference mixtures so that 29.7% bond strength recovery is obtained for SAP-contained mixtures. Results also show that SAP particles are more efficient in SCC mixtures as compared to NC mixtures to heal cracks at the rebar-concrete interface.
- Results show that the self-healing performance of small crack widths is higher than large ones so that entirely bond recovery is obtained for a damaged specimen with 0.10 mm crack width after 28-day healing periods.

- Improvement factors for self-sealing of cracks are considerably higher than the self-healing one so that in the case of NCSAP2 samples, 29.7% and 50.4% improvement factors are obtained for bond strength recovery and crack closure respectively.

CONCLUSIONS

A comprehensive experimental study was carried out in the present thesis to determine the effect of the pre-cracking phenomenon on bond behaviour of steel rebar emebedded in normal concrete (NC), air-entraining concrete (AE concrete), and self-consolidating concrete (SCC). Crack widths ranging from 0.10 mm to 0.5 mm were studied in the thesis. A simplified analytical model along with a proposed bond-slip nvelope curve was proposed for pre-cracked specimens. Also, a practical approach was used to mitigate internal damage at rebar-concrete interface by an accelerated self-healing method using superabsorbent polymer (SAP). Generally, the present thesis intendes to emphasize the effect of concrete compsotion on uncracked, pre-cracked, and healed specimens. Different dosages (and types) of SAP and healing periods were considered in the experimental program. Finally, the following conclusions are obtained from experimental, analytical, and statistical studies of the current dissertation:

- A literature review done from the previous studies revealed that concrete composition has a considerable impact on bond properties of steel reinforcing rebar embedded in concrete (Chapter 1). Moreover, in the case of SAP concrete, the total water-to-cement ratio, including additional water, plays a major role in predicting the compressive strength of mixture.
- The pre-cracking phenomenon has a significant impact on bond properties, especially residual bond stress. However, small crack widths ($w \leq 0.15\ mm$) have less influence (Chapter 2). The pre-cracking phenomenon can often change the failure mode of rebar from pull-out to a splitting failure mechanism. The simplified analytical model presented in Chapter 3 shows that surface separation along with opening crack width (simultaneously) leads to the propagation of bond failure after the pre-cracking phenomenon. Rebar rib geometry plays a critical role in this context.
- Concrete with higher flowability (high slump value) is less sensitive to the pre-cracking phenomenon so that strength reduction factors of SCC and NC with higher slump values are lower than NC with a slump in the range of 100±15 mm. (Chapter 4).

- Using superabsorbent polymers (SAP) to accelerate autogenous the crack-healing is efficient especially for a higher dosage of SAP. Although the higher dosage of SAP leads to bond reduction due to the macro voids after releasing water by polymer, a high improvement factor is found for 1.0% SAP, especially for lower crack widths (Chapter 5). Calcium carbonate precipitations are confirmed by performing SEM images of healed products from crack surfaces. SAP with larger size (SAP-2) is more efficient for all statuses of uncracked, pre-cracked, and healed concrete. 28 days of wet-dry cycles are more efficient, as compared to the 14-day healing periods.
- Using air-entraining admixture in concrete has a positive impact on the self-healing method by SAP (Chapter 6). Statistical analysis of all experimental tests revealed that crack width, SAP percentage, healing period, AE dosage, and SAP type are the main parameters affecting the self-healing method performance.
- Similar to the NC, SCC concrete containing SAP show higher healing performance at the rebar-concrete interface (Chapter 7), as compared with concrete without SAP. General results show that 0.25% SAP is optimal and acceptable for retaining the current strength and increasing the healing performance of concrete mixtures. Results also show that SAP particles are more efficient in SCC mixtures as compared to NC mixtures for healing cracks at the rebar-concrete interface.

RECOMMENDATIONS FOR FUTURE STUDIES

Despite the extensive efforts made in the current dissertation, more experimental studies are necessary for future investigations to confirm and extend the obtained observations. The author's recommendations about future studies necessary to complement this study and better investigate the subject are as follows:

- In the case of the pre-cracking phenomenon, confined concrete by transverse reinforcement should be studied to control the crack opening. This surrounding steel or FRP confinement can also help for self-healing cracks by SAP.
- Moreover, non-steel rebars or corrosion protected rebars are necessary to be studied for extending the healing period for more than 1 month. Large crack widths ($w > 0.15\ mm$) needs more time to regain bond strength. Also, steel fiber may be more efficient to provide a bridge between two sides of the crack lip for improving the self-healing method.
- Only two types of superabsorbent polymer are tested in the present dissertation. More experimental tests are essential to study the effect of SAP chemical type on self-healing at the rebar-concrete interface.
- Only one regime of healing, wet-dry cycles, is considered for the present experimental study, and more tests are needed to be performed for other regimes. Also, the effect of the water pH on self—healing should be studied in future research.
- As mentioned in Chapters 6 and 7, SAP concrete has closer macro voids to the rebar edge. Due to the enriched quantity of calcium hydroxide at the steel-concrete interface (SCI), these macro voids can be efficient to provide more conditions of the lime cycle to generate calcium carbonate precipitation. Additionally, calcium hydroxide in the vicinity of SCI changes the pH value at a relatively higher level. This can affect the performance of SAP for self-healing. Hence, both pullout strength and SCI properties are necessary to be examined by future studies.
- Regarding SEM and microscopic results presented in Chapters 5 and 6, an analytical solution is necessary to optimize SAP dosage around the rebar edge for improving self-healing performance, using different types of concrete composition. The author of the present thesis recommends the classical problem of the probability, "Buffon needle", so

that SAP locations can intersect the path of the crack to precisely accelerate the self-healing approach.

- The monotonic pull-out test is considered for the experimental program. Future works can expand the study of the pre-cracking phenomenon and the self-healing method to cyclic loadings.
- To confirm the promising results obtained in the present thesis, macro studies are necessary such as real internal or external beam-column joints. In these members, a practical technique should be used to pre-crack the joint, and then using wet-dry cycles for healing this region. The same process can be used for shear wall, column, and foundation. However, a practical way of pre-cracking and exposing wet-dry cycles are challenging for these types of studies.

APPENDIX I

EFFECT OF SAP ON THE REDUCTION OF THE COMPRESSIVE STRENGTH

Table-A I-1 Collected test specimens for SAP mixtures in the literature

References	SAP (%)	w/c	w_e/c	w_T/c	f'_c (MPa)	day	Strength reduction (%)	SAP size (mm)
Lam & Hooton (2005)	0	0.35	0	0.35	51.11	7	0	0
	0.30	0.35	0.10	0.45	34.51	7	-32.48	0.80
	0.60	0.35	0.10	0.45	40.65	7	-20.46	0.80
	0	0.35	0	0.35	56.86	28	0	0
	0.30	0.35	0.10	0.45	41.177	28	-27.59	0.80
	0.60	0.35	0.10	0.45	44.05	28	-22.53	0.80
Igarashi & Watanabe (2006)	0	0.25	0	0.25	86.30	7	0	0
	0.35	0.25	0.04	0.29	78.00	7	-9.62	0.20
	0.70	0.25	0.09	0.34	67.00	7	-22.36	0.20
	0	0.25	0	0.25	97.40	28	0	0
	0.35	0.25	0.04	0.29	94.20	28	-3.29	0.20
	0.70	0.25	0.09	0.34	76.10	28	-21.87	0.20
Piérard et al. (2006)	0	0.35	0	0.35	97	7	0	0
	0.30	0.35	0.02	0.37	84	7	-13.40	0.85
	0.60	0.35	0.04	0.39	76	7	-21.65	0.85
	0	0.35	0	0.35	107	28	0	0
	0.30	0.35	0.02	0.37	99	28	-7.48	0.85
	0.60	0.35	0.04	0.39	93	28	-13.08	0.85
Lura et al. (2006)	0	0.31	0	0.31	76.82	7	0	0
	0	0.31	0	0.31	87.42	28	0	0
	0.40	0.31	0.05	0.36	70.19	7	-8.62	0.25
	0.40	0.31	0.05	0.36	89.74	28	2.65	0.25
	0	0.32	0	0.32	84.11	7	0	0
	0	0.32	0	0.32	111.92	28	0	0
	0.40	0.32	0.05	0.37	81.79	7	-2.76	0.25
	0.40	0.32	0.05	0.37	117.22	28	4.73	0.25
Mechtcherine et al. (2006)	0	0.25	0	0.25	132	28	0	0
	0.40	0.25	0.04	0.29	129	28	-2.27	0.25

Table-A I-1 Collected test specimens for SAP mixtures in the literature (continued)

References	SAP (%)	w/c	w_e/c	w_T/c	f'_c (MPa)	day	Strength reduction (%)	SAP size (mm)
Esteves et al. (2007)	0	0.35	0	0.35	52.32	7	0	0
	0	0.30	0	0.30	66.19	7	0	0
	0	0.25	0	0.25	77.44	7	0	0
	0.20	0.35	0.05	0.40	48.66	7	-7	0.25
	0.20	0.3	0.05	0.35	56.25	7	-15.02	0.25
	0.20	0.25	0.05	0.30	62.53	7	-19.26	0.25
	0	0.35	0	0.35	60.96	28	0	0
	0	0.30	0	0.30	75.35	28	0	0
	0	0.25	0	0.25	84.24	28	0	0
	0.20	0.35	0.05	0.40	49.97	28	-18.03	0.25
	0.20	0.3	0.05	0.35	62.53	28	-17.01	0.25
	0.20	0.25	0.05	0.30	70.64	28	-16.15	0.25
Dudziak & Mechtcherine (2008)	0	0.24	0.05	0.29	132	28	0	0
	0.40	0.24	0.05	0.29	129	28	-2.27	0.20
	0	0.25	0.03	0.28	140	28	0	0
	0.40	0.25	0.03	0.28	140	28	0	0.20
	0	0.24	0.05	0.29	172	28	0	0
	0.40	0.24	0.05	0.29	150	28	-12.79	0.20
	0	0.25	0.03	0.28	163	28	0	0
	0.40	0.25	0.03	0.28	150	28	-7.98	0.20
Craeye & De Schutter (2008)	0	0.32	0	0.32	108.69	28	0	0
	0.04	0.32	0.06	0.38	91.30	28	-16.00	0.80
	0.06	0.32	0.08	0.4	79.80	28	-27.00	0.80
	0.08	0.32	0.10	0.42	75.00	28	-31.00	0.80
Dudziak & Mechtcherine (2009)	0	0.22	0	0.22	122	7	0	0
	0.40	0.22	0	0.22	112	7	-8.19	0.15
	0.30	0.22	0.04	0.26	111	7	-9.02	0.15
	0.30	0.22	0.05	0.27	108	7	-11.48	0.15
	0.40	0.22	0.07	0.29	94	7	-22.95	0.15
	0	0.22	0	0.22	141	28	0	0
	0.40	0.22	0	0.22	134	28	-4.96	0.15
	0.30	0.22	0.04	0.26	137	28	-2.84	0.15
	0.30	0.22	0.05	0.27	142	28	0.71	0.15
	0.40	0.22	0.07	0.29	120	28	-14.89	0.15

Table-A I-1 Collected test specimens for SAP mixtures in the literature (continued)

References	SAP (%)	w/c	w_e/c	w_T/c	f'_c (MPa)	day	Strength reduction (%)	SAP size (mm)
Dudziak & Mechtcherine (2009)	0	0.27	0	0.27	225	28	0	0
	0.30	0.27	0.04	0.31	207	28	-8	0.15
	0	0.22	0	0.22	127	7	0	0
	0.40	0.22	0	0.22	118	7	-7.09	0.15
	0.30	0.22	0.04	0.26	121	7	-4.72	0.15
	0.30	0.22	0.05	0.27	125	7	-1.57	0.15
	0.40	0.22	0.07	0.29	95	7	-25.19	0.15
	0	0.27	0	0.27	117	7	0	0
	0.30	0.27	0.04	0.31	109	7	-6.84	0.15
	0	0.22	0	0.22	160	28	0	0
	0.40	0.22	0	0.22	156	28	-2.50	0.15
	0.30	0.22	0.04	0.26	155	28	-3.13	0.15
	0.30	0.22	0.05	0.27	147	28	-8.13	0.15
	0.40	0.22	0.07	0.29	128	28	-20	0.15
	0	0.27	0	0.27	188	28	0	0
	0.30	0.27	0.04	0.31	181	28	-3.72	0.15
Wang et al. (2009)	0	0.34	0	0.34	64.60	28	0	0
	0.30	0.34	0.04	0.38	62.40	28	-3.41	0.50
	0.50	0.34	0.04	0.38	62.40	28	-3.41	0.50
	0.70	0.34	0.04	0.38	56.60	28	-12.38	0.50
	0	0.30	0	0.30	71.80	28	0	0
	0.50	0.30	0.02	0.32	68.50	28	-4.59	0.50
	0.50	0.30	0.04	0.34	66.30	28	-7.66	0.50
	0.50	0.30	0.06	0.36	63.80	28	-11.14	0.50
Hasholt et al. (2010)	0.60	0.35	0.07	0.42	58.86	7	-6.61	-
	0.40	0.35	0.05	0.40	62.41	7	-0.97	-
	0	0.35	0	0.35	63.02	7	0	-
	0.20	0.35	0.02	0.37	64.72	7	2.69	-
	0.10	0.35	0.01	0.36	65.65	7	4.16	-
	0.60	0.35	0.07	0.42	67.04	28	-8.43	-
	0	0.35	0	0.35	73.21	28	0	-
	0.40	0.35	0.05	0.40	73.52	28	0.42	-
	0.20	0.35	0.02	0.37	75.06	28	2.53	-
	0.10	0.35	0.01	0.36	75.52	28	3.16	-
	0.60	0.40	0.07	0.47	47.96	7	-16.46	-

Table-A I-1 Collected test specimens for SAP mixtures in the literature (continued)

References	SAP (%)	w/c	w_e/c	w_T/c	f'_c (MPa)	day	Strength reduction (%)	SAP Size (mm)
Hasholt et al. (2010)	0.30	0.40	0.03	0.43	52.39	7	-8.76	-
	0.10	0.40	0.01	0.41	56.35	7	-1.86	-
	0.20	0.40	0.02	0.42	56.80	7	-1.06	-
	0	0.40	0	0.40	57.42	7	0	-
	0.60	0.40	0.07	0.47	57.66	28	-15.80	-
	0.30	0.40	0.03	0.43	62.39	28	-8.90	-
	0.10	0.40	0.01	0.41	65.44	28	-4.45	-
	0.20	0.40	0.02	0.42	65.74	28	-4.01	-
	0	0.40	0	0.40	68.49	28	0	-
	0.60	0.50	0.07	0.57	36.36	7	-17.12	-
	0.20	0.50	0.02	0.52	38.91	7	-11.29	-
	0.40	0.50	0.05	0.55	39.23	7	-10.56	-
	0.30	0.50	0.03	0.53	42.27	7	-3.64	-
	0	0.50	0	0.5	43.87	7	0	-
	0.60	0.50	0.07	0.57	43.71	28	-14.12	-
	0.20	0.50	0.02	0.52	46.10	28	-9.42	-
	0.40	0.50	0.05	0.55	46.74	28	-8.16	-
	0.30	0.50	0.03	0.53	49.94	28	-1.88	-
	0	0.5	0	0.50	50.89	28	0	-
Craeye et al. (2011)	0.42	0.32	0.19	0.51	59.72	7	-28.02	0.15
	0.33	0.32	0.15	0.47	67.55	7	-18.59	0.15
	0.23	0.32	0.11	0.43	71.99	7	-13.25	0.15
	0	0.32	0	0.32	82.98	7	0	0
	0.42	0.32	0.19	0.51	70.61	28	-27.39	0.15
	0.33	0.32	0.15	0.47	75.69	28	-22.17	0.15
	0.23	0.32	0.11	0.43	82.66	28	-15.00	0.15
	0	0.32	0	0.32	97.25	28	0	0
Schröfl et al. (2012)	0	0.30	0	0.30	73.33	7	0	0
	0	0.30	0	0.30	101.37	28	0	0
	0.30	0.30	0.03	0.33	65.78	7	-10.29	0.32
	0.30	0.30	0.03	0.33	81.15	28	-19.95	0.32
	0.30	0.30	0.04	0.34	66.86	7	-8.82	0.58
	0.30	0.30	0.04	0.34	80.07	28	-21.01	0.58
	0.30	0.30	0.06	0.36	70.09	7	-4.41	0.63
	0.30	0.30	0.06	0.36	77.38	28	-23.67	0.63

Table-A I-1 Collected test specimens for SAP mixtures in the literature (continued)

References	SAP (%)	w/c	w_e/c	w_T/c	f'_c (MPa)	day	Strength reduction (%)	SAP size (mm)
Schröfl et al. (2012)	0.30	0.30	0.26	0.56	36.39	7	-50.37	0.63
	0.30	0.30	0.26	0.56	52.30	28	-48.40	0.63
	0.30	0.30	0.06	0.36	64.44	7	-12.13	0.90
	0.30	0.30	0.06	0.36	79.80	28	-21.28	0.90
	0.20	0.30	0.04	0.34	74.14	7	1.10	0.90
	0.20	0.30	0.04	0.34	97.06	28	-4.25	0.90
	0.10	0.30	0.02	0.32	76.03	7	3.68	0.90
	0.10	0.30	0.02	0.32	95.98	28	-5.32	0.90
	0.30	0.30	0.05	0.35	73.60	7	0.37	1.06
	0.30	0.30	0.05	0.35	98.68	28	-2.66	1.06
	0.30	0.30	0.02	0.32	80.07	7	9.19	0.59
	0.30	0.30	0.02	0.32	101.37	28	0	0.59
Olawuyi & Boshoff (2013)	0	0.25	0	0.25	89.53	7	0	0
	0.20	0.25	0.06	0.31	79.24	7	-11.49	0.008
	0.30	0.25	0.09	0.34	76.76	7	-14.26	0.008
	0.40	0.25	0.11	0.36	67.89	7	-24.17	0.008
	0.60	0.25	0.16	0.41	49.38	7	-44.84	0.008
	0.20	0.25	0.07	0.32	79.85	7	-10.81	0.01
	0.30	0.25	0.10	0.35	71.68	7	-19.94	0.01
	0.40	0.25	0.13	0.38	64.06	7	-28.45	0.01
	0.60	0.25	0.19	0.44	51.79	7	-42.15	0.01
	0	0.25	0	0.25	106.12	28	0	0
	0.20	0.25	0.06	0.31	97.81	28	-7.83	0.008
	0.30	0.25	0.09	0.34	93.41	28	-11.98	0.008
	0.40	0.25	0.11	0.36	86.66	28	-18.34	0.008
	0.60	0.25	0.16	0.41	66.73	28	-37.12	0.008
	0.20	0.25	0.07	0.32	92.00	28	-13.31	0.01
	0.30	0.25	0.10	0.35	84.65	28	-20.23	0.01
	0.40	0.25	0.13	0.38	80.64	28	-24.01	0.01
	0.60	0.25	0.19	0.44	65.74	28	-38.05	0.01
Mechtcherine et al. (2014)	0	0.30	0	0.30	84.70	7	0	0
	0.30	0.30	0.03	0.33	79.10	7	-6.61	0.58
	0.30	0.30	0.04	0.34	79.10	7	-6.61	0.32
	0	0.30	0	0.30	103.20	28	0	0
	0.30	0.30	0.03	0.33	94.40	28	-8.53	0.58

Table-A I-1 Collected test specimens for SAP mixtures in the literature (continued)

References	SAP (%)	w/c	w_e/c	w_T/c	f'_c (MPa)	day	Strength reduction (%)	SAP size (mm)
Mechtcherine et al. (2014)	0.30	0.30	0.04	0.34	95.50	28	-7.46	0.32
Laustsen et al. (2015)	0	0.45	0	0.45	63.00	28	0	0
	0.07	0.45	0.03	0.48	57.00	28	-9.52	0.06
	0.15	0.45	0.06	0.51	55.00	28	-12.69	0.06
	0.30	0.45	0.13	0.58	43.00	28	-31.75	0.06
Wang et al. (2013)	0	0.35	0	0.35	60.98	28	0	0
	0.10	0.35	0	0.35	69.68	28	14.27	0.16
	0.20	0.35	0	0.35	70.58	28	15.74	0.16
	0.30	0.35	0	0.35	70.46	28	15.55	0.16
	0.60	0.35	0	0.35	67.1	28	10.04	0.16
	0	0.35	0	0.35	60.98	28	0	0
	0.10	0.35	0	0.35	66.14	28	8.46	0.07
	0.20	0.35	0	0.35	69.68	28	14.27	0.07
	0.30	0.35	0	0.35	70.04	28	14.86	0.07
	0.60	0.35	0	0.35	72.92	28	19.58	0.07
Snoeck et al. (2014)	0	0.50	0	0.50	52.25	7	0	0
	0.50	0.50	0	0.50	51.35	7	-1.72	0.47
	1	0.50	0	0.50	48.11	7	-7.93	0.47
	0.50	0.50	0.04	0.54	40.90	7	-21.72	0.47
	1	0.50	0.09	0.59	40	7	-23.45	0.47
	0.50	0.50	0	0.50	35.31	7	-32.41	0.10
	0.50	0.50	0.15	0.65	32.25	7	-38.28	0.10
	1	0.50	0	0.50	30.81	7	-41.03	0.10
	1	0.50	0.30	0.80	20.36	7	-61.03	0.10
	0	0.50	0	0.50	61.98	28	0	0
	0.50	0.50	0	0.50	59.28	28	-4.36	0.47
	1	0.50	0	0.50	58.56	28	-5.52	0.47
	0.50	0.50	0	0.50	52.25	28	-15.69	0.10
	0.50	0.50	0.04	0.54	50.81	28	-18.02	0.47
	1	0.50	0.09	0.59	50.81	28	-18.02	0.47
	1	0.50	0	0.5	43.24	28	-30.23	0.10
	0.50	0.50	0.15	0.65	41.62	28	-32.85	0.10
	1	0.50	0.30	0.8	28.83	28	-53.49	0.10

Table-A I-1 Collected test specimens for SAP mixtures in the literature (continued)

References	SAP (%)	w/c	w_e/c	w_T/c	f'_c (MPa)	day	Strength reduction (%)	SAP size (mm)
Justs et al. (2015)	0	0.15	0	0.15	154.29	7	0	0
	0.21	0.15	0.03	0.18	133.37	7	-13.56	0.06
	0.31	0.20	0	0.20	122.91	7	-19.52	0.06
	0	0.20	0	0.20	152.72	7	0	0
	0	0.15	0	0.15	182.53	28	0	0
	0.21	0.15	0.03	0.18	166.32	28	-8.88	0.06
	0.31	0.20	0	0.20	149.58	28	-18.52	0.06
	0	0.20	0	0.20	183.58	28	0	0
Kong et al. (2015)	0	0.29	0	0.29	69.26	7	0	0
	0.20	0.29	0.05	0.34	64.43	7	-6.97	0.42
	0.40	0.29	0.10	0.39	32.29	7	-53.39	0.42
	0	0.29	0	0.29	84.19	28	0	0
	0.20	0.29	0.05	0.34	80.23	28	-4.69	0.42
	0.40	0.29	0.10	0.39	49.61	28	-41.07	0.42
Van Tittelboom et al. (2016)	0	0.27	0	0.27	58.40	28	0	0
	1	0.27	0.07	0.34	47.70	28	-18.32	0.60
Shen et al. (2016)	0	0.33	0	0.33	64.00	28	0	0
	0.05	0.33	0.01	0.34	62.50	28	-2.34	0.15
	0.15	0.33	0.03	0.36	59.40	28	-7.19	0.15
	0.26	0.33	0.05	0.38	57.30	28	-10.47	0.15
Mechtcherine et al. (2017)	0	0.45	0	0.45	61.00	28	0	0
	0.15	0.45	0.05	0.50	56.10	28	-8.03	0.30
	0.15	0.45	0.05	0.50	56.50	28	-7.38	0.15
	0	0.45	0	0.45	56.00	28	0	0
	0.12	0.45	0.05	0.50	51.40	28	-8.21	0.30
	0.13	0.45	0.05	0.50	50.80	28	-9.29	0.15
	0	0.45	0	0.45	43.20	28	0	0
	0.15	0.45	0.05	0.50	43.30	28	0.23	0.30
	0.15	0.45	0.05	0.50	41.00	28	-5.09	0.15
	0	0.45	0	0.45	50.00	28	0	0
	0.6	0.45	0.05	0.50	40.10	28	-19.80	0.30
	0.6	0.45	0.05	0.50	41.90	28	-16.20	0.15
	0	0.45	0	0.45	57.00	28	0	0
	0.15	0.45	0.05	0.50	51.70	28	-9.29	0.30
	0.15	0.45	0.05	0.50	47.80	28	-16.14	0.15

Table-A I-1 Collected test specimens for SAP mixtures in the literature (continued)

References	SAP (%)	w/c	w_e/c	w_T/c	f'_c (MPa)	day	Strength reduction (%)	SAP size (mm)
Mechtcherine et al. (2017)	0	0.42	0	0.42	37.00	28	0	0
	0.40	0.42	0.07	0.49	36.90	28	-0.27	0.30
	0.40	0.42	0.07	0.49	36.20	28	-2.16	0.15
	0	0.45	0	0.45	50.50	28	0	0
	0.16	0.45	0.05	0.50	40.10	28	-20.59	0.30
	0.16	0.45	0.05	0.50	43.70	28	-13.47	0.15
	0	0.45	0	0.45	43.50	28	0	0
	0.15	0.45	0.05	0.50	36.10	28	-17.01	0.30
	0.15	0.45	0.05	0.50	33.20	28	-23.68	0.15
	0	0.45	0	0.45	48.20	28	0	0
	0.15	0.45	0.05	0.50	46.90	28	-2.69	0.30
	0.15	0.45	0.05	0.50	43.10	28	-10.58	0.15
	0.18	0.45	0	0.45	47.20	28	-2.07	0.15
	0	0.45	0	0.45	57.80	28	0	0
	0.15	0.45	0.05	0.50	48.60	28	-15.92	0.30
	0.15	0.45	0.05	0.50	48.00	28	-16.96	0.15
	0	0.45	0	0.45	57.80	28	0	0
	0.15	0.45	0.05	0.50	49.00	28	-15.22	0.30
	0.15	0.45	0.05	0.50	48.60	28	-15.92	0.15
	0.15	0.45	0	0.45	58.00	28	0.35	0.30
	0.15	0.45	0	0.45	50.00	28	-13.49	0.15
	0	0.45	0	0.45	47.30	28	0	0
	0.15	0.45	0.05	0.50	47.00	28	-0.63	0.30
	0.15	0.45	0.05	0.50	43.30	28	-8.46	0.15
	0	0.45	0	0.45	56.70	28	0	0
	0.15	0.45	0.05	0.50	48.70	28	-14.11	0.30
	0.15	0.45	0.05	0.50	53.30	28	-5.99	0.15

APPENDIX II

EXPLANATIONS OF THE WATER ABSORPTION TESTS OF SAP

This supplementary file gives additional information regarding the details of tests conducted to measure the water absorption of SAP used in the experimental tests. Regarding the recommendations provided by RILEM TC 260-RSC (Snoeck et al., 2018), the tea bag method is implemented to measure the water absorption of SAP (Figure-A II-1).

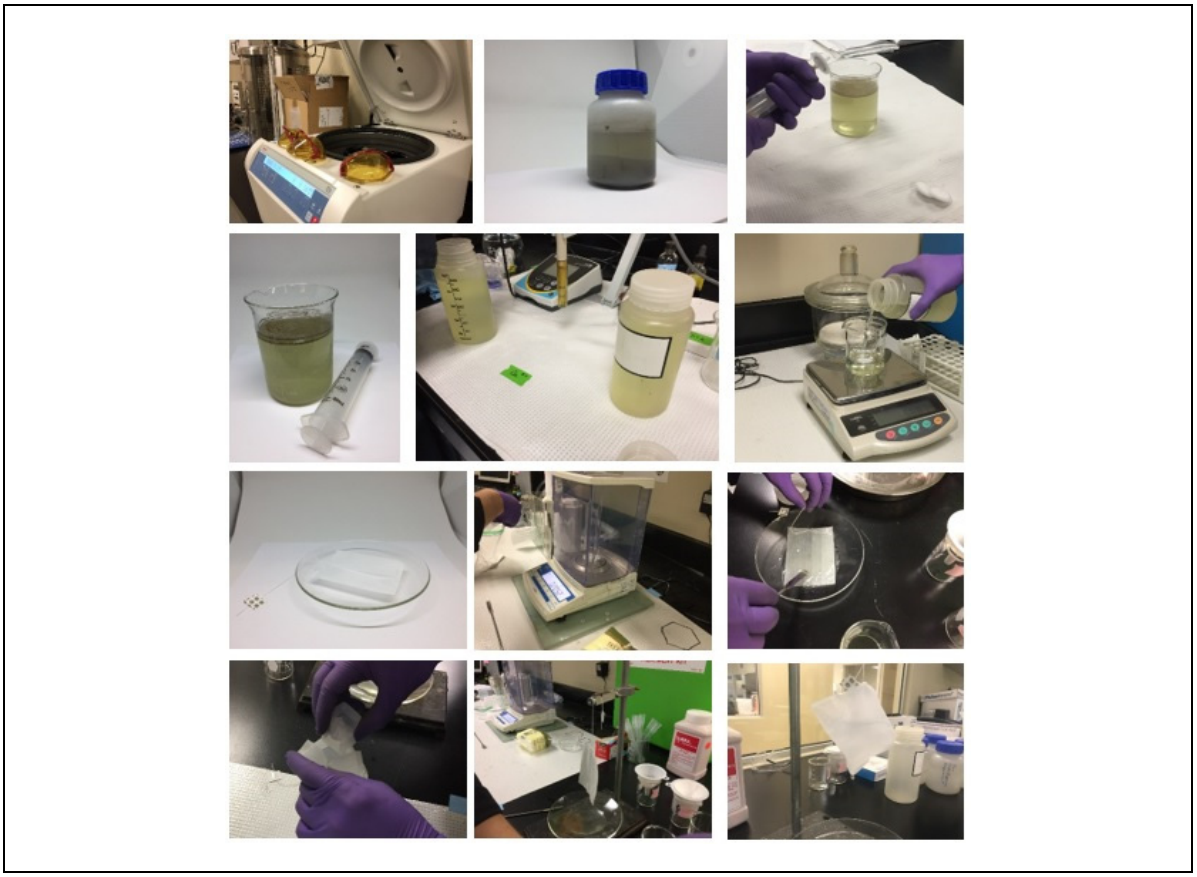

Figure-A II-1 Tea bag method for measuring water absorption of SAP

In addition to the value of water absorption results obtained by the Tea bag method (Table-A II-1), absorption capacity is also adjusted by slump flow tests, which are summarized in Table 6.1 of the manuscript. Finally, the value of 25 g water per g of dry SAP is selected for both SAP to maintain the slump value in a constant range. This value is slightly lower than the results of the Tea bag method (Table-A II-1). Similar trend has been recommended by RILEM TC 260-RSC (Snoeck et al., 2018).

Table-A II-1 Absorption of SAP (g fluid/g SAP) by the tea bag method

Series	1 min	5 min	10 min	30 min	1h	3h	24h
pore solution (pH=12.8 for w/c=1.0)							
SAP1-A	21.3	26.5	26.8	25.4	24.9	27.4	26.1
SAP1-B	26.5	30.7	29.7	29.3	28.6	29.6	31.7
SAP2-A	12.6	24.4	24.4	24.5	26.2	30.2	34.9
SAP2-B	10.1	22.0	25.1	25.0	25.4	29.5	32.4
deionized water (pH=6.5)							
SAP1-A	109.0	210.9	236.0	249.4	259.8	269.4	302.5
SAP1-B	81.7	289.2	216.4	232.1	236.5	248.3	294.5
SAP2-A	26.0	61.3	93.3	158.4	182.7	218.4	232.7
SAP2-B	29.7	61.9	80.4	122.3	156.8	206.9	238.2

* A and B show cross-checked.

However, as illustrated in Table 6.1 of the manuscript, high dosage of superplasticizer is used for mixture containing 1.0% SAP-1 compared to other mixtures. To check the accuracy of the water absorption capacity for higher dosage of SAP, an approach proposed by Schröfl et al. (2012) is conducted for small trial batch of mixture. Based on this method, water absorption capacity can be obtained by just gradually adding water during mixing to retain the slump constant. For these trial batches (10 litre), the value of **24.97** g water per g dry SAP (i.e., 98.63/3.95) is obtained for SAP-1 in high dosage content (1.0% SAP) (Table-A II-2), which is so close to value used in the experimental tests. Results also indicate that for having the same slump (225 mm), more superplasticizer is necessary for higher dosage of SAP. Finally, similar to SAP-2, the value of 25 g/g is used as an additional water for mixtures containing SAP-1.

Table-A II-2 Mean absorption of SAP (g fluid/g SAP) by slump test (10 litre trial batches)

Mix	Cement	Sand	Gravel 5/10	Gravel 10/14	Water	Add water	SP	SAP	Slump	W_T/C	SAP type
	(kg/m^3)							%	mm	(-)	
RT	395	788	822	258	187	0	14	0	225	0.47	-
100ST1	395	788	822	258	187	98.63	14	1.0	210	0.72	SAP-1

*Note: Add=additional water, SP=superplasticizer, W_T/C=total water to cement ratio, SAP= % wt. of cement.

Although the same slump value is obtained without increasing superplasticizer for trial batch of 1.0% SAP-1 (for 10 litre mixture), high dosage of superplasticizer is used to keep the slump in the same range of the reference concrete for the main batch (55 litre concrete, Table 6.1). Similar issue is reported by Van Tittelboom et al. (2016) in which for mixture containing

0.50% SAP, a high amount of superplasticizer compared to the reference mix is used. It can be attributed to the fact that controlling slump flow in mixtures containing high dosage of SAP without using high amount of superplasticizer is difficult. Hence, more experimental tests are necessary to address this issue by using different types and dosages of superplasticizer for concrete containing high amount of SAP.

APPENDIX III

SEM IMAGE ANALYSIS OF STALACTITES OBSERVED AT THE EXTERNAL LIP OF CRACKS

Other examples of EDS results are summarized here as follows:

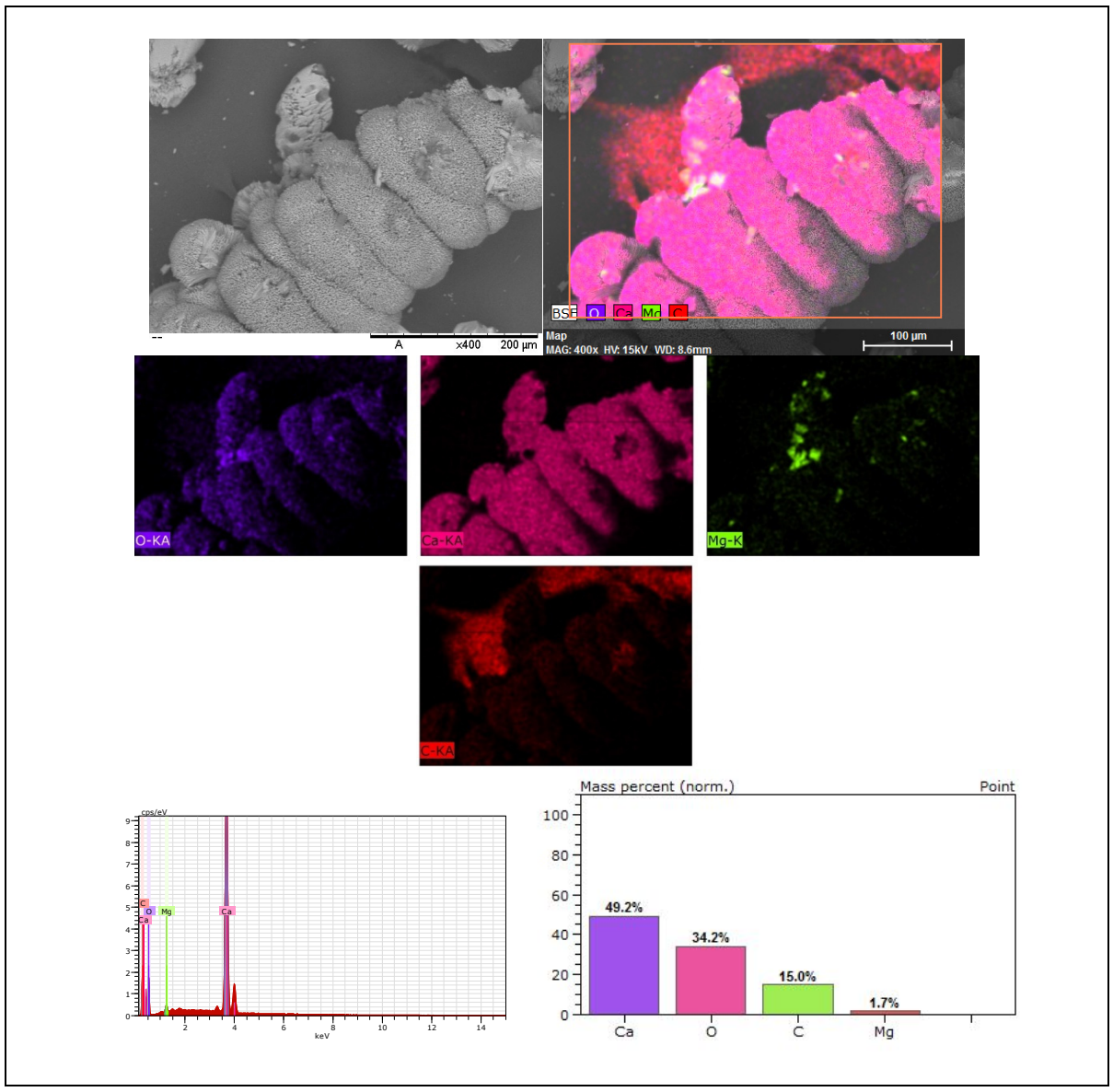

Figure-A III-1 SEM image analysis of stalactites - Second sample

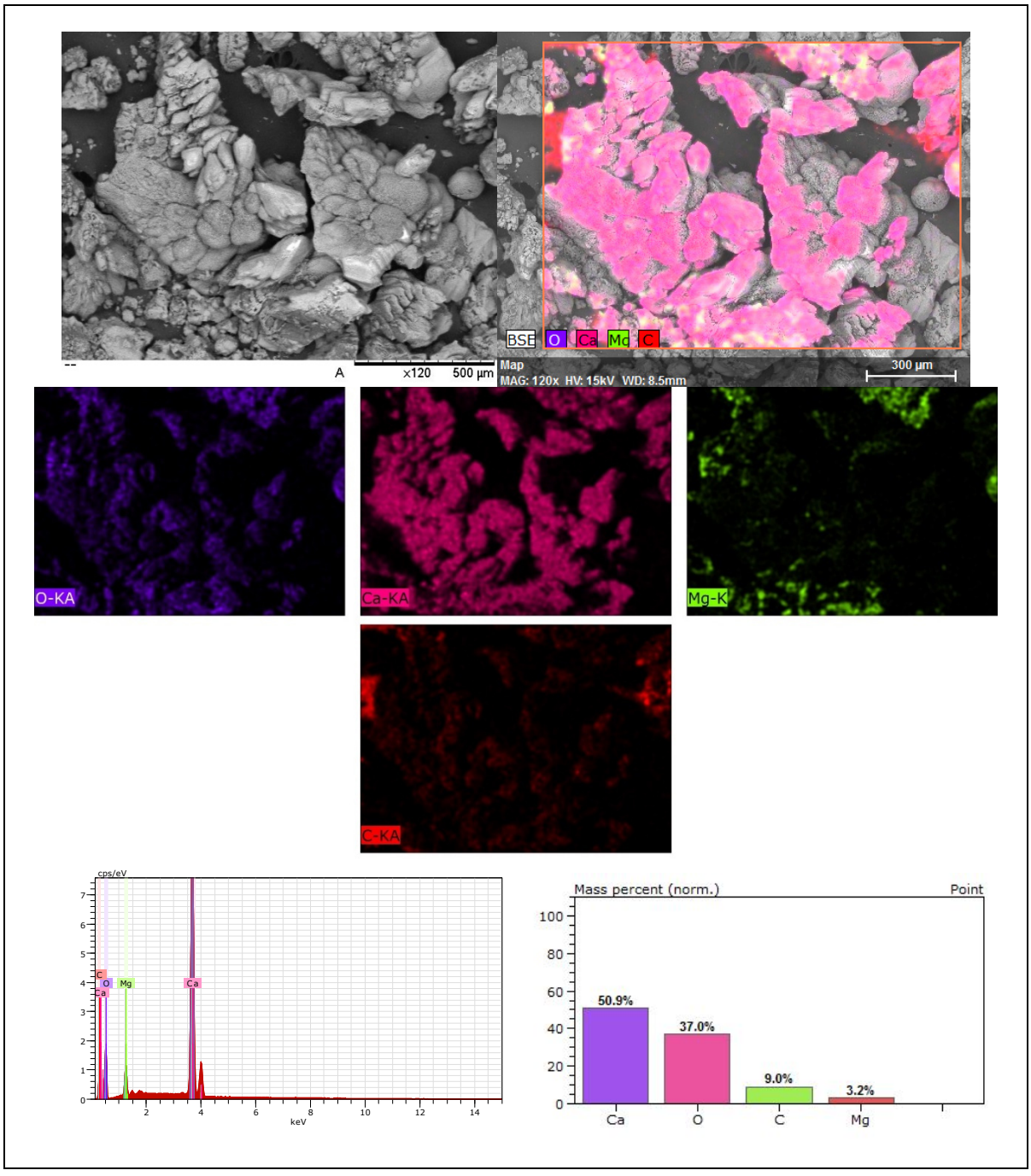

Figure-A III-2 SEM image analysis of stalactites - Third sample

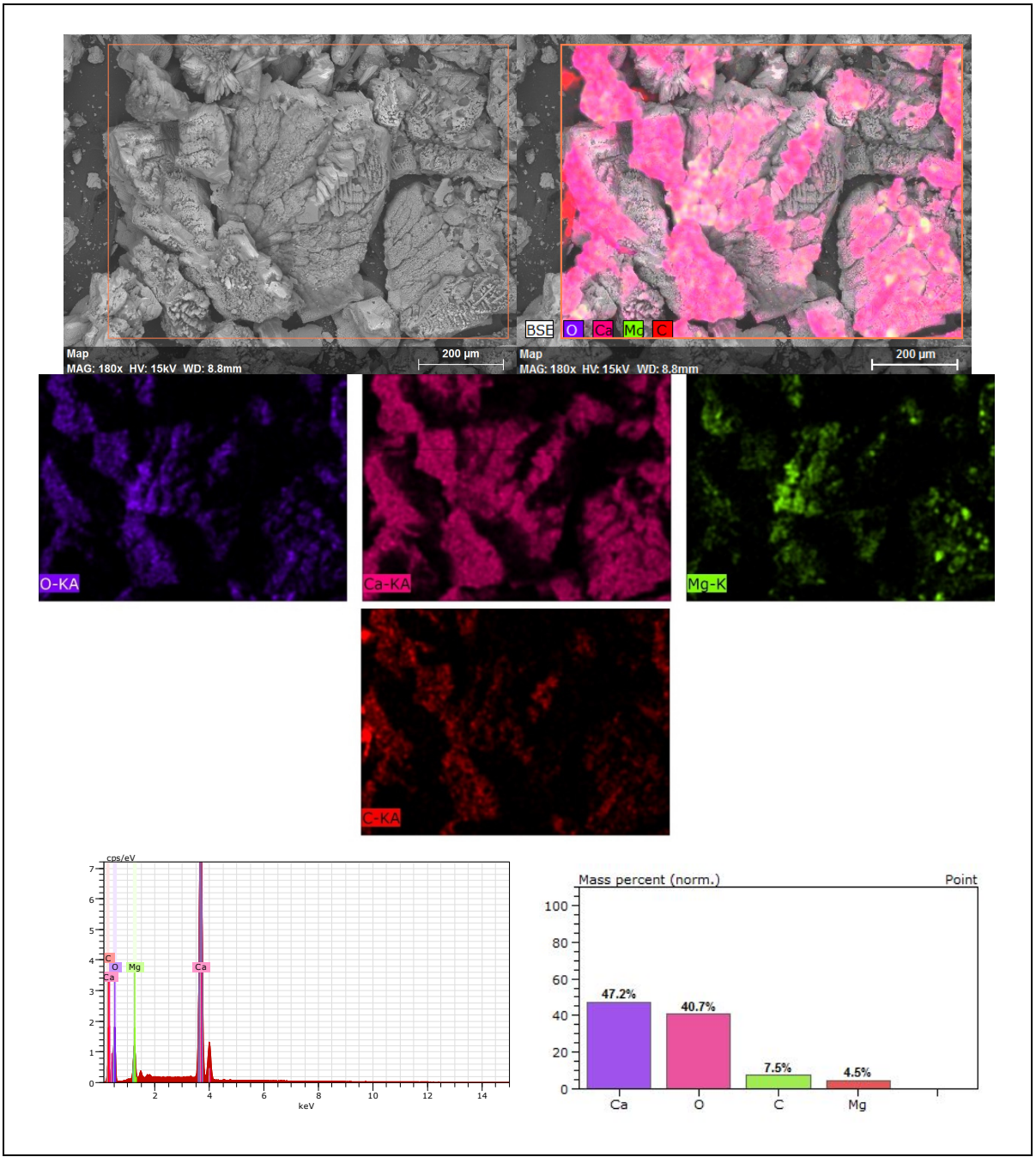

Figure-A III-3 SEM image analysis of stalactites- Fourth sample

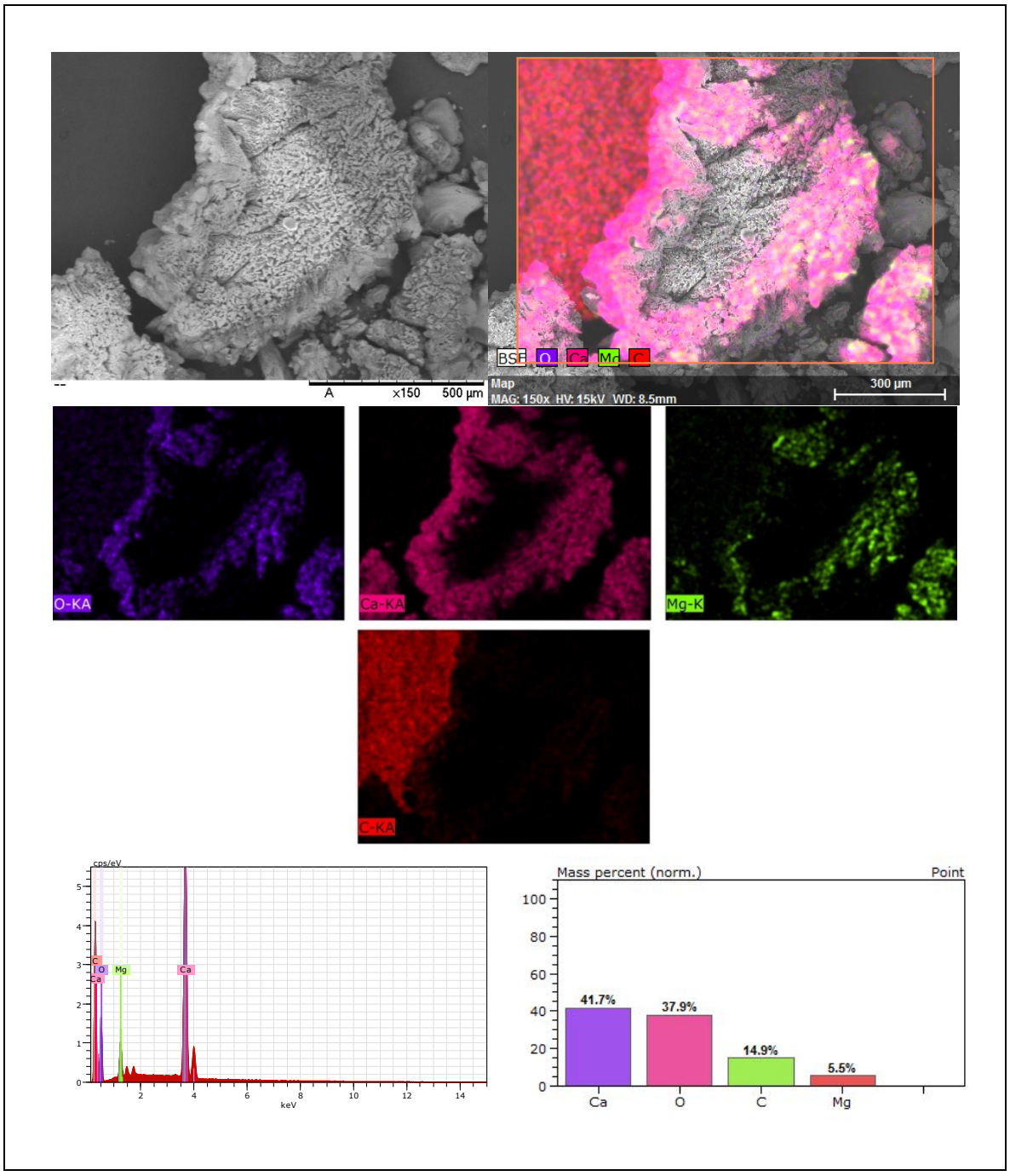

Figure-A III-4 SEM image analysis of stalactites- Fifth sample

APPENDIX IV

SUMMARY OF SIX SAMPLES FOR SIZE AND DISTANCE OF MACRO VOIDS FROM REBAR EDGE

Table-A IV-1 Distance and size of macro voids around the rebar (μm)

Concrete type	SAP (%)	1	2	3	4	5	6	Diameter/Distance ratio		
								Average	Max	Min
RU	0	1055.4	1635.6	1030.8	1718.4	974.4	1413.6	0.17	1.74	0.019
25S1U	0.25	1789.8	2152.8	1830	2001.6	1190.4	2292.6	0.42	2.19	0.053
50S1U	0.5	1584	2094	2383.2	2526	2081.4	3037.8	0.38	2.31	0.058
100S1U	1.0	2706.6	1905.6	3094.8	3530.4	3264	2178.6	0.42	2.91	0.069

APPENDIX V

STATISTICAL ANALYSIS OF ALL HEALING RESULTS

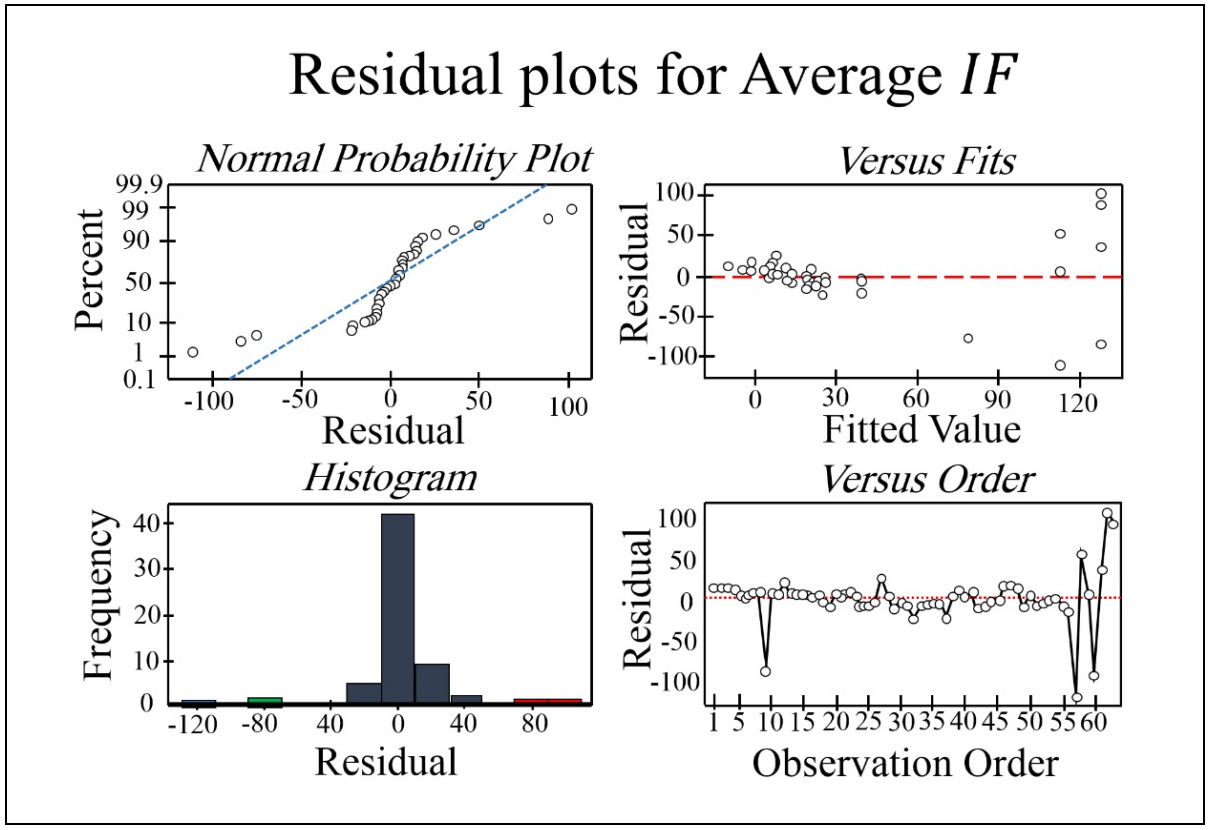

Figure-A V-1 Residual plot for average bond stress IF (IF_{ave})

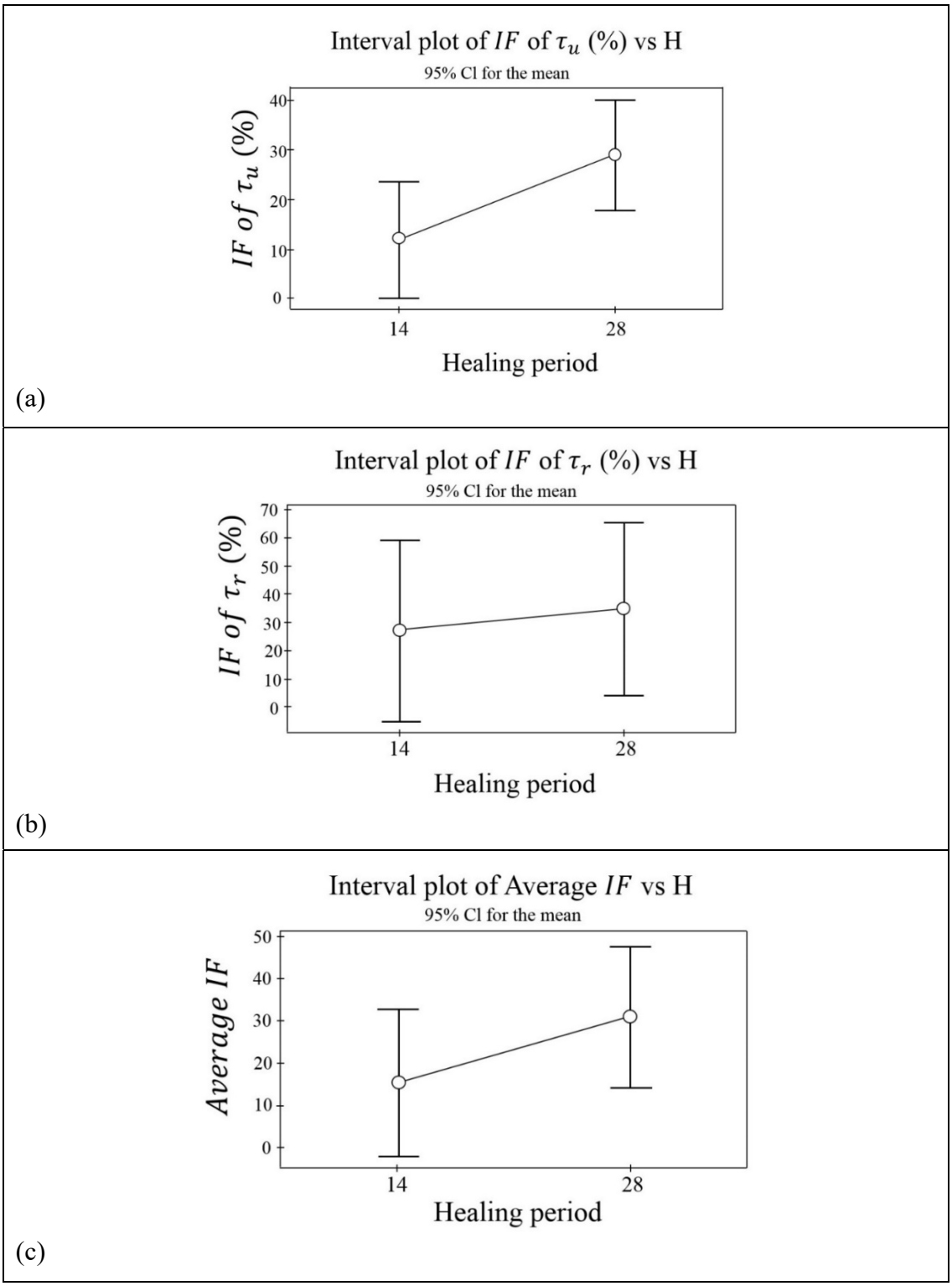

Figure-A V-2 Interval plot of improvement factors with respect to healing periods: (a) IF of bond strength; (b) IF of residual bond stress; (c) average improvement factor

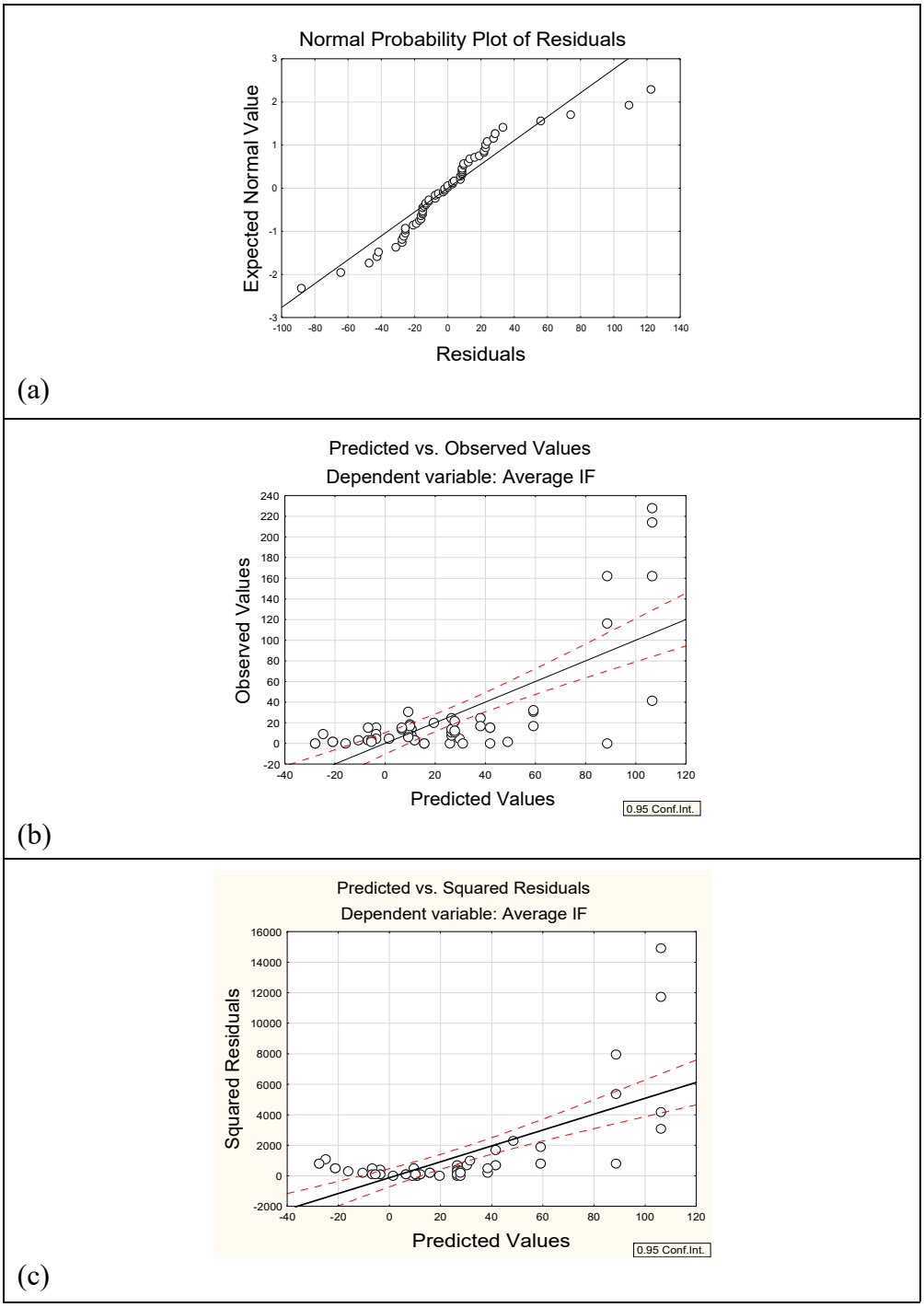

Figure-A V-3 Performance of Eq. (6.11) for IF_{ave}

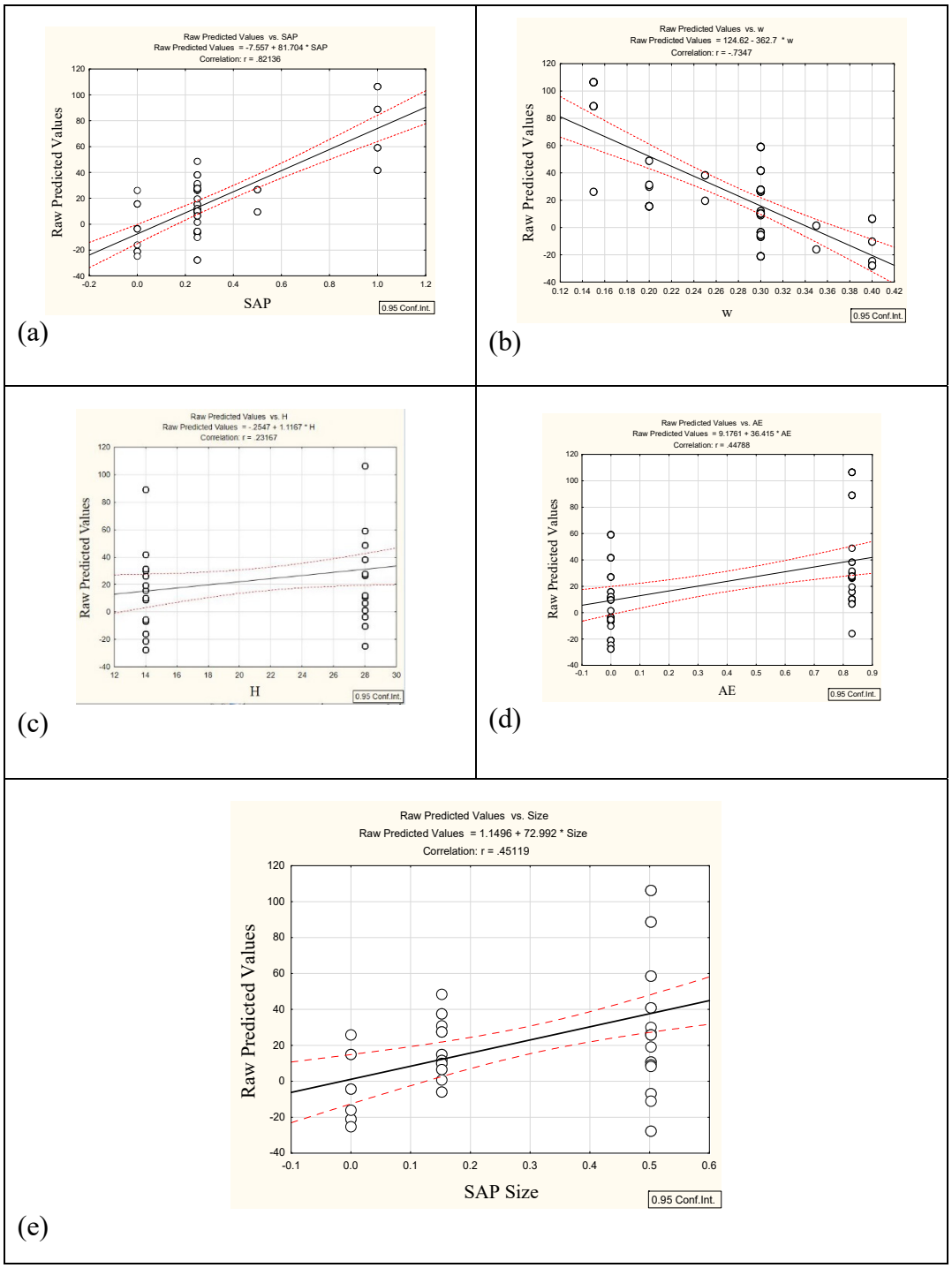

Figure-A V-4 Main effect of variables on IF_{ave} based on multilinear regression in STATISTICA: (a) SAP%; (b) w; (c) H; (d) AE; (e) SAP size (type)

LIST OF REFERENCES

Canadian Standards Association. (2014). *Design of Concrete Structures*. CSA Standard A23.3-14. Mississauga, ON, Canada, 290 pp: Canadian Standards Association.

Abadjiev, P., Panayotov, K. & Petrov, S. (1993). Influence of condensed silica fume as admixture to concrete on the bond to the reinforcement. *Construction and Building Materials*, *7*(1), 41-44. DOI: 10.1016/0950-0618(93)90023-6

Abdel-Jawad, Y. & Haddad, R. (1992). Effect of early overloading of concrete on strength at later ages. *Cement and concrete research*, *22*(5), 927-936. DOI: 10.1016/0008-8846(92)90116-D

American Concrete Institute. (2007). *Self-Consolidating Concrete*. ACI Standard 237R-07. Farmington Hills, Michigan: American Concrete Institute.

American Concrete Institute. (2014). *Building code requirements for structural concrete*. ACI Standard 318-14. Farmington Hills, Michigan: American Concrete Institute.

American Concrete Institute. (2003). *Bond and Development of Straight Reinforcing Bars in Tension*. ACI Standard 408R-03. Detroit, Michigan: American Concrete Institute.

American Concrete Institute. (2008). *Guide to Durable Concrete*. ACI Standard 201.2R-08. Farmington Hills, Michigan: American Concrete Institute.

Ahmad, S., Pilakoutas, K., Rafi, M. M., Khan, Q. U. Z. & Neocleous, K. (2018). Experimental investigation of bond characteristics of deformed and plain bars in low strength concrete. *Scientia Iranica*, *25*(6), 2954-2966. DOI: 10.24200/sci.2017.4570

Aïtcin, P. C. (2016), Entrained air in concrete: Rheology and freezing resistance. In P. C. Aïtcin & R. J. Flatt (Eds.), *Science and Technology of Concrete Admixtures* (pp. 87-95). DOI: 10.1016/B978-0-08-100693-1.00006-0

Aitcin, P. C. & Lessard, M. (1994). Canadian experience with air-entrained high-performance concrete. *Concrete International*, *16*(10), 35-38. Retrieved from https://www.concrete.org/publications/internationalconcreteabstractsportal/m/details/id/4257

Akinpelu, M. A., Odeyemi, S. O., Olafusi, O. S. & Muhammed, F. Z. (2019). Evaluation of splitting tensile and compressive strength relationship of self-compacting concrete. *Journal of King Saud University-Engineering Sciences*, *31*(1), 19-25. DOI: 10.1016/j.jksues.2017.01.002

Al-Hubboubi, S., al-Attar, T., Al-Badry, H., Abood, S., Mohammed, R. & Haddhood, B. (2018). Performance of super-absorbent polymer as an internal curing agent for self-compacting concrete. *MATEC Web of Conferences*, *162*, 02023. DOI: 10.1051/matecconf/201816202023

Al-Nasra, M. (2013). Optimizing the use of sodium polyacrylate in plain concrete. *International Journal of Engineering Research and Applications (IJERA), 3*(3), 1058–1062. Retrieved from https://www.ijera.com/papers/Vol3_issue3/FX3310581062.pdf

Al-Nasra, M. & Daoud, M. (2013). Investigating the use of super absorbent polymer in plain concrete. *International Journal of Emerging Technology and Advanced Engineering*, *3*(8), 598-603. Retrieved from http://www.ijetae.com/files/Volume3Issue8/IJETAE_0813_92.pdf

Al Khalaf, M. & Page, C. (1979). Steel/mortar interfaces: microstructural features and mode of failure. *Cement and Concrete Research*, *9*(2), 197-207. DOI: 10.1016/0008-8846(79)90026-7

Alex, C. N. P. C. (2019). Effect of light weight aggregate and super absorbent polymer as internal curing agent on SCC. *International Research Journal of Engineering and Technology (IRJET)*, 6(5), 7360-7366. Retrieved from https://www.irjet.net/archives/V6/i5/IRJET-V6I51060.pdf

Aliko-Benítez, A., Doblaré, M. & Sanz-Herrera, J. (2015). Chemical-diffusive modeling of the self-healing behavior in concrete. *International Journal of Solids and Structures*, *69*, 392-402. DOI: 10.1016/j.ijsolstr.2015.05.011

Als, W. S. P. & Beton, Z. F. H. (2005). Water saturated super-absorbent polymers used in high strength concrete. *Otto-Graf-Journal*, *16*, 193. Retrieved from https://www.mpa.uni-stuttgart.de/institut/publikationen/otto-graf-journal/new_downloadgallery/2005/2005_beitrag_moennig.pdf

Alva, G. M. S. & de Cresce El, A. L. H. (2013). Moment–rotation relationship of RC beam-column connections: Experimental tests and analytical model. *Engineering Structures*, *56*, 1427-1438. DOI: 10.1016/j.engstruct.2013.07.016

Amura, h. o. & Ouchi, m. (1999), Self-compacting concrete. development, present use and future. In Å. Skarendahl & Ö. Petersson (Eds.), *1st International RILEM Symposium on Self-Compacting Concrete, Stockholm, Sweden, September 13* (pp. 3-14). RILEM Publications. Retrieved from https://www.rilem.net/publication/publication/12?id_papier=1275

Arezoumandi, M., Looney, T. J. & Volz, J. S. (2015). Effect of fly ash replacement level on the bond strength of reinforcing steel in concrete beams. *Journal of Cleaner Production*, *87*, 745-751. DOI: 10.1016/j.jclepro.2014.10.078

Arezoumandi, M., Wolfe, M. H. & Volz, J. S. (2013). A comparative study of the bond strength of reinforcing steel in high-volume fly ash concrete and conventional concrete. *Construction and Building Materials*, *40*, 919-924. DOI: 10.1016/j.conbuildmat.2012.11.105

Arslan, G. (2004). Mesh size effect on load carrying capacity of the reinforced concrete beams without stirrups by using drucker-prager and cracking concrete fracture criteria. *Sigma Journal of Engineering and Natural Sciences*, *22*(3), 34-42. Retrieved from http://eds.yildiz.edu.tr/AjaxTool/GetArticleByPublishedArticleId?PublishedArticleId=1565

Arya, S., Das, B. & Goudar, S. K. (2019). Microstructural Study of Steel-Concrete Interface and Its Influence on Bond Strength of Reinforced Concrete. *Advances in Civil Engineering Materials*, *8*(1), 171-189. DOI: 10.1520/ACEM20180133

ASTM International. (2009). *Standard test method for slump flow of self-consolidating concrete*. ASTM Standard C1611/C1611M-09be1. Retrieved from https://www.astm.org/DATABASE.CART/HISTORICAL/C1611C1611M-09BE1.htm

AzariJafari, H., Kazemian, A., Rahimi, M. & Yahia, A. (2016). Effects of pre-soaked super absorbent polymers on fresh and hardened properties of self-consolidating lightweight concrete. *Construction and Building Materials*, *113*, 215-220. DOI: 10.1016/j.conbuildmat.2016.03.010

Baloch, H., Usman, M., Rizwan, S. A. & Hanif, A. (2019). Properties enhancement of super absorbent polymer (SAP) incorporated self-compacting cement pastes modified by nano silica (NS) addition. *Construction and Building Materials*, *203*, 18-26. DOI: 10.1016/j.conbuildmat.2019.01.096

Baltay, P. & Gjelsvik, A. (1990). Coefficient of friction for steel on concrete at high normal stress. *Journal of Materials in Civil Engineering*, *2*(1), 46-49. DOI: 10.1061/(ASCE)0899-1561(1990)2:1(46)

Bassuoni, M. & Nehdi, M. (2005). The case for air-entrainment in high-performance concrete. *Proceedings of the Institution of Civil Engineers-Structures and Buildings*, *158*(5), 311-319. DOI: 10.1680/stbu.2005.158.5.311

Beaupré, D., Lacombe, P. & Khayat, K. (1999). Laboratory investigation of rheological properties and scaling resistance of air entrained self-consolidating concrete. *Materials and Structures*, *32*(3), 235-240. DOI: 10.1007/BF02481521

Belarbi, A. & Hsu, T. T. (1994). Constitutive laws of concrete in tension and reinforcing bars stiffened by concrete. *Structural Journal*, *91*(4), 465-474. DOI: 10.14359/4154

Belarbi, A. & Hsu, T. T. C. (1991). *Constitutive laws of reinforced concrete in biaxial tension-compression* (Report No. UHCEE 91-2). Houston: Department of Civil & Environmental Engineering, University of Houston.

Bentz, D. P., Geiker, M. & Jensen, O. M. (2002), On the mitigation of early age cracking. In B. Persson & G. Fagerlund (Eds.), *Proceedings of the 3rd International Seminar on Self-Desiccation and Its Importance in Concrete Technology* (pp. 195-203). Lund, Sweden: Division of Building Materials, LTH, Lund University.

Bentz, D. P. & Weiss, W. J. (2011). *Internal curing: a 2010 state-of-the-art review* (Report No. NISTIR 7765). Maryland: US Department of Commerce, National Institute of Standards and Technology Gaithersburg.

Bergmeister, K. (1988). *Stochastik in der Befestigungstechnik mit realistischen Einflussgrößen* [Stochastic in fastening technology under realistic variables]. (Doctoral thesis, Universität Innsbruck, Austria).

Beushausen, H. & Gillmer, M. (2014). The use of superabsorbent polymers to reduce cracking of bonded mortar overlays. *Cement and Concrete Composites*, *52*, 1-8. DOI: 10.1016/j.cemconcomp.2014.03.009

Beushausen, H., Gillmer, M. & Alexander, M. (2014). The influence of superabsorbent polymers on strength and durability properties of blended cement mortars. *Cement and Concrete Composites*, *52*, 73-80. DOI: 10.1016/j.cemconcomp.2014.03.008

Biolzi, L., Cattaneo, S., & Mola, F. (2014). Bending-shear response of self-consolidating and high-performance reinforced concrete beams. *Engineering structures*, *59*, 399-410. DOI: 10.1016/j.engstruct.2013.10.043

Biuriani, E. & Plizzari, G. (1985). Legami locali dell'aderenza in presenza di fessure di «splitting». *Studi e ricerche—Corso di perfezionamento per le costruzioni in cemento armato Fratelli Pasenti,* 7, 57-118. Retrieved from https://pascal-francis.inist.fr/vibad/index.php?action=getRecordDetail&idt=8094419

Bompa, D. & Elghazouli, A. (2017). Bond-slip response of deformed bars in rubberised concrete. *Construction and Building Materials*, *154*, 884-898. DOI: 10.1016/j.conbuildmat.2017.08.016

Brantschen, F. (2016). *Influence of bond and anchorage conditions of the shear reinforcement on the punching strength of RC slabs*. (Doctoral thesis, École polytechnique fédérale de Lausanne (EPFL), Lausanne, Switzerland).

Brantschen, F., Faria, D., Fernández Ruiz, M. & Muttoni, A. (2016). Bond behaviour of straight, hooked, U-shaped and headed bars in cracked concrete. *Structural Concrete*, *17*(5), 799-810. DOI: 10.1002/suco.201500199

Brettmann, B. B., Darwin, D. & Donahey, R. C. (1986). Bond of Reinforcement to Superplasticized Concrete. *ACI JOURNAL Proceedings*, *83*(1), 98-107. DOI: 10.14359/1743

Bruere, G. (1967). *Fundamental actions of air-entraining agents*. Paper presented at International Symposium on Admixture for Mortar and Concrete, RILEM Publications, Brussels, Belgium (pp. 7-23).

British Standards Institution. (1997). *Structural use of concrete, part 1. Code of practice for design and construction*. BS 8110-1:1997. London, England: British Standards Institution (BSI).

Bubshait, A. A. & Tahir, B. (1997). Effect of silica fume on the concrete-steel bond. *Building Research & Information*, *25*(6), 365-369. DOI: 10.1080/096132197370183

Burge, T. A. (1983). High strength lightweight concrete with condensed silica fume. *Special Publication*, *79*, 731-746. Retrieved from https://www.concrete.org/publications/internationalconcreteabstractsportal.aspx?m=details&ID=6722

Cairns, J. (2015). Bond and anchorage of embedded steel reinforcement in fib Model Code 2010. *Structural Concrete*, *16*(1), 45-55. DOI: 10.1002/suco.201400043

Cairns, J. & Abdullah, R. B. (1996). Bond strength of black and epoxy-coated reinforcement-a theoretical approach. *ACI Materials Journal*, *93*(4), 362-369. DOI: 10.14359/9823

Cairns, J. & Jones, K. (1995). Influence of rib geometry on strength of lapped joints: an experimental and analytical study. *Magazine of Concrete Research*, *47*(172), 253-262. DOI: 10.1680/macr.1995.47.172.253

Canadian Standard Association. (2009). *Carbon steel bars for concrete reinforcement*. CSA Standard G30.18-09. Mississauga, Ontario, Canada: Canadian Standard Association

Carvalho, E. P., Miranda, M. P., Fernandes, D. S. & Alves, G. V. (2018). Comparison of test methodologies to evaluate steel-concrete bond strength of thin reinforcing bar. *Construction and Building Materials*, *183*, 243-252. DOI: 10.1016/j.conbuildmat.2018.06.109

Castel, A., Vidal, T., Viriyametanont, K. & François, R. (2006). Effect of reinforcing bar orientation and location on bond with self-consolidating concrete. *ACI Materials Journal*, *103*(4), 559. DOI: 10.14359/16432

Castro, J., de la Varga, I., Golias, M. & Weiss, J. (2010, February). *Extending internal curing concepts (using fine LWA) to mixtures containing high volumes of fly ash*. Paper presented at 2010 Concrete Bridge Conference: Achieving Safe, Smart & Sustainable

Bridges, Phoenix, Arizona.

Cela, J. J. L. (1998). Analysis of reinforced concrete structures subjected to dynamic loads with a viscoplastic Drucker–Prager model. *Applied Mathematical Modelling*, *22*(7), 495-515. DOI: 10.1016/S0307-904X(98)10050-1

Cervenka, V. (1985). Constitutive model for cracked reinforced concrete. *ACI Structural Journal, 82*(6), 877-882. DOI: 10.14359/10409

Chen, F., Li, C. Q., Baji, H. & Ma, B. (2019). Effect of design parameters on microstructure of steel-concrete interface in reinforced concrete. *Cement and Concrete Research*, *119*, 1-10. DOI: 10.1016/j.cemconres.2019.01.005

Choi, O. & Yang, S. (2010, May). *Bond analysis model of deformed bars to concrete*. Paper presented at 7th International Conference on Fracture Mechanics of Concrete and Concrete Structures, Korea Concrete Institute, Seoul (pp. 811-815).

Choi, O. C., Choi, H. & Hong, G. (2010). Bearing Angle Model for Bond of Reinforcing Bars in Concrete. *ACI Structural Journal*, *14*(1), 245-253. DOI: 10.14359/51689256

Choi, O. C. & Lee, W. S. (2002). Interfacial bond analysis of deformed bars to concrete. *ACI Structural Journal*, *99*(6), 750-756. DOI: 10.14359/12339

Choi, Y., Lee, H.-K., Chu, S., Cheong, S. & Jung, W. (2012). Shear behavior and performance of deep beams made with self-compacting concrete. *International Journal of Concrete Structures and Materials*, *6*(2), 65-78. DOI: 10.1007/s40069-012-0007-y

Chung, C. (1981). Application of the Buffon needle problem and its extensions to parallel-line search sampling scheme. *Journal of the International Association for Mathematical Geology*, *13*(5), 371-390. DOI: 10.1007/BF01079642

Collepardi, M. & Corradi, M. (1979). Influence of naphthalene-sulfonated polymer based Superplasticizers on the strength of ordinary and lightweight concretes. *Special Publication*, *62*, 315-336. Retrieved from https://www.concrete.org/publications/internationalconcreteabstractsportal/m/details/id/17731

Coronelli, D. & Mulas, M. G. (2001). Local–global approach in the seismic analysis of R/C frames including bond slip effects. *Engineering Structures*, *23*(8), 911-925. DOI: 10.1016/S0141-0296(00)00116-4

Craeye, B. (2006). *Reduction of autogenous shrinkage of concrete by means of internal curing* [in Dutch]. (Master's dissertation, Magnel Laboratory for Concrete Research, Ghent Univerity, Ghent, Belgium).

Craeye, B., Cockaerts, G. & Kara De Maeijer, P. (2018). Improving Freeze–Thaw Resistance of Concrete Road Infrastructure by Means of Superabsorbent Polymers. *Infrastructures*, *3*(1), 4. DOI: 10.3390/infrastructures3010004

Craeye, B. & De Schutter, G. (2008, September & October). *Experimental evaluation of mitigation of autogenous shrinkage by means of a vertical dilatometer for concrete*. Paper presented at Eight International Conference on Creep, Shrinkage and Durability Mechanics of Concrete and Concrete Structures, Ise-Shima, Japan (pp. 909-914).

Craeye, B., Geirnaert, M. & De Schutter, G. (2011). Super absorbing polymers as an internal curing agent for mitigation of early-age cracking of high-performance concrete bridge decks. *Construction and Building Materials*, *25*(1), 1-13. DOI: 10.1016/j.conbuildmat.2010.06.063

Cross, D., Stephens, J. & Vollmer, J. (2005, April). *Structural applications of 100 percent fly ash concrete*. Paper presented at World of Coal Ash (WOCA), Lexington, Kentucky.

Crouch, L., Sauter, H. J. & Williams, J. A. (2000). 92-MPa air-entrained high-performance concrete using Tennessee materials. *Transportation research record*, *1698*(1), 24-29. DOI: 10.3141/1698-04

Canadian Standards Association. (2014). *Concrete materials and methods of concrete construction/Test methods and standard practices for concrete*. CSA Standard A23.1-14/A23.2-14. Mississauga, Ontario, Canada: Canadian Standards Association.

Daczko, J. A. (2012). *Self-consolidating concrete: applying what we know* (1st ed.). Boca Raton, Florida: Spon Press (pp. 289).

Dakhil, F. H., Cady, P. D. & Carrier, R. E. (1975). Cracking of fresh concrete as related to reinforcement. *ACI Journal Proceedings*, *72*(8), 421-428. DOI: 10.14359/11145. Retrieved from https://www.concrete.org/publications/internationalconcreteabstractsportal/m/details/id/11145

Darwin, D. & Graham, E. K. (1993). Effect of deformation height and spacing on bond strength of reinforcing bars. *ACI Structural Journal*, *90*(6), 646-657. DOI: 10.14359/4459

Dawood, N. & Marzouk, H. (2012). Cracking and tension stiffening of high-strength concrete panels. *ACI Structural Journal*, *109*(1), 21-30. DOI: 10.14359/51683490

de Almeida Filho, F. M., Mounir, K. & El Debs, A. L. H. (2008). Bond-slip behavior of self-compacting concrete and vibrated concrete using pull-out and beam tests. *Materials and Structures*, *41*(6), 1073-1089. DOI: 10.1617/s11527-007-9307-0

Dehestani, M., Asadi, A. & Mousavi, S. (2017). On discrete element method for rebar-concrete interaction. *Construction and Building Materials*, *151*, 220-227. DOI: 10.1016/j.conbuildmat.2017.06.086

Dehestani, M. & Mousavi, S. (2015). Modified steel bar model incorporating bond-slip effects for embedded element method. *Construction and Building Materials*, *81*, 284-290. DOI: 10.1016/j.conbuildmat.2015.02.027

Deng, P. & Matsumoto, T. (2018). Determination of dominant degradation mechanisms of RC bridge deck slabs under cyclic moving loads. *International Journal of Fatigue*, *112*, 328-340. DOI: 10.1016/j.ijfatigue.2018.03.033

Desnerck, P., De Schutter, G. & Taerwe, L. (2010). Bond behaviour of reinforcing bars in self-compacting concrete: experimental determination by using beam tests. *Materials and Structures*, *43*(1), 53-62. DOI: 10.1617/s11527-010-9596-6

Desnerck, P., Lees, J. M. & Morley, C. T. (2015). Bond behaviour of reinforcing bars in cracked concrete. *Construction and Building Materials*, *94*, 126-136. DOI: 10.1016/j.conbuildmat.2015.06.043

Desnerck, P., Lees, J. M. & Morley, C. T. (2017). The effect of local reinforcing bar reductions and anchorage zone cracking on the load capacity of RC half-joints. *Engineering Structures*, *152*, 865-877. DOI: 10.1016/j.engstruct.2017.09.021

Dhir, R., Jones, M., Ahmed, H. & Seneviratne, A. (1990). Rapid estimation of chloride diffusion coefficient in concrete. *Magazine of Concrete Research*, *42*(152), 177-185. DOI: 10.1680/macr.1990.42.152.177

Dhir, R., Jones, M. & Senerirathe, A. (1991). Diffusion of chlorides into concrete influence of PFA quality. *Cement and concrete research*, *21*(6), 1092-1102. DOI: 10.1016/0008-8846(91)90069-t

Dhir, R., McCarthy, M., Limbachiya, M., El Sayad, I. & Zhang, D. (1999). Pulverized fuel ash concrete: air entrainment and freeze/thaw durability. *Magazine of Concrete Research*, *51*(1), 53-64. DOI: 10.1680/macr.1999.51.1.53

Dhir, R. K., Sangha, C. M. & Munday, J. G. (1973). Strength and deformation properties of autogenously healed mortars. *ACI Journal Proceedings*, *70*(3), 231-236. DOI: 10.14359/11202

Deutsches Institut für Normung. (2001). *Tragwerke aus Beton, Stahlbeton und Spannbeton. Teil 1: Bemessung und Konstruktion*. DIN Standard 1045-1. Berlin: Deutsches Institut für Normung.

Dolch, W. L. (1996), Air-entraining admixtures. In V.S. Ramachandran (Ed.), *Concrete Admixtures Handbook: Properties, Science, and Technology* (2nd Edition, pp. 518-557). Elsevier. DOI: 10.1016/b978-081551373-5.50012-x

Domone, P. (2006). Self-compacting concrete: An analysis of 11 years of case studies. *Cement and concrete composites*, *28*(2), 197-208. DOI: 10.1016/j.cemconcomp.2005.10.003

Dudziak, L. & Mechtcherine, V. (2008), Mitigation of volume changes of ultra-high performance concrete (UHPC) by using super absorbent polymers. In E. Fehling, M. Schmidt, & S. Stürwald (Eds.), *2nd international symposium on ultra high performance concrete, Kassel, Germany, March 05-07* (pp. 425-432). Kassel: Kassel University Press.

Dudziak, L. & Mechtcherine, V. (2009), Reducing the cracking potential of ultra-high performance concrete by using Super Absorbent Polymers (SAP). In G. van Zijl & W.P. Boshoff (Eds.), *Advances in Cement-Based Materials: Proc. Int. Conf. Advanced Concrete Materials, November 17-19, 2009, Stellenbosch, South Africa* (pp. 11-19). London: Taylor & Francis Group.

Dybeł, P. & Furtak, K. (2015). The effect of ribbed reinforcing bars location on their bond with high-performance concrete. *Archives of Civil and Mechanical Engineering*, *15*(4), 1070-1077. DOI: 10.1016/j.acme.2015.03.008

European federation of national trade associations representing producers and applicators of specialist building products. (2002). *Specification and guidelines for self-compacting concrete*. EFNARC . Retrieved from http://www.efnarc.org/pdf/SandGforSCC.PDF

Eibl, J., Idda, K. & Lucero-Cimas, H.-N. (1999). Verbundverhalten bei Querzug. *KURZBERICHTE AUS DER BAUFORSCHUNG*, 40(1). Retrieved from https://trid.trb.org/view/963179

Einpaul, J., Brantschen, F., Fernández Ruiz, M. & Muttoni, A. (2016). Performance of punching shear reinforcement under gravity loading: Influence of type and detailing. *ACI Structural Journal*, *113*(4), 827-838. DOI: 10.14359/51688630

El-Feky, M.S., Serag, M.I., Yasien, A.M. & Elkady, H. (2016). Bond strength of nano silica concrete subjected to corrosive environments. *ARPN Journal of Engineering and Applied Sciences, 11*(23), 13909-13924. Retrieved from http://www.arpnjournals.org/jeas/research_papers/rp_2016/jeas_1216_5472.pdf

Eligehausen, R. & Bozenhardt, A. (1989). *Crack widths as measured in actual structures and conclusions for the testing of fastening elements* (Research report No. 1/42-89/9). University of Stuttgart, Stuttgart, Germany: Institute of Construction Materials.

Eligehausen, R., Popov, E. P. & Bertero, V. V. (1983). *Local Bond Stress-Slip Relationships of Deformed Bars under Generalized Excitations* (Research report No. UCB/EERC-83/23). University of California, Berkeley, California.

Eom, T.-S., Hwang, H.-J. & Park, H.-G. (2015). Energy-Based Hysteresis Model for Reinforced Concrete Beam-Column Connections. *ACI Structural Journal*, *112*(3). DOI: 10.14359/51687404

Esfahani, M. R. & Kianoush, M. R. (2005). Development/splice length of reinforcing bars. *ACI structural journal*, *102*(1), 22-30. DOI: 10.14359/13527

Esfahani, M. R., Lachemi, M. & Kianoush, M. R. (2008). Top-bar effect of steel bars in self-consolidating concrete (SCC). *Cement and Concrete Composites*, *30*(1), 52-60. DOI: 10.1016/j.cemconcomp.2007.05.012

Esfahani, M. R. & Rangan, B. V. (1998). Bond between normal strength and high-strength concrete (HSC) and reinforcing bars in splices in beams. *Structural Journal*, *95*(3), 272-280. DOI: 10.14359/545

Esteves, L. P., Cachim, P. & Ferreira, V. M. (2007). Mechanical properties of cement mortars with superabsorbent polymers. *Advances in Construction Materials 2007*, Springer, 451-462. DOI: 10.1007/978-3-540-72448-3_45

Falikman V.R. (2020), Effect of SAP on the Freeze-Thaw Resistance of Concrete: Tests According to Russian Standards. In W. Boshoff, R. Combrinck, V. Mechtcherine & M. Wyrzykowski (Eds.), *3rd International Conference on the Application of Superabsorbent Polymers (SAP) and Other New Admixtures Towards Smart Concrete* (Vol. 24, pp. 57-64). Cham, Skukuza, South Africa: RILEM Bookseries, Springer. DOI: 10.1007/978-3-030-33342-3_7

Fallah, M. M., Shooshtari, A. & Ronagh, H. R. (2013). Investigating the effect of bond slip on the seismic response of RC structures. *Structural Engineering and Mechanics*, *46*(5), 695-711. DOI: 10.12989/sem.2013.46.5.695

Feng, Q., Visintin, P. & Oehlers, D. J. (2015). Deterioration of bond–slip due to corrosion of steel reinforcement in reinforced concrete. *Magazine of Concrete Research*, *68*(15), 768-781. DOI: 10.1680/jmacr.15.00217

Fernandes, C., Varum, H. & Costa, A. (2013). Importance of the bond–slip mechanism in the numerical simulation of the cyclic response of RC elements with plain reinforcing bars. *Engineering Structures*, *56*, 396-406. DOI: 10.1016/j.engstruct.2013.05.013

Fernández Ruiz, M., Hars, E. & Muttoni, A. (2005). *Bond mechanics in structural concrete. Theoretical model and experimental results* (Research report No. IS-BETON). Lausanne, Switzerland: Ecole Polytechnique Federale de Lausanne.

The Fédération internationale du béton (CEB-FIP). (2000). *Bond of reinforcement in concrete: state-of-art report* (Research fib Bulletin No. 10, pp. 434). Lausanne, Switzerland: Fédération Internationale du Béton. DOI: 10.35789/fib.BULL.0010

fédération internationale du béton. (2013). *fib Model Code for Concrete Structures 2010*. fib Model Code 2010. Lausanne: fédération internationale du béton/International Federation for Structural.

Filip, C. & Ahmad, I. (1988). *Nonlinear analysis of reinforced concrete frames under cyclic load reversals* (Research report No. UCB/EERC-88/12). Berkeley, Calif: Earthquake Engineering Research Center, University of California.

Fu, X. & Chung, D. (1998). Combined use of silica fume and methylcellulose as admixtures in concrete for increasing the bond strength between concrete and steel rebar. *Cement and concrete research*, *28*(4), 487-492. DOI: 10.1016/s0008-8846(98)00016-7

Fu, X. & Chung, D. (1998). Effects of Water-Cement Ratio, Curing Age, Silica Fume, Polymer Admixtures, Steel Surface Treatments and Corrosion on the Bond between Concrete and Steel Reinforcing Bar. *Materials Journal*, *95*(6), 725-734. DOI: 10.14359/417

Gagné, R. (2016). Air entraining agents." *Science and Technology of Concrete Admixtures*, Elsevier, 379-391. DOI: 10.1016/B978-0-08-100693-1.00017-5

Gagne, R., Pigeon, M. & Aitcin, P. (1991). Deicer salt scaling resistance of high strength concretes made with different cements. *Special Publication*, *126*, 185-200. DOI: 10.14359/9759

Gambarova, P. & Karakoç, C. (1981). In tema di aderenza fra barre nervate e calcestruzzo, in presenza di fissure longitudinali da spacco. *Studi e Ricerche*, *3*, 143-176.

Gambarova, P., Rosati, G. & SUFI, E. (1993). Aderenza armatura-calcestruzzo e fessurazione longitudinale per barre di piccolo diametro. *Studi e ricerche-Politecnico di Milano. Scuola di specializzazione in costruzioni in cemento armato, 14*, 1-27. Retrieved from https://pascal-francis.inist.fr/vibad/index.php?action=getRecordDetail&idt=3563200

Gambarova, P. & Zasso, B. (1985). Aderenza armatura-calcestruzzo e fessurazione longitudinale da spacco: una sintesi di alcuni recenti risultati sperimentali. *Studi e ricerche—Corso di perfezionamento per le costruzioni in cemento armato Fratelli Pasenti, 7*, 7-54. Retrieved from https://pascal-francis.inist.fr/vibad/index.php?action=getRecordDetail&idt=8042184

Gambarova, P. G., Rosati, G. P. & Zasso, B. (1989). Steel-to-concrete bond after concrete splitting: test results. *Materials and Structures*, *22*(1), 35-47. DOI: 10.1007/BF02472693

Gardner, N., Sau, P. & Cheung, M. (1986). Strength development and durability of CSA Type 30 cement/slag/fly-ash concretes for arctic marine applications. *Durability of building materials*, *4*(2), 179-200. Retrieved from https://www.osti.gov/etdeweb/biblio/6761183

Geiker, M. R., Bentz, D. P. & Jensen, O. M. (2004). Mitigating autogenous shrinkage by internal curing. In *High-Performance Structural Lightweight Concrete, American Concrete Institute Special Publication*, 143-154. Retrieved from https://www.researchgate.net/profile/D_Bentz/publication/238607657_Mitigating_Autogenous_Shrinkage_by_Internal_Curing/links/00b4951c04b9d34741000000/Mitigating-Autogenous-Shrinkage-by-Internal-Curing.pdf

Gibbs, J. & Zhu, W. (1999), Strength of hardened self-compacting concrete. In *1st International RILEM Symposium on Self-Compacting Concrete (PRO 7), Stockholm, Suede* (pp. 199-209). RILEM Publications S.A.R.L.

Giuriani, E., Plizzari, G. & Schumm, C. (1991). Role of stirrups and residual tensile strength of cracked concrete on bond. *Journal of Structural Engineering*, *117*(1), 1-18. DOI: 10.1061/(asce)0733-9445(1991)117:1(1)

Giuriani, E. & Plizzari, G. A. (1998). Interrelation of splitting and flexural cracks in RC beams. *Journal of Structural Engineering*, *124*(9), 1032-1049. DOI: 10.1061/(asce)0733-9445(1998)124:9(1032)

Gjorv, O. E., Monteiro, P. J. & Mehta, P. K. (1990). Effect of condensed silica fume on the steel-concrete bond. *Materials Journal*, *87*(6), 573-580. DOI: 10.14359/2527

Gopalakrishnan, S., Lakshmanan, N., Rajamane, N., Krishnamoorthy, T., Neelamegam, M., Chellappan, A., AnniePeter, J., Balasubramanian, K., Prabhakar, J. & Bharatkumar, B. (2005). *Demonstration of utilising high volume fly ash based concrete for structural applications* (A report Prepared for Confederation of Indian Industry (CII)). India. Retrieved from https://serc.res.in/demonstration-utilising-high-volume-fly-ash-based-concrete-structural-applications

Granger, S., Loukili, A., Pijaudier-Cabot, G. & Chanvillard, G. (2007). Experimental characterization of the self-healing of cracks in an ultra high performance cementitious material: Mechanical tests and acoustic emission analysis. *Cement and Concrete Research*, *37*(4), 519-527. DOI: 10.1016/j.cemconres.2006.12.005

Guizani, L., Chaallal, O. & Mousavi, S. S. (2017). Local bond stress-slip model for reinforced concrete joints and anchorages with moderate confinement. *Canadian Journal of Civil Engineering*, *44*(3), 201-211. DOI: 10.1139/cjce-2015-0333

Hadidi, R. & Saadeghvaziri, M. A. (2005). Transverse cracking of concrete bridge decks: State-of-the-art. *Journal of Bridge Engineering*, *10*(5), 503-510. DOI: 10.1061/(asce)1084-0702(2005)10:5(503)

Hakuto, S., Park, R. & Tanaka, H. (1999). Effect of deterioration of bond of beam bars passing through interior beam-column joints on flexural strength and ductility. *Structural Journal*, *96*(5), 858-864. DOI: 10.14359/740

Hamad, B. (2000). Overview of Anchorage Problems of Reinforcing Bars in High-Performance Silica Fume Concrete. *Special Publication*, *193*, 847-870. Retrieved from https://www.concrete.org/publications/internationalconcreteabstractsportal/m/details/id/9964

Hamad, B. & Machaka, M. (1999). Effect of transverse reinforcement on bond strength of reinforcing bars in silica fume concrete. *Materials and Structures*, *32*(6), 468-476. DOI: 10.1007/bf02482719

Hamad, B. S. & Itani, M. S. (1998). Bond strength of reinforcement in high performance concrete: role of silica fume, casting position, and superplasticizer dosage. *ACI Materials Journal, 95*(5), 499-511. DOI: 10.14359/392

Hamad, B. S. & Sabbah, S. M. (1998). Bond of reinforcement in eccentric pullout silica fume concrete specimens. *Materials and Structures*, *31*(10), 707-713. DOI: 10.1007/BF02480448

Han, J., Fang, H. & Wang, K. (2014). Design and control shrinkage behavior of high-strength self-consolidating concrete using shrinkage-reducing admixture and super-absorbent polymer. *Journal of sustainable cement-based materials*, *3*(3-4), 182-190. DOI: 10.1080/21650373.2014.897268

Han, J., Wang, S., Chen, Y. & Cao, C. (2018). Analytical derivation of rib bearing angle of reinforcing bar subject to axial loading. *Magazine of Concrete Research*, *71*(4), 175-183. DOI: 10.1680/jmacr.17.00329

Hang, M. Y. & Zhang, W. (2011). Efficiency air-entraining water-reducing agent in concrete Study on the freeze-thaw resistance. *Applied Mechanics and Materials*, *71*, 3566-3571. DOI: 10.4028/www.scientific.net/amm.71-78.3566

Harajli, M. (2009). Bond stress–slip model for steel bars in unconfined or steel, FRC, or FRP confined concrete under cyclic loading. *Journal of structural engineering*, *135*(5), 509-518. DOI: 10.1061/(asce)0733-9445(2009)135:5(509)

Harajli, M., Hout, M. & Jalkh, W. (1995). Local bond stress-slip relationship of reinforcing embedded in fiber reinforced concrete. *ACI Materials Journal*, *92*(4), 343-354. DOI: 10.14359/999

Hashemi, S. & MirzaeiMoghadamb, I. (2014). Influence of Nano-silica and Polypropylene Fibers on Bond Strength of Reinforcement and Structural Lightweight Concrete. *International Journal of Engineering*, *27*(2B), 269-276.

DOI: 10.5829/idosi.ije.2014.27.02b.10. Retrieved from http://www.ije.ir/article_72252.html

Hashemi, S. & Sedighi, H. (2016). Nanosilica effects on mechanical properties of concrete in crude oil products environment. *Scientia Iranica. Transaction A, Civil Engineering*, *23*(6), 2557-2564. DOI: 10.24200/sci.2016.2314

Hasholt, M. T., Jensen, O. M., Kovler, K. & Zhutovsky, S. (2012). Can superabsorent polymers mitigate autogenous shrinkage of internally cured concrete without compromising the strength?. *Construction and Building Materials*, *31*, 226-230. DOI: 10.1016/j.conbuildmat.2011.12.062

Hasholt, M. T., Jespersen, M. H. S. & Jensen, O. M. (2010, August). *Mechanical properties of concrete with SAP part I: Development of compressive strength*. Paper presented at International RILEM Conference on Use of Superabsorbent Polymers and Other New Additives in Concrete, Technical University of Denmark, Denmark. Retrieved from https://pdfs.semanticscholar.org/0d40/d5de5464091750c1ad4bc3691d19fb6e0a9a.pdf

Hasholt, M. T., Jespersen, M. H. S. & Jensen, O. M. (2010, August). *Mechanical properties of concrete with SAP. Part II: Modulus of elasticity*. Paper presented at International RILEM Conference on Use of Superabsorbent Polymers and Other New Additives in Concrete, Technical University of Denmark, Denmark. Retrieved from https://pdfs.semanticscholar.org/508f/6d403eba0b0617597f95464e44681aaa5bb4.pdf

Haskett, M., Oehlers, D. J. & Ali, M. M. (2008). Local and global bond characteristics of steel reinforcing bars. *Engineering Structures*, *30*(2), 376-383. DOI: 10.1016/j.engstruct.2007.04.007

Hazaree, C., Ceylan, H. & Wang, K. (2011). Influences of mixture composition on properties and freeze–thaw resistance of RCC. *Construction and Building Materials*, *25*(1), 313-319. DOI: 10.1016/j.conbuildmat.2010.06.023

Heikal, M., Morsy, M. S. & Aiad, I. (2006). Effect of polycarboxylate superplasticizer on hydration characteristics of cement pastes containing silica fume. *Ceramics Silikaty*, *50*(1), 5-14. Retrieved from http://www.ceramics-silikaty.cz/index.php?page=cs_detail_doi&id=527

Helland, S., Acker, P., Gram, H. E. & Sellevold, E. J. (Eds.). (1988). *Condensed silica fume in concrete. State of Art Report* (pp. 37). London: Thomas Telford Ltd, Fédération internationale de la précontrainte (FIP). DOI: 10.1680/csfic.13735

Holschemacher, K. & Klug, Y. (2002). A database for the evaluation of hardened properties of SCC. *Leipzig Ann. Civ. Eng. Rep., Germany (LACER), 7*, 124-134.

Hong, G. & Choi, S. (2017). Rapid self-sealing of cracks in cementitious materials incorporating superabsorbent polymers. *Construction and Building Materials*, *143*, 366-375. DOI: 10.1016/j.conbuildmat.2017.03.133

Hong, S. & Park, S.-K. (2012). Uniaxial bond stress-slip relationship of reinforcing bars in concrete. *Advances in Materials Science and Engineering*, *2012*, 1-12. DOI: 10.1155/2012/328570

Horne, A., Richardson, I. & Brydson, R. (2007). Quantitative analysis of the microstructure of interfaces in steel reinforced concrete. *Cement and Concrete Research*, *37*(12), 1613-1623. DOI: 10.1016/j.cemconres.2007.08.026

Hossain, K. M. A. & Lachemi, M. (2008). Bond behavior of self-consolidating concrete with mineral and chemical admixtures. *Journal of Materials in Civil Engineering*, *20*(9), 608-616. DOI: 10.1061/(asce)0899-1561(2008)20:9(608)

Hou, J. & Chung, D. (2000). Effect of admixtures in concrete on the corrosion resistance of steel reinforced concrete. *Corrosion Science*, *42*(9), 1489-1507. DOI: 10.1016/s0010-938x(99)00134-1

Hwang, S. J., Lee, Y.-Y. & Lee, C.-S. (1994). Effect of silica fume on the splice strength of deformed bars of high-performance concrete. *Structural Journal*, *91*(3), 294-302. DOI: 10.14359/4360

Idda, K. (1999). *Verbundverhalten von Betonrippenstählen bei Querzug*. (Doctoral thesis, Institut fuer Massivbau und Baustofftechnologie, University of Karlsruhe, Germany).

Iemura, H., Takahashi, Y. & Sogabe, N. (2004, August). *Development of unbonded bar reinforced concrete structure*. Paper presented at 13th World Conference on Earthquake Engineering, Vancouver, British Columbia, Canada (Paper No. 1537). Retrieved from https://www.iitk.ac.in/nicee/wcee/article/13_1537.pdf

Igarashi, S.-i. & Watanabe, A. (2006), Experimental study on prevention of autogenous deformation by internal curing using super-absorbent polymer particles. In O. M. Jensen, P. Lura & K. Kovler (Eds.), *International RILEM Conference on Volume Changes of Hardening Concrete: Testing and Mitigation, Lyngby, Denmark, August 20-23* (pp. 77-86). RILEM Publications SARL. Retrieved from https://www.rilem.net/gene/main.php?base=500218&id_publication=57&id_papier=2240

Ismael, R., Silva, J., Carmo, R., Soldado, E., Lourenço, C., Costa, H. & Júlio, E. (2016). Influence of nano-SiO 2 and nano-Al 2 O 3 additions on steel-to-concrete bonding. *Construction and Building Materials*, *125*, 1080-1092. DOI: 10.1016/j.conbuildmat.2016.08.152

Jacobs, F. & Hunkeler, F. (1999), Design of self-compacting concrete for durable concrete structures. In Å. Skarendahl & Ö. Petersson (Eds.), *1st International RILEM Symposium on Self-Compacting Concrete Stockholm, Sweden* (pp. 397-407). Rilem Publications. Retrieved from https://www.rilem.net/publication/publication/12?id_papier=1307

Jacobsen, S. & Sellevold, E. J. (1996). Self healing of high strength concrete after deterioration by freeze/thaw. *Cement and Concrete Research*, *26*(1), 55-62. DOI: 10.1016/0008-8846(95)00179-4

Jensen, O. M. (2013). Use of superabsorbent polymers in concrete. *Concrete international*, *35*(1), 48-52. Retrieved from https://www.concrete.org/publications/internationalconcreteabstractsportal.aspx?m=details&id=51684343

Jensen, O. M. & Hansen, P. F. (2002). Water-entrained cement-based materials: II. Experimental observations. *Cement and Concrete Research*, *32*(6), 973-978. DOI: 10.1016/s0008-8846(02)00737-8

Jiang, C., Wu, Y.-F. & Dai, M.-J. (2018). Degradation of steel-to-concrete bond due to corrosion. *Construction and Building Materials*, *158*, 1073-1080. DOI: 10.1016/j.conbuildmat.2017.09.142

Joergensen, H. B. & Hoang, L. C. (2015). Strength of loop connections between precast bridge decks loaded in combined tension and bending. *Structural Engineering International*, *25*(1), 71-80. DOI: 101686614x14043795570697

Johannesen, I. G. (2008). The Buffon needle problem revisited in a pedagogical perspective. *Mathematica Journal*, *11*(2), 284. DOI: 10.3888/tmj.11.2-9

Jones, W. A. & Weiss, W. J. (2014), Freeze thaw durability of internally cured concrete made using superabsorbent polymers. In Jan Olek & Jason Weiss (Eds.), *4th International conference on the durability of concrete structures, Purdue University, West Lafayette, Tippecanoe County, Indiana, July 24–26* (pp. 3-11). Doi: 10.5703/1288284315376

Japan Society of Civil Engineers. (1999). *Recommendation for self-compacting concrete.* JSCE Concrete Engineering Series *31*, 77pp, Tokyo, Japan. Retrieved from http://www.jsce.or.jp/committee/concrete/e/newsletter/newsletter01/recommendation/selfcompact/document.htm

Justs, J., Wyrzykowski, M., Bajare, D. & Lura, P. (2015). Internal curing by superabsorbent polymers in ultra-high performance concrete. *Cement and Concrete Research*, *76*, 82-90. DOI: 10.1016/j.cemconres.2015.05.005

Kamiyama, H. (1972). Cracks in concrete and corrosion of steel bars. *JCA Proceedings of Cement & Concrete*, 491-493 (in Japanese).

Karahan, O., Hossain, K. M., Ozbay, E., Lachemi, M. & Sancak, E. (2012). Effect of metakaolin content on the properties self-consolidating lightweight concrete. *Construction and Building Materials*, *31*, 320-325. DOI: 10.1016/j.conbuildmat.2011.12.112

Karatas, M., Turk, K. & Ulucan, Z. C. (2010). Investigation of bond between lap-spliced steel bar and self-compacting concrete: the role of silica fume. *Canadian Journal of Civil Engineering*, *37*(3), 420-428. DOI: 10.1139/l09-159

Khalaf, J., Huang, Z. & Fan, M. (2016). Analysis of bond-slip between concrete and steel bar in fire. *Computers & Structures*, *162*, 1-15. DOI: 10.1016/j.compstruc.2015.09.011

Khayat, K. H. & Guizani, Z. (1997). Use of viscosity-modifying admixture to enhance stability of fluid concrete. *Materials Journal*, *94*(4), 332-340. DOI: 10.14359/317

Khedr, S. A. & Abou-Zeid, M. N. (1994). Characteristics of silica-fume concrete. *Journal of Materials in Civil Engineering*, *6*(3), 357-375. DOI: 10.1061/(asce)0899-1561(1994)6:3(357)

Kim, J., & Schlangen, E. (2010), Super absorbent polymers to simulate self healing in ECC. In K. van Breugel, G. Ye & Y. Yuan (Eds.), *2nd International Symposium on Service Life Design for Infrastructures, Delft, Netherlands, October 4-6* (pp. 849-858). Retrieved from https://www.rilem.net/publication/publication/74?id_papier=3747

Kim, M.-J., Kim, H.-G., Lee, J.-M., Lee, Y.-J. & Kim, K.-H. (2018). A prediction model for bond deterioration in RC members. I: bond stress-slip behavior for splitting failure. *Journal of Structural Engineering*, *144*(3), 04018002. DOI: 10.1061/(asce)st.1943-541x.0001966

Kim, Y. J. & Wang, J. (2016). Interfacial Behavior of Glass Fiber-Reinforced Polymer Bars Embedded in Concrete with Internal Curing Agents. *ACI Structural Journal*, *113*(3), 595-604. DOI: 10.14359/51688068

Kodeboyina, G. B. (2018). *High Performance Self-consolidating Cementitious Composites.* Boca Raton: CRC Press, Taylor & Francis Group. DOI: 10.1201/9781315161310-1

Kollegger, J. & Mehlhorn, G. (1990). *Experimentelle Untersuchungen zur Bestimmung der Druckfestigkeit des gerissenen Stahlbetons bei einer Querzugbeanspruchung* (Research report No. 413). Berlin, Germany: Deutscher Ausschuß für Stahlbeton Deutscher Ausschuss für Stahlbeton.

Kong, X.-m., Zhang, Z.-l. & Lu, Z.-c. (2015). Effect of pre-soaked superabsorbent polymer on shrinkage of high-strength concrete. *Materials and Structures*, *48*(9), 2741-2758. DOI: 10.1617/s11527-014-0351-2

König, G., Holschemacher, K., Dehn, F. & Weibe, D. (2001), Self-compacting concrete-time development of material properties and bond behaviour. In K. Ozawa & M. Ouchi (Eds.), *2nd International RILEM Symposium on Self-Compacting Concrete (Pro 33), Tokio, Japan* (pp. 507-516). COMS Engineering Corporation.

Kotsovos, G. M., Vougioukas, E. & Kotsovos, M. D. (2013). Reducing steel congestion without violating seismic performance requirements. *ACI Structural Journal*, *110*(3), 427-436. DOI: 10.14359/51685600

Krishna, A., Rao, B. K. & Rajagopal, A. (2010). Effect of different sizes of coarse aggregate on the properties of NCC and SCC. *International journal of engineering science and technology*, *2*(10), 5959-5965. Retrieved from https://pdfs.semanticscholar.org/7c7b/b0487ba46b2b27b3f3ac66bbbb3d7457d458.pdf

Kwak, H.-G. & Kim, J.-K. (2006). Implementation of bond-slip effect in analyses of RC frames under cyclic loads using layered section method. *Engineering structures*, *28*(12), 1715-1727. DOI: 10.1016/j.engstruct.2006.03.003

Kwak, H.-G. & Kim, S.-P. (2010). Simplified monotonic moment–curvature relation considering fixed-end rotation and axial force effect. *Engineering Structures*, *32*(1), 69-79. DOI: 10.1016/j.engstruct.2009.08.017

Lam, H. & Hooton, R. (2005), Effects of internal curing methods on restrained shrinkage and permeability. In B. Persson, D. P. Bentz & L. O. Nilsson (Eds.), *4th international seminar on self-desiccation and its importance in concrete technology,* Lund, Sweden (pp. 210–228). Lund University.

Lauer, K. R. & Slate, F. O. (1956). Autogenous healing of cement paste. *ACI Material Journal Proceedings*, *52*(6), 1083–1097. DOI: 10.14359/11661. Retrieved from https://www.concrete.org/publications/internationalconcreteabstractsportal.aspx?m=details&ID=11661

Laustsen, S., Hasholt, M. T. & Jensen, O. M. (2015). Void structure of concrete with superabsorbent polymers and its relation to frost resistance of concrete. *Materials and Structures*, *48*(1-2), 357-368. DOI: 10.1617/s11527-013-0188-0

Łaźniewska-Piekarczyk, B. (2013). The type of air-entraining and viscosity modifying admixtures and porosity and frost durability of high performance self-compacting concrete. *Construction and Building Materials*, *40*, 659-671. DOI: 10.1016/j.conbuildmat.2012.11.032

Lee, H., Wong, H. & Buenfeld, N. (2010). Potential of superabsorbent polymer for self-sealing cracks in concrete. *Advances in Applied Ceramics*, *109*(5), 296-302. DOI: 10.1179/174367609x459559

Lee, H., Wong, H. & Buenfeld, N. (2016). Self-sealing of cracks in concrete using superabsorbent polymers. *Cement and Concrete Research*, *79*, 194-208. DOI: 10.1016/j.cemconres.2015.09.008

Lee, H. X. D., Wong, H. S. & Buenfeld, N. (2010), Self-sealing cement-based materials using superabsorbent polymers. In O. M. Jensen, M. T. Hasholt & S. Laustsen (Eds.), *International RILEM Conference on Use of Superabsorbent Polymers and Other New Additives in Concrete (*PRO 74*), Lyngby, Denmark*, August 15-18 (pp. 171–178). Technical University of Denmark: RILEM Publications S.A.R.L.

Lee, H. X. D., Wong, H. S. & Buenfeld, N. (2010), Estimating the swelling ratio of superabsorbent polymers in cement-based materials. In O. M. Jensen, M. T. Hasholt & S. Laustsen (Eds.), *International RILEM Conference on Use of Superabsorbent Polymers and Other New Additives in Concrete (*PRO 74*), Lyngby, Denmark*, August 15-18 (pp. 163-170). Technical University of Denmark: RILEM Publications S.A.R.L.

Limkatanyu, S. & Spacone, E. (2003). Effects of reinforcement slippage on the non-linear response under cyclic loadings of RC frame structures. *Earthquake engineering & structural dynamics*, *32*(15), 2407-2424. DOI: 10.1002/eqe.334

Lin, H., Zhao, Y., Ožbolt, J. & Reinhardt, H.-W. (2017). Bond strength evaluation of corroded steel bars via the surface crack width induced by reinforcement corrosion. *Engineering Structures*, *152*, 506-522. DOI: 10.1016/j.engstruct.2017.08.051

Lin, J., Chen, H., Lv, Z. & Wang, Y. (2018). Analytical solution on dosage of self-healing capsules in materials with two-dimensional multi-shaped crack patterns. *Science and Engineering of Composite Materials*, *25*(6), 1229-1239. DOI: 10.1515/secm-2017-0256

Lindorf, A., Lemnitzer, L. & Curbach, M. (2009). Experimental investigations on bond behaviour of reinforced concrete under transverse tension and repeated loading. *Engineering Structures*, *31*(7), 1469-1476. DOI: 10.1016/j.engstruct.2009.02.025

Lindorf, C. (2011). *Bond fatigue in reinforced concrete under transverse tension*. (Doctoral thesis. Dresden University).

Litvan, G. G. (1988), The mechanism of frost action in concrete: Theory and practical implications. In *Workshop on Low Temperature Effects on Concrete, Sapporo, Hokkaido, Japan* (pp. 115-134). Montreal, Canada: National Research Council Canada, Institute for Research in Construction.

Lobo, P. S. & Almeida, J. (2015). RC fiber beam–column model with bond-slip in the vicinity of interior joints." *Engineering Structures*, *96*, 78-87. DOI: 10.1016/j.engstruct.2015.04.005

Lorrain, M. & Daoud, A. (2002), Bond in self-compacting concrete. In *RILEM International Symposium Bond in Concrete from Research to Standards, November, Budapest* (pp. 529-536). Budapest University of Technology and Economics.

Lotze, D. (1987). *Untersuchungen zur Frage der Wahrscheinlichkeit, mit der Dübel in Rissen liegen – Einfluß der Querbewehrung* [Investigations on the Probability of Fasteners being Located in Cracks – Influence of Transverse Reinforcement] (Bericht Nr. 1/24-87/6). Stuttgart, Germany: Institut für Werkstoffe im Bauwesen, Universität Stuttgart.

Lura, P., Durand, F., Loukili, A., Kovler, K. & Jensen, O. M. (2006), Compressive strength of cement pastes and mortars with superabsorbent polymers. In O. M. Jensen, P. Lura & K. Kovler (Eds.), *International RILEM Conference on Volume Changes of Hardening Concrete: Testing and Mitigation, Lyngby, Denmark, August 20-23* (pp. 117-125). RILEM Publications SARL. Doi: 10.1617/2351580052.013. Retrieved from https://www.rilem.net/publication/publication/57?id_papier=2244

Lutz, L. A. & Gergely, P. (1967). Mechanics of bond and slip of deformed bars in concrete. *ACI Journal Proceedings*, *64*(11), 711-721. DOI: 10.14359/7600

Mahrenholtz, C. (2012). *Seismic bond model for concrete reinforcement and the application to column-to-foundation connections*. (Doctoral thesis, Institut für Werkstoffe im Bauwesen der Universitat Stuttgart, Univ. of Stuttgart, Stuttgart, Germany).

Mahrenholtz, C. & Eligehausen, R. (2017). Cyclic Tests on Concrete Reinforcement for Development of Seismic Bond Model. *ACI Materials Journal*, *114*(4), 571-579. DOI: 10.14359/51689777

Martí-Vargas, J., García-Taengua, E. & Serna, P. (2013). Influence of concrete composition on anchorage bond behavior of prestressing reinforcement. *Construction and Building Materials*, *48*, 1156-1164. DOI: 10.1016/j.conbuildmat.2013.07.102

Martí-Vargas, J., Serna, P., Navarro-Gregori, J. & Bonet, J. (2012). Effects of concrete composition on transmission length of prestressing strands. *Construction and Building Materials*, *27*(1), 350-356. DOI: 10.1016/j.conbuildmat.2011.07.038

Matsumoto, K., Wang, T., Hayashi, D. & Nagai, K. (2016). Investigation on the Pull-out Behavior of Deformed Bars in Cracked Reinforced Concrete. *Journal of Advanced Concrete Technology*, *14*(9), 573-589. DOI: 10.3151/jact.14.573

Comite Euro-International Du Beton. (1993). *Model code for concrete structures*. CEB-FIP Model Code 1990, Bulletin d'information. Lausanne, Switzerland: International Federation for Structural Concrete;. DOI: 10.1680/ceb-fipmc1990.35430

Mechtcherine, V., Dudziak, L. & Hempel, S. (2009), Mitigating early age shrinkage of ultra-high performance concrete by using super absorbent polymers (SAP). In T. Tanabe, K.

Sakata, H. Mihashi, R. Sato, K. Maekawa & H. Nakamura (Eds.), *Creep, Shrinkage and Durability Mechanics of Concrete and Concrete Structures (CONCREEP 8), Ise-Shima, Japan, 30 September-2 October 2008* (pp. 847-853). CRC Press.

Mechtcherine, V., Dudziak, L., Schulze, J. & Staehr, H. (2006), Internal curing by super absorbent polymers (SAP)–Effects on material properties of self-compacting fibre-reinforced high performance concrete In O. M. Jensen, P. Lura & K. Kovler (Eds.), *International RILEM Conference on Volume Changes of Hardening Concrete: Testing and Mitigation, Lyngby, Denmark, August 20-23* (pp. 87-96). RILEM Publications SARL. DOI: 10.1617/2351580052.010

Mechtcherine, V., Gorges, M., Schroefl, C., Assmann, A., Brameshuber, W., Ribeiro, A. n. B., Cusson, D., Custˇdio, J., da Silva, E. F. & Ichimiya, K. (2014). Effect of internal curing by using superabsorbent polymers (SAP) on autogenous shrinkage and other properties of a high-performance fine-grained concrete: results of a RILEM round-robin test. *Materials and structures*, *47*(3), 541-562. DOI: 10.1617/s11527-013-0078-5

Mechtcherine, V. & Reinhardt, H.-W. (2012). *Application of super absorbent polymers (SAP) in concrete construction: state-of-the-art report prepared by Technical Committee 225-SAP*, Springer Netherlands. DOI: 10.1007/978-94-007-2733-5

Mechtcherine, V., Schröfl, C., Wyrzykowski, M., Gorges, M., Lura, P., Cusson, D., Margeson, J., De Belie, N., Snoeck, D. & Ichimiya, K. (2017). Effect of superabsorbent polymers (SAP) on the freeze–thaw resistance of concrete: results of a RILEM interlaboratory study. *Materials and Structures*, *50*(1), 14. DOI: 10.1617/s11527-016-0868-7

Mechtcherine, V., Snoeck, D., Schröfl, C., De Belie, N., Klemm, A. J., Ichimiya, K., Moon, J., Wyrzykowski, M., Lura, P. & Toropovs, N. (2018). Testing superabsorbent polymer (SAP) sorption properties prior to implementation in concrete: results of a RILEM Round-Robin Test. *Materials and Structures*, *51*(1), 28. DOI: 10.1617/s11527-018-1149-4

Meng, B. (2019). Testing and Modeling of Compressive and Tensile Viscoelastic Effects in High Performance Concrete. (Doctoral thesis, University of Michigan). Retrieved from https://deepblue.lib.umich.edu/bitstream/handle/2027.42/150020/mengbo_1.pdf?sequence=1

Menzel, C. (1939). Some factors influencing results of pull-out bond tests. *ACI Journal Proceedings*, *35*(6), 517-542. DOI: 10.14359/8507

Metelli, G. & Plizzari, G. A. (2014). Influence of the relative rib area on bond behaviour. *Magazine of Concrete Research*, *66*(6), 277-294. DOI: 10.1680/macr.13.00198

Mielenz, R. C. (1968), Use of surface-active agents in concrete. In *Fifth International Symposium on Chemistry of Cement, Tokyo* (Vol. 4, pp. 22-24).

Mignon, A., Snoeck, D., Dubruel, P., Van Vlierberghe, S. & De Belie, N. (2017). Crack mitigation in concrete: superabsorbent polymers as key to success?. *Materials*, *10*(3), 237. DOI: 10.3390/ma10030237

Mignon, A., Snoeck, D., Schaubroeck, D., Luickx, N., Dubruel, P., Van Vlierberghe, S. & De Belie, N. (2015). pH-responsive superabsorbent polymers: A pathway to self-healing of mortar. *Reactive and Functional Polymers*, *93*, 68-76. DOI: 10.1016/j.reactfunctpolym.2015.06.003

Mihashi, H. & Nishiwaki, T. (2012). Development of engineered self-healing and self-repairing concrete-state-of-the-art report. *Journal of Advanced Concrete Technology*, *10*(5), 170-184. DOI: 10.3151/jact.10.170

Mikame, A., Uchida, K. & Noguchi, H. (1991), A study of compressive deterioration of cracked concrete. In *International Workshop on Finite Element Analysis of Reinforced Concrete, Columbia Univ., New York, June 2-5.* Reston: ASCE publication.

Minitab, I. (2014). Minitab (Version release 17) [Statistical Computer Software]. State College, PA: Minitab, Inc. Retrieved from (www. minitab. com).

Mo, K. H., Alengaram, U. J., Jumaat, M. Z. & Yap, S. P. (2015). Feasibility study of high volume slag as cement replacement for sustainable structural lightweight oil palm shell concrete. *Journal of Cleaner Production*, *91*, 297-304. DOI: 10.1016/j.jclepro.2014.12.021

Molero, M., Aparicio, S., Al-Assadi, G., Casati, M., Hernández, M. & Anaya, J. (2012). Evaluation of freeze–thaw damage in concrete by ultrasonic imaging. *Ndt & E International*, *52*, 86-94. DOI: 10.1016/j.ndteint.2012.05.004

Monteiro, P. J., Gjorv, O. & Mehta, P. K. (1989). Effect of condensed silica fume on the steel-cement paste transition zone. *Cement and Concrete Research*, *19*(1), 114-123. DOI: 10.1016/0008-8846(89)90071-9

Monti, G. & Spacone, E. (2000). Reinforced concrete fiber beam element with bond-slip. *Journal of Structural Engineering*, *126*(6), 654-661. DOI: 10.1061/(asce)0733-9445(2000)126:6(654)

Montoya, E., Vecchio, F. & Sheikh, S. (2001). Compression field modeling of confined concrete. *Structural Engineering and Mechanics*, *12*(3), 231-248. DOI: 10.12989/sem.2001.12.3.231

Mor, A. (1993). Steel-concrete bond in high-strength lightweight concrete. *ACI Materials Journal*, *89*(1), 76-82. DOI: 10.14359/1248

Moreau, M. (1973). Contribution to the study of adhesion between the hydrated constituents of artificial Portland cement and embedded steel. *Revenue mater*, *674*, 4-17.

Mousavi, S., Dehestani, M. & Mousavi, K. (2017). Bond strength and development length of steel bar in unconfined self-consolidating concrete. *Engineering Structures*, *131*, 587-598. DOI: 10.1016/j.engstruct.2016.10.029

Mousavi, S., Dehestani, M. & Mousavi, S. (2016). Bond strength and development length of glass fiber-reinforced polymer bar in unconfined self-consolidating concrete. *Journal of Reinforced Plastics and Composites*, *35*(11), 924-941. DOI: 10.1177/0731684416632930

Mousavi, S., Ouellet-Plamondon, C. & Guizani, L. (2019), Effect of superabsorbent polymer on mitigating damages at steel bar-concrete interface. In *CSCE Annual Conference, Laval, Quebec, Canada, June 12-15*. Canadian Society for Civil Engineering (CSCE). Retrieved from http://www.csceproceedings.ca/index.cfm?CID=855&AbID=4122

Mousavi, S. S., Guizani, L. & Ouellet-plamondon, C. (2020). A simplified analytical model for interfacial bond strength of deformed steel rebar embedded in pre-cracked concrete. *Journal of structural Engineering*, *146*(8), 04020142. DOI: 10.1061/(ASCE)ST.1943-541X.0002687

Mousavi, S. S., Guizani, L. & Ouellet-Plamondon, C. M. (2019). On bond-slip response and development length of steel bars in pre-cracked concrete. *Construction and Building Materials*, *199*, 560-573. DOI: 10.1016/j.conbuildmat.2018.12.039

Mousavi, S. S., Mousavi Ajarostaghi, S. S. & Bhojaraju, C. (2020). A critical review of the effect of concrete composition on rebar–concrete interface (RCI) bond strength: A case study of nanoparticles. *SN Applied Sciences*, *2*(5), 893. DOI: 10.1007/s42452-020-2681-8

Murata, J. & Kawai, T. (1984). Studies on bond strength of deformed bars by pull-out tests. *Doboku Gakkai Ronbunshu*, *348*, 113-122. DOI: 10.2208/jscej.1984.348_113

Murcia-Delso, J. & Benson Shing, P. (2014). Bond-slip model for detailed finite-element analysis of reinforced concrete structures. *Journal of Structural Engineering*, *141*(4), 04014125. DOI: 10.1061/(asce)st.1943-541x.0001070

Musser, P. L., Carrasquillo, R. L., Jirsa, J. O. & Klingner, R. E. (1985). *Anchorage and Development of Reinforcement in Concrete Mode Using Superplasticizers* (Research Report 3-5-84-383). Texas: State Department of Highways and Public Transportation, The University of Texas at Austin. Retrieved from https://library.ctr.utexas.edu/digitized/texasarchive/phase2/383-1-ctr.pdf

Nagataki, S. & Fujiwara, H. (1995). Self-compacting property of highly flowable concrete. *Special Publication*, *154*, 301-314. Retrieved from https://www.concrete.org/publications/internationalconcreteabstractsportal/m/details/id/960

Naik, T. R., Singh, S., Sivasundaram, V. & Energy, M. (1989). Concrete compressive strength, shrinkage and bond strength as affected by addition of fly ash and temperature. *The University of Wisconsin–Milwaukee*, Milwaukee, WI.

Nakamura, H. & Ogawa, S. (2000). Influence of interaction between sand and superplasticizer on the fluidity of concrete. *Transactions of the Japan Concrete Institute*, *21*, 15-20. Retrieved from https://ci.nii.ac.jp/naid/10007250726/en/

Nasiri, E. & Liu, Y. (2017). Development of a detailed 3D FE model for analysis of the in-plane behaviour of masonry infilled concrete frames. *Engineering Structures*, *143*, 603-616. DOI: 10.1016/j.engstruct.2017.04.049

Consiglio Superiore dei Lavori Pubblici. (2008). *Nuove Norme Tecniche per le Costruzioni (in Italian)*. NTC-08. Roma, Italy: Ministero delle Infrastrutture.

Okada, K. & Miyagawa, T. (1980). Chloride Corrosion of Reinforcing Steel in Cracked Concrete. *ACI Symposium Publication*, *65*, 237-254. DOI: 10.14359/6356

Olawuyi, B. & Boshoff, W. (2013), Compressive strength of high-performance concrete with absorption capacity of Super-Absorbing-Polymers (SAP). In A. Zingoni (Ed.), *Research and Applications in Structural Engineering, Mechanics and Computation–Zingoni (Ed.), Fifth International Conference on Structural Engineering, Mechanics and Computation (SEMC 2013), Cape Town, South Africa, 2-4 September* (pp. 1679-1683). London: Taylor & Francis Group.

Page, C. (1975). Mechanism of corrosion protection in reinforced concrete marine structures. *Nature*, *258*(5535), 514-515. DOI: 10.1038/258514a0

Page, C. & Treadaway, K. (1982). Aspects of the electrochemistry of steel in concrete. *Nature*, 297(5862), 109-115. DOI: 10.1038/297109a0

Pandey, G. R. & Mutsuyoshi, H. (2004), Seismic damage mitigation of reinforced concrete bridge piers by unbonding longitudinal reinforcements. In *13th World Conference on Earthquake Engineering, Vancouver, BC, Canada, Augus 1-6* (Paper No. 154). Retrieved from http://www.iitk.ac.in/nicee/wcee/article/13_154.pdf

Pandurangan, K., Kothandaraman, S. & Sreedaran, D. (2010). A study on the bond strength of tension lap splices in self compacting concrete. *Materials and structures*, *43*(8), 1113-1121. DOI: 10.1617/s11527-009-9570-3

Papadrakakis, M., Fragiadakis, M. & Plevris, V. (Eds.). (2013), *Computational methods in earthquake engineering*. Berlin, Germany: Springer. DOI: 10.1007%2F978-94-007-0053-6

Peng, G.-F., Ma, Q., Hu, H.-M., Gao, R., Yao, Q.-F. & Liu, Y.-F. (2007). The effects of air entrainment and pozzolans on frost resistance of 50–60 MPa grade concrete. *Construction and Building Materials*, *21*(5), 1034-1039. DOI: 10.1016/j.conbuildmat.2006.02.002

Perenchio, W., Kress, V. & Breitfeller, D. (1990). Frost Lenses? Sure, but in Concrete?. *Concrete International*, *12*(4), 51-53. Retrieved from https://www.concrete.org/publications/internationalconcreteabstractsportal.aspx?m=details&ID=2084

Pérez, G., Calvo, J. G., Carballosa, P., Allegro, V. R., Gaitero, J., Erkizia, E. & Guerrero, A. (2015), Efficiency of an Innovative Self-Healing System in Ultra-High-Strength Concrete under a Salt Spray Test. In C. Hellmich, B. Pichler & J. Kollegger (Eds.), *10th International Conference on Mechanics and Physics of Creep, Shrinkage, and Durability of Concrete and Concrete Structures (CONCREEP 10), Vienna, Austria, September 21-23* (pp. 919-928). RILEM and the Engineering Mechanics Institute of ASCE . DOI: 10.1061/9780784479346.110

Persson, B. (2001). A comparison between mechanical properties of self-compacting concrete and the corresponding properties of normal concrete. *Cement and concrete Research*, *31*(2), 193-198. DOI: 10.1016/s0008-8846(00)00497-x

Petersen, L., Lohaus, L. & Polak, M. A. (2007). Influence of freezing-and-thawing damage on behavior of reinforced concrete elements. *ACI Materials Journal*, *104*(4), 369-378. DOI: 10.14359/18826

Piérard, J., Pollet, V. & Cauberg, N. (2006). Mitigating autogenous shrinkage in HPC by internal curing using superabsorbent polymers. In O. M. Jensen, P. Lura & K. Kovler (Eds.), *International RILEM Conference on Volume Changes of Hardening Concrete: Testing and Mitigation, Lyngby, Denmark, August 20-23* (pp. 97-106). RILEM Publications SARL. DOI: 10.1617/2351580052.011

Pop, I., De Schutter, G., Desnerck, P. & Onet, T. (2013). Bond between powder type self-compacting concrete and steel reinforcement. *Construction and Building Materials*, *41*, 824-833. DOI: 10.1016/j.conbuildmat.2012.12.029

Pop, I., De Schutter, G., Desnerck, P. & Szilagy, H. (2015). Influence of self-compacting concrete fresh properties on bond to reinforcement. *Materials and Structures*, *48*(6), 1875-1886. DOI: 10.1617/s11527-014-0280-0

Powers, T. C. & Brownyard, T. L. (1946). Studies of the Physical Properties of Hardened Portland Cement Paste. *ACI Journal Proceedings*, *43*(9), 469-504. DOI: 10.14359/15302

Purainer, R. (2005). *Last-und Verformungsverhalten von Stahlbetonflächentragwerken unter zweiaxialer Zugbeanspruchung* (Doctoral thesis, Universität der Bundeswehr München, Universitätsbibliothek).

Rabbat, B. & Russell, H. (1985). Friction coefficient of steel on concrete or grout. *Journal of Structural Engineering*, 111(3), 505-515. DOI: 10.1061/(asce)0733-9445(1985)111:3(505)

Ramachandran, V. S. (Ed.). (1996), *Concrete admixtures handbook: properties, science and technology* (pp. 1183). Park Ridge, New Jersey: Noyes Publications.

Ramadan, K. Z. & Haddad, R. H. (2017). Self-healing of overloaded self-compacting concrete of rigid pavement. *European Journal of Environmental and Civil Engineering*, *21*(1), 63-77. DOI: 10.1080/19648189.2015.1090931

Rehm, G. (1957), The fundamental law of bond. In T. H. Rotaprinttrychkeri (Ed.), *Symposium on Bond and Crack Formation in Reinforced Concrete (Stockholm), Stockholm, Sweden* (pp. 491-498). Paris, France: RILEM, International Laboratories Union for Estimation of Materials.

Rehm G., R., E. & B., N. (1978). Rationalisierung der Bewehrungstechnik im Stahlbetonbau. *Vereinfachte Schubbewehrung in Balken. Betonwerk+Fertigteil-Technik*, *44*(3&4), 147–155. Institut für Werkstoffe im Bauwesen, Universität Stuttgart.

Reinhardt, H.-W., Assmann, A. & Mönnig, S. (2008), Superabsorbent polymers (SAPs)-an admixture to increase the durability of concrete. In W. Sun, K. van Breugel, C. Miao, G. Ye & H. Chen (Eds.), *1st International Conference on Microstructure Related Durability of Cementitious Composites, Nanjing, China, October 13-15* (pp. 313-322). RILEM publications. Retrieved from https://www.rilem.net/images/publis/pro061-034.pdf

Ruiz, M. F., Muttoni, A. & Sagaseta, J. (2015). Shear strength of concrete members without transverse reinforcement: A mechanical approach to consistently account for size and strain effects. *Engineering structures*, *99*, 360-372. DOI: 10.1016/j.engstruct.2015.05.007

Ruiz, M. F., Plumey, S. & Muttoni, A. (2010). Interaction between bond and deviation forces in spalling failures of arch-shaped members without transverse reinforcement. *ACI Structural Journal*, *107*(3), 346-354. DOI: 10.14359/51663700

Saadeghvaziri, M. A. & Hadidi, R. (2005). Transverse cracking of concrete bridge decks: effects of design factors. *Journal of Bridge Engineering*, *10*(5), 511-519. DOI: 10.1061/(asce)1084-0702(2005)10:5(511)

Saatcioglu, M. & Alsiwat, J. (1996), Significance of anchorage slip on dynamic inelastic response of R/C frame structures. In *11th World Conf. on Earthquake Engineering, Acapulco, Mexico, June 23-28.* Sociedad Mexicana de Ingeniería Sísmica. Retrieved from http://www.iitk.ac.in/nicee/wcee/article/11_1854.PDF

Saatcioglu, M., Alsiwat, J. M. & Ozcebe, G. (1992). Hysteretic behavior of anchorage slip in R/C members. *Journal of Structural Engineering*, *118*(9), 2439-2458. DOI: 10.1061/(asce)0733-9445(1992)118:9(2439)

Saatcioglu, M. & Ozcebe, G. (1989). Response of reinforced concrete columns to simulated seismic loading. *Structural Journal*, *86*(1), 3-12. DOI: 10.14359/2607

Sabău, M., Pop, I. & Oneţ, T. (2016). Experimental study on local bond stress-slip relationship in self-compacting concrete. *Materials and Structures*, *49*(9), 3693-3711. DOI: 10.1617/s11527-015-0749-5

Sadawy, M. M. & Elsharkawy, E. (2016). Effect of Nano-Tio2 addition on Mechanical Properties of Concrete and Corrosion Behavior of Reinforcement Bars. Int. J ournal of Engineering Research and Application. *6*(10), 61-65. Retrieved from https://www.ijera.com/papers/Vol6_issue10/Part-1/L0610106165.pdf

Sagoe-Crentsil, K. & Glasser, F. (1990), Analysis of the Steel/Concrete Interface. In C.L. Page, K.W.J. Treadaway & P.B. Bamforth (Eds.), *3rd Symp Corrosion of Reinforcement in Concrete* (pp. 74-86). London: Elsevier Science Publishers.

Şahin, R., Taşdemir, M. A., Gül, R. & Çelik, C. (2007). Optimization Study and Damage Evaluation in Concrete Mixtures Exposed to Slow Freeze–Thaw Cycles. *Journal of materials in civil engineering*, *19*(7), 609-615. DOI: 10.1061/(asce)0899-1561(2007)19:7(609)

Şahmaran, M. (2007). Effect of flexure induced transverse crack and self-healing on chloride diffusivity of reinforced mortar. *Journal of Materials Science*, *42*(22), 9131-9136. DOI: 10.1007/s10853-007-1932-z

Şahmaran, M., Keskin, S. B., Ozerkan, G. & Yaman, I. O. (2008). Self-healing of mechanically-loaded self consolidating concretes with high volumes of fly ash. *Cement and Concrete Composites*, *30*(10), 872-879. DOI: 10.1016/j.cemconcomp.2008.07.001

Sahmaran, M., Yildirim, G. & Erdem, T. K. (2013). Self-healing capability of cementitious composites incorporating different supplementary cementitious materials. *Cement and Concrete Composites*, *35*(1), 89-101. DOI: 10.1016/j.cemconcomp.2012.08.013

Said, A., & Nehdi, M. (2007). Behaviour of reinforced self-consolidating concrete frames. *Proceedings of the Institution of Civil Engineers-Structures and Buildings*, *160*(2), 95-104. DOI: 10.1680/stbu.2007.160.2.95

Sancak, E., Hossain, K. M. A. & Lachemi, M. (2016). Bond Loss between Metakaolin-Incorporated Structural Lightweight Self-Consolidating Concrete and Corroded Steel Reinforcement. *Journal of Materials in Civil Engineering*, *29*(5), 04016283. DOI: 10.1061/(asce)mt.1943-5533.0001811

Sancak, E. & Simsek, O. (2011), The bond strength of structural lightweight pumice aggregate concrete with/without silica fume.In *International Balkans Conference on Challenges of Civil Engineering (BCCCE), EPOKA University, Tirana, Albania, May 19-21* (pp. 1-12). Retrieved from http://dspace.epoka.edu.al/handle/1/515

Sasi, A. T. D. (2018). Study on Effectiveness of Self-Healing Technique for Self Compacting Concrete. *IJISET - International Journal of Innovative Science, Engineering & Technology*, *5*(4). Retrieved from http://ijiset.com/vol5/v5s4/IJISET_V5_I04_28.pdf

Schiessl, A. & Zilch, K. (2001, October). *The effect of the modified composition of SCC on shear and bond behavior*. Paper presented at the 2nd International Symposium on Self-Compacting Concrete, Tokyo, Japan (pp. 501-506).

Schröfl, C., Mechtcherine, V. & Gorges, M. (2012). Relation between the molecular structure and the efficiency of superabsorbent polymers (SAP) as concrete admixture to mitigate autogenous shrinkage. *Cement and concrete research*, *42*(6), 865-873. DOI: 10.1016/j.cemconres.2012.03.011

Seki, H. & Maruyama, H. (1973). Corrosion of steel bars at crack of reinforced concrete exposed to sea environments. *The Report of Port and Airport Research Institute*, *12*(3), 203-225. Retrieved from https://www.pari.go.jp/en/report_search/detail.php?id=1973090120305

Serag, M. I., Yasien, A. M., El-Feky, M. S. & Elkady, H. (2017). Effect of nano silica on concrete bond strength modes of failure. *International Journal of GEOMATE*, *12*(29), 2892-2899. DOI: 10.21660/2017.29.160412

Sezen, H. & Setzler, E. J. (2008). Reinforcement slip in reinforced concrete columns. *ACI Structural Journal*, *105*(3), 280-289. DOI: 10.14359/19787

Sfikas, I. P. & Trezos, K. G. (2013). Effect of composition variations on bond properties of self-compacting concrete specimens. *Construction and building materials*, *41*, 252-262. DOI: 10.1016/j.conbuildmat.2012.11.094

Shang, H.-S. & Yi, T.-H. (2013). Freeze-thaw durability of air-entrained concrete. *The Scientific World Journal*, 1-6. DOI: 10.1155/2013/650791

Shang, H., Song, Y. & Ou, J. (2009). Behavior of air-entrained concrete after freeze-thaw cycles. *Acta Mechanica Solida Sinica*, *22*(3), 261-266. DOI: 10.1016/s0894-9166(09)60273-1

Shen, D., Wang, X., Cheng, D., Zhang, J. & Jiang, G. (2016). Effect of internal curing with super absorbent polymers on autogenous shrinkage of concrete at early age. *Construction and Building Materials*, *106*, 512-522. DOI: 10.1016/j.conbuildmat.2015.12.115

Shi, C., Liu, J., Lv, K., Ma, X., Zhang, J. & Wu, Z. (2016), Effect of Super-Absorbent Polymer on Shrinkage and Permeability of Self-Compacting Concrete (SCC). In K. H. Khayat (Ed.), *8th International RILEM Symposium on Self-Compacting Concrete, Washington, D.C., May 15-18* (pp. 73-88). RILEM Publications SARL. Retrieved from https://www.rilem.net/publication/publication/459?id_papier=10779

Shirai, N. & Noguchi, H. (1989), Compressive deterioration of cracked concrete. In *ASCE Struct. Congress: Design, analysis, and testing, San Francisco, CA, May 1-5* (pp. 1-10). New York, N.Y.: ASCE.

Sikora, k. s. & Klemm, a. j. (2014). The effect of superabsorbent polymers on performance of fly ash cementitious mortars exposed to accelerated freezing/thawing conditions. *International Journal of Computational Methods and Experimental Measurements*, *2*(3), 255-268. DOI: 10.2495/cmem-v2-n3-255-268

Simons, I. N. (2007). *Verbundverhalten von eingemörtelten Bewehrungsstäben unter zyklischer Beanspruchung* [Bond behaviour of post-installed reinforcing bars under cyclic loading]. (Doctoral thesis, Institut für Werkstoffe im Bauwesen der Universität Stuttgart, Stuttgart).

Skorobogatov, S. M., & Edwards, A. D. (1979). The influence of the geometry of deformed steel bars on their bond strength in concrete. *Proceedings of the Institution of Civil Engineers, 67*(2), 327-339. DOI: 10.1680/iicep.1979.2460

Snoeck, D. (2018). Superabsorbent polymers to seal and heal cracks in cementitious materials. *RILEM Technical Letters*, *3*, 32-38. DOI: 10.21809/rilemtechlett.2018.64

Snoeck, D. & De Belie, N. (2013), The influence of superabsorbent polymers on the microstructure and permeability of cementitious materials. In Z. J. Li, W. Sun, C. W. Miao, K. Sakai, O. E. Gjørv & N. Banthia (Eds.), *7th international conference on concrete under severe conditions–environment and loading. Nanjing, China, September 23-25* (pp. 363-373).

Snoeck, D. & De Belie, N. (2015). Repeated autogenous healing in strain-hardening cementitious composites by using superabsorbent polymers. *Journal of Materials in Civil Engineering*, *28*(1), 04015086. DOI: 10.1061/(asce)mt.1943-5533.0001360

Snoeck, D. & De Belie, N. (2019). Autogenous healing in strain-hardening cementitious materials with and without superabsorbent polymers: an 8-year study. *Frontiers in Materials*, *6*, 48. DOI: 10.3389/fmats.2019.00048

Snoeck, D., De Schryver, T. & De Belie, N. (2018). Enhanced impact energy absorption in self-healing strain-hardening cementitious materials with superabsorbent polymers. *Construction and Building Materials*, *191*, 13-22. DOI: 10.1016/j.conbuildmat.2018.10.015

Snoeck, D., Dubruel, P. & De Belie, N. (2014), How to seal and heal cracks in cementitious materials by using superabsorbent polymers. In V. Mechtcherine & C. Schroefl (Eds.), *Application of Superabsorbent Polymers and Other New Admixtures in Concrete Construction (PRO 95), Dresden, Germany, September 14-17* (pp. 375-384). Bagneux: RILEM Publications. Retrieved from https://biblio.ugent.be/publication/5705654

Snoeck, D., Pel, L. & De Belie, N. (2018). Superabsorbent polymers to mitigate plastic drying shrinkage in a cement paste as studied by NMR. *Cement and Concrete Composites*, *93*, 54-62. DOI: 10.1016/j.cemconcomp.2018.06.019

Snoeck, D., Schaubroeck, D., Dubruel, P. & De Belie, N. (2014). Effect of high amounts of superabsorbent polymers and additional water on the workability, microstructure and strength of mortars with a water-to-cement ratio of 0.50. *Construction and Building Materials*, *72*, 148-157. DOI: 10.1016/j.conbuildmat.2014.09.012

Snoeck, D., Schroefl, C. & Mechtcherine, V. (2018). Recommendation of RILEM TC 260-RSC: testing sorption by superabsorbent polymers (SAP) prior to implementation in cement-based materials. *Materials and Structures*, *51*(5), 116. DOI: 10.1617/s11527-018-1242-8

Snoeck, D., Steuperaert, S., Van Tittelboom, K., Dubruel, P. & De Belie, N. (2012). Visualization of water penetration in cementitious materials with superabsorbent polymers by means of neutron radiography. *Cement and Concrete Research*, *42*(8), 1113-1121. DOI: 10.1016/j.cemconres.2012.05.005

Snoeck, D., Van Tittelboom, K., De Belie, N., Steuperaert, S. & Dubruel, P. (2012), The use of superabsorbent polymers as a crack sealing and crack healing mechanism in cementitious materials. In M. G. Alexander, H. Beushausen, F. Dehn & P. Moyo (Eds.), *Concrete Repair, Rehabilitation and Retrofitting III: 3rd International Conference on Concrete Repair, Rehabilitation and Retrofitting (ICCRRR-3), Cape Town, South Africa, September 3–5* (pp. 152-157). London: CRC Press.

Snoeck, D., Van Tittelboom, K., Steuperaert, S., Dubruel, P. & De Belie, N. (2014). Self-healing cementitious materials by the combination of microfibres and superabsorbent polymers. *Journal of Intelligent Material Systems and Structures*, *25*(1), 13-24. DOI: 10.1177/1045389x12438623

Sonebi, M. & Bartos, P. (1999), Hardened SCC and its bond with reinforcement. In Å. Skarendahl & Ö. Petersson (Eds.), 1st *International RILEM Symposium on Self-Compacting Concrete, Stockholm, Sweden, September 13-14* (pp. 275-289). Retrieved from https://www.rilem.net/publication/publication/12?id_papier=1298

Song, C., Choi, Y. C., & Choi, S. (2016). Effect of internal curing by superabsorbent polymers–internal relative humidity and autogenous shrinkage of alkali-activated slag mortars. *Construction and Building Materials*, *123*, 198-206. DOI: 10.1016/j.conbuildmat.2016.07.007

Songpiriyakij, S., Pulngern, T., Pungpremtrakul, P. & Jaturapitakkul, C. (2011). Anchorage of steel bars in concrete by geopolymer paste. *Materials & Design*, *32*(5), 3021-3028. DOI: 10.1016/j.matdes.2011.01.048

Soretz, S. & Holzenbein, H. (1979). Influence of rib dimensions of reinforcing bars on bond and bendability. *ACI Journal Proceedings, 76*(1), 111-128. DOI: 10.14359/6939

Soutsos, M. (Ed.). (2010). *Concrete durability: a practical guide to the design of durable concrete structures*. London : Thomas Telford.

St John, D. A., Poole, A. B. & Sims, I. (Eds.). (1998). *Concrete petrography: a handbook of investigative techniques* (2nd ed.). London: CRC Press. DOI: 10.1201/b18688

StatSoft, I. N. C. (2011). STATISTICA, data analysis software system (Version 10) [Computer software]. Tulsa, Oklahoma: StatSoft Inc.

Takagi, E., Lima, M. & Helene, P. (2015), Self-healing of self-compacting concretes made with brazilian blast furnace slag cements activated by crystalline catalyst. In M. Quattrone & V. M. John (Eds.), *XIII International Conference on Durability of Building Materials and Components (XIII DBMC), September 2-5, Sao Paulo, Brazil* (pp. 633-640). RILEM publications. Retrieved from https://www.rilem.net/publication/publication/435?id_papier=10147

Tan, Y., Chen, H., Wang, Z., Xue, C. & He, R. (2019). Performances of Cement Mortar Incorporating Superabsorbent Polymer (SAP) Using Different Dosing Methods. *Materials*, *12*(10), 1619. DOI: 10.3390/ma12101619

Tanyildizi, H. (2009). Fuzzy logic model for the prediction of bond strength of high-strength lightweight concrete. *Advances in Engineering Software*, *40*(3), 161-169. DOI: 10.1016/j.advengsoft.2007.05.013

Tassios, T. P. (1979), Properties of bond between concrete and steel under load cycles idealizing seismic actions. In *Comite´ Euro-International du Beton (AICAP-CEB) Symposium, Paris, France, Apr* (CEB Bulletin No. 131, pp. 67-122).

Tastani, S. & Pantazopoulou, S. (2009). Direct tension pullout bond test: Experimental results. *Journal of Structural Engineering*, *136*(6), 731-743. DOI: 10.1061/(asce)st.1943-541x.0000159

Tastani, S. P., Konsta-Gdoutos, M. S., Pantazopoulou, S. J. & Balopoulos, V. (2015, May). *The effect of Carbon NanoTubes/Polypropylene Fibers on Bond of Reinforcing Bars in ECC*. Paper presented at Fifth International Symposium on Nanotechnology in Construction (NICOM5), Chicago. Retrieved from https://www.researchgate.net/profile/Souzana_Tastani/publication/308481225_The_effect_of_Carbon_NanoTubesPolypropylene_Fibers_on_Bond_of_Reinforcing_Bars_in_ECC/links/57e4f02408ae06097a0e2915.pdf

Tastani, S. P., Konsta-Gdoutos, M. S., Pantazopoulou, S. J. & Balopoulos, V. (2016). The effect of carbon nanotubes and polypropylene fibers on bond of reinforcing bars in strain resilient cementitious composites. *Frontiers of Structural and Civil Engineering*, *10*(2), 214-223. DOI: 10.1007/s11709-016-0332-3

Réunion Internationale des Laboratoires et Experts des Matériaux (RILEM). (1994). *RILEM recommendations for the testing and use of constructons materials, RC 6 Bond test for reinforcement steel. 2. Pull-out test*. RILEM TC. Retrieved from https://www.rilem.net/publication/publication/4

Thrane, L., Pade, C., Idzerda, C. & Kaasgaard, M. (2010), Effect of rheology of SCC on bond strength of ribbed reinforcement Bars. In K. Khayat & D. Feys (Eds.), *Design, Production and Placement of Self-Consolidating Concrete, Montreal, Canada, September 26-29* (pp. 367-377). Dordrecht: RILEM Bookseries. DOI: 10.1007/978-90-481-9664-7_31

Trezos, K. G., Sfikas, I. P. & Orfanopoulos, K. (2014). Bond of self-compacting concrete incorporating silica fume: Top-bar effect, effects of rebar distance from casting point and of rebar-to-concrete relative displacements during setting. *Construction and Building Materials*, *73*, 378-390. DOI: 10.1016/j.conbuildmat.2014.09.113

Tu, W., Zhu, Y., Fang, G., Wang, X. & Zhang, M. (2019). Internal curing of alkali-activated fly ash-slag pastes using superabsorbent polymer. *Cement and Concrete Research*, *116*, 179-190. DOI: 10.1016/j.cemconres.2018.11.018

Turk, K., Caliskan, S. & Yildirim, M. S. (2005). Influence of loading condition and reinforcement size on the concrete/reinforcement bond strength. *Structural Engineering and Mechanics*, *19*(3), 337-346. DOI: 10.12989/sem.2005.19.3.337

Turk, K., Karatas, M. & Ulucan, Z. C. (2010). Effect of the use of different types and dosages of mineral additions on the bond strength of lap-spliced bars in self-compacting concrete. *Materials and structures*, *43*(4), 557-570. DOI: 10.1617/s11527-009-9511-1

Usher, P. M., Angles, J. G., Rixom, R. M. & Ryle, R. K. (1980). *Guide to Chemical Admixtures for Concrete* (Technical Report No. 18). London: The Cement Admixtures Association, Concrete Society.

Valcuende, M. & Parra, C. (2009). Bond behaviour of reinforcement in self-compacting concretes. *Construction and Building Materials*, *23*(1), 162-170. DOI: 10.1016/j.conbuildmat.2008.01.007

Van Tittelboom, K., & De Belie, N. (2013). "Self-healing in cementitious materials—A review." *Materials*, 6(6), 2182-2217. DOI: 10.1016/j.conbuildmat.2008.01.007

Van Tittelboom, K., Gruyaert, E., Rahier, H. & De Belie, N. (2012). Influence of mix composition on the extent of autogenous crack healing by continued hydration or calcium carbonate formation. *Construction and Building Materials*, *37*, 349-359. DOI: 10.1016/j.conbuildmat.2012.07.026

Van Tittelboom, K., Wang, J., Araújo, M., Snoeck, D., Gruyaert, E., Debbaut, B., Derluyn, H., Cnudde, V., Tsangouri, E. & Van Hemelrijck, D. (2016). Comparison of different approaches for self-healing concrete in a large-scale lab test. *Construction and building materials*, *107*, 125-137. DOI: 10.1016/j.conbuildmat.2015.12.186

Vecchio, F. J. & Collins, M. P. (1986). The modified compression-field theory for reinforced concrete elements subjected to shear. *ACI Journal Proceedings*, *83*(2), 219-231. DOI: 10.14359/10416

Vecchio, F. J. & Collins, M. P. (1993). Compression response of cracked reinforced concrete. *Journal of structural engineering*, 119(12), 3590-3610. DOI: 10.1061/(asce)0733-9445(1993)119:12(3590)

Volz, J. S., Myers, J., Richardson, D. N., Arezoumandi, M., Beckemeier, K., Davis, D., Holman, K., Looney, T. & Tucker, B. (2012). *Design and evaluation of high-volume fly ash (HVFA) concrete mixes* (Research No. TRyy1110, cmr 13-008). Missouri: Center for Transportation Infrastructure and Safety/NUTC program, Dept. of Transportation, 2012. Missouri University of Science and Technology.

Walker, P., Batayneh, M. & Regan, P. (1997). Bond strength tests on deformed reinforcement in normal weight concrete. *Materials and Structures*, *30*(7), 424. DOI: 10.1007/bf02498566

Wang, D. Z., Zhang, Y. Y. & Meng, Y. F. (2014). Study on Adding Super Absorbent Polymer to Improve the Frost Resistance of Concrete. *Applied Mechanics and Materials*, *584*, 960-963. DOI: 10.4028/www.scientific.net/amm.584-586.960

Wang, F., Zhou, Y., Peng, B., Liu, Z. & Hu, S. (2009). Autogenous shrinkage of concrete with super-absorbent polymer. *Materials Journal*, *106*(2), 123-127. DOI: 10.14359/56458

Wang, W. B., Liu, J. P., Tian, Q., Wang, Y. J. & Li, L. (2013). Effects of Water Absorption and Size of Superabsorbent Polymers on Internal Curing of Cement Paste. *Materials Science Forum, 743-744*, 193-197. DOI: 10.4028/www.scientific.net/msf.743-744.193

Wang, Z.-H., Li, L., Zhang, Y.-X. & Wang, W.-T. (2019). Bond-slip model considering freeze-thaw damage effect of concrete and its application. *Engineering Structures*, *201*, 109831. DOI: 10.1016/j.engstruct.2019.109831

Welch, G. B. & Patten, B. J. Bond strength of reinforcement affected by concrete sedimentation. *ACI Journal Proceedings*, *62*(2), 251-264. DOI: 10.14359/7690

Wu, C. & Chen, G. (2015). Unified Model of Local Bond between Deformed Steel Rebar and Concrete: Indentation Analogy Theory and Validation. *Journal of Engineering Mechanics*, *141*(10), 04015038. DOI: 10.1061/(asce)em.1943-7889.0000945

Wu, C., Chen, G., Volz, J. S., Brow, R. K. & Koenigstein, M. L. (2012). Local bond strength of vitreous enamel coated rebar to concrete. *Construction and Building Materials*, *35*, 428-439. DOI: 10.1016/j.conbuildmat.2012.04.067

Wu, Y.-F. & Zhao, X.-M. (2012). Unified bond stress–slip model for reinforced concrete. *Journal of Structural Engineering*, *139*(11), 1951-1962. DOI: 10.1061/(asce)st.1943-541x.0000747

Wyrzykowski, M., Lura, P., Pesavento, F. & Gawin, D. (2012). Modeling of water release from superabsorbent polymers during internal curing. *Journal of Materials in Civil Engineering*, *24*(8), 1006-1016. DOI: 10.1061/(asce)mt.1943-5533.0000448

Xia, J.-W., Wang, S. X., Chang, H. F., Peng, H.-Q., Jiang, L. & Ding, P. (2006). Study on strength and bond characteristics of GGBS concrete. *Key Engineering Materials*, *302*, 561-566. DOI: 10.4028/www.scientific.net/kem.302-303.561

Yao, Y., Zhu, Y. & Yang, Y. (2012). Incorporation superabsorbent polymer (SAP) particles as controlling pre-existing flaws to improve the performance of engineered cementitious composites (ECC). *Construction and Building Materials*, *28*(1), 139-145. DOI: 10.1016/j.conbuildmat.2011.08.032

Yerlici, V. A. & Ozturan, T. (2000). Factors affecting anchorage bond strength in high-performance concrete. *Structural Journal*, *97*(3), 499-507. DOI: 10.14359/4645

Yuan, X. L., Li, B. X. & Zhou, S. H. (2011). Freeze-thaw and de-icing salt resistance of concrete containing mineral admixtures and air-entraining agent. *Advanced Materials Research*, *163*, 3122-3127. DOI: 10.4028/www.scientific.net/amr.163-167.3122

Yue, L. & Shuguang, H. (2001). The microstructure of the interfacial transition zone between steel and cement paste. *Cement and Concrete Research*, *31*(3), 385-388. DOI: 10.1016/s0008-8846(01)00452-5

Zayed, A. M. (1991). The Nature of the Concrete-Steel Rebar Interface in Plain and Silica Fume Concrete. *MRS Proceedings*, *245*, 341-347. DOI: 10.1557/proc-245-341

Zhang, S., Fan, Y. & Li, N. (2015). Bonding behavior between steel bars and concrete modified with nano-kaolinite clay. *J. Southeast Univ. (Nat. Sci. Ed.) 45*(2), 382–386. Retrieved from http://en.cnki.com.cn/Article_en/CJFDTotal-DNDX201502032.htm

Zhao, W. & Zhu, B. (2017). Basic parameters test and 3D modeling of bond between high-strength concrete and ribbed steel bar after elevated temperatures. *Structural Concrete*, *18*(5), 653-667. DOI: 10.1002/suco.201600005

Zhao, W. & Zhu, B. (2018). Theoretical model for the bond–slip relationship between ribbed steel bars and confined concrete. *Structural Concrete*, *19*(2), 548-558. DOI: 10.1002/suco.201700008

Zheng, X. H., Ge, Y. & Yuan, J. (2013). Influence of air content and vibration time on frost resistance of air entrained concrete. *Advanced Materials Research*, *857*, 110-115. DOI: 10.4028/www.scientific.net/amr.857.110

Zhu, W., Sonebi, M. & Bartos, P. (2004). Bond and interfacial properties of reinforcement in self-compacting concrete. *Materials and structures*, *37*(7), 442-448. DOI: 10.1007/bf02481580

Ziaei-Nia, A., Tadayonfar, G.-R. & Eskandari-Naddaf, H. (2018). Effect of air entraining admixture on concrete under temperature changes in freeze and thaw cycles. *Materials Today: Proceedings*, *5*(2), 6208-6216. DOI: 10.1016/j.matpr.2017.12.229

Ziari, H., Hayati, P. & Sobhani, J. (2017). Air-entrained air field self-consolidating concrete pavements: strength and durability. *International Journal of Civil Engineering*, *15*(1), 21-33. DOI: 10.1007/s40999-016-0104-4

Zilveti, A., Sooi, T. K., Klingner, R. E., Carrasquillo, R. L. & Jirsa, J. (1985). *Effect of Superplasticizers on the Bond Behavior of Reinforcing Steel in Concrete Members* (Research report No. FHWA/TX-86/36+383-2F). Austin, Texas: Center For Transportation Research, University of Texas. Retrieved from https://library.ctr.utexas.edu/digitized/texasarchive/phase2/383-2f-ctr.pdf